

AD-A021 526

MICRO NAVIGATOR (MICRON) PHASE 2A. VOLUME I.  
TECHNICAL REPORT

Joseph M. Miller

Rockwell International Corporation

Prepared for:

Air Force Avionics Laboratory

February 1976

DISTRIBUTED BY:

**NTIS**

National Technical Information Service  
U. S. DEPARTMENT OF COMMERCE

## **DISCLAIMER NOTICE**

**THIS DOCUMENT IS BEST QUALITY  
PRACTICABLE. THE COPY FURNISHED  
TO DTIC CONTAINED A SIGNIFICANT  
NUMBER OF PAGES WHICH DO NOT  
REPRODUCE LEGIBLY.**

AFAL-TR-75-210  
Volume I

071106

# MICRO NAVIGATOR (MICRON) PHASE 2A

## VOLUME I TECHNICAL REPORT

Autonetics Group  
Rockwell International  
Aneheim, California

February 1976

Technical Report AFAL-TR-75-210, Volume I Final Report  
for the Period 1 April 1974 through 1 August 1975

Approved for public release; distribution unlimited



NATIONAL TECHNICAL  
INFORMATION SERVICE



Air Force Avionics Laboratory  
Air Force Wright Aeronautical Laboratories  
Air Force Systems Command  
Wright-Patterson Air Force Base, Ohio

## UNCLASSIFIED

SECURITY CLASSIFICATION OF THIS PAGE (When Data Entered)

REPORT DOCUMENTATION PAGE		READ INSTRUCTIONS BEFORE COMPLETING FORM
1 REPORT NUMBER AFAL-TR-75-210	2 GOVT ACCESSION NO.	3 RECIPIENT'S CATALOG NUMBER
4 TITLE (and Subtitle) MICRO NAVIGATOR (MICRON) PHASE 2A VOLUME I - TECHNICAL REPORT; Technical Report AFAL-TR-75-210, Volume I Final Report for the Period 1 April 1974 thru 1 Aug 75		5 TYPE OF REPORT & PERIOD COVERED Technical Report - Final, 1 April 1974 thru 1 Aug 1975
7 AUTHOR(s)		6 PERFORMING ORG REPORT NUMBER C74-455/201
Joseph M. Miller, et al		8 CONTRACT OR GRANT NUMBER(s) F33615-74-C-1099
9 PERFORMING ORGANIZATION NAME AND ADDRESS Autonetics Group, Rockwell International 3370 Miraloma Avenue Anaheim, California 92803		10 PROGRAM ELEMENT PROJECT TASK AREA & WORK UNIT NUMBERS Project No. ADP 666A Task No. 666A03
11 CONTROLLING OFFICE NAME AND ADDRESS Air Force Wright Aeronautical Laboratories (AFSC) Air Force Avionics Laboratory Wright-Patterson AFB, Ohio 45433 AFAL/RWM-666A		12 REPORT DATE February 1976
14 MONITORING AGENCY NAME & ADDRESS (if different from Controlling Office)		13 NUMBER OF PAGES <del>101</del> 530
		15 SECURITY CLASS (of this report) Unclassified
16 DISTRIBUTION STATEMENT (of this Report) Approved for public release, distribution unlimited		
17 DISTRIBUTION STATEMENT (of the abstract entered in Block 20, if different from Report)		
18 SUPPLEMENTARY NOTES		
19 KEY WORDS (Continue on reverse side if necessary and identify by block number) Angle Calibration Optimization    Mass Unbalance Modulation    N57A Flights Tests Cost of Ownership    Micro Electrostatic Gyro    Small Gap Gyro Drift Model Improvement    Micro Electrostatic Gyro Accelerometer    Vac Ion Pump Elimination Getter Gyro    MOS Device Development Gyro Fast Reaction    Navigation Performance		
20 ABSTRACT (Continue on reverse side if necessary and identify by block number) The Micro Navigator (MICRON) is a low-cost highly reliable, and moderately accurate strapdown inertial navigator. The heart of the MICRON system is the micro-electrostatic gyro (MESG), an instrument which incorporates an all-attitude, whole-angle readout from an electrostatically suspended rotor. Under previous Air Force contracts two developmental navigation systems (N57A-1 and N57A-2) were developed.		



UNCLASSIFIED

SECURITY CLASSIFICATION OF THIS PAGE(When Data Entered)

20. ABSTRACT (Cont)

The objective of the MICRON Phase 2A contract was to test N57A-1 and N57A-2; to design, fabricate and integrate two gyro subassemblies and one gyro test station; to test gyros and gyro subassemblies; and to perform analyses, studies and trade-offs for use in defining the MICRON system.

Both N57A systems were flight tested and the capability of the system to meet the position accuracy requirement was demonstrated. N57A-1 was used to demonstrate in-motion polhode damping. System reliability screen, Scorsby and heading sensitivity tests were successfully conducted on N57A-2.

Two gyro subassemblies and one gyro test station were designed, fabricated, and integrated. One subassembly was used for MESGA development testing and one was used for 4-plate gyro and electronics development.

Getter gyros were fabricated and tested. A gyro design evolved which meets the fast reaction requirement. A "small gap" gyro was developed which reduces the cost of gyro suspension electronics.

System analyses, studies, and trade-offs were made which resulted in circuit simplification, reduced costs, and partitioning to meet maintainability and producibility requirements.

UNCLASSIFIED

SECURITY CLASSIFICATION OF THIS PAGE(When Data Entered)

## FOREWORD

This report was prepared under Air Force Contract F33615-74-C-1099, Project No. ADP 666, Task Number 666A03. The report covers work performed by the Autonetics Group of Rockwell International, 3370 Miraloma Avenue, Anaheim, Ca 92803, for the Air Force Avionics Laboratory, Wright-Patterson Air Force Base, Ohio. This final report consists of two volumes of which this is Volume I. The titles of the volumes are:

Volume I    Technical Report

Volume II   Appendices

The purpose of this MICRON Phase 2A contract was to test the N57A system and gyros; to design, fabricate, and integrate two gyro subassemblies and one gyro test station; and to perform analyses, studies, and tradeoffs for use in defining the MICRON system. This program was conducted from April 1974 through July 1975. It was directed by the MICRON Program Manager, J. A. Schwarz and the Engineering Manager, L. B. Romine. The principal contributors to this report were A. P. Andrews, T. F. Brasher, H. L. Bump, K. J. Gibson, A. G. Gross, F. R. Hall, R. B. Hall, D. W. Homes, L. E. Johnsen, J. F. Klinchuch, J. M. Miller, M. J. Rupert, A. L. Sattler, W. P. Thoennes, and C. C. Whang, Jr. The contractors final submittal date was February 1976.

This report has been assigned the Internal Rockwell Control Number, C74-455/201. All correspondence relating to this document should reference this number.

The cognizant Air Force Project Manager on this phase of the MICRON program was Captain Walter Peterson, Jr., AFAL/RWM-666A.

## TABLE OF CONTENTS

	<u>Page</u>
1. Introduction and Summary .....	1
1.1 Introduction .....	1
1.2 Summary .....	2
1.2.1 Highlights and Conclusions .....	2
1.2.2 Summary by Statement of Work Tasks .....	3
2. Task 1, Prime Mission Product .....	7
2.1 Inertial Measuring Unit (IMU) .....	7
2.1.1 Error Analysis/Error Budget .....	7
2.1.2 Design Evaluation Models .....	8
2.2 Software .....	26
2.2.1 In-Motion Polhode Damping .....	26
2.2.2 Test Station Software .....	30
2.2.3 Define DPU Parameters .....	32
2.2.4 Define CCU Parameters .....	32
2.3 Aerospace Ground Equipment (AGE) .....	32
2.3.1 Gyro Test Station CI Specification .....	32
2.3.2 Design Gyro Test Station .....	34
2.3.3 Fabrication of Gyro Test Station .....	34
2.3.4 Integration of Gyro Test Station .....	38
3. Task 2, Test and Evaluation .....	39
3.1 Test Plans .....	39
3.1.1 Gyro and Gyro Subassembly Test Plans .....	39
3.1.2 EMI /Grounding Test Plans .....	39
3.1.3 Design Evaluation Model Test Plan .....	39
3.1.4 N57A-1/HAFB GSA Test Plans .....	40
3.2 Laboratory Tests .....	41
3.2.1 N57A-2 Lab Tests .....	41
3.2.2 Gyro Testing .....	43
3.2.3 Laboratory Test DEM .....	70
3.2.4 N57A-1/HAFB GSA Tests .....	70
3.2.5 Test Gyro Subassemblies .....	74
3.2.6 Test Northrop Rotors and Cavities .....	75

Preceding page blank

## TABLE OF CONTENTS (Cont)

	<u>Page</u>
3.3 Flight Test Engineering .....	78
3.3.1 Flight Test Support .....	78
3.3.2 Post Flight Analysis .....	79
3.4 Flight Test Operations .....	94
4. Task 3, Support Equipment .....	96
4.1 Gyro Subassembly .....	96
4.1.1 CI Specification for Gyro Subassembly .....	96
4.1.2 Design Gyro Subassemblies .....	96
4.1.3 Fab/Integrate GSA and GSA Spares .....	100
4.2 Support Hardware .....	100
4.2.1 Define Integrable MICRON Configuration .....	100
4.2.2 Define Stand-Alone MICRON Configuration .....	101
4.3 Repair .....	101
4.3.1 Gyros .....	101
4.3.2 N57A Systems .....	103
4.3.3 Refurbish N57A-1 System and Test Equipment .....	107
5. Task 4, Training .....	102
5.1 Manuals .....	108
5.1.1 Operating Manual .....	108
5.1.2 Interface Drawings .....	108
5.1.3 Training Plan .....	108
5.2 Hardware .....	108
5.3 Services .....	109
5.3.1 Support LAX Flight Tests .....	109
5.3.2 Support HAFB Gyro Subassembly .....	109
5.3.3 Install and C/O N57A-2 at HAFB .....	113
5.3.4 Support HAFB Flight Tests .....	114
5.3.5 Training .....	122

## TABLE OF CONTENTS (Cont)

	<u>Page</u>
6. Task 5, System Management Engineering .....	123
6.1 Program Management .....	123
6.1.1 Design Reviews .....	123
6.1.2 Program Plans .....	134
6.1.3 Work Breakdown Structure .....	135
6.1.4 Grounding and EMI Guidelines .....	135
6.1.5 Second Source Rotors and Cavities .....	135
6.1.6 Angle Readout Model .....	143
6.2 Cost of Ownership .....	144
6.2.1 Baseline IMU .....	144
6.2.2 IMU Production Processes/Techniques .....	150
6.2.3 PRM Tradeoff Studies .....	166
6.2.4 Reliability .....	195
6.2.5 Maintainability .....	216
6.2.6 Cost-of-Ownership Model .....	233
6.2.7 Parts Program .....	235
6.2.8 Beam Lead Development .....	236
6.2.9 MOS Device Development .....	238
6.3 System Engineering .....	252
6.3.1 Develop 8-Plate MESGA .....	252
6.3.2 Vacion Pump Elimination .....	259
6.3.3 Develop Four-Plate Gyro .....	281
6.3.4 Perform Mechanization and Modeling Improvements .....	287
6.3.5 Develop Hardware and Software Improvements .....	319
6.3.6 Design Alternatives .....	381
6.4 Applications Engineering .....	446
6.4.1 Applications Engineering Trip to Wright-Patterson Air Force Base (23-25 October 1974) .....	446
6.4.2 Applications Engineering Trip to General Dynamics, Martin-Marietta, and McDonnell Douglas (6-8 November 1974) .....	447
6.4.3 Applications Engineering Trip to Northrop Corp. (12 November 1974) .....	447
6.4.4 Applications Engineering Trip to Army ECOM, Sikorsky, Grumman, Fairchild-Republic, and Boeing Vertol (19-21 November 1974) .....	448

## TABLE OF CONTENTS (Cont)

	<u>Page</u>
7. Task 6, Data .....	449
8. Program Schedule .....	453
9. References .....	460

## LIST OF ILLUSTRATIONS

Figure		Page
2-1.	Position CEP vs Time .....	16
2-2.	North, East, and Radial Velocity Error vs Time .....	17
2-3.	Conduction Cooled Design Evaluation Model .....	18
2-4.	Liquid Cooled Design Evaluation Model .....	20
2-5.	Comparison of Module Clamp Thermal Conductance for MICRON 2A Test Demonstrator Conduction Model .....	21
2-6.	MICRON Liquid Model, Airflow Requirements .....	23
2-7.	MICRON Liquid Model Fast Reaction Heat Required .....	24
2-8.	MICRON Liquid Model Control Heater Power Required vs Insulation Thickness .....	25
2-9.	Conduction DEM, GAU Fast Reaction Response, Heaters on Chassis Only .....	27
2-10.	Conduction DEM, GAU Fast Reaction Response, Heaters on Chassis and Modules .....	28
2-11.	Conduction DEM, GAU Fast Reaction Response, Heaters on Chassis and Modules-Critical Electronics Control Power Increased to 120 Watts .....	29
2-12.	MESGA Acceleration Readout Variation Over 24 Hours .....	33
2-13.	Gyro Test Station Layout .....	35
2-14.	Gyro Test Console (02710-727-1) .....	36
2-15.	Computer Console (02720-717-1) .....	37
3-1.	Time Constant Determination Test - Gyro A012Y .....	57
3-2.	Thermal Response: Gyro -012Y Time Constant for Rotor Warm- Up with Rotor Suspended .....	58
3-3.	Thermal Response: Gyro A012Y Time Constant for Rotor Cool-Down with Rotor Suspended .....	59
3-4.	Thermal Response: Gyro A012Y Time Constant for Rotor Cool-Down with Rotor Desuspended .....	60
3-5.	N57A-1 CEP Time History .....	83
3-6.	N57A-2 CEP Time History .....	84
3-7.	CEP vs Time, 7 N57A-1 LAX Flights .....	86
3-8.	CEP Rate vs Time; N57A-1 LAX Flights .....	87
3-9.	Per Channel Time RMS Velocity Error vs Time; 7 N57A-1 LAX Flights .....	88
3-10.	Per Channel RMS Velocity Error vs Time; 7 N57A-1 Flights .....	89
3-11.	CEP vs Time; 5 N57A-2 LAX Flights .....	90
3-12.	CEP Rate vs Time; 5 N57A-2 LAX Flights .....	91
3-13.	Per Channel Time RMS Velocity Error vs Time; 5 N57A-2 LAX Flights .....	92
3-14.	Per Channel RMS Velocity Error vs Time; 5 N57A-2 LAX Flights .....	93
4-1.	Gyro Subassembly .....	98
4-2.	Interface Block Diagram (MICRON Concept) .....	102
4-3.	Interface Block Diagram (ACF Concept) .....	102
5-1.	N57A-2 CEP Time History .....	116
6-1.	CPS Flow .....	151
6-2.	CPC Assembly/Test Flow .....	152

## LIST OF ILLUSTRATIONS (Cont)

Figure		Page
6-3.	CPC Assembly/Test Flow .....	153
6-4.	CPC Assembly/Test Flow .....	154
6-5.	CPC Test-Yield-Reflow .....	155
6-6.	MICRON Phase 2A Production Flow Packaging Design Alternate No. 1 .....	157
6-7.	MICRON Phase 2A Production Flow - Pkg. Alt. 2 .....	158
6-8.	MICRON Phase 2A Production Flow - Pkg. Alt. 3 .....	159
6-9.	MICRON Phase 2A Production Flow - Pkg. Alt. 4 .....	160
6-10.	MICRON Phase 2A Production Flow - Pkg. Alt. 5 .....	161
6-11.	MICRON Phase 2A Production Flow Design Alternate No. 6 .....	162
6-12.	MICRON Phase 2A Production Flow Design Alternate No. 7 .....	163
6-13.	Production Flow - Stand Alone MICRON System .....	164
6-14.	Electronics Cost Target/Estimate Comparison .....	167
6-15.	Suspension Electronics Cost Target/Estimate Comparison .....	168
6-16.	MUM and Digitizer Electronics Cost Target/Estimate Comparison .....	169
6-17.	Spin Motor Electronics Cost Target/Estimate Comparison .....	170
6-18.	Support Electronics Cost Target/Estimate Comparison .....	171
6-19.	Reliability Sensitivity Cost Comparison .....	173
6-20.	Module Repair/Discard Indifference Curve of Module Price vs Failure Rate Normalized to the Baseline Estimates .....	177
6-21.	Module Repair/Discard Indifference Curve of Module Size vs Failure Rate Normalized to the Baseline Estimates .....	178
6-22.	Diagram of 8-Plate Dual Frequency Suspension System .....	183
6-23.	Cost Comparison - Beam Lead Parts vs Fly Wire Parts .....	186
6-24.	Suspension Servo Loop Block Diagram .....	189
6-25.	Electronics Cost vs Parts Per Module .....	192
6-26.	Parts Per Module vs Parts Yield .....	193
6-27.	Electronics Cost vs Number of Electronic Modules .....	194
6-28.	Computer Prediction Printout .....	200
6-29.	Predicted Reliability vs Part Temperature .....	206
6-30.	Expected Failures per Active Device During CPC Hybrid Testing (As a Function of BL Mix) .....	210
6-31.	IMU Logistics Costs as a Function of Unit Cost and Reliability .....	217
6-32.	Maintenance Action Generation Sources .....	218
6-33.	Histogram of <u>MIL-HDBK-217 MTBF Prediction</u> Sample Data .....	219
	Field MTBF	
6-34.	Maintenance Concept Comparisons .....	224
6-35.	E-2 M-1 Maintenance Concept vs Calibration Stability .....	225
6-36.	MICRON Test and Fault Isolate Requirements .....	228
6-37.	Unit Support Cost vs BIT Confidence .....	229
6-38.	IMU Removals vs BIT Confidence E-2/M-1 System .....	231
6-39.	Block Diagram of TRGC Device .....	240
6-40.	CASC Block Diagram .....	242
6-41.	Block Diagram of QIRFG Device .....	244
6-42.	DMAC Device Block Diagram .....	245



## LIST OF ILLUSTRATIONS (Cont)

Figure	Page
6-43. Functional Block Diagram of 65008 Chip .....	250
6-44. Functional Block Diagram of Spin Control MOS Chip .....	251
6-45. Block Diagram of Pulsewidth Modulation Suspension Electronics .....	255
6-46. Block Diagram of MESGA 8-Plate Suspension Electronics and Acceleration Digitizer .....	257
6-47. RGA Spectrum .....	261
6-48. RGA Calibration .....	262
6-49. Speed Change of Gyro 118 .....	264
6-50. Speed Change of Gyro No. 118 .....	265
6-51. Speed Change of Gyro 118 .....	267
6-52. Speed Change of Gyro 154 .....	268
6-53. Speed Change of Gyro 156 .....	271
6-54. Speed Change of Gyro 156 .....	273
6-55. Speed Changes from Internal Effects in Gettered Gyros .....	274
6-56. "10-14" Leak Detector Schematic .....	280
6-57. Helium Pressure vs Time .....	281
6-58. Welded Gyro Design .....	282
6-59. Four-Plate Gyro Electrode Configuration .....	284
6-60. Four-Plate Suspension Electronics Block Diagram .....	285
6-61. Typical Four-Plate Waveforms .....	286
6-62. RMS Angle Readout Compensation Error vs Number of Calibration Samples .....	288
6-63. RMS Angle Compensation Error vs Number of Calibration Samples .....	289
6-64. Composite Histograms of Individual Drift Rate Model Magnitudes, Models Evaluated Independently .....	298
6-65. Histograms of Marginal Drift Model Coefficients after Orthonormalization of Five Models .....	300
6-66. Histograms of Marginal Drift Model Coefficients after Orthonormalization of Ten Models .....	301
6-67. Histograms of Marginal Drift Model Coefficients after Orthonormalization of Twenty Models .....	302
6-68. Histograms of Marginal Drift Model Coefficients after Orthonormalization of all 35 Models .....	304
6-69. Histograms of Marginal Drift Model Coefficients in Sequence of Maximum Marginal Compensation .....	305
6-70. Magnitude of rms Marginal Drift Rate Compensation vs Number of Drift Model Coefficient Used .....	306
6-71. Comparison of K44WR and K44W Marginal Compensation .....	310
6-72. MESGA Test Setup, T'S W .....	325
6-73. Gyro 124 Harmonic Analysis .....	327
6-74. Gyro X-Axis Stability Data .....	328
6-75. Gyro Y-Axis Stability Data .....	329
6-76. Gyro 124 Z-Axis Stability Data .....	330
6-77. Gyro 96 Y Residuals .....	333
6-78. Gyro 96 Y Residuals (Bias and Trend Removed) .....	334

## LIST OF ILLUSTRATIONS (Cont)

<u>Figure</u>	<u>Page</u>
6-79. Gyro 96 Y Residual Autocorrelation Function .....	335
6-80. Gyro 68 X Axis Transient .....	335
6-81. Gyro 68 Y Axis Transient .....	337
6-82. Gyro 68 Z Axis Transient .....	338
6-83. Gyro 68 Noise Before Transient .....	339
6-84. Gyro 68 Noise After Transient .....	340
6-85. GSA Acceleration Pickoff Block Diagram .....	354
6-86. X Acceleration Component vs Time; 7-15-75, +Z Vertical Position .....	359
6-87. Y Acceleration Component vs Time; 7-15-75, +Z Vertical Position .....	360
6-88. Z Acceleration Component vs Time; 7-15-75 +Z Vertical Position .....	361
6-89. X Acceleration Component vs Time; 7-16-75; +1 Vertical Position .....	362
6-90. Y Acceleration Component vs Time; 7-16-75, +1 Vertical Position .....	363
6-91. Z Acceleration Component vs Time; 7-16-75, +1 Vertical Position .....	364
6-92. X Acceleration Component vs Time; 7-16-75, -3 Vertical Position .....	365
6-93. Y Acceleration Component vs Time; 7-16-75, -3 Vertical Position .....	366
6-94. Z Acceleration Component vs Time; 7-16-75, -3 Vertical Position .....	367
6-95. X Acceleration Component vs Time; 7-16-75, 7-17-75, Z Horizontal Position .....	368
6-96. Y Acceleration Component vs Time; 7-16-75, 7-17-75, Z Horizontal Position .....	369
6-97. Z Acceleration Component vs Time; 7-16-75, 7-17-75, Z Horizontal Position .....	370
6-98. X Acceleration Component vs Time; 7-17-75, 7-18-75, +Y Vertical Position .....	371
6-99. Y Acceleration Component vs Time, 7-17-75, 7-18-75, +Y Vertical Position .....	372
6-100. Z Acceleration Component vs Time; 7-17-75, 7-18-75, +Y Vertical Position .....	373
6-101. X Acceleration Component vs Time; 7-17-75, 7-18-75, +Z Vertical Position .....	374
6-102. Y Acceleration Component vs Time; 7-17-75, 7-18-75, +Z Vertical Position .....	375
6-103. Z Acceleration Component vs Time; 7-18-75, +Z Vertical Position .....	376
6-104. Electrostatic Gyro (MICRON) .....	383
6-105. Electrostatic Gyro - MICRON (Outline Drawing) .....	384
6-106. "Sure-Start" Modification .....	389
6-107. Pin Brazed into Beryllium Oxide Wafer .....	392

## LIST OF ILLUSTRATIONS (Cont)

<u>Figure</u>	<u>Page</u>
6-108. Pin Brazed into Beryllium Oxide Wafer . . . . .	392
6-109. Feedthrough Brazements: Cracking in BeO Wafers . . . . .	394
6-110. Cooling Air Flow Requirements . . . . .	404
6-111. Design Alternative No. 1 - Approximate Volume 416 in <sup>3</sup> W/O Thermal Insulation . . . . .	405
6-112. Design Alternative No. 2, Approximate Volume 486 In <sup>3</sup> W/O Thermal Insulation . . . . .	406
6-113. Design Alternative No. 3, Approximate Volume 397 In <sup>3</sup> W/O Thermal Insulation, Approximate Weight 15 Lb . . . . .	409
6-114. Instrument Assembly . . . . .	410
6-115. Gyro Assembly Unit (GAU) . . . . .	411
6-116. Liquid Cooling Loop Flow Schematic . . . . .	412
6-117. Design Alternative No. 4 - Approximate Volume 397 In <sup>3</sup> Approximate Weight 15 Lb . . . . .	413
6-118. Design Alternative No. 5 - Approximate Volume 429 In <sup>3</sup> W/O Insulation . . . . .	414
6-119. Instrument Assembly . . . . .	415
6-120. Design Alternative No. 6 Volume 498 In <sup>3</sup> Estimated Weight 18 Lb . . . . .	417
6-121. Design Alternative No. 7 Volume 434 in <sup>3</sup> Estimated Weight 15 Lb, LRU No. 1 of 2 . . . . .	418
6-122. Alternative MESG Design No. 1 . . . . .	435
6-123. Alternative MESG Design No. 2 . . . . .	436
6-124. Alternative MESG Design No. 3 . . . . .	437
6-125. Alternative MESG Design No. 4 . . . . .	438
6-126. Dual Gyro, Single Pump Brazed to Beryllium Base . . . . .	439
6-127. Dual Gyro, Single Pump E-Beam Welded to Inconel Adapter . . . . .	440
6-128. Dual Gyro, Single Pump Sealed to Beryllium Base with Gold Gasket . . . . .	441
6-129. Captured Seal Design - Using .020 Diameter Wire . . . . .	442
6-130. Captured Seal Design . . . . .	443
6-131. Captured Seal Design - Conflat 0.030(t) x 0.089(w) Gasket . . . . .	444
7-1. Phase 2A MICRON Data Schedule . . . . .	450
8-1. Program Schedule . . . . .	454
8-2. Standard Milestone Symbols . . . . .	459

## LIST OF TABLES

<u>Tables</u>	<u>Page</u>
2-1. Segments Approximating INS Route No. 6 .....	7
2-2. Budgeted Error Sources and Tabulated Errors at 256 Minutes .....	9
3-1. Summary of Test Results, N57A-2 Heading Sensitivity Tests, July 1974 .....	42
3-2. Summary of Test Results N57A-2 Turn-on Repeatability Tests .....	43
3-3. Summary of Test Station IV Activity .....	45
3-4. Comparison of Drift Rates Due to Interelectrode Grooves: Gyro 136 vs 144 .....	55
3-5. Summary of Cavity-to-Rotor Time Constant Tests .....	61
3-6. Summary of Z-Coil-Only Rotor Heating Characterization Studies Using 5 kHz Excitation Frequency .....	62
3-7. Z-Coil-Only Rotor Heating Tests Gyro A-012Y, Tabulation of Tests ..	64
3-8. Summary of Z-Coil Heating Test Results, Gyro A-012Y, Categorized by Power Supply Used .....	65
3-9. Gyro Motor Temperature Tests .....	66
3-10. Summary of Rotor Heating Tests - Gyro No. 059 .....	67
3-11. N57A-1 Flight Test Summary .....	80
3-12. N57A-2 Flight Test Summary .....	81
3-13. CEP Rates and Velocity Errors .....	82
3-14. N57A LAX Flight Test Results .....	85
3-15. Summary of Maneuvers, N57A-2 Flight 3 .....	95
3-16. Summary of Maneuvers, N57A-2 Flight 4 .....	95
4-1. GSA Electronics Modules .....	97
4-2. GSA Housing - Drawing List .....	99
4-3. History of MESA Assembly Activity .....	104
5-1. Angle Calibration Results .....	112
5-2. Drift Calibration Results .....	112
5-3. Summary of N57A-2 HAFB Flight Data .....	114
5-4. HAFB Helicopter and Laboratory Data Summary .....	118
5-5. HAFB Laboratory and Helicopter Data Summary for March 7 through March 27, 1975 .....	120
5-6. HAFB C-141 and Laboratory Data Summary .....	121
6-1. Systems Electronics Unit (SEU) .....	145
6-2. Gyro Accelerometer Unit (GAU) .....	146
6-3. Baseline System Ten Year Ownership Costs .....	148
6-4. Phase 2A Recurring Price Estimates .....	149
6-5. Baseline/Update Comparisons .....	166
6-6. Conditions for Cost-of-Ownership Prediction - Reliability Sensitivity Study .....	172
6-7. Reliability Sensitivity Cost Comparisons .....	172
6-8. Reliability Tradeoff Maintenance Costs .....	174
6-9. Matrix of Conditions for Module Price Discard-Repair Study .....	175
6-10. Matrix of Conditions for Module Size Discard-Repair Study .....	175
6-11. MICRON Packaging Alternative Matrix .....	180
6-12. Packaging Alternate Analysis .....	181
6-13. Suspension System Comparison .....	184
6-14. Price Comparisons .....	184

## LIST OF TABLES (Cont)

<u>Tables</u>	<u>Page</u>
6-15. PDA No. 6 Vs (E-3)/(M-1) Price Comparison .....	187
6-16. Phase 2A Configuration Comparisons .....	196
6-17. Ten Year Ownership Costs .....	197
6-18. Matrix of MICRON Configurations Evaluated .....	198
6-19. Reliability Screening Comparisons .....	207
6-20. Hybrid CPC Screen Evaluation - Estimated Failures (in%) .....	208
6-21. Reliability Prediction/MICRON Design Configuration Matrix .....	211
6-22. Reliability Prediction Summary .....	213
6-23. Eight Lowest Cost Baseline System Maintenance Concepts Listed in Ascending Cost Order .....	221
6-24. "Goal" System Definition .....	223
6-25. Mini-ORLA Results .....	223
6-26. Basic Fault Isolate Characteristic Definitions .....	227
6-27. Classes of Removal Causes .....	230
6-28. Module Fault Isolation vs BITE Confidence .....	232
6-29. Selected 2A Model Improvements .....	234
6-30. MOS Devices Utilized in the Input/Output .....	238
6-31. Rise Time and Propagation Delay Sensitivity to Temperature Variations for the Charge Amplifier First Stage .....	254
6-32. Gyro 154 After Getter Reactivation .....	270
6-33. Variations in Design/Fabrication of Gettered Gyros .....	275
6-34. Gyro 158C .....	277
6-35. MESG Angle Calibrations Used in Determining Initial Uncertainty of Calibration Coefficients .....	289
6-36. Comparison of IBM 1130 Results with HP2100 Results from Angle Parameter Comparison Program (CMPZE) .....	291
6-37. Comparison of Angle Calibration Parameters from Standard (230-Sample) Calibration and Optimized (165-Sample) Calibration .....	293
6-38. Drift Rate Data Bank Description .....	295
6-39. Functional Formulas for Drift Model K44W .....	296
6-40. Five Least Significant Drift Models .....	307
6-41. Ordering of K44WR Models Compared to K44W Models .....	309
6-42. Ordering of K45 Models Compared to K44WR .....	313
6-43. Functional Formulas for Drift Model K46 .....	316
6-44. Marginal Utility Ordering of Model K46 .....	317
6-45. Allowable Variations for MESGA .....	321
6-46. MESGA Error Budget (PAM) .....	322
6-47. MESGA Error Budget (PWM) .....	323
6-48. MESGA T/S IV Test Summary .....	326
6-49. Gyro 96 Calibration Data .....	331
6-50. Gyro 102 Data .....	341
6-51. Angle and Drift Calibration Data .....	342
6-52. MESGA Error Budget (PWM) .....	344
6-53. MESGA Errors .....	345
6-54. MESGA Errors - Recent Test Data .....	346
6-55. Summary of Revised MESGA Test Plan .....	350
6-56. MESGA Test Log Summary .....	351

## LIST OF TABLES (Cont)

<u>Tables</u>	<u>Page</u>
6-57. MESGA Calibration Table Angles . . . . .	353
6-58. GSA MESGA Calibration Data, Gyro 14Y . . . . .	355
6-59. GSA MESGA Calibration Parameter Shifts . . . . .	356
6-60. Stability Test Summary . . . . .	357
6-61. Feedthrough Brazements: Cleaning Practices for Beryllium Oxide . .	391
6-62. Feedthrough Brazements: Relative Thermal Contraction . . . . .	395
6-63. Magnetic Susceptibility of Cavities . . . . .	399
6-64. Microprobe Analyses of Inconel X750 Coatings . . . . .	401
6-65. Memory Configurations . . . . .	420
6-66. Baseline MICRON Semiconductor Memory Power Requirements . . . .	421
6-67. MICRON Semiconductor Memory Alternate No. 1 Power Requirements . . . . .	421
6-68. MICRON Semiconductor Memory Parts Count Summary . . . . .	422
6-69. DPU Component Reduction Summary . . . . .	425
6-70. Baseline DPU Parts Summary . . . . .	427
6-71. Discrete Packaging, Baseline DPU Parts List . . . . .	429

## LIST OF SYMBOLS AND ABBREVIATIONS

AB	Accumulator and Buffer
AC	Algorithm Control
ACF	Air Combat Fighter
A/D	Analog to Digital
AGE	Aerospace Ground Equipment
AIU	Analog Interface Unit
ALU	Arithmetic Logic Unit
ASALM	Advanced Strategic Air Launched Missile
ASD	Automatic Shutdown
BAP	Buffer and Parity
BIT	Built-in Test
BITE	Built-in Test Equipment
BLC	Bus Logic and Clock
BLSJ	Beam Lead Sealed Junction
CAS	Counter and Automatic Sequencer
CASC	Counter and Automatic Sequencer Control
CCU	Central Computer Unit
CDRL	Contract Data Requirements List
CDU	Control Display Unit
CEP	Circle Error, Probable
C/M	Charge Monitor
CMOS	Complementary Metal Oxide Semiconductors
COO	Cost of Ownership
CPC	Ceramic Printed Circuit
CPS	Ceramic Printed Substrate

## LIST OF SYMBOLS AND ABBREVIATIONS

CPU	Central Processor Unit
CSDL	Charles Stark Draper Laboratory
D/A	Digital-to-Analog
DEM	Design Evaluation Model
DISAG	Dielectric Isolation Self-Aligning Gate
DMA	Direct Memory Access
DMAC	Direct Memory Access Control
DPU	Dedicated Processor Unit
EAROM	Electrically Alterable Read Only Memory
EMA	Electromagnetic Accelerometer
EMC	Electromagnetic Compatibility
EMO	Electromagnetic Interference
ESG	Electrostatic Gyro
FTP	Flight Test Panel
GAU	Gyro Accelerometer Unit
GSA	Gyro Subassembly
HAFB	Halloman Air Force Base
IAU	Instrument Assembly Unit
IC	Integrated Circuit
IMU	Inertial Measuring Unit
INS	Inertial Navigation Set
INT	Interrupt
I/O	Input/Output
IOU	Input/Output Unit
LAD	Logic and Adder
LAX	Los Angeles International Airport



## LIST OF SYMBOLS AND ABBREVIATIONS

LCC	Life Cycle Cost
LED	Light Emitting Diode
LRU	Line Replaceable Unit
LSI	Large Scale Integration
MESG	Micro Electrostatic Gyro
MESGA	Micro Electrostatic Gyro Accelerometer
MHU	Mechanical Housing Unit
MIB	Master Interconnect Board
MICRON	Micro Navigator
MLB	Multi-layer Board
MMC	Martin Marietta Corporation
MNOS	Metal-Nitride Oxide-Semiconductor
MOS	Metal Oxide Semiconductor
MPC	Micro Program Control
MSI	Medium Scale Integration
MSA	Moving Spin Axis
MTBF	Mean Time Between-Failures
MTU	Multiplex Terminal Unit
MUAR	Mass Unbalance Attitude Readout
MUM	Mass Unbalance Modulation
MUX	Multiplex
MXF	Multiplexer Four
NMOS	Nitride Metal Oxide Semiconductor
NRTS	Not Repairable This Station
OJT	On the Job-Training
ORLA	Optimum Repair Level Analysis
PAM	Pulse Amplitude Modulation

## LIST OF SYMBOLS AND ABBREVIATIONS

PCT	Program Counter and Timer
PCU	Program Control Unit
PDA	Production Design Alternative
PIO	Parallel Input/Output
PPM	Parts Per Million
PSU	Power Supply Unit
PWM	Pulse Width Modulation
QRFG	Quasi-Reference Frequency Generator
RADC	Rome Air Development Center
RAM	Radome Access Memory
RCA	Radio Corporation of America
RGA	Residual Gas Analyzer
RMS	Root-Mean-Square
ROM	Read Only Memory
RSA	Rotor Spin Axis
RSS	Root-Sum Square
RTOK	Retes* OK
RWM	Read/Write Memory
SAMUS	State Space Analysis of Multisensor Systems
SEU	System Electronics Unit
SF	Scale Factor
SIO	Serial Input/Output
SMC	Spin Motor Control
SMPA	Spin Motor Power Amplifier
SOW	Statement of Work
SRU	Shop Replaceable Unit
SSI	Small Scale Integration

## LIST OF SYMBOLS AND ABBREVIATIONS

TA	Table Angle
TASC	The Analytic Sciences Corporation
TD	Torque Disturbance
TM	Technical Memorandum
TRG	Timing Reference Generator
TRGC	Timing Reference Generator Control
T/S	Test Station
TTL	Transistor-Transistor Logic
WBS	Work Breakdown Structure

## I. INTRODUCTION AND SUMMARY

### 1.1 INTRODUCTION

The objective of the MICRON Phase 2A contract was to test the N57A system; to design, fabricate, and integrate two gyro subassemblies; to test gyros; to design, fabricate, and integrate one gyro test station; and to perform analyses, studies, and tradeoffs for use in defining the MICRON System

The design goals of the MICRON IMU are low cost, high reliability, and moderate accuracy. The MICRON IMU will output inertially derived reference data at the proper rate and format to be used for guidance, navigation, weapon delivery, cargo delivery, reconnaissance sensor pointing, and radar stabilization. Typical MICRON applications will include strategic cruise missiles, interceptors, fighter-bombers, transports, close air support aircraft, helicopters, drones, and remotely piloted vehicles. The design goals for the MICRON IMU are a size of 3278 cu cm, a weight of 4.5 kg, and a position error of 1.8 km/hr on each axis.

Under previous Air Force contracts gyro drift rate calibration programs have been developed and performance tests of the gyro and its suspension and MUM pickoff electronics have been performed. A developmental navigation system, designated the N57A, has been designed, fabricated, and tested in the laboratory, in the Air Force Mobile Laboratory, and in the environmental laboratory.

The Phase 2A program began in April 1974 under Contract F33615-74-C-1099. In August 1974, the contract was modified by P00003 to augment Phase 2A with additional tasks and funding. In January 1975 the contract was modified by P00007 which realigned the Phase 2A program to more closely support ACF. The realigned program deleted those tasks not critical to ACF while placing additional emphasis on tasks critical to ACF. In anticipation of the realigned program, tasks not critical to ACF were terminated by a stop work directive in December 1974.

Under the Phase 2A contract the following tasks were performed:

1. Prime Mission Product - IMU, Software, AGE
2. Test and Evaluation
3. Support Equipment
4. Training
5. System Management Engineering
6. Data

This report is arranged according to tasks.

## 1.2 SUMMARY

### 1.2.1 Highlights and Conclusions

Highlights of the technology studies of Phase 2A and the conclusions drawn from these studies are summarized in the following paragraphs.

The flight test results on the N57A-1 and N57A-2 systems demonstrated the capability of the system to meet the position accuracy requirement. The N57A-1 was flight tested in the Sabreliner at LAX and the N57A-2 was flight tested in the Sabreliner at LAX and in the C-141 aircraft and the UH-1 helicopter at HIAFB.

The packaging studies have shown that a housing divided into a temperature controlled (high temperature) and a non-temperature controlled (lower temperature) compartment satisfies the performance requirements and the lower temperature of a large portion of the electronics results in improved INU reliability.

The getter has proven to be capable of handling the internal gas loads in support of eliminating the Vaclon pump from the gyro. Effort remains to determine means for sealing the gyro parts so that external leaks are acceptably low.

A gyro design has evolved which has the thermal characteristics which support fast reaction. The 80% min warm-up rate and time constants of less than 30 sec have been demonstrated.

A gyro design termed "narrow gap" (approximately 225  $\mu$ -in gap) together with its associated electronics has evolved which significantly reduces the cost of gyro suspension electronics.

The MESGA testing has proven this task to be extremely complex and not a viable candidate for system application at this time. In addition to providing a very difficult technical problem the MESGA as presently understood does not result in the cost saving once thought possible, in fact, the MESGA has been shown to be more expensive than the basic gyro and EMA combination.

The four plate gyro has been shown to be a difficult technical problem and also the associated PWM electronics are more expensive than those associated with the basic 8-plate gyro.

The DPU memory tradeoffs have proven that the solid state memory technology will support MICRON requirements. This results in significant cost savings over the plated wire memory in the original MICRON DPU.

Tradeoffs in the development of the system electronics and the DPU I/O have resulted in the digital system I/O being combined with the DPU I/O. This combination results in circuitry which lends itself to the use of a MOS technology with the attendant size reduction and cost reduction.

Parts standardization efforts have resulted in a part type reduction of approximately 20 percent and a total parts count reduction of approximately 30 percent. These reductions resulted in significant cost reductions and reliability improvements.

### 1.2.2 Summary by Statement of Work Tasks

Under Task 1, Prime Mission Product, error analysis models were developed for MESGA acceleration error mechanisms and an error budget was developed for a MICRON instrument configuration including the MESGA multisensor. The error budget establishes allowable MESGA acceleration error characteristics for meeting the MICRON navigational performance requirements. Two IMU design evaluation models were designed to be used for shock, vibration, thermal, and packaging studies. One model was a conduction cooled version and one was a liquid cooled version. Fast reaction heating electronics, temperature controllers, and temperature monitors for the design evaluation models were designed, fabricated, and tested. A specification for the gyro test station was developed and one gyro test station was designed, fabricated, and integrated. This station approximates potential MICRON product assurance test equipment by including automatic polhode damping, failure recording, self-contained calibration, and automatic startup and shutdown. Software for in-motion polhode damping was programmed in the D-216 computer and demonstrated on the N57A-1 system. Software for data sampling and processing on the GSA test station was developed and operated satisfactorily.

Under Task 2, Test and Evaluation, test plans were developed for gyros, gyro subassemblies, design evaluation models, N57A-1, and the HAFB GSA. EMI and grounding test plans were also developed. System reliability screen, Scorsby, and heading sensitivity tests were conducted on the N57A-2. Test Station IV was in continuous use in test and evaluation of MESG units in support of N57A-1, N57A-2, and the HAFB gyro subassembly. Developmental tests were also performed both at the system and gyro level including evaluation of fast reaction, self calibration, low speed damping, Inconel X/Paliny pin vacuum enclosure, getter gyro, narrow electrode separation groove, and small gap gyro. Thermal analyses and tests on the design evaluation models were initiated. The N57A-1 was used to demonstrate in-motion polhode damping. Eight-plate GSA testing was performed and the results are discussed in Para 3.2.5.1. All second source rotor and cavity critical parameters were tested at the component level and two complete sets were evaluated in the assembled instrument configuration. Second source master tooling parts were also evaluated. Flight testing of the N57A-1 and N57A-2 was conducted at LAX. Seven N57A-1 flights and five N57A-2 flights were completed. Post flight analysis was performed including statistical characterization of position error rates and velocity errors. The computed CEP rates were 1.09 nm/hr on N57A-1 flights and 0.42 nm/hr on N57A-2 flights compared to the goal for MICRON of 1 nm/hr.

Under Task 3, Support Equipment, a CI development specification was developed for the Gyro Subassembly. Two gyro subassemblies (an 8-plate and 4-plate) were designed, fabricated, and integrated. Spares for these gyro subassemblies were also fabricated and tested. One subassembly was used for MESGA development testing and one was used for 4-plate gyro and electronics development. A definition of a baseline MICRON system which would be integrable with other avionics and a definition of a MICRON system which would be operated in a stand-alone configuration were initiated. Hardware fabricated in Phase 1B and Phase 2A was maintained and repaired as required. The N57A-1 was refurbished to the N57A-2 configuration including D-216 controlled automatic start-up and polhode damping.

Under Task 4, Training, an Operation Instruction Manual, interface drawings, and a Training Plan were prepared in support of the N57A-2 flight test program at Holloman AFB. Phase 1B and Phase 2A hardware was used to support training as set forth in the Training Plan. Engineering services were furnished in support of the LAX flight testing of the N57A-1 and N57A-2. Support to HAFB gyro subassembly testing was provided including on-site support, consultation, and data analysis. The N57A-2 was installed in the laboratory at HAFB and HAFB personnel were instructed how to operate the equipment. Support was provided during N57A-2 flight testing and laboratory testing at HAFB. Fourteen C-141 flights and 10 UH-1 helicopter flights were completed. Results of these flight tests are discussed in Para 5.3.4. Preparations were made for RF-4C flight testing of the N57A-2 including performance of 24 Nav verification runs and a fit check in the RF-4C.

Under Task 5.1, Program Management, 10 informal design reviews and a System Requirements Review were conducted at Autonetics. The System Design Review will be held in October 1975. Program plans, including a system engineering management plan, personnel, marketing, financial, facilities, and contract data management plans, were developed and modified as necessary. A contract work breakdown structure was also developed. Grounding and EMI guidelines were developed and documented. Engineering support was provided to second source for rotors and cavities. Documentation relative to second source is reported in Para 6.1.5. The MESA angle readout model was documented and submitted to AFAL.

Under Task 5.2, Cost of Ownership, producibility, reliability, and maintainability trade-offs were made and the results incorporated into the final Phase 2A configuration. Included in this configuration were the results of design improvements E-1 through E-3 which were aimed at circuit simplification, elimination of high cost parts and processes, and partitioning to meet maintainability and producibility requirements. This configuration also included modification of the A/D converter, spin motor, and temperature control electronic circuits. The interface between the DPU and SEU was redesigned into MOS circuits for simplicity and decreased costs. Three EMA's were incorporated into the system as a result of the MESA/EMA trade-off which showed a favorable cost reduction in favor of the EMA's. A repair/discard criteria was established for the hybrid electronic packages. Military specifications discourage the repair of sealed hybrid packages, therefore a cost effective discard concept was desired. This final configuration meets this desired criteria.

Significant progress was made in several categories during Phase 2A. The recurring acquisition price showed a steady improvement from \$64,778 to \$54,011, especially considering that the baseline configuration did not have a workable acceleration sensing mechanization. The life cycle cost also improved due in part to the acquisition price and maintenance concept. The decrease in the average price per hybrid module made the discard maintenance concept feasible which acted to drive the life cycle cost down. The average parts per module and the average active parts per module decreased due to simplifications and partitioning changes. This in turn made the system more producible and acted to lower the acquisition price. Several other areas have been identified that will further decrease the acquisition and life cycle costs. These include further simplifications in the charge amplifiers, more application of MOS technology, make or buy considerations, and continued activity on elimination of high cost parts and processes.

In support of the cost of ownership task, parts standardization, alternate parts, and alternate part technology trade-offs were continuously undertaken during Phase 2A. Standardized specification formats were developed which will expedite final specification release. Beam lead device development and beam lead carrier development programs were conducted during Phase 2A. A contract for the development of a high performance operational amplifier was placed with RCA and parts delivery is expected early in Phase 2B. The development of four new MOS devices was initiated to simplify the IMU/DPU electronics. The design implemented represented a savings of 14 MOS devices over the original design. Development of an improved MOS A/D converter and a MOS circuit for the spin motor control was also initiated to significantly reduce cost and complexity of the electronics.

Under Task 5.3, System Engineering, an 8-plate MESGA multisensor and a 4-plate MESG were developed and means were investigated to eliminate the VacIon pump. MESG/MESGA design alternatives were investigated to update the instrument design as required to assure adequacy of the MESG to perform in the MICRON system environment. Alternatives studied pertained to fast reaction, 180°F rotor operational temperature, brazing process to fabricate the Pump and Housing Assembly, and cavity plating. Mechanization and modeling improvements were made including angle calibration optimization and drift model improvement.

After early Phase 2A analyses and tests showed that MESGA was orders of magnitude away from required performance, MESGA development effort continued on the GSA and GSA test station. The test data obtained on the GSA and GSA test station were between two and three orders of magnitude worse than the acceleration sensing requirements. It is concluded that the work on the GSA and GSA test station has not brought MESGA within the realm of the practicable.

MICRON external cooling alternative studies determined that the only reasonable external cooling concept is by forced convection by vehicle supplied coolant. Seven MICRON internal package design alternatives were created and subjected to cost-of-ownership studies of Task 5.2 to identify cost sensitivities of the various design features.

DPU design trade-offs were conducted with the objectives of reducing recurring costs, size, and power. A semiconductor memory was configured in lieu of plated wire memory. EAROM devices were evaluated and characterized. A simplified DPU/SEU interface was defined and portions of the SEU electronics were studied and remechanized to reduce total parts and part types used. Alternate methods of packaging the DPU were examined.

In simplifying the gyro electronics, designs have been developed for the suspension and MUM electronics which reduce the number of parts and eliminate high cost parts. In simplifying the gyro mechanical design, the principal areas of effort have been the small gap gyro, 1/2-impedance motor, potential new MESG configurations, dual instrument on a single base, and replacement of gold o-ring seals. Trade-off studies were initiated for the power supplies and definitions of a hybrid version and an all discrete version were completed. The input/output design alternatives task consisted of trade-off studies directed toward obtaining the lowest cost digital/synchro converters and linear DAC.



Under Subtask 5.4, Application Engineering, four trips were made in which more than 20 companies or agencies were visited representing over 30 different programs. The purpose of these trips was to inform the various audiences of the MICRON Program status and plans and to solicit feedback information from the various programs regarding their program objectives and requirements related to a navigation system for their application.

Under Task 6, Data, 72 Phase 2A data items were submitted on schedule through 1 September 1975. A schedule of all CDRL data items is given in Section 7.

A complete schedule of the major milestones of the Phase 2A program by task is given in Section 8.

## 2. TASK 1, PRIME MISSION PRODUCT

### 2.1 INERTIAL MEASURING UNIT (IMU)

In Task 1.1, IMU, Autonetics (1) conducted an error analysis and developed an error budget for the MICRON IMU, (2) designed, fabricated and integrated IMU design evaluation models and (3) investigated several design alternatives. The error analysis was performed to derive error models and performance sensitivities to different time constants during alignment and fast reaction. The design of the design evaluation models was such that they could be used for shock, vibration, thermal and packaging studies. Several design alternatives were investigated; these included liquid cooling of the instruments and electronics, ambient air as the only cooling and use of cooling air as specified in the design goals. Each of the above areas is discussed in detail in the following sections.

#### 2.1.1 Error Analysis/Error Budget

The MICRON version of the SAMUS error analysis computer program was reconstructed from FORTRAN and Assembly Language source decks, and was made operational. It was used to analyze MICRON performance along a specific flight path originating at Holloman AFB. The particular flight path selected was INS Route No. 6 from Holloman AFB to Miramar Naval Air Station to Bakersfield. To allow a longer navigation period, this profile was extended to Sacramento, then back to Holloman. Table 2-1 lists the flight segments used to simulate the profile.

Table 2-1. Segments Approximating INS Route No. 6

Segment Segment	Duration (Sec)	Heading (Deg)	Velocity (fps)	Destination
1	336	0	0	(Alignment, Holloman AFB)
2	60	165	220	(Enter Nav, Takeoff)
3	600	220	400	Las Cruces, New Mexico
4	1800	267	735	Tucson, Arizona
5	900	300	735	Gila Bend, Arizona
6	1800	269	735	Miramar NAS, California
7	3300	329	735	Sacramento, California
8	6900	33	735	Holloman AFB

The SAMUS error analysis computer program was used to analyze MICRON performance using budgeted MESGA error sources in place of accelerometer error sources. Budgeted MESGA error sources are the performance goals and do not correspond to MESGA test data reported elsewhere in this report.

As anticipated, the system performance with budgeted MESGA errors is nearly the same as that with accelerometers. Only a slight degradation occurs. Table 2-2 provides the error budget, the individual error contributions, and the resulting total system error upon return to Holloman AFB. The error budget is broken down into five major groups: MESG drift rate, MESG angle read out, MESGA acceleration, miscellaneous, and initial conditions. Individual error sources are listed under these headings together with their contribution to navigation errors. Total navigation errors due to all error sources within each of the major blocks is also listed.

Plots of position CEP and velocity error are shown in Figures 2-1 and 2-2, respectively. Performance measures were computed at 3 and 4 hours after alignment, as follows:

$$\text{Least-Squares CEP Rate} = \begin{cases} .85 \text{ nm/hr over 3 hours} \\ .80 \text{ nm/hr over 4 hours} \end{cases}$$

$$\text{Time - RMS Velocity Error} = \begin{cases} 7.37 \text{ fps over 3 hours} \\ 7.82 \text{ fps over 4 hours} \end{cases}$$

Also, some minor changes were made in output format for error budget tabulation, and the SAMUS program deck setups were documented and filed. A planned update of the MESGA acceleration error budget, based upon test results, was not completed due to unavailability of data in time to complete the update.

## 2.1.2 Design Evaluation Models

The task defined for Design Evaluation Models (DEM) consisted of two housing versions -- a conduction cooled model and a liquid cooled model depicted in Figure 2-3 and 2-4 respectively.

The conduction cooled model was defined as the basic design evaluation model configuration. For this DEM, two alternate module configurations were considered; one with wedge clamps and one with a simpler bolted flange joint. Both module configurations featured self-aligning connectors while providing positive mechanical retention with low thermal resistance. Figure 2-5 compares the thermal conductance for the two configurations.

A potential requirement for a cooling air control valve design for the ultimate MICRON IMU was identified to be compatible with the specified cooling air supply. This condition did not impact the design evaluation model per se since it was planned to control the test air flow by external means so the model did not need a valve. Analytical studies were made which showed the need for precise air flow control to avoid excessive heater power consumption. Based on these studies, heater control requirements were defined. A requirement for six proportional control and two on off control channels was specified for the test model. It was expected that test results would indicate whether fewer or more channels will be required in the ultimate MICRON.

The MESGA/charge amp assembly was suspended by a c.g. shock mount configuration rather than with focalized shock mounts to minimize the introduction of rotational modes into the suspended assembly. However this approach required the use of all-attitude shock mounts and required more volume.

Table 2-2. Budgeted Error Sources and Tabulated Errors at 256 Minutes.  
MESGA Errors Included - Holloman INS Route No. 6 (Sheet 1 of 7)

SOURCE SOURCE	MAGNITUDE MPS/AXIS	CORRELATION	POSITION EAST	POSITION NORTH	TIME 256.00 MIN CUMULATIVE EAST	TIME 256.00 MIN CUMULATIVE NORTH	TILT EAST	TILT NORTH	TILT EAST	TILT NORTH	POSITION VELOCITY EAST	POSITION VELOCITY NORTH	POSITION VELOCITY EAST	POSITION VELOCITY NORTH
MESG DRIFT RATE														
SPHERICAL - SPHERICAL														
MESG 1 AXIS 1	0.00500 D/M		5701.3	4252.4	1.23	0.63	38.2	0.2	0.6	0.2	0.0	0.0	0.0	0.0
MESG 2 AXIS 1	0.00500 D/M		2727.0	555.9	0.28	0.06	0.0	0.0	0.0	0.0	0.0	0.0	0.0	0.0
MESG 3 AXIS 1	0.00500 D/M		2610.1	012.7	0.15	0.04	0.0	0.0	0.0	0.0	0.0	0.0	0.0	0.0
MESG 4 AXIS 1	0.00500 D/M		4155.0	1007.7	0.51	0.15	0.0	0.0	0.0	0.0	0.0	0.0	0.0	0.0
SPHERICAL - SPHERICAL														
MESG 1 AXIS 1	0.00500 D/M		4267.7	2306.3	0.78	0.07	0.0	0.0	0.0	0.0	0.0	0.0	0.0	0.0
MESG 2 AXIS 1	0.00500 D/M		342.7	106.7	0.04	0.01	0.0	0.0	0.0	0.0	0.0	0.0	0.0	0.0
MESG 3 AXIS 1	0.00500 D/M		330.5	205.1	0.07	0.11	0.3	0.1	0.2	0.2	0.0	0.0	0.0	0.0
MESG 4 AXIS 1	0.00500 D/M		2261.2	341.2	0.17	0.05	0.0	0.0	0.0	0.0	0.0	0.0	0.0	0.0
MESG 5 AXIS 1	0.00500 D/M		1495.3	506.9	0.25	0.07	0.0	0.0	0.0	0.0	0.0	0.0	0.0	0.0
MESG 6 AXIS 1	0.00500 D/M		126.2	074.9	0.29	0.07	0.0	0.0	0.0	0.0	0.0	0.0	0.0	0.0
SPHERICAL - SPHERICAL														
MESG 1 AXIS 1	0.00500 D/M		4141.6	2367.0	0.70	0.63	38.2	0.2	0.6	0.2	0.0	0.0	0.0	0.0
MESG 2 AXIS 1	0.00500 D/M		321.9	106.7	0.04	0.01	0.0	0.0	0.0	0.0	0.0	0.0	0.0	0.0
MESG 3 AXIS 1	0.00500 D/M		330.5	205.1	0.07	0.11	0.3	0.1	0.2	0.2	0.0	0.0	0.0	0.0
MESG 4 AXIS 1	0.00500 D/M		1562.6	78.0	0.01	0.06	0.0	0.0	0.0	0.0	0.0	0.0	0.0	0.0
MESG 5 AXIS 1	0.00500 D/M		1504.4	216.9	0.02	0.06	0.0	0.0	0.0	0.0	0.0	0.0	0.0	0.0
MESG 6 AXIS 1	0.00500 D/M		1400.4	176.7	0.01	0.10	0.0	0.0	0.0	0.0	0.0	0.0	0.0	0.0
SPHERICAL - SPHERICAL														
MESG 1 AXIS 1	0.00500 D/M		1000.0	630.7	0.07	0.03	19.3	1.0	0.8	0.1	0.0	0.0	0.0	0.0
MESG 2 AXIS 1	0.00500 D/M		398.4	0.0	0.11	0.06	0.0	0.0	0.0	0.0	0.0	0.0	0.0	0.0
MESG 3 AXIS 1	0.00500 D/M		675.2	123.6	0.10	0.02	11.3	0.5	0.8	0.2	0.0	0.0	0.0	0.0
MESG 4 AXIS 1	0.00500 D/M		887.1	280.0	0.15	0.04	15.0	0.1	0.7	0.0	0.0	0.0	0.0	0.0
MESG 5 AXIS 1	0.00500 D/M		377.3	172.4	0.10	0.01	7.9	0.0	0.8	0.0	0.0	0.0	0.0	0.0
SPHERICAL - SPHERICAL														
MESG 1 AXIS 1	0.01000 D/M		462.4	54.9	0.00	0.04	1.9	0.1	0.2	0.1	0.0	0.0	0.0	0.0
MESG 2 AXIS 1	0.01000 D/M		1006.7	5.4	0.00	0.00	1.2	0.0	0.1	0.0	0.0	0.0	0.0	0.0

Table 2-2. (Cont) (Sheet 2 of 7)

BEAD-ANALYSIS, EMM SOURCE									
TIME = 250.00 MIN									
EMM SOURCE	MAGNITUDE MAG/AXIS	CORRELATION TIME SEC	POSITION NORTH EAST	CUMULATIVE NORTH EAST	VEL NORTH EAST	DEL NORTH EAST	AZIMUTH DEG	TILT IN	POSITION VELOCITY X IN Y IN
*****									
MISC DRIFT RATE									
AXIAL-BIAS-UNBALANCE									
MISC 1	0.00700 0.00700		724.0	449.0	0.15	0.01	8.3	0.0	0.0
MISC 2	0.00600 0.00400		724.0	449.0	0.15	0.01	8.3	0.0	0.0
RANDOM-BIAS-BUILDING-EFFECT									
MISC 1 AND 2	0.00300 0.00400	0.00	1405.0	1406.1	0.94	0.92	12.5	7.0	2.0
MANUALLY-SET RATE									
MISC 1	0.00300 0.00700	1400	1514.2	2352.0	0.99	0.90	0.2	0.2	0.0
MISC 2	0.00300 0.00700	1400	1514.2	2352.0	0.99	0.90	0.2	0.2	0.0
*****									
DRIFT-ONLY-SUM-TOTAL									
			12270.5	6084.0	2.51	2.00	150.0	14.5	4.4
*****									
MISC ANGLE HEAD-101									
SEVERAL-BEAM-NO.									
MISC 1 AXIS X-Y	1.000 MHA0	0	2400.2	1071.5	1.24	1.37	17.4	10.9	2.9
MISC 2 AXIS X-Y	1.000 MHA0	0	1536.0	765.5	0.82	0.70	11.8	6.1	4.0
MISC 1 AXIS Z-Y	1.000 MHA0	0	74.6	221.1	0.08	0.05	0.1	0.1	0.1
MISC 2 AXIS Z-Y	1.000 MHA0	0	211.7	38.4	0.24	0.15	0.6	0.5	0.5
MISC 1 AXIS X-Z	1.000 MHA0	0	1458.4	913.0	0.73	0.68	11.4	5.3	2.8
MISC 2 AXIS X-Z	1.000 MHA0	0	737.6	381.2	0.47	0.40	5.3	2.1	1.0
MISC 1 AXIS Y-Z	1.000 MHA0	0	110.2	187.9	0.14	0.10	0.0	0.3	0.0
MISC 2 AXIS Y-Z	1.000 MHA0	0	52.0	119.1	0.10	0.15	0.0	1.5	1.1
MISC 1 AXIS X-Y	1.000 MHA0	0	135.2	94.1	0.14	0.10	0.0	1.2	0.8
MISC 2 AXIS X-Y	1.000 MHA0	0	235.3	21.6	0.14	0.10	0.0	1.2	0.8
MISC 1 AXIS X-Z	1.000 MHA0	0	1080.4	634.3	0.70	0.68	8.9	7.9	2.0
MISC 2 AXIS X-Z	1.000 MHA0	0	591.4	259.1	0.42	0.42	4.4	5.1	0.6
MISC 1 AXIS Y-Z	1.000 MHA0	0	10.1	10.1	0.07	0.04	0.0	0.5	1.1
MISC 2 AXIS Y-Z	1.000 MHA0	0	10.1	10.1	0.07	0.04	0.0	0.5	1.1

Table 2-2. (Cont) (Sheet 3 of 7)

EARTH SURFACE	WATER SURFACE	COMPLAINT POSITION	POSITION	TIME	VEL	TIME 2 270-00 MIN		TILT	TILT	POSITION	VELOCITY
						PSI	ZN	IN	YN	ZN	ZN
MSG ANGLE HEAD-OUT											
MSG 2 SIN AXIS 2	0.042 mmi	110.2	210.2	0.04	0.10	0.0	0.0	2.4	1.1	0.4	0.0
MSG 2 SIN AXIS 3	0.042 mmi	21.2	210.2	0.07	0.14	0.0	0.0	2.3	0.2	0.5	0.0
MSG 2 COS AXIS 2	0.042 mmi	461.3	210.2	0.25	0.17	0.1	0.1	0.6	2.5	0.1	0.0
MSG 2 COS AXIS 3	0.042 mmi	107.2	122.4	0.05	0.06	0.5	0.5	0.4	0.5	0.2	0.0
MSG 2 COS AXIS 3	0.042 mmi	3.7	130.5	0.16	0.05	0.0	0.0	0.4	0.5	0.1	0.0
SCALE 2 (100-1000)											
MSG 1 AXIS 2	0.00010 PIS/PI	39.2	102.1	1.00	0.07	0.0	0.0	0.4	1.3	1.7	0.0
MSG 1 AXIS 3	0.00010 PIS/PI	430.6	120.6	0.73	0.07	1.0	1.0	0.5	5.9	1.5	0.0
MSG 2 AXIS 2	0.00010 PIS/PI	100.2	100.2	0.25	0.26	1.4	1.4	2.6	1.0	2.2	0.0
MSG 2 AXIS 3	0.00010 PIS/PI	70.4	100.2	0.43	0.16	0.6	0.6	0.7	0.1	0.5	0.0
MSG 2 AXIS 3	0.00010 PIS/PI	91.6	101.9	0.10	0.10	2.0	2.0	3.3	1.0	0.5	0.0
SCALE 2 (100-1000)											
MSG 1 AXIS 1-1	2.1 mm	14.7	70.3	0.11	0.01	0.0	0.0	1.0	0.2	0.0	0.0
MSG 1 AXIS 1-2	2.1 mm	110.0	19.0	0.05	0.12	0.1	0.1	0.5	1.2	0.1	0.0
MSG 1 AXIS 1-3	2.1 mm	103.5	51.3	0.05	0.12	0.0	0.0	0.7	0.1	0.2	0.0
MSG 1 AXIS 2-1	2.1 mm	92.4	11.2	0.08	0.01	0.1	0.1	1.1	0.3	0.0	0.0
MSG 1 AXIS 2-2	2.1 mm	42.5	132.5	0.03	0.07	0.2	0.2	0.7	0.7	0.2	0.0
MSG 1 AXIS 2-3	2.1 mm	13.5	72.1	0.05	0.09	0.0	0.0	0.3	0.0	0.1	0.0
MSG 2 AXIS 1-1	2.1 mm	21.1	17.4	0.11	0.02	0.1	0.1	0.2	0.0	0.1	0.0
MSG 2 AXIS 1-2	2.1 mm	21.1	17.4	0.03	0.03	0.0	0.0	0.3	0.1	0.0	0.0
MSG 2 AXIS 1-3	2.1 mm	3.2	17.6	0.03	0.03	0.0	0.0	0.3	0.1	0.1	0.0
MSG 2 AXIS 2-1	2.1 mm	7.9	1.1	0.05	0.02	0.1	0.1	0.3	0.1	0.0	0.0
MSG 2 AXIS 2-2	2.1 mm	10.1	15.9	0.01	0.01	0.0	0.0	0.4	0.1	0.0	0.0
MSG 2 AXIS 2-3	2.1 mm	130.0	160.6	0.35	1.39	4.6	4.6	13.2	3.2	3.7	0.1
MSG 1 IN 100-1000	0.00100 PIS/PI	152.4	3	30.0	1.39	0.35	0.35	1.3	1.5	0.2	0.0
MSG 2 IN 100-1000	0.00100 PIS/PI	210.2	250.5	0.36	0.36	0.0	0.0	1.0	1.2	0.2	0.0
MSG 2 IN 100-1000	0.00100 PIS/PI	315.1	24.7	0.24	0.24	2.1	2.1	1.6	1.2	0.2	0.0
MSG 2 QUADANTUM	0.00100 PIS/PI										

Table 2-2. (Cont) (Sheet 1 of 7)

[illegible]





Table 2-2. (Cont) (Sheet 6 of 7)

SHIP SOURCE	ACQUISITION	MEASUREMENT	COMPARISON	POSITION				TIME 250.00 MIN				TILT				POSITION VELOCITY			
				North	East	Down	Alt	North	East	Down	Alt	IN	EN	DN	UP	IN	EN	DN	UP
MESG ACCELERATION				75	1174.9	531.1	0.07	0.05				0.5				0.1			0.0
SCALE FACT X-AXIS		26.0 ppm		75	1301.4	134.6	0.06	0.00				0.5				0.1			0.0
SCALE FACT Y-AXIS		26.0 ppm		75	1301.4	134.6	0.06	0.00				0.5				0.1			0.0
SCALE FACT Z-AXIS		26.0 ppm		75	1301.4	134.6	0.06	0.00				0.5				0.1			0.0
QUANTILE DIFFERENCES																			
MESG X-AXIS		10.00 uin			224.5	208.2	0.05	0.01				1.1				0.2			0.0
MESG Y-AXIS		10.00 uin			205.3	181.5	0.05	0.01				1.1				0.2			0.0
MESG Z-AXIS		10.00 uin			205.3	181.5	0.05	0.01				1.1				0.2			0.0
SCALE FACT X-AXIS		26.0 ppm			205.3	181.5	0.05	0.01				1.1				0.2			0.0
SCALE FACT Y-AXIS		26.0 ppm			205.3	181.5	0.05	0.01				1.1				0.2			0.0
SCALE FACT Z-AXIS		26.0 ppm			205.3	181.5	0.05	0.01				1.1				0.2			0.0
ANGLE MEASUREMENTS																			
MESG 1 ABOUT 2		10.00 S/C			96.7	303.3	0.05	0.03				0.7				1.0			0.1
MESG 2 ABOUT 3		10.00 S/C			96.7	303.3	0.05	0.03				0.7				1.0			0.1
MESG 3 ABOUT 4		10.00 S/C			96.7	303.3	0.05	0.03				0.7				1.0			0.1
MESG 4 ABOUT 5		10.00 S/C			96.7	303.3	0.05	0.03				0.7				1.0			0.1
MESG 5 ABOUT 6		10.00 S/C			96.7	303.3	0.05	0.03				0.7				1.0			0.1
MESG 6 ABOUT 7		10.00 S/C			96.7	303.3	0.05	0.03				0.7				1.0			0.1
MESG 7 ABOUT 8		10.00 S/C			96.7	303.3	0.05	0.03				0.7				1.0			0.1
MESG 8 ABOUT 9		10.00 S/C			96.7	303.3	0.05	0.03				0.7				1.0			0.1
MESG 9 ABOUT 10		10.00 S/C			96.7	303.3	0.05	0.03				0.7				1.0			0.1
MESG 10 ABOUT 11		10.00 S/C			96.7	303.3	0.05	0.03				0.7				1.0			0.1
MESG 11 ABOUT 12		10.00 S/C			96.7	303.3	0.05	0.03				0.7				1.0			0.1
MESG 12 ABOUT 13		10.00 S/C			96.7	303.3	0.05	0.03				0.7				1.0			0.1
MESG 13 ABOUT 14		10.00 S/C			96.7	303.3	0.05	0.03				0.7				1.0			0.1
MESG 14 ABOUT 15		10.00 S/C			96.7	303.3	0.05	0.03				0.7				1.0			0.1
MESG 15 ABOUT 16		10.00 S/C			96.7	303.3	0.05	0.03				0.7				1.0			0.1
MESG 16 ABOUT 17		10.00 S/C			96.7	303.3	0.05	0.03				0.7				1.0			0.1
MESG 17 ABOUT 18		10.00 S/C			96.7	303.3	0.05	0.03				0.7				1.0			0.1
MESG 18 ABOUT 19		10.00 S/C			96.7	303.3	0.05	0.03				0.7				1.0			0.1
MESG 19 ABOUT 20		10.00 S/C			96.7	303.3	0.05	0.03				0.7				1.0			0.1
MESG 20 ABOUT 21		10.00 S/C			96.7	303.3	0.05	0.03				0.7				1.0			0.1
MESG 21 ABOUT 22		10.00 S/C			96.7	303.3	0.05	0.03				0.7				1.0			0.1
MESG 22 ABOUT 23		10.00 S/C			96.7	303.3	0.05	0.03				0.7				1.0			0.1
MESG 23 ABOUT 24		10.00 S/C			96.7	303.3	0.05	0.03				0.7				1.0			0.1
MESG 24 ABOUT 25		10.00 S/C			96.7	303.3	0.05	0.03				0.7				1.0			0.1
MESG 25 ABOUT 26		10.00 S/C			96.7	303.3	0.05	0.03				0.7				1.0			0.1
MESG 26 ABOUT 27		10.00 S/C			96.7	303.3	0.05	0.03				0.7				1.0			0.1
MESG 27 ABOUT 28		10.00 S/C			96.7	303.3	0.05	0.03				0.7				1.0			0.1
MESG 28 ABOUT 29		10.00 S/C			96.7	303.3	0.05	0.03				0.7				1.0			0.1
MESG 29 ABOUT 30		10.00 S/C			96.7	303.3	0.05	0.03				0.7				1.0			0.1
MESG 30 ABOUT 31		10.00 S/C			96.7	303.3	0.05	0.03				0.7				1.0			0.1
MESG 31 ABOUT 32		10.00 S/C			96.7	303.3	0.05	0.03				0.7				1.0			0.1
MESG 32 ABOUT 33		10.00 S/C			96.7	303.3	0.05	0.03				0.7				1.0			0.1
MESG 33 ABOUT 34		10.00 S/C			96.7	303.3	0.05	0.03				0.7				1.0			0.1
MESG 34 ABOUT 35		10.00 S/C			96.7	303.3	0.05	0.03				0.7				1.0			0.1
MESG 35 ABOUT 36		10.00 S/C			96.7	303.3	0.05	0.03				0.7				1.0			0.1
MESG 36 ABOUT 37		10.00 S/C			96.7	303.3	0.05	0.03				0.7				1.0			0.1
MESG 37 ABOUT 38		10.00 S/C			96.7	303.3	0.05	0.03				0.7				1.0			0.1
MESG 38 ABOUT 39		10.00 S/C			96.7	303.3	0.05	0.03				0.7				1.0			0.1
MESG 39 ABOUT 40		10.00 S/C			96.7	303.3	0.05	0.03				0.7				1.0			0.1
MESG 40 ABOUT 41		10.00 S/C			96.7	303.3	0.05	0.03				0.7				1.0			0.1
MESG 41 ABOUT 42		10.00 S/C			96.7	303.3	0.05	0.03				0.7				1.0			0.1
MESG 42 ABOUT 43		10.00 S/C			96.7	303.3	0.05	0.03				0.7				1.0			0.1
MESG 43 ABOUT 44		10.00 S/C			96.7	303.3	0.05	0.03				0.7				1.0			0.1
MESG 44 ABOUT 45		10.00 S/C			96.7	303.3	0.05	0.03				0.7				1.0			0.1
MESG 45 ABOUT 46		10.00 S/C			96.7	303.3	0.05	0.03				0.7				1.0			0.1
MESG 46 ABOUT 47		10.00 S/C			96.7	303.3	0.05	0.03				0.7				1.0			0.1
MESG 47 ABOUT 48		10.00 S/C			96.7	303.3	0.05	0.03				0.7				1.0			0.1
MESG 48 ABOUT 49		10.00 S/C			96.7	303.3	0.05	0.03				0.7				1.0			0.1
MESG 49 ABOUT 50		10.00 S/C			96.7	303.3	0.05	0.03				0.7				1.0			0.1
MESG 50 ABOUT 51		10.00 S/C			96.7	303.3	0.05	0.03				0.7				1.0			0.1
MESG 51 ABOUT 52		10.00 S/C			96.7	303.3	0.05	0.03				0.7				1.0			0.1
MESG 52 ABOUT 53		10.00 S/C			96.7	303.3	0.05	0.03				0.7				1.0			0.1
MESG 53 ABOUT 54		10.00 S/C			96.7	303.3	0.05	0.03				0.7				1.0			0.1
MESG 54 ABOUT 55		10.00 S/C			96.7	303.3	0.05	0.03				0.7				1.0			0.1
MESG 55 ABOUT 56		10.00 S/C			96.7	303.3	0.05	0.03				0.7				1.0			0.1
MESG 56 ABOUT 57		10.00 S/C			96.7	303.3	0.05	0.03				0.7				1.0			0.1
MESG 57 ABOUT 58		10.00 S/C			96.7	303.3	0.05	0.03				0.7				1.0			0.1
MESG 58 ABOUT 59		10.00 S/C			96.7	303.3	0.05	0.03				0.7				1.0			0.1
MESG 59 ABOUT 60		10.00 S/C			96.7	303.3	0.05	0.03				0.7				1.0			0.1
MESG 60 ABOUT 61		10.00 S/C			96.7	303.3	0.05	0.03				0.7				1.0			0.1
MESG 61 ABOUT 62		10.00 S/C			96.7	303.3	0.05	0.03				0.7				1.0			0.1
MESG 62 ABOUT 63		10.00 S/C			96.7	303.3	0.05	0.03				0.7				1.0			0.1
MESG 63 ABOUT 64		10.00 S/C			96.7	303.3	0.05	0.03				0.7				1.0			0.1
MESG 64 ABOUT 65		10.00 S/C			96.7	303.3	0.05	0.03				0.7				1.0			0.1
MESG 65 ABOUT 66		10.00 S/C			96.7	303.3	0.05	0.03				0.7				1.0			0.1
MESG 66 ABOUT 67		10.00 S/C			96.7	303.3	0.05	0.03				0.7				1.0			0.1
MESG 67 ABOUT 68		10.00 S/C			96.7	303.3	0.05	0.03				0.7				1.0			0.1
MESG 68 ABOUT 69		10.00 S/C			96.7	303.3	0.05	0.03				0.7				1.0			0.1
MESG 69 ABOUT 70		10.00 S/C			96.7	303.3	0.05	0.03				0.7				1.0			0.1
MESG 70 ABOUT 71		10.00 S/C			96.7	303.3	0.05	0.03				0.7				1.0			0.1
MESG 71 ABOUT 72		10.00 S/C			96.7	303.3	0.05	0.03				0.7				1.0			0.1
MESG 72 ABOUT 73		10.00 S/C			96.7	303.3	0.05	0.03				0.7				1.0			0.1
MESG 73 ABOUT 74		10.00 S/C			96.7	303.3	0.05	0.03				0.7				1.0			0.1
MESG 74 ABOUT 75		10.00 S/C			96.7	303.3	0.05	0.03				0.7				1.0			0.1
MESG 75 ABOUT 76		10.00 S/C			96.7	303.3	0.05	0.03				0.7				1.0			0.1
MESG 76 ABOUT 77		10.00 S/C			96.7	303.3	0.05	0.03				0.7				1.0			0.1

Table 2-2. (Cont) (Sheet 7 of 7)

[illegible]

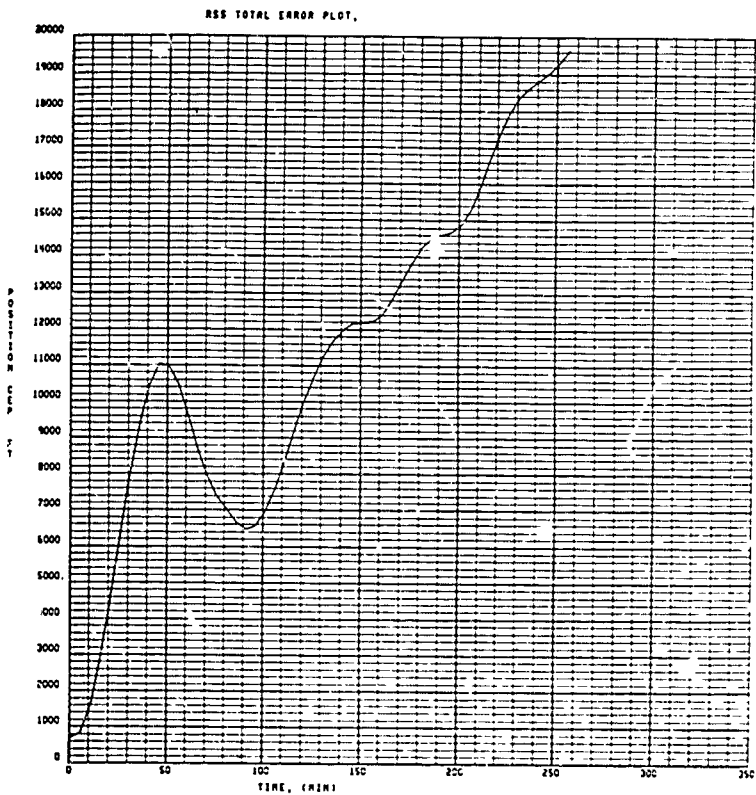


Figure 2-1. Position CEP vs Time

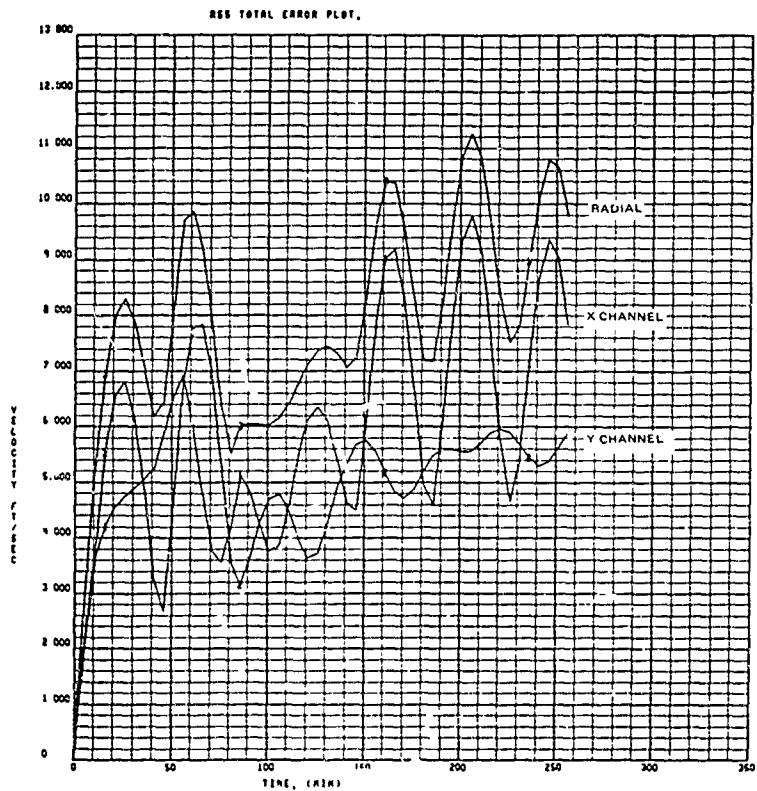
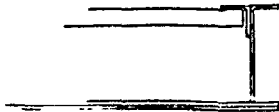
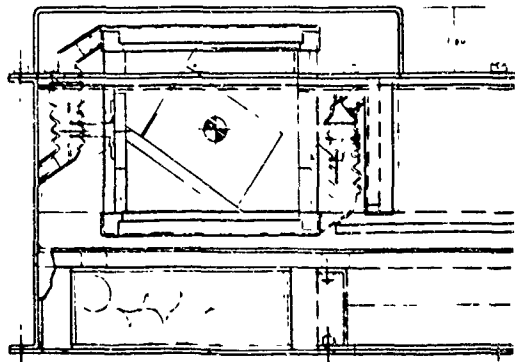
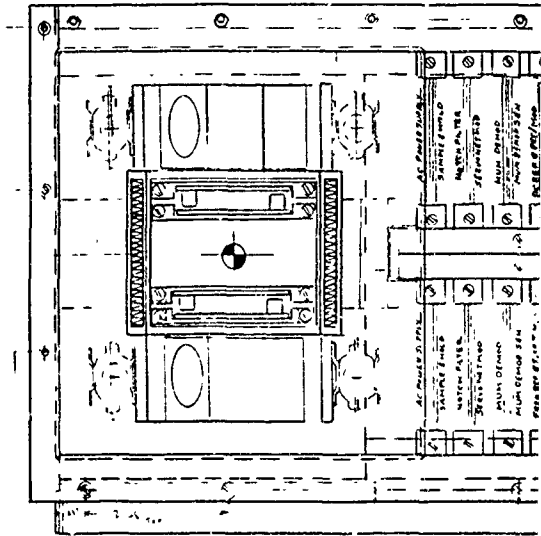


Figure 2-2. North, East, and Radial Velocity Error vs Time





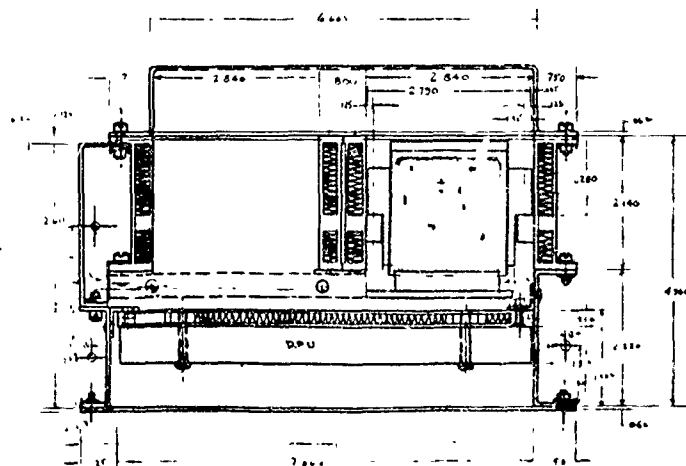
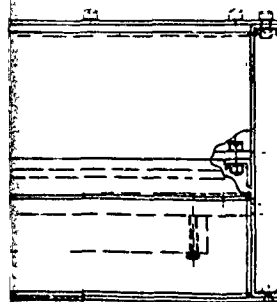
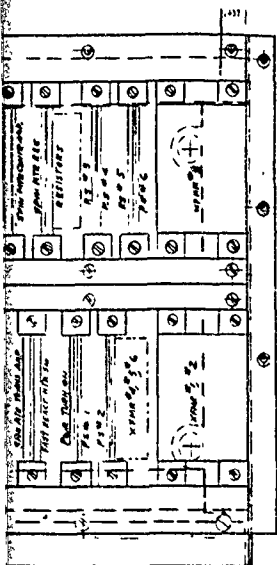


Figure 2-3. Conduction Cooled Design Evaluation Model.

Preceding page blank







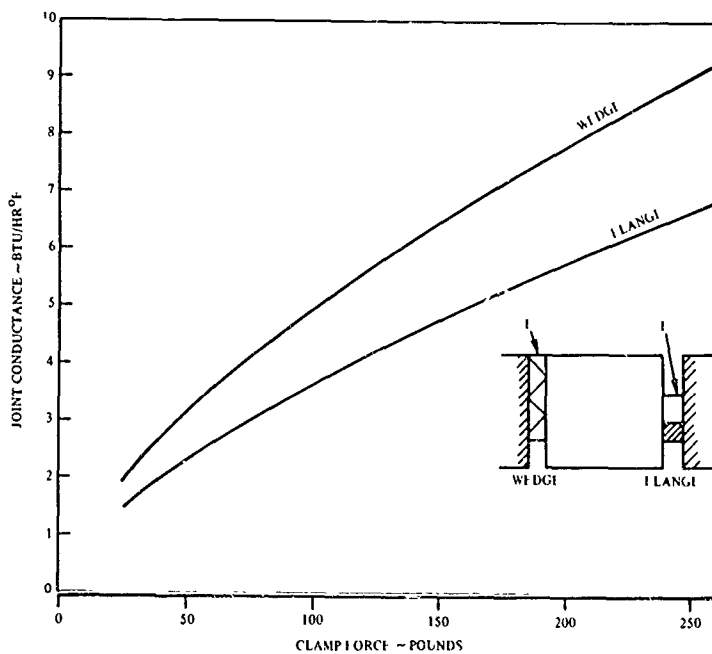


Figure 2-5. Comparison of Module Clamp Thermal Conductance for MICRON 2A Test Demonstrator Conduction Model

The battery module was relocated from the IMU cover to the outlet end of the DPU cold plate. This change made better use of available space and potentially eliminated the need for a separate battery heater.

The fast reaction heating system, capable of furnishing up to 7 KW of power, was designed, fabricated and tested. Input to the controller is 208 V, 3  $\phi$ , 60 Hz power. Output is SCR-controlled 3  $\phi$  power into a delta load. Power is removed from the load when the temperature reaches approximately 170°F. A "reset" action is required to reapply heat.

Six channels of precision temperature control, four for the charge amplifiers and two for the control of the critical electronics, were designed, fabricated and tested. The temperature setpoint was 176°F. Four of the controllers can furnish up to five watts of power while the other two can furnish 10 watts. A control bandwidth of  $\pm 0.035^\circ\text{F}$  on four channels and  $\pm 0.5^\circ\text{F}$  on the other two was the design goal. This accuracy was not verified since the DEM task was terminated. (Temperature control requirements on the latest system designs are not nearly so stringent since the MESGA design has been discarded — see Para 6.3.5.5).

An oven, which can be optionally operated, was provided for the six controllers. A pulse-width modulation technique was incorporated into the controllers so as to minimize hot spots otherwise created by power transistors. A six-channel temperature indicator was fabricated to monitor the areas controlled by the six temperature controllers to get an approximate idea when control had been reached.

By December 1974, fabrication and integration of the conduction cooled DEM and its associated power control equipment was completed. Fabrication and procurement of parts for the liquid cooled DEM was completed except for the blank ceramic substrates and the heaters. No further effort was expended on this task due to the Stop Work Order received in December 1974.

In parallel with design and fabrication of the two DEM's, computer analyses of the models were conducted using the XF 0011 thermal analyzer program. These efforts focused primarily on evaluation of power and control requirements to achieve the specified fast reaction time from -65°F. Results of the analyses for the liquid cooled DEM are given by Figures 2-6, 2-7, and 2-8.

For the conduction DEM, it was found that very precise distribution of heater power and cooling air flow control were essential to bring the MESGA and critical electronics modules up to operating temperature and into thermal stabilization within the required time. The entire GAU must be heated from -65°F to operating temperature at 80°F per minute within three minutes to leave time for suspension, spin up, polhode damping, thermal settling and alignment of the system. For this heating rate analytical results showed that the fast reaction heater power must be applied directly to the GAU modules, as well as to the heat exchangers, in order to avoid excessive thermal lag. Results also showed it was difficult to synchronize the heating of the MESGA's with the charge amplifiers and critical electronics in the GAU without using multiple sensors to control the fast reaction heater turn-off points. Additionally, once the fast reaction heaters turned off, the system was greatly affected by the inrush of cooling air as the flow control valve starts to modulate. This was particularly true of the critical electronics which are upstream of the MESGA and charge amplifiers and thus experience greater fluctuations in cooling air temperature.

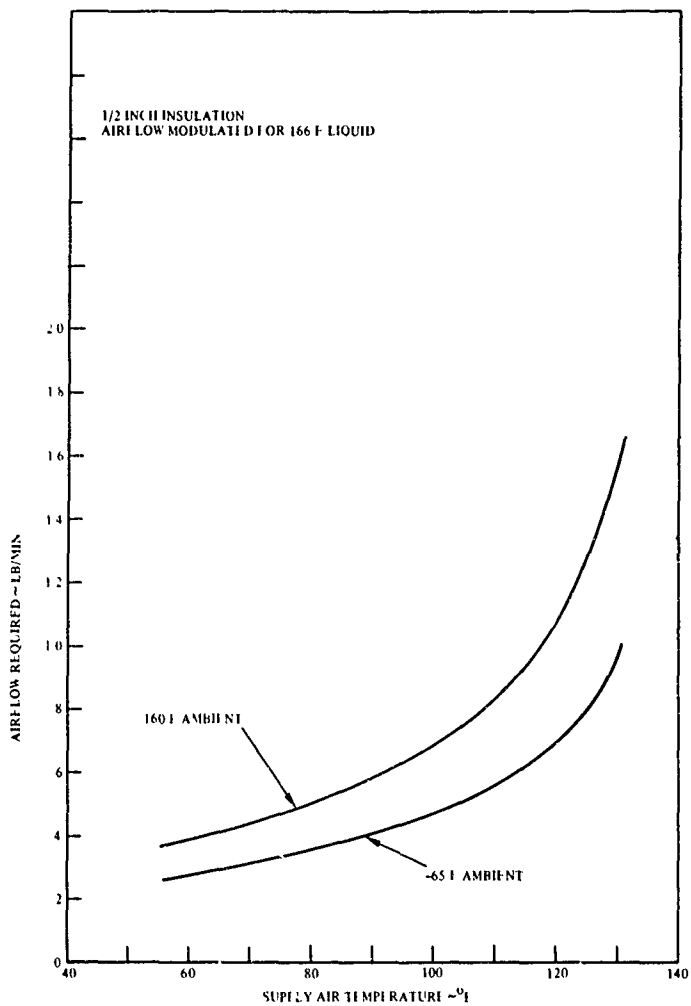


Figure 2-6. MICRON Liquid Model, Airflow Requirements

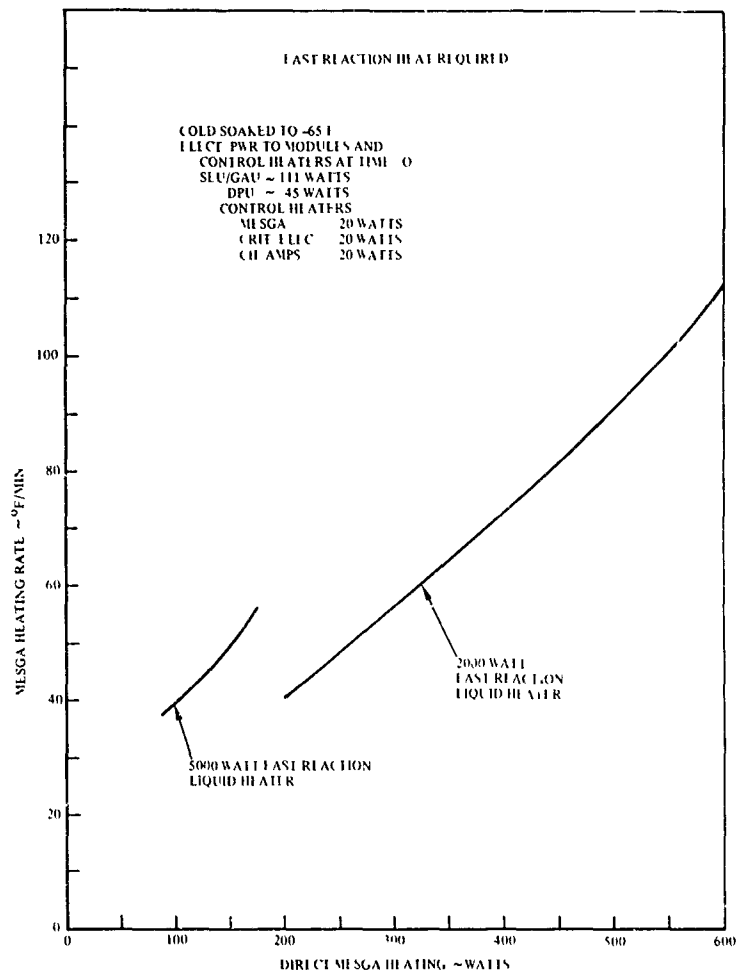


Figure 2-7. MICRON Liquid Model Fast Reaction Heat Required

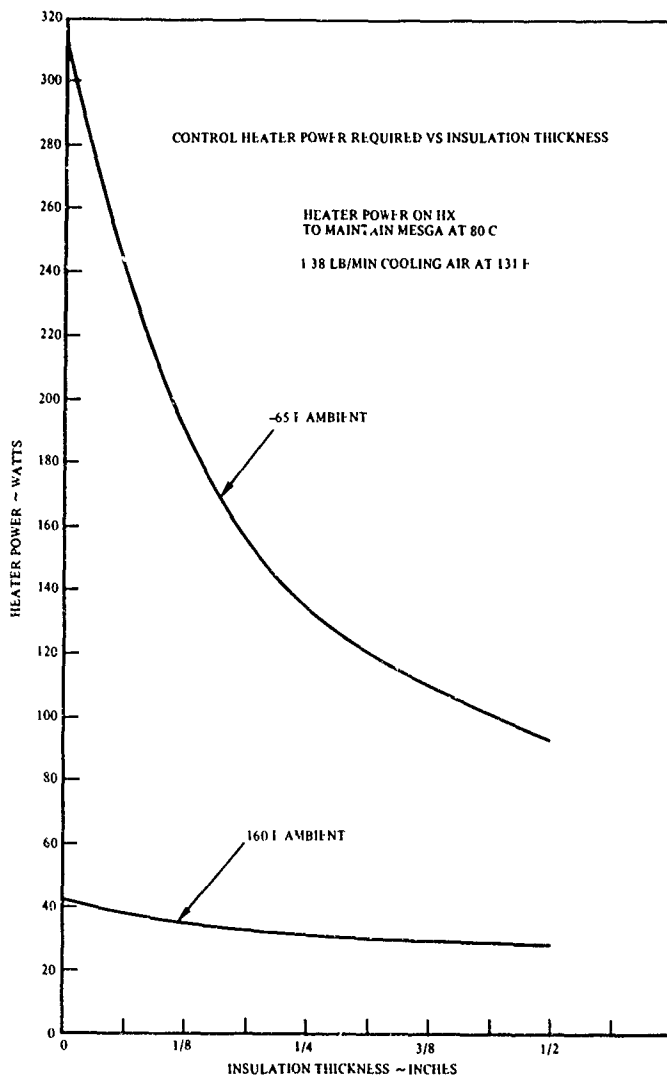


Figure 2-8. MICRON Liquid Model Control Heater Power Required vs Insulation Thickness

Figures 2-9 through 2-11 show the temperature response of the MESGA, charge amplifiers and critical electronics in successive attempts to accomplish the desired reaction time for the conduction DEM.

In Figure 2-9 the fast reaction heaters are located on the GAU heat exchanger surfaces and are controlled by a single thermostat located on the MESGA mounting bracket. Total input power was 5,184 watts. Figure 2-10 shows the effect of adding fast reaction heaters directly to the MESGA, charge amplifier and critical electronics modules and using individual control thermostats. The critical electronics limit cycle was caused by overcooling after the control valve opens, thus driving the critical electronics fast reaction thermostat below its lower turn on limit of 161°F. This indicates that the 80 watt critical electronics control heater power was insufficient. Total input power was 4,871 watts.

After redistributing the fast reaction heater power and increasing the critical electronics control heater power to 120 watts, the response was obtained as shown in Figure 2-11 which was very close to the desired performance. Total input power was 4,324 watts.

## 2.2 SOFTWARE

In Task 1.2, Software, Autonetics developed the necessary software for in-motion polhode damping and developed the software for gyro test station data acquisition.

### 2.2.1 In-Motion Polhode Damping

Polhode damping tests were conducted in the simulated environment of an aircraft in nominally straight and level flight. The Goerz three-axis table was used to generate Scorsby motion of 15 deg about each axis with 12 sec period. The entire automatic start up procedure was performed with the Scorsby motion. The automatic start up modes are Z coil heat, spin up, damp, temperature stabilization, and degauss. No external attitude information was provided to the computer. The N57A-1 navigation system was used in the tests.

Z coil heating, spin up, temperature stabilization, and degauss modes operated satisfactorily. No difficulties were anticipated.

Polhode damping proceeded satisfactorily and completely damped both gyros. However, while damping gyro 1, the damping complete logic would not pass in the presence of Scorsby motion. The Scorsby motion was briefly halted and the damping complete logic passed immediately and exited the damp gyro 1 mode. Gyro 2 damping terminated normally without halting the Scorsby motion. However terminal control took longer than usual and required an extra phase reversal before it damped in gyro 2.

In order to understand the difficulty with terminal control and the damping complete logic, recall that polhode damping attempts to minimize the variations in MUM magnitude which are caused by polhode motion. The MUM magnitude variations are very large except during terminal control and so noise causes no problem except during terminal control. If the MUM magnitude noise is larger than the termination threshold the damping will not terminate and may apply incorrect control.

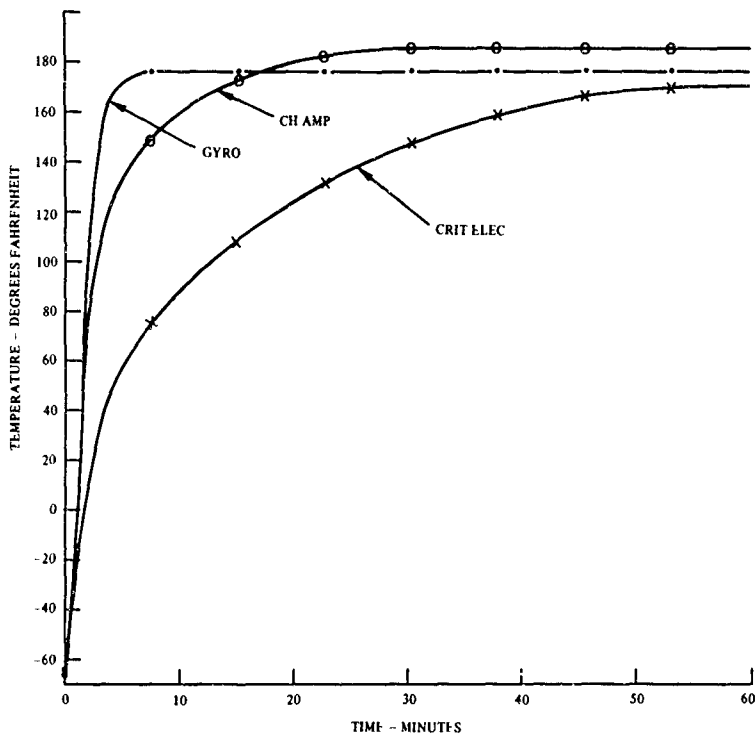


Figure 2-9. Conduction DEM, CAU Fast Reaction Response, Heaters on Chassis Only



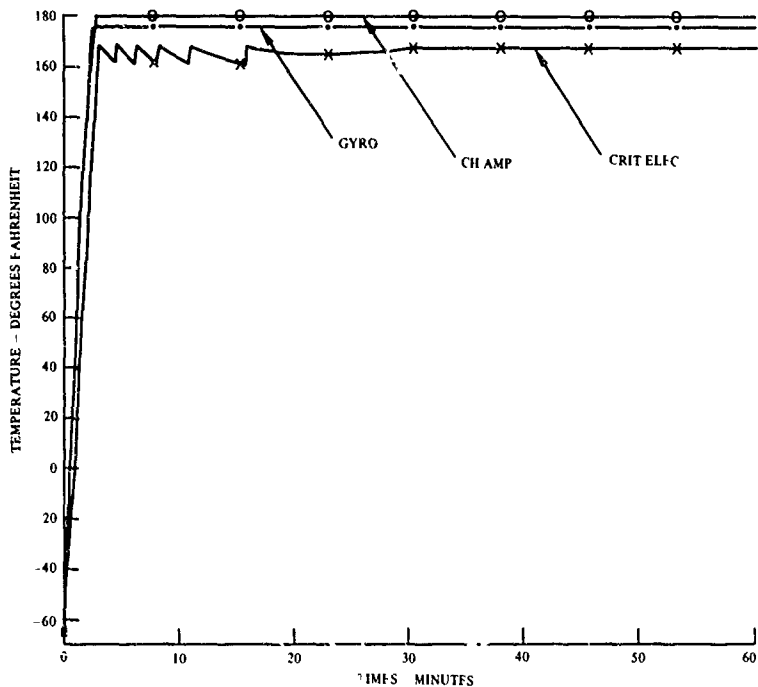


Figure 2-10. Conduction DEM GAU Fast Reaction Response, Heaters on Chassis and Modules

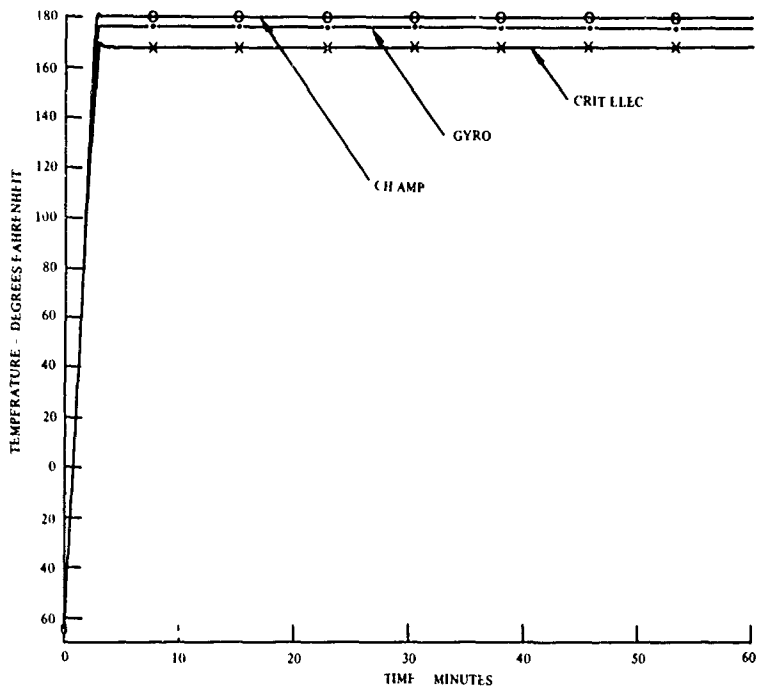


Figure 2-11. Conduction DEM, GAU Fast Reaction Response, Heaters on Chassis and Modules-Critical Electronics Control Power Increased to 120 watts

The additional MUM magnitude noise during Scorsby motion was produced by 3-space angle readout gains that were unbalanced by 6 percent on gyro 1 and 12 percent on gyro 2. Compensation of the 3-space gain unbalance is part of the normal angle readout compensation during navigation. Gain unbalance is not compensated during polhode damping. The gain unbalance will cause uncompensated MUM magnitude to change with attitude change and thus be confused with polhode motion. Future computer mechanizations will apply 3-space gain and phase compensation during automatic start up as well as during navigation. Other angle readout terms are significantly less than the 3-space gain and phase terms. Therefore it is expected that this modification will eliminate the difficulties encountered in terminating polhode damping.

The modification has been made in the mechanization equations. However, N57A-1 development testing was terminated in December by a Stop Work Order. Consequently, final verification of this task was not completed on the hardware.

### 2.2.2 Test Station Software

The objective of this task was to develop the software for testing and processing of test data on the test stations being developed under Phase 2A.

The major programs which perform data sampling and processing were coded on the HP 2100 computers. These include the data sampling programs for collecting calibration data (for angle readout and drift rate) and the angle readout and drift rate.

Drift calibration batch processing programs were coded, using N.A. Carlson's "Fast Triangular Square-Root Mechanization" for the Kalman filter. These programs require less memory and less time than the comparable programs on the IBM 1130 computers.

The programs configured for the 16K-word background memory size (for the distributed system software) were verified on actual data. Data sampled on the Holloman Cyro Subassembly was used for verification, because angle calibration data from the GSA test station was not yet available.

Verification of on-line real-time programs proceeded as the test station hardware checkout progressed. Sampling and smoothing of MESGA acceleration data was first demonstrated with a dummy load (capacitance circuit) in place of the MESGA multisensor element. This data was used for a baseline in characterizing output noise of the MESGA multisensor. Some special-purpose data reasonableness programs were programmed for noise evaluation.

The programs for real-time sampling and smoothing of MESGA acceleration readout were then verified using a non-spinning "proof mass" on the GSA test station. The only problem experienced was a precision limitation on the real-time noise estimates. These had been generated by the "one-pass" estimator of RMS noise given below.

$$\begin{aligned} \text{RMS} &= \left\{ \frac{1}{N-2} \sum_{i=1}^N [Q_i - Q_0 - iR]^2 \right\}^{1/2} \\ &= \left\{ \frac{1}{N-2} \left[ \sum_{i=1}^N Q_i^2 - 2 \sum_{i=1}^N i Q_i - 2Q_0 \sum_{i=1}^N Q_i \right. \right. \\ &\quad \left. \left. + N Q_0^2 + N(N+1) Q_0 R + \frac{N(N+1)(2N+1) R^2}{6} \right] \right\}^{1/2} \end{aligned}$$

where

$R$  is the least-squares estimated output rate (in pulses per sampling period)

$Q_0$  is the pulse counter value prior to start of sampling (a real number)

$Q_i$  is the pulse counter value on the  $i^{\text{th}}$  sample (an integer)

The sums in the second equation involve only  $Q_i$  and  $i$ . Therefore, they can be computed in one pass through the data ( $Q_i$ ). This estimation method has one defective trait, however. That is that the individual terms are very large compared to the value of the whole expression. It was estimated that the 40-bit "mantissa" of extended precision (IIP 2100) arithmetic would be sufficient for a sample size of about 4000 samples (about 1 minute of real-time data). However, the results obtained on live data showed precision-induced errors in the estimates from such a sample size. This problem was solved by limiting the noise estimation algorithm to 100 samples.

Evaluation of the data used for software verification yielded the following MESGA characteristics:

1. Scale Factor is  $\sim 0.0056$  ft/sec per pulse (3-space)
2. 4-space bias pulse rate is  $\sim 20,050$  pulses per second (design goal was 20,000 pps)
3. The zero-mean short term noise (periods in the order of several seconds) is about half a pulse per sample, rms (which is excellent)
4. There are output rate variations of about 70 parts per million (if it is scale factor) or 70 micro-g's (if it is bias), rms, with periods in the order of several minutes. Cause unknown.

5. There was a slow exponential decline of output pulse rates, with about 5 percent total variation in 24 hours and a 4-hour time constant. The cause is most likely thermal settling of the rotor. This trend is shown in Figure 2-12. The shorter-than-usual time constant may be due to the condition of the proof mass and electrodes used in this test (both "very frosty" caused by excessive sparking during suspension testing).

After the 24-hour stability and noise evaluation, two MESGA calibrations were conducted with a non-spinning rotor, and the data were used for verification of the calibration software. Some zero-divisor problems were encountered, similar to those found in the angle parameter comparison program (see Para 6.3.4.1). They were corrected in the same way, also. Final verification with a spinning rotor was not completed, due to a low speed (~400 Hz) rotor drop during test. (The cause of the drop was accidental shock due to mis-meshing the Ultradex table setting teeth.)

The calibrations with a non-spinning rotor showed anomalous scale-factor/misalignment parameters, which were caused by an error in a coordinate conversion algorithm. During July 1975 the cause of the anomaly was resolved by sampling four-space data, and the results were corrected.

MESGA tests on the GSA and GSA test station are described in detail in Para 6.3.5.5.

### 2.2.3 Define DPU Parameters

This task was started in December 1974, and then terminated in compliance with the Stop-Work Order. Work was started in determining the minimum cycle time requirements for parts of the angle readout compensation, to see whether a whole-angle compensation algorithm could be done real time if all compensation were performed after the cross-product mechanization.

### 2.2.4 Define CCU Parameters

- This task was started in December 1974, and then terminated by the Stop Work Order. Initial investigation was started in compiling a list of functions to be performed by the CCU.

## 2.3 AEROSPACE GROUND EQUIPMENT (AGE)

In Task 1.3, AGE, Autonetics developed a configuration item (CI) specification for the gyro test station and designed, fabricated, and integrated one gyro test station. This station approximates potential MICRON product assurance test equipment by including automatic polhode damping, failure recording, self-contained calibration, and automatic startup and shutdown. The gyro test station was used to test the gyro subassemblies designed on this contract.

### 2.3.1 Gyro Test Station CI Specification

The Gyro Test Station CI Specification, AJ00071, was submitted in October 1974 as CDRL Item A009. This specification defines the functional design requirements for the test station and the detail interface signal characteristics between the test station and the GSA.

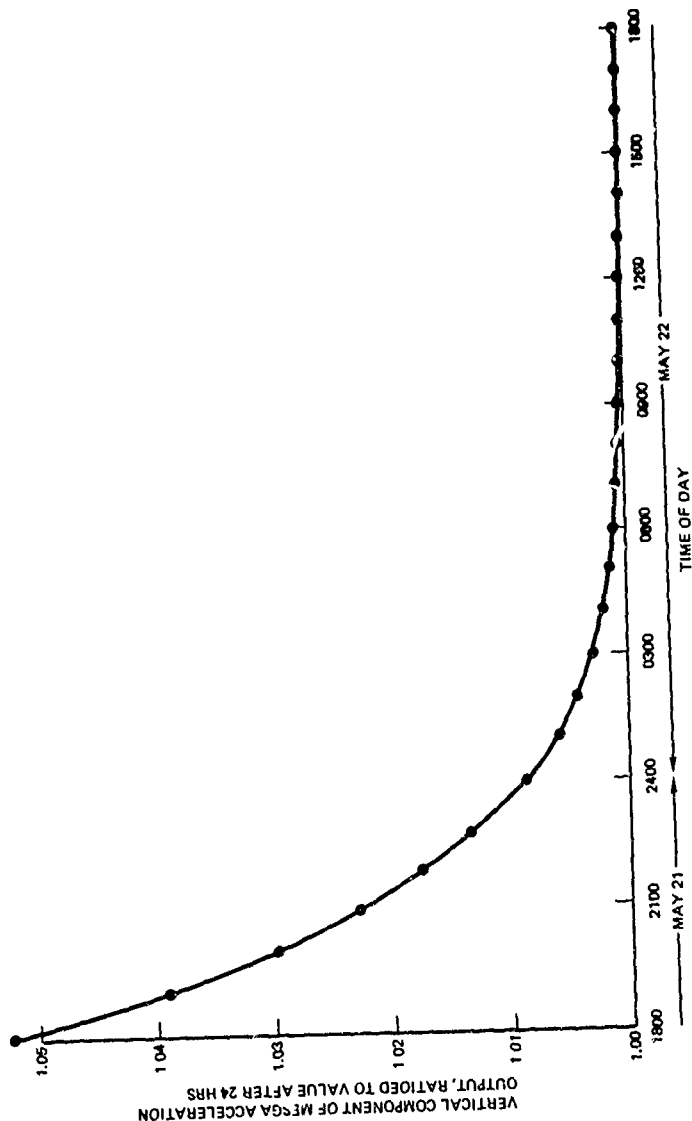


Figure 2-12. MESA Acceleration Readout Variation Over 24 Hours

### 2.3.2 Design Gyro Test Station

The Gyro Test Station basic design activity began in May 1974, paralleling the development of the CI specification, and was completed in October 1974. All drawings for the test station were submitted in October 1974 as CDRL Item A00F. Design update and drawing maintenance was continued throughout the fabrication and integration tasks.

The layout of the Gyro Test Station is shown in Figure 2-13. The test station consists of the following major pieces of equipment:

1. Test Console (2 bays)
2. Computer Console (1 bay)
3. Test Stand and 2-axes manual tilt table
4. Computer Peripherals.
  - a. CRT/Keyboard
  - b. Card Reader
  - c. Terminal Printer
  - d. CRT Mount
5. Support Electronics
6. Interconnect Cabling

The functional characteristics of these equipments are defined in the Gyro Test Station CI Specification, AJ00071.

Figure 2-14, Gyro Test Console, depicts the final panel and equipment arrangement within the test console along with appropriate part numbers. Figure 2-15, Computer Console, depicts the final equipment arrangement within the console along with the Computer Input/Output (I/O) module assignments.

### 2.3.3 Fabrication of Gyro Test Station

Fabrication of the Gyro Test Station began in late June 1974 and was completed in February 1975. The fabrication task included the ordering of commercial equipment and piece part materials, detail fabrication of modules and panel assemblies, assembly of consoles, and basic checkout of wiring and self-contained panels. In general, the following quantities and classes of equipment were fabricated or procured

#### 3 Major Assemblies/Consoles

- Test Console
- Computer Console
- Support Electronics

#### 38 Modules

- 34 in-house fabricated
- 4 commercial

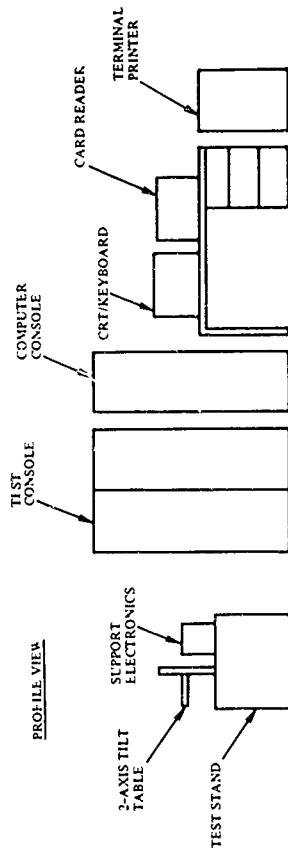
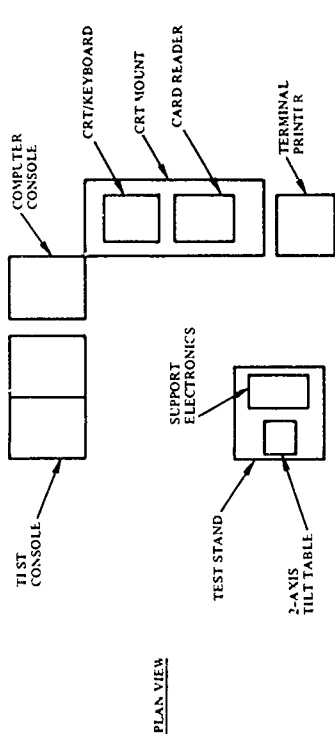


Figure 2-13. Gyro Test Station Layout



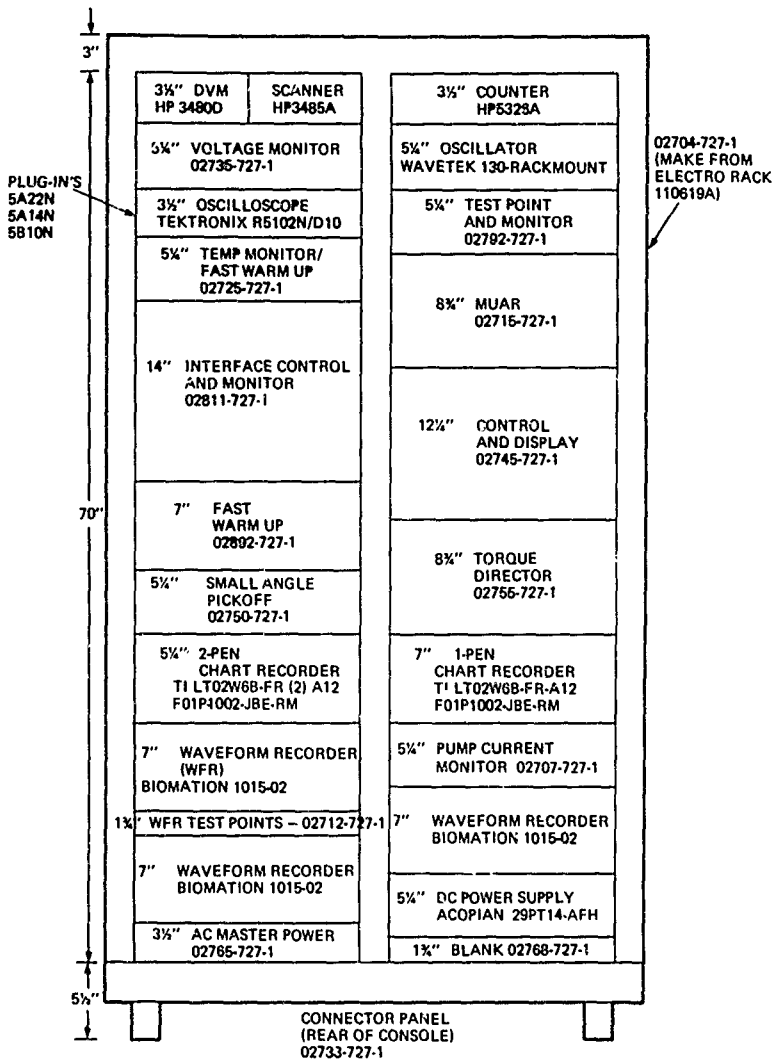
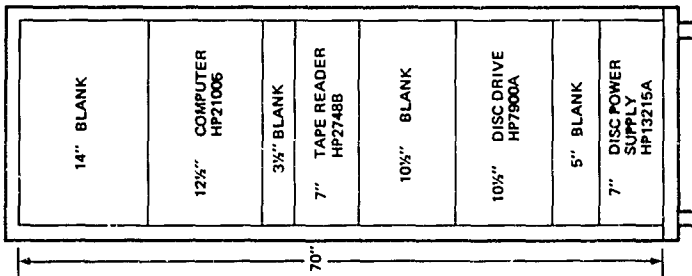


Figure 2-14. Gyro Test Console (02710-727-1)



# COMPUTER I/O ASSIGNMENTS

<u>I/O SLOT NO.</u>	<u>MODULE</u>	<u>FUNCTION</u>
10	HP3485A	SCANNER INTERFACE
11	HP3485D	DMM INTERFACE
12	HP12331C	TERMINAL PRINTER INTERFACE
13	SPARE	
14	HP12925A	TAPE READER INTERFACE
15	HP12960A	DISC DRIVE, WRITE INTERFACE
16	HP12960A	DISC DRIVE, READ INTERFACE
17	HP12868H	CARD READER INTERFACE
18	HP12860A	CRT/KEYBOARD INTERFACE
19	HP12604B	DATA SOURCE - COUNTER INTERFACE
20	HP12639B	TIME BASE GENERATOR
21	HP12566B	MICROCIRCUIT DUPLEX REGISTER - REMOTE CONTROL
22	HP12566B	MICROCIRCUIT DUPLEX REGISTER - MICROCIRCUIT DUPLEX REGISTER - CONTROL & MONITOR DATA
23	HP12566B	MICROCIRCUIT DUPLEX REGISTER - MICROCIRCUIT DUPLEX REGISTER - CONTROL & MONITOR CONTROL

Figure 2-15. Computer Console (O2720-727-1)

- 8 Secondary Commercial Power Supplies
  - 13 Panels/Subassemblies
    - All in-house fabricated
  - 16 Major Pieces of Commercial Equipment
- 2.3.4 Integration of Gyro Test Station

Integration of the Gyro Test Station began in late January 1975, overlapping the completion of the fabrication activity, and was completed in March 1975. This integration task consisted of verifying that all test station electronics functioned properly and verifying the test station interface to the GSA units. Modifications to the test station were made as required for proper operation.

### 3. TASK 2, TEST AND EVALUATION

#### 3.1 TEST PLANS

In Task 2 1, Test Plans, Autonetics developed gyro, gyro subassembly, design evaluation model, N57A-1, and EMI/Grounding test plans.

##### 3.1.1 Gyro and Gyro Subassembly Test Plans

The Gyro and Gyro Subassembly Test Plan, C74-980/201, was submitted to the customer in October 1974 as CDRL Item A00T. This document defined the tests to be performed on the MESG units and the MESG/MESGA subassemblies during the Phase 2A contract. The test plan included developmental testing of the instrument, performance evaluation of instruments, and evaluation of second source instruments. The Gyro and Gyro Subassembly Test Plan document included:

1. Gyro Subassembly (GSA) and Gyro Subassembly-to-Test Station Integration Test Plan
2. MESGA Test Plan
3. ESG Test Plan

##### 3.1.2 EMI/Grounding Test Plans

The following EMI and grounding test plans were prepared during Phase 2A. These test plans were completed during the first two quarters of Phase 2A and were published internally.

1. MICRON Prototype Power Supply Mutual Capacitance Measurement Test Plan
2. MICRON Power Supply Transformer Primary to Secondary Mutual Capacitance Measurement Test Plan
3. Magnetic Field Susceptibility Testing of the Gyro Test Plan
4. Special EMI and Grounding Testing of MICRON Prototype Printed Circuits Test Plan
5. Alternate Method of Special EMI and Grounding Testing of MICRON Prototype Ceramic Printed Circuits Test Plan
6. Prototype MICRON IMU Subsystem Electromagnetic Compatibility Test Plan
7. Prototype MICRON IMU Subsystem Grounding Test Plan

##### 3.1.3 Design Evaluation Model Test Plan

The Design Evaluation Model Test Plan, C74-990/201, was submitted in October 1974 as CDRL item A00V. This document defined the tests that were to be performed on the design evaluation models during the Phase 2A contract. The test plan included temperature, vibration, and mechanical shock tests.

### 3.1.4 N57A-1/HAFB GSA Test Plans

#### 3.1.4.1 N57A-1 Test Plan

The N57A-1 was intended to provide an in-house system test bed in support of the N57A-2 HAFB flight tests and as a development test vehicle.

The test plan for the N57A-1 was completed in October 1974. The test plan covered those development test activities required to resolve problems associated with an operational MICRON system. Specifically, these items included:

- Gap Monitoring Error Sources
- In-Motion Polhode Damping
- Calibration Repeatability
- Polar versus Moving Spin Axis Drift Calibration
- Navigation Performance with Gyros Spun-Up in Body Fixed Coordinates
- Long Term Navigation
- Attitude Readout Accuracy
- Automatic Polhode Damping of Three-Wire Rotor Gyro
- Fast Alignment
- Program Checkout Support

Subsequent to completion of the test plan, the following were added to the list of tests for future incorporation into the test plan:

- Navy Scorsby Test (Funded by Marine Systems Division for Navy with Air Force Permission)
- 12-Bit Demodulator Reference Performance Evaluation
- Calibration Diagnostic Development and Evaluation
- Non-Vertical Plate Center No. 1 Performance Evaluation

A new test plan had to be written for the HAFB Subassembly since the N57A-1 testing was discontinued in December 1974 per the Stop Work Order and replaced by development testing of the HAFB Subassembly.

#### 3.1.4.2 HAFB Gyro Subassembly Test Plan

A test plan was written for the HAFB Gyro Subassembly which incorporated those tests originally scheduled on the N57A-1 system which could be performed on the Gyro Subassembly. Tests originally scheduled for the Gyro Subassembly were retained to the extent possible considering test priority and scheduling. In addition, "Gyro Characterization" and evaluation of the small gap gyro and its associated lower cost suspension electronics were included.

The HAFB GSA was chosen as the test vehicle for evaluation of the small gap gyro and electronics (see Para 6.3.6.5) because the GSA is suitable for the G-capability and environmental testing required. A detailed plan for this evaluation was prepared. The test plan contained three major phases. They were: Phase 1 - Feasibility Evaluation with Existing Hardware, Phase 2 - G-Capability Determinations,

and Phase 3 - Associated Lower Cost Suspension Electronics Evaluation. The test plan defined the test equipment to be used, the necessary preparation, the testing and evaluation, and the decisions required for each phase.

The test items in the final HAFB GSA Test Plan were:

1. Short Term Calibration Repeatability
2. Gyro Characterization
  - a. Baseline angle calibration
  - b. Baseline drift calibration
  - c. Measure MUM magnitude
3. Calibration Diagnostic Development and Evaluation
4. HP 2100 Program Checkout in Support of GSA Software
5. Module Problem Isolation
6. Polar vs Moving Spin Axis Drift Calibration Evaluation
7. Small Gap Gyro Evaluation

It was anticipated that these tests would be performed as required and approximately in the order indicated; however, no firm schedule was established for completion of these tests. This was due to gyro availability and the fact that this testing must be suspended during periods when the N57A-2 system was in the Autonetics laboratory for repair and/or recalibration.

### 3 2 LABORATORY TESTS

In Task 2.2, Laboratory Tests, Autonetics conducted system reliability screen, Scorsby, and heading sensitivity tests on N57A-2, tested gyros; initiated thermal analyses and tests on the design evaluation models, used N57A-1 to demonstrate in-motion polhode damping; tested the gyro subassemblies, and tested second source rotors and cavities.

#### 3 2 1 N57A-2 Lab Tests

Integration of the second N57A system, which was initiated in Phase 1B, continued through May 1974 according to plan. Gyro magnetization and degaussing tests were completed. These tests indicated that magnetization levels induced under normal operating conditions could be successfully degaussed automatically during the system start-up sequence.

The instrument cube operating temperature was raised to 170°F and a new 400 Hz heater thermal switch (170°F) was installed to reduce the system warm-up time.

The system was calibrated and Heading Sensitivity tests per the Phase 1B test plan were completed on 12 July 1974 and Scorsby tests were completed on 25 July 1974. A summary of the test results is shown in Table 3-1. These results showed that there was no alignment sensitivity due to initial system heading.

The system was then used to support checkout of the navigation program to be used for HAFB flight tests. Computer reliability delayed the flight test program and integration of the D216 into the N57A-2 system. System level checkout of the automatic turn-on portion of the navigation program for HAFB flight test was completed on 13 August 1974.

Minor modifications to system wiring and structure were required to permit installation of the D216 computer into the IMU housing. The computer interface had to be completely rewired to be compatible with the system connectors. Computer integration progressed smoothly with the only major problem being intermittent computer halts.

Table 3-1. Summary of Test Results,  
N57A-2 Heading Sensitivity Tests, July 1974

Run No.	Alignment Hdg	Duration (Hrs)	Radial Error Rate	RMS Vel. Error	Remarks
1	90°	.6	-	-	Computer Halted
2	0°	4.2	0.01	2.69	90° Hdg Rotation @ 2 hr
3	45°	2.8	0.78	1.73	
4	90°	4.0	0.27	1.55	10° Roll Rotation @ 2 hr
5	135°	5.3	0.88	2.68	
6	180°	2.0	0.59	3.02	10° Pitch During Align
7	0°	2.0	1.52	2.34	
8	225°	2.0	0.74	1.94	15° Roll and Pitch During Align
9	313°	2.0	0.50	1.20	
10	270°	2.0	0.53	1.13	10° Roll During Align
11	270°	2.6	0.66	2.05	
12	315°	9.0	1.20	3.80	Computer Halt
13	315°	2.4	0.82	1.64	
14	90°	.9	-	-	Computer Ck Sum
15	90°	1.4	-	-	
16	90°	5.0	0.60	1.51	Scorsby Motion 4 hrs

Reliability screen tests were started on 29 August 1974 and 12 of the 24 hours had been completed when a malfunction of the test chamber required discontinuance of the test. The remaining 12 hours were completed on 3 September 1974. There were no problems other than the computer halt problem. The computer halt problem was worked after the completion of the Reliability Screen Tests and cured by electrically isolating the computer from the IMU Housing.

In preparation for the continuation of the Sabreliner flight tests at LAX and the HAFB flight tests, gyros 134 and 96 were installed, the system calibrated, and seven repeatability runs were made with a power cycle between each run. Each run had two turns of 90 deg each 40 min apart. Table 3-2 contains a summary of the repeatability test results. These results showed good system performance and that the system was ready to be flight tested.

The system was moved to LAX on 26 September 1974 and installed and checked out aboard the Sabreliner in preparation for the flight tests to be performed in October.

Further reporting of N57A-2 activities is covered in the flight testing and flight test support sections of this report.

Table 3-2. Summary of Test Results  
N57A-2 Turn-on Repeatability Tests

Date	Alignment Heading	Duration Hours	Radial Error Rate nm/hr	Ave/Channel Vel Error f/s Time rms
9-23-74	270°	2	0.77	4.16
9-23-74	270°	2	0.79	4.62
9-24-74	270°	2	0.79	3.19
9-25-74	0°	2	1.16	4.93
9-25-74	0°	2	0.46	2.05
9-25-74	180°	4	0.56	3.57
9-26-74	270°	2	0.81	3.35

### 3.2.2 Gyro Testing

Test Station IV (T/S IV) was in continuous use for test and evaluation of MMSG units in support of N57A-1, N57A-2, and the HAFB gyro subassembly. Developmental tests were also performed to evaluate the following:

1. Stability of the MMSG cavity configuration in the fast reaction environment (motor functions)
2. Inconel X/Palmer pin vacuum enclosures



3. Getter gyros
4. Self calibration feasibility
5. Three wire fast reaction rotor
6. Low speed (500 Hz) polhode damping capability/feasibility
7. Baseline testing on "standard" MESH in anticipation of narrow (5 mil) electrode separation, groove
8. Small gap gyros
9. Fast Reaction of Beryllium Base gyros
10. Fast Reaction using -Z-coil-only rotor heating
11. Stycast Motor Heating tests
12. Beryllium-oxide support ring evaluation

A chronological summary of T/S IV test activity is presented in Table 3-3. A brief summary of test results is presented below.

#### 3.2.2.1 Test Results

##### 1. Cavity Stability in the Fast Reaction Environment

The latest configuration N57A type MESH units were exposed to this series of tests. MESH Units No. 096, 134, and 136 were used in support of the investigation. Each unit was exposed to normal operating conditions and an angle calibration and drift calibration. The unit was then spun down (but not desuspended) and the case heaters were turned off and the unit was permitted to stabilize over night. The next sequence of tests on the gyro included fast rotor warm up (80°F/min), fast spin up (12 sec) and rapid polhode damping (motor "on time" < 20 sec) followed by a standard angle calibration. The spin down was again accomplished and the series of tests was again repeated after rotor desuspension. In summary, there was no detectable cavity shift across any or all exposures.

##### 2. Inconel X/Palinea Pin Vacuum Enclosure

The reported problem of magnetic material in the MESH vacuum housing which caused problems in the N57A automatic spin up/polhode damping environment was corrected by material changes. The vacuum housing material was changed from stainless steel to Inconel X. The feedthrough pins were changed to Palinea 7 type material. The MESH units were exposed to tests on T/S IV and on N57A-1 and N57A-2 systems, as well as component testing to assure that the problem had been corrected and had not degraded instrument performance in any other respect. All MESH units will have this latest configuration vacuum enclosure.

Table 3-3. Summary of Test Station IV Activity

Date	Activity	Gyro
4/1/74	MESGA Tests	124
4/1	Charge Monitor, Spin Up, Gyro Check	116
4/2-23	ECOM Testing - Temperature Tests and Rotor Heating, Drift Cal	124
4/23-25	Getter Gyro Tests	118
4/26-29	Getter Gyro Tests	112
4/29	Charge Monitor	096
5/1-16	MESGA Testing, Temperature and Rotor Heating Tests, Angle and Drift Calibrations. "Angle-Cal-Orama"	096
5/16-17	Gyro, Charge Monitor Check	126
5/17	Charge Monitor and Gyro Check	132
5/17-20	Charge Monitor	126
5/20-21	Gyro Check - Heating Check	132
5/21-22	Charge Monitor and Case Heating Test	124
5/23-28	Gyro Checks - Speed Notch	126
5/28	Getter Gyro Test	118
5/29-31	Thermal Response Tests	132
5/31	Gyro Check	126
5/31	Getter Gyro Test	118
6/3	Getter Gyro Test	118
6/3-4	Charge Monitor, Gyro Check	126
6/4-10	ECOM Tests - Heating Tests	128
6/11	Gyro Check	132
6/12-13	Gyro Check	128
6/13-19	T/S Modified - New MUAR Installed	-
6/19-20	MESGA Tests	126
6/20-21	Charge Monitor, Speed Notch Checks	128
6/24-25	Charge Monitor - T/S Checkout	007
6/25	Charge Monitor Heating Check	126
6/25-28	MESGA Testing	068

Table 3-3. (Cont)

Date	Activity	Gyro
7/1/74	Mount Gyro Charge Monitor, Spin up polhode damp, temperature stabilize overnight	102
7/2	Angle Cal, Drift Cal preparatory to MESGA Test Program (approx 1 week)	102
7/3	MESGA Testing - Cavity misalignment evaluation, MESGA Cal, "Noise" test, start 40 hr stability test	102
7/5	End 40 hr stability test, MESGA Cal, "Noise" test, Angle Cal, start 65 hr stability test	102
7/8	End 65 hour stability test, "Noise" test, MESGA Cal	102
7/9	Troubleshooting/repairing test equipment problems. Remove Gyro.	102
	Mount getter gyro for speed notch tests, remove gyro.	118
	Mount gyro, Charge Monitor	124
7/10	Spin up, polhode damp, Angle Cal, Drift Cal	124
7/11	Remove gyro	124
	Mount gyro, charge monitor overnight	135
7/12	Spin up, polhode damp, observe polhode motion and period, remove gyro.	135
7/12	Mount gyro, charge monitor	128
7/15	Spin up, polhode damp, set equilibrium angle, spin down and remove gyro	128
	Mount gyro, charge monitor	137
7/16	Spin up, polhode damp, observe polhode motion and action vs temperature (75°F to 105°F) Spin down, remove gyro	137
	Mount gyro charge monitor	135
7/17	Spin up, polhode damp, observe polhode motion and action vs temperature (75°F to 105°F) spin down, remove gyro	135
	Mount gyro, charge monitor, spin up, polhode damp, set equilibrium angle.	134
7/18	Start Cavity Stability Test Program per the test plan - "Palmer Gyros 096, 131 and 136"	134
7/31	Continuing Cavity Stability Tests	136

Table 3-3. (Cont)

Date	Activity	Gyro
8/1	Continuation of Cavity Stability Test Program - per Test Plan	136
8/2	Quick check of integrity of gyros sustaining full-speed ball drop on N57A-1 System. Both unable to suspend	130 098
	Resume Cavity Stability Testing	136
8/6	Spin up and polhode damp at approximately 500 rps to observe 'minimal' amount of heating required to lamp. Angle cal.	068
8/8	Getter Gyro Tests	118
8/9	Resume Cavity Stability Testing, with third candidate	096
8/13	Trouble-shooting computer-interface equipment problem (Multiverter - DVM)	
8/19	Conclude Cavity Stability Testing	096
	Modify Suspension Electronics for self-calibration feasibility studies	
8/20	Self Calibration Feasibility - per Test Plan. Checkout T/S and Software	068
	Checking and trouble shooting software and test equipment problems	
8/26	Second modification of electronics, to improve signal-to-noise ratio	
	Resume checkout preliminary to testing	068
9/3 - 9/9	Functional tests, then support self calibration feasibility tests	068
9/9 - 9/10	Getter gyro testing	118
9/10	First test of 3-wire rotor. Measured polhode period (1.38 sec)	100
9/10 - 9/13	Support self calibration feasibility tests	086
9/16 - 9/23	Functional tests and week-end cross-polar tests for "wide groove" baseline tests	136

Table 3-3. (Cont)

Date	Activity	Gyro
9/30	Angle Calibration	112
10/1-4	Drift Cal, Support Self-Cal feasibility studies. Trouble-shoot temperature controller.	112
10/4	Charge monitor gyro from N57A system	102 110
10/4	Trouble-shooting ECOM power supply and ECOM motor problems. Rotor sustained a low speed de-suspension. ECOM motor developed internal short beyond repair. ECOM power supply required repair.	132
10/7	Charge monitor - determining low-power rotor spin up characteristics.	140
10/8	Charge monitor - recheck gyro (Beryllium Base MESG)	132
10/9	Getter gyro testing	118
10/9-14	First tests of gyro with narrow cavity grooves and a 3-wire rotor. Angle cal, drift cal special torquing sensitivity tests. Week-end cross polar drift tests.	144
10/14	Vacclon pump voltage sensitivity tests.	068
10/15-24	Vacclon pump voltage sensitivity tests. Comparison of angle and drift cals made at full pump excitation and rotor speeds compared to reduced pump excitation and resultant reduced rotor speed.	144
10/24	Getter gyro test	118
10/25-28	Test new ECOM motor for Z coil only rotor heating capability. Polhode period vs rotor temperature sensitivity test.	145
10/29-31	Check ECOM motor capability for rapid warmup on "Standard" gyro.	142
10/31-11/1	Angle Cal and Drift Cal	102

Table 3-3. (Cont)

Date	Activity	Gyro
11/1-5	Angle Cal, Drift Cal; Repeat series of short angle calcs - Troubleshooting	102
11/5-6	Getter Gyro Testing	118
11/6	Polhode Motion Studies	135
11/6-14	Angle Cal, Drift Cal; Repeat Angle Cal, 50 Hour Cross-Polar Drift Test	144 118
11/14	Getter Gyro (New) Testing - Charge Monitor	154
	Getter Gyro Testing	118
11/14-18	Charge Monitor - At Room Temp	71
11/18	Getter Gyro Testing	154, 118
11/22	Getter Gyro Testing	154
11/26	Getter Gyro Testing	154
11/27	Getter Gyro Testing	118
12/2	Getter Gyro Testing	154
12/3	Getter Gyro Testing	156
12/6	Getter Gyro Testing-Repeat	*56, 118, 154
12/6-9	Charge Monitor - Weekend (160°F)	156
12/9	Getter Gyro Testing	156, 154
12/10-12	Functional Testing (Trouble-shooting)	142
12/12-13	Charge Monitor - Room Temperature	077
12/13-16	Polhode Period vs Temperature	149
12/16	Getter Gyro Testing	154, 156
12/16	Charge Monitor	066
12/17	Getter Gyro Testing	118
12/17-19	Repeat Functional Test	142
12/19	Polhode Period vs Temperature	151
12/19-20	Repeat Drift Cal Tests	142

Table 3-3. (Cont)

Date	Activity	Gyro
01/02/75	Getter Gyro Tests	154
01/03/75	Getter Gyro Tests	156
01/03/75	Getter Gyro Tests	118
01/09/75	Getter Gyro Tests	154
01/09/75	Getter Gyro Tests	156
01/10/75	Getter Gyro Tests	118
01/13/75	Charge Monitor	101
01/14/75		
01/15/75	Charge Monitor - Gyro Checkout Test	135
01/16/75	Getter Gyro Tests	154
01/16/75	Getter Gyro Tests	156
01/17/75	Getter Gyro Tests	118
01/23/75	Polhode Motion Tests	153
01/24/75	First Beryllium Base MICRON Gyro Gyro Warmup Tests Temperature Response (Time Constant) Tests Z-Coil Heating Tests - New Power Supply	A012Y
02/3-6/75	Thermal Response Tests; Thermal Ramps, Z-Coil Heating, Time Constant Determinations, Angle and Drift Cals	A012Y
02/6-7/75	Getter Gyro Tests - (Repeat Tests)	118
02/07/75	Getter Gyro Tests - (Repeat Tests)	156
02/10/75	Getter Gyro Tests - (Repeat Tests)	154
02/10/75	Getter Gyro Tests - New Gyro, Initial Test	158
02/11/75	Getter Gyro Tests - (Repeat Test)	158
02/11-21/75	"Small Gap" Gyro Tests, Angle & Drift Cals, Cross-Polar Drift Run	124
02/24/75	Gyro Check-out Tests	155
02/25/75	Charge Monitor Check	086
02/26/75	Getter Gyro Tests (Repeat Tests)	156
		154
02/27/75	Getter Gyro Tests (Repeat Tests)	118
02/28/75	Getter Gyro Tests (Repeat Tests)	154
	Charge Monitor Check	073

Table 3-3. (Cont)

Date	Activity	Gyro
03/3-5/75	Charge Monitor - Suspected Charger	073
03/5-7/75	Getter Gyro Tests - "Rebuilt" Getter Gyro - Reactivating Getter	158
03/7-10/75	Getter Gyro Tests	118
03/11/75	Getter Gyro Tests	156
03/11-12/75	VacUon Pump "Sure-Start" Preliminary Test	059
03/12-17/75	Getter Gyro Tests	154
03/17/75	Getter Gyro Tests	156
03/17-18/75	Getter Gyro Tests - "Rebuilt" Getter Gyro, "Double Reactivation" Series	158
03/18/75	Recheck MUM Signals - Amplitude	136
03/19-20/75	Getter Gyro Tests	158
03/20-31/75	Beryllium Base Gyro Tests Thermal Responses, Time Constants Z-Coil Heating Rate Tests	A012Y
04/1-9	Beryllium Base Gyro Testing Thermal Response Tests; Time-Constant Tests (Rotor Suspended and De-Suspended) Z-Coil Heating Rates vs Motor Power Supplies and Power Input Variations	A012Y
04/9	Charge Monitor Check	142
04/10	Charge Monitor Check	148
04/11	Getter Gyro Tests Getter Gyro Tests Thermal Response Tests	156 118 A012Y
04/14	De-Activate T/S for Move to New Lab	
04/15-24	Re-locate T/S, Integrate and Interface with new Computer and I/O, Align Test Stand and Calibrate Axes and Orientations	
04/25-28	Checkout T/S with Suspension-Grade Gyros	015 & 024
04/29	Final T/S Checkout - Charge Monitor	086
04/30	Getter Gyro Test - Rotor Dropped Trouble-Shoot T/S for Probable Cause of Rotor Drop	158



Table 3-3. (Cont)

Date	Activity	Gyro
05/1	Trouble-Shooting Test Station with Suspension-Grade Instruments	007 & 126
05/2-14	Continued Trouble-Shooting with a "Stable" (Non-Charging) Suspension-Type Gyro: a. Repetitive Suspending and De-suspending b. Charge Monitoring a. Various TDY Input Levels and Durations c. Incremental Spin up to Full Speed, Overnight Runs, Weekend Runs d. Angle and Drift Cal Runs e. Repetitive Spin Ups and Spin Downs	015
05/14	Getter Gyro Testing	118
05/15-16	Getter Gyro Testing	156
05/20	Charge Monitor Checkouts	A020Y A021Y 007 & 015
05/21	Small Gap Gyro Tests - Rotor Dropped	124
05/21-30	Trouble Shooting Test Station with Suspension Grade Gyros, Refurbishing and Updating Consoles	024, 146 & 015
06/2-19	Repairing and Refurbishing Console, Updating Test Station and Documentation	
06/19	Console Checkout, Including Repeated Spin-ups and Spin-Downs for Confidence Checks	126
06/20-23	Spin-up, Polhode Damp, Spin-Down, Charge Monitor Over Week-end	126
06/23-24	Checkout of Cabling and Circuitry Modifications	126
06/24-25	Checkout of Test Station Configuration and Software Checkout	059
06/26-27	Z-Coil Heating Rate Tests, Spin-up, Polhode Damp, Charge Monitor Overnight	059
06/27-30	Two Angle Cals, Spin-Down, Charge Monitor Over Weekend	059
06/30	Spin-up, Polhode Damp, Temperature Stabilize for Drift Cal	059

Table 3-3. (Cont)

Date	Activity	Gyro
7/1-2	Tests of Gyro without Cavity Clamp Ring, Charge Monitor, Angle & Drift Calibrations	059
7/2	Charge Monitor Checks	A-022Y A-021Y
7/3	Getter Gyro Test	118
7/7-8	Getter Gyro Tests	156 118
7/8	Getter Gyro Test, Rotor Drop (Non-Spinning) T/S Checkout with Suspension Grade Gyro	154 126
7/9	Charge Monitor Checks	154 A-022Y
7/10	Charge Monitor Check Narrow Gap Gyro - Suspension & Charge Monitor Check	A-020Y 116
7/11-14	T/S Checkout, Suspension & Triggering Checks	024
7/14-17	Small Gap Gyro Charge Monitor, Rotor Drop (Non-Spinning) T/S Checkout with Suspension Grade Gyros Replaced Charge Amp Connector	116 126 024
7/18-21	Suspension Checks & Charge Monitor Over Weekend	116
7/21	T/S Heater Circuit Checkout	126
7/22-25	Small Gap Gyro, Angle & Drift Calibrations	116
7/25-30	Second Source Gyro, Charge Monitor Over Weekend Angle & Drift Calibrations	N-0005
7/30	Getter Gyro Tests	118 156
7/31-	Second Source Gyro, Angle & Drift Cals.	N-0006

### 3. Getter Gyro Evaluation

A discussion of getter gyro tests and evaluation is presented in Section 6.3.

### 4. Self Calibration Feasibility

A discussion of this test activity is presented in Section 6.3.

### 5. Three Wire Fast Reaction Rotor

The first rotors of the three wire type were tested during this reporting period. Two rotors were evaluated

<u>Rotor</u>	<u>MUM Amplitude</u>	<u>Speed</u>	<u>Polhode Period</u>	<u>Polhode Pattern</u>
B <sub>7</sub>	3.1 V <sub>p-p</sub>	2433	1.38 sec	Per Design
B <sub>1</sub>	3.0 V <sub>p-p</sub>	2441	1.18 sec	Per Design

The above table summarizes the initial evaluation. The polhode pattern is distinctive and should be quite adequate for computerized polhode damping and the short period is desirable for Fast Reaction capability

### 6. Low Speed Damping

Two MESH units were properly damped at approximately 500 Hz. No problems were encountered during this manual function. The rotor temperature change was less than 1°F which is a more ideal value for "Fast Turnaround" environment, than the 9°F presently induced.

### 7. Narrow Groove Evaluation

Two gyros, each with different interelectrode groove widths, were tested for the purpose of comparing their performance. The first gyro, No. 136, with the then standard 10 mil groove width, was tested as a baseline test. The second gyro, No. 144, with narrow 5 mil grooves, was then tested in the same manner. The tests consisted of an angle cal, drift cal, and then RSA cross-polar testing for a 48 hour period with infrequent case position changes. The results are listed in Table 3-4. All gyro cavity parts are now being fabricated with 5 mil interelectrode groove widths.

### 8. Small Gap MESH Evaluation

A small gap gyro (~235  $\mu$ -in. radial gap) No. 121 was also tested. The calibration results from the small gap gyro were within the envelope of results obtained from other gyros. An additional moving-RSA drift calibration of about 48 hr was also conducted. This data was used in modeling studies (see Para 6.3.4), on the theory that the small gap may

Table 3-4. Comparison of Drift Rates Due to Interelectrode Grooves:  
Gyro 136 vs. 144

Rotor Shape Harmonic (Order)	Calibrated Drift Rates Due to Interelectrode Grooves Coupled with Rotor Shape Harmonics (Deg/hr)	
	Gyro 136 (10 mil grooves)	Gyro 144 (5 mil grooves)
4th	0 014	0 003
6th	0 197	0.010
8th	0 053	0.000
10th	0 010	0.002
12th	0 010	0 009
14th	0.002	0.001
16th	0.007	0.002
RMS	0.078	0.005
Raw Drift Rate RMS	0.231	0.092

accentuate drift rate mechanisms that are present but less observable on all nominal gap (300  $\mu$ -in. radial gap) gyros.

A second small gap gyro ( $\sim 160 \mu$ -in. radial gap) No 116 was also tested. The results of the angle cal and drift cal were also within the envelope of results obtained from other gyros. The additional moving RSA drift cal, of 48 hours duration, was not conducted at this time. It is planned to conduct this test during Phase 2B and include the gyro data in the modeling studies as reported in Para 6.3.2.

#### 9. Fast Reaction Tests (Beryllium Base Gyro)

The first beryllium base gyro for MICRON, Gyro No A-012Y, was subjected to preliminary temperature response testing. The gyro was mounted on Test Station IV with three thermosensors attached to the gyro and

mounting bracket combination. The "Deep Probe" Thermosensor was located approximately 5/16 in from the cavity. The second thermosensor was located in the center of the mounting adapter. The third thermosensor was located in the base of the gyro. The gyro was initially stabilized at room ambient (73°F), then the case heaters were turned on full power for an 8 min interval, during which time the gyro gap and the three temperatures were recorded. The results of the initial test, shown in Figure 3-1, indicate that the time constant between the gyro mounting interface and cavity is less than 30 sec.

Additional temperatures ramp response tests were conducted using approximately one-half power input to the case heaters and varying the duration of heat input. The results were very predictable, based on information from the full power results. In all of these tests the time constant from the cavity to the case never exceeded 30 seconds. Thus one of the various design goals for achieving Fast Reaction Capability, discussed later in Paragraph 6.3.6.1, was successfully met.

In conjunction with the temperature ramp tests, the cavity-to-rotor time constant ( $\tau_{c-r}$ ) determination tests were conducted, per previously established test plans, first with the rotor suspended and later with the rotor de-suspended.

The tests for time constants, with the rotor suspended, are relatively straight-forward. The gyro is at a steady-state temperature, then the temperature controller is either turned off, or the controlling setpoint increased. In the test with the rotor de-suspended the gyro was at a steady-state operating temperature then the temperature controller was turned off and the gap monitored for one (1) minute, then the rotor was de-suspended for 14 minutes to allow de-suspended cooling. At the end of 14 minutes, the rotor was suspended and the gap monitored for one minute, then de-suspended for 14 minutes, and the 15 minute cycle repeated until the end of the test.

The results are shown in Figures 3-2 to 3-4 and summarized in Table 3-5.

The determination of  $\tau_{c-r}$  was done using the graphical method as shown in Figures 3-2 to 3-4 vis., a tangent to the gap curve at a time after steady state temperature was achieved on the cavity, extended to intercept the steady state (nominal) gap value.

The results were per expectations, based on earlier tests with gyro No. 124, with the exception of the rotor de-suspended results. During Phase 2B, it is planned to repeat the time constant checks on a second beryllium gyro to verify the results. Additional test duration time will be allowed, particularly in the rotor de-suspended tests, to fully characterize the gap curves.

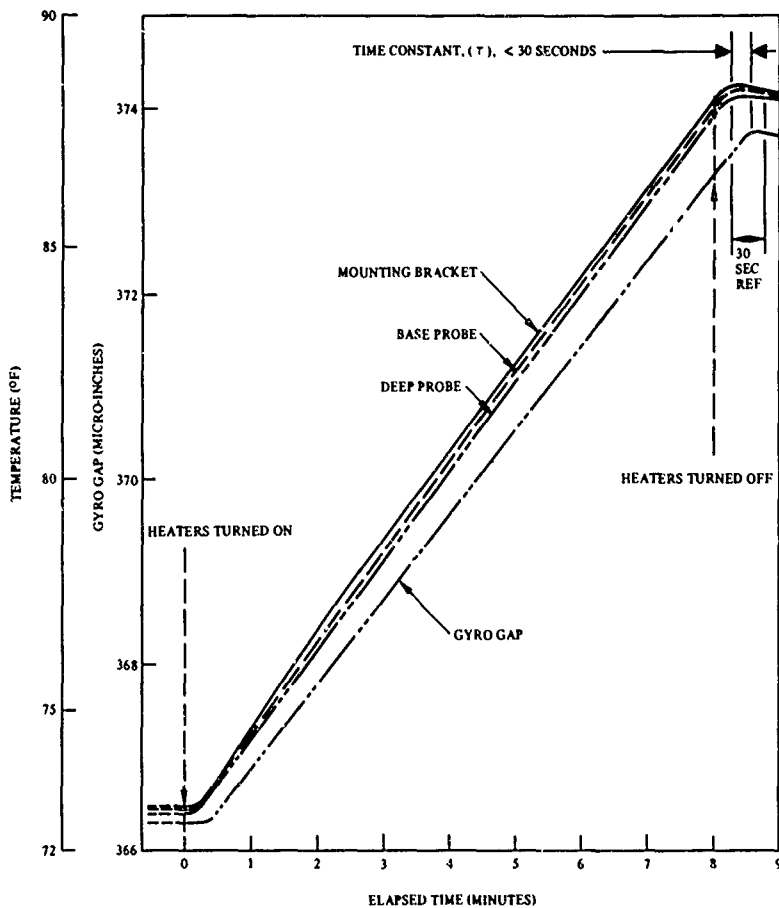


Figure 3-1. Time Constant Determination Test - Gyro A012Y

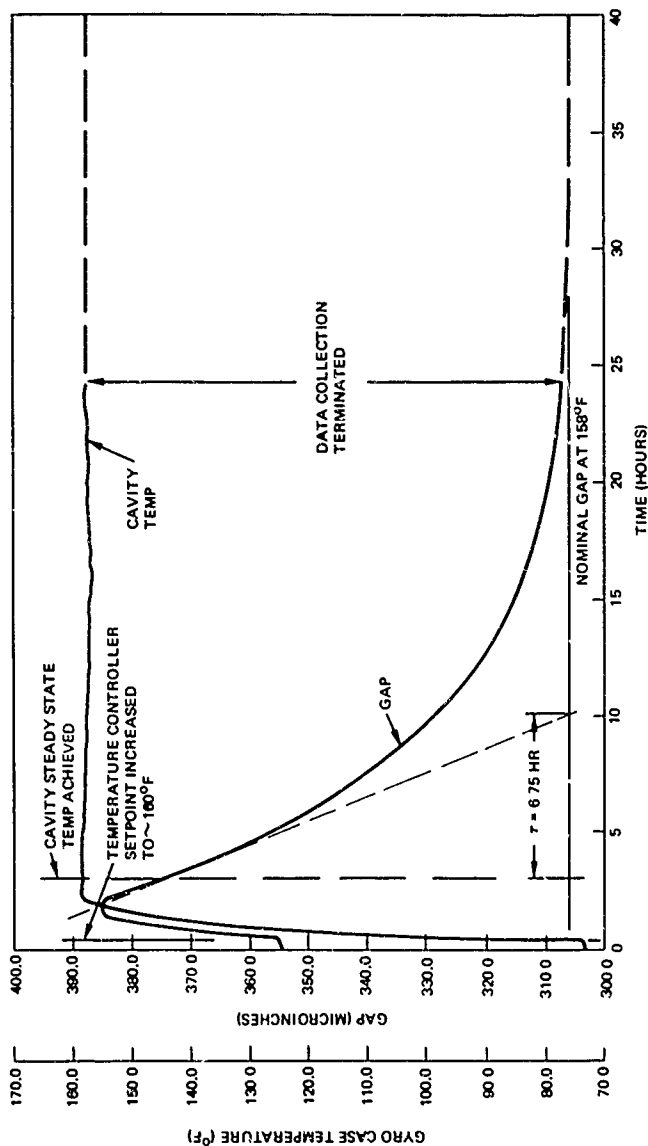


Figure 3-2. Thermal Response: Gyro -012Y Time Constant for Rotor Warm-Up with Rotor Suspended

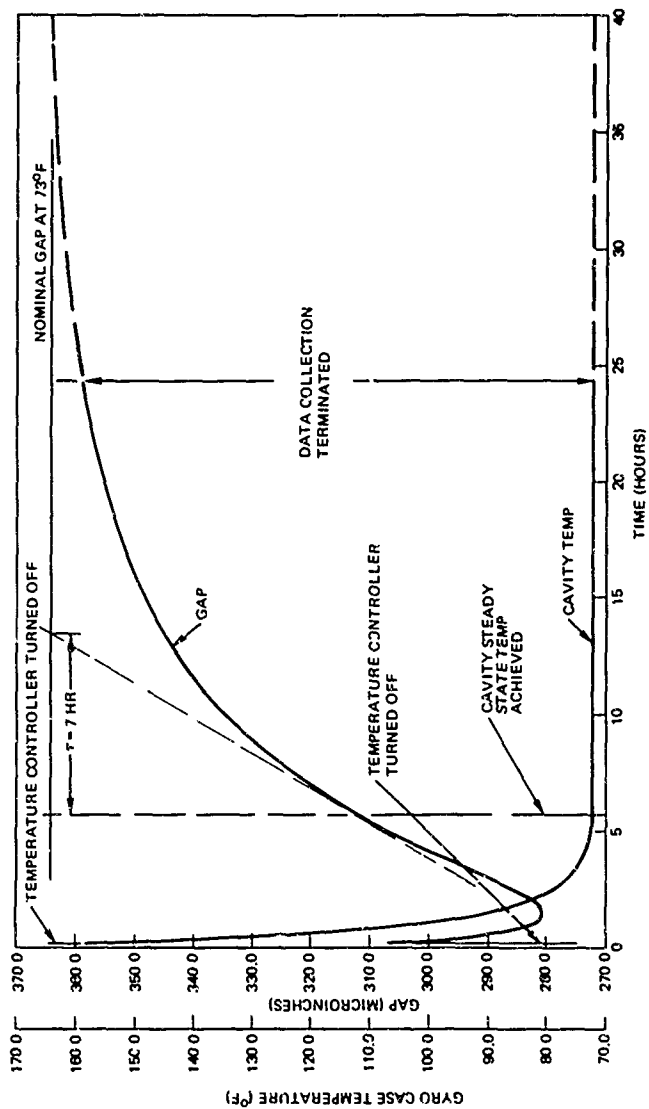


Figure 3-3. Thermal Response: Gyro A012V Time Constant for Rotor Cool-Down with Rotor Suspended



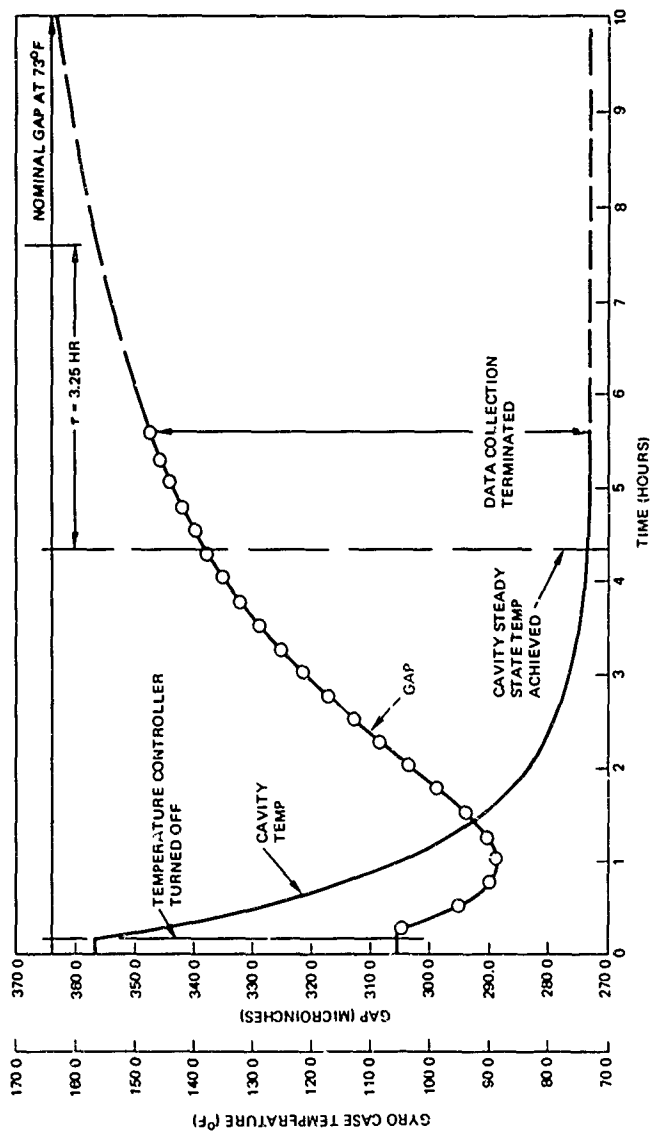


Figure 3-4. Thermal Response: Gyro A012Y Time Constant for Rotor Cool-Down with Rotor DeSuspended

Table 3-5. Summary of Cavity-to-Rotor Time Constant Tests

Response Test		Time Constant Cavity-to-Rotor $\tau_{c-r}$ Hrs
Thermal Mode	Rotor Mode	
Heating (73° to 158°)	Suspended	6.75
Cooling (158° to 73°)	Suspended	7
Cooling (157° to 73°)	De-Suspended	3.25

#### 10. Fast Reaction Tests - Z-Coil-Only Rotor Heating Tests

Another requirement of the Fast Reaction mode, for the gyro, is that the rotor must be heated at a rate of 80°F/minute. This goal was achieved on N57A type gyros by applying 5.74 amps-rms at an excitation frequency of 5 kHz for a limited duration to the then existing gyro motor. However this rate could not be maintained for sustained durations (~10 seconds maximum) due to possibly excessive coil heating and subsequent danger of destructive damage to motor windings. The motor had not been designed at the time to withstand or dissipate the excessive heat generated. The motors were redesigned to be capable of withstanding the heating for the requisite durations by using a thermally conductive potting compound (STYCAST 2850 FT). After several modifications and testing, a rotor heating capability of 80°F/min was achieved by applying 9-amp-rms at 5 kHz to the Z coil of the new Fast Reaction Motor (ECOM type). The new current requirement exceeded the capabilities of the motor power supply, requiring design changes and modifications to the existing power supply.

Throughout Phase 2A combinations of motors, power supplies and and gyros, modified to complement and evaluate design changes for Fast Reaction gyro development, were tested. An overall summary is given in Table 3-6.

The tests were generally conducted using 5 kHz excitation frequency and the "normal" 9-amp-rms of Z-coil current. In the few instances where the "normal" 9-amp current was not used, the results were normalized to a 9-amp condition to ease the compilation of the summary and comparison of results. A discussion of the means used to provide comparisons of different tests is given in later paragraphs.

In all these instances, the desired improvements to the gyro were achieved (i.e., time constants were reduced, spin up and polhode time reduced) however the rotor heating rate decreased. The substantial loss of heating effectivity as a result of the beryllium base was believed to be attributable to Eddy Current losses in the beryllium base. Therefore the base was

Table 3-6. Summary of Z-Coil-Only Rotor Heating Characterization Studies  
Using 5 kHz Excitation Frequency

Test Date	Gyro/Configuration/Remarks	Heating Rate (HE) °F/min	Heating Effectivity (HE) °F/min/amp <sup>2</sup>	Current Req'd (Ir) for 80°F/min Amps
5/21/74	Gyro 124 - N57A Type	83.7	1.033	8.8
5/17/74	Gyro 132 - Beryllium Base - Unslotted	39.1	.483	12.9
5/21/74	Gyro 132 - Beryllium Base - Unslotted	43.7	.539	12.2
9/24/74	Gyro 132 - Beryllium Base - Slotted	45.9	.567	11.9
10/29/74	Gyro 132 - Beryllium Base - Slotted, Cavity Clamp Ring Removed	44.6	.550	12.1
1/28/75	Gyro A-012Y - Beryllium Gyro - Latest Configuration - Slotted (Sinusoid Wave Shape)	40.4 46.6	.586 .660	11.7 11.0
1/31/75	Gyro A-012Y - Same as above Using GSA Motor Power Supply (~"Square" Wave)	62.9	.777	10.1

"slotted" to break up the Eddy Current losses in the beryllium base. With the use of the "slotted" base there was approximately a 5 to 10 percent heating rate improvement. The removal of the beryllium copper cavity clamp ring had little effect on the heating rate. The tests with the beryllium gyro (A-012Y) established the current requirement of ~11 amp rms in order to heat at 80°F/minute. A test with the GSA motor power supply, using modified wave shapes, indicated an improvement of heating rate. The wave shape was changed from a sinusoid shape to an approximate square wave.

It was theorized that more efficient induction heating of the rotor might be achieved at a higher excitation frequency. Tests were conducted to investigate the idea, using gyro A012Y, and the breadboard GSA Motor Power Supply. The result of various tests, at varying frequencies greater than 5 kHz, did not exhibit a marked improvement of heating rates, worthy enough to warrant a change from the existing 5 kHz excitation frequency.

Since the induction heating of the rotor is a function of the applied current squared ( $I^2R$  effect) the following relationships apply:

$$\frac{(I_a)^2}{(HR_a)} = \frac{(I_r)^2}{(HR_r)}$$

and

$$I_r = I_a \sqrt{\frac{(HR_r)}{(HR_a)}}$$

where;

$I_i$  = Z-coil current applied; amps rms

$HR_i$  = Heating rate (of rotor) achieved for the applied  $I_i$ ; °F/min.

the subscripts;

a = applied values

r = required values

and;

$HR_r = 80^\circ\text{F/min}$

The column headed "Current Required for 80°F/min" in Tables 3-6 through 3-8 is a listing of equivalent currents required to achieve the goal, using the above stated relationships. The different Z-coil currents were achieved by varying the input voltages to the motor power supply, or adjusting the outputs to specific multiples of the "required" level, as a cross-check of the  $I^2R$  effects.

A convenient means of comparing relative inductive heating "efficiencies", for varying input parameters, is provided by comparing the various Heating Effectivity (HE) values, where:

$$HE = \frac{HR_a}{(I_a)^2}$$

This value of HE is useful for determining the required current ( $I_r$ ) for any required heating rate ( $HR_r$ ) by the relationship:

$$I_r = \sqrt{\frac{HR_r}{HE}}$$

Table 3-7. Z-Coil-Only Rotor Heating Tests Gyro A-012Y, Tabulation of Tests

Test Parameters			Results				
Excit. Freq. kHz	Z Coil Current Amps	Test Duration Secs	Gap Change $\mu$ in.	Heating Rate $^{\circ}$ F/min	Heating Effectivity $^{\circ}$ F/min/A <sup>2</sup>	Current Required for 80 $^{\circ}$ F/min	Rotor Spin up RPS
2.5*	9.34	20	11.5	26.2	.300	16.3	-
	9.34	20	12.5	28.4	.326	15.7	-
	10.25	20	13.5	30.7	.292	16.6	440
	12.1	20	18.0	40.9	.279	16.9	-
3.75*	9.2	20	10.5	23.9	.282	16.8	200
	9.2	20	14.5	33.0	.390	14.3	200
	9.5	-10	13.0	59.1	.655	11.1	-
	10.16	20	16.0	36.4	.353	15.1	210
5.0*	8.1	30	18.0	27.3	.416	13.9	-
	8.1	30	17.5	26.5	.404	14.1	-
	8.6	20	12.5	28.4	.384	14.4	95
	9.3	20	15.5	35.2	.407	14.0	-
5.0	5.65	15	9.5	28.8	.902	9.4	-
	8.2	15	15.0	45.5	.677	10.9	250
	8.3	20	19.5	44.3	.643	11.2	-
	9.5	15	21.0	63.7	.706	10.6	161
	10.83	20	32.5	73.9	.630	11.3	301
	11.2	20	35.5	80.7	.643	11.2	345
	11.3	20	39.5	89.8	.703	10.7	445
	11.3	10	17.5	79.6	.623	11.3	161
	11.37	20	34.5	70.5	.607	11.5	388
6.0	11.38	15	28.0	84.9	.656	11.0	236
	7.65	20	18.5	42.1	.719	10.5	-
	7.65	30	29.5	44.7	.764	10.2	195
	10.02	20	30.5	69.4	.691	10.8	185
7	10.6	20	32.0	72.8	.648	11.1	197
	7.1	30	24.0	36.4	.722	10.5	112
7.5	6.85	20	15.0	34.1	.727	10.5	-
8.0	6.6	30	19.5	29.6	.680	10.9	-
8.0	6.6	15	10.5	31.8	.730	10.5	130
9.0	6.13	32	19.0	27.0	.719	10.5	84
9.0	6.15	5	2.8	25.5	.674	10.9	-
10.0	5.65	20	11.5	26.2	.821	9.9	300

\*Tests conducted with a 'modified' GSA Motor Power Supply

A "modified" design of the motor power supply was used to test at excitation frequencies below 5 kHz together with several repeat 5 kHz 'baseline' checks. The resultant decreased effectivity of rotor heating is shown in Table 3-7. The table is a complete tabulation of all Z-coil heating tests conducted on Gyro A-012Y.

A summary of all Z-coil testing results is shown in Table 3-8 categorized by the specific motor power supply used. The average HE for each excitation frequency grouping is given, together with the accompanying  $I_r$  to achieve the required heating rate of 80°F/min. It can be seen that the "modified" motor power supply was less efficient, approximately 30% less efficient in the 5 kHz gabeline tests, than the GSA power supply. Also, there was a degeneration of HE with a lowering of frequency, as was expected.

Table 3-8. Summary of Z-Coil Heating Test Results, Gyro A-012Y,  
Categorized By Power Supply Used

Power Supply Used	Z-Coil Excitation Frequency kHz	Heating Effectivity (HE) °F/Min/Amp <sup>2</sup>	Current Req'd ( $I_r$ ) For 80°F/Min Amps
'Modified' GSA	2.5	.299	16.4
Motor P/S	3.75	.420	14.3
(Breadboard)	5.0	.403	14.1
GSA Motor Power Supply	5.0	.679	10.9
	6.0	.706	10.7
	7.0	.722	10.5
	7.5	.727	10.5
	8.0	.705	10.7
	9.0	.697	10.7
	10.0	.821	9.9

It appears that the rotor heating rates are affected by the saturation levels of the various transistors in the motor power supply circuit and/or the harmonic content of the Z-coil current. More detailed studies and tests are planned in phase 2B to investigate these parameters and improve the effectivity of the induction current to heat the rotor.

## 11. Stycast Motor - Motor Heating Tests

An imperfect gyro motor, deemed unreliable for use in a system (bare wires) exposed during processing to final configuration) was tested to determine the temperature rise of the windings as a function of Z-coil current and the duration of Z-coil excitation. The motor windings were potted in Stycast 2850 FT.

The test was purposely conducted under adverse conditions. The motor assembly housing was placed on an aluminum plate with only the base of the assembly (shield ring) acting as a thermal conductive path to the aluminum plate. Two thermocouples were attached to the inside diameter of the assembly, viz., vacuum housing/motor assembly interface, directly on the Stycast surface. Three tests, all at 5 kHz excitation frequency, were conducted and the results are summarized in Table 3-9.

Table 3-9. Gyro Motor Temperature Tests

Test Number	Z-Coil Current Amperes	Test Duration (sec)	Temperature Data		
			Initial	Final	$\Delta$ Temp.
1	9.3	60 sec	82°F	180°F	98°F
2	9.3	120	78	260	182
3	11.25	120	79	357	278

Immediately after termination of power input in the third test, the integrity of the Stycast potting was checked and it exhibited no physical degradation, viz, tackiness or softening of the Stycast potting. Additional, more severe tests, possibly to destruction, are planned during Phase 2B to ascertain endurance limits.

## 12. Beryllium-Oxide Support Ring Evaluation

Gyro No. 059 was reassembled to a new configuration. The new assembly includes a beryllium-oxide supporting ring without a cavity clamp ring. The gyro was subjected to Z-coil heating tests to determine the effect of the new configuration on rotor heating rates.

No previous rotor heating rates had been determined for gyro No. 059, in its old 'standard' (N57A type) configuration. The nominal Z-coil-only rotor heating rate for the N57A type gyro is  $-80^{\circ}\text{F}/\text{min}$  with 9.3 amps rms at a Z-coil excitation frequency of 5 kHz.

The results of the rotor heating tests are summarized in Table 3-10.

The results indicate that the configuration changes have a net improvement of ~8 percent on rotor heating. Additional tests will be conducted during Phase 2B to verify the results at various current levels, and possibly various excitation frequencies.

Table 3-10. Summary of Rotor Heating Tests - Gyro No. 059

Current Applied $I_a$ Amps	Test Duration $t_a$ Sec	Heating Rate HR $^{\circ}\text{F}/\text{min}$	Heating Effectivity HE $^{\circ}\text{F}/\text{min}/\text{A}^2$	Current Required $I_r$ For $80^{\circ}\text{F}/\text{min}$ Amps
4.65	40	22.6	1.045	8.75
4.65	40	22.9	1.059	8.69
4.65	60	25.0	1.156	8.32

### 3.2.2.2 Relocation of Test Station IV

Although the MICRON Test Lab was moved to new quarters earlier, the relocation of Test Station IV was delayed until mid-April 1975. The delay served several purposes: (1) allowed utilization of the last of three IBM 1130 Computers remaining at the termination of a lease contract (the lease terminated April 20), (2) allowed real-time gyro gap plotting and concurrent accumulation of temperature data, and (3) allowed additional time for interfacing the new computer and I/O devices with the other test stations in the new lab.

During the process of relocating and repositioning the test stand, and subsequent calibration of the table axes orientations, the feed-through wires for the gyro and associated suspension electronics were damaged, necessitating extensive repairs and wire replacement. Following the repair activity the test station was thoroughly exercised, using suspension-grade instruments for proofing the test station prior to declaring the test station 'ready' for use to test inertial-grade instruments.

The following paragraphs are a chronology of events that followed.



3.2.2.2.1 Testing of Gyro 158 - Getter Tests. The new-build getter gyro No. 158 was mounted, suspended and charge-monitored for an adequate length of time. All precautions, normally observed during initial spin-ups of new instruments, were taken and pertinent signals were monitored and found to be "normal." The rotor was spun up to ~1250 rps, at which time a precautionary check of applicable test signals was made. Noting that all signals looked and checked "normal," the decision was made to spin up to full speed (2430 rps) and polhode damp the rotor. At the time that rotor spin up was to occur, the rotor was suddenly de-suspended.

Functional testing activity came to a halt following the catastrophic failure of Getter Gyro No. 158. Testing activity centered around troubleshooting the test station using suspension-grade instruments. The various activities addressed the problem of locating the probable cause for the rotor de-suspension.

Initially it was discovered that the "Master" Biomation recorder, which records the MUM signals, did not function properly at the time of the rotor drop. Although it did trigger the "slave" Biomation recorder, the "master" itself did not properly record its assigned signals. The defective recorder was replaced and an additional four-channel unit was put into service. The additional unit enabled monitoring a total of 12 signals in the process of further exercising the test station. The additional four channels were used to monitor the four MLAR signals directly at the Suspension Electronic test points and isolate a possible fault in the intervening amplifier stages.

The test station-to-computer interface and data links were tested and exercised via a simulated angle calibration with suspender gyro No. 015. The simulated angle calibration was conducted with the TD frequency near speed notch frequency (~2430 Hz). Subsequent to the simulated angle calibration, the gyro was cautiously spun up, in selected increments, to full speed. All pertinent signals were monitored at the incremental speed levels prior to the next increase. Once the gyro achieved full speed it was polhode damped and allowed to stabilize preparatory to conducting an angle calibration. Following this angle calibration, a drift calibration run was made. Throughout both calibration runs no potential de-suspension problems manifested themselves in either the test stand-to-console or test station-to-computer interfaces.

During the test station troubleshooting procedures, minor problems, including an open heater winding and a defective scanner board (reading gap voltages) in the computer data link, were discovered and the problems resolved. Throughout the investigation and troubleshooting, no direct cause for the rotor drop was found.

As a final exercise, suspender gyro No. 015 was subjected to several iterations of suspending, spinning up to full speed, de-spinning and de-suspending, in a fast turnaround mode and all without incident. The station was then considered safe for testing navigation-grade instruments.

In the interim period before the planned testing of gyro No. 121, getter gyros No. 118 and 158 were successfully tested without incident.

3.2.2.2.2 Testing Gyro No. 124 - Small Gap Gyro. Upon completion of its pre-functional tests, the Small Gap Gyro No. 124, was mounted on Test Station IV, suspended and charge monitored. The gyro was assembled with an oversize rotor designed to provide a gap of  $\sim 150 \mu\text{-in.}$  at operating temperature,  $160^\circ\text{F.}$  The gyro gap was monitored as the case temperature was raised to  $160^\circ\text{F.}$  Z-coil heating was used to heat the rotor to a point where the gap was  $\sim 170 \mu\text{-in.}$ , after the case temperature had reached a stable condition. A servo response test of the suspension servo was made at this junction via TD inputs at varying frequencies. The servo exhibited responses within accepted limits and it was considered that conditions were right to proceed with rotor spin-up. Once the decision was made to proceed with spin-up, all external appendages and cables, with the exception of the spin motor connections and the No. 3 Charge Amplifier monitor lead were removed from the test stand. The removals included the four suspension electronics signal monitor lines going to the Biomation recorder. This action was in keeping with normal precautions to preclude transmission of physical transients to the test stand. The test station was fully prepared for a rotor spin-up.

The rotor was spun up to  $\sim 1250$  rps and damped into a "C" family to minimize MUM amplitude, as a precaution in spinning through servo resonance, prior to spinning up to full speed. The rotor was then spun up to approximately notch speed for polhode damping. The rotor was 'undamped' from the "C" family and was proceeding satisfactorily into the "A" family. During one of the polhode cycles, at a time when no damping current was being applied, the rotor experienced a catastrophic drop.

The visual evidence of the drop consisted of: (1) the loss of recorder signals used in polhode damping, (2) the Vaclon pump current monitor went off scale, (3) the loss of MUM signals on the console oscilloscopes. Neither the ASD Fault Light nor the Biomation recorders were triggered by the rotor drop.

Following the rotor drop of gyro No. 124, an intensive investigation was launched to determine the reason for the lack of a triggering signal for the Biomation Recorders, the lack of the Fault Light to indicate a fault and ultimately find the cause for the second rotor drop within a span of three weeks.

The conclusion reached in the subsequent investigation was that the triggering threshold for the MUM amplitude detector was improperly set. The improper limit setting is attributed to a mistake in scaling of the detector circuitry, the small gap was not properly accounted for.

The MUM amplitude trigger circuit is normally set for a nominal  $300 \mu\text{-in.}$  gap, with the trigger level set near the threshold of the suspension stiffness. The threshold stiffness is approached when the rotor (MUM amplitude) makes an excursion approaching 120 to  $150 \mu\text{-in.}$  into the radial gap. In the case of gyro No. 124, the magnitude of MUM signal required to trigger the ASD Fault Light and Biomation recorder (set for a nominal  $300 \mu\text{-in.}$  gap) far exceeded the threshold of suspension stiffness, with catastrophic results.

Corrective measures have been taken to preclude similar mishaps, in future testing of small gap gyros.

3.2.2.2.3 Updating and Refurbishment of Test Station IV. The investigations that ensued, as a result of the two rotor drops within a three-week period following relocation of the Test Stand, brought to light potential problem areas in the test station. The two failures, coupled with these potential problem areas, brought to a sharp focus by the close scrutiny in the investigations, caused great concern over the functional integrity of the Test Station. After a thorough analysis of the situation, and discussion of the circumstances surrounding the failures, it was decided to suspend further gyro testing. The decision entailed shutting down the test station to enable refurbishment of the station as required to update its capabilities and documentation. A series of tests were performed, using suspension-grade gyros, to re-establish a high confidence level of gyro testing in order to resume testing of navigation-grade gyros.

After an interval of testing of navigation grade gyros, during which Gyro No. 059 and two getter gyro retests were successfully completed, there were two non-spinning rotor drops in mid-July 1975. The circumstances surrounding these drops focused attention on the charge amp connectors. Upon dismantling the suspension electronics package (required for access to repair/inspect the charge amp connector), various electronic modules were rechecked and an additional test point (servo network) was added as an aid to fault monitoring. The charge amp connector had a badly corroded solder connection that was highly suspect of being intermittent, particularly when heated. The entire charge amp connector was replaced, the Test Station has been functioning reliably since then, and various gyros have been tested, including:

1. Small Gap Gyro No. 116 (results reported in Para. 3.2.2.1)
2. Two getter gyro retests (results reported in Para. 6.3.2)
3. Two Second Source gyros.  
Nos. N 0005 and N 0006 (results reported in Para. 3.2.6)

### 3.2.3 Laboratory Test DEM

Testing of the DEM began in early December 1971 in accordance with the test plan submitted as CDRL item A00V (see Paragraph 3.1.1). The DEM, conduction-cooled version, was installed in the temperature test chamber and airflow-pressure drop calibration runs were made and the required orifice plate was fabricated to provide correct airflow distribution to each DEM cold plate. Steady state, room temperature operation runs were started to evaluate normal temperature control characteristics. The temperature controller was found to be deficient in both gain and setpoint level adjustment and was returned to the electronics laboratory for modification. Upon its return to the test laboratory it was found to have sufficient gain in all channels, but still required a slight increase in setpoint adjustment range on the two charge amplifier channels. At this point the test was terminated in compliance with the Stop Work Directive received in December 1971 with no significant test data having been obtained.

### 3.2.4 N57A-1/HAFB GSA Tests

#### 3.2.4.1 N57A-1 Tests

The N57A-1 was to be used for developmental testing in accordance with the test plan covered in Section 3.1.1.1 upon completion of flight testing and refurbishment.

Automatic polhode damping of a 3-wire rotor gyro (~1 sec polhode period) was demonstrated using instrument serial number 100.

Gyros S/N 112 and S/N 86 were installed on the system in the number 1 and 2 positions respectively. Parameters for automatic operation using these instruments were established.

The N57A-1 System Test Console was used to support N57A-2 from 1 November to 15 November. On 11 November the No. 2 gyro suspension and MUM read-out modules were swapped between N57A-1 and N57A-2 to correct a calibration noise problem on N57A-2.

From 15 November through the beginning of December, successive drift calibrations (partial and complete) were conducted in an effort to isolate the calibration noise problem (which came from the modules swapped from the N57A-2) to a particular module. The intermittent nature of the problem accounted for the long time required for fault isolation.

Modules were interchanged from channel-to-channel in groups and singularly between the drift data collections to isolate down to the X-Servo Network module as being the cause of the noisy data.

During this period, the gyro in the No. 1 slot dropped due to a faulty Charge Amplifier. The Charge Amplifier had a metallic object shorting a conductive pad to the lid.

On 10 December with the system installed on the Goertz Table and oscillatory motion of  $\pm 5$  degrees with a period of 13 seconds on each axis, the demonstration of in-motion polhode damping was accomplished, i.e., polhode motion was damped to a level less than or equal to that observed after polhode damping a stationary system.

On 11 December, a damped inertial navigation mechanization (developed on Marine Systems Division funding for the Navy) was evaluated for the first time, however there were definite breaks in velocity which coincided with shifts in indicated gap of gyro No. 2. This problem was traced to charge amplifiers although a single charge amplifier could not be pin-pointed as the cause. Therefore, all eight charge amplifiers were swapped with those in the HAFB subassembly.

In the course of rebalancing charge amps and recalibrating the system, one gyro was sparked, and one gyro incurred a full speed drop. The sparking was caused by an intermittent charge amplifier in the -4 position. The full speed drop was caused by a thermally sensitive modulator.

After cleaning up the above problems, the system was running well, had undergone calibration, and a 24 hour Scorsby run with the damped inertial mechanization.

Future activities called out in the test plan were discontinued per the Stop Work Order received in December.

Near the end of March 1975, Air Force permission was granted to use the N57A-1 system for non-developmental testing. Tests conducted during April 1975, included HP 2100 calibration software checkout, spare module checkout, automatic polhode damping of low-extrusion ratio rotors, and testing related to the preparation of the N57A-2 system for RF-4C flight testing.

Since the HAFB Gyro Subassembly has no accelerometers, the N57A-1 system was used to debug the EMA calibration portion of the software developed for the new HP 2100 system. This effort was completed on 28 March 1975.

The N57A-1 system was used to verify the operation of the spare Spin Motor Power Amplifier (SMPA), the Spin Motor Control electronics, and the Spin Motor Timing electronics. The interchangeability of the electronic modules with the Spin Motor Power Amplifier was also verified. This consisted of measuring the dc voltages applied to the motor by the SMPA when all the computer inputs are in the "ZERO" state. With all combinations of the SMPA and electronic boards, the dc voltages were less than the 5 mv required for successful motor degaussing during the spin-up sequence. Concurrently, the operation of the spare Demod Reference Generator was checked out. This effort was completed 15 April 1975.

During the period of 16 April 1975 through 25 April 1975, the N57A-1 system was used to perform tests in support of the up-coming RF-4C flight testing of the N57A-2 system. These tests included verifying the operation of the cold plate air flow valve and thermal tests to optimize the location of the gyro case temperature sensor. Since minimal environmental control was available in the RF-4C, it was necessary to minimize gyro case temperature variation due to cold plate temperature changes. To determine the corrective action to be taken on the N57A-2 system, temperatures were monitored on the gyros during rotor spin-up and damping while varying the cold plate temperature. The results of this testing indicated that the gyro case temperature sensors should be moved from the bracket holding the suspension electrode on the gyro to the middle of the Vacion pump housing near the spin motor. Also, the steps required to make the cold plate air flow valve operational were determined.

During the course of the thermal testing, A/D Converter S N A003Y was tested several times after attempts to correct a problem related to reading out the gyro No. 1 gap voltage. This problem has not yet been resolved. In addition, several attempts were made to automatically polhode damp gyros containing low-extrusion ratio rotors. The rotors were successfully damped on only 25% of the attempts. In order to correct this problem, a major software modification of the polhode damping program would be required. It is not intended that this modification will be performed because there are presently sufficient spare system gyros with the "W" series rotors (not low-extrusion ratio rotors). The thermal tests were concluded on 25 April 1975.

On 7 May 1975, the inertial instruments, MIB assembly, spin-motor power amplifier, power supply and all electronic modules were removed from the N57A-1 system housing. The N57A-1 housing was then sent to Kirtland AFB for a physical fit check in the RF-4C pallet. The housing remained at Kirtland AFB until it was returned to Autonetics on 24 June 1975.

Upon inspecting the N57A-1 housing, after its return from Kirtland AFB, it appeared that it had been dropped on its left side. The IMU handle/support brackets had dents on them and the back-up battery connector was loose. The battery protective cover was damaged and had been repaired. Further battery tests revealed eleven bad cells.

The battery unit was repaired and the system was reassembled and returned to operational status.

Due to the cancellation of RF-4C tests of the N57A-2 because of aircraft unavailability, the N57A-1 system was set aside and used for spares for the N57A-2.

#### 3.2.4.2 HAFB Gyro Subassembly Tests

A series of seven angle calibrations in support of the Short Term Calibration Repeatability testing was completed on 4 February 1975. This testing was done on the Goerz table and between each of the calibrations the gyro subassembly was shut down, allowed to reach room temperature, and then restarted. An associated drift calibration was also taken with each angle calibration, except for the last one. During the seventh drift calibration a +5 vdc power supply in the Goerz table electronics failed necessitating test termination. However, the seven angle calibrations and six drift calibrations provided a sufficient data sample to accomplish the objectives of the testing. The results of these tests are presented in Appendix A.

After the Goerz table electronics were repaired, testing was resumed on 17 February 1975. This testing supported the HP 2100 software checkout. Testing was suspended when the N57A-2 system returned for recalibration on 21 February 1975.

Testing resumed on 28 February 1975. The test effort was directed toward characterizing the spare system gyros. Characterization consists of a gyro operational check-out followed by an RSA polar angle and drift calibration. Six gyros underwent this testing during March.

The Gyro Subassembly was also used to support the checkout of HP 2100 software required for the eight-plate GSA. This was done concurrently with gyro characterization.

During April, the primary effort was directed toward characterizing spare system gyros. This included a complete functional check, charge monitoring, MUM magnitude measurement, and baseline angle and drift calibration. Drift data was also taken over many 24 hr periods to be used in the evaluation of the Polar vs MSA Drift Calibration. During the course of this testing, the HAFB GSA was periodically used for checkout of the HP 2100 software in support of GSA testing.

From 28 April 1975 through 16 June 1975 the N57A-2 system was at Autonetics for modification and recalibration prior to RF-4C flight testing. During the first half of this period, the HAFB GSA was used to characterize Gyro No. 136. An RSA polar angle calibration and drift calibration were performed. This was completed on 12 May 1975.

From 12 May 1975 through 16 June 1975 the data acquisition console was used to support the N57A-2 recalibration effort, hence, no further gyro tests were performed

on the HAFB GSA. However, this opportunity was taken to modify a set of electronics required to support the small gap gyro evaluation. The modified modules were installed in the GSA and thoroughly checked-out.

Preparation for small gap gyro testing resumed on 17 June 1975. In order to optimize the probability of successful suspension of the small gap gyro, a normal gap suspender gyro was installed on the GSA. Several unsuccessful attempts were made to suspend the normal gap gyro. Since the gyro was cold the gap was of the order of 370 micro-inches. The gyro was heated with the rotor desuspended in order to decrease the gap to approximately 300 micro-inches. Attempts to suspend at this gap were successful about 50 percent of the time. It is believed that with the small gap gyro (170 micro-inch) suspension should be successful.

A small gap gyro became available in late July 1975. This gyro will be tested early in Phase 2B in accordance with the Paragraph 3.1.4.2 Test Plan.

### 3.2.5 Test Gyro Subassemblies

#### 3.2.5.1 Eight-Plate GSA

Fabrication and checkout of the eight-plate GSA and GSA Test Station were completed during February and March 1975. Integration of the GSA and Test Station proceeded to the point of servo loop verification with a capacitive load. Suspension with a suspension grade gyro was not attempted at this time due to noise pickup on critical signals. The eight-plate GSA was removed from the Test Station and returned to the electronics laboratory where fixes were incorporated to eliminate noise and noise susceptibility. While the eight-plate GSA was in the electronics laboratory, the GSA Test Station was utilized to integrate the four-plate GSA and integration proceeded to the point of servo loop verification with a suspended suspension grade gyro.

During April, the eight-plate GSA was returned to the GSA Test Station from the electronics laboratory. Three different suspension grade gyros were levitated but difficulties were encountered in obtaining consistently good lift offs. The lift off problem was solved by a combination of timing, electronic changes and de-activation of all-attitude lift-off in favor of sine wave lift-off. Charge monitoring techniques were developed and a software program to access and plot MESGA data was developed and utilized. During computer data access it was noted that the GSA servo loop was shocked into the high "G" mode.

The problem of servo loop shock during computer data access was solved in early May when non-terminated ground lines between the computer and GSA Test Station were discovered and properly grounded. MESGA data was taken from suspended, non spinning gyros during 24 hour periods when gyro temperature was stabilized at +160°F. It became apparent during this time period that the Ultradex Table must be operated with extreme care to prevent table induced shock inputs which exceeded the suspension servo capability.

The table was instrumented with accelerometers to determine the magnitude of these inputs which turned out to be 9-g's at a frequency between 300 and 1000 Hz. The 9-g's was the highest level and caused by the index control lever on the outer table axis. Dampers were installed, and this high polhode was minimized for this source of shock input. Shock caused by gear teeth engagement of the Ultradex tables was correctable only by having the table operator exercise caution when engaging gear teeth.

In early June it was concluded that certain unexplained, intermittent shut downs were being caused when the GSA switched from the low to the high "G" mode. This problem was solved by disabling the high "G" mode while increasing the low "G" mode by 1.5 times to 170 volts.

Two non spinning MESGA calibrations were accomplished and evaluated. Manual spin-up and polhode damping occurred at frequencies below 1 kHz. Frequency response of the servo loop was such that charge amplifier saturation occurred at about 1 kHz and rotor spinning above 700 Hz may have caused loss of control and gyro damage.

During early July gyro damage occurred while a spinning MESGA calibration was in progress. Shut down was caused by striking a gear tooth during positioning of the Ultradex Table. The GSA was moved to an Imperial Table where testing continued after gyro repair. No additional problems were encountered and the required MESGA test data was acquired. These test results are given in Para. 6.3.5.5.

#### 3.2.5.2 Four-Plate GSA

During March 1975, the four-plate GSA was checked out and integrated with the eight-plate GSA Test Station. Integration proceeded through servo loop verification with a suspended suspension grade gyro.

Upon completion of servo loop verification with the suspension grade gyro, the four-plate GSA was set aside so that the GSA Test Station could be dedicated to eight-plate GSA checkout. It was intended to resume four-plate GSA testing when the second GSA Test Station was completed. This test station was completed and verified. However, no further testing of the four-plate GSA with the station was performed. Four-plate GSA testing was deemphasized because cost projections showed PWM 4-plate electronics costs to be higher than standard 8-plate electronic costs.

#### 3.2.6 Test Northrop Rotors and Cavities

The testing of Northrop rotors and cavities is complementary to the task of developing Northrop as a second source (see Para. 6.1.5). The initiation of the task depended upon the receipt of parts which were to be processed thru final fabrication sequences by Northrop. The cavity items were originally furnished to Northrop by Autonetics in a condition ready for plating and the rotors had been eloxed and were ready for lapping. Northrop processed the parts through the final stages of fabrication. The delivery of the parts from Northrop to Autonetics was:

<u>No. of Sets</u>	<u>Month</u>
1	February 1975
1	March 1975
2	April 1975
2	May 1975



Measurements and evaluation were completed on the items and the results and evaluations were transmitted to Northrop. All data were formally transmitted to Northrop through AFAL. In addition to the above activity, Northrop master cavity parts and rotors were evaluated at Autonetics for size and roundness. The results were documented and sent to Northrop via AFAL.

### 3.2.6.1 Northrop Cavity/Rotor Evaluation Summary

1. Cavities - The first four sets of cavities as finished by Northrop were of nearly adequate quality for instrument use except for the following:
  - a. Plating Surface Finish. The general appearance of the plating was good but there were deep random lapping scratches which were judged too deep for instrument use. The scratches were a result of final lapping using the hand lap tool.
  - b. Equatorial Location. There were discrepancies between Autonetic's and Northrop's measurement of equatorial location. There is an indication that Northrop was missing the location by about 10  $\mu$ -inches.
  - c. Slots. The separating slots between electrodes were not cleaned up properly. It is assumed this problem was caused by the slot cutting tool material. Cavity set N0002 showed some indication of lifted plating at the slot edges. It is currently thought that this anomaly was caused by the two step chrome gold plating sequence Northrop was using or excessive pressures/forces used during slot lapping.
  - d. Plating. Plating material extended from the electrode area through the spring-button cavity holes to the back side of the cavities. The plating could cause electrode short circuit to ground and to each other (through ground).
2. Rotor - The first rotors as finished by Northrop were of nearly adequate quality for instrument use except for the following:
  - a. The rotors were not symmetrically out of round with respect to the axis of anisotropy. Extended pitch lapping at Northrop was the assumed reason for the discrepancy.
  - b. Surface discrepancies ("dings") were noted on the rotors as provided by Northrop. This defect was assumed to be caused by handling during processing.

The last two sets of parts delivered by Northrop (N0005/Z23 and N0006/Z20) looked good and were considered adequate for navigational grade instruments.

N0005/Z23 and N0006/Z20 were assembled into N57A type MESSG units and successfully passed the prefunctional test, bake out and cold soak. The units were

then functionally tested on T/S IV after the relocation and repair of the test station. The results of angle calibration and drift calibration were:

	Angle Cal Residuals	Drift Cal Residuals
N0005/Z23	0.126 mrad	0.006 deg/hr
N0006/Z20	0.060 mrad	0.006 deg/hr

These results are considered to be good.

N0003, Z16 was assembled into an instrument (beryllium base configuration) and used as a levitator unit in support of MESGA test station evaluation. A request was made by Northrop for Autonetics metrology unit to measure their three master cavities. This effort was conducted to resolve the slight difference in dimensional measurement between Autonetics and Northrop. The three master cavities, two made from beryllia and one from stainless steel, were measured at room temperature and again at 68°F. The measured values at both temperatures were recorded and the coefficient of expansion, evaluated at the nominal cavity size, was extrapolated. This effort will continue until all problems concerning measurements between Autonetics and second source are resolved.

Information gathered to date is encouraging. All assembled units (N0006/Z20, N0005, Z23, and N0003, Z16) were mechanically and electrically cavity aligned without problem. Prefunctional test was accomplished in a normal manner. No problems were experienced in the functional test of N0005 and N0006.

There was an intentional omission of the originally planned electrode to BeO adhesion test as called out in the test plan. The omission was verbally reported to AFAL in a Telecon. The reason for the omission was that only the last two cavity sets provided by Northrop were processed in a single step chrome gold plating operation and therefore are typical of parts to be fabricated in the future. Since these are the only two "typical" sets of parts and since Autonetics is committed to evaluation of two full-up instrument configurations, a destructive adhesion test could not be performed at the present time.

Autonetics conducted an evaluation of Northrop parts for rotor min-max size, roundness check, cavity sphericity, depth, and equator location. All measurements were documented and sent to Northrop via AFAL.

The serial number of parts subjected to the above are:

<u>Cavities</u>	<u>Rotors</u>
N0001	No. 2
N0002	No. 7
N0003	Z13
N0004	Z16
N0005	Z20

<u>Cavities</u>	<u>Rotors</u>
N0006	Z21
Master No. 7	Z22
BeO Master	Z23
Master N-1	

### 3.3 FLIGHT TEST ENGINEERING

In Task 2.3, Flight Test Engineering, Engineering supported Flight Operations in the operation, testing, and maintenance of the N57A-1 and N57A-2 systems during LAX flight testing. Autonetics conducted post flight analysis on the N57A data.

#### 3.3.1 Flight Test Support

##### 3.3.1.1 N57A-1 Flight Test Support

N57A-1 flight testing at LAX began in June 1974 and continued into July 1974. A total of seven N57A-1 flights were completed.

A high speed taxi run was made on 6 June 1974 and system performance was acceptable. A short (1 + hours) flight was made on 7 June. It was noted during the flight that the altitude was incorrect. Post flight investigation disclosed that Aircraft/ System wiring to the altitude transducer was incorrect. In effect the output was floated and read zero at all times. The wiring was corrected.

Flight No. 1 (FT1) was the initial checkout flight. The results of the second flight were generally very good; however, the altitude problem persisted. Indications were that the bias for the transducer output was incorrect. The results of the third flight were somewhat degraded with respect to the previous flight. Post flight investigation disclosed that the altitude transducer had failed. It was replaced by a transducer that has a maximum altitude of 20 K ft. All future flights were limited to this altitude until a replacement 50 K ft transducer could be obtained. Flight No. FT7 was terminated due to a computer halt during the flight.

Flight testing of the N57A-1 system was considered completed after Flight 7 so that the N57A-1 could undergo refurbishment. LAX flight testing was completed on the N57A-2 system prior to its going to HAFB for flight testing.

##### 3.3.1.2 N57A-2 Flight Test Support

A total of five N57A-2 flights were completed at LAX. Flights 1 and 2 were relatively benign and similar to those conducted during N57A-1 flight testing. Flights 3 and 4 were aggravated flights, i.e., with maneuvers, and simulated an F-4 environment within the capability of the T-39 Sabreliner. The sequence of maneuvers is further detailed in Section 3.4. Flight 5 was a transport flight to HAFB. Upon arrival at HAFB, the N57A-2 system, flight test panel, flight rack, and associated cables and hardware were removed from the T-39 Sabreliner and moved into the laboratory at HAFB.

The actual checkpoint data was incorporated into the N57A-2 LAX Flight test data error computations. The checkpoint data is that data which is derived from the pictures of VOR stations taken at the same instant that N57A-2 position data was recorded. This data existed for all flights except Flight No. 5 from LAX to HAFB and was provided for use during Post Flight Analysis.

During this flight testing, no significant problems were encountered. These tests completed the LAX flight testing of the N57A systems.

### 3.3.2 Post Flight Analysis

This task includes the compilation of position error history plots, time interpolation to a standard time reference, and interpolation to define error distribution quantiles (CEP and 90th percentile). Least-squares straight-line fits to the quantile curves were used for summarizing systems performance.

Flight testing of the N57A systems at Los Angeles International Airport was completed in October, 1974. Seven flights were made with the N57A-1 system and five flights were made with the N57A-2 system. The test results for the N57A-1 flights are summarized in Table 3-11. Similarly, Table 3-12 is a summary of the N57A-2 test results. The time RMS Velocity Error is the average for the two channels and is only for the pre- and post-flight portion of the navigation run since no accurate reference velocity was available during flight. Range error plots for the N57A-1 Flights are shown in Figures U-1 through U-7 of Appendix U. Figures U-8 through U-12 of Appendix U present similar data for the N57A-2 Flights.

The CEP and CEP rate were computed for the set of seven N57A-1 flights and the set of five N57A-2 flights. The rms of the average per channel velocity errors has also been computed for the same sets of data. The CEP rates and velocity errors are presented in Table 3-13.

The CEP time history of the seven N57A-1 flights is shown in Figure 3-5. The CEP time history of the five N57A-2 flights is shown in Figure 3-6.

Numerous requests were received for velocity error data on N57A flights conducted at LAX. No velocity error plots had been generated because the only velocity error data available was that taken prior to and just after the flight. During the actual flight, no velocity reference was available and, hence, no velocity error data.

As a part of the data reduction effort required for the C-141 and UH-1 flight testing at HAFB, the HAFB personnel developed a computer program which estimates velocity error based upon the position error data obtained during flight. This program was supplied to Autonetics by HAFB and was modified to run on Autonetics' HP 2100 computers.

While modifying the velocity estimation program, a number of desirable features were added. The program computes the radial error rate and the time rms velocity error for each flight using both the actual data as well as the estimated position and velocity data.

For the data set in question the program computes:

1. CEP vs Time - The CEP at a given time is computed for the data set in question.

Table 3-11. N57A-1 Flight Test Summary

N57A-1 LAX Flight Test Results							
Flight No.	Date	Radial Error Rate (nm/hr)	Pre and Post Flight Time RMS Velocity Error (ft/sec)			Flight Time	Route/ Destination/Remarks
			Average Per Channel	North	East		
Ft 1	6-07-74	2.37	17.96	20.09	15.55	1 Hr 10 Min	E-W/Blythe (Initial checkout flight)
Ft 2	6-26-74	0.36	5.30	6.20	4.22	3 Hr 20 Min	N-S/Medford
Ft 3	6-27-74	1.12	11.17	13.21	8.65	2 Hr 5 Min	E-W/Phoenix
Ft 4	7-05-74	0.90	2.08	1.34	2.61	2 Hr 35 Min	NE-SW/Bryce Canyon
Ft 5	7-08-74	1.75	6.69	8.07	4.93	2 Hr 50 Min	NE-SW/Bryce Canyon
Ft 6	7-09-74	0.36	4.71	4.55	4.86	2 Hr 45 Min	NE-SW/Bryce Canyon
Ft 7	7-10-74	3.05	1.85	1.92	1.79	2 Hr 10 Min	Rect/Sar Diego, Phoenix, G. C. (computer failure)

Table 3-12. N57A-2 Flight Test Summary

N57A-2 LAX Flight Test Results.						
Flight No.	Date	Radial Error Rate (nm/hr)	Pre and Post Flight Time RMS Velocity Error (ft/sec)			Flight Time
			Average Per Channel	North	East	
Ft 1	9-30-74	0.47	3.17	2.23	3.89	2 Hr 40 Min
Ft 2	10-1-74	0.45	5.66	4.49	6.63	2 Hr 35 Min
Ft 3	10-2-74	0.37	3.08	1.79	3.97	1 Hr 20 Min
Ft 4	10-3-74	0.23	2.49	1.76	3.05	1 Hr 20 Min
Ft 5	10-7-74	0.97	4.09	4.37	3.79	1 Hr 55 Min
						NE-SW/ Bryce Canyon
						Rect/San Diego, Gila Bend, Grand Canyon, LAX
						Aggravated Flight
						Aggravated Flight
						E/HAFB

Table 3-13. CEP Rates and Velocity Errors

Data Sample	CEP Rate (nm/hr)	AVE/Channel Time rms Velocity Error (ft/sec)
N57A-1 (7 Flights)	1.09	8.86
N57A-2 (5 Flights)	0.42	3.86

2. CEP Rate vs Time - A least square fit is done on the CEP vs Time data from Time = 0 to the time in question. This fitted line is forced to pass through the origin.
3. Time RMS Velocity Error vs Time - An ensemble Time RMS Velocity Error from Time = 0 to the time in question is computed.
4. RMS Velocity Error vs Time - An RMS Velocity Error is computed vs Time for the data set under consideration.

In the above four cases, the computations are done using the estimated position and/or velocity data output from the program

This program was run using two sets of data. Namely, the seven N57A-1 flights at LAX and the five N57A-2 LAX flights. The estimated radial error rate and time RMS velocity for each individual flight is presented in Table 3-14. The numbers in parentheses are those obtained using the actual position errors and the actual pre- and post-flight velocity data. This corresponds to the flight data presented in Tables 3-11 and 3-12. In all cases the time increment between estimated data points is five minutes.

Figures 3-7 through 3-10 present (1) CEP vs Time, (2) CEP Rate vs Time, (3) Per Channel Time RMS Velocity Error vs Time, and (4) Per Channel RMS Velocity Error vs Time for the seven N57A-1 flights at LAX. Figures 3-11 through 3-14 present similar data for the set of five N57A-2 flights at LAX.

The plots of CEP vs Time (Figures 3-7 and 3-11) should allow comparison to ACF requirements regarding position accuracy. In addition, the plots of RMS Velocity Error vs Time should relate directly to the ACF velocity requirements.

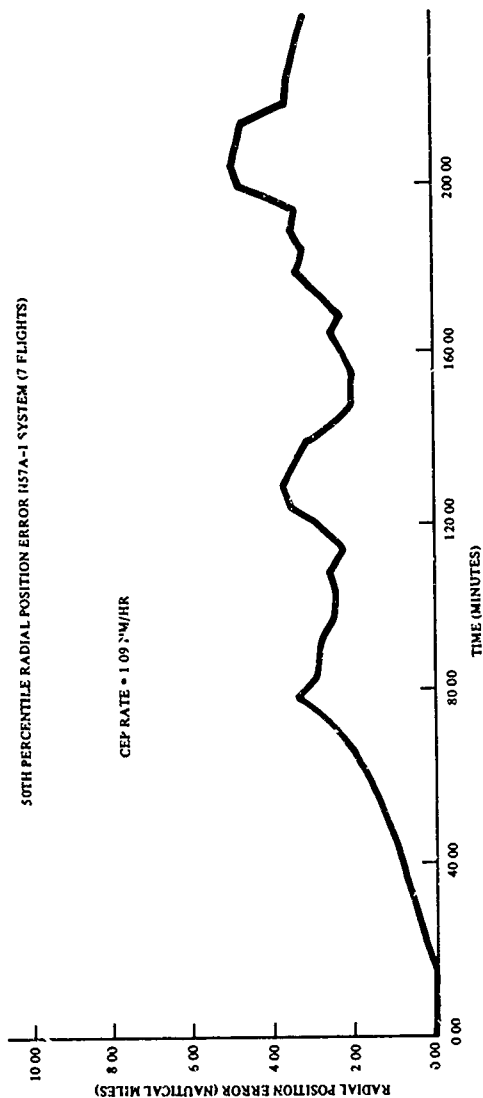


Figure 3-5. N57A-1 CEP Time History



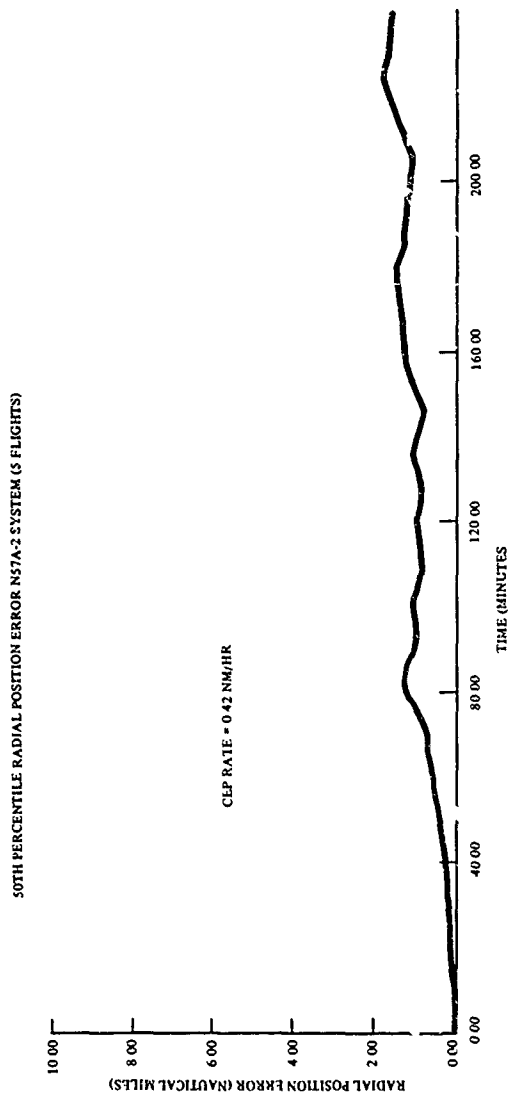


Figure 3-6. N57A-2 CEP Time History

Table 3-14. N57A LAX Flight Test Results

FLIGHT NO.	DATE	RADIAL ERROR RATE (NM/HR)	TIME RMS VELOCITY ERROR (ft/sec)			FLT HRS	NAV HRS	ROUTE/ DESTINATION/ REMARKS
			AVG PER CHANNEL	NORTH	EAST			
N57A-1-1	6-07-74	3.204 (2.971)	22.623 (17.970)	25.740 (20.098)	19.001 (15.553)	1.17	2.83	E-W/Blythe (initial checkout flight)
-2	6-26-74	0.413 (0.364)	5.113 (5.307)	5.221 (6.204)	5.405 (4.224)	3.33	5.42	N-S/Medford
-3	6-27-74	1.170 (1.121)	10.71 (11.170)	12.932 (13.216)	7.924 (8.653)	2.08	3.58	E-W/Phoenix
-4	7-05-74	1.101 (0.907)	7.631 (2.082)	5.301 (1.345)	9.409 (2.619)	2.58	4.17	NE-SW/Bryce Canyon
-5	7-08-74	2.019 (1.757)	12.208 (6.691)	11.992 (8.074)	12.421 (4.933)	2.83	4.58	NE-SW/Bryce Canyon
-6	7-09-74	0.441 (0.367)	6.038 (4.714)	6.057 (4.560)	6.018 (4.863)	2.75	5.25	NE-SW/Bryce Canyon
-7	7-10-74	3.613 (3.053)	7.527 (3.851)	8.697 (4.130)	6.139 (3.551)	2.17	1.60	Rect/San Diego, Phoenix, Grand Canyon (computer failure)
N57A-2-1	9-30-74	0.416 (0.479)	3.458 (3.177)	2.752 (2.236)	4.044 (3.897)	2.67	5.30	NE-SW/Bryce Canyon
-2	10-01-74	0.425 (0.454)	4.933 (5.668)	4.061 (4.493)	5.672 (6.638)	2.58	4.92	Rect/San Diego, Gila Bend, Grand Canyon, LAX
-3	10-02-74	0.410 (0.379)	3.605 (3.084)	2.825 (1.799)	4.244 (3.974)	1.33	3.73	Aggravated Flight
-4	10-03-74	0.259 (0.254)	2.446 (2.495)	1.773 (1.761)	2.970 (3.058)	1.33	4.17	Aggravated Flight
-5	10-07-74	1.036 (0.979)	6.974 (4.093)	5.711 (4.370)	8.041 (3.795)	1.92	4.00	E/HAFB

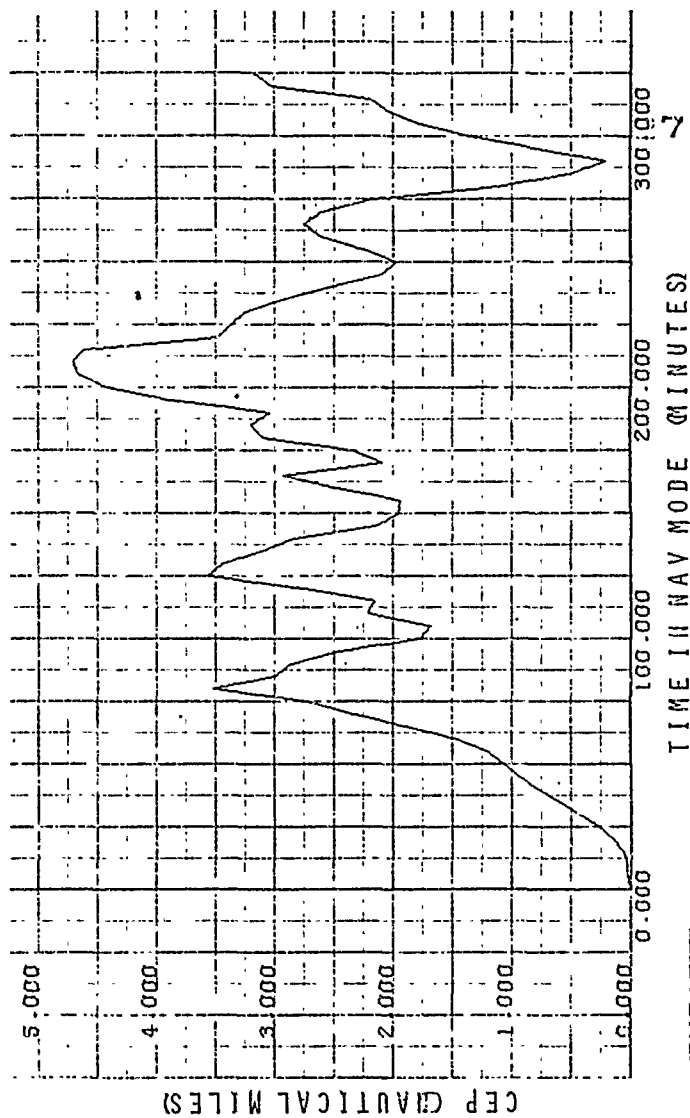


Figure 3-7. CEP vs Time: 7 N57A-1 LAX Flights

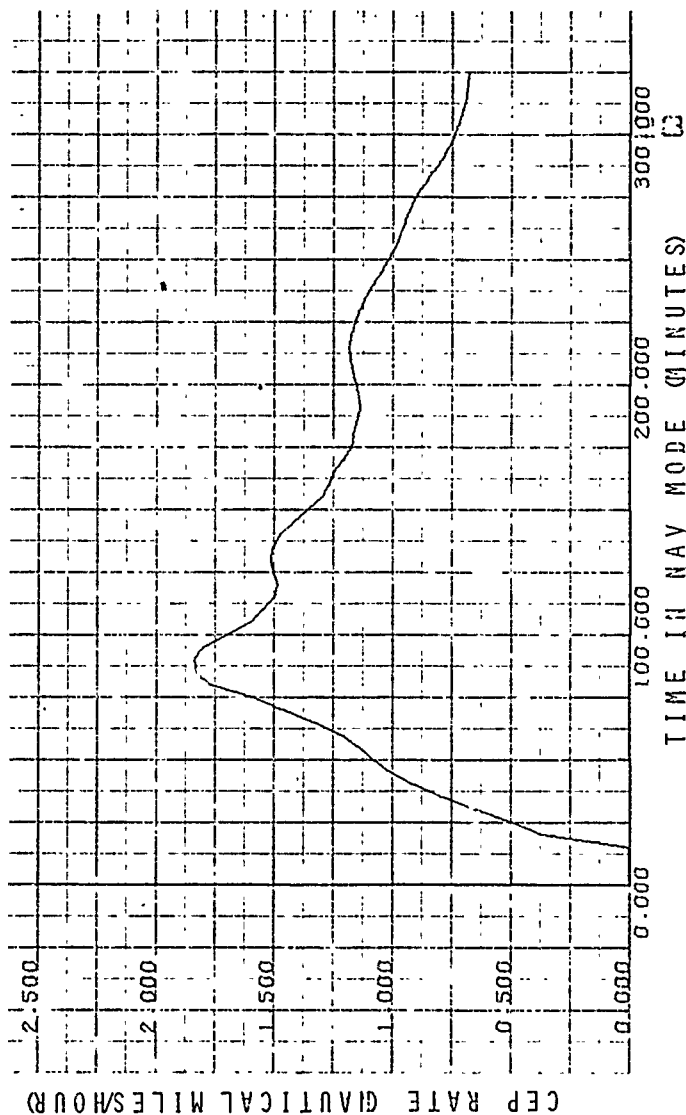


Figure 3-8.. CEP Rate vs Time; 7 N57A-1 LAX Flights

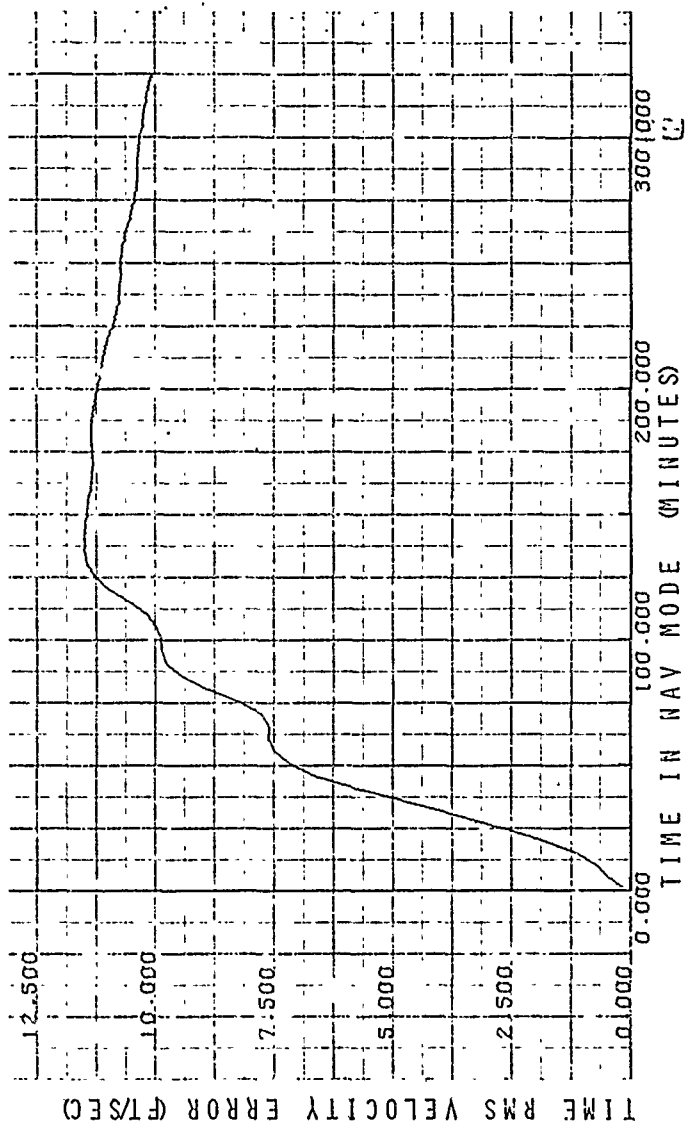


Figure 3-9. Per Channel Time RMS Velocity Error vs Time; 7 N57A-1 LAX Flights

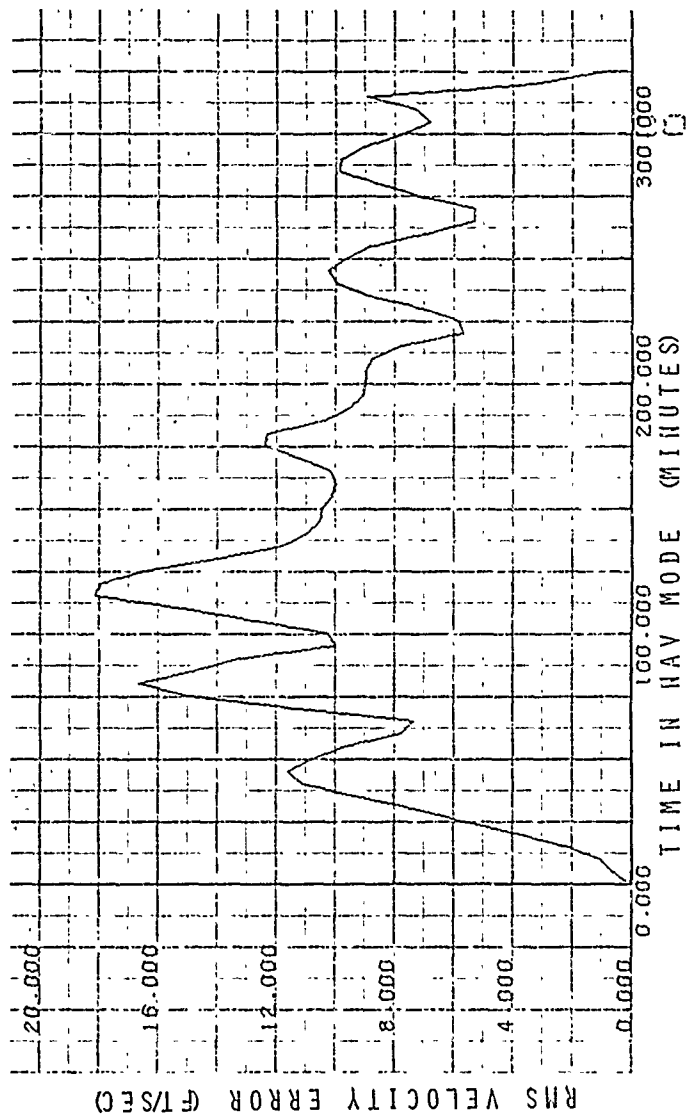


Figure 3-10. Per Channel RMS Velocity Error vs Time; 7 N57A-1 Flights

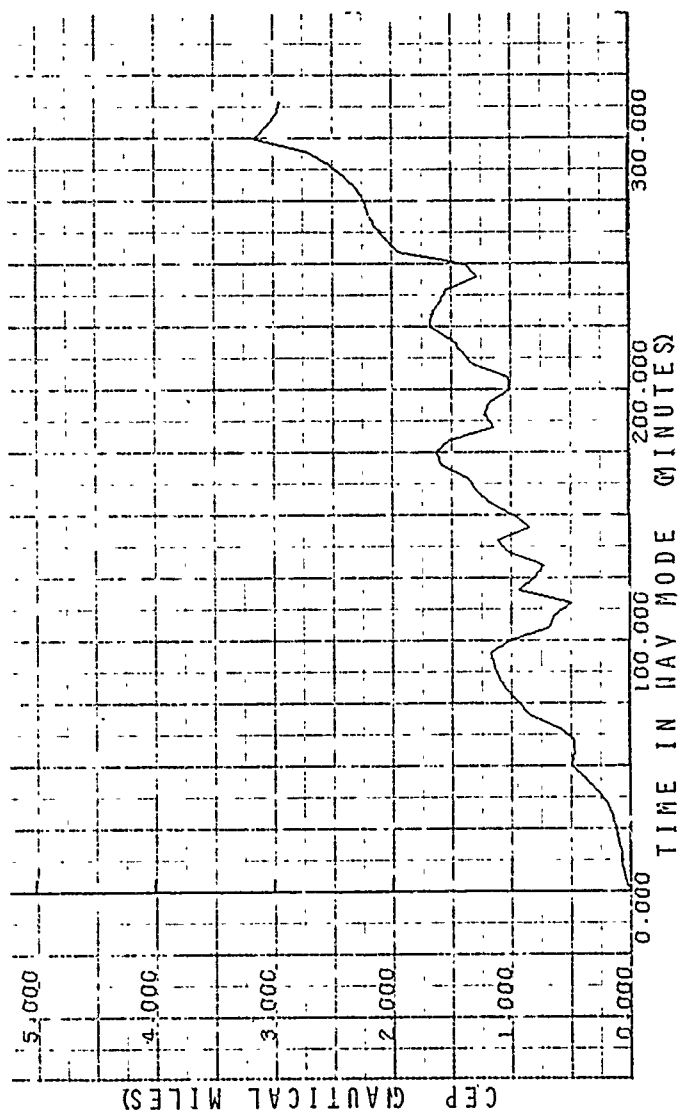


Figure 3-11. CEP vs Time; 5 N37A-2 LAX Flights

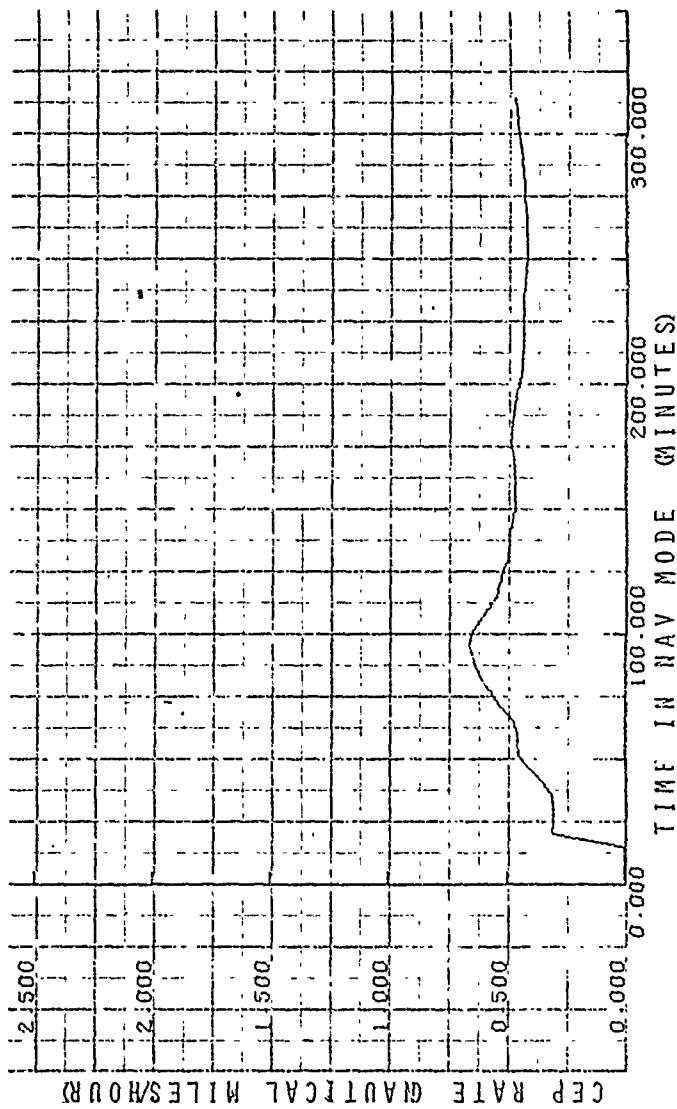


Figure 3-12. CEP Rate vs Time; 5 N57A-2 LAX Flights



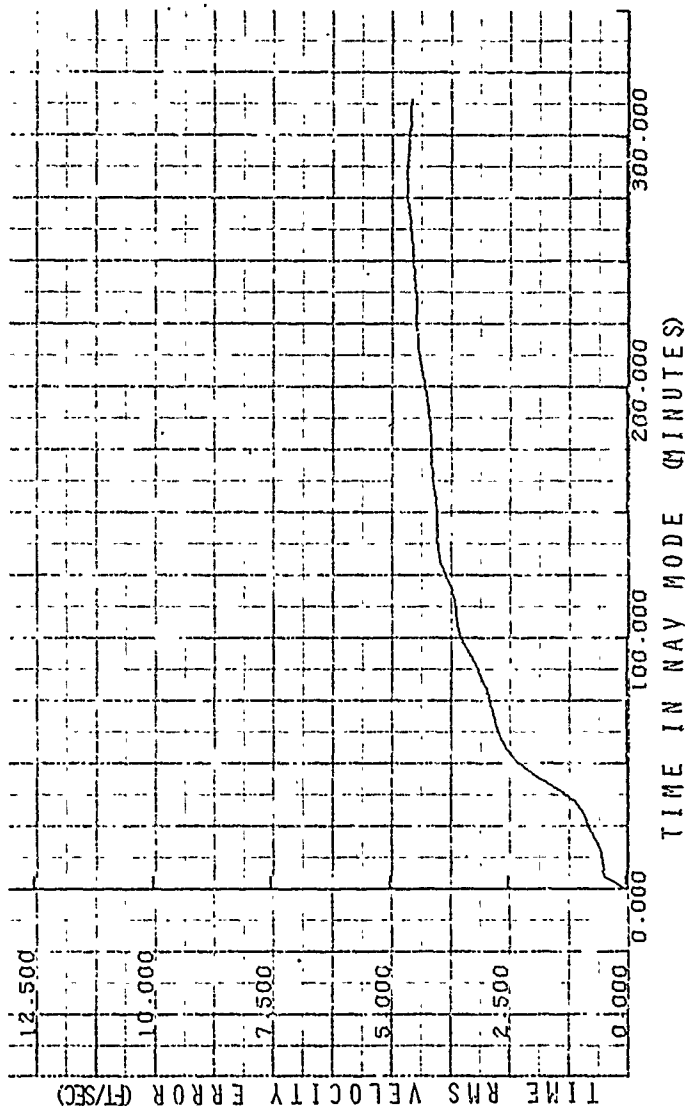


Figure 3-13. Per Channel Time RMS Velocity Error vs Time; 5 N57A-2 LAX Flights

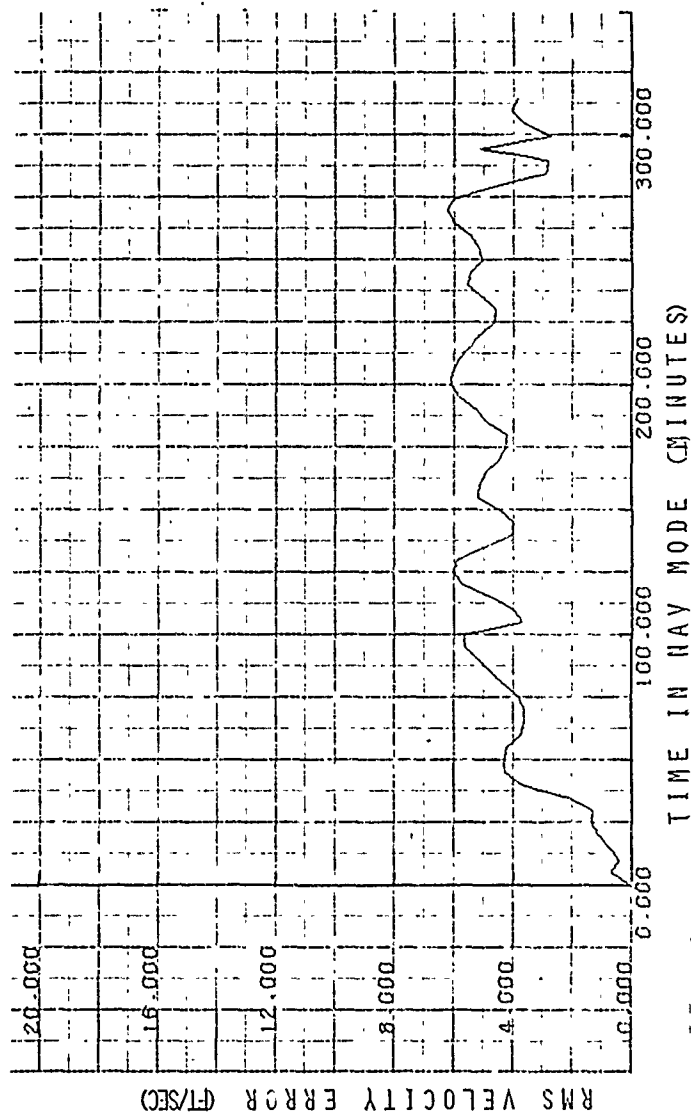


Figure 3-14. Per Channel RMS Velocity Error vs Time; N57A-2 LAX Flights

### 3.4 FLIGHT TEST OPERATIONS

In Task 2.4, Flight Test Operations, Autonetics flight tested N57A-1 and N57A-2 at Los Angeles International Airport (LAX).

During May 1974 all aircraft modifications for flight testing the N57A-1 System at LAX and the flight test plans were completed. The N57A-1 System was received on 16 May and installed into the T39 aircraft on 21 May 1974. The aircraft reserve power and the power transfer system malfunctioned during the initial checkout testing. The cause was located and corrected. The N57A-1 system was removed as discussed in Para 5.3.1 from the aircraft and reinstalled on May 31. Dummy load tests and power transfer tests were run successfully. Checkout testing was completed and flight testing was started in June.

Seven flights were completed with the N57A-1 installed in the T-39 aircraft. Details of the flights are discussed in Section 3.3 of this report.

Five flights were completed with the N57A-2 installed in the T-39 aircraft. Details of the flight are discussed in Section 3.3 of this report. MICRON flights 10 and 11 (N57A-2 flights 3 and 4) were aggravated flights. A list of maneuvers performed during these flights is summarized in Tables 3-15 and 3-16.

This series of flight tests on the N57A-2 system completed the planned flight test program on the two N57A systems at Los Angeles International Airport (LAX). The T-39 aircraft was refurbished to its configuration prior to the N57A flight test program.

Table 3-15. Summary of Maneuvers, N57A-2 Flight 3

Maneuver Number	Description of Maneuver	Airspeed (knots)	Peak Acceleration (g's)
1	Left aileron roll, 60 deg/sec	300	1.75
2	Right aileron roll, 60 deg/sec	300	1.8
3	Left max rate roll, 120 deg/sec	200	1.05
4	Right max rate roll, 120 deg/sec	200	0.85 to 1.1
5	Loop left	N/A	4.0
6	Loop right	N/A	4.0
7	360° turn left; 70° bank angle	N/A	3.2
8	360° turn right; 75° bank angle	N/A	3.5
9	Wing-over left	N/A	1.2 to 0.5
10	Wing-over right	N/A	1.2 to 0.5
11	40° pitch-up stall	N/A	0.6
12	Max deceleration: 400 knots to 200 knots in 10 sec	-	-

Table 3-16. Summary of Maneuvers, N57A-2 Flight 4

Maneuver Number	Description of Maneuver	Airspeed (knots)	Peak Acceleration (g's)
1	Left aileron roll, 60 deg/sec	300	2.0
2	Right aileron roll, 60 deg/sec	300	2.0
3	Left max rate roll, 120 deg/sec	200	1.0
4	Right max rate roll, 120 deg/sec	200	1.2
5	Loop left	N/A	4.1
6	Loop right	N/A	4.15
7	360° turn left; 60° bank angle	N/A	4.0
8	360° turn right; 60° bank angle	N/A	3.75 to 4.0
9	Wing-over left	N/A	2.8 to 0.25
10	Wing-over right	N/A	2.7 to 0.25
11	40° pitch-up stall	N/A	0.5
12	Max deceleration: 400 knots to 200 knots in 11 sec.	-	-

## 4. TASK 3, SUPPORT EQUIPMENT

### 4.1 GYRO SUBASSEMBLY

In Task 3.1, Gyro Subassembly, Autonetics developed a CI specification for the gyro subassemblies and designed, fabricated, and integrated two gyro subassemblies. These subassemblies included automatic thermal stabilization and shutdown and a variable demodulator reference. One subassembly was used for MESGA development testing and one was used for 4-plate gyro and electronics development. Autonetics also fabricated and tested spares for the gyro subassemblies.

#### 4.1.1 CI Specification for Gyro Subassembly

The CI Development Specification for the Gyro Subassembly, AJ00072, was submitted to the customer in October 1974 as CDRL Item A008. This specification establishes the performance, design, development, and test requirements for the MICRON Gyro Subassembly configuration item. Due to the large amount of commonality between the Four-plate and Eight-plate GSA configurations, this specification presents requirements for both.

#### 4.1.2 Design Gyro Subassemblies

##### 4.1.2.1 Design GSA Electronics

This task included the design and printed circuit board layout of the eight-plate and four-plate GSA Electronics. The GSA Electronics include the Charge Amplifiers, Suspension Electronics, MUM Electronics, Computer Interface Electronics, Signal Buffers, Timing Generator, and for the MESGA, it also includes the Acceleration Digitizer. A list of all GSA Electronics modules is shown in Table 4-1. Development cost was reduced by maintaining as much commonality as possible between the four-plate and eight-plate designs.

The packaging scheme for the GSA Electronics utilized hybrid thick-film substrates mounted along with discrete components onto aluminum core multilayer boards or fiberglass boards.

All drawings for the GSA Electronics were submitted to the customer in October 1974 as CDRL Item A00E.

##### 4.1.2.2 Design GSA Housing

The design of the GSA Housing Assembly was supported with thermal and structural analysis. The GSA Housing consists of two packages as shown in Figure 4-1; a MESG/Charge Amplifiers package and a GSA Electronics package. Each package mounts on its own coldplate and has its own insulated environmental housing. The eight-plate and four-plate GSA Housings are identical except for the internal wire harness in the Electronics package.

Table 4-2 lists the drawings which comprise the GSA Housing. All drawings for the GSA Housing were submitted to the customer in October 1974 as CDRL Item A00E.

Table 4-1. GSA Electronics Modules

Nomenclature	Module Type	Quantity Required for 8-Plate GSA	Quantity Required for 4-Plate GSA	Quantity for Spares	Total Quantity
Precision Charge Amplifier ( $\pm 2$ )	Hybrid	8	4	4	16
Suspension Servo Module (XN-77)	AI Core	1	1		2
Notch Filter (XN-77)	Hybrid	1	1	1	3
Precision Sample & Hold ( $\phi 2$ )	Hybrid	2	2	2	6
50 kHz Buffer (XN-77)	Hybrid	1	1	1	3
Servo Network/Modular (XN-77)	Hybrid	1	1	1	3
MUX/Timing Elec. Module (XN-77)	AI Core	1	1		2
MUM & EMA Tim. Gen. (XN-77)	Hybrid	1	1	1	3
MUM Demodulator (XN-77)	Hybrid	1	1	1	3
MUM Demodulator S&H (XN-77)	Hybrid	1	1	1	3
A/D Converter (XN-77)	Hybrid	1	1	1	3
Precision GAP Monitor ( $\pm 2$ )	Hybrid	1	1	2	4
Interface Electronics Module	AI Core	1	1		2
MESSA Counter ( $\pm 2$ )	Hybrid	1	1		2
Computer Interface (XN-77)	Hybrid	1	1	1	3
Frequency Generator (XN-77)	Hybrid	1	1	1	3
Quasi Ref Gen (XN-77)	Hybrid	1	1	1	3
Gap & Charge Monitor (XN-77)	Hybrid	1	1	2	4
Auto Sequencer (XN-77)	Hybrid	1	1	2	4
Acceleration Digitizer ( $\pm 2$ )	Fiberglass	1	0		1
Acceleration Preprocessor	Hybrid	1	0	1	2
EMA Digitizer Ckt (XN-77)	Hybrid	4	0	1	5
Signal-Buffer & Sinewave Lin. In/ff	Fiberglass	1	1		2
Signal Buffer	Hybrid	2	2	1	5
Timing Generator ( $\pm 2$ )	Fiberglass	1	1	1	3
Sign & Magnitude (PWM No. 1)	Fiberglass	1	1		2
8 Plate PWM Logic (PWM No. 2)	Fiberglass	1	0		1
PWM Output (PWM No. 3)	Fiberglass	1	1		2
Output Control Logic	Hybrid	2	2	1	5
Modulator, Logic & Pul Generator	Fiberglass	1	1		2
Q Ref, Max Channel & Max Sense	Hybrid	1	1	1	3
PWM Converter (PWM No. 4)	Fiberglass	1			1
4 Plate Pulsewidth Generator	Fiberglass	0	1		1

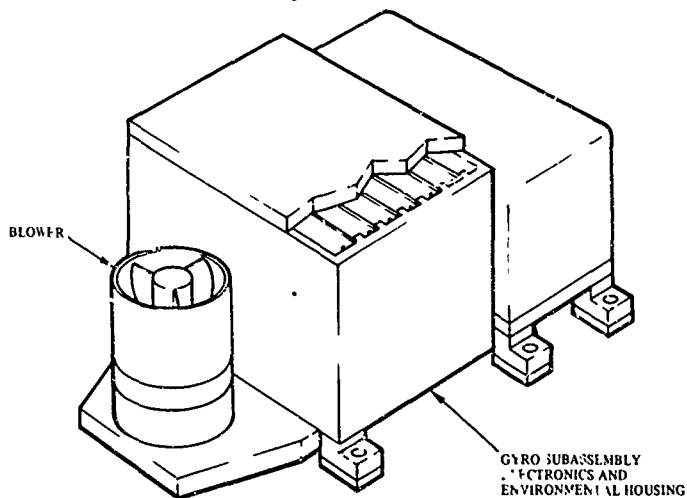
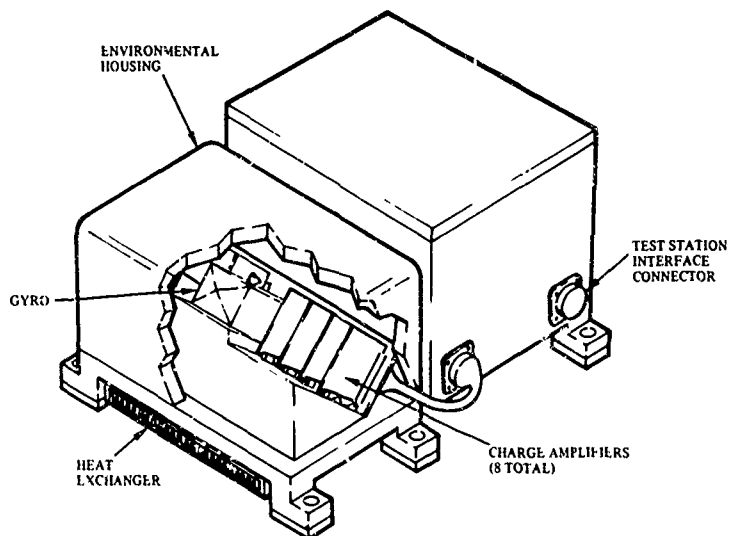


Figure 4-1. Gyro Subassembly

Table 4-2. GSA Housing - Drawing List

Part Number	Title
02710-707	Gyro Subassembly
02711-707	Interconnecting Diagram
02712-707	Plate, Adapter
02713-707	Heat Exchanger, Gyro
02714-707	Heat Exchanger, Electronics
02715-707	Electronics Assembly
02716-707	Connector Bracket
02717-707	Base Plate, Electronics
02718-707	Side Plate
02719-707	End Plate
02720-707	Cover, Electronics'
02721-707	Heat Exchanger Assembly
02722-707	Heat Exchanger Mounting Rail
02723-707	Mounting Plate, Blower
02724-707	Shock Mount, Blower
02725-707	Gyro Assembly
02726-707	Schematic
02727-707	Base Plate, Gyro
02728-707	Mount, Gyro and Charge Amplifiers
02729-707	Cover, Gyro
02730-707	PWB Assembly, Gyro
02731-707	PWB, Gyro
02732-707	Spacer, Gyro PWB
02733-707	Wedge Clamp Assembly
02734-707	Nut, Wedge Clamp
02735-707	Screw, Wedge Clamp
02736-707	Wedge, Full
02737-707	Wedge, Half
02738-707	(Unassigned)
02739-707	(Unassigned)



#### 4. 1. 3 Fab/Integrate GSA and GSA Spares

##### 4. 1. 3. 1 MESG

The intent of this task was to fabricate MESG/MESGA units in support of instrument development tasks and in support of GSA/Electronics development tasks. The task has complimented other tasks such as Develop eight-plate MESGA, Develop four-plate gyro, Vacuon pump elimination, and the multiple objectives of the design alternatives task.

Five beryllium base MESG units, A012 through A016, were fabricated to evaluate eight-plate MESGA, four-plate MESG, and eight-plate MESG. The evaluation of the multiple efforts in the design alternatives task was accomplished by use of the new beryllium base units (fast reaction for example) and standard N57A type MESG units (second source component evaluation, small gap, four-plate MESG, and new three wire rotor material). In addition to the above, seven assemblies were fabricated in support of gettered MESG test and evaluation.

All new beryllium base units included a fast thermal time constant base, three-wire rotor, a thermal sensor near the cavity members, and a fast reaction motor.

The first new gyro, A012Y (beryllium base), was tested on Test Station IV on 24 January 1975, approximately nine months after contract go-ahead, and consisted of parts which had been totally redesigned and fabricated during the nine month period. The test information on A012Y is included in Section 3. 2. 2.

##### 4. 1. 3. 2 GSA Electronics

The GSA Electronics modules, and the quantities of each, which were fabricated and testing during Phase 2A, are listed in Table 4-1.

##### 4. 1. 3. 3 GSA Housing

Fabrication of the first GSA Housing (eight-plate version) was completed and was integrated with its test station. Fabrication of the second GSA Housing (4-plate version) was also completed but integration with its test station was not completed.

#### 4. 2 SUPPORT HARDWARE

In Task 3. 2, Support Hardware, Autonetics initiated the definition of a baseline MICRON system which would be integrable with other avionics and a MICRON system which would be operated in a stand-alone configuration.

##### 4. 2. 1 Define Integrable MICRON Configuration

This activity was initiated in December 1974 and was dependent upon information derived from the Applications Engineering studies (Task 5. 4).

Preliminary results from the Applications Engineering studies indicated that the primary potential application for the MICRON system was the Air Force and Navy ACF programs. These programs demanded a low-cost, lightweight, medium accuracy inertial navigation system for which MICRON is ideally suited.

With this in mind, initial system definition studies were directed toward the ACF application. Figure 4-2 illustrates the MICRON system as initially conceived. In this configuration the IMU communicates with the CDU and CCU through a digital data bus as defined by MIL-STD-1553. In the initial ACF application, the IMU was required to communicate directly with the CDU (Figure 4-3). In addition, the CCU is required to be a part of the IMU which then communicates with the ancillary equipment through the digital data bus.

Further effort on this task was discontinued in accordance with the Stop Work Order received in December 1974.

#### 4.2.2 Define Stand-Alone MICRON Configuration

This activity was initiated in December 1974 and was dependent upon information derived from the Applications Engineering studies (Task 5.4). This effort was conducted in parallel with that of Para 4.2.1.

For the configuration shown in Figure 4-2, a special purpose IOU would allow communication directly between the IMU and the CDU. Where both integrated and stand-alone operational capability may be required, a system configuration similar to that of Figure 4-3 may be more desirable in that an operational data bus is not required.

Further effort on this task was discontinued in accordance with the Stop Work Order received in December 1974.

#### 4.3 REPAIR

In Task 3.4, Repair, Autonetics repaired and maintained hardware fabricated in Phase 1B and Phase 2A. Autonetics refurbished N57A-1 to N57A-2 configuration including D-216 controlled automatic start-up and polhode damping.

##### 4.3.1 Gyros

The intent of this repair task was to maintain MESSG units in an operational condition in order to support the various design and evaluation tasks and to support continued testing on two N57A systems, the Holloman Gyro subassembly and the eight-plate MESSG, eight-plate MESSG and the four-plate MESSG subassembly. The repair task also included refurbishment of levitator units required for troubleshooting and initial check-out of systems, test stations and electronics in the electronics development lab. Tasks were also accomplished which were not originally anticipated such as (1) fab of nonmagnetic vacuum housings with Poliney pins which required instrument reassembly and burn-in after the new housings were installed and (2) rework of Vacion pumps to assure a positive mechanical tie-down of the titanium buttons.

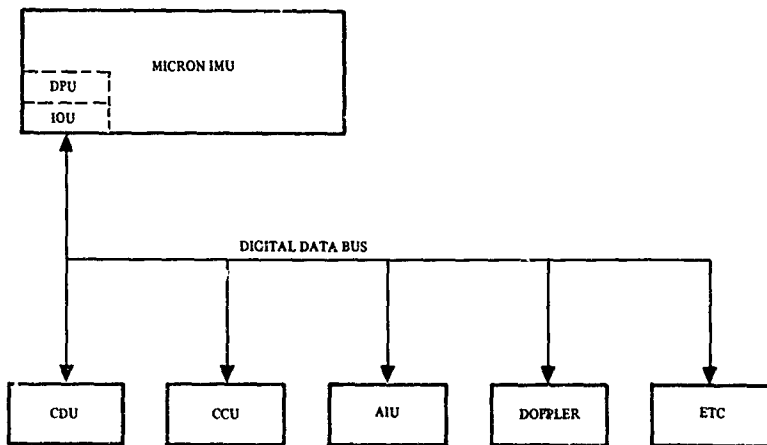


Figure 4-2. Interface Block Diagram (MICRON Concept)

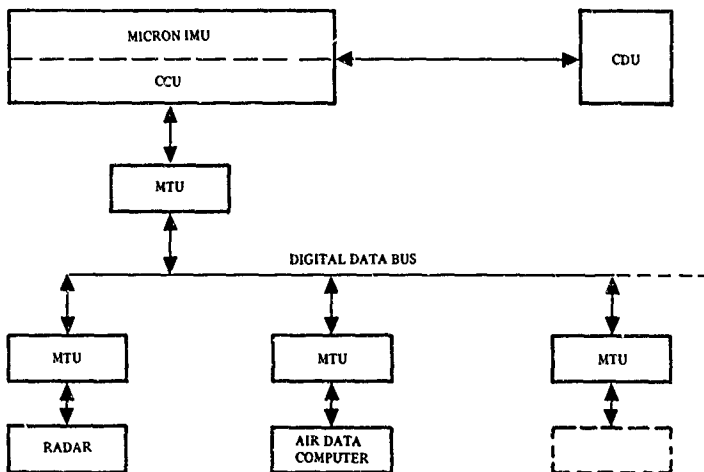


Figure 4-3. Interface Block Diagram (ACF Concept)

Typical MESG repair normally consists of two category types:

1. Repair after full speed rotor drop
2. Repair after non-spinning rotor drop

The first category requires an anticipated failure rate and a start of fabrication of spare parts months prior to the actual failure. The rotor and cavity are normally destroyed which requires instrument disassembly, reassembly, and one week of pre-functional burn-in followed by bakeout and cold soak.

The second category may normally be repaired by instrument disassembly, kiss lap of rotor and cavity, resizing, reassembly, and one week of prefunctional burn in followed by bakeout and cold soak.

A history of the assembly activity during Phase 2A is shown in Table 4-3.

#### 4.3.2 N57A Systems

For this report, each contract quarter has been delineated with respect to the maintenance and repair activities occurring within that quarter.

The repair activities during the first quarter were primarily for the D-216 computer rework. Both computers exhibited intermittent problems which appeared to be in the memory as opposed to the CPU portion of the computer. These problems manifested themselves as memory scrambles of varying degrees. Identification of the cause of these problems was associated with a bit (No. 8) being one-set in all memory locations.

An EMA required rework and this was included under this task.

During the second quarter, maintenance and repair included retest of a charge amplifier from the N57A-1 which was thought to be operating improperly, and replacement of a defective part on the On/Off Sequencer which was installed on the N57A-1. An EMA was removed from the N57A-2 for repair.

A significant activity dealt with the continued retest and repair of D216 computers and in particular with computer memories. The computer memories have displayed a problem of an intermittent nature which appears as a bit lockup in various memory locations. This problem was alleviated by adding a memory refresh routine to the software.

During the third quarter, rework and retest was performed on the N57A-1 CDU and Spin Motor Power Amp, a spare modulator, and a spare temperature controller. Diagnostic testing followed by corrective action repair was accomplished on a MUM Demodulator and one A/D Converter. These modules came out of the N57A-2 during its retest and recalibration period at Anaheim. EMA S/N A009Y, which was also removed from the N57A-2, was tested (verified large bias shift) diagnostically, disassembled, cleaned and retested. Particle contamination was the suspected cause of the large bias shift.

Table 4-3. History of MESH Assembly Activity

Assembly Date	MESH No.	Type
6/13/74	102 W33	N57A
6/24/74	138 L011	Getter
6/25/74	124 L03	N57A
7/3/74	66 W17	N57A
7/5/74	134 W35	N57A
7/5/74	136 W36	N57A
7/17/74	12 Y16	Levigator
7/25/74	56 Z8	N57A
7/25/74	122 Z3	4 Plate
7/26/74	96 W27	N57A
8/6/74	112 W26	N57A
8/22/74	86 W37	N57A
8/22/74	136 W36	N57A
8/23/74	12 Y16	Levigator
8/29/74	100 B7	N57A
9/17/74	140 W38	N57A
9/24/74	142 W39	N57A
9/26/74	144 B2	N57A
9/27/74	132 B8R	ECOM
10/2/74	24 W13	Levigator
10/2/74	142 W39	N57A
10/14/74	7U 28	Levigator
10/14/74	15 Z2	Levigator
10/14/74	102 W33	N57A
10/14/74	110 W30	N57A
10/30/74	15 Z2	Levigator
11/1/74	154 L017	Getter
11/21/74	156 L019	Getter
12/16/74	104 W34	N57A
1/9/75	104 W35	N57A
1/10/75	104 W35	N57A
1/15/75	132 B1	BE Base (3 wire rotor)
1/17/75	136 W40	N57A
1/21/75	102 W41	N57A
1/21/75	15 Z2	Levigator
1/23/75	104 W35	N57A
1/24/75	124 B8	N57A
1/27/75	146 W42	N57A
1/27/75	148 W43	N57A
1/30/75	102 W41	N57A
1/31/75	134 W35	N57A
2/4/75	120 V33	4-Plate
2/7/75	59 V18	N57A Sure Start
2/17/75	122 Z3	4 Plate
2/18/75	122 Z3	4 Plate
2/19/75	96 W27	N57A
2/25/75	102 W41	N57A
2/27/75	15 Z2	Levigator
3/5/75	158 L015	Getter
3/6/75	122 Z1	4 Plate
3/7/75	146 W42	Levigator
3/13/75	122 Z1	4 Plate
3/13/75	24 Z13	Levigator
3/14/75	7U 28	Levigator

Table 4-3. (Cont)

Assembly Date	MSG No.	Type
3/18/75	15 Z2	Levitor
3/19/75	104 W34	N57A
3/21/75	104 L025	N57A
3/24/75	59 V18	N57A Sure Start Test Unit
4/4/75	24 W13	Levitor
4/4/75	122 Z1	4 Plate
4/7/75	59 V18	Sure Start
4/8/75	104 L025	N57A
4/10/75	86 W37	N57A
4/10/75	122 Y38	4 Plate
4/15/75	158 L018	Getter
4/16/75	136 W44	N57A
4/16/75	96 W27	N57A
4/18/75	96 W27	N57A
4/18/75	142 W39	N57A
4/22/75	102 W41	N57A
4/25/75	122 Z4	4 Plate
4/30/75	126 Z9	Levitor
5/9/75	59 L05	Filament & BeO Support Ring
5/13/75	134 B14	Small Gap
5/21/75	102 W41	N57A
5/21/75	150 L022	N57A
5/28/75	116 B17	Small Gap
5/29/75	7 V28	Levitor
5/30/75	N0005 Z23	Northrop Cavity & Rotor
5/30/75	24 Q13	Levitor
6/7/75	N0003 Z16	Northrop Cav. & Rot. Levitor
6/5/75	126 Z9	Levitor
6/12/75	N0003 Z16	Northrop Levitor
6/13/75	15 Z2	Levitor
7/3/75	12 Y16	Levitor
7/3/75	N0006 Z20	N57A Northrop Cavity & Rotor
7/7/75	138 B16	Be Base, 3 Wire Rotor
7/7/75	102 W14	N57A
7/8/75	164 L024	E Beam Welded Getter
7/17/75	N0003 Z16	Northrop Levitor
7/29/75	170 B9	Be Base, 3 Wire Rotor

During the fourth quarter, the D-216 Computer Word Module was repaired and retested. This module was removed from the N57A-2 System.

In order to support N57A-2 testing at HAFB, a set of non-calibration sensitive module spares was prepared to be sent to HAFB. Sufficient spares were also prepared for the laboratory to support testing activities.

The following list represents those modules that are non-calibration sensitive and which were prepared as spares for HAFB.

- Computer Interface
- Demod Reference Generator
- Accelerometer Preprocessor
- Auto Sequencer
- A/D Converter
- Gap Monitor S/H
- Spin Motor Timing
- Spin Motor Controller
- Spin Motor Power Amp
- Alt/Vel Signal Conditioner

Note that a spare Alt/Vel Signal Conditioner Module was never fabricated before but was completed at this time. This module goes into the original spare slot and contains the Altimeter Signal Conditioning and the Halt and Reset Control circuitry for the D-216 Computer.

There are other non-calibration sensitive modules which were recommended for sparing at Holloman. These include the D-216 Computer and the Power Cube.

In February, a Computer Interface module, a Demod Reference Generator module and an A/D Converter module was shipped to HAFB as spares.

During the last month of the fourth quarter, repair was accomplished on the Computer Control Panel that was damaged at HAFB. A tape reader control switch and an indicator light were replaced.

The A/D Converter removed from the N57A-2 system at HAFB during February, was tested at the module level. The failure was verified as a broken fly-wire in the sample-and-hold portion of the circuitry on the A/D converter. This module was repaired.

While using the N57A-1 system to check out spare modules for the N57A-2 system, a modulator failed. The problem was identified as a failed HI-1800 device. The device was replaced and the modulator operated correctly. Also, a MIB problem occurred. A high resistance between the -2 Charge Amp output and the -2 suspension electrode was found in the MIB circuitry. The MIB was repaired.

During the fifth quarter of Phase 2A, an A/D converter S/N A003Y which had repeatedly failed when tested at the system level was thoroughly bench tested and a tentative repair was made (a multiplex device was changed). The A/D converter passed functional testing at the component level but performance at the system level was not yet verified due to the unavailability of the system for the required testing.

The N57A-2 system had a speed control problem on the No. 2 gyro which was traced to the X-Servo Network. The module was removed and retested at the component level and found to be within functional test specification tolerances.

During recalibration of the N57A-2 system in May and June, a "Z" Servo Network and a MUM Demod were removed from the system because of poor system calibration results. These modules are to be tested at the module level.

One of the MIB housing heater control transistors on the HAFB GSA failed during this reporting period. The transistor was replaced and HAFB GSA testing resumed.

#### 4.3.3 Refurbish N57A-1 System and Test Equipment

The refurbishment of the N57A-1 and test equipment consisted of two things: (1) updating the wiring in the N57A-1 to include the modification that went into the N57A-2, and (2) thoroughly investigating the grounding and EMI that had been causing noise problems and poor performance and correct any discrepancies found.

The wiring modifications were performed first. Then EMI tests were performed on the N57A-1 system configuration. The test results show the greatest source of EMI current flows through the 28 vdc primary power conductors. This EMI current is due to the 28 vdc to 6 vdc converter located in the Control Display Unit (CDU). The peak-to-peak spike current amplitude is proportional to the brightness of the L. E. D. display, the spikes being maximum at maximum brightness. No voltage spikes appeared at the 6 vdc output of the converter.

Within the N57A-1 Auxiliary Test Console, the switch located on the recorder used for recording charge monitor data, was identified as a source of EMI signals in this console. The EMI is generated whenever the switch is rapidly switched from either the "On" to "Standby" or the "Standby" to "Off" position. The auxiliary large gap detector and automatic shutdown circuit, at times, was susceptible to this EMI. Tests showed the EMI was conducted from the recorder via the AC power high, return and safety conductors through the plug mold, to which both the recorder and the auxiliary control panel are connected, into the auxiliary control panel internal wiring harness. Because both the AC power conductors and the monitored MUM signal conductors are routed together in the same harness, the EMI signals coupled from the AC power conductors into the shields and the monitored MUM signal conductors that connect to the inputs of the susceptible circuit.

EMI decoupling capacitors were added in the 115 VAC circuitry of the auxiliary control panel. This modification eliminated false shutdown due to the EMI signals being conducted via the AC power circuit into the automatic shutdown circuit.

With the successful verification of the EMI reduction modifications, the refurbishment task was completed.



## 5. TASK 4, TRAINING

### 5.1 MANUALS

In Task 4.1, Manuals, Autonetics prepared an operating manual, interface drawings, and a training plan for the N57A-2.

#### 5.1.1 Operating Manual

Autonetics prepared an Operation Instructions Manual, UTM-285-MICRON-01, and submitted it to the customer in July 1974 as CDRL Item A00U. This manual provides operation and system maintenance instructions in support of the N57A-2 flight test program at Holloman Air Force Base.

#### 5.1.2 Interface Drawings

The N57A-2 and CDU interface drawing 02259-727 was prepared and submitted to the customer in June 1974 as CDRL Item A00H.

#### 5.1.3 Training Plan

The Training Plan to support training of Holloman AFB personnel was completed and submitted to the customer in July 1974 as CDRL Item A00U. The Training Plan provided schedule, location, course outline, and other pertinent information necessary to present Autonetics' approach to N57A-2 program training requirements.

### 5.2 HARDWARE

In Task 4.2, Hardware Autonetics utilized Phase 1B and Phase 2A hardware to support training as set forth in the Training Plan prepared in Task 4.1.

During the laboratory portion of the training course, students were given "hands-on" exposure to the MICRON airborne equipment (N57A-2) and laboratory and flight test equipment.

The following items of hardware were used during the training course:

1. Inertial Measurement Unit (IMU), Part Number 80085-101-1
2. Control Display Unit (CDU) Part Number 11995-502-1
3. Flight Test Panel (FTP), Part Number 02630-727
4. Two-pen recorder, SERVO/ITER II
5. D216 Computer Support Console

### 5.3 SERVICES

In Task 4.3, Services, Autonetics supported the LAX flight tests, maintained the N57A-1 system, supported the Holloman Gyro subassembly tests, and supported the HAFB flight tests. Autonetics installed and checked out the N57A-2 in the laboratory at HAFB and instructed the HAFB personnel how to operate the equipment. Autonetics developed and supplied training course materials and conducted training classes.

#### 5.3.1 Support LAX Flight Tests

##### 5.3.1.1 N57A-1 Flight Testing

The bulk of N57A-1 System testing during April 1974, was directed toward solving the heading sensitivity problem. A series of angle and drift calibrations followed by navigation performance runs showed that automatic spin-up, damping, etc. caused the MESSG cases to become magnetized resulting in an apparent heading sensitivity. Procedures were worked out which would allow manual operation during the Flight Test Program. At the same time, system operation with the Flight Test Panel was also verified.

During the first of May 1974, the system was calibrated prior to shipment to LAX for integration with the aircraft for Flight Testing. On May 16, after system calibration and after obtaining a series of successful navigation runs, the N57A-1 and its support equipment was shipped to LAX.

System and aircraft integration began on May 17. During integration the rotor of one of the MESSG's suffered a non-spinning drop. The details of this rotor drop are given in Appendix B.

The system was removed from the aircraft and returned to Anaheim for gyro replacement and recalibration. This was accomplished and the system was returned to LAX on May 31, 1974, and flight tests started the first week of June. N57A-1 maintenance activities and flight information are discussed in Para 3.3 of this report.

##### 5.3.1.2 N57A-2 Flight Testing

Autonetics Engineering provided support to Flight Test Operations in the flight testing of the N57A-2 system. This activity is discussed in Para 3.3 of this report.

#### 5.3.2 Support HAFB Gyro Subassembly

During the first three weeks of April 1974, support was provided to HAFB in the form of data analysis. Gyro subassembly test data was received by Autonetics and processed using the regular angle and drift programs. The data indicated that there was a hardware and/or software problem associated with the stepping demodulator reference. While this problem was being investigated, a gyro rotor drop was experienced at HAFB.

During 22-26 April, 1974, a trip to Holloman Air Force Base was made to verify the rotor drop and to determine and correct the cause. A detailed account of the trip is included in Appendix C. The rotor drop was verified and it is suspected the rotor drop was caused as a result of charge build-up on the ball.

On 30 May 1974, Autonetics Engineer, J. A. North, arrived at Holloman Air Force to provide on-site support for Gyro Subassembly Testing.

On 3 June 1974, Mr. North installed a modification in the Motor Torque Director. The purpose of this modification was to eliminate current transients in the gyro motor windings when the Torque Director was turned on or off. It was found during N57A-1 testing that the extraneous current pulses could magnetize the MESH housing, making this modification necessary.

On 5 June 1974, a set of angle and drift calibration data taken on the Gyro Subassembly at HAFB was received. The data were reduced with the following results:

Angle cal residuals - 0.296 mr rms/axis  
Drift cal residuals - 0.05198 deg/hr rms/axis

Three problems associated with the data acquisition were noted. They were:

1. Loss of phase lock in the MUAR - this resulted from having the MUAR locked on MUM I which, at certain table positions, was too small a signal to maintain phase lock.
2. Data truncation error - in the data processing programs written at HAFB, the raw data were being truncated thereby limiting resolution to approximately 0.3 mr.
3. 3-Axis table positioning - the actual intermediate table axis position and that used in the data reduction program were not the same.

After taking into account the incorrect table positioning, the drift and angle cal residuals are consistent with what should be expected due to the truncation error.

Information concerning these problems and their solutions was transmitted to HAFB personnel. A new set of angle and drift data, taken after correcting the above problems, was received on 17 June 1974. The angle calibration data were questionable due to a data acquisition computer problem and were not reduced. However, the reduction resulted in a drift calibration residual of 0.01457 deg/hr rms/axis. These data were reduced using the angle calibration coefficients from the first data set. Considering the angle calibration residuals (0.296 mr rms/axis) the drift calibration residuals indicate that the truncation problem and the other problems were corrected and that the Gyro Subassembly was performing correctly.

On 21 June 1974, a third set of data was received. Attempts to reduce these data were totally unsuccessful. The indication was that it was a hardware problem.

A series of tests were performed on the Gyro Subassembly to isolate the problem. It appears that the problem was associated with the A/D converter or one of the two computer interface boards in the Subassembly. It was intended that these boards will be returned to Autonetics for repair or replacement.

The month of July 1974 was devoted primarily to troubleshooting to determine why the gyro subassembly was unable to provide reasonable angle and drift calibrations. After extensive testing, it was discovered that the drivers in the HP 2100 computer were being synchronized to the leading edge of the input pulse, whereas, they should be on the trailing edge. This problem was corrected in the HP 2100. The system and the HP 2100 were rechecked for proper operation.

Emergency power was made available for the Gyro Subassembly fans and Subassembly Auxiliary Test Equipment for power black-outs. This gives the capability of shutting the system off during a power failure.

On 22 July 1974, the gyro was spun-up, damped, and heated and an angle calibration was performed one hour later for verification of data being accepted properly by the computer. The results were satisfactory. After a 24-hr stabilization period, an angle and drift calibration was performed on 23 July 1974. Another set of calibration data was taken on 24 July. The gyro subassembly was kept operating between these two sets of calibrations. Following the second drift calibration, the system was turned off. On 25 July the system was restarted and allowed to stabilize prior to taking the third set of calibration data on 26 July 1974. These data were received from Holloman Air Force for reduction at Autonetics. These data were taken after all the hardware and software problems had been resolved. The intent of the data reduction effort at Autonetics was to verify proper operation of the hardware and software in use at HAFB. When this was accomplished, no further data reduction at Autonetics was to be performed.

The end of July 1974 concluded the offsite support provided by Autonetics Engineer, J. A. North.

A summary of the angle calibration residuals is given in Table 5-1. These are the calibration residuals after table positioning errors have been taken into account. In order to allow for table errors, the data reduction program was modified to allow removal of an inertial vector for each rotation in the data acquisition process. This is roughly equivalent in modeling a TA1 error peculiar to each rotation.

A summary of the drift calibration residuals is given in Table 5-2. No results were obtained for the 23 July 1974 calibration because of a formatting problem which occurred during data tape duplication at HAFB. This was due to a HAFB computer malfunction and, based on the results obtained from the other two calibrations, it was decided not to generate the software required to recover these data. However, this data does still exist in proper format at HAFB if reduction were deemed necessary.

Table 5-1. Angle Calibration Results

Data of Calibration	Calibration Residuals (mr-rms/axis)
7/23/74	0.078
7/24/74	0.205
7/26/74	0.099

Table 5-2. Drift Calibration Results

Data of Calibration	Calibration Residuals (deg/hr - rms/axis)
7/23/74	No Results
7/24/74	0.01680
7/26/74	0.01819

After removing the effect of tilt table positioning, both the angle and drift calibration residuals were acceptable. This, of course, does not include the results of the second angle calibration. No acceptable explanation of this data set has been found. It was understood that during the total calibration sequence, the data acquisition computer at HAFB had problems relating to its internal clock and/or timing. The timing problem may have contributed to the poor results of the second angle calibration but there was no way to substantiate that possibility.

Successful angle and drift calibrations with a minimum of data editing require the tilt table to be accurately positioned. Tilt table mispositioning was by no means an uncommon occurrence. Moving TA1 when it should be TA3, or vice versa, was very easily done. This will probably occur until all calibrations are done on an automatic table. It is believed that this was the cause of the bad data points observed in the drift calibrations.

The angle calibration is even more sensitive to table positioning than the drift calibration. The problems in the angle calibration data appear to be associated with difficulty in accurately positioning TA1. The angle calibration results, prior to accounting for TA1 errors, would indicate table positioning errors of the order of 40 to 80 sec of arc. This information was related to HAFB personnel who optically checked the tilt table. Their results indicate TA1 accuracies of the order of 15 sec of arc, peak-to-peak. This dilemma was not resolved.

It was noted during August that several power losses at HAFB necessitated emergency shutdown of the GSA. If during one of these shutdowns the ball was sparked, the gyro would probably become a charger.

On 5 September 1974, it was determined the rotor of the gyro on the GSA was picking up a charge. Repeated turn-on cycles did not correct this condition. Servo checks were performed which verified that the instrument had indeed become a charger. Further testing was discontinued pending a decision by the Air Force as to which gyro should be sent to HAFB as a replacement. Subsequently, the Air Force made the decision to return

the GSA and Test Console to Autonetics. It was understood that all additional subassembly testing would be performed at the Anaheim facility. Support continued to be provided to HAFB in the form of consultation concerning the analysis of data taken at HAFB.

Since the GSA was returned to Autonetics on 15 October 1974, no further activity was planned under this task. Subsequent GSA testing is reported under Task 2.2, Laboratory Tests.

### 5.3.3 Install and C/O N57A-2 at HAFB

On 7 October 1974, the N57A-2 system arrived at HAFB aboard the T-39 Sabreliner. The system was removed from the aircraft and moved into the laboratory at HAFB. All associated cabling and the flight rack were also removed from the aircraft. October 8 and 9 were devoted to installing the system and the other equipment in the pallet. Also the 400 Hz and 60 Hz power to the pallet was checked out.

On 10 October 1974, the system was powered up for the first time. In checking the +28 vdc input power to the system, it was found that the voltage at the system was +23.5 vdc under load (+29 vdc at no load). This was, in part, due to the +3 vdc line drop from the generator to the laboratory outlet. After removing the battery back-up protection diode in the FTP the voltage at the system was +24.8 vdc.

The system was then allowed to continue through the automatic starting sequence. The system operated normally until the final heating mode was initiated. After waiting approximately 45 min, this mode was exited manually and the starting sequence was manually completed.

The final heat mode was not automatically completed because the gyro case temperatures settled at a higher temperature than that previously stored in the computer. The higher case temperatures were probably due to (1) the HAFB laboratory being warmer than the laboratory at Autonetics and (2) the position of the case temperature sensor in that it is somewhat sensitive to cold plate temperature.

The alignment mode was commanded and after a 20 min alignment, the system was put into the navigate mode for a short checkout run. Both the alignment and the navigation run results were acceptable.

October 11 and 14 were devoted primarily to tying up interconnection cables within the pallet in preparation for Air Force Quality Control inspection.

At 1700 hrs on 14 October, the system was powered up for a navigation run. Due to the previous case temperature problem, new case temperature values were calculated and keyed into the computer. Two alignments, each followed by a one hour nav run, were performed with acceptable results.

On 15 October 1974, one week after being delivered to HAFB, the N57A-2 system was installed on the C-141 for the first test flight later in the day. The results of this and subsequent flights are detailed in Para 5.3.4.

It is significant to note that the first successful C-141 flight test was accomplished one week after arrival of the N57A-2 system at HAFB. This was in a large part due to the cooperation received from the Air Force personnel, especially TSgt's McCormack and Mathis and their crews in the work done to get the pallet ready for Air Force Q. C. inspection.

This effort completed this task. Subsequent activity of this type was covered as part of the HAFB flight test support.

#### 5.3.4 Support HAFB Flight Tests

Support was provided by Autonetics during N57A-2 flight and laboratory testing at HAFB. A total of five C-141 flights were completed before the C-141 returned to Wright-Patterson AFB for maintenance. A summary of the flight data is shown in Table 5-3. These data are "quick-look" data and as such are not corrected for actual aircraft position at the checkpoints.

Table 5-3. Summary of N57A-2 HAFB Flight Data

Flight No.	Date	Radial Error Rate (nm/hr)	Pre and Post Flight Time RMS Velocity Error (ft/sec)		
			Avg/Channel	North	East
1	10/15/74	0.53	2.75	2.00	3.54
2	10/16/74	0.70	13.43	14.31	12.49
3	10/18/74	0.67	7.77	8.52	6.96
4	10/21/74	1.40	17.35	16.20	18.43
5	10/23/74	1.08	10.85	10.09	11.56

Due to the priority of the B-1 system test program, the C-141 flight schedule, profiles, and duration were at their discretion. It was intended that the N57A-2 system would be on as many flights as possible prior to the C-141 leaving HAFB for maintenance. Consequently, flights 3 through 5 were flown in spite of the prior indication of a system problem.

Because of the poor velocity error results, the system was moved back into the laboratory at HAFB on 25 October 1974. The results of an alignment and nav run in the laboratory indicated an apparent calibration parameter shift. This, in addition to the apparent instrument cube temperature increase, made it necessary to return the N57A-2 system to Autonetics for repair and recalibration. The system was shipped from HAFB on 30 October 1974.

The N57A-2 system was received at Autonetics on 31 October 1974. The system was repaired and recalibrated and a total of three nav verify runs were made, all with acceptable results. A detailed analysis of the system problems encountered is included as Appendix D.

The system was returned to HAFB for continued testing on 15 November 1974. On 18 November 1974, the system was installed on a helicopter pallet in preparation for flight testing in a UH-1 Helicopter. Several navigation verification runs were performed in the laboratory at HAFB with marginal results. It was determined that the gyro case temperatures were changing and were directly related to ambient air and hence, cold plate temperature. When the cold plate temperature was relatively stable, the nav verify results were acceptable. It was noted that the HAFB laboratory temperature, and thus the N57A-2 inlet cooling air temperature, varies from a low of 65°F in the morning to a high of 84 to 86°F in the afternoon. This high temperature is above the system's design criteria. When the system performance was marginal the cold plate temperature was high and the laboratory ambient was at its high temperatures.

The system was installed in the helicopter and the first flight was performed on 29 November 1974. The results of this flight were poor and subsequent analysis indicated a problem in one of the Electromagnetic Accelerometers (EMA). The EMA problem was verified in the HAFB laboratory and the system was returned to Autonetics Anaheim where the EMA problem was also verified. The Y-EMA was replaced and the system was successfully recalibrated. Navigation verification runs were made with acceptable results and the system was returned to HAFB on 13 December 1974. An analysis of this system failure is included as Appendix E.

When the system was received at HAFB, a six-hour navigation run was performed with the system on a Scorsby table. The radial error rate was 0.84 nm/hr and the average per channel time RMS velocity error was 1.81 ft/sec. The per channel time RMS velocity errors were 2.18 ft/sec and 1.34 ft/sec for the North and East channels, respectively.

Upon completion of the Scorsby test, the system was prepared for reinstallation in the UH-1 helicopter. At this time, a problem in loading the computer was encountered. Tests performed at HAFB could not isolate the problem to either the D216 computer or the Computer Control Panel.

The N57A-2 system was returned to Autonetics on 2 January 1974 for repair and recalibration as required.

Laboratory testing at Autonetics verified the computer loading problem. It was found that address bit No. 12 was "true" at all times resulting in incorrect filling of locations involving that bit. The voltage on MA12P, the address bit No. 12 output line from the "Word Module" to memory, was always +1.8 VDC (false state is 2.0 VDC to 5.0 VDC). The Word Module was replaced and the computer operated normally. Bench testing of the failed Word Module revealed IC Z37 (type MC 3100) had failed. The IC was replaced and the spare Word Module operated correctly. At the time of the failure the computer had undergone 639 hours of operation inside the housing and in excess of 2000 hours prior to installation in the housing.

The system was recalibrated and subsequent navigation verification runs indicated excellent performance. The system was returned to Holloman AFB on 13 January 1975.

While the system was at Autonetics, the flight data from the five C-141 flights was subjected to additional analysis. The CEP rate for this data was computed and is 0.84 nm/hr. The CEP time history for this data is shown in Figure 5-1. The only velocity data available to Autonetics was the velocity errors before and after the flight periods. Therefore, no presentation of velocity error data is made here.



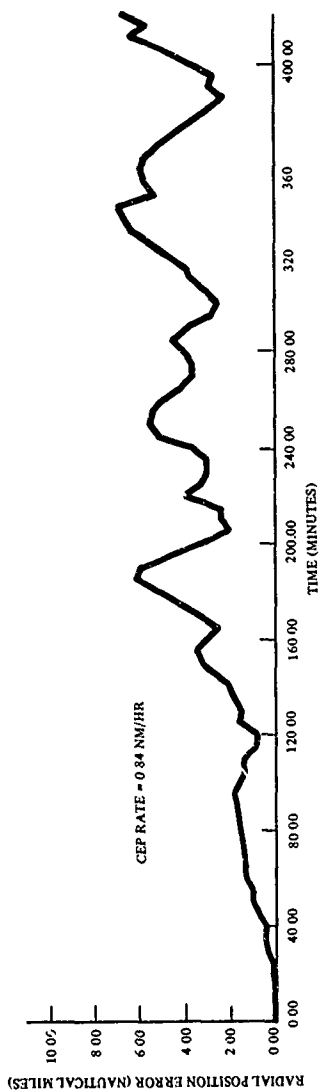


Figure 5-1. N57A-2 CEP Time History

On 15 January 1975, the system was installed on the helicopter pallet and a navigation verification run was performed in the HAFB laboratory. The results of the nav run were acceptable. After installation in the helicopter, a turn-on sequencing problem was encountered. Numerous tests were performed at HAFB to isolate the problem. It was determined that either the On/Off Sequencer or the Control Display Unit was malfunctioning.

On 21 January 1974, a spare On/Off Sequencer and the system No. 1 CDU were sent to HAFB. By interchanging the CDU and Sequencer, the problem was isolated to the Sequencer.

On 22 January 1974, a second laboratory nav verify run was performed. This run repeated the results of the 16 January run. At this time, the HAFB computer interface was also checked out. During an attempt to run a third nav verify run the next day, the system shut down due to a "BITE" malfunction. The indicated bite was the negative A/C high voltage monitor. After hooking up the Auxiliary Test Console, no problems could be found with the system. It appears that this shutdown was due to an erroneous "BITE" indication. The system was again turned-on and, during a short nav run, the hardware functioned correctly.

On 24 January 1974, another navigation verification run was planned prior to installation in the helicopter. At system turn-on it was noted that the spin motor voltages during coarse heating were abnormal. This condition persisted through a system shutdown. It was determined that the problem was due to a Spin Motor Power Amplifier malfunction, in particular a stuck relay contact. A spare Spin Motor Power Amplifier and its associated electronic boards were sent to HAFB from Autonetics, Anaheim. These modules were installed on 27 January 1975 and, during system check-out, it was noted that Gyro No. 1 rotor was charging. Numerous power cycles did not cure the problem. Since the gyro had to be replaced, the system was returned to Autonetics for repair. The system arrived at Anaheim on 28 January 1975.

After replacing both gyros and correcting the problems identified at HAFB, the system was recalibrated and navigation verification runs indicated acceptable performance. The system was returned to HAFB on 4 February 1975 aboard the Rockwell International T-39 Sabreliner. A detailed discussion of the repair actions at Autonetics is included as Appendix F.

After return to HAFB, helicopter testing resumed on the N57A-2 system. Three flights were performed with marginal system performance. Laboratory runs at HAFB were made and they confirmed the flight performance. A summary of the helicopter flight data and the subsequent HAFB laboratory runs is given in Table 5-4.

It was noted during start-up for the first and second helicopter flights that RSA magnitude software BITES occurred. The BITES cleared themselves prior to alignment. It was suspected that a MUX located on the A/D converter board may have been operating with an intermittent condition. For this reason a spare A/D Converter was sent to HAFB. After installation in the system, a second lab run was made. System performance was not improved but no software BITES occurred. Subsequent lab testing of the suspect A/D converter at Anaheim revealed a broken fly-wire in the sample-and-hold portion of the circuitry on the substrate. The fly-wire was repaired and the A/D converter was made available as a spare.

Table 5-4. HAFB Helicopter and Laboratory Data Summary

Data Summary						
Run Number	Date	Radial Error Rate (nm/hr)	Time RMS Velocity Error (ft/sec)			Comments
			Ave/Channel	North	East	
1	2/8/75	1.60	11.42	7.15	14.48	Helicopter Flight No. 1 - N/S
2	2/11/75	1.93	8.36	2.71	11.52	Helicopter Flight No. 2 - N/S
3	2/12/75	1.76	5.03	1.01	7.05	Helicopter Flight No. 3 - N/S
4	2/13/75	1.01	6.37	5.95	6.76	Lab Run Simulating N/S Flight
5	2/14/75	1.44	5.73	7.00	4.07	Same as Run No. 4 after changing A/D Converter
6	2/18/75	1.68	10.91	13.56	7.37	Lab Run Simulating E/W Flight

Due to the marginal performance, it was decided to return the system to Autonetics, Anaheim, for problem diagnosis and recalibration. During the course of the problem diagnosis, the system was recalibrated and subsequent nav verify runs again gave marginal performance. A thorough review of the system data and other data pertaining to Gyro S/N 142 indicated that the performance problem could be attributed to the gyro. The gyro was removed and replaced with Gyro S/N 110.

The system was again recalibrated and five subsequent navigation verification runs indicated excellent system performance. A detailed account of the action taken during the period of 21-28 Feb, 1975 and a summary of the performance data for the five nav verify runs are included in Appendix G. The system was packed for shipment to HAFB on 3 March 1975.

It is significant to note that, as anticipated, changing Gyro S/N 142 materially improved system performance. Prior to this time, the majority of system performance problems had been rightly attributed to the electronics. Since Gyro S/N 142 had been calibrated numerous times on the system and on the HAFB Gyro Subassembly in addition to the navigation runs on the N57A-2 system, sufficient data was available to directly correlate system navigation performance with instrument calibration data. The insight into this correlation provided by reviewing this gyro data aided in evaluating future system performance.

The N57A-2 system arrived at HAFB on 5 March 1975 and was reinstalled in the helicopter pallet for laboratory nav runs and continued helicopter flight testing. Two laboratory navigation runs were made in addition to seven additional helicopter flights. The flight results were very good and are summarized in Table 5-5 along with the laboratory test data.

After Helicopter Flight No. 10, the system was removed from the helicopter and installed in the 4-bay pallet in preparation for resumption of C-141 flight testing. A lab nav verification run was performed at HAFB on 27 March 1975. The results of this test are also included in Table 5-5.

On-site support to the HAFB flight test program was provided by Autonetics personnel during the week of 10 March 1975 and the week of 24 March 1975.

During April, additional C-141 flight testing at HAFB was completed. A total of nine additional flights were accomplished. One stationary navigation run in the C-141 and three HAFB laboratory runs were also performed. The results of the flight tests are summarized in Table 5-6 along with the laboratory test data.

With the exception of an aborted flight test on 15 April 1975, the N57A-2 system performed throughout this portion of the test program with a minimum of problems. Prior to the 15 April 1975 flight, an apparent computer problem was encountered. This problem manifested itself in abnormal system turn-on sequencing. Numerous power cycles, computer resets, and reloading of the computer did not correct this condition. The system was shut down and the flight was made with the system off.

In preparation for the next C-141 flight, 16 April 1975, the CDU was checked to ensure that there were no improperly seated electronic boards. It did not appear that any boards were loose. After this check, however, the system was turned-on and the start-up sequence was normal. Other than the reseating of the CDU boards, no satisfactory explanation of the abnormal system behavior has been found.

The last C-141 flight was accomplished on 16 April 1975. The system was then moved into the HAFB laboratory for stationary navigation runs. The results of these tests are also included in Table 5-6.

A number of N57A-2 system modifications were identified as necessary to prepare the system for RF-4C flight testing. The system was returned to Autonetics on 28 April 1975 to accomplish these modifications and for recalibration. The required modifications and the subsequent system testing and recalibration effort is detailed in Appendix H.

On 14 June 1975 an acceptable navigation verification was obtained on the N57A-2 system. In order to support the RF-4C integration the system was packed for shipment to Kirtland AFB on 16 June 1975.

The system arrived at Kirtland AFB on 17 June 1975, accompanied by Autonetics engineers. Prior to checking the system installation in the RF-4C, all the adapter cables were continuity checked. The only problem identified was that 20 AWG wire was used to provide +28 vdc to the system. The 20 AWG wires were replaced with 14 AWG wires. System power checks in the RF-4C were completed at Kirtland AFB on 19 June 1975. The system was then transported to Holloman AFB for checkout of the HAFB data acquisition equipment, and performance of a nav verify run with the system in the RF-4C pallet in the laboratory prior to RF-4C flight testing.

Table 5-5. HAFB Laboratory and Helicopter Data Summary  
for March 7 through March 27, 1975

Data Summary

Run Number	Date	Radial Error Rate*(nm/hr)	Time RMS Velocity Error**(ft/sec)			Comments
			Ave/Channel	North	East	
1	3/7/75	0.58	2.28	1.52	2.84	Lab Run - 90° turns 40 min apart
2	3/10/75	0.91	7.54	4.02	9.87	Lab Run - Simulating N/S Flight
3	3/12/75	0.62	3.92	3.98	3.85	Helicopter Flight No. 4 - N/S
4	3/13/75	0.70	6.52	1.23	9.14	Helicopter Flight No. 5 - N/S
5	3/14/75	0.72	5.37	6.62	3.72	Helicopter Flight No. 6 - N/S
6	3/17/75	1.08	1.95	2.29	1.53	Stationary run in helicopter - no turns
7	3/18/75	1.58	8.01	8.92	6.99	Helicopter Flight No. 7 - E/W
8	3/19/75	0.66	4.10	2.95	5.00	Helicopter Flight No. 8 - E/W
9	3/20/75	0.68	4.39	2.92	5.48	Helicopter Flight No. 9 Terrain Following (E/W)
10	3/21/75	0.83	6.08	8.27	2.38	Helicopter Flight No. 10 - N/S
11	3/27/75	1.20	3.72	4.59	2.49	Lab run - C-141 pallet 90 turns, 40 min apart

\*Based on preliminary checkpoint data provided by HAFB

\*\*Based on only pre- and post flight data provided by HAFB

Table 5-6. HAFB C-141 and Laboratory Data Summary

Run Number	Date	Radial Error Rate* (nmi/hr)	Time RMS Velocity Error** (ft/sec)			Comments
			AVE/Channel	North	East	
1	4/1/75	0.26	1.97	1.91	2.03	C-141 Flight No. 5 - E/W
2	4/2/75	0.56	3.79	2.86	4.54	C-141 Flight No. 7 - E/W
3	4/3/75	0.51	4.20	5.03	3.16	C-141 Flight No. 8 - E/W
4	4/4/75	0.51	2.22	2.78	1.44	C-141 Flight No. 9 - E/W
5	4/7/75	0.56	0.98	1.00	0.96	Stationary run in C-141, no turns
6	4/8/75	0.31	4.69	4.86	4.51	C-141 Flight No. 10 - E/W
7	4/9/75	0.57	3.77	5.12	1.48	C-141 Flight No. 11 - N/S
8	4/10/75	0.56	10.70	14.18	5.27	C-141 Flight No. 12 - E/W
9	4/14/75	0.45	2.20	2.97	0.93	C-141 Flight No. 13 - N/S
10	4/16/75	0.67	11.95	5.34	16.03	C-141 Flight No. 14 - W-N/S-E
11	4/18/75	0.81	2.94	3.08	2.78	Baseline Hdg. Sens Lab Run - no turns
12	4/21/75	0.28	1.92	2.21	1.59	HAFB Lab Hdg Sens Test
13	4/22/75	1.45	5.24	6.06	4.28	HAFB Lab Run 2 turns

\*Based on preliminary check-point data provided by HAFB.

\*\*Based on only pre- and post-flight data provided by HAFB.

The period of 20 June 1975 through 24 June 1975 was devoted to checking out the communications link between the N57A-2 system D216 computer and the HAFB parallel-to-serial converter and tape deck data acquisition equipment. No major problems were encountered during the checkout of the data link.

A nav verify run was performed in the HAFB laboratory on 25 June 1975. This run was performed with the N57A-2 system and the data acquisition equipment installed in the RF-4C pallet. The results were:

Radial error rate:	1.40 nm/hr
Time RMS velocity error	
Per channel:	3.06 ft/sec
North:	1.92 ft/sec
East:	3.87 ft/sec

Although the radial error rate was greater than 1.0 nm/hr, the tilt and drift errors due to heading changes were not excessive. Therefore, the system was pronounced ready for RF-4C shake down flight. The shake down flight was scheduled for 30 June 1975. However, on 27 June 1975 word was received that the RF-4C flight testing had been postponed until mid-July 1975 due to other commitments of the RF-4C test aircraft.

On 8 July 1975, the Air Force notified Autonetics of the loss of the RF-4C and discontinuation of any further N57A-2 flight testing. The N57A-2 along with all support equipment were prepared for return to Autonetics. The N57A-2 was returned to Autonetics on 21 July 1975 where it was set up to evaluate the previously monitored nav tape problem.

Four nav verification runs were performed using the Dec 6 and Feb 6 nav tapes. System performance progressively got worse. Two EMA calcs and two polar angle calcs were performed using both nav tapes and a polar drift cal was performed with the Dec 6 nav tape only. Calibration repeatability between the nav tapes was good. Three nav runs were performed using both nav tapes. Performance was poor but repeatable.

The open ground from W1(PR) to J8-C was repaired. This open was first noted at Holloman AFB prior to the scheduled RF-4C flight tests. The system was recalibrated using the Dec 6 nav tape and three nav runs were performed. The first nav run was very good but the results of the two succeeding runs again got progressively worse.

The plan is now to change four suspected charge amps, recalibrate and perform nav verification runs. This will be done early in Phase 2B.

### 5.3.5 Training

During September 1974 six Air Force personnel (five from Holloman AFB and one from AFAL, Wright-Patterson AFB) completed a two week training course held at the Autonetics Anaheim facility. The course curriculum included classroom and laboratory training intended to familiarize Air Force personnel with N57A-2 equipment operation.

A trained Autonetics service representative was assigned to HAFB to provide On-the-Job Training (OJT) and technical assistance during installation and checkout of the N57A-2 in the C-141, and UH-1 helicopter. Technical assistance was provided during temporary installation of the N57A-2 in the RF-4C aircraft. Assistance was also provided in support of the verification runs to determine system accuracy.

## 6. TASK 5, SYSTEM MANAGEMENT ENGINEERING

### 6.1 PROGRAM MANAGEMENT

In Task 5.1, Program Management, Autonetics provided program management and project engineering to assure achieving a balanced MICRON design. Autonetics conducted 10 informal design reviews, one system requirements review, and will conduct one system design review. Autonetics developed MICRON grounding and EMI guidelines; developed a detailed work breakdown structure; provided documentation and engineering support related to establishing a second source for MESH rotors and cavities; developed and modified as necessary a system engineering management plan; developed and modified as necessary personnel, marketing, financial, facilities, program, and contract data management plans; and documented the MESH angle readout model.

#### 6.1.1 Design Reviews

##### 6.1.1.1 Informal Design Reviews

A total of ten (10) informal design reviews were conducted during the course of the Phase 2A contract. All these design reviews were held at Autonetics.

6.1.1.1.1 First Informal Design Review. The first informal design review was held on 30 April through 2 May 1974. Personnel in attendance from organizations other than Autonetics were Capt R. R. Warzynski and Capt G. C. Radic, both of AFAL/666A. The agenda for this design review was as follows:

#### Tuesday, April 30

10:30	2nd Source Rotor/Cavity Data Pack	H. L. Bump
1:30	N57A-1 Status and Data Review	L. B. Romine/J. C. Pinson
3:00	N57A-2 Integration/Calibration	T. F. Brasher
4:00	ECOM Gyro Tests	H. L. Bump

#### Wednesday, May 1

9:00	Holloman Subassembly	D. Holmes
10:00	Final $\phi$ 1B Report	R. B. Higley/L. B. Romine
10:30	LAX Flight Test Preparation Status	G. A. Bloomstadt/T. F. Brasher
1:30	DPU Status Review	W. P. Thoennes
2:00	MESGA Analysis and Test Data	R. B. Hall/D. T. Friest
3:00	Parts Program Review	A. L. Sattler
4:00	Design Evaluation Model Plans	W. A. Thompson



Thursday, May 2

9:00	Getter Gyro	J. C. Boltinghouse
9:45	Phase 2A Cost Proposal	J. A. Schwarz/C. M. Wardman/ G. E. Runyon

6.1.1.1.2 Second Informal Design Review. The second informal design review was held on 14 through 17 May 1974. The following personnel from organizations other than Autonetics Anaheim attended this design review:

<u>Name</u>	<u>Organization</u>
Capt R. R. Warzynski	AFAL/666A
Capt G. C. Radic	AFAL/666A
Sgt R. Acosta	AFAL/666A
R. W. Burrows	Martin Marietta
R. A. Holtz	Martin Marietta

The agenda for the second informal design review was as follows:

Tuesday, May 14

Morning	1. Phase 2A Material Questions	G. E. Runyon
	2. Phase 2A data cost estimate by CDRL item	J.W. MacDonald
	3. Phase 2A Travel backup info	J.W. MacDonald/ G. E. Runyon
Afternoon	1. Phase 1B P0013 SOW Change	J. A. Schwarz/ J. Terry
	2. Field Engr Training/Mockup for N57A-2 support at Holloman	J. A. Schwarz/ G. E. Runyon
	3. Questions on Phase 2A Mgmt Volume	J. A. Schwarz/ L. B. Romine

Wednesday, May 15

Morning	Appendix I (MICRON IMU Spec)	J. A. Schwarz/ G. E. Runyon
Afternoon	Phase 1B Final Report	R. Hitley/L. Romine

Thursday, May 16

Morning	Richard Burrows/Ray Holtz Visit	J. A. Schwarz/
	Martin Marietta-Denver	L. B. Romine
	Reliability Associate Contractor	G. E. Runyon
Afternoon	Phase 2B SOW, CDRL, Schedule and Funding	J. A. Schwarz/ G. E. Runyon G. W. Sargent

Friday, May 17

Morning	1. Parts Tab Questions	A. Sattler/J. Klinchuch
	2. Parts Program (including vendor bids)	A. Sattler

Afternoon Baseline MICRON System Definition M. Rupert/L. Romine

6.1.1.1.3 Third Informal Design Review. The third informal design review was held on 25 through 28 June 1974. Personnel in attendance from organizations other than Autonetics were Capt R. R. Warzynski and Capt G. C. Radic, both of AFAL/666A. The agenda for this design review was as follows:

Tuesday, June 25

1:30	HAFB Flight Testing	Daryl Crouse
2:30	HAFB GSA	Don Holmes

Wednesday, June 26

9:00	Electronics Thermal Dissipation (XN-77/MICRON)	Jack Klinchuch Hiroshi Kamei Bill Thompson
1:30	Phase 2A Prime	Jerry Schwarz Gerry Runyon John Terry

Thursday, June 27

9:00	Parts Program	Art Sattler
10:30	ECOM Fast Reaction Results	Pete Bump
1:30	Reliability	Ray Holtz
2:30	Getter Gyros	Joe Boltinghouse
3:30	MESGA	Bob Hall

Friday, June 28

9:00	Cost of Ownership	Milt Rupert
10:30	XN-77	G. Sargent

6.1.1.1.4 Fourth Informal Design Review. The fourth informal design review was held on 23 through 25 July 1974. In addition to reviewing the MICRON Phase 2A status, the purpose of this meeting was to get all associates/primes together with all government personnel involved to:

1. Meet the personnel from the various organizations
2. Establish points of contact

3. Coordinate all efforts to avoid overlap/duplication
4. Understand what each associate/prime SOW involves

The following personnel from organizations other than Autonetics Anaheim attended this meeting:

<u>NAME</u>	<u>ORGANIZATION</u>	<u>POSITION</u>
Capt Bob Warzynski	AFAL (NVA/666A)	MICRON Project Engineer
Lt Col Jim Canaday	AFAI (NVA/666A)	666A Program Manager
Capt G. C. Radic	AFAL (NVA/666A)	Project Engineer
Sgt R. D. Acosta	AFAL (NVA/666A)	Flight Test Engineer
Maj Ralph W. Holm	AFAL (NVA/666A)	NVA/666A (Future Program Manager)
George A. Langston	AFAL/NVA	Branch Technical Assistant
R. M. Werner	AFAL/TEA W-PAFB	Project Engineer
Lt Co. Ewald	AF/RDPN	PEM 63203F
George E. Himes	WPAFB 4950-PMEB	Procuring Contract Officer
Capt L. F. Sandler	6585 TG/GDP	Test Director
Capt B. Montgomery	6586 TG/GDOA	Project Engineer
Jerry Durant	AFPRO Q. A.	Q. A. Supervisor
Jack Faradjollah	AFPRO IEN	Project Engineer
K. Bell	AFPRO, R/I	Procurement
G. E. Atkisson	AFPRO/TMD	ACO AF
Ray Clark	USA ECOM-Ft Monmouth	Project Engineer
Jim Shields	TASC	Project Engineer
Chuck Ormsby	TASC	Project Engineer
Ted Blaschke	TASC	Project Engineer
Ed Toohey	TASC	Project Engineer
R. W. Burrows	Martin-Marietta	Reliability Program Manager
Ray A. Holtz	Martin-Marietta	Technical Director
John Bouchard	Northrop	Reliability Analysis
W. G. Merritt	Northrop	Director
R. O. Westhaver	Northrop	Program Manager
Julius Feldman	CS Draper Laboratory	Project Engineer

The agenda for the fourth informal design review was as follows:

Tuesday, July 23

9:00	MICRON Program Overview	Capt Warzynski
10:00	Autonetics Status Overview	J. A. Schwarz
11:00	MIT Non-Destructible Gyro Overview	Julius Feldman
11:30	TASC Software Overview	Ted Blaschke
1:30	Northrop MESH 2nd Source Overview	Bob Westhaver
2:00	Martin Marietta Reliability Overview	Dick Burrows

2:45	Holloman AFB Flight Test Overview	Capt Sandlin
3:15	Autonetics Engineering Overview	G. E. Runyon
3:45	MICRON Laboratory Tour	L. B. Romine

Wednesday, July 24

9:00	Mechanization, Modeling and Software Status	Gus Andrews
9:30	Electronics Design Status	Paul Ito/Tom Wada/ Bob Jones
10:30	Electronic Parts Program	Arnold Fanzoi
11:15	Design Evaluation Models	Bill Thompson
1:30	Test Equipment Plans/Status	Charlie Whang
2:00	Gyro Design and Test	Pete Bump
2:30	MESGA	Bob Hall
3:00	System Engineering and System Test	Tom Brasher
3:30	Cost of Ownership	Milt Rupert/Lee Johnson F. R. (Bob) Hall/ Ray Holtz (MMC)/ Keith Gibson

6.1.1.1.5 Fifth Informal Design Review. The fifth informal design review was held on 3 through 5 September 1974. Personnel in attendance from organizations other than Autonetics were Capt R. R. Warzynski and Capt G. C. Radic, both of AFAL/666A, and R. A. Holtz of Martin Marietta. The agenda for this design review was as follows:

Tuesday, September 3

10:30	XN77	Jim Cross
11:00	Monthly Status Report	Joe Miller/
	Content	Larry Romine
	DID	
1:00	N57A-2 Status	Tom Brasher
2:00	2nd Source Data Pack	Pete Bump
2:30	New ESG Fabrication Facility	Pete Bump
3:00	DI-E-3101 Modification for General System Specification (Data Sequence No. B002)	Tom Brasher
4:00	Beam Lead Parts Costs	Jerry Schwarz
4:30	HAFB Gyro Subassembly	Don Holmes

Wednesday, September 4

8:30	Cost of Ownership - Cost Status	Jim Cross/Milt Rupert Lee Johnsen
10:15	Call George Himes regarding: Phase 2A Prime	Jerry Schwarz
10:30	In-Motion Polhode Damping	A. P. Andrew ,
11:00	Self Calibration	J. Wauer
1:00	Applications Engineering	Schwarz/Romine
2:00	Phase 2A Schedule (including Phase 2A Prime + Option)	Romine/Miller
3:30	Temperature Specification Range on Electronic Parts (deviate for cost benefits?)	Sattler/Brasher/ Klinchuch/Romine

Thursday, September 5

8:30	Funding Schedule Phase 2A Phase 2A Prime Option	Jerry Schwarz
9:30	Cost of Ownership - Reliability Status	Hall/Holtz
10:30	Martin Marietta Status	Ray Holtz
1:30	Discussions on Design Evaluation Models	Whang/Thompson

6.1.1.1.6 Sixth Informal Design Review. The sixth informal design review was held on 16 through 18 October 1974. The following personnel from organizations other than Autonetics Anaheim attended this design review:

<u>Name</u>	<u>Organization</u>
Capt R. R Warzynski	AFAL/666A
Capt G. C. Radic	AFAL/666A
Don Vanderstoep	TASC
Jim Shields	TASC
Ed Toohey	TASC
Chuck Ormsby	TASC

The agenda for the sixth informal design review was as follows:

Wednesday, October 16

9:00	N57A-2 Flight Test (LAX and Holloman)	Brasher
10:00	Getter Gyro	Gross/Bump
11:00	Parts Program	Sattler

1:30	Applications Engineering	Romine/Runyon/ Brasher/Rupert
3:30	Design Evaluation Models/Packaging	Whang/Thompson

Thursday, October 17

8:30	Cost of Ownership	Cross/Rupert/ Johnsen/Hall/Gibson
10:30	Cost of Reduction via MOS	Schmidt/Romine/ Klinchuch/Gunckel
1:00	MESGA	J. C. Pinson
2:30	Gyro Improvements Status	Boltinghouse/Bump
3:30	Fast Reaction	Friest/Fisher

Friday, October 18

8:30	CFY 75 MESG IR&D	Romine/Klinchuch
9:30	XN77 IMU Status	Cross
11:00	Phase 2A Cost Status	Schwarz/Runyon

6.1.1.1.7 Seventh Informal Design Review. The seventh informal design review was held on 11 through 13 November 1974. Personnel in attendance from organizations other than Autonetics Anaheim were Capt R. R. Warz, aski of AFAL/666A and Mr. J. C. Barron, Rockwell International, Washington, D.C. There was no formal agenda for this design review.

6.1.1.1.8 Eighth Informal Design Review. The eighth informal design review was held on 17 through 19 December 1974. Personnel in attendance from organizations other than Autonetics were Maj R. W. Holm and Capt R. R. Warzynski, both of AFAL/666A, and J. J. Szalona of AFPRO/EN. The agenda for this design review was as follows:

Tuesday, December 17

2:00	Phase 2A Status Overview	G. E. Runyon
3:00	MESG Rotor & Cavity Fabrication Times	L. E. Johnsen
3:30	Conformal Coating of Substrates	J. J. Licari
4:00	Status on CPC Producibility Studies	L. F. Johnsen
4:30	Parts Program	A. L. Sattler

Wednesday, December 18

8:00	Answers to Monthly Report Comments	L. B. Romine
8:30	N57A-2 Status	T. F. Brasher
9:00	Autonetics Recommendation for Restructuring MICRON Program for ACF	J. A. Schwarz/G. W. Sargent L. B. Romine/G. E. Runyon

1:00 Continue Reconstructed Program Discussions

Thursday, December 19

8:30 Lab Tour

D. W. Holmes

9:30 AFAL/AFPRO Discussions

Joe Szalona

10:00 Continue Reconstructed Program Discussions

J. A. Schwarz/G. W. Sargent  
L. B. Romine/G. E. Runyon

1:00 Restructured Program Conclusions

J. A. Schwarz/G. W. Sargent  
L. B. Romine/G. E. Runyon

6.1.1.1.9 Ninth Informal Design Review. The ninth informal design review was held on 15 through 17 January 1975. Personnel in attendance from organizations other than Autonetics were Capt R. R. Warzynski and Capt G. C. Radic, both of AFAL/666A. The agenda for this design review was as follows:

Wednesday, January 15

2:00 Realigned Phase 2A Cost Discussions

J. K. Terry/J. MacDonald  
L. B. Romine/G. E. Runyon

Thursday, January 16

8:30 Velocity Error Specifications

A. P. Andrews

9:30 Realigned Phase 2A Cost Discussions

J. K. Terry/J. MacDonald  
L. B. Romine/G. E. Runyon

1:30 Review MICRON System  
Comparison/Evolution Chart

L. B. Romine/M. J. Rupert  
K. J. Gibson/L. E. Johnsen

2:30 Phase 2B Program Discussions

L. B. Romine/G. E. Runyon  
J. K. Terry

Friday, January 17

8:30 AFAL Questions on November Status  
Report

L. B. Romine/  
J. Miller

10:00 Realigned Phase 2A Cost Discussions

J. K. Terry/J. MacDonald  
L. B. Romine/G. E. Runyon

1:30 Phase 2B Program Discussions

L. B. Romine/G. E. Runyon  
J. K. Terry

6.1.1.1.10 Tenth Informal Design Review. The tenth informal design review was held on 28 through 30 April 1975. Personnel in attendance from organizations other than Autonetics were Capt R. R. Warzynski and Capt. W. Peterson, both of AFAL/666A. The agenda for this design review was as follows:

Monday, April 28

9:00	Gyro Development	H. L. Bump
11:00	Electronics Development	J. F. Klinchuch
1:30	Electronics Development (Cont)	J. F. Klinchuch
2:30	GSA Test Stations	C. C. Whang, Jr.
3:00	MICRON Packaging Studies	C. C. Whang, Jr.
3:30	Rotating MICRO	C. C. Whang, Jr.
4:00	Alternate Computer	A. P. Truban

Tuesday, April 29

8:00	AFPRO	Capt Moore
9:00	Dedicated Processor Unit	W. P. Thoenes
10:00	MOS Development	W. P. Thoenes
11:00	EMA's	K. K. Jin
1:30	Alternate Computer, Alternate Accelerometer	A. P. Truban
2:30	Test Activities	T. F. Brasher/D. W. Holmes
4:00	System Engineering	T. F. Brasher

Wednesday, April 30

9:00	System Analysis	A. P. Andrews
10:30	Parts Program	A. L. Sattler
1:30	Monthly Questions	J. M. Miller
2:30	Cost of Ownership	M. J. Rupert, et al

6.1.1.2 Phase 1B Final Fee Evaluation Review

On 17 February 1975, the Phase 1B Final Fee Evaluation Review was held at Autonetics. This meeting was prepared and conducted on Phase 1B funding.

The following personnel from organizations other than Autonetics Anaheim attended this meeting:

<u>Name</u>	<u>Organization</u>
Maj Ralph W. Holm	AFAL/666A
Capt Robert R. Warzynski	AFAL/666A
Capt Carl L. Moore	AFPRO/EN
Capt Theta Y. Brentnall	4950/PMP
Capt George Radic	AFAL/666A
George E. Himes	4950/PMEB
J. O. Roberts	Rockwell Central Region Office
J. H. Gilmore	Rockwell Northeastern Dist Office



The agenda for the Phase 1B Final Fee Evaluation Review meeting is presented below:

8:30	Introduction	Capt Warzynski/ J. A. Schwarz
9:00	X-Ray Testing Results (Task 7)	T. F. Brasher
9:45	Mechanization Improvements and Additional Testing (Tasks 17 and 18)	T. F. Brasher
10:45	Fabrication, Integration, and Testing of 2nd N57A System (Tasks 12, 14, 15, and 16)	D. W. Holmes
11:30	Flight Test Planning/Preparation (Task 19)	D. W. Holmes
1:00	Delivery (Hardware/Data)	G. E. Runyon
1:30	Contract Administration	
	Cost	E. Ghironzi
	Administrative Aspects	J. K. Terry
2:15	Summary	J. A. Schwarz
3:00	Fee Evaluation Board Meeting (Govt only)	

#### 6.1.1.3 System Requirements Review

On 18 through 21 February 1975, the System Requirements Review was held at Autonetics in conjunction with the first Phase 2A fee evaluation meeting.

The following personnel from organizations other than Autonetics Anaheim attended this meeting:

<u>Name</u>	<u>Organization</u>
Maj Ralph W. Holm	AFAL/666A
Capt Robert R. Warzynski	AFAL/666A
Howard Steenberg	AFAL/TEA
John M. Blasingame	AFAL/TEA-3
Capt Carl L. Moore	AFPRO/EN
Capt John A. Krumm	HAFB/GDAG, 6585TG
Capt Theta Y. Brentnall	4950/PMP
Ray A. Holtz	Martin Marietta
R. W. Burrows	Martin Marietta
Anthony D. Pettinato	RADC/Rel and Maintenance
J. J. Szalona	AFPRO/EN
J. L. Cook	AFAL/APA-4
Lt Stephen Ringlee	ASD/ACCC
Ray Clark	ECOM
George E. Himes	4950/PMEB
Capt George Radic	AFAL/666A
James D. Shields	TASC
Charles C. Ormsby	TASC

Name  
P. R. Kerrigan  
R. O. Westhaver  
J. O. Roberts  
J. H. Gilmore

Organization  
Draper Lab  
Northrop Corporation  
Rockwell Centre Region Office  
Rockwell North Western District Office

The agenda for the Phase 2A First Fee Evaluation/Design Review Meeting is presented below:

**Tuesday, February 18**

8:30	Introduction	Capt R. Warzynski/ J. A. Schwarz
9:00	Autonetics Overview	G. E. Runyon
9:45	*TASC Presentation	J. Shields
11:00	*Martin Presentation	R. Burrows/R. A.
1:00	*Northrop Presentation	R. O. Westhaver
2:00	*CSDL Presentation	P. Kerrigan
2:45	DPU Design Tradeoffs (Task 5.3)	W. P. Thoenes
3:45	Parts Program (Task 5.2)	A. L. Sattler
4:30	*XN77 Status	A. P. Truban

\*Information Only - Not subject of this Fee Evaluation Review

**Wednesday, February 19**

8:30	Design, Fab, Integrate Gyro Test Station (Task 1.3)	J. D. Courtier
9:00	Test Planning (Task 2.1)	T. F. Brasher
9:15	N57A-2 Laboratory Testing (Task 2.2)	T. F. Brasher
10:00	N57A-1 and -2 Flight Test at LAX (Task 2.3, 2.4 and 4.3)	D. W. Holmes
10:45	Gyro Subassembly Design and Fab (Task 3.1)	J. F. Klinchuch
1:00	N57A-1 Refurbishment (Task 3.4)	A. J. Orsak
1:15	Grounding and EMI Guidelines (Task 5.1)	A. J. Orsak
1:45	N57A-2 Training Program (Tasks 4.1, 4.2 and 4.3)	F. L. Wood
2:15	Holloman Gyro Subassembly Testing at Holloman (Task 4.3)	D. W. Holmes
2:30	N57A-2 Flight Tests at Holloman AFB (Task 4.3)	D. W. Holmes

3:15	Cost of Ownership (Task 5.2)	M. J. Rupert
	Producibility	L. E. Johnser.
	Reliability	F. R. Hall
	Maintainability	K. J. Gibson

#### Thursday, February 20

8:30	MESGA (Task 5.3)	J. C. Pinson
9:00	Vacuum Pump Elimination (Task 5.3)	A. G. Gross
9:45	4-Plate Gyro (Task 5.3)	J. C. Boltinghouse
10:15	Error Analysis/Error Budget/Software (Task 1.1 and 1.2)	R. W. Fisher/ A. P. Andrews
11:15	Software Improvements (Task 5.3)	A. P. Andrews/ J. C. Wauer
1:00	Hardware Improvements (Task 5.3)	H. L. Bump
1:45	Design, Fabricate, Integrate and Test Design Evaluation Models (Tasks 1.1, 2.1, 2.2 and 5.3)	C. C. Whang, Jr.
3:00	Design (Packaging) Alternatives (Task 5.3)	C. C. Whang, Jr.
4:00	Applications Engineering (Task 5.4)	D. W. Holmes
4:30	Data (Task 6)	J. M. Miller

#### Friday, February 21

8:30	Technical Summary	G. E. Runyon
9:30	Contract Administration	
	Cost	E. Ghironzi
	Administrative Aspects	J. K. Terry
10:45	Summary	J. A. Schwarz
1:30	Fee Evaluation Board (Government only)	

#### 6.1.1.4 System Design Review

The System Design Review will be held at Autonetics in October 1975 in conjunction with the Final Fee Evaluation Review.

#### 6.1.2 Program Plans

The MICRON Phase 2A System Engineering Management Plan was originally submitted to the customer in June 1974 as CDRL Item A00S. This plan was subsequently revised to reflect modification P00003 to Contract F33615-74-C-1099 and was submitted to the customer in October 1974 as CDRL Item A00S.

The Contract Data Management Plan was originally submitted to the customer in May 1974 as CDRL Item A003. This plan was subsequently revised to reflect modification P00003 to the contract and was submitted to the customer in August 1974 as CDRL Item A003.

Other MICRON Phase 2A program plans including personnel, marketing, financial, facilities and program plans were submitted to the customer in June 1974. These plans were subsequently revised to reflect modification P00003 to Contract F33615-74-C-1099. The revised personnel, financial, and facilities plans were submitted in October 1974. The revised program plan was submitted in November 1974.

#### 6.1.3 Work Breakdown Structure

The Work Breakdown Structure (WBS) for MICRON Phase 2A was submitted to the customer in May 1974 as CDRL Item A004. The WBS was revised to reflect modification P00003 to Contract F33615-74-C-1099 and submitted to the customer in September 1974 as CDRL Item A004.

#### 6.1.4 Grounding and EMI Guidelines

The interdependence of disciplines in the area of cabling, connectors, electrical bonding, grounding, shielding, and filtering basic to electromagnetic compatibility (EMC), required combining the Grounding and EMI Guidelines into one document. This document, "Micro Navigator (MICRON) Phase 2A Electromagnetic Compatibility, Grounding, and EMI Guidelines" (C74-919/201) was submitted to the customer in October 1974.

These grounding and EMI guidelines present techniques, for MICRON IMU grounding circuit design, that can maximize the electromagnetic compatibility and minimize the susceptibility to EMI of the MICRON IMU when it is operating in an avionics system environment. These techniques encompass disciplines in the areas of cabling, connectors, electrical bonding, grounding, filtering, and shielding.

#### 6.1.5 Second Source Rotors and Cavities

Specifications and drawings were produced and updated throughout Phase 2A as required to reflect the latest materials, processes, tooling, and MESG parts configuration. This effort was in support of the second source task and CDRL Items A00B, A00C, and A00D. This effort was intended to establish a second source capability for fabrication of rotors and cavities from the point of raw material purchase. Latest definition of parts includes five mil electrode separation, small equatorial chamfer, and three wire rotor configurations.

The Phase 2A second source development activities consisted of five primary areas of effort; namely,

1. Autonetics fabrication and delivery of parts
2. Drawings and specifications
3. Telephone conversations

4. In-house visits by second source personnel

5. Test and evaluation of the parts

Each of the first four activities listed are summarized below. The fifth activity listed was performed under Task 2, Test and Evaluation, and is discussed in Para 3.2.6.

6.1.5.1 Autonetics Fabrication and Delivery of Parts

Autonetics fabricated and delivered ten (10) cavity sets ready for plating and twelve (12) rotors which were in the eloxed condition and ready for the finishing processes. Eight rotors were delivered to AFAL for use by the Charles Stark Draper Laboratory (CSDL). The rotors were of proper size and had been used in MESG instruments previously.

6.1.5.2 Drawings and Specifications

All drawings, specifications, and supporting documents necessary to fabricate cavities and rotors were sent to second source via AFAL.

An initial submittal of four specifications and 78 drawings was made in June 1974 as CDRL items A00B, A00C, and A00D. These drawings were necessary to define the early tooling equipments. The equipments include: Rotor lapping machine, cavity spherometer comparator, cavity equator comparator, cavity equator chamfer comparator, ring and disc set masters, slot lapping fixture, and a cavity lapping machine.

The intent for early submittal of drawings and specifications was to establish, as early as possible, the second source capability to fabricate rotors and cavities from the material items provided by Autonetics.

A second drawing and specification package (CDRL items A00B, A00C, and A00D) was submitted in December 1974 which permitted Northrop to fabricate rotor and cavity parts from the raw material state. The package also defined the raw materials. A list of MESG material suppliers was also transmitted to second source. The list included (1) name or stock number, (2) dimensions and type of material per Autonetics specification number, and (3) suppliers name and address. Preliminary documentation was also provided to Northrop which permitted initial contact with their sources for purchase of BeO cavity material, beryllium rotor material, and beryllium billet extrusion processing.

Drawings and specifications with regards to MESG rotors, cavities and tooling were in continuous change and update during the developmental program. All changes and/or updates in drawings and specifications were forwarded to Northrop during the contract.

Fabrication, process and supporting documents used in fabrication of ESG rotors and cavities, sent to second source, are as follows:

AA0103-004	Electrical Discharge Machining
AA0104-001	Marking of Elec & Mech Items
AA0109-009	Deposition of an Elect Nickel-Phosphorous Plate
AA0109-023	Preparation of Basis Mat for Final Plating
AA0109-050	Sputter Deposition of Chromium & Gold on BeO
AA0109-051	Electroless Deposition of Nickel-Phosphorous Plate on Gold
AA0110-008	Cleaning of Beryllium
AA0115-003	Det of Mag Suscept for Plat Used in Prec Inst
AA0117-004	Handling of Flam & Dangerous Liquids & Chemicals
AA0117-005	Safety & Environ Health Req for Mach & Handling of Be Alloys & Compositions
AA0110-035	Solvent & Deterg Clean of Inertial Instrument Components
AA0111-003	Thermal Treatment of Beryllium
AB0115-006	Ceramic, BeO Dense
AB0170-067	Beryllium, Extruded (for Precision Instrument Application)
AB0210-007	Solvent, Trichlorotrifluoroethane (Type TF) Inert Inst Grade
AB0210-008	Solvent, Petroleum
ST0115AA0010	Mach Parts; Tol, Surface Finish Stand Config
ST0115AA00103	Req of Cleanroom, Clean Work Station & Controlled Area
ST0140AB0012	Grease Ball & Roller Bearings, Sodium Base
ST0170AB002	Be Billet, Bar & Shaves; Hot Pressed Powder or Flake
ST0115AA0089	Radiographic Inspection
ASTM B365-70	Tantalum Wire Spec
AL70030	Rotor, Auto P/N 12504-302; Hot Lapping Procedure
AL70032	Cavity, Rotor; Auto Dwg No. 12700-302 Lapping Procedure

The following drawings, in support of the ESG program, were sent to second source:

12504-302	ROTOR			
12698-302	CAVITY, ROTOR			
12699-302	CAVITY, ROTOR (PLATED)			
12700-302	CAVITY, ASSY, ROTOR			
10000-207	ROTOR LAPPING MACHINE - ESG			
10001-207	BASE	ROTOR LAPPING MACHINE		
10002-207	CARTRIDGE HOLDER	"	"	"
10003-207	INSULATOR	"	"	"
10004-207	SHAFT	"	"	"
10005-207	CAP	"	"	"
10006-207	SPINDLE	"	"	"
10007-207	BODY	"	"	"
16308-207	BUSHING	"	"	"
10009-207	CLAMP	"	"	"
10010-207	ADAPTER	"	"	"
10011-207	PIN	"	"	"
10012-207	LAP	"	"	"
10013-207	LOCK PIN, CARTRIDGE	"	"	"
10014-207	WASHER	"	"	"
10015-207	PLATE	"	"	"
10016-207	WHEEL	"	"	"
10017-207	TRUNNION	"	"	"
10018-207	SHAFT, CRANK	"	"	"
10019-207	SPACER	"	"	"
10020-207	BLOCK	"	"	"
10021-207	SLIDE	"	"	"
10022-207	WAY	"	"	"
10023-207	CLAMP	"	"	"
10024-207	HANDLE	"	"	"
10025-207	BUSHING	"	"	"
10026-207	BLOCK, STOP	"	"	"
10027-207	PULLY, MOTOR	"	"	"
10028-207	CAM, SLIDE	"	"	"
10029-207	SHIM, MOTOR	"	"	"
10030-207	BRACKET	"	"	"
10031-207	SHIELD	"	"	"
10032-207	COMPARATOR, CAVITY SPHEROMETER - ESG			
10033-207	HEAD,	SPHERICAL DIA COMPARATOR		
10034-207	TIP	"	"	"
10035-207	TIP AND WEIGHT	"	"	"
10036-207	SUPPORT RING	"	"	"
10037-207	NUT, COLLET	"	"	"
10038-207	CARTRIDGE HOLDER	"	"	"
10039-207	COMPARATOR, CAVITY EQUATOR - ESG			

10040-207	HEAD	COMPARATOR CAVITY EQUATOR		
10041-207	TIP	"	"	"
10042-207	COMPARATOR, CAVITY EQUATOR CHAMFER - ESG			
10043-207	HEAD	CAVITY EQUATOR CHAMFER		
10044-207	PIN	"	"	"
10045-207	GAGE	"	"	"
10046-207	RING, SET MASTER, CAVITY COMPARATOR - ESG			
10047-207	DISC,	"		
10048-207	SLOT LAPPING FIXTURE			
10049-207	HOLDER, SLOT LAPPING FIXTURE			
10050-207	BASE,	"	"	"
10051-207	RETAINER	"	"	"
10052-207	ROTATOR	"	"	"
10053-207	ALIGNMENT GAGE, SLOT LAPPING FIXTURE			
10054-207	CUTTER	"	"	"
10055-207	SLIDE	"	"	"
10056-207	CAVITY LAPPING MACHINE			
10057-207	HOLDER, CAVITY LAPPING MACHINE			
10058-207	LAP,	"	"	"
10059-207	SPINDLE	"	"	"
10060-207	DRIVER	"	"	"
10061-207	COLLAR, DRIVE	"	"	
10062-207	ADAPTER	"	"	
10063-207	STANDOFF	"	"	
10064-207	PLATE SIDE	"	"	
10065-207	GUSSET, CAVITY LAPPING MACHINE			
10066-207	ARM, CONNECTING	"		
10067-207	BRACKET, ASSY	"		
10068-207	INDICATOR,	"		
10069-207	CRANK,	"		
10070-207	ARM,	"		
10071-207	BLOCK, PILLOW,	"		
10072-207	SHAFT,	"		
10073-207	BRACKET,	"		
10074-207	BASE,	"		
10075-207	POT CHUCK FIXTURE			
10076-207	ELECTRODE, ELOX			
10077-207	CAVITY TOOL, HAND LAPPING			
10078-207	MASK, SPUTTER			
10079-207	CAVITY HOLDER - TALYROND			
10080-207	CAVITY GRIND FIXTURE			
10081-207	SUPPORT-TEMP CONTROLS	ROTOR LAPPING MACHINE		
10082-207	COVER	"	"	"
10083-207	PROBE-TEMP	"	"	"
10084-207	SHIELD	"	"	"
10089-207	ROTOR MEASURING FIXTURE - TALYROND			
10090-207	BAKE FIXTURE, ROTOR			
12795-302	BILLET, EXTRUSION, ROTOR			
12796-302	EXTRUSION, ROTOR			



### 6.1.5.3 Telephone Conversations

Telephone conversations, their dates and substance are summarized as follows:

<u>Date</u>	<u>Substance</u>
2 August 1974	<p>Comments with regard to the discrepancies on parts as furnished by Autonetics to the second source.</p> <p>Autonetics' anticipated delivery date of the remaining four cavity sets to the second source.</p> <p>Autonetics anticipated delivery date of additional specifications requested by the second source.</p>
5 Sept 1974	<p>Discussed content of letter sent through AFAL with regard to discrepancy of parts as measured by Northrop.</p> <p>Northrop also indicated no intent to measure components at 140°F.</p>
18 Sept 1974	<p>Discussed/set up Northrop visit on 24, 25 and 26 September 1974.</p>
11 Nov 1974	<p>Mr. Ron Pagels called to determine the meaning of the "Information Only" stamp on the face of a specification. It was explained that the intent of the stamp is to inform the user that the particular copy would not be automatically updated by the print control crib.</p>
14 Jan 1975	<p>Conversation with Northrop regarding (1) billet design change, (2) "STARBURST" pattern on rotor surface finish, and (3) cavity BeO surface finish.</p>
16 Jan 1975	<p>Conversation with Northrop regarding (1) why different lapping compounds were used for the room temperature lapping and the 147°F lapping, (2) Mikrokator force (rotor size measurement) and (3) methods of parts packaging for shipment to Autonetics.</p>
23 Jan 1975	<p>Conversation with Northrop regarding (1) room temperature out of roundness of hot lapped rotors and (2) Mikrokator forces present/used when measuring rotor size.</p>
30 Jan 1975	<p>Discussion with Northrop regarding</p> <ol style="list-style-type: none"><li>1. The data package which was sent to Northrop via AFAL on 12-20-74. Northrop indicated that a specification (MAB-205-M) was not included in the package. The specification is available through the Materials Advisory Board, National Academy of Sciences National Research Council, Washington, D. C. A copy however was located in</li></ol>

Autonetics Central Library which was reproduced and sent to Northrop via Capt Radic AFAL.

2. A cavity set which was near completion. The plating on one part lifted at/near a plate edge/corner. There had been an apparent separation at the chrome to gold interface.

6 Feb 1975

Mr. R. Westhaver of Northrop called to inform Autonetics that the first rotor (Z16) and cavity set (A0001) had been shipped on 5 February 1975. The intended testing on these parts was discussed.

#### 6.1.5.4 In-house Visits by Second Source Personnel

The following is a summary of the visits made to Autonetics by second source personnel:

11 Sept 1974

Charles Stark, Draper Lab personnel (Mr. K. Taylor and Mr. J. McCuen) visited Autonetics for a full day discussion of cavity and rotor fabrication. A shop tour was conducted to familiarize them with Autonetics plating technique (nickle chrome, gold), beryllium extrusion process, rotor and cavity fabrication techniques and instrument assembly technique. The primary discussion was with regards to cavity fabrication. A series of drawing and specs were provided at the request of CSDL.

24 through  
26 Sept 1974

Northrop personnel (Mr. F. A. Hallock, Mr. R. D. Pagels and Mr. K. Milo) visited Autonetics. All aspects of cavity and rotor fabrication were covered during the three days and included shop tours, plating technique (nickle, chrome, gold), beryllium extrusion process, and instrument assembly.

17 Jan 1975

In-house discussions were held between Capt Radic, L. B. Romine and H. L. Bump with regard to:

1. Northrop suggestions given to AFAL with respect to process improvements.
2. Northrop problem areas alluded to in the 1-14-75 telecon listed above.
3. Method of the in-house Air Force AFPRO buy off of parts as provided by Northrop. The buy off will essentially be one of "parts count only." It was agreed that Northrop should deliver the first parts at the time of the design review (2-17-75) in order to preclude shipping handling problems and to also ease the method of AFPRO buy off.

4. Provision of four additional cavity halves to Northrop. It was suggested that, since Northrop is required to deliver only six sets of the 10 provided by Autonetics and since there is little or no probability of parts damage of the 10 sets in Northrop's processing, strip and replating of problem parts could be accomplished to achieve final quantity goals. The strip and replating method was included in the data package provided to Northrop.
5. Provision of two additional rotors (eloxed condition) to Northrop. The two units were given to Capt Radic on 1-17-75 for delivery to Northrop.

18 through  
20 Feb 1975

During the period of the System Requirements Review, discussions were held with Northrop, CSDL, and Martin Marietta. These discussions are summarized below.

Initial size measurements on Northrop rotor and cavity set and Northrop master rotor and cavity parts were discussed with Northrop. Cavity set No. 87 was returned to Northrop. This particular cavity set was fabricated by Northrop and was installed in an instrument in March 1973. Contamination found on A0001 cavity set as received by Autonetics was also discussed.

Rotor and cavity fabrication techniques were discussed with Mr. Paul Kerrigan of CSDL. A rough tour of the shop was conducted to expose Mr. Kerrigan to Autonetics' processes.

Initial discussions were held with Mr. Lyle Berquist of Martin Marietta regarding getter efforts and Vac Ion pump sure start.

13 through  
15 May 1975

The last two sets of Northrop rotors and cavities were hand carried to Autonetics by Mr. R. Westhaver and Mr. R. Pagels on 13 May 1975. The parts were taken to the dust controlled area where comments by Engineering with regard to the parts, and AFPRO and Autonetics inspection observations were documented in the presence of the Northrop personnel. In addition to the inspection of the last parts delivered, a comparison inspection was made of the first four sets of parts which were delivered by Northrop. It was felt that the discussions at the time of parts inspection were excellent and a definite indication of progress was experienced as the first parts were compared to the final parts. The results and observations with regard to the parts have been forwarded to Northrop via AFAL.

This visit by Mr. Westhaver and Mr. Pagels was very productive. In summary the agenda was:

13 May 1975

R. Westhaver, R. Pagels, H. L. Bump, M. Kohno, AFPRO Rep and Autonetics inspection spent much of the day inspecting

and commenting on all parts which were delivered by Northrop. Problem areas were pointed out and possible corrective action was discussed.

Parts were sent to the Beryllium shop for stabilization in anticipation of parts measurements to be taken on the following day.

14 May 1975      Measured all parts in the Beryllium shop. The parts consisted of:

Cavity Set      N0005  
                    N0006

BeO Master  
440C Master N-7

Rotor Z-23  
Rotor Z-13

Those participating in the measurements of parts were R. Westhaver, R. Pagels, H. L. Bump, K. Lund, J. Kuhn, J. Greene and J. Boltinghouse.

The parts were then sent to Metrology for roundness evaluation. Those participating in the measurements were R. Westhaver, R. Pagels, K. Lund, J. Kuhn, and H. Bump.

Processes and techniques, such as slot lapping, cavity lapping, and rotor lapping were reviewed on this date.

15 May 1975      Review of measurements taken on the previous day was made by R. Westhaver, R. Pagels, K. Lund, and H. Bump. At the conclusion of the review, it appeared that there was agreement between Autonetics and Northrop measurements to within a couple of microinches. It is noted however, that later evaluation and documentation revealed a rotor size discrepancy which will require further understanding and correction.

#### 6.1.6 Angle Readout Model

Autonetics began the development of the angle readout compensation software in 1968, under company funding. Over a period of about four years Autonetics improved the angle readout error compensation capability to the required 200 to 1 improvement factor, and developed calibration and compensation software. In the MICRON Phase 2A contract, Autonetics prepared a technical document which details the derivation and interpretation of these angle readout models. The technical report on the Angle Readout Model (Report No. C74-753/201) was submitted to the customer in July 1974 as CDRL Item A00Q.

## 6.2 COST OF OWNERSHIP

In Task 5.2, Cost of Ownership, Autonetics defined a baseline MICRON IMU, partitioned the functions of the IMU into modules/subassemblies for packaging purposes, and defined potential automated production techniques for the baseline IMU to support cost-of-ownership tradeoffs. Autonetics traded off producibility, reliability, and maintainability to arrive at a balanced MICRON design which exhibits minimum cost of ownership and will satisfy the widest possible range of potential applications. Autonetics developed a MICRON cost-of-ownership model and used it to predict MICRON cost-of-ownership parameters. Autonetics initiated an electronic parts development program; defined and developed specifications for electronic components; initiated development of a carrier and test procedures for reliability screen testing of beam lead components; and initiated development of beam lead devices.

### 6.2.1 Baseline IMU

The purpose of the Cost of Ownership Task 5.2, during the Phase 2A program, was to arrive at a balanced MICRON IMU design which would exhibit a minimum cost of ownership. To accomplish this task, a baseline system was defined and used as a basis for conducting producibility, reliability and maintainability trade-offs.

The initial approach to the program was to update the Phase 1B MICRON IMU definition, functionally partition the IMU to the subassembly and module level, and acquire mechanical and electrical definition. From this definition production processes and techniques were defined. Also costs were calculated in terms of direct labor hours and basebill of material dollars. Failure rates for each module were also calculated.

The Phase 1B MICRON IMU was updated and functionally partitioned to the following subassembly level:

1. Mechanical Housing Unit (MHU)
2. Systems Electronics Unit (SEU)
3. Gyro Accelerometer Unit (GAU)
4. Dedicated Processor Unit (DPU)
5. Input/Output Unit (IOU)

The baseline definition of the MHU included conduction cooling of all modules via a heat exchanger using forced air cooling. It included the capability of internally shock mounting the microelectrostatic gyro-accelerometers (MESGA's). It also provided means for plug-in 2 in. x 2 in. electronic modules.

The SEU was defined to include the support electronics, the spin motor electronics, the power supply, and a battery. Partitioning to the module is shown in Table 6-1.

Table 6-1. Systems Electronics Unit (SEU)

	Quantity per System
Support Electronics	
Temperature Controller	1
Frequency Generator	1
Quasi Reference Generator	1
Frequency Reference and Suspension Timing Generator	1
MUM Timing Generator	1
Preload Reference Modulator	1
Auto Sequencer	1
Gap Monitor	1
Computer Interface	1
Accelerometer Counter	1
Spin Motor Electronics	
Spin Motor Control	1
D/A Converter	1
Spin Motor Control Power Amp	1
Spin Motor Regulator	1
Spin Motor Transistor Power Amplifier	3
Power Supply	1
Battery	1

The GAU was defined to include the MESGA's, the suspension electronics, the MUM electronics, and the acceleration digitizer. Partitioning to the module level is shown in Table 6-2.

Table 6-2. Gyro Accelerometer Unit (GAU)

	Quantity per System
MESGA	2
Charge Amplifiers	8
Sample and Hold	2
Notch Filter	2
Servo Modulator	2
Transformation/Buffer	2
A/D Converter	1
MUM Demodulator	2
MUM Demodulator Sample and Hold	2
Acceleration Digitizer	3

From the functional partitioning of the IMU to the subassembly and module level, as described previously, production processes and techniques were defined. Process flow of the detail electronics, i.e., CPS (ceramic printed substrate) and CPC (ceramic printed circuit) or module assembly were essentially the same as considered during the Phase 1B program. Subsequent screen tests were modified and more extensive. The addition of stabilization bake, thermal cycle, and burn-in (bias power) at the module level (CPC) added another functional test to the flow. Preliminary standards (estimated) for these operations were developed.

Labor and material estimates were completed on the baseline product description. The data was inputted into the cost-of-ownership model. The direct labor hour content was increased by 10 percent relative to the Phase 1B estimate. The increase was the result of additional screen tests at the CPC or module level and the use of chip and fly wire devices in place of previously assumed beam lead devices. Additionally, material costs increased drastically since Phase 1B. This was due primarily to the hi-rel testing requirements and specifications being imposed at the component level. In turn the suppliers did not presently have the capability to accomplish the required screens and test. This uncertainty caused the suppliers to render conservative quotes.

Life Cycle Cost predictions for the Phase 2A baseline system were completed and analyzed. The baseline system definition included the following:

#### Baseline Hardware Description

##### Hardware Breakdown

- 43-2 x 2 Ceramic Hybrid Thick Film Circuits
- Digital Processor Unit
- Power Supply
- Battery
- Mechanical Housing Unit
- 2-MESGA

##### Circuit Types

- Pulse Amplitude Suspension
- N77 Spin Motor Electronics
- Purchased DPU

#### Baseline Manufacturing Location

##### Anaheim

- System Assembly and Test
- MESGA Fab and Test

##### West Virginia

- Ceramic Circuit Fab and Test

#### Baseline Maintenance Concept

##### Organizational Maintenance

- Remove and Replace IMU

##### Intermediate Maintenance

- Verify GO/NO-GO Condition

##### Depot Maintenance

- IMU and Subsequent Repair

The resultant 10 year ownership costs are shown in Table 6-3. Base dollar rates for 1973, 1974, 1977, and 1978 are shown for comparison.



Table 6-3. Baseline System Ten Year Ownership Costs

	Base Year Dollars			
	1973	1974	1977	1978
Production Nonrecurring	4000.	4320.	5440.	5880.
Production Recurring	61222.	64778.	68245.	69907.
Acquisition Cost	65222.	69098.	73685.	75787.
Initial Spares	37089.	29248.	41376.	42388.
Initial Inv. Management	15.	17.	21.	22.
Initial Support Equip.	4780.	4780.	4780.	4780.
Manuals	312.	341.	421.	443.
Initial Maintenance Trng.	2274.	2492.	3077.	3239.
Support Equip. Install	238.	238.	238.	238.
Initial Logistics Cost	44710.	47118.	49914.	51113.
Corrective Maintenance	22161.	23047.	25123.	25903.
Support Equip. Maintenance	4779.	4779.	4779.	4779.
Inventory Management	153.	167.	206.	218.
Maintenance Training	4105.	4498.	5555.	5848.
Maintenance Facilities	273.	300.	337.	389.
Preventive Maintenance	1504.	1649.	2609.	2144.
Repair Transport	2586.	2874.	3544.	3736.
Maintenance Cost	35564.	37317.	41589.	43023.
Cost of Ownership	145496.	153534.	165189.	169924.

Analysis of the data shows that recurring hardware costs is the prime factor in the excessive delta between the goals and the above predictions. These costs show up not only in the Acquisition but also in the Spares Cost and materials cost in Corrective Maintenance.

Table 6-4 shows a break out of the estimated recurring prices to the functional level for the baseline system. Analysis of the data shows that the high price of the GAU and SEU was due to the high cost of electronic parts.

In order to reduce the price of the electronic modules, the following efforts were pursued during Phase 2A:

1. Analyzed electronic circuits to eliminate high cost parts and simplify the circuits.
2. Continued contact with the part suppliers to obtain more realistic quotes.
3. Examined the circuits to determine if a single MOS device could be used to replace discrete parts.
4. Performed cost trade-offs.

Table 6-4. Phase 2A Recurring Price Estimates

System Calibration and Functional Test	\$3,064
MHU	7,331
GAU	28,830
SEU	15,430
DPU	9,235
I/O	888
Totals	<u>\$64,778</u>

Analysis of electronic circuits was accomplished by feeding back to each responsible engineer the costs and cost targets of his circuits. Each engineer was also supplied with a system electronics component parts list with unit costs, a parts list with component costs for each circuit, and a breakdown of each circuit into material and labor costs. The output from this analysis resulted in both circuit simplification and substitutions for high cost parts. This information was used to generate and update cost estimates. This process was continued throughout the Phase 2A Program.

### 6.2.2 IMU Production Processes/Techniques

The task of defining production processes during the Phase 2A program has included the continuation of cost visibility and projections for the MICRON production system. The development of process and system flow charts initially determines the production process. Analysis of this data displays and identifies potential producibility problems and high cost processes. This also provides visual indications of fruitful areas for the application of automated production techniques. Iterations of these data will serve as the primary guide to manufacturing personnel for later detailing of the processes and planning to fabricate, assemble, and test the production MICRON IMU.

The Ceramic Printed Substrate (CPS) process has been analyzed in the thick film fabrication shop and at the assembly level. Design guidelines and specific process specifications were reviewed and compared to actual shop practice. The CPS Flow depicted in Figure 6-1 is the present process projected for MICRON production. Specific ink requirements compatible to thermo-compression and ultra sonic bonding and meeting electrical parameters have been determined. Projected costs for the CPS has become a very small part of the total electronics cost. Improved materials and equipment within the thick film industry have contributed. The next level of interconnection and the requirement for hermetic sealing of the Ceramic Printed Circuit (CPC) is not resolved design wise and could, potentially, pose some process problems to the extent of requiring a special ink for the seal ring and interconnection pads.

The Assembly and Test of the CPC (hybrid electronic circuit) has been exercised extensively and continually during this program. The decision to back off from the conceptual 100 percent beam lead system, due primarily to the unavailability and associated cost of developing beam leads, has impacted the electronics packaging drastically. The mix of beam lead and fly wire devices has necessitated the revising of the assembly and test flow. Additionally, the reliability requirements for screens and tests at the component and hybrid level have been a major impact on the process flow and cost.

The CPC Assembly and Test Flow charts depicted in Figures 6-2, 6-3, and 6-4 indicate the major progression in production requirements for the hybrid circuits. Figure 6-2 is essentially the flow for a 100 percent beam lead circuit with a conformal coating for environmental and handling protection. Figure 6-3 depicts the flow prior to the extensive tradeoffs involving predictions of piece part reliabilities due to the level of screen testing at the component level. Figure 6-4 is the assembly and test flow presently considered for production. This flow utilizes a standard gold plated kovar butterfly type package and allows the alternative of using either the thin or thick film process for the substrate. This flow is not necessarily considered the ultimate in that the functional test between temperature cycling and the 168 hr burn may be eliminated if the yield at this point is high enough to make it cost effective. Additionally, the high and low temperature functional tests after burnin are still in the evaluation stage wherein the "low temp" test may be eliminated.

Figure 6-5 is a preliminary test, yield, and reflow matrix denoting points in the flow at which failures will be detected. By applying predicted yields at each of these points a total rework effort may be determined. Predicting the various yields is a function of the design, the component mix, the type of component (previous screen tests), and the capability of the test equipment to fully test and fault isolate. Preliminary

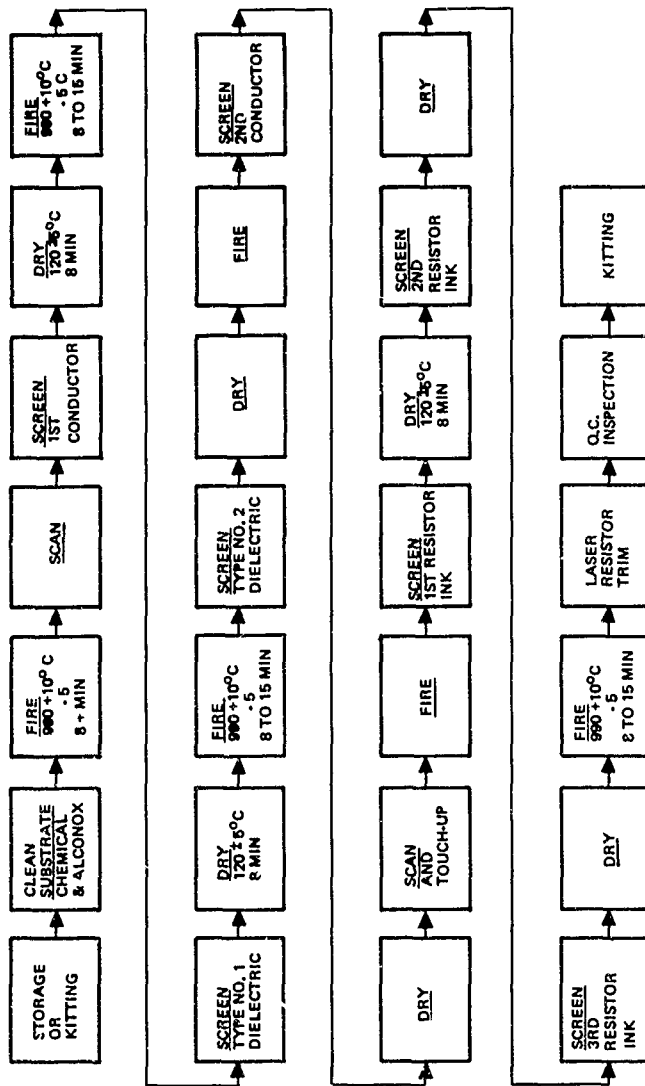


Figure 6-1. CPS Flow

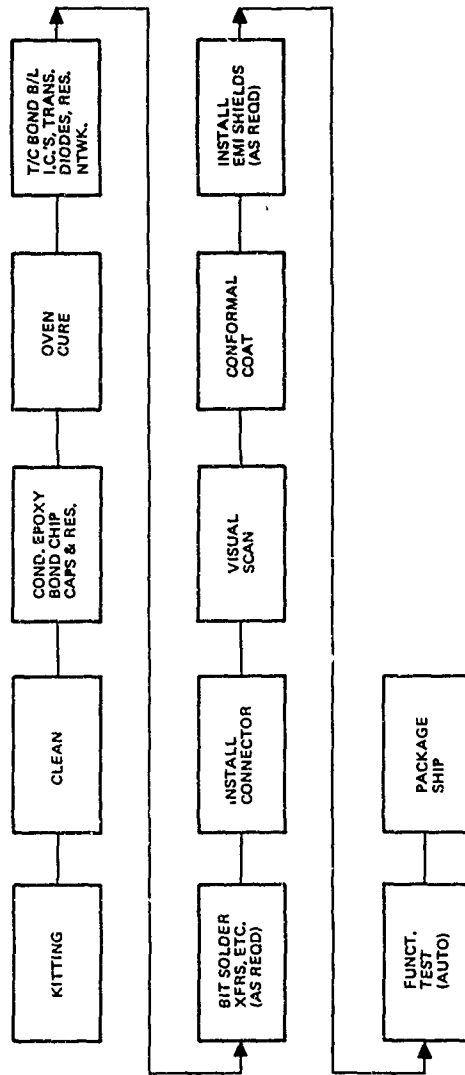


Figure 6-2. CPC Assembly/Test Flow

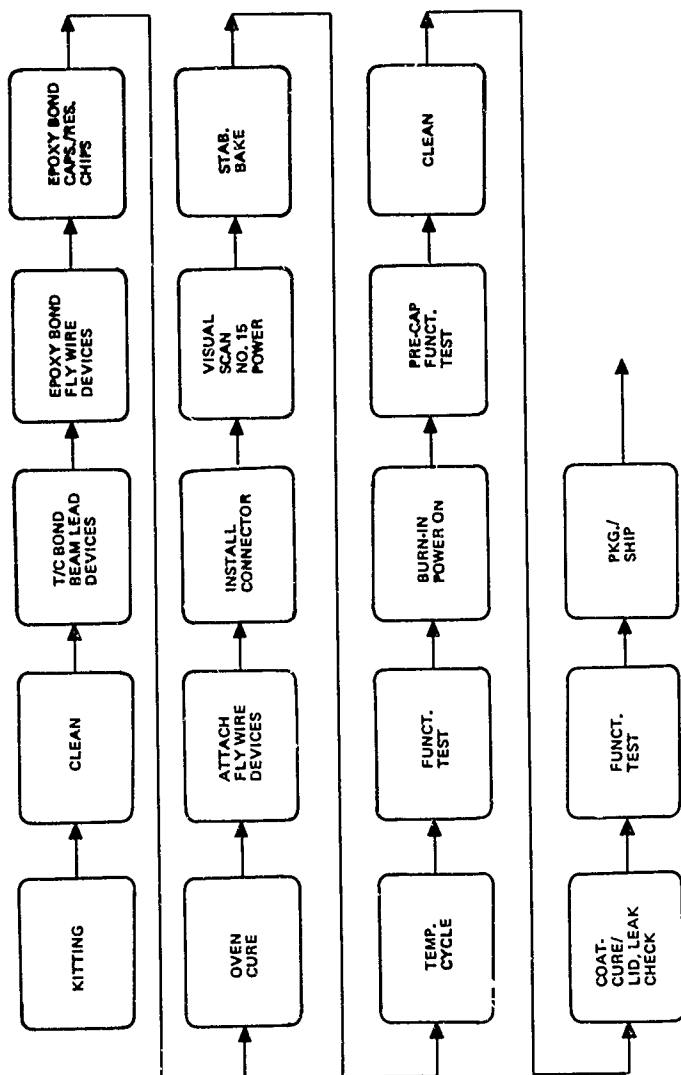


Figure 6-3. CPC Assembly/Test Flow

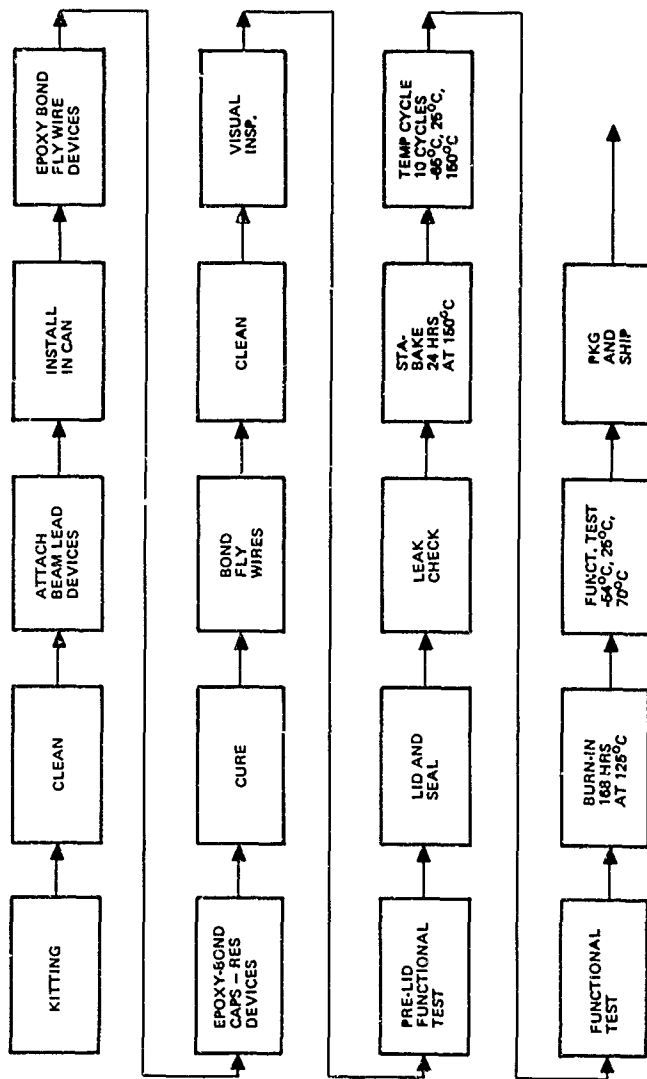


Figure 6-4. CPC Assembly/Test Flow

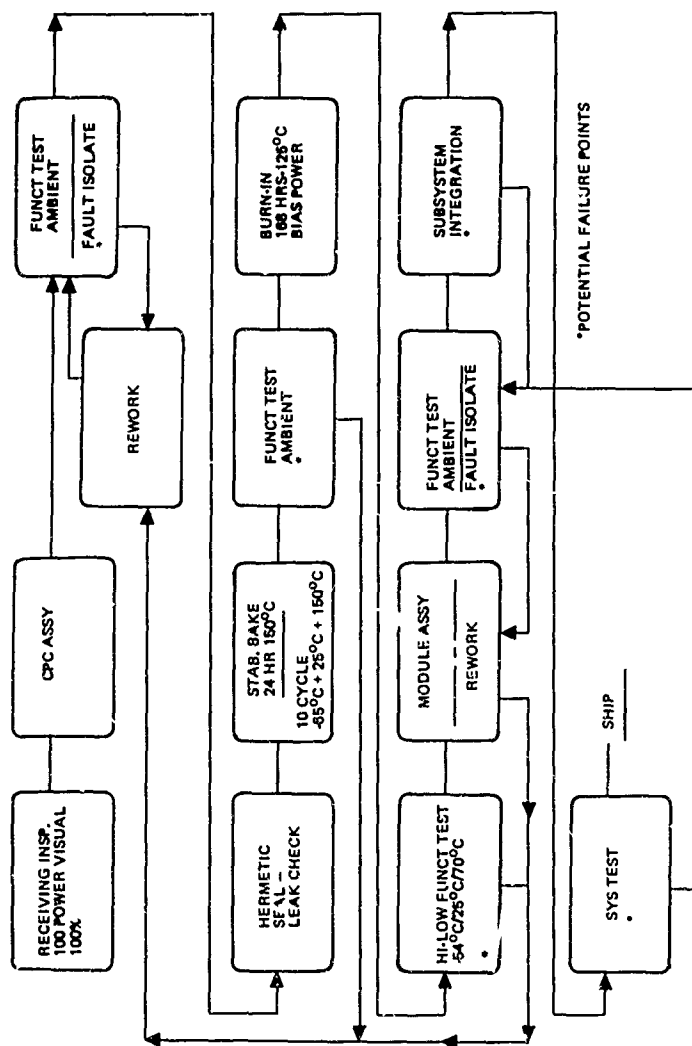


Figure 6-5. CPC Test-Yield-Reflow



effort in this area has resulted in working with Reliability and Design Engineering (Systems and Test) in an effort to better quantify the many variables. The number of recycles per part not only affect the direct cost and equipment but require more parts in the pipeline and lengthen flow time. Utilizing arbitrary yields at all points allows an evaluation of the impact of the various tests on costs. This will allow decisions to be made based on cost, performance, and reliability requirements.

Meeting the requirements of MIL-STD-883 and MIL-M-38510 has been and still is a grey area. It appears that all hybrid houses meet the intent of these specifications but take exceptions in some areas. Determining how other hybrid houses meet these requirements is very difficult to do. Each customer or program may have its own requirements and thus a hybrid supplier adjusts his processes and flow accordingly. Determining our specific requirements is still a tradeoff between reliability and cost. The longer the test flow (screen tests, etc.), the lower the factory yield becomes. Optimizing this hybrid test flow to minimize failures in later assemblies is the producibility goal.

The assembly of the CPC (Ceramic Printed Circuit) as presently designed for the GSA was evaluated in the manufacturing area on a small run of circuits used in the Phase 2A GSA. Special tooling and equipment requirements for device attachment to substrates is minimum and within the present state of art. However, it was observed that beam lead devices of the same type from two suppliers can vary enough in die size to pose a problem for the TC wobble bond process. Standardization of die size between multiple sources is a necessity. Evaluation of standard hour applications for device attachment presently used in cost-of-ownership estimates indicates the basic standards are good. Rework will require some special tooling for production.

The Packaging Design Alternates developed by Engineering required a major effort to develop the production process and techniques for each alternate. This essentially entailed the development of a production plan for each alternate. Figures 6-6 through 6-12 depict the production flow for these alternate system packages. Detail flow for critical processes (CPS, CPC, etc.) was developed as required to support the system level. This gives the basis for all production planning and cost estimating. Cost predictions were developed for all packaging alternates and are addressed in Para. 6.2.3. and Table 6-11.

Figure 6-13 depicts the system production flow for the most recent complete system description. This is the E3 (Engineering Redesign No. 3), M3 (Material Pricing Exercise No. 3) configuration for a stand alone system (basic MICRON). Cost predictions and discussions are addressed in Para. 6.2.3., Tables 6-16 and 6-17.

The hybrid circuit has and is being exercised thoroughly by the MICRON team for component count, mix, package size, package sealing, and optimum size for mounting to the next level interconnection boards. This design is not finalized because the package size (physical) presently being considered is not a production standard size and is also impacted by the system packaging configuration. Guidelines for component count and mix have been developed and the design group is complying. Definitive cost tradeoffs in this area will be continued in the next phase of the program.

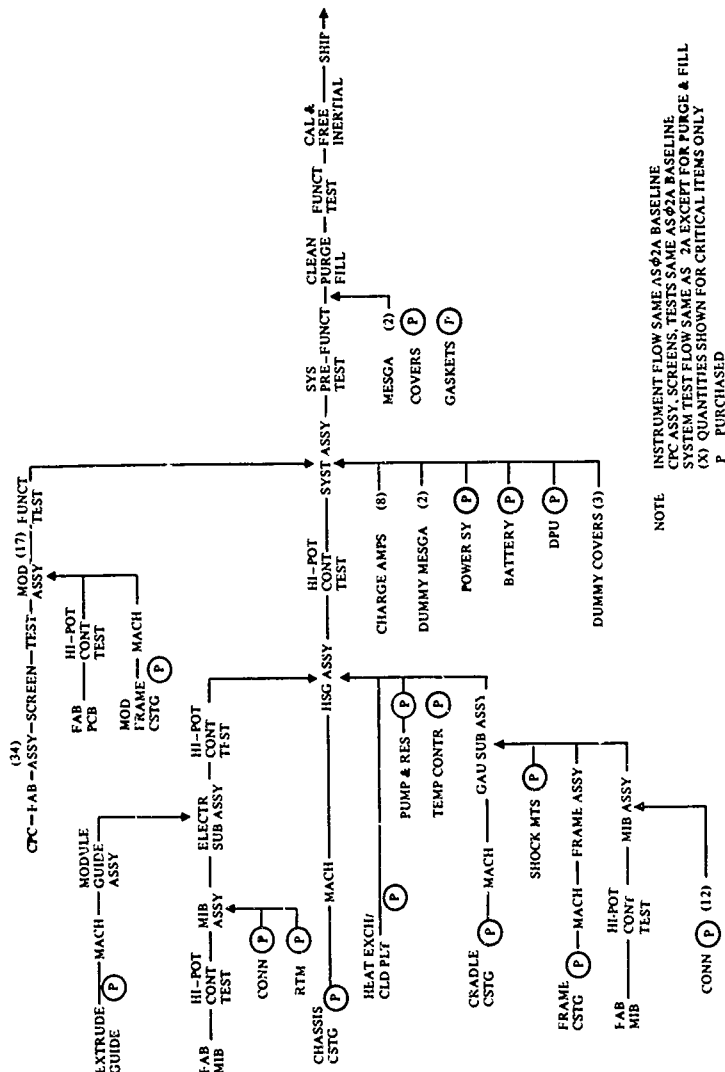


Figure 6-6. MICRON Phase 2A Production Flow Packaging Design Alternate No. 1



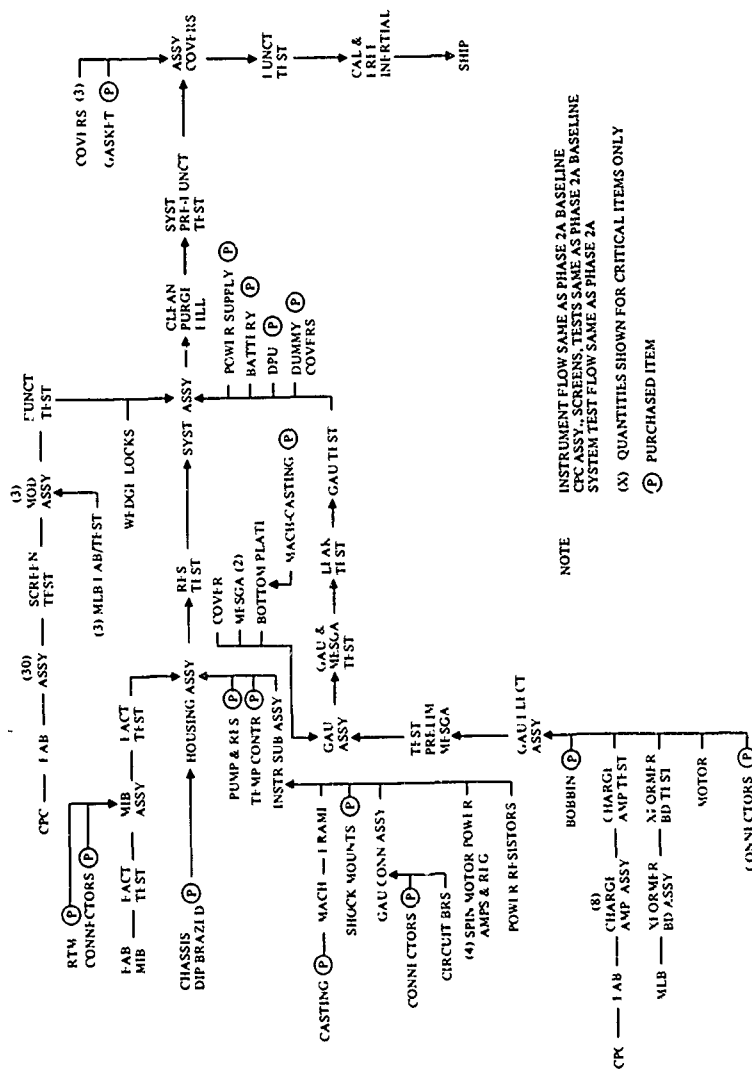


Figure 6-8. MICRON Phase 2A Production Flow - Pkg. Alt. 3



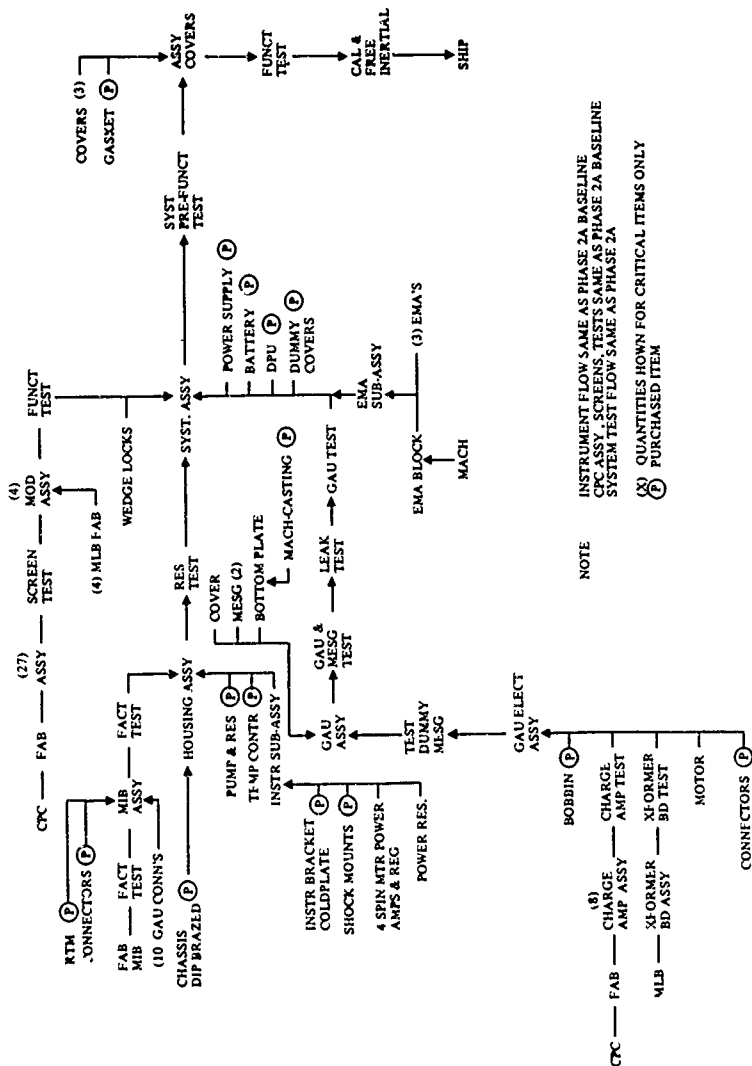


Figure 6-10. MICRON Phase 2A Production Flow - Pkg. Alt. 5







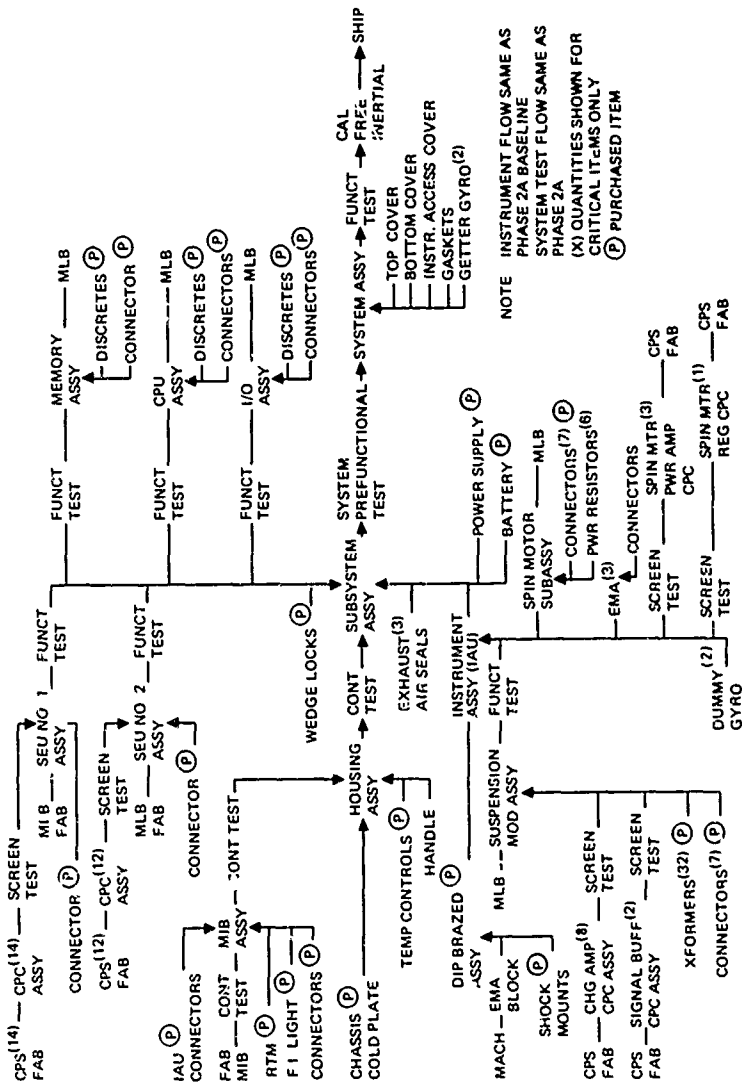


Figure 6-13. Production Flow - Stand Alone MICRON System

The mounting of the hybrid circuits on the multi-layer interconnect boards influences the board design and the hybrid package. The present concept of a planar, hermetic sealed package appears to be optimum assuming the new Hughes bar bonder or equivalent equipment is utilized. This allows one or both sides of the hybrid to be reflow soldered in one step. Available information indicates no hot spots or damage to the board occurs. This has not been verified by in house test programs but is planned for the next phase in the program.

The drawing packages for the MESH and the EMA have been processed through the Work Measurement group for application of standards to all details and assembly operations. Evaluation of this data and the drawings to improve tooling requirements and methods, to recommend make or buy, and to recommend design changes to reduce cost is just beginning. This effort will be continued in Phase 2B.

### 6.2.3 PRM Tradeoff Studies

#### 6.2.3.1 Design Improvement Trade-offs

Feedback of cost information to responsible engineers resulted in design improvements termed E-1 and E-2. (Engineering updates 1 and 2) These engineering updates were aimed at simplifying electronic circuits, reducing the number of parts, reducing the number of types of parts, and substituting for high cost parts.

Concurrent with the above activity, new quotes from parts suppliers were acquired. This new cost information was used to update the priced bill of material and was labeled M-1 (Material update 1).

Table 6-5 summarizes the key comparisons of the baseline system to the updates. The cost-of-ownership dollar values are for the maintenance concept of all depot repair. For each of the three cases, a more cost effective maintenance concept can be used. These are discussed in Para 6.2.3.12. For the comparisons in Table 6-5 to be valid, the maintenance concept was not varied.

Table 6-5. Baseline/Update Comparisons

	Baseline System	(E-1)/(M-1) Update	(E-2)/(M-1) Update
Cost-of-Ownership	153,534	129,237	120,902
Recurring Acquisition Cost	64,778	54,352	50,913
Electronics Parts Cost	15,030	9,565	7,648
Number of Electronic Parts	2,055	1,979	1,795
Cost Per Electronic Part	\$7.31	\$4.83	\$4.26
System MTBF	917	1,101	1,254
Total Material Cost	26,195	20,729	18,812
Direct Labor Hours	811	785	761

The decrease in the unit price was due entirely to changes in the electronics resulting from new parts costs, circuit simplifications, and substitution for high costs parts.

Figure 6-14 depicts the comparison of the electronics cost target to the baseline estimate, the (E-1)/(M-1) update and the (E-2)/(M-1) update in terms of material costs and direct labor hours. The cost target is shown as a constant cost line. Any estimate of a given material and labor mix to the right of and above the cost target line exceeds the cost target and indicates that action must be taken to bring the estimate to the left of and below the cost target line. The overall electronics cost problem is mainly material cost.

Figures 6-15 through 6-18 are a subset of Figure 6-14 for the functional partitioning of the electronics.

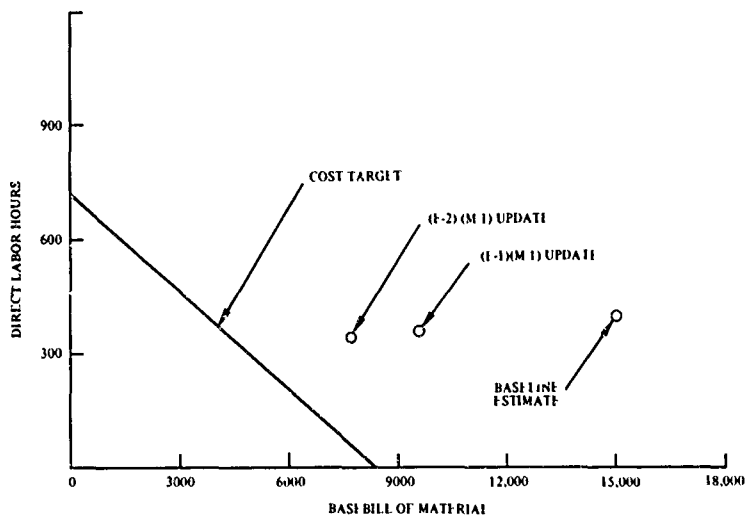


Figure 6-14. Electronics Cost Target/Estimate Comparison

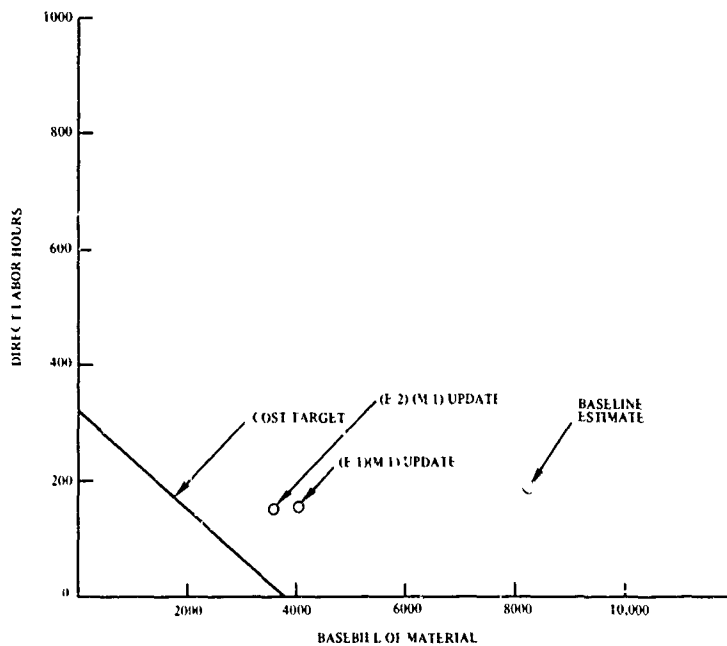


Figure 6-35. Suspension Electronics Cost Target/Estimate Comparison

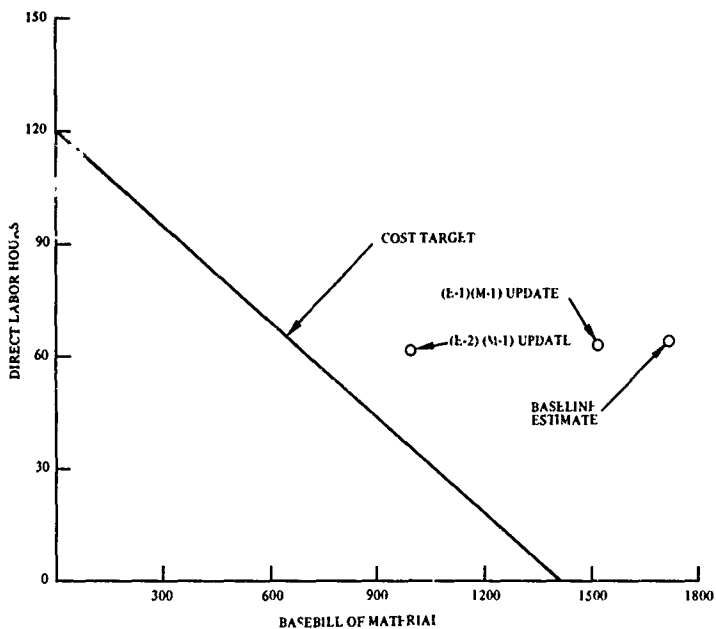


Figure 6-16. MUM and Digitizer Electronics Cost Target/Estimate Comparison

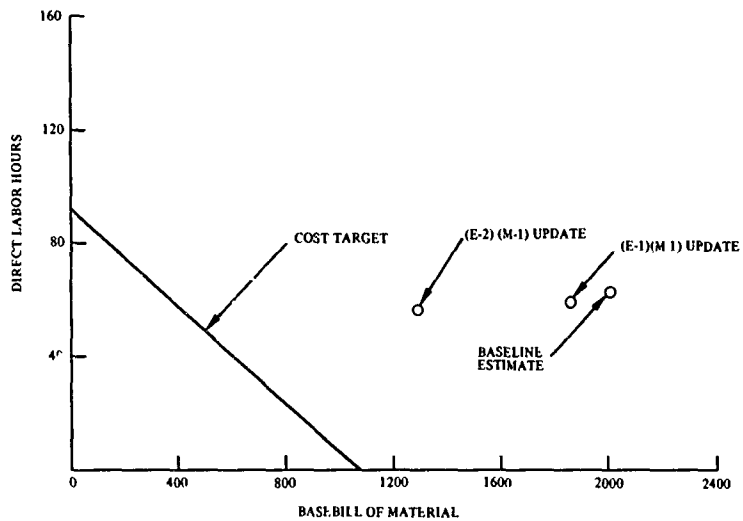


Figure 6-17. Spin Motor Electronics Cost Target/Estimate Comparison

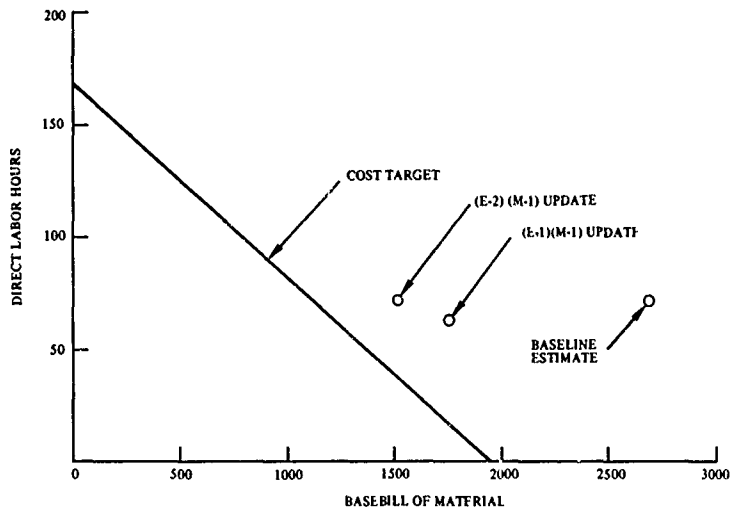


Figure 6-18. Support Electronics Cost Target/Estimate Comparison



### 6.2.3.2 Reliability/Cost Sensitivity Study

A trade-off study was conducted to determine the reliability/cost sensitivity to screens applied to electronic parts and to the hybrid level CPC. For this study, four cost-of-ownership predictions were made. Conditions for these predictions are shown in Table 6-6.

Table 6-6. Conditions for Cost-of-Ownership Predictions - Reliability Sensitivity Study

Prediction No. Conditions	1	2	3	4
Vendor Screened Parts	X	X		
Vendor Unscreen Parts			X	X
Maximum Hybrid Screens	X		X	
Minimum Hybrid Screens		X		X

The screening levels may be interpreted as follows: (1) screened parts have received the equivalent MIL-M-38510 level B and MIL-S-19500 JANTX testing by the vendor; the unscreened part receives no vendor screen testing beyond the normal visual and DC electrical probe test; (2) maximum hybrid screen is the equivalent MIL-STD-883B, Class B testing at the CPC level; the minimum hybrid screen includes a visual, 100 percent bond pull, and electrical functional test at 25°C.

The results of these predictions are given in Table 6-7 and depicted in Figure 6-19. The initial conclusion that can be drawn from this study is that it is more cost effective to use unscreened parts and apply screens at the hybrid level. Further studies are required to validate this conclusion as it is dependent upon the accuracy of the data inputted to the prediction model. For the present, however, the study does indicate that the minimum life cycle cost occurs for the case of unscreened parts and application of screens at the hybrid level. The study also shows the high sensitivity of maintenance cost to MTBF.

Table 6-7. Reliability Sensitivity Cost Comparisons

	Vendor Screened Pts		Vendor Unscreened Pts Class C or Commercial		Corrected Baseline Prediction
	Max Hybrid Screen	Min Hybrid Screen	Max Hybrid Screen	Min Hybrid Screen	
IMU MTBF	1101 hr	707 hr	1037 hr	523 hr	946 hr
IMU Unit Price	\$54,352	\$54,113	\$50,563	\$49,359	\$64,788
IMU 10Y LOC	129,237	151,372	125,201	163,773	153,534

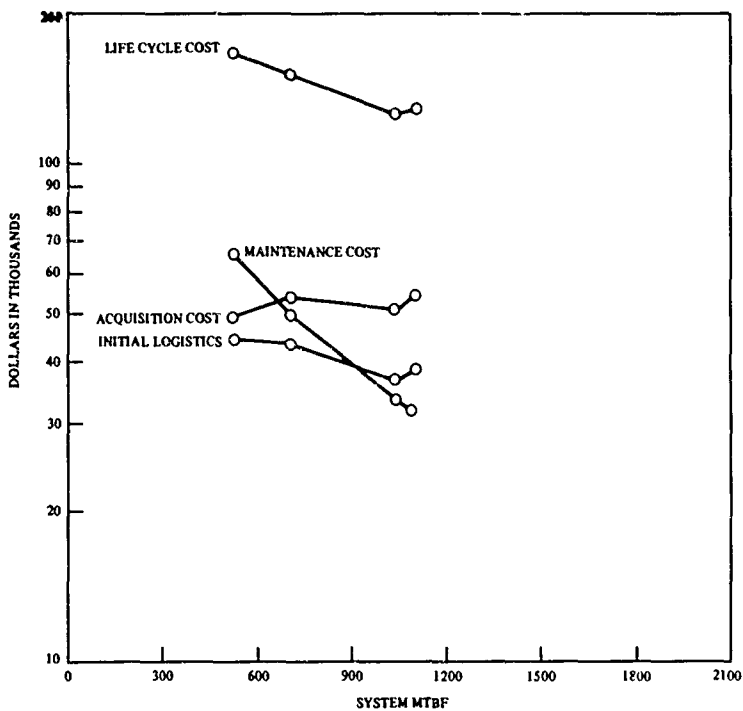


Figure 6-19. Reliability Sensitivity Cost Comparison

The Trade Studies showed the significant impact unit price and reliability have on support costs. Reliability alternatives involving parts screening, burn-in, etc. not only impact the expected maintenance rate but also change the unit cost for spares and repair material costs. Some of the maintenance factors of the reliability trade-off are shown in Table 6-8.

Table 6-8. Reliability Tradeoff Maintenance Costs

Cost Category	Average Dollars per System EI-MI Design - 1974 Base Rates - West Virginia Module Fab - Depot IMU Repair			
	Vendor Screened Parts		Unscreened Parts	
	Max. Hybrid Screen	Min. Hybrid Screen	Max. Hybrid Screen	Min. Hybrid Screen
Average Cost per Maintenance Action	\$ 1,104	\$ 1,158	\$ 1,118	\$ 1,209
Initial Spares	31,020	35,050	29,240	36,100
Support Equipment (Including Installation and Maintenance)	9,280	10,310	9,280	10,820
Training (Initial and Recurring)	6,860	7,200	6,900	7,580
Corrective Maintenance	18,350	34,270	19,730	48,340
Reparable Transportation	2,470	3,840	2,620	5,200

#### 6.2.3.3 Repair/Discard Trade-off Study

The object of this study was to determine the criteria for the repair or discard of the failed electronic modules. The baseline system data was used for these initial comparisons.

The approach taken was to make repair and discard life cycle cost projections for the baseline system factoring the predicted reliability and module price/size by various constants.

Cost projections were made for module prices ranging from 25 percent to 100 percent of the baseline estimates. For each of these prices the reliability was varied over the range of 0.1 to 2.0 times the predicted module failure rates. The matrix of conditions is shown in Table 6-9. Also, cost projections were made for module sizes ranging from the full baseline size of four square inches to one-fifth of that size. For each of these sizes the reliability was varied over a range of 2.0 to 0.1 times the predicted module failure rate. The matrix of conditions is shown in Table 6-10.

Table 6-9. Matrix of Conditions for Module Price  
Discard-Repair Study

Failure Rate	Maintenance Concept		Module Price
	Discard	Repair	
2X → .1X	X		1
2X → .1X		X	1
2X → .1X	X		3/4
2X → .1X		X	3/4
2X → .1X	X		1/2
2X → .1X		X	1/2
2X → .1X	X		1/4
2X → .1X		X	1/4

Table 6-10. Matrix of Conditions for Module Size  
Discard-Repair Study

Failure Rate	Maintenance Concept		Module Size
	Discard	Repair	
2X → .1X	X		1
2X → .1X		X	1
2X → .1X	X		1/2
2X → .1X		X	1/2
2X → .1X	X		1/3
2X → .1X		X	1/3
2X → .1X	X		1/4
2X → .1X		X	1/4
2X → .1X	X		1/5
2X → .1X		X	1/5

The cost of repair was then compared to the cost of discard for each module price/size. For each, there are those failure rates which would cause a repair decision (the cost of discard is higher than the cost of repair) and those which would enable a discard decision (the cost of repair is higher than the cost of discard). The failure rate at which the cost is the same for repair or discard is a reliability indifference point for that module price/size. Figures 6-20 and 6-21 show plots of these indifference points for the module price/sizes of significance.

From the information generated during this study it can be concluded that any of the following conditions could enable a discard policy:

1. For the baseline module price/size; achieve an average failure rate of 57.5 percent or less than that predicted for the baseline system.
2. For the baseline predicted module failure rates; reduce the module price/size to 62.5 percent of the baseline price/size.
3. Achieve some other price/size/failure rate combination on or below the indifference curve.

It should be noted that the position of the curves is strictly a function of the baseline system parameters. The curves have the general characteristics of the equation:

$$y = a + \frac{b}{x}$$

Specifically it is a plot of:

$$M_c F = R_c F + K$$

Where:

$y = M_c$  = the module cost

$x = F$  = number of module failures

$a = R_c$  = the cost to repair a module

$b = K$  = initial cost of module test equipment + cost to maintain the test equipment + training cost + manual cost + . . .

Over a limited number of failures  $K$  remains constant. If the module failures reach a frequency great enough to saturate the test equipment utilization, then more test equipment, training, etc is required and the value of  $K$  increases.

The value of  $K$  for the baseline system and the curve shown has been found to be approximately \$6,200,000. \$5,200,000 of this has been identified as initial and recurring training costs. Further investigation into these high costs is planned for the future.

Decreasing the value of  $K$  will cause the curve to move toward the origin. A new criteria for repair/discard then exists as a function of the failure rate and the module price/size.

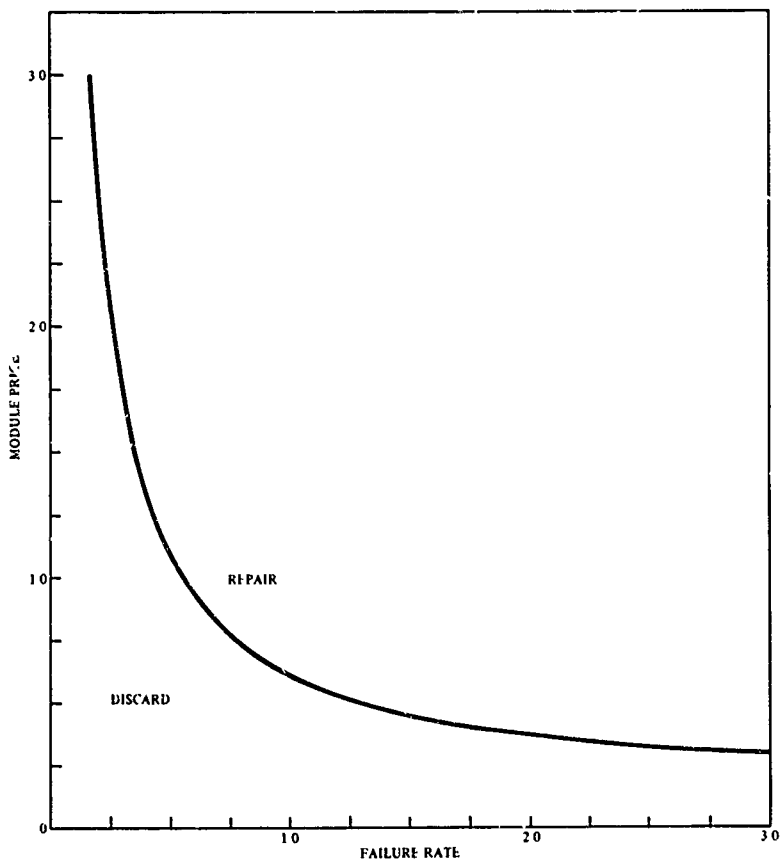


Figure 6-20. Module Repair/Discard Indifference Curve of Module Price vs Failure Rate Normalized to the Baseline Estimates

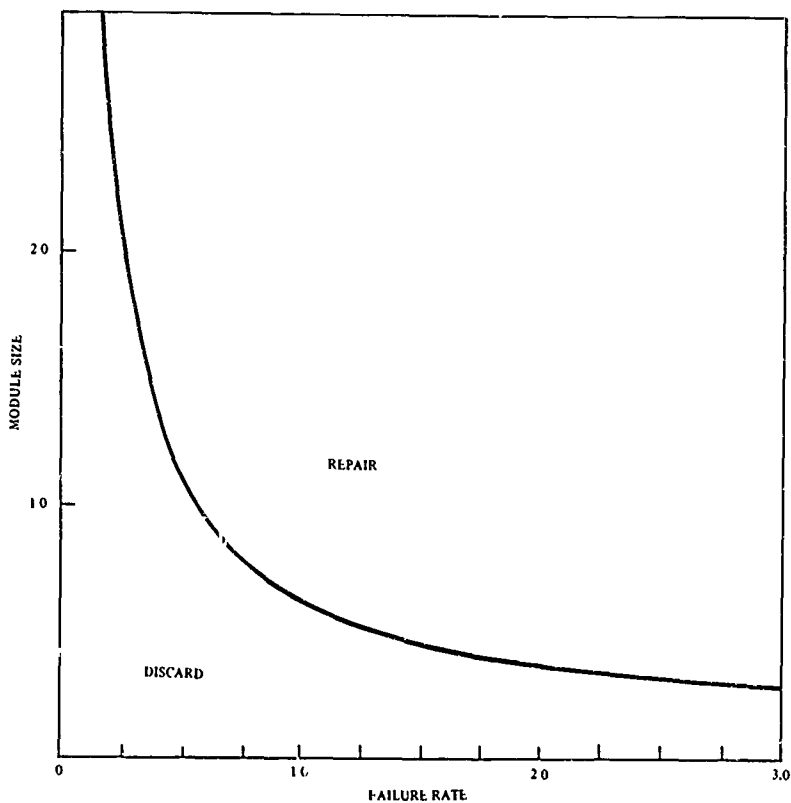


Figure 6-21. Module Repair/Discard Indifference Curve of Module Size vs Failure Rate Normalized to the Baseline Estimates

#### 6.2.3.4 Packaging Alternative Studies

Cost of ownership evaluations were conducted for the seven candidate IMU designs developed under the design alternative task (see Para 6.3.6.2). The goal of this evaluation was to determine the best features of each design and incorporate these into the final recommended packaging concept. The first step toward this goal was the evaluation, quantification of the producibility, reliability, and maintainability features of each design and the prediction of resultant life cycle costs for each. This was completed and the results are summarized in Table 6-11 and 6-12.

The producibility analysis included development of production flow charts, labor and material estimates by item, and other producibility considerations. Flow charts for designs one through seven are shown in Figures 6-6 through 6-13.

The circuit mechanization was held constant to the extent possible for all alternatives. Only where EMA's and Vaclon MESG were added were the electronic components changed. The reliability estimate changes were thus mainly the result of temperature variations, the number of interconnections (connectors, bonds, etc.), and electro-mechanical parts (fluid pumps, EMA, etc.). Electronic temperatures ranged from 80°C to 60°C depending upon cooling design and isolation from the power supply and instrument assemblies.

The maintenance concept was also held constant in evaluating the alternatives Depot IMU and electronics repair was the concept used. Studies with additional variations such as electronics discard will add insight into the pro and cons and development of the recommended approach.

The range of the end predicted numbers (both average unit price and life cycle cost) is very small. Comparison at only the top level may thus lead to the erroneous conclusion that packaging design is unimportant. This small range is the result of the several variations between alternatives counteracting each other. For example, many of the good maintenance features were in design number 2 which was also run at a high temperature. The result was a lower reliability which overshadowed the wet design (No. 1) which helped to balance out the cost of liquid handling.

#### 6.2.3.5 Dual Frequency Suspension Initial Cost Trade-off

The conceptual design of the dual frequency suspension system was given an initial evaluation from a cost and reliability standpoint. This was done for both an 8-Plate and 6-Plate gyro. A diagram of the 8-Plate dual frequency suspension system is shown in Figure 6-22. The 6-Plate version would eliminate the four to three transformation in the pickoff amplifier, the three to four transformation in the summing amplifier and one half of a charge amplifier including the associated transformer. The results of this initial trade-off indicate a strong preference for the 6- or 8-Plate dual frequency system over 8-Plate pulse amplitude system from a cost and reliability standpoint. The comparison is shown in Table 6-13.

This cost trade-off shows a potential cost reduction of approximately \$3900 per system, however the time required to fully develop and prove this suspension system will prohibit its inclusion into the initial MICRON design.



Table 6-11. MICRON Packaging Alternative Matrix

Packaging Alternative	Number	(E-2)(M-1) at 55° C	(E-2)(M-1) at 70° C	PDA-1	PDA 2	PDA-3	PDA-4	PDA-5	PDA-6	7
Description		Air Cooled 1 CPC/Module Minimal Distortion MESG/Gutter		Liquid Cooled 2 CPC/Module MESG/Gutter	Air Cooled 1 CPC/Module MESG/Gutter	Liquid MESGA 12 CPC/Module MESG/Gutter	Liquid MESGA 15 CPC/Module MESG/Gutter	EMA 8 CPC/Module MESG/Gutter	EMA 8 CPC/Module MESG/Gutter	Same as No. 6 Except 2 LRT
Temperature	Instruments	55° C	70° C	70° C	70° C	70° C	70° C	70° C	70° C	70° C
	"Electronics"	55° C	70° C	70° C	80° C	55° C	55° C	55° C	55° C	55°/80°
Maintenance Concept	IMU Repair	Depot	Depot	Depot	Depot	Depot	Depot	Depot	Depot	Depot
	Circuit Repair	Depot	Depot	Depot	Depot	Depot	Depot	Depot	Depot	Depot
Total Direct Labor (hours)		764.2	764.2	1,023.7	1,133.8	957.3	942.4	997.7	958.19	1,030.5
Total Direct Material Dollars		18,811	18,811	18,907	19,532	17,973	17,853	18,468	21,368	24,714
Average Unit Price		\$50,913	\$50,913	\$56,280	\$58,967	\$58,498	\$55,750	\$58,037	\$59,800	\$66,816
Predicted MTBF (hr)		1,254	983	987	882	1,052	1,052	1,047	979	943
Average Repair Cost per Failure		\$1,112	\$ ,066	\$ 1,130	\$1,123	\$1,228	\$1,239	1,221	1,177	996
Initial Spares Cost per System		\$28,552	\$29,694	\$32,813	\$36,287	\$33,777	\$33,465	34,612	35,436	29,363
Initial Support Equipment per System		\$4,530	\$4,530	\$4,810	\$4,780	\$4,840	\$4,840	4,820	4,740	4,540
Corrective Maintenance Cost per System		\$16,236	\$19,846	\$20,951	\$23,384	\$21,371	\$21,563	21,352	22,006	20,235
Total LCC per System		\$120,902	\$126,226	\$137,106	\$144,131	\$137,644	\$138,777	140,234	144,047	142,565

Table 6-12. Packaging Alternate Analysis (Sheet 1 of 2)

	PDA-1		PDA-2		PDA-3		PDA-4	
	LCC \$/System	Notes	LCC \$/System	Notes	LCC \$/System	Notes	LCC \$/System	Notes
Prod. Nonrecurring	4320		4320		4320		4320	
Prod. Recurring	56280		56957		56498		56750*	
Acquisition Cost	60600		63287		60818		63070*	
Initial Spares	32813		36287		33777		33465	561 IMU and 472 Subassy
Initial Inv. Mgt.	29		20*		26		26	Liquid Handling
Initial Support Eq.	4810	Liquid Handling	4780		4840		4840	
Manuals	385		355*		372		372	
Init. Maint. Trng.	2955		2627*		2819		2819	
Support Eq. Install	240		238		241		241	
Initial Logistics Cost	41234		48308		42078		41786	
Corrective Maint.	20561		23324	Lower MTBF	21371		21563	Higher Module Cost
Support Eq. Maint.	4809		4779		4839		4839	
Inventory Mgmt.	276		198*		254		254	
Maine Training	5533		4745*		5092		5092	
Maint. Facilities	320		300		360		360	
Precedent Maint.	1878		1598*		1721		1721	
Repair Transport	1890		1587		1108		1108	
Maintenance Cost	35271		36524		34748		34940	
Cost of Ownership	137105		144131		137644		136777*	
				*Notes: lowest cost of that category				
Mature Reliability (MTBF)	987 Hours		882 Hours		1053 Hours		1052 Hours	
Remarks	Corrective maint low because of no solder seal can and medium high MTBF.		Lowest cost per repair High corrective maint due to lower reliability		Lower subassembly spares cost overshadowed by higher IMU price (compared to PDA 4) Cost of GAU spars overshadowed by lower IMU price (Co noted to PDA 2) Variations may further reduce some alternatives.		Improved module fault isolation overshadowed by higher module price.	
Maintenance Advantages	Easy module repair due to no hermetic seal.		No liquid handling Lowest module price		Separate GAU and multi CPC modules are an advantage and disadvantage. They make maintenance and increase condemnation costs. They make fault isolation (first level) easier and are more adaptable to Base IMU repair.			
Maintenance Disadvantages	Liquid handling for each LRU repair		CPC mounting is costly. Hermetic can.					

Table 6-12. Packaging Alternate Analysis (Sheet 2 of 2)

	PDA-5		PDA-6		PDA-7	
	LCC \$/System	Notes	LCC \$/System	Notes	LCC \$/System	Notes
Prod. Nonrecurring Proc. recurring	4320 58037		4320 59800		4320 68516	
Acquisition Cost Initial Spares	62357 34812	582 IMU 481 Subassembly	64120 35435	568 IMU 393 Subassembly	70936 29383*	653 LRU 393 Subassembly
Initial Inv. Mgt. Initial Support Eq	27 4820		32 4740		36 4540*	One less Cal. Station
Manuals	383		404		421	
Init. Maint. Trng.	2506		1072		3219	
Support Eq Install Initial Logistics Cost	240 42951		236 43922		226* 37808*	
Corrective Maint. Support Eq. Maint.	21352 4819		22006 4739		20235* 4539*	Reduced test for LRU 2
Inventory Maint.	263		304		353	
Maint. Training	5253		5546		5805	
Maint. Facilities	365		305		295*	
Preventive Maint.	1716		1673		1614	
Repair Transport	1113		1429		977*	
Maintenance Cost	34886		36004		33820*	
Cost of Ownership	140234		144057		142565	
	*Notes lowest cost of that Category					
Mature Reliability (MTBF)	1,047 hrs		979 hrs		943 hrs	
Remarks	Adds EMA's but eliminates liquid cooling for gyro assemblies.	Adds Vac-ion pump and power supply				Two LRU configuration is by far the best from a logistics viewpoint. This is offset by higher system cost and lower reliability as now defined.
Maintenance Advantages	Eliminates liquid cooling	No intermediate higher cost instrument GAO's.				Lower cost/LRU
Maintenance Disadvantages	Still has high cost gyro assemblies.	Most complicated intru ment assembly - poor access				No Navigation test for LRU No. 2 Failures Higher LRU removal rate More spare items

Note: All alternatives were evaluated with same maintenance concept. Variations may further reduce some alternatives.

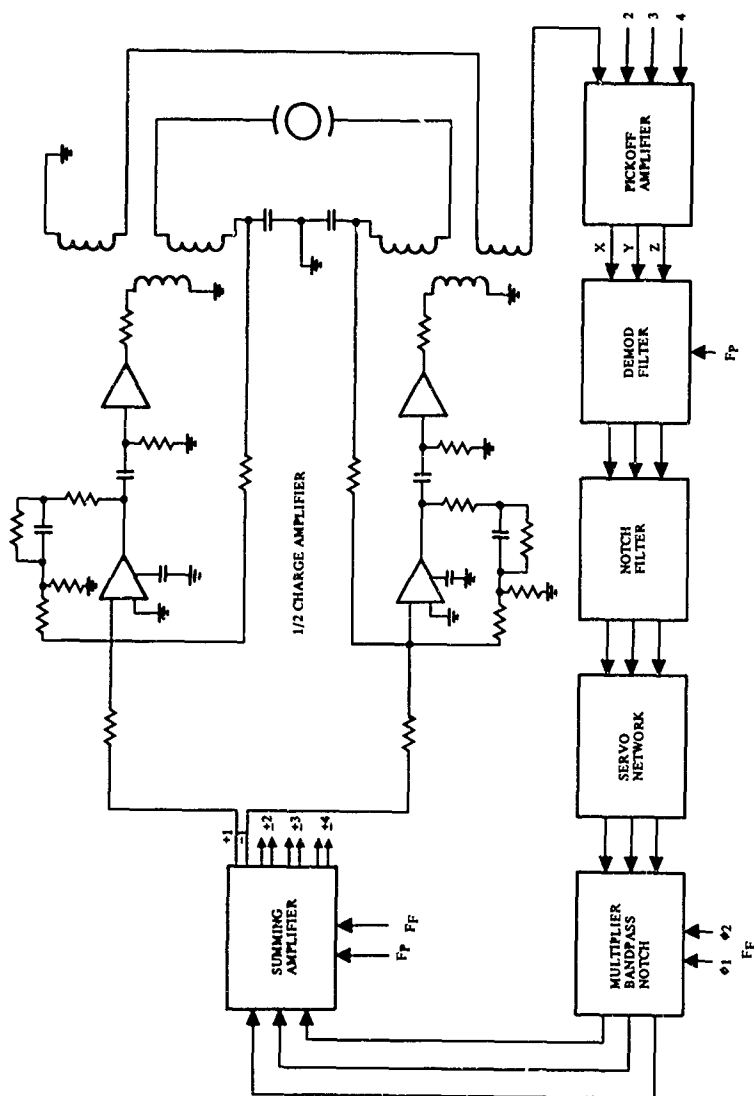


Figure 6-22. Diagram of 8-Plate Dual Frequency Suspension System

Table 6-13. Suspension System Comparison

	Pulse Amplitude Suspension/8-Plate	Dual Frequency Suspension	
		8-Plate	6-Plate
Price-Two Suspension Systems	\$9771	\$7022	\$5622
Number of Modules	16	17	13
Types of Modules	6	8	3
Discrete Parts	981	542	464
Failure Rate - %/1000 hr	24	17	14

## 6.2.3.6 Cost Trade-Offs of Proposed Redesigns

Several proposed redesigns were evaluated from a cost standpoint to determine if they should be pursued. Those that showed a favorable result were design changes to the A/D converter, the Spin Motor Control and the Temperature Controller. The results are shown in Table 6-14. The dollar values in the table are for recurring costs only. These redesigns are being pursued and incorporated into the MICRON design.

Table 6-14. Price Comparisons

	Estimate (E-2)/(M-1)	Redesign Estimate
A/D Converter	\$746	\$567
Spin Motor Control	\$670	\$360
Temperature Control	\$444	\$268

## 6.2.3.7 Cost Tradeoff of Proposed Interface Redesign

Preliminary cost evaluation of a proposed redesign of the interface between the DPU/SEU, GAU, and I/O indicates a favorable cost advantage for the redesign. Technical details of this proposed redesign are given in Para 6.3.6. In short, it involves incorporating the functions on eight and one half modules in the SEU, GAU, and I/O into the DPU. This is done by designing three new MOS chips to accomplish the functions and then incorporating the MOS chips into the DPU/IO design. The estimated recurring cost advantage is \$1800/system. Based on this cost advantage, the design of the MOS chips was initiated. The redesign of the interface utilizing these MOS chips will be incorporated into the MICRON system design.

#### 6.2.3.8 Beam Lead/Flywire Parts Trade-off

A cost tradeoff was conducted in an attempt to determine the cost effectiveness of using beam lead parts versus fly wire parts. The following equation was used to compare the costs associated with the beam lead and fly wire parts:

$$\text{Cost} = \text{Installation Cost} + \text{Rework Cost} \left( \frac{1 - \text{Yield}}{\text{Yield}} \right)$$

Where:

Installation Cost = Material Cost + Part Placement Labor Cost

Rework Cost = [Fault Isolation + Removal + Replacement + Test + Material] Costs

Yield = The expected device yield

The costs in the above equation were determined for both the fly wire and beam lead parts. The costs associated with the placement, removal, and replacement of fly wire parts were calculated as a function of the number of leads per part since the leads must be attached and removed individually. For the beam lead parts, only the removal and replacement were calculated as a function of the number of leads. The initial installation would be done as a single operation with a wobble bonder that is independent of the number of leads. The replacement was assumed to be done with a thermal compression bonder, one lead at a time.

The yields were assumed to be 95 percent for the beam lead devices and 75 percent for the fly wire devices. The 75 percent yield for fly wire devices is the approximate yield experienced by hybrid houses surveyed. The 95 percent yield for beam lead devices was projected due to proposed component testing. It was assumed this would improve the quality by 20 percent. Using these yields, costs were determined as a function of the material parts costs for parts having one, two, four, eight and 16 leads. Equating the costs associated with beam lead parts to those associated with fly wire parts and plotting the results, the graphs in Figure 6-23 were obtained. Graph A is for single lead parts, Graph B is for two lead parts, Graph C is for four lead parts, Graph D is for eight lead parts, and Graph E is for 16 lead parts.

To use the graph, given the material parts cost for a fly wire and beam lead part, find the coordinates of the point relating the material costs on the graph. If the point is below and to the right of the plot for an equivalent lead device, then the beam lead part is more cost effective. If the point is above and to the left of the plot, the fly wire is more cost effective.

#### 6.2.3.9 Design Improvement E-3

Producibility, reliability, and maintainability parameters were estimated and used as inputs to the cost-of-ownership model to support the design improvement (E-3).

Due to normal delay in getting new material quotes, the design improvements of (E-3) were run with the old (M-1) material quotes. This was done to make a comparison to the previous design (E-2)/(M-1), which was incorporated into Design Alternate No. 6 (PDA No. 6). Table 6-15 shows this comparison.

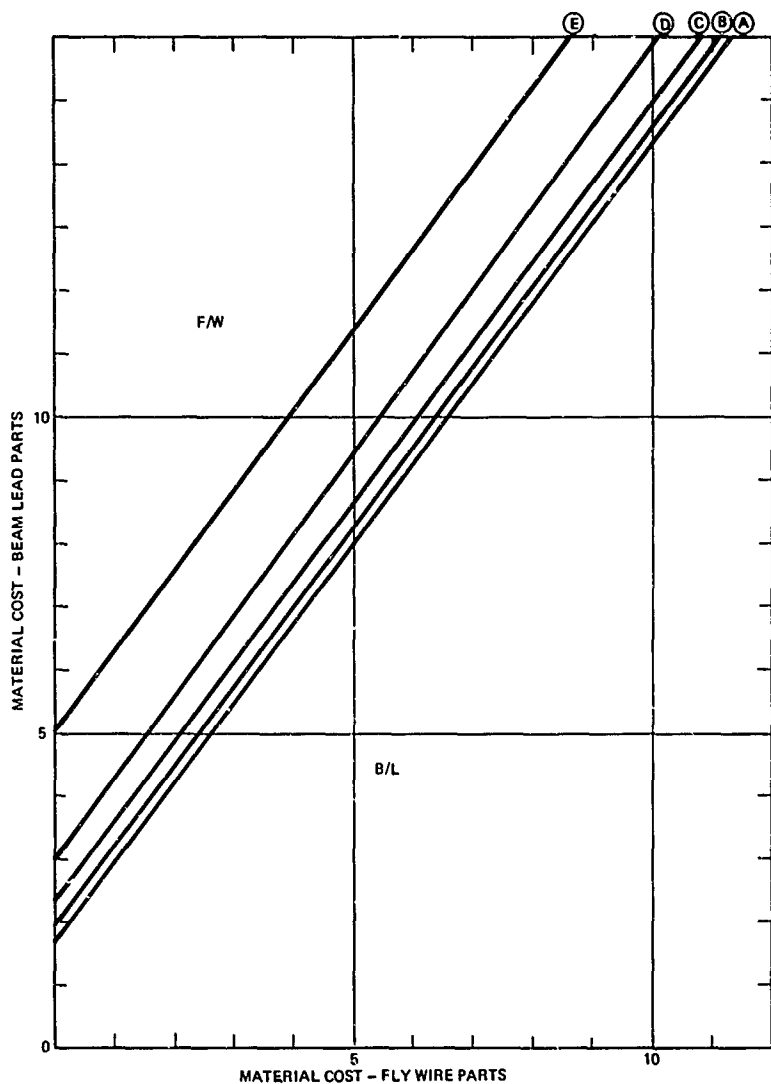


Figure 6-23. Cost Comparison - Beam Lead Parts vs Fly Wire Parts

Table 6-15. PDA No. 6 Versus (E-3)/(M-1) Price Comparison

	PDA No. 6			(E-3)/(M-1)		
	\$59,800	2,431 5,428 25,779	716 9,207 4,124 9,032 2,700	\$53,666	2,374 6,240 20,929	1,093 6,144 4,194 6,599 2,899
MICRON						
Calibration and F/T						
Housing						
Instrument Assy.						
Chassis, Assembly, and Test						
Gyros						
EMA's						
Suspension Module						
Spin Motor Module						
Support Electronics		12,542			7,248	
DPJ		9,235			12,488	
Power Supply		4,255			4,255	
Battery		130			131	



The net decrease in the estimated price is \$6134. As can be seen in the table, some of the estimates increased and some decreased. The price increase in the system housing and the instrument assembly chassis was due to more complete definition of the parts involved. This was also true of the Spin Motor Module. In PDA No. 6 the module was not defined as a complete assembly, all of the parts were defined but the method and hardware required to tie them together was lacking.

The decrease in the gyro price was due to assuming gettered gyros instead of gyros with VaeIon pumps.

Simplifications in the suspension electronics (reduced high voltage transistors by one-half and eliminated high voltage diodes) accounted for the decrease of \$2433 in the price of the Suspension Module. The incorporation of the proposed modified interface electronics into the Dedicated Processor Unit (DPU) and other circuit simplifications accounted for the decrease in the estimated price for the Support Electronics and the increase in the DPU price.

After the new (M-3) electronic material quotes were received, a cost comparison was made between the M-1 and M-3 quotes. The base bill of material for the Suspension, Spin Motor, and Support Electronics increased by \$863 for M-3 compared to M-1. This increase in cost was due to better definition of the testing required on the parts. It now remains to determine the cost effectiveness of these parts test.

#### 6.2.3.10 MESGA/EMA Cost Trade-offs

Two MESGA vs EMA cost trade-offs were completed during this program. The initial one showed a cost advantage in favor of the system using EMA's of \$5,024. The updated one showed a greater cost advantage for the system using EMA's of \$5,526.

The initial trade-off was limited to a comparison of an eight plate Pulse Width Modulation (PWM) suspension system with MESGA's vs an eight plate Pulse Amplitude Modulation (PAM) system with EMA's. The following assumptions were made:

1. The suspension servo loop is the same for the PWM and the PAM with the exception of the modulator. The servo loop is shown in Figure 6-24.
2. The acceleration preprocessor and digitizer can be represented by one Sample and Hold Module and three EMA Digitizer Modules.
3. The balance of the system is considered essentially the same for both cases.

The third assumption was made so that the initial comparison could be limited to that which was best defined at that time. It should also be stated that Figure 6-24, modulator case 1, Present-PAM, was the configuration for the cost-of-ownership Baseline System, E-1, and E-2.

It was assumed at the time the Baseline System was defined, that acceleration could be accurately sensed at the output of the PAM modulator. The validity of that assumption has since been proven false. The system definition was updated to include EMA's at the time Packaging Design Alternate No. 5 was defined and have been included in all subsequent system definitions.

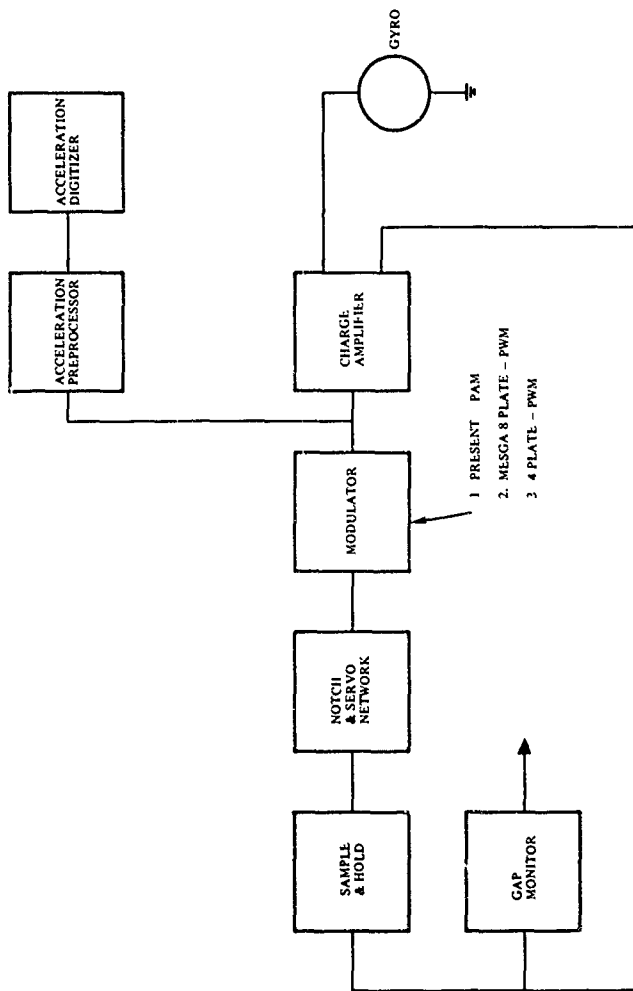


Figure 6-24. Suspension Servo Loop Block Diagram

The initial cost estimate for the MESGA electronics was \$11,154. This was compared to the estimated cost of three EMA's and the PAM modulator of 6130. This yielded an initial difference of \$5,024 in favor of the system using EMA's.

The updated estimate of the MESGA electronics included the modulator, the acceleration preprocessor and digitizer, and the support electronics. These were compared to the estimated cost of the PAM modulator electronics, support electronics, and three EMA's. The updated estimate for the MESGA electronics was \$11,768 as compared to \$6,242 for the EMA's and associated electronics, a difference of \$5,526 in favor of the latter.

#### 6.2.3.11 Electronics Packaging Study

An electronics packaging study was conducted to determine the most cost effective means of partitioning the MICRON electronics. The results are also to be used as a criteria for evaluating the present and future electronics partitioning.

To accomplish this, the E-3 electronics definition and the parts lists for thirty-six of the electronic modules was used as a basis. A cost model was then defined and used to determine the MICRON electronics cost (C) as a function of:

1.  $C_I$  - the initial material, fabrication, and test costs.
2.  $C_R$  - the recycle or rework cost
3.  $Y$  - the electronics module yield

The model used was:

$$C = C_I + C_R \frac{(1-Y)}{Y}$$

where:

$$C_I = A n + B$$

$$Y = y^p$$

and:

A was the labor cost associated with the number of modules, or in this case, hybrid circuits.

n was the number of modules

B was the fixed cost for material

y was the average active device yield

p was the average number of active devices per module

The assumption was made that the material cost would remain constant as the partitioning or the number of modules was varied. It was also assumed that the recycle cost,  $C_R$ , would remain constant.

Since there were thirty-six (36) substrates and three hundred eighty seven (387) active electronic parts in the definition, the following constraint was used:

$$n = \frac{387}{P}$$

The results of this study are shown in Figures 6-25, 6-26, and 6-27. Figure 6-25 shows the relationship of the electronics cost vs the number of active parts per hybrid module for various device yields. It is interesting to note that the cost estimate of the electronics made independent of this study was \$13,060 and that the average number of active parts per hybrid was 10.75. If this study is valid, then the device yield after being placed on a hybrid circuit must be about 89% for the estimate of \$13,060 to be valid. With the proposed testing and screening of the electronic parts a device yield of about 90% is expected during the MICRON production program.

Figure 6-26 shows the most cost effective number of active parts per module as a function of the parts yield. This curve is a plot of the minimum cost points of each curve in Figure 6-25. This curve also shows that for 10.75 active parts per module (the E average) the device yield should be between 89% and 90% for the partitioning to be cost effective.

Figure 6-27 is a family of curves showing the electronics cost vs the number of electronic modules for various parts yield. Again, these curves show that a device yield of 89% to 90% is required for the E-3 definition to be cost effective.

The results of this study show that the cost of the electronics for the MICRON system are and will be greatly influenced by the parts yield. It also shows that it is important to concentrate on all methods and/or procedures that will insure a high device yield.

#### 6.2.3.12 Final Phase 2A Configuration (July 1975)

Producibility, reliability, and maintainability trade-offs have been made and the results incorporated into the final Phase 2A configuration. Included in this configuration are the results of design improvements E-1 through E-3 which were aimed at circuit simplification, elimination of high cost parts and processes, and partitioning to meet maintainability and producibility requirements. It also included modification of the A/D converter, spin motor, and temperature control electronic circuits. The interface between the DPU and SEU was redesigned into MOS circuits for simplicity and decreased costs. Three EMA's were incorporated into the system as a result of the MESGA/EMA trade-off which showed a favorable cost reduction in favor of the EMA's. A repair/discard criteria was established for the hybrid electronic packages. Military specifications discourage the repair of sealed hybrid packages, therefore a cost effective discard concept was desired. This final configuration meets this desired criteria. Referring to the repair/discard criteria in Figure 6-20, the hybrid package price and failure rate of this final Phase 2A configuration yield a point at:

Module Price = 0.47

Failure Rate = 0.21

This point is well within the discard area and thus gives the desired result.

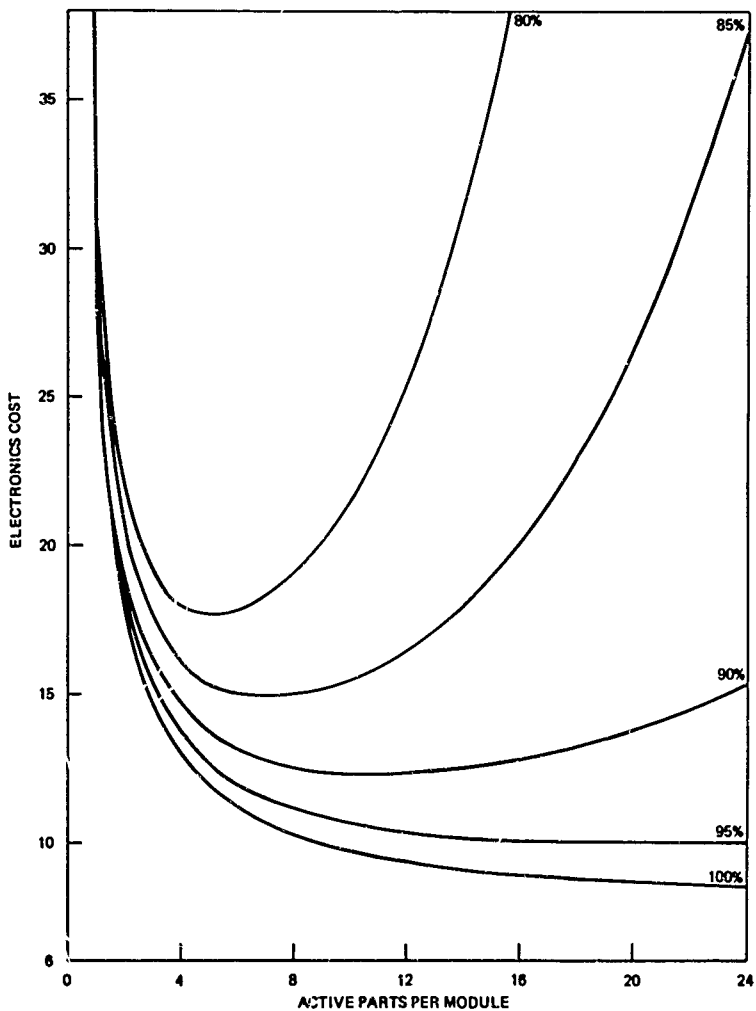


Figure 6-25. Electronics Cost vs Parts Per Module

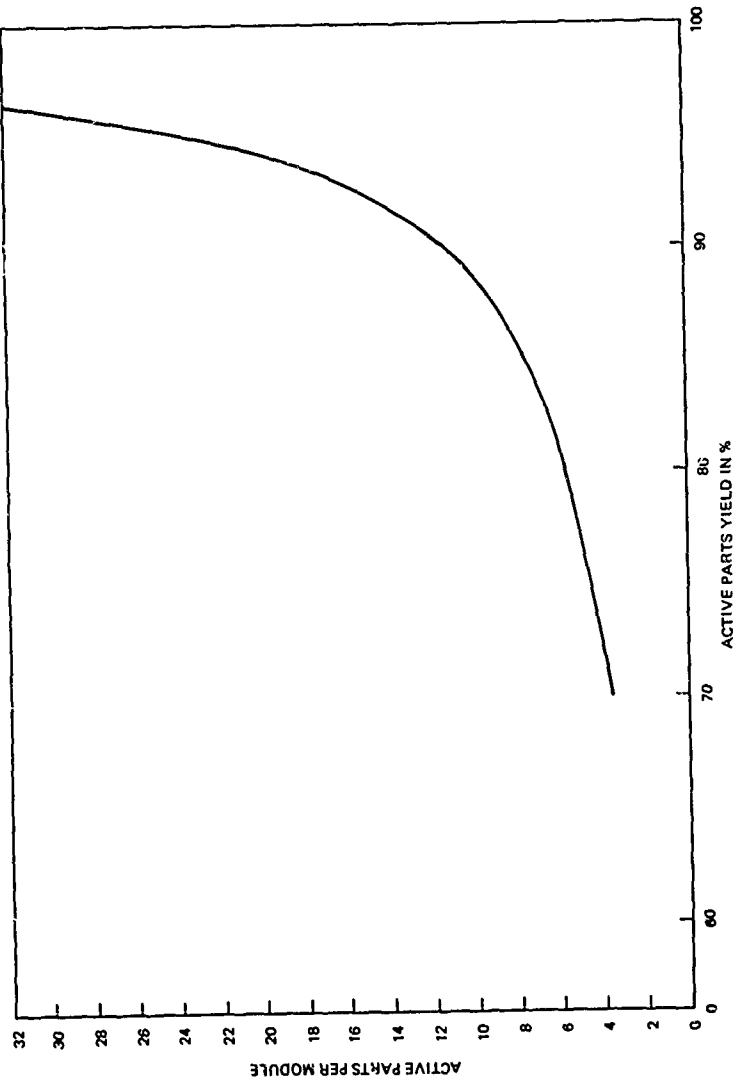


Figure 6-26. Parts Per Module vs Parts Yield

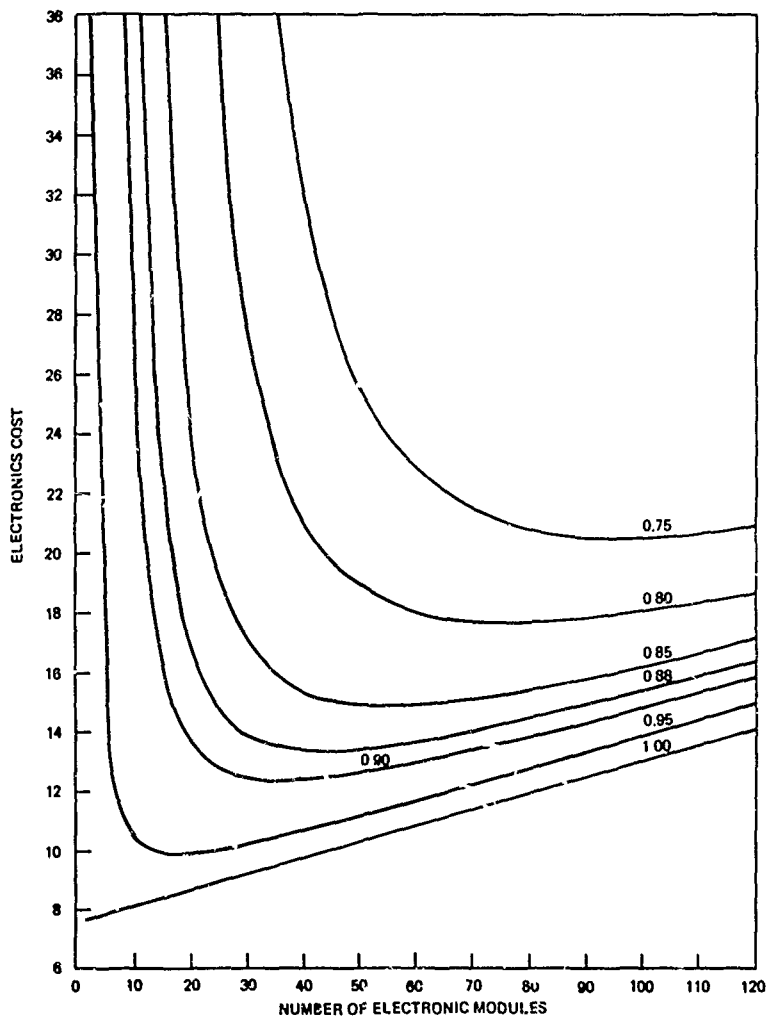


Figure 6-27. Electronics Cost vs Number of Electronic Modules

Table 6-16 indicates some of the progress made in several categories during this phase. The recurring acquisition price showed a steady improvement, especially considering that the baseline configuration did not have a workable acceleration sensing mechanization, which if one had been incorporated would act to increase the price by more than \$3,000. The life cycle cost also improved due in part to the acquisition price and maintenance concept. The decrease in the average price per hybrid module made the discard maintenance concept feasible, which as indicated acted to drive the life cycle cost down. The average parts per module and the average active parts per module decreased due to simplifications and partitioning changes. This in turn made the system more producible and acted to lower the acquisition price.

Table 6-16 shows the recurring acquisition cost allocations to the major sub-assembly and the estimates to the same level for the Baseline System and the Final Phase 2A system configuration. As indicated in previous paragraphs the major cost reductions were accomplished in the electronics. In the Baseline System 74.5 percent of the cost was in the electronics. The Final Phase 2A system has just 64.4 percent of the cost in the electronics. This represents a decrease of \$13,520 in electronics costs.

The acquisition and life cycle cost targets have not as yet been achieved, even though much progress has been made. Several areas have been identified that will decrease the above estimates. These include further simplifications in the charge amplifiers, more application of MOS technology, make or buy considerations, and continued activity on elimination of high cost parts and processes.

The resultant 10 year ownership costs are shown in Table 6-17. Base dollar rates are for 1973, 1974, and 1977 and are shown for comparison.

#### 6.2.4 Reliability

The reliability activities of Phase 2A have been conducted to specifically support the Cost of Ownership (COO) task of performing trade-offs with reliability, producibility, and maintainability to arrive at a low cost, high reliability MICRON design. The principal reliability activity has been to perform the reliability prediction study which will enable the iterative design process to be evaluated and quantified for further trade-offs with producibility and maintainability utilizing the COO model. The paragraphs which follow summarize the prediction study and its results, and discuss the related reliability activities performed during the period of Phase 2A.

##### 6.2.4.1 MICRON Configurations Evaluated

Four major IMU design configurations were subjected to a detailed prediction evaluation during Phase 2A. They included: (1) MICRON baseline; (2) E-1, M-1; (3) E-2, M-1, and (4) E-3, M-3. The latter IMU configuration was also utilized to evaluate the MICRON IMU design for the ACF (F16) application. A matrix of the MICRON configurations evaluated and their significant design difference is shown in Table 6-18.



Table 6-16. Phase 2A Configuration Comparisons

System Configuration	Recurring Acquisition Price	Life Cycle Cost	Average Price per Module	Parts per Module (Total/Active)	System MTBF
Baseline	\$64,778	\$153,534	\$806	48/21.1	946
PDA No. 6	\$59,800	\$144,047	\$469	42/18.5	979
Final Phase 2A (July 75 Configuration)	\$54,011	\$112,607	\$377	26/10.5	1577

	Allocation		Baseline System		Final Phase 2A System	
		\$		\$		\$
System Assembly & Test	\$ 3,600		\$ 3,093		\$ 3,015	
MHU	3,160		7,331		5,915	
IAU	10,695		21,398		20,241	
Gyro's		4,500		6,072		6,139
EMA's		① 4,320		① 11,920		4,180
Suspension Module		1,875		3,406		7,023
Spin Motor Module						2,899
SEU	8,420		19,336		11,406	
DPU	9,000		9,235		9,047	
Power Supply	3,375		4,385		4,387	
Totals	\$38,250		\$64,778		\$54,011	

① Baseline System and Allocation assumed MESGA and Pulse Amplitude Modulation Suspension System compatible for acceleration sensing. Assumption proved false. EMA's added instead of more expensive electronics (Ref Para 6.2.3.10).

Table S-17. Ten Year Ownership Costs

	Base Year Dollars		
	1973	1974	1977
Production Nonrecurring	4000.	4320.	5440.
Production Recurring	50838.	54011.	58122.
Acquisition Cost	54838.	58331.	63562.
Initial Spares	12206.	12959.	13903.
Initial Inv. Management	47.	51.	64.
Initial Support Equip.	9390.	9390.	9390.
Manuals	117.	128.	158.
Initial Maintenance Trng.	910.	998.	1232.
Support Equip. Install	469.	469.	469.
Initial Logistics Cost	23140.	23995.	25216.
Corrective Maintenance	25193.	26322.	28659.
Support Equip. Maintenance	246.	246.	246.
Inventory Management	70.	768.	947.
Maintenance Training	1628.	1784.	2203.
Maintenance Facilities	358.	392.	487.
Preventive Maintenance	397.	435.	530.
Repair Transport	300.	334.	412.
Maintenance Cost	28823.	30281.	35483.
Cost of Ownership	106801.	112607.	122260.

Table 6-18. Matrix of MICRON Configurations Evaluated

MICRON Configuration Evaluated	Instruments	Support Electronics	Power Supply	Dedicated Processor	Input/Output	
					Analog	Digital
Baseline IMU	MESGA (Getter)	Hybrid CPC's	N57A Power Cube Discretes	Autonetics Hybrid CPC design W/8K Memory	N/A	N/A
E-1, M-1 IMU	"	"	"	"	"	"
E-2, M-1 IMU	MESG (Getter) EMA's	"	"	"	"	"
E-3, M-3 IMU	"	"	"	Autonetics/ MMI Discrete Design W/ 17K Memory	"	"
E-3, M-3 IMU	"	"	"	"	Autonetics Hybrid/ Discrete Design	SCI Discrete (MIL-STD- 1553) Design

#### 6.2.4.2 Reliability Prediction Study

6.2.4.2.1 MTBF Goal. The mean time between failure (MTBF) goal established for the MICRON IMU is 2000 hours. It is important to recall here that this goal was established during the prior MICRON development phases, and it was carried forward as a Phase 2A reliability MTBF goal. Also, it should be remembered that this MTBF goal was considered achievable (in the aircraft environment) based on the projected gains in reliability offered through a maximum utilization of beam lead sealed junction (BLSJ) active devices in lieu of chip and flywire devices in the electronics design. However, as is discussed in Para. 6.2.4.2.4, achieving a near 100 percent BLSJ electronics design would prove a most difficult and costly, if not impossible, goal to attain during the MICRON design window. Also, the potential gains in predicted reliability (reduced failure rate) for BLSJ technology, compared to chip and flywire technology, have been substantially diminished or negated when using the hybrid prediction techniques contained in the current issue of MIL-HDBK-217B. On the other hand, utilization of the more sophisticated hybrid microcircuit prediction models contained in MIL-HDBK-217B offers a distinct improvement in the accuracy of predictions performed for the MICRON IMU hybrid electronics design. Considering the above, a predicted reliability in excess of 2000 hours MTBF can be calculated for a MICRON IMU configured with the basic hybrid electronics DPU design which featured an 8-K memory capacity. It should be emphasized, however, that lowering the MTBF goal is worthy of consideration for the IMU and INU MICRON configurations since both utilize a DPU with 17K memory in the current E-3 electronics design.

6.2.4.2.2 Reliability Prediction Iterations. Nearly forty (40) separate prediction iterations were performed during Phase 2A in support of the COO trade-off task. Approximately 75 percent of these prediction iterations were performed using the part class and part type techniques similar to that described in MIL-HDBK-217A, and previously utilized to perform the preliminary prediction included in the MICRON Phase 2 proposal. The remainder of the prediction iterations (approximately 25 percent) were performed utilizing both the part stress and parts count techniques described in MIL-HDBK-217B. The hybrid prediction model contained in the parts stress analysis section of MIL-HDBK-217B was utilized to perform the prediction for the hybrid electronics portion of the MICRON design.

The majority of the prediction iterations performed (prior to implementing MIL-HDBK-217B) were accomplished utilizing a Computer Prediction Model and a computer program developed by Autonetics. A sample printout of a prediction for one CPC is shown in Figure 6-28. Utilization of this program permitted a faster and more accurate analysis of part, circuit, and/or subassembly design changes under evaluation by the COO team. It is possible to alternately vary the prediction influencing factors such as: part reference temperatures, flywire vs BLSJ part technology, part and hybrid CPC level screening, and part costs. Similar computer programs have been developed by outside agencies to generate predictions per MIL-HDBK-217B. However, these computer techniques were not utilized for MICRON due to cost considerations during the final months of the Phase 2A program.

6.2.4.2.3 Prediction Math Models. The mathematical models utilized to generate the prediction iterations completed during Phase 2A are briefly described in the following paragraphs.

MICRON PREDICTION (V-1.5-3)(DA 6) VSCR + HYMAN SCR\*\* DATE\* 3-24-75

CPC NUMBER 9 SLEVO NA SCHLIN=FULL HYSKIL TEMPERATURE = 65.

PART TYPE	PART CLASS	CATEGORY	QUANTITY	FAILURE CONTRIBUTION	RELATIVE COST
QW4131BL	IC L	1.	3.	NO. SPIN	12.75
CA3130A	IC L	1.	1.	0.010921	0.00046
CD4053	IC L	3.	1.	0.041909	0.00030
CDR01BP100RK	CCMP	7.	2.	0.040994	0.000175
CDR01BP101BF	CCMP	7.	2.	0.001016	0.000003
CDR01BP475RK	CCMP	7.	1.	0.001016	0.000003
CDR01BX122RK	CCMP	7.	1.	0.000508	0.000001
CDR01BX472AK	CCMP	7.	1.	0.000508	0.000001
CDR01BX103RK	CCMP	7.	2.	0.001016	0.000003
CDR02HX123AK	CCMP	7.	2.	0.001016	0.000003
CDR04BP152CF	CCMP	7.	2.	0.001016	0.000003
CDR05BP472HF	CCMP	7.	2.	0.001016	0.000003
XA(1)	RNET	3.	1.	0.000000	0.000000
XD(25X)	RNET	3.	1.	0.000000	0.000000
XH 1-RP-165K	RNET	3.	1.	0.000000	0.000000
WSCRREE	-SC	7.	15.	0.000000	0.000000
WAG & LID 1	SKG	7.	1.	0.000000	0.000000
SUMSTAT	SUR5	7.	1.	0.000000	0.000000
SINGLE SUBSTRATE TOTAL = 0.157362					0.000000
CU = 1.00 KE = 0.50					0.000000
ADJUSTED SINGLE SUBSTRATE TOTAL = 1.022304					0.000000
TIMES 6. SUBSTRATES					0.137129

ALIGNED AVE A3. COST = 4. ACTIVE DEVICE = 0.090037  
 MISSED AVE A3. COST FOR PASSIVE DEVICE = 0.000024  
 AVERAGE PERMINUTUAL COST = 1.011901

Figure 6-28. Computer Prediction Printout

#### a. Autonetics Computer Predictions

As previously mentioned, approximately 75 percent of the prediction iterations were performed using the Autonetics developed computer prediction technique. The reliability model utilized for these predictions was previously described in the Phase 2 proposal. It is repeated in this report in Equation (1) below. The equipment failure rate ( $\lambda_s$ ) in Equation (1) is the sum of the failure rates contributed by each part type ( $n_i \lambda_i$ ) where there are  $n_i$  parts of a given type and  $i$  part types in the equipment. This sum is multiplied by the (MIL-STD-756A) use environment factor ( $K_E$ ). The factor  $K_Q$  in Equation (1) is used to adjust the equipment failure rate for quality, workmanship, and related failures which are not accounted for in the parts inherent failure rates. The adjustment is made as a percentage of part failures. (NOTE: For a mature MICRON MTBF, this  $K_Q$  factor is assigned a value of 1.0).

$$\lambda_s = K_Q K_E \sum_{i=1}^m n_i \lambda_i, \quad K_Q, K_E \geq 1 \quad \text{Eq. (1)}$$

Part failure rates ( $\lambda_i$ ) are calculated for each part type by adjusting the base failure rate for the part type ( $\lambda_{i0}$ ) for average applied electrical stress ( $K_s$ ) and average operating case temperature ( $K_T$ ) as shown in Equation (2).

$$\lambda_i = \lambda_{i0} K_s K_T \quad \text{Eq. (2)}$$

The relationship between equipment failure rate and MTBF is given in Equation (3).

$$M = \frac{1}{\lambda_s} \quad \text{Eq. (3)}$$

**Autonetics Predicted Failure Rates.** The failure rates used in the Autonetics computer prediction were taken from a failure rate data set maintained by Autonetics. The failure rates are based largely on achieved data for cased devices, from Autonetics hardware in past and current programs. A set of base failure rates, adjusted for the average applied electrical stress, was utilized in the computer prediction program. The computer program contains factors to account for vendor screening, part quality, hybrid screening, and of course, the  $K_Q$  and  $K_E$  terms of Equation (1). The Autonetics failure rate model does not, however, account for micro-circuit and semiconductor devices in the uncased die format. As such, it may provide less optimistic prediction results than a prediction model that does, such as the hybrid prediction model contained in MIL-HDBK-217B.

#### b. MIL-HDBK-217B Predictions

The reliability prediction iterations performed using MIL-HDBK-217B utilized the models contained therein for calculating hybrid device and monolithic device failure rates. The hybrid device failure rate ( $\lambda_p$ ) is given in Equation (4):

$$\lambda_p = \lambda_b (\pi_T \times \pi_E \times \pi_Q \times \pi_F) \quad \text{Eq. (4)}$$

where

$\lambda_b$  = the base failure rate for the hybrid circuit

$\pi_T$  = temperature acceleration factor for the hybrid circuit

$\pi_E$  = environmental factor for in service condition

$\pi_Q$  = quality level or screening class factor

$\pi_F$  = circuit function factor (digital, linear, both)

The hybrid circuit failure rate ( $\lambda_b$ ) is given in Equation (5).

$$\lambda_b = \lambda_s + A_s \lambda_c + (\Sigma \lambda_{RT} N_{RT}) + (\Sigma \lambda_{DC} N_{DC}) + (\lambda_{PF} \pi_{PF}) \quad \text{Eq. (5)}$$

where:

$\lambda_s$  = failure rate due to substrate type

$A_s \lambda_c$  = failure rate due to network complexity and substrate area

$\Sigma \lambda_{RT} N_{RT}$  = summed film resistor failure rate

$\Sigma \lambda_{DC} N_{DC}$  = summed failure rate for all attached devices

$\lambda_{PF} \pi_{PF}$  = failure rate of hybrid package (size and type)

The hybrid device failure rate ( $\lambda_{DC}$ ) is determined from a table of calculated values for most chip devices including resistors, capacitors, inductors, diodes, and transistors. The calculation of  $\lambda_{DC}$  for bipolar and MOS device chips is accomplished using Equation (6), the general failure rate model for monolithic microcircuit devices

$$\lambda_P = \pi_L \pi_Q (C_1 \pi_T + C_2 \pi_E) \quad \text{Eq. (6)}$$

where:

$\pi_L$  = learning factor for hybrid production phase

$\pi_Q$  = factor for quality level or screening class

$C_1$  = circuit complexity factor

$\pi_T$  = temperature acceleration factor for device technology

$C_2$  = circuit complexity factor

$\pi_E$  = environmental factor for in service environment

In applying the general failure rate model to the calculations of failure rates of hybrid devices ( $\lambda_{DC}$ ), the value of  $\pi_L$  is set to 1.0; and the value of  $\pi_Q$  to 2.0 per MIL-HDBK-217B hybrid model use instructions. Similar to Autonetics prediction model, the MICRON system reliability in terms of MTBF is given by Equation (7).

$$MTBF = \frac{1}{\lambda_P} \quad \text{Eq. (7)}$$

where

$\lambda_P$  = summed hybrid circuit failure rates

6.2.4.2.4 Reliability Trade-Off Considerations. During Phase 2A major emphasis was placed on trade-offs concerning: beam lead sealed junction (BLSJ) devices, part operating temperatures, part/device quality and screening levels; and screen testing of hybrid microcircuits. The following paragraphs briefly summarize the evaluation and analysis conducted for these trade-off areas.

#### a. Application of Beam Lead Devices

Since the early phases of the MICRON program, Autonetics has pursued a goal of maximum utilization of beam lead sealed junction (BLSJ) active devices in the IMU design. This goal was established to take advantage of the higher reliability and lower manufacturing/assembly costs potentially available from this new technology.

During Phase 2A Autonetics intensified its efforts to investigate the application of beam lead devices with the emphasis placed on trade-offs which were consistent with the MICRON design-to-cost and reliability goals. Because of their direct influences on these goals, device availability and testing capability were identified as the most immediate areas of concern to begin the trade-off analysis.

Utilizing the design engineer's parts/circuit requirements, component engineering conducted an analysis to determine device availability; and generated a parts list for the baseline IMU configuration. BLSJ devices appearing on this initial parts list represented the optimum selection for the availability trade-off factors considered for the analysis. These factors included considerations such as: catalog and production status; delivery times, alternate and/or second sourcing; device cost; screen and sampling test costs, standardization, and development/technical risk (if any). On the basis of this initial trade-off analysis, a beam lead versus fly-wire active device mix of 46% was identified for the baseline IMU design.



Through the co-operative efforts of component engineering, design engineering and the reliability/cost of ownership disciplines, additional devices were identified as candidates for potential beam lead development on the basis of their usage in the MICRON IMU baseline configuration. Included were: The 1800 MOS switch; the HA 2620 op-amp; and the SN 54LS193 up-down counter. Together these three devices accounted for roughly 40 percent of the fly-wire active devices in the baseline configuration. Subsequent trade-offs, plus part substitution and circuit redesign, reduced the number of potential candidates, and development funding was authorized to design the 2620 op-amp in the equivalent beam lead format. Converting the 2620 devices to a beam lead format had the effect of increasing the BLSJ versus fly-wire mix. Also, developing this device in beam lead format had the positive effect of increasing the predicted MTBF from 808 hours to approximately 1088 using the Autonetics prediction model.

Beam lead devices currently account for approximately 32 percent of the total active devices identified with E-3 MICRON IMU configuration (and 50 percent of the IAU and SEU electronics design). The major contributors to the overall reduction in beam lead device usage are identified with: (1) the increased use of MOS (fly-wire) in the SEU digital circuits; and (2) the substitution of discrete, cased devices for the beam lead uncased devices in the DPU design identified with the baseline, E-1, and E-2 configurations. The MOS activity has a positive reliability contribution, because the overall MICRON electronic parts count is reduced.

The development of a beam lead device carrier for conducting electrical testing, including MIL-STD-883 reliability screening tests, was also authorized during Phase 2A. (For the beam lead development status see para. 6.2.8.) Based on the limited industry experience/data available, indications are that the implementation of this test carrier will serve to enhance device reliability and device yield during hybrid manufacturing/assembly and test operations.

As indicated previously, Autonetics has utilized the hybrid prediction model and failure rates per MIL-HDBK-217B for the current MICRON IMU and ACF IMU predictions. Using this hybrid prediction model does impose a 2 to 1 failure rate penalty for the predicted reliability calculated for beam lead digital SSI/MSI devices compared to fly-wire devices. Since less than 3% of the total beam lead active devices used in the ACF IMU design fall in the digital SSI/MSI category, the impact of this failure rate penalty is minimized. Using MIL-HDBK-217B prediction techniques, the MTBF calculated for the MICRON ACF IMU exceeds the specified MTBF requirement, reference Table 6-22.

#### b. Part Temperatures

Electronic part temperatures of 55°C were assumed for the MICRON baseline and the E-1 configuration. A higher temperature (65°C) was applied to power devices utilized in the charge amplifier and spin motor electronic circuits.

During the period of evaluation for the E-2 configuration, seven packaging design alternatives (PDA's) were explored. Reliability vs temperature benefits for each of the packaging design alternatives were analyzed. For example, methods were sought to improve the thermal isolation between the instrument assembly unit (IAU) and the

support electronics unit (SEU). Packaging Design Alternate (PDA) No. 6 emerged from this phase of the study with this thermal design feature. This design included mounting the charge amplifiers, high voltage switch, and the power circuits of the spin motor electronics in the IAU.

The benefit of the PDA No. 6 package design is that it minimizes the thermal influence of the spin motor power transistor electronics on the rest of the SEU electronics during spin-up, damping and braking (spin-down). Also, it tends to promote another dual benefit: (1) the spin motor power transistors operate at a lower temperature since the heat generated is more readily dissipated to the instrument mass; and (2) the heating effect in turn reduces the instrument heater requirements and warm-up time.

The reference part temperatures utilized for the E-3, M-3 design configuration are based on preliminary calculations of expected operating temperatures for the MICRON engineering model electronics. Reliability predictions for the IMU/INU have been referenced to the temperatures indicated below:

<u>IMU/INU Subassembly</u>	<u>Temp °C</u>
MHU	70
IAU	70
SEU	55
DPU	55
PSU	70
Conv. (analog I/O)	45
MUX (digital I/O)	50

A plot of reliability failure rate vs part temperatures is shown in Figure 6-29. The top curve illustrates the baseline IMU (updated), and the lower curves the E-3 IMU configurations. In the lower two curves (E-3, M-3) the temperatures for the MHU, IAU and I/O have been held constant while the temperature is varied for SEU, DPU, and PSU subassemblies. Inspection of the E-3, M-3 curves indicates lower part temperatures are one means of achieving a higher reliability for the INU and IMU configurations, respectively.

#### c. Part Quality and Screening

A prediction evaluation which traded-off part quality and screening levels was initiated early in Phase 2A. This evaluation was conducted utilizing the E-1, M-1 IMU configuration. Table 6-19 summarizes the MTBF's determined for combinations of unscreened and screened parts, combined with a minimum or a maximum hybrid microcircuit screen (CPC level). The screening levels may be interpreted as follows: (1) screened parts have received the equivalent MIL-M-38510 level B and MIL-S-19500 JANTX testing by the vendor; the unscreened part receives no vendor screen testing beyond the normal visual and LC electrical probe test; (2) maximum hybrid screen is the equivalent MIL-STD-883B, Class B testing at the CPC level; the minimum hybrid screen includes a visual, 100 percent bond pull, and electrical functional test at 25°C.

The initial conclusion that can be drawn from the results shown in Table 6-19 is that it may be more cost effective to use unscreened parts and apply screens only at the hybrid CPC level. Further studies are needed to evaluate the validity of this

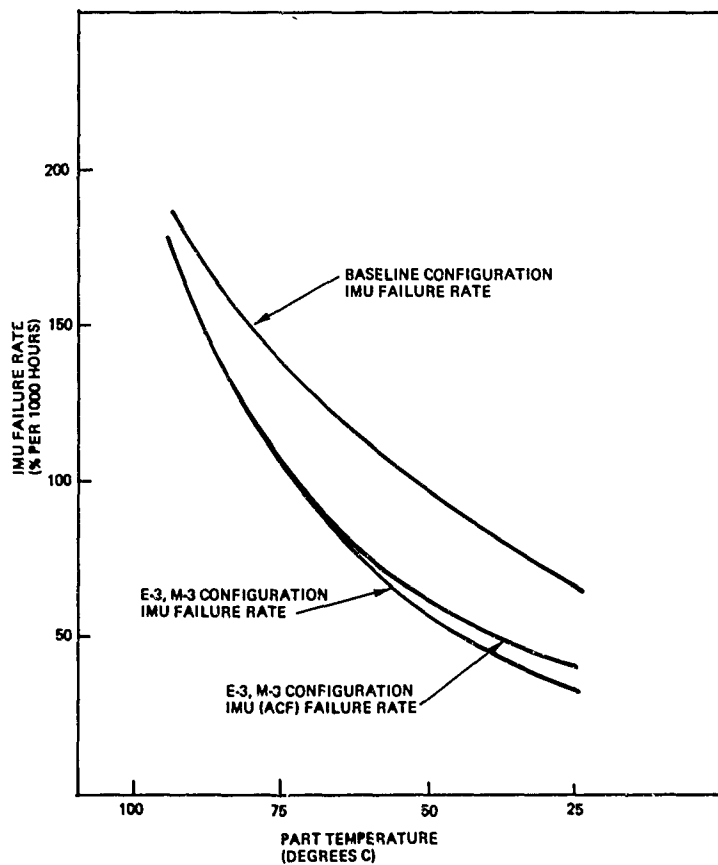


Figure 6-29. Predicted Reliability vs Part Temperature

Table 6-19. Reliability Screening Comparisons

	Vendor Screened Pts		Vendor Unscreened Pts Class C or Commercial	
	Max Hybrid Screen	Min Hybrid Screen	Max Hybrid Screen	Min Hybrid Screen
IMU MTBF	1101 hrs	707 hrs	1037 hrs	523 hrs

conclusion. However, it should be noted that the predicted MTBF's calculated here utilize the Autonetics earlier prediction model and failure rates. In the hybrid prediction model of MIL-HDBK-217B (currently used for the E-3 IMU/INU productions) the microcircuit failure rate calculation for attached devices ( $\lambda_{DC}$ ) assumes the part quality ( $\pi_Q$ ) level is equivalent to a MIL-M-38510, level B screened device. With the promise of a test and screening capability using beam lead device carriers, it would appear that BLSJ device failure rates, calculated per MIL-HDBK-217B, maybe subject to evaluation and improvement.

Autonetics initiated a preliminary IID spec development effort during MICRON Phase 2A. This effort has assumed a successful development of the carrier will enable more thorough electrical test and burn-in screens to be accomplished for BLSJ devices. For the spec. development status see para 6.2.7.2.

#### d. Reliability Screen Testing of Hybrid Microcircuits (CPC's)

Commencing with the Phase 2A go-ahead, a preliminary evaluation of the effectiveness of various possible combinations of screening inspections and tests for hybrid microcircuits was initiated. The results of this preliminary evaluation were utilized to perform reliability trade-offs in support of the COO task.

This evaluation assumes there will be a mix of beam lead and non-beam lead devices; and that it will be necessary to employ CPC screens that are equivalent to a MIL-STD-883, Class C and/or Class B level of testing. Thus far, cost tradeoffs have been limited in scope to a rather gross estimate for conducting the MIL-STD-883 equivalent screen testing at the hybrid CPC level. Estimates of the gross nature were necessary since there is little, if any, data available with which to make specific determinations of the effectiveness of a particular screen test or combination of screen tests. The results of the evaluation are intended to permit an assessment of the failure fallout as a result of employing selected screens and to evaluate cost impact on material costs and production flow.

The expected percentage of devices (IC's, transistors, diodes, capacitors, and resistors) which have been estimated to fail during the various screen tests for CPC's is summarized in Table 6-20. Since preliminary information was indicated that the testing and costs attendant to high-low functional testing is of particular concern, the data in Table 6-20 reflects the results of screening with and without this screen consideration. Estimates are also reflected for the percentage of latent failures which are not expected to be detected by the CPC screen tests. These undetected defects

Table 6-20. Hybrid CPC Screen Evaluation - Estimated Failures (in %)

Step	Hybrid Screen	Percentage Fail-Out for Device Type															
		Integrated Circuits - ICs						Transistors and Diodes						Capacitors		Resistors	
		Beam Leaded			Fly Wire			Beam Leaded			Fly Wire						
		C-B	C-C	B-B	B-C	C-B	C-C	C-B	C-C	B-B	B-C	C-B	C-C	ER-B	ER-C	ER-B	ER-C
1.	Band Pull	1.4	1.4					5.3	5.3								
2.	Internal Visual	3.7	3.7	0.7	0.7	0.7	0.7	3.4	3.4	0.7	0.7	0.7	0.7				
3.	Stabilization Bake Temperature Cycle Int/Final Elect (125°C)	5.3	5.3	0.5	0.5	0.5	0.5	3.5	3.5	0.4	0.4	0.4	0.4				
4.	Burn-In Final Elect (+25°C) Final Elect (-55°C) Final Elect (-125°C)	8.0		0.5		1.9		4.6		0.6	1.5						
5.	External Visual	0.2	0.2	0.1	0.1	0.1	0.1	0.2	0.2	0.1	0.1	0.1	0.1				
Total Failout- (%)																	
a. With Ht./Lo Elect		18.6		1.9		3.3		17.0		1.8	2.7						
b. Without Ht./Lo Elect		15.1	10.7	1.6	1.3	2.5	1.4	14.9	12.4	1.5	1.2	2.0	1.2	0.50	0.47	0.8 0.75	
Total Failures (%) (Latent Failures not revealed)																	
a. With Ht./Lo Elect		4.3		1.7		4.1		4.3		0.4	2.0						
b. Without Ht./Lo Elect		11.9	10.3	1.9	2.1	4.9	5.9	6.3	8.8	0.7	1.0	2.7	3.5	0.02	0.08	0.05 0.07	

will be therefore carried over into next assemblies (MLB-module assembly and/or IMU-system), and possibly go undetected prior to delivery of the hardware.

The estimated percentage for the fallout of the generic types of devices, when mounted on a hybrid ceramic printed substrate (CPS), are based on an extrapolation of data from the screening of cased devices. Industry publications and technical papers (and data summarized therein), and Autonetics experience data provide the necessary baselines needed to perform the extrapolation. The established baselines are:

1. Weighting factors for the determination of the general effectiveness of the "MIL-STD-883" type screens.
2. Device failure modes/mechanisms and their relative occurrence.
3. Sensitivity of each screen type in detecting specific failure modes/mechanisms.
4. Manufacturers' yield percentages for screened and unscreened cased devices.

The resultant model for the screening effectiveness of cased devices permits an assessment of the relative effectiveness of the possible screen programs for the uncased devices mounted on a CPS. For non-beam lead active devices, two (2) screen programs at the hybrid level are possible. They are:

1. MIL-M-38510, Class C integrated circuits and MIL-S-19500 JAN semi-conductors purchased from vendors and subjected to a "MIL-STD-883 Class B" type hybrid screen. In Table 6-20 this program is identified as C-B.
2. Parts purchased as in 1) above but subjected to "MIL-STD-883, Class C" type hybrid screen. This program is identified as C-C in Table 6-20.

Four (4) screen programs are possible for beam-lead active devices. They are achieved by subjecting either Class B or C and JAN or JAN TX devices to hybrid Class B or C screens. The combinations are identified as B-B, B-C, C-B, and C-C in Table 6-20. Two possibilities exist for capacitors and resistors. They are subjecting established reliability (ER) parts to either the B or C hybrid screen.

Figure 6-30 depicts the expected failures for the various combinations of Hybrid CPC screens, as a function of the beam lead active device mix. As one may expect, the larger the contribution of beam lead active devices to the total active device usage, the fewer the expected failures.

The data generated during this evaluation must be considered preliminary and subject to continual review as the MICRON development program progresses; and updating as actual hybrid CPC test results become available. However, the data does permit tradeoffs involving screen testing of hybrid CPC's to continue. The data results are expected to prove particularly useful in estimating the expected quantities of devices required to support manufacturing assembly and test operation for various combinations of CPC screen tests under consideration.

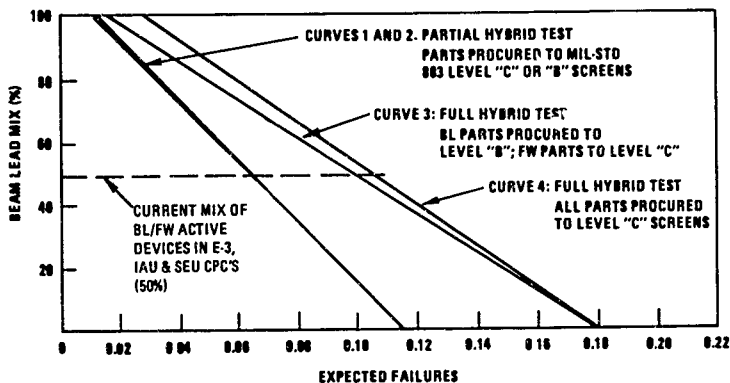


Figure 6-30. Expected Failures Per Active Device During CPC Hybrid Testing  
(As a Function of BL Mix)

#### 6.2.4.2.5 Reliability Prediction Summary

A tabulation of the reliability prediction iterations completed during the course of the MICRON Phase 2A study are shown in Table 6-21.

The upper half of Table 6-21 identifies the major MICRON hardware configurations evaluated for reliability. Also included is pertinent detail information regarding: (1) type of instruments (e.g., getter or Vactron gyro) including when EMA's are utilized; (2) the reference temperature, (3) the electronic parts count, (4) the number of active devices, and (5) the percentage of active devices which are of the BLSJ format.

The lower half of Table 6-21 provides a failure rate prediction summary for each major configuration analyzed. The subassembly abbreviations are as follows:

MHU	Mechanical Housing Unit
IAU	Instrument Assembly Unit
SEU	System Electronics Unit
PSU	Power Supply Unit
DPU	Dedicated Processor Unit

Table 6-21. Reliability Prediction/MICRON Design Configuration Matrix

CONFIGURATION DESIGN IDENT.	1	2	3	4	5	6	7	8	9
	BASLINE IMU	BASLINE UPDATED	E-1, M-1 IMU	E-2, M-1 IMU	E-2, M-1 UPDATED	E-3, M-1 IMU	E-3, M-1 UPDATE (217-8)	E-3, M-3 IMU	E-3, M-3 ACF (F16)
INSTRUMENT TYPE	MESGA (GETTER)	MESGA (GETTER)	MESGA (GETTER)	MESGA (GETTER)	MESG (VAC-ION) EMAs	MESG (GETTER) EMAs	MESG (GETTER) EMAs	MESG (GETTER) EMAs	MESG (GETTER) EMAs
REF. Instruments	70	70	70	70	70	70	70	70	70
TEMP °C	55	55	55	55	65	65/60	65/60	55/70	45/50/55/70
ELECTRONIC PARTS COUNT	2442	2442	2351	2179	2259	1715	1715	1366	1458
ACTIVE DEVICES	1189	1189	1105	1045	1068	899	899	645	680
% BLSJ DEVICES	46	48	54	58	56	51	51	32	32
RELIABILITY PREDICTION SUMMARY (FAILURE RATES IN %/1000 HOURS)									
MHU	37	7.0	7.0	7.0	11.2	7.3	5.3	5.3	3.4
IAU (GAU)	72.8	57.3	39.5	33.7	26.4	36.7	21.5	15.8	15.8
SEU	20.0	14.3	17.3	12.0	34.1	23.2	8.2	8.7	8.7
PSU	10.0	9.8	9.8	9.8	11.0	8.6	5.6	10.0	10.0
DPU	17.2	17.2	17.2	17.2	19.4	50.0	22.0	23.6	23.6
MTU (DIG I/O)	-	-	-	-	-	-	-	-	6.2
CONV (ANAL I/O)	-	-	-	-	-	-	-	-	1.9
SYSTEM	F/R	123.7	50.8	79.7	102.1	125.8	63.6	63.4	69.6
TOTALS	MTBF	808	1101	1254	979	754	1571	1576	1436



MTU            Multiplex Terminal Unit  
(MIL-STD-1553 MUX; referred to elsewhere in text as digital I/O)

CONV          Converter Unit (Referred to elsewhere in text as analog I/O)

As previously mentioned, the reliability predictions beginning with the E-3, M-1 update have been performed using the hybrid prediction model and failure rates as provided in MIL-HDBK-217B. The MIL-HDBK-217B failure rates and prediction models have also been utilized where discrete device or miscellaneous (and low population) item predictions were required. Also, all predictions performed have considered the MICRON airborne environment in the final MTBF calculations.

The prediction for the E-3, M-3 INU configuration has been baselined to include MTBF's based on vendor reliability estimates for the power supply unit, and the multiplex terminal unit (MIL-STD-1553 MUX). Autonetics is in process of updating the power supply design. However, detail reliability predictions remain to be completed for both of the above two subassemblies.

Also, the predictions for all of the IMU configurations include a prediction estimate for a battery unit as part of the MHU calculation. The prediction for the E-3, M-3 ACF (F16) application does not include a battery as part of the INU configuration. Therefore, the reliability failure rate estimate for the MHU is adjusted, accordingly.

Table 6-22 provides a CPC/module level breakdown of the reliability predictions completed for the last iteration of the E-3, M-3 IMU and INU configurations. As noted above, the MHU failure rate does not reflect a battery unit for the INU.

The reliability allocation performed early in Phase 2A for the IMU is indicated below:

IMU Subassembly	Phase 2A Allocated Failure Rate (%/10 <sup>3</sup> Hr)
MHU	2.33
IAU	16.67
SEU	11.00
(Includes Battery and Power Supply)	
DPU	20.00
Total Failure Rate (%/10 <sup>3</sup> Hr)	50.00
MTBF (Hours)	2000

The allocated failure rates shown for each major subassembly may be compared with the final Phase 2A predicted results summarized for the E-3, M-3 INU configuration shown in Table 6-22. As indicated above, the SEU allocation includes the battery and power supply. In the final IMU configuration (E-3), the prediction estimate for the battery is included in the MHU calculation; and the power supply became a separate subassembly.

Table 6-22. Reliability Prediction Summary

	MICRON IMU APPLICATION			ACF (F-16) MICRON INU APPLICATION		
	E-3, M-3 Configuration Failure Rate (%/10 <sup>3</sup> Hr)			E-3, M-3 Configuration Failure Rate (%/10 <sup>3</sup> Hr)		
• Mechanical Housing Unit (MHU)			5 329			3 433
• Instrument Assembly Unit (IAU)			15 801			15.801
• Instrument Assembly		8.294			8 294	
• MESGs	2.167			2 167		
• EMAs	6.127			6 127		
• Suspension Electronics		5 172			5 172	
• Charge Amps	4.220			4 220		
• Signal Buffers	0 952			0 952		
• Spin Motor Electronics		0 647			0 647	
• SM Transistor P/A	0 504			0 504		
• SM Regulator	0.143			0.143		
• IAU Assy Misc		1 688			1 688	
• Support Electronics Unit (SEU)			8 695			8.695
• SEU Module "A"		4 539			4 539	
• Servo Network	1 520			1 520		
• Modulator Input	0 585			0 585		
• Modulator Output	0 406			0 406		
• DC Ref and P/Load Modulator	0 389			0 389		
• Freq Ref, T/S Gen, & Auto Seq	0 225			0 225		
• High Voltage Switch	1.184			1.184		
• Precision Crystal Oscillator	0 230			0.230		
• SEU Module "B"		4 156			4 156	
• Gap Monitor	0.256			0.256		
• MUM Demodulator	0 445			0 445		
• MUM Demod Filter	0.076			0 076		
• MUM Demod S&H	0 837			0 837		
• A/D Converter	0 358			0 358		
• Spin Motor/Temp Control	0.778			0 776		
• SM Power Control Amp	0 077			0 077		
• Quasi RG, MUM/EMA Timing, & RG	0 541			0 541		
• Temperature Compensation	0 788			0.788		
• Dedicated Processor Unit (DPU)			23 610			23 610
• DPU Module No. 1 (CPU)		5.010			5 010	
• DPU Module No. 2 (Memory)		17.160			17 160	
• DPU Module No. 3 (I/O)		1 440			1 440	
• Power Supply Unit (PSU)			10 000			10 000
• Multiplex Terminal Unit (MTU) (MIL-STD-1553 MUX)			N/A			6 240
• MUX Module No. 1					3.120	
• MUX Module No. 2					3.120	
• Converter Module			N/A			1 872
• SYSTEM TOTALS						
• Failure Rate (€/10 <sup>3</sup> Hr)			63 435			69.051
• MTBF			1576			1436

#### 6.2.4.3 Supplemental Phase 2A Reliability Activities

6.2.4.3.1 Associate Contractor Interface. During the course of the Phase 2A program, a continuous technical interface has been maintained with representatives of the Martin Marietta Corporation (MMC), the associate contractor for MICRON reliability.

Autonetics reliability representative attended a formal technical interchange meeting at MMC's plant in Denver, Colorado on 26 August, 1974. Technical discussions were held at this time on the subjects of: failure rates, reliability prediction models, reliability design guidelines, and reliability demonstration testing. A discussion of reliability demonstration testing was entered into in considerable detail since MMC was about to prepare a formal plan for MICRON testing to be conducted per MIL-STD-781B, during Phase 2B. Autonetics informally reviewed the experience data results generated during F-111 reliability demonstration testing conducted per MIL-STD-781B test conditions. During the ensuing discussions, emphasis was placed on the evaluation of the proposed test assets and appropriate MIL-STD-781B test plans which appeared applicable for MICRON during Phase 2B.

Subsequent to this technical interchange meeting, Autonetics reviewed and provided informal comments to a reliability test plan submitted to AFAL by MMC. On a more informal basis, Autonetics reviewed the reliability design guidelines document and a reliability program plan document prepared by MMC and submitted to AFAL for application on the MICRON reliability program.

It is appropriate to also note that MMC's on-site representative at Autonetics has performed in a most co-operative and professional manner throughout the Phase 2A period. The most significant contributions have been assisting in performing reliability predictions; and in supporting the hardware failure and failure data assessment requirements generated through N57A system testing.

6.2.4.3.2 RADC Technical Interchange Meetings. Autonetics reliability representative joined the MMC (Denver) reliability representative in technical discussions held at Rome Air Development Center (RADC) in Rome, N. Y. during the period 28-29 August 1974.

At RADC, technical discussions and interchange meetings were conducted with representatives responsible for reliability predictions (MIL-STD-217B); reliability demonstration (MIL-STD-781B); and reliability screening (MIL-STD-883 and MIL-M-38510). Overall, these discussions were very informative regarding the general cost-of-ownership and test constraints facing reliability during the development of the MICRON IMU. A specific example which may be cited concerned the availability of devices in a beam lead (BL) format. Investigation of this problem had apparently prompted Ft. Monmouth (Army) to go out with some contracts to vendors to encourage early development of BL devices. RADC indicated the unavailability of BL devices has discouraged their use on many new hardware programs (not identified).

An overview of the type of reliability screening for parts and hybrid microcircuits, being considered for the MICRON IMU, was presented to the RADC personnel. In general, they were most receptive to the approach to testing to assure reliability at these levels.

Copies (unreleased at the time of this visit) of the MIL-HDBK-217B and MIL-STD-883, Method 5004 (screening procedures) were provided by RADC personnel for information only. They agreed to mail out copies of the released documents as soon as available.

During the course of the Phase 2A Design Review Meeting held at Autonetics during 18-21 February 1975, the Autonetics reliability representative was invited to participate in two splinter meetings with the RADC and MMC reliability representatives in attendance. At these splinter sessions, the RADC comments to the MMC Reliability Program Plan and Test Plan documents were reviewed and discussed in some detail.

In addition the RADC representative requested a copy of the Autonetics and MMC predictions, and the E2/M1 parts list. The Autonetics data, upon approval of program management (and AFAL), was provided (as was the MMC data). The basis for this request was that RADC would like to perform their own independent prediction and review the results with AFAL. Autonetics' representatives concluded that these splinter sessions were mutually beneficial and served to establish a valuable technical interchange link with RADC and the MICRON reliability task.

6.2.4.3.3 AFAL Interface. Autonetics reliability representative supported the COO team interface meetings with AFAL representatives during monthly program review visits. As required, data was prepared on reliability activities of interest to status the MICRON program progress for AFAL. As much as possible, the technical interchange and data presentations were kept on an informal basis.

The MICRON Design Review Meetings held at Autonetics during Phase 2A were supported on a formal basis. Reliability data pertinent to statusing the Phase 2A activity is contained in the formal publications submitted for these reviews.

6.2.4.3.4 Formal Activity Reports. Status inputs and data generated from Phase 2A reliability activities was provided in support of the cost of ownership section of each MICRON Phase 2A monthly report submitted to AFAL.

## 6.2.5 Maintainability

The maintainability aspects of the cost of ownership team are concerned with minimizing life cycle costs by developing the optimum combination of MICRON hardware support features and maintenance concepts. This includes the estimation of quantitative support characteristics for evaluating design, producibility, and reliability alternatives as well as developing/evaluation maintainability alternatives.

Phase 2A activity has encompassed both of these areas. The trade studies discussed in the previous sections show the significant impact unit price reliability and packaging have on support costs. Reliability alternatives involving parts screening, burn-in, etc not only impact the expected maintenance rate but also change the unit cost for spares and repair material costs. The effect of parts procurement/screening on maintenance costs, as an example, is shown in the earlier section of this report which covers that subject. The evaluation of alternative packaging approaches was another task reported above wherein the resultant maintenance features greatly impacted life cycle costs.

The maintainability trade studies accomplished covered the subjects of repair level analysis, repair/discard trade-offs, hybrid circuit sizes, calibration stability period, calibration labor requirements, built in test confidence, total test requirements, instrument assembly packaging, and IMU repair access characteristics. Most of these subjects were treated on each major system configuration identified. Initially this work was done using a baseline definition derived from the Phase 1B work. Subsequent definitions used included two additional hardware mechanizations, three or more different material cost exercises, two reliability prediction models, and several packaging approaches. As each maintainability topic is further discussed below the impact of these changes will be seen.

The identification of major logistics cost drivers to be studied and worked was accomplished early in the program by comparing the baseline system to one which met the unit price and reliability goals. This identified the maintenance characteristics and associated costs independent of the achieved producibility and reliability. The top level life cycle cost results are graphed in Figure 6-31. It shows that if one could extrapolate the current baseline system and maintenance concept to a 2,000 hour MTBF, 35 thousand dollar system the logistics costs would still exceed current goals. More importantly, the detail of the analyses provided data which was used to identify and work the major cost drivers. Trade studies covering these specific cost drivers were subsequently conducted for the various hardware configurations developed in Phase 2A. These studies have identified characteristics which will enable meeting the logistics goals. Later paragraphs discuss these results.

### 6.2.5.1 MICRON Logistics "K" Factor

An important but rather subjective factor used in predicting maintenance rates and subsequent life cycle cost is referred to as the logistics K factor. This K factor is the number used to predict the MICRON maintenance rate in the using environment with the predicted failure rate as a basis. It is expressed as the Multiplier by which predicted failure rate is increased to get a maintenance rate. Initial MICRON studies used a K factor of 1.50. This number was established early in the MICRON program as being appropriate to use with the failure rate model. The subsequent change to MIL-HDBK-217B reliability prediction techniques necessitated further study of the K value. This study

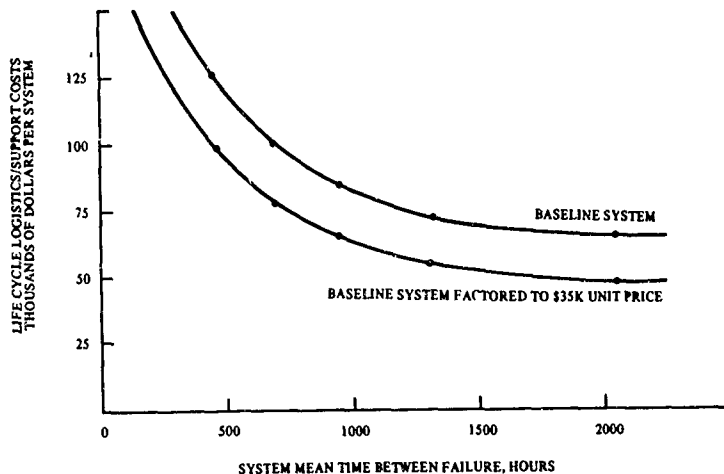


Figure 6-31. IMU Logistics Costs as a Function of Unit Cost and Reliability

yielded a new K factor which is a function of BIT and test set capabilities as well as increasing it to correspond with the more optimistic reliability predictions. The analysis also developed relationships between the IMU K factor and module/subassembly K factors. The resultant value for the MICRON IMU at the predicted test probabilities is 2.91. This new factor has been used for all studies with the July 1975 hardware configuration.

Figure 6-32 demonstrates the reason why a K factor is needed. Maintenance actions are caused by many reasons summarized in this figure under four categories. First are the primary or relevant failures. These are failures which the reliability model attempts to predict. Depending upon the prediction accuracy, there may be additional failures as listed because of variations from the norm. The second two categories are maintenance actions generated because of errors in testing, diagnostics, handling, etc. These are a function of the system design and support system compatibility.

The development of a K factor for a specific system in a specific environment is a subjective task. It is a matter of (a) trying to project the reliability prediction to the operational environment and (b) identifying hardware and support characteristics which will cause maintenance "errors."

One can look at past history in attempting (a) above (i.e., projecting predicted failure rates to the operational environment). There is at hand a significant amount of data relating to predicted reliability and realized maintenance rates. The data are

# PRIMARY MAINTENANCE ACTIONS ARE CAUSED BY:

## PRIMARY FAILURES

### Predicted Failures

Based on average part histories considering expected temperature and electrical stresses and "Normal" failure modes

+

### Failures Not Predicted

Accounts for variations from Norm:  
Operating hours per on/off cycle  
Operating exceeding expected stress  
Non-operating effects (Age, Handling, storage)  
Maintenance induced failure (Not obvious)  
Environmental stresses not accounted for

## AND OTHER MAINTENANCE REQUIREMENTS

### Maintenance

Maintenance when no failure exists  
Maintenance which does not correct failure

+

### Gross Physical Damage

Handling, Overstressing, Improper storage, etc.

Figure 6-32. Maintenance Action Generation Sources

quickly muddled, however, by variations in the prediction model, incomplete user data, and design changes between the prediction and field measurement. In August of 1973 Autonetics Logistics conducted a survey of 17 agencies including Commercial Airlines, RADC, Air Force and Contractors. The results indicated the use of K factors ranging from 0.1 to 10 (maintenance rate equals 0.1 to 10 times the predicted failure rate). The most used factors were grouped in the range of 3 to 6. A survey of F-111 avionics at the same time indicated a mean K factor across all MK II LRU's of 8.3 and a median factor of 5.2. Another comparison is a report by Grumman Aerospace Corporation (RADC-TR-74-266). This report is mainly directed toward accounting for the disparity between demonstrated and field reliability. Included in the approach however, was a MIL-HDBK-217B prediction for each of the 95 equipment types surveyed plus a sanitized field reliability measurement accounting for all failures but excluding all "maintenance error" type removals. This is the exact comparison needed to relate to the (a) portion of K factor development above.

Figure 6-33 shows a histogram of data extracted from that report. The data is based on 95 different equipment types including RF receiver transmitters, signal and data processor, indicators and controls, and power devices. For each of these equipments the ratio of predicted MTBF to field MTBF was computed from the report data. Statistics on the resultant ratio is as follows:

Ratio Range	0.05 to 1481
Median Ratio	3.1

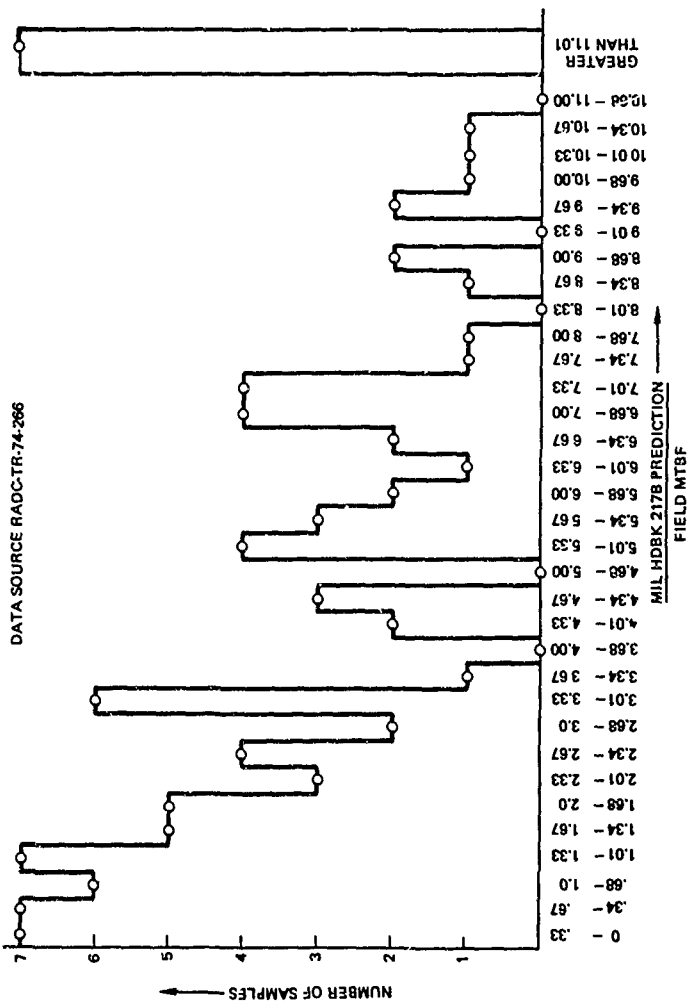


Figure 6-33. Histogram of MIL-HDBK-217 MTBF Prediction Sample Data



Mean Ratio 30.36

Mean Ratio excluding 3.6  
all data over a value  
of 11.0 (7 samples of  
the 95 were excluded)

Part b, estimating the "maintenance error" portion of the K factor, relates to characteristics such as Built in Test, fragility, human interpretation of performance, adjustments required, handling requirements, operating environment, support resource adequacy, etc. Inertial navigators have a peculiar characteristic in this category which is repeatability, i.e., some runs can exhibit errors without exceeding the average overall specification. The major portion of this consideration can be expressed quantitatively in terms of the following probabilities at each level of maintenance.

Probability of fault detection and isolation

Probability of fault indication with no failure

Probability of removal with no indication nor failure

Previous MICRON work in evaluating BIT cost effectiveness established the analytical relationship of these factors depending upon the maintenance concept used.

From the above and other analysis it is concluded that a new K factor relating predicted failure rate to field failure rate should be 2.8. This is 10% less than the Median of the Grumman data. In addition this should be increased as a function of the testability characteristics. This results in a total K factor of 2.91 given the following conditions. Changes in any of this data will be reflected into new factors as applicable.

95% probability of BIT flagging of failures

1% probability of false BIT flag (no failure)

Depot IMU repair with no base verification

Depot repair station capabilities:

2% probability passing bad unit not flagged by BIT

1% probability not passing a good unit

0% probability passing bad unit flagged by BIT

#### 6.2.5.2 Optimum Repair Level and Repair/Discard Analysis (ORLA)

A complete ORLA was performed early in Phase 2A. The baseline system configuration was used for this analysis. The detailed results were published in report C74-1008/201 dated October 16, 1974 and submitted to the customer as CDRL data item A00L. The ORLA followed the approach and intent of AFLCM/AFSCM 800-4,

however the MICRON life cycle cost prediction model was used for all cost projections. This made these tradeoffs compatible with all others performed throughout and assured that all pertinent MICRON characteristics were evaluated.

Fourteen potential maintenance concepts were evaluated for the Phase 2A baseline system. These concepts ranged from complete repair at each intermediate shop to contractor repair to assembly discard. The eight lowest cost approaches are summarized in Table 6-23. The approaches are listed in ascending cost order.

A series of sensitivity projections were also made as part of the ORLA to determine what maximum average hybrid circuit price would provide a discard at maintenance policy at a lower life cycle cost than the lowest cost repair policy. This latter subject is treated in Para 6.2.3.3 above both for the baseline system and the final July 75 configuration.

Table 6-23. Eight Lowest Cost Baseline System Maintenance Concepts Listed in Ascending Cost Order

Maintenance Concept				Total Projected Life Cycle Cost Dollars Per System
Items Repaired At			Items Discarded	
Base Shop	Depot	Contractor		
IMU	All Sub Assys		Battery	135,265
IMU	Housing MESGA Power Supply DPU		Battery Electronic Modules	140,230
IMU	Housing MESGA Power Supply DPU		Battery	151,417
Electronic Modules	IMU All Sub Assys		Battery	153,534*
	IMU, Housing, Electronic Modules Power Supply, and DPU	MESGA	Battery	153,861
	IMU	All Sub Assys	Battery	155,491
	IMU, Housing, MESGA, DPU, and Power Supply		Battery Electronic Modules	158,115
	IMU, Housing, DPU, Power Supply, and Elect Modules		Battery MESGA	162,729

\*Baseline Maintenance Concept.

Many conclusions may be drawn from the ORLA. Some of the more significant are:

1. Base Shop IMU repair is dramatically less costly than Depot Repair (the baseline concept) for the baseline system.
2. An average module price of less than 62.5 percent of the baseline price would be required before module discard is less costly than repair.
3. The least costly approach is still about twice the MICRON Life Cycle cost goal. Calibration and test equipment requirements constitute the major maintainability deterrents to goal achievement.
4. Contractor repair (not considering repair quality or design improvements) is not effective.

Subsequent to conducting the baseline ORLA, mini-ORLA's were performed on three additional IMU designs; the E-2/M-1 concept described in earlier paragraphs of this section, the July 1975 configuration, and a hypothetical system which meets all of the quantitative Producibility, Reliability, and Maintainability goals of Appendices II, III, and IV (Reference 3). A description of the Goal System is listed in Table 6-24. Predicted Life Cycle Costs for each of the alternative maintenance concepts are listed in Table 6-25 and compared graphically to the other designs in Figure 6-34.

The increase in costs for the July 1975 configuration is attributable to increases in unit price and maintenance rate. Also the differential between base and depot repair is broadened due to a reduction in test equipment repair cost estimates.

The desired maintenance concept for the MICRON program is Depot IMU repair and hybrid circuit discard. It is interesting to note that the E-2/M-1 and July 1975 designs achieve the last portion of this (i.e., module discard) while the goal system almost achieves this concept in total.

#### 6.2.5.3 Calibration Stability

The first major logistics cost driver identified is the calibration period of the IMU. Regardless of hardware price and reliability, calibrations constitute a major logistics cost. In fact, as the reliability is improved, calibration costs increase if the stability period remains constant. This is due to fewer calibrations being performed as part of corrective maintenance actions and more on a "scheduled" basis.

With the mean time between corrective maintenance (MTBCM) in the range predicted for MICRON (836 hrs for E-2/M-1 and 542 hours 7/75 system) life cycle costs are sensitive to the calibration stability period up to about one year. Improvements in stability beyond that do not yield much savings unless the MTBCM is also increased. A Depot IMU repair concept is also much more sensitive than when the IMU are repaired at each base. The results of LCC studies including all spares, TE, etc investigating this are graphed in Figure 6-35.

The early studies on the E-2/M-1 system showed a crossover between base and depot repair with a one year stability period. That crossover no longer exists with the July 1975 system. This is due in part to the increased maintenance rate of the

Table 6-24. "Goal" System Definition

Average IMU Unit Price	\$38,250
Mature Reliability	2000 hr MTBF
IMU Weight	10 lb
Packaging Configuration	Same as baseline
Calibration Period	750 days
Manhours per Calibration	.8 hr
Manhours per Repair (Including Calibration)	
System	1/2 hr
IMU	1 hr
Assys/Sub Assys	Same as baseline
IMU Re-Test OK Rates (as applicable)	
Base Verification	8 percent
Depot Repair	1 percent
Test Equipment Costs	
Base Shop Verification	100K
Depot IMU Repair	200K
MESGA and Module Repair	175K

Table 6-25. Mini-ORLA Results

Maintenance Concept	Predicted Life Cycle Cost (1974 dollars)		
	E-2/M-1	7/75 Conf.	Goal System
Base IMU Repair, Hybrid Circuit discard, and Depot repair of all other assemblies.	108,871	112,607	62,456
Base IMU Repair and Depot Repair of all assemblies to the piece part.	111,011	114,914	66,687
Depot Repair of IMU and all Sub Assys except Hybrid Circuits. Discard Hybrid Circuits.	118,320	123,315	64,688
Depot Repair of IMU and All Sub Assys. Note: All alternatives include battery discard.	120,902	125,859	68,908

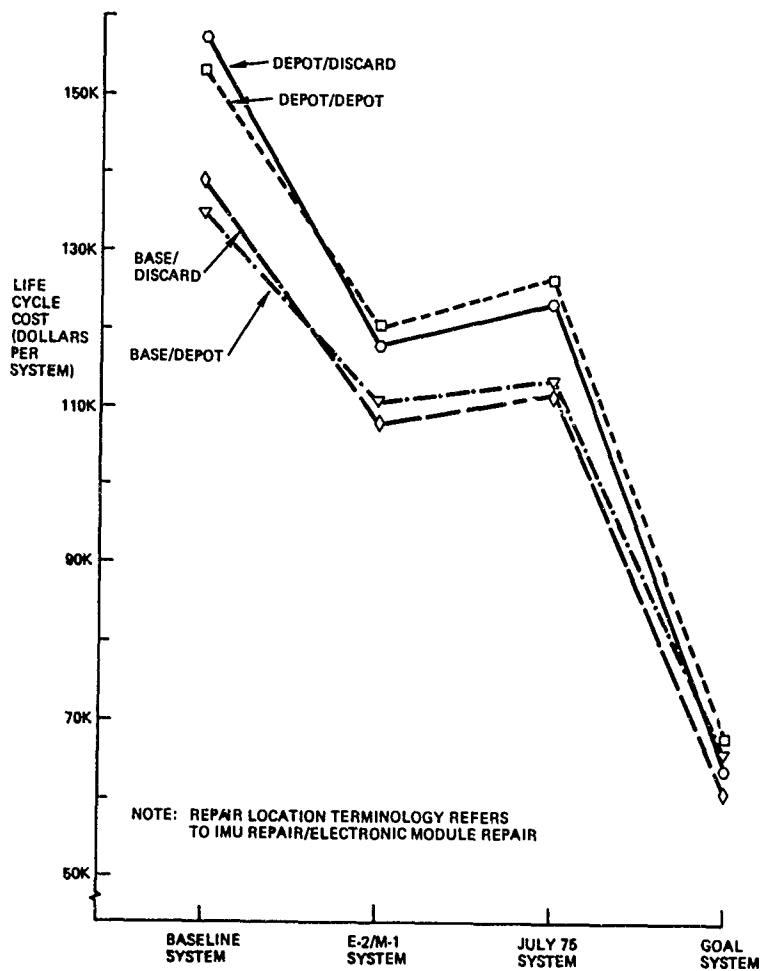


Figure 6-34. Maintenance Concept Comparisons

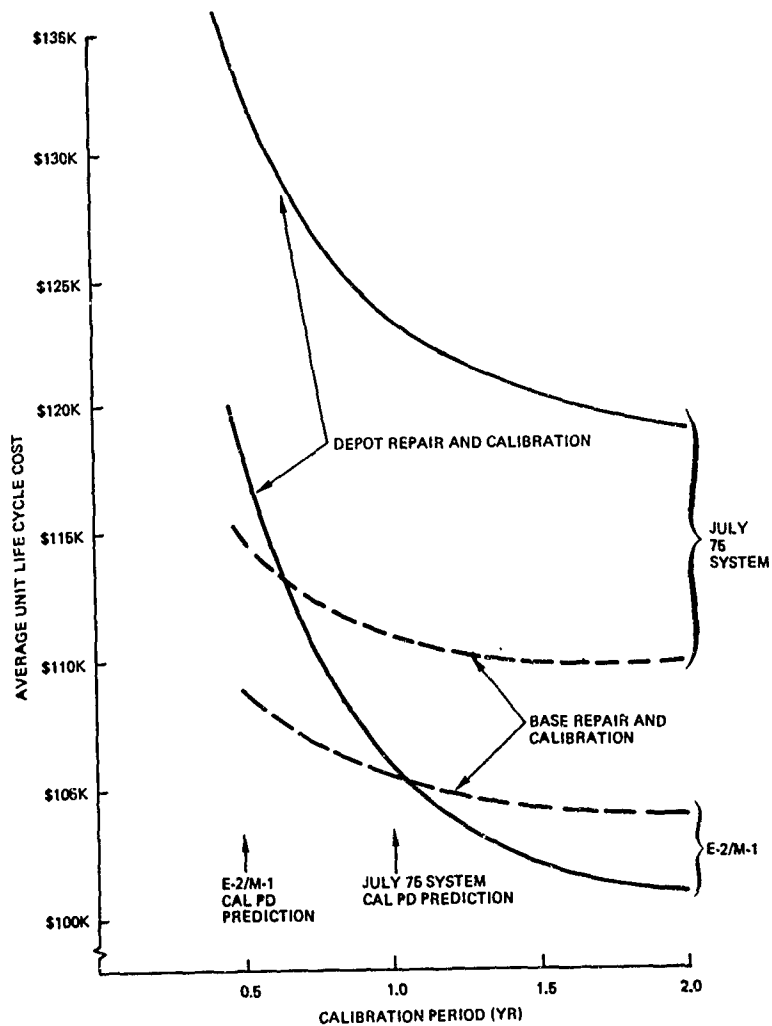


Figure 6-35. E-2/M-1 Maintenance Concept vs Calibration Stability

latter system. It is more heavily influenced however by a reduction in test equipment maintenance costs probably in error for the E-2/M-1 system. These high maintenance costs benefitted a depot repair concept unduely.

#### 6.2.5.4 Built In Test and Other Test Requirements

System testability has been discussed extensively throughout the MICRON team during Phase 2A. The direction of these discussions were documented in two letters which were prepared and distributed identifying the malfunction isolation requirements and philosophy for MICRON. The first presented an initial survey of specified MICRON and ACF requirements. This was prepared by engineering as a result of a survey of MICRON SOW and model specifications, F16 INS specifications, and F17 specifications. The second was prepared by maintainability/cost of ownership in an attempt to bring together some of the points in the first letter and the results of MICRON studies into a cohesive basic philosophy. This letter also contained some basic definitions so that common terminology is used. These definitions are listed in Table 6-26.

The test and fault isolate requirements identified are summarized in Figure 6-36. The data presented is basic and straight forward, however, it is important (as stressed in the text of the referenced letter) that the required capability, but no more, exists in the final design.

The amount of IMU Built In Test (BIT) capability is a significant maintainability question to be answered prior to final IMU design. A preliminary sensitivity study using the E-2/M-1 design was conducted to determine the impact of varying the BIT confidence levels on initial and recurring support costs. This analysis required the definition of IMU removal rates, test equipment capabilities, and module removal/repair all in terms of the BIT confidence. The BIT confidence was then varied from 0 to 99 percent with the resultant maintenance factors and rates input to the Life Cycle Cost prediction model. The model output provided a prediction of the initial Logistics and Support Costs as a function of BIT confidence. The result is graphed in Figure 6-37. In summary it shows that the E-2/M-1 system and the baseline maintenance concept (base verification and depot repair) the potential Life Cycle Cost advantage of BITE is almost 8 thousand dollars per system. The July 1975 system with its revised K factor etc has a potential of over 11 thousand dollars using its lowest cost maintenance philosophy, Base IMU repair. The next question to be answered is what cost is required to achieve these probabilities for BIT. With that data one can develop the optimum requirement.

The E-2/M-1 portion of Figure 6-37 also shows the impact of base verification. If a depot repair only concept were selected the cost of verification only pays off at the lower BIT confidences. This considers all applicable costs such as test equipment and spares acquisition, support, manpower, training, facilities, etc.

Test equipment capabilities were held constant. These test confidences were as follows.

#### Base Verification Test Set

- 5% probability of passing bad unit not flagged by BIT
- 1% probability of not passing a good unit

Table 6-26. Basic Fault Isolate Characteristic Definitions

Built In Test (BIT)

The self contained capability of a system to detect malfunctions and isolate them to some equipment level. BIT includes:

**Self Test:** That portion of BIT which operates continuously and automatically in conjunction with the normal item operation. Self test is usually the major technique for fault detection. Otherwise an undetected fault could exist waiting for the time an operator initiated test is conducted. Tests initiating shutdown must be of this category.

**Operator Initiated:** Supplemental tests initiated by the system operator or maintenance technician. These tests are typically conducted following the fault detection above to obtain further fault isolation information.

Built In Test Equipment (BITE)

Often used synonymously with BIT. Specifically it refers to the hardware (equipment) included in the prime items to perform the BIT function. It may be expanded to include test points, etc., but this is not the usual conotation.

Test Points

Electrical connection points identified to provide circuit access for the attachment of the test equipment (AGE). Test points may be nothing more than a circuit node marked and accessible. Manual probing is not desired, however. MICRON test points are thus considered points for positive mating of AGE connectors.

Fault Detection/Isolation Software

Special software used in conjunction with BIT or AGE for detection and/or isolation. Software may be resident in the DPU or AGE. It may be loaded into the DPU by the AGE for use only during testing.

**IMU and Module Repair Stations**

2% probability of passing bad unit not flagged by BIT

1% probability of not passing a good unit

all IMU which are bad and flagged by BIT are checked as bad by both test sets.

Defining the IMU removal rate as a function of BIT was accomplished by dividing removal causes into 5 classes. The impact of BIT on each of these was then easily assessed. Table 6-27 lists these classes, their removal rates, and associated terms and definitions. The removal rate terms shown correspond with the increased K factor now being used. These differ from the previously published values. The sum of all five classes of removals equals the total IMU replacements. These are plotted in Figure 6-38 for the E-2/M-1 portion of the study. For the July 1975 system with its new MIL-HDBK-217B failure rate, the removal rate ranged from 2.85λ to 4.27λ.



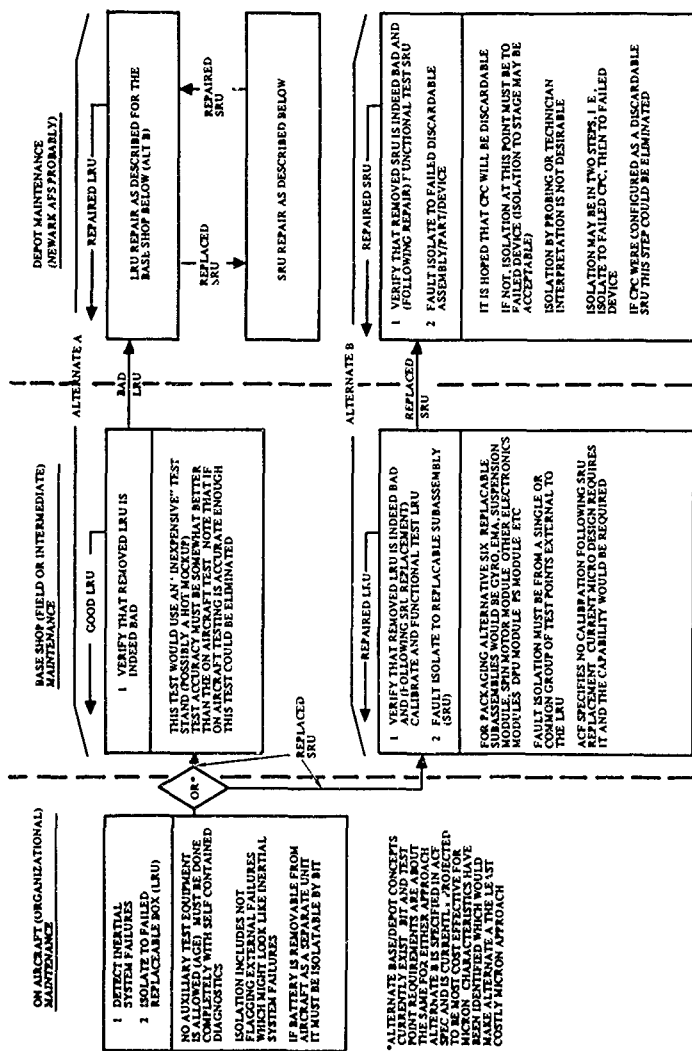


Figure 6-36. MICRON Test and Fault Isolate Requirements

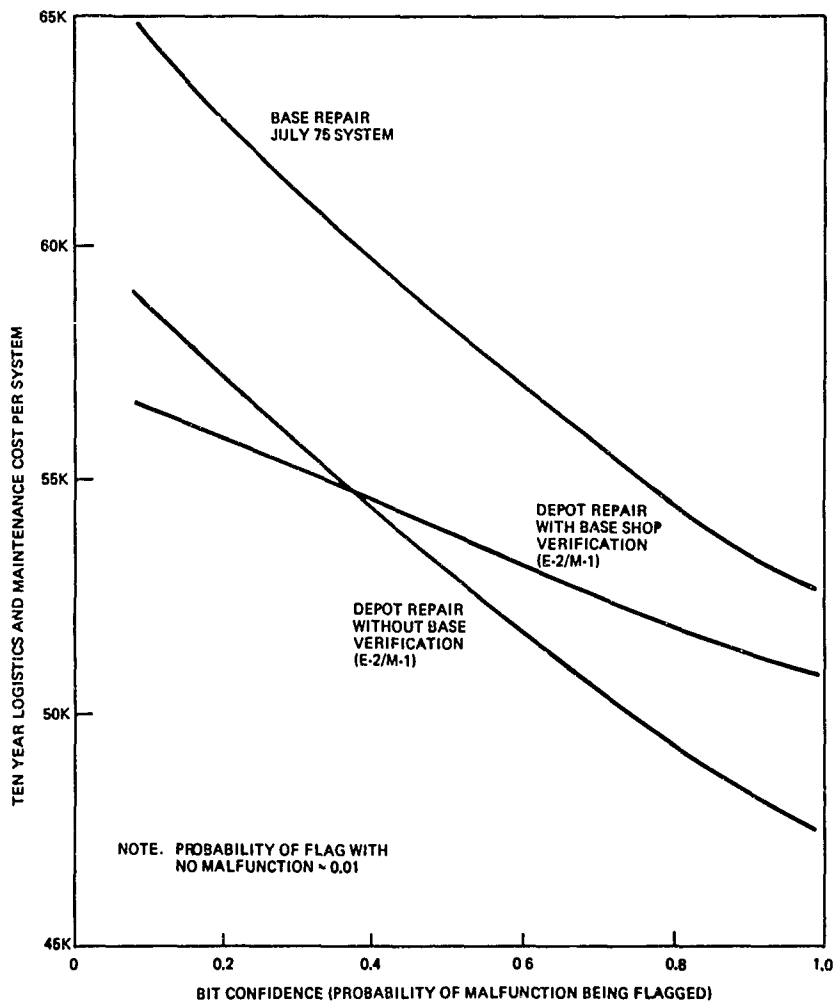


Figure 6-37. Unit Support Cost vs BIT Confidence

Table 6-27. Classes of Removal Causes

Removal Cause	Removal Rate	Remarks
a. IMU has failed and is flagged by BITE	$2.8 \lambda \times P_{BC}$	Malfunction rate times the BITE Confidence.
b. IMU has failed, not flagged by BITE, but replaced anyhow.	$2.8 \lambda \times (1 - P_{BC})$	All other malfunctions.
c. IMU is good but flagged as bad by BITE.	$\frac{P_{BFI} \times P_{BC} \times 2.8 \lambda}{1 - P_{BFI}}$	Ratio of the probability of a flag when good to all flags.
d. IMU is good, not flagged by BITE, but thought bad and replaced.	$1.4 \lambda \times (1 - P_{BC})$	Assumed at a rate of one-half the failed but not flagged rate.
e. IMU was bad when it was installed. (Not previously repaired or "failed in storage".	$\lambda \times (.066 - .056 P_{BC})$	Calculated from test equipment capabilities. Also assumes a storage failure rate of .01.

#### TERMS AND DEFINITIONS

- $\lambda$  = Malfunctions predicted by the reliability failure rate.
- $2.8 \lambda$  = All malfunctions including those predicted by the failure rate plus malfunctions due to storage, improper handling, etc.
- $P_{BC}$  = BITE Confidence = Probability that when a malfunction occurs it will be flagged by BITE.
- $P_{BFI}$  = BITE false indication probability = probability that when a BITE flag exists the system will be good. ( $P_{BFI}$  was held constant at 0.1 for all studies to date)

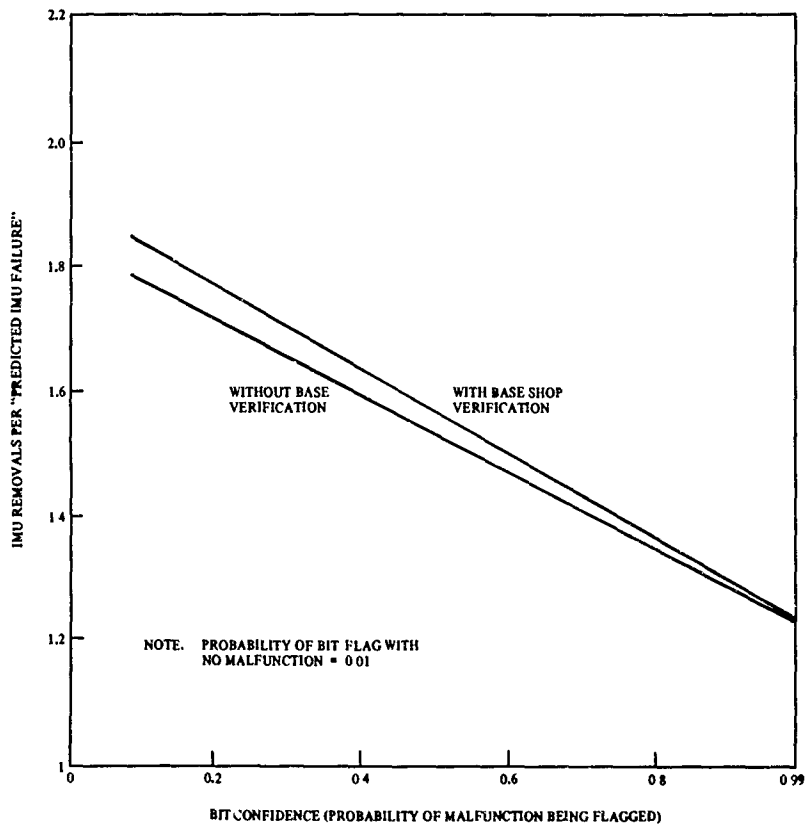


Figure 6-38. IMU Removals vs BIT Confidence E-2/M-1 System

Decreased BIT confidence increases the removal rate not only because of improper actions when a malfunction occurs, but also because of increased removals when the unit is good. High confidence in BIT will tend to preclude removals because of one bad navigation run, etc. It is also interesting to note that removals are increased slightly with base verification. This is due to the lower capability of the verification test set to detect all failures. It was assumed to have a 5 percent probability of passing a bad unit not flagged by BIT whereas the depot station will only pass 2 percent of bad units not flagged. Thus, with verification we have more bad units returning to the vehicle. Increased removals just to check the unit because verification is readily accessible were not considered.

The degree of accuracy in isolating IMU faults to the proper module is also a function of the BIT circuitry. While good fault isolation using a functional test station is not necessarily dependent upon BIT it does follow that the more complete the BIT the more accurate the fault isolation. This consideration was included in the BIT study by assuming faults flagged by BIT were better isolated than those not. The actual isolation percentages used are shown in Table 6-28. A similar analysis for hybrid circuits yielded average CPC removal rates of 1.19 per bad module and 0.02 per good module tested.

Table 6-28. Module Fault Isolation vs BITE Confidence

IMU Condition When Placed on Repair Station	Percent of Fixes Vs Number of Modules Replaced			
	0 Modules	1 Module	2 Modules	3 Modules
Bad IMU and flagged by BITE		80%	20%	
Bad IMU but not flagged by BITE	1%	61%	20%	18%
Good IMU but fixed anyhow			100%	

NOTE: Subsequent module RTOK rate was assumed to be 25% of the excess modules replaced.

#### 6.2.5.5 IMU Repairability

The design activities of Phase 2A have developed a packaging approach generally accepted for the engineering model of Phase 2B. Because of the many critical requirements imposed on the instrument assembly, this packaging approach is somewhat more complex than earlier mockups. Several alternatives have been and are being evaluated from a maintainability/life cycle cost view point. These alternatives include such things as:

- a. Division of the suspension module into two identical assemblies
- b. A combined gyro/suspension assembly consisting of one gyro and a half suspension module defined in a.
- c. Single charge amps rather than dual packages now used.

Preliminary studies show that item (b) does not yield significant savings. (a) and (c) combined however have a potential of \$1,200,000 program savings. If additional improvements could be made making the instrument area as easily repairable as module replacement, an additional \$400,000 could be saved. In both cases the above dollars do not include the cost of incorporating the changes presented. Studies must be conducted to determine if implementation costs are less than the potential savings.

#### 6.2.6 Cost-of-Ownership Model

The goal of this task is to develop a Cost-of-Ownership prediction model applicable to Phase 2 and then use that model in evaluating various design/support alternatives. The MICRON cost model developed in Phase 1 provided the basis for the Phase 2 model.

The first effort under this task was a complete review of the Phase 1 model in light of the detail, trade-offs, and information applicable to Phase 2A. Changes were then identified which made the model sensitive to the trade-offs expected and more complete in its considerations.

The selected model improvements are outlined in Table 6-29. The first category of improvements relate to the prediction of prime hardware costs. In the previous model unit prices were computed external to the model. The improved model accepts base labor and material factors for each subitem as input and computes the unit price. Variable base dollar years and manufacturing locations (i.e., different labor rates, etc.) can be selected. Inputs also allow for the consideration of reliability/recycle rates on production cost. In correlation with the variable base dollar year used to predict hardware price, variable year customer cost rates are also available. Cost factors as published in AFSCM/AFLCM 200-4 may also be used. While these factors are generally accepted as out of date they are official values for use if desired.

Estimating algorithms for six of the output cost categories have been improved. Generally the changes in these algorithms are directed to the input considerations applicable to Phase 2A.

Retest OK and split repair levels are now easily considered by the model. Estimates of RTOK and NRTS are accepted as input variables.

The final model improvements are those in the output report formatting. New reports have been added to correspond with the above changes. Most output reports of the previous model remain with minor changes as applicable.

The model was initially programmed on the IBM 1130. Later in the phase it was reprogrammed to operate on both the MICRON Lab HP 2100 computer system and Rockwell's central IBM 370 data processing system. This change was required because of the release of the IBM 1130 computers formerly used in the MICRON Lab.

The required model changes to effect this change were (a) report reformatting for 80 character maximum line lengths, (b) elimination of data switches for report selection, sensitivity studies, etc., and (c) the incorporation of Hewlett-Packard peculiar coding techniques. Steps (a) and (b) were accomplished using the IBM 370

Table 6-29. Selected 2A Model Improvements

1. Increased Producibility Sensitivity

Unit Fab Labor, Test Labor, Base Material Inputs

Selectable yearly labor and material cost factors (1973 through 1977)

Varying Manufacturing location rates

Potential for varying rework considerations

(Unit Price Input Override)

2. Selectable Base Year Customer Cost Factors (1973 through 1977)

Repair Labor Rate

Training Cost

Manpower Attrition Rates

Transportation Rates

Inventory Management Cost

Tech Pubs Page Cost

Facilities Cost

(AFSCM/AFLCM 800-4 Override)

3. More Complete Cost Estimating Algorithms

Repairable/Serviceable Item Transportation - New Cost Category

Training - Now only includes corrective maintenance manpower

- Considers only equivalent heads

Facilities - Now only includes Depot facilities

- Estimated based on complexity factory - relate to test equipment

Test Equipment Maintenance - Consider T. E. Failure Rates rather than percentage

Spares Inventory Mgt - Need to add Field Administration cost

Initial Test Equipment - Easier more accurate method

4. Testability/Partial Repairability Sensitivity

RTOK Consideration (Retest OK)

NRTS Rate Consideration (Not Repairable this Station)

5. Related Report Format Improvements

batch processing system. This enabled the major changes to be made on a completely defined system (rather than the more fluid laboratory systems) plus it now gives two machines which can be used as conditions warrant.

Subsequent to transferring the model to the HP 2100 system, that version was also resegmented allowing greater detail in the input hardware definition. The model will now accept a hardware breakdown of up to 120 line items.

Appendix I to this report provides a general description of the model including a sample of each report type which may be generated by the prediction model. The actual reports produced for a given run are selectable by the input data.

A subtask of this effort is the continuing awareness of prediction model activities in the inertial community, particularly maintaining compatibility with other models which might be used to evaluate MICRON. In this regard, participation in the joint data exchange for inertial systems Life Cycle Cost task group has continued throughout this phase. Autonetics representative is currently serving on the executive board of this group.

#### 6.2.7 Parts Program

##### 6.2.7.1 Parts Commonality

The parts selection and commonality studies during the Phase 2A contract have been directed toward part type reduction of piece parts. A strong "push" has been made toward alternates to costly parts; changes in technology (i.e., beam lead vs fly wire vs packaged, bipolar vs MOS), and changes in procurement techniques. The tradeoffs have been considered by design groups, operations, reliability and program/project management. As an example of possible changes in procurement technique it may be possible to omit Group B and C testing from fly wire die specifications. These tests are related to device packages and omission would result in a savings of approximately 10 percent per part. Rationale exists for deleting these tests when cost and reliability are traded. Implementation of the results of these studies will be made when the specification development and release takes place during Phase 2B.

Component engineering supported the efforts to obtain 800 volt NPN and PNP transistors for use in MICRON. PNP transistors received from Fairchild semiconductor perform satisfactorily. Three shipments of NPN transistors and two trips to Fairchild were required to obtain an initial quantity of satisfactory devices. Fairchild attributes the problems to sensitive process techniques now under control and expects to complete the order early in Phase 2B.

##### 6.2.7.2 Parts Specifications

Preliminary beam lead device specification outlines patterned after MIL-M-38510 Class B were negotiated with potential suppliers and tentative agreement reached related to die screening capability. While the concepts and necessity of testing were generally acceptable to the suppliers, commitment cannot be accomplished until a beam lead carrier is available for supplier evaluation tests.



As part of the Phase 2A contract, 25 device specifications were prepared at the start of the phase. These specifications cover 10 integrated circuits, 3 transistors, 4 diodes, 2 capacitors and 6 resistors. Many of the devices covered by these documents are no longer required because of the increased use of the MOS, LSI, and other circuit changes. Effort to develop specifications for additional devices has slowed until the numerous technology studies and configuration trade-offs are completed.

A firm specification format and standardization of specification common pages and paragraphs was finalized and put into work. This effort will benefit the program more effectively as identification of final devices becomes known.

#### 6.2.8 Beam Lead Development

##### 6.2.8.1 Beam Lead Devices

The use of fully screened and tested beam lead devices will increase system reliability and reduce assembly costs. To increase the availability of beam lead devices several requests for quotation were sent to potential suppliers for development of high usage parts in beam lead form. The part types considered were:

High Performance Operational Amplifier  
(similar to Harris HA2620)

CMOS Quad Analog Switch with Driver  
(similar to Harris HI1500 or RCA CD4053)

Synchronous 4 Bit Digital Counter  
(similar to TI SN54LS193)

Custom High Stability Resistor Networks

A contract was placed with RCA for the High Performance Operational Amplifier on 28 June 1974. The first parts were produced and found unsatisfactory. A redesign and process changes were accomplished and the next parts are expected early in Phase 2B. Preliminary results appear favorable but latest production part cost estimates are higher than desired.

Contracts were not placed for any other devices. The resistor networks are still in a state of flux due to circuit trade-off studies. The synchronous counter is no longer used since the counting function has been incorporated in new MOS, LSI circuits. The CMOS quad analog switch development effort was stopped due to the high risk and high costs associated with the new technology development for beam leads on MOS devices.

##### 6.2.8.2 Beam Lead Carrier

6.2.8.2.1 Autonetics Development Program. A modified 16 lead "Barnes" type carrier to accommodate either a 4, 10, 14, or 16 beam chip was under development during Phase 2A. The carrier will consist of a Kapton flexible circuit cemented to the Barnes base and a spring retained glass lid. The carrier will allow full Class B integrated circuit or TXV level semiconductor screening and testing of beam lead die.

Ten prototype (hand-made) carriers were made at Autonetics and beam lead chips with 16 beams (Texas Instruments BL54LS00Y) were purchased. Electrical testing was performed with the prototypes using standard automatic test and handling equipment.

Based on the initial test data a specification was prepared and 100 carriers purchased from ITT, Cannon Electric Division. Testing of the Cannon carriers indicated problems with the design and specification.

Test equipment to carrier interface mating problems occurred with the 25 mil wide contact areas on the carriers. New Kapton with 40 mil wide contact areas was purchased and installed on the carrier bases. Testing showed the wide gold has significantly improved the measuring equipment contact problem. However, another problem surfaced which was associated with relative movement of the Kapton/beam lead device/glass (which "holds" the device) during semiautomatic equipment handling and testing. There was apparently a strong affinity of the device for the glass which sometimes moved the beams from contact with the Kapton gold.

Based on test results new drawings were prepared for two improved slightly different carrier designs. One includes a resilient pad beneath the Kapton-with-gold circuitry. The other uses a selectively conductive resilient pad on top of the circuitry. The first design was submitted to industry for quotations and/or comment. It is expected that replies will be forthcoming soon enough to allow placing orders early in Phase 2B. The selectively conductive design will be the subject of further study.

6.2.8.2.2 Outside Supplier Development Programs. Lockheed's Missile Systems Division initiated a carrier program in September 1973 for the Trident program. Lockheed pursued an in-house program and also funded three beam lead chip suppliers (RCA, Motorola and Raytheon) to develop a carrier. Autonetics was in contact with Lockheed and its suppliers and is aware of their current progress.

Autonetics representatives attended a conference on beam lead device carriers at Bendix, Kansas City Division, Kansas City, Mo., on 12 June 1974. The other attendees were representatives from Lockheed Missiles and Space Company, Hughes Aircraft Company, Raytheon, Sandia Laboratories, RCA, Texas Instruments, Harris Semiconductor, Motorola, ITT Cannon and Bendix.

A second conference was attended at Lockheed, Sunnyvale, Ca., on 25 April 1975. Representatives from Texas Instruments, Raytheon, Motorola, RCA, JPL, Bendix and Sandia Labs also attended.

Conclusions from the meetings indicated that Lockheed had not finalized a design and was still funding three separate developments at Motorola, RCA and Texas Instruments. Testing performed by Lockheed and its subcontractors had been hand testing on the bench. Autonetics had done more testing with actual automated handling and testing equipment.

Several attempts were made to obtain carriers developed for Lockheed for evaluation at Autonetics. All available carriers were being used by Lockheed for evaluation. Motorola, however, accepted a purchase order for 50 carriers to the design developed for Lockheed. The Motorola carriers are due for delivery early in Phase 2B. Evaluations and comparison with Autonetics designs will begin at that time.

## 6.2.9 MOS Device Development

### 6.2.9.1 IMU/DPU MOS Electronics

During March, 1975, development of a number of MOS devices was initiated which are expected to reduce systems cost. Primary emphasis during March and April 1975 was placed on defining total system requirements in terms of interface signals and the timing of these signals. This effort consisted of development of detailed block diagrams, detailed timing, apportionment to MOS devices and preliminary sizing of each MOS device type.

The implementation and logic design was initiated using the mechanization arrived at in December 1974 as a result of design tradeoffs completed at that time. In evaluating the detailed timing requirements, it was determined that some changes in the mechanization could reduce the number of MOS devices required without increasing the development costs. In particular, the December 1974 mechanization required 23 MOS devices of seven types. These included three new designs and two ROM's. In addition, 36 bipolar devices were required. This mechanization used 8.5 watts of power. In contrast, the same three new designs, are required for the new mechanization, but only eight total devices of four types are used. This has been accomplished due to several factors. The most significant one is that the frequency reference generator logic was able to be incorporated on one of the new control devices. Also, the number of discrete outputs required to be under CPU control was reduced from 32 to 16. Also, the above changes reduced the function of the remaining BAP and MXF devices to that of buffers and latches. They were, therefore, replaced with tri-state bipolar devices which offered cost advantages. This mechanization should only require 6 watts.

It was determined that one of the new control devices would be exceptionally large, approximately 250 mils x 250 mils. A recommendation was made, and is being implemented, to divide this device into two smaller devices. This resulted in development of four new MOS devices. However, the only additional nonrecurring costs incurred is the development of a mask set and a fabrication run.

The eight MOS devices utilized in the input/output are identified in Table 6-30:

Table 6-30. MOS Devices Utilized in the Input/Output

Designation		Qty
1. Program Counter Timer	(PCT)	3
2. Timing and Reference Generator	(TRGC)	1
3. Counter and Sequencer	(CASC)	1
4. Quasi Reference Generator	(QRFG)	2
5. Direct Memory Access Control	(DMAC)	1
Total		8

Device number 1, PCT, has been developed and applied in the prototype MICRON dedicated processor unit. Device numbers 2 through 5 are the new MOS devices currently being designed. A brief description of each device and development status is provided subsequently.

a. TRGC Device Functional Description. The logic in this device consists primarily of frequency dividing counters used to generate fixed frequencies and timing signals. The 1 MHz clock frequency is divided down to provide outputs of 33-1/3 kHz (square wave), 40K PPS and a 320 Hz signal. The dividing continues to 32 Hz. A strap input is used to select whether the 32 Hz or 64 Hz will be used for the fast cycle interrupt. Three other signals are generated with fixed delays from the selected fast cycle interrupt. These signals are used to control the sampling of the MUM demod signals. Finally, a small block of logic is included which is used to condition the asynchronous EMA signals to asynchronous increment commands for the EMA counters. Figure 6-39 is a block diagram of this device. A functional description of each of the interface signals follows.

<u>Signal</u>	<u>Signal Description</u>
SIO	Controls resetting the sample and hold circuits. Occurs 400 $\mu$ sec before the end of "ST" and has a pulse width of 400 $\mu$ sec.
STDLYD	Marks the start of the MUM demod sample window. This signal occurs 500 $\mu$ sec after "ST."
X	Count signal from the EMA's. These are 40K PPS signals
Y	which are modulated by the acceleration. Pulse width
Z	is 1 $\mu$ sec with a 25 $\mu$ sec period. Count once for each pulse.
BITE/EMA	A discrete input signal which selects between counting EMA pulses or counting the 40K PPS pulses.
XINC	Issued to PYC input of the PCT's (EMA counters) to
YINC	cause an increment.
ZINC	
A	This is a strap input used to select a 64/sec or 32/sec fast cycle.
320 Hz	Frequency output used for generating a triangular waveform. Period is 3125 $\mu$ sec. Low for 1.875 ms and high for 1.250 msec.
33-1/3 kHz	Symmetrical square wave output.
64 Hz	Fast cycle interrupt may be programmed to be either 64/sec or 32/sec by strapping input "A."
ST	Controls the multiplexers for the MUM demod sample and hold circuits. "ST" occurs 1.5 msec after the fast cycle interrupt and is a 2 msec pulse.

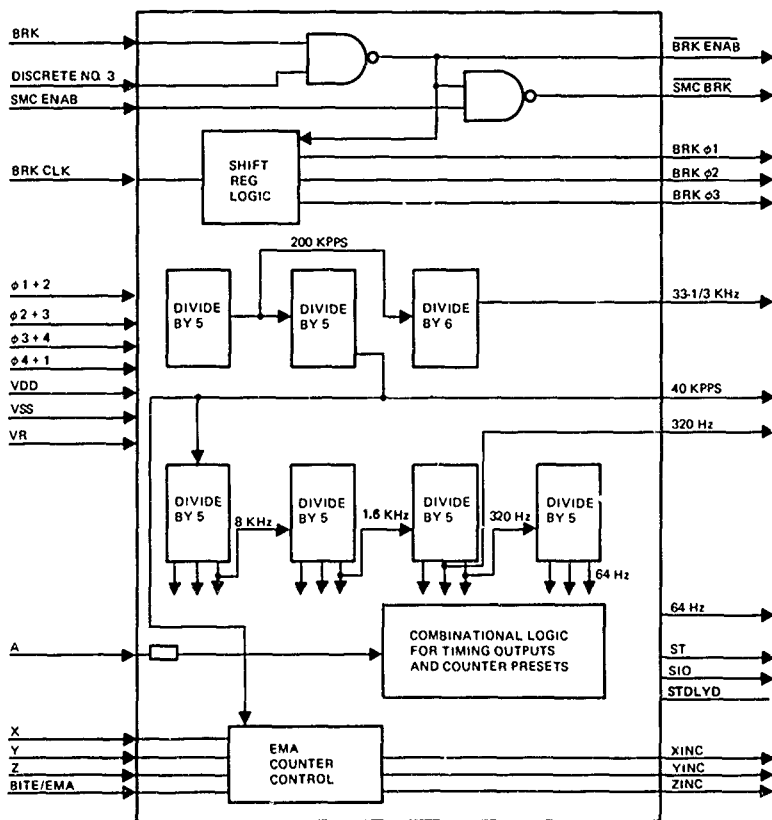


Figure 6-39. Block Diagram of TRGC Device

40K PPS	Frequency output to the EMA's.
BRK BRKCLK DISCRETE NO. 3	Inputs to the spin motor brake logic from the CASC device.
SMC ENAB	Discrete input to the SMC brake logic
<u>BRK ENAB</u> SMC BRK	Outputs to the spin motor brake circuits
BRKØ1 BRKØ2 BRKØ3	

b. CASC Functional Description. The CASC device mechanizes the functions of the automatic sequencer and the frequency reference and suspension timing logic. The 1 MHz clock is counted down to provide frequencies of 100 kHz, 20 KPPS and 10 kHz. Two additional 10 kHz signals designated QUASI A and QUASI B are also generated. These frequencies have set phase relationships. A 50 kHz signal is also generated but is gated with discrete logic. The counting chain continues from 10 kHz to 208 sec, if enabled by the CLK INHIBIT signal. The timing chain from 25.6 msec to 208 sec is reset with the occurrence of any of three shutdown discretes. The remaining outputs of this device are used for sequencing the suspension/desuspension and are generated as combinations of the input control discretes and the timing counter outputs. Figure 6-40 is a block diagram of the CASC device. A functional description of the interface signals follows.

<u>Signal</u>	<u>Signal Description</u>
<u>CLOCK INHIBIT</u>	Inhibits the automatic sequencer timing counter.
INITC	Initializes the counters and sets the outputs to the proper state.
CCSHTDWN	Shutdown discrete from the control computer.
<u>PCSHTDWN</u>	Shutdown discrete from the power control.
<u>MALFSHTDWN</u>	Shutdown Discrete from BITE logic.
SUSPEND	Discrete input command which is part of turn on sequence.
SHORT T/OFF	Discrete input which commands the short turn off sequence.
LONG	Discrete input which commands the long turn off sequence.
RECYCLE	Discrete input which commands cycle down and back up.
CL/LO(B)	Lift off signal output.
100 kHz	Square wave timing output.

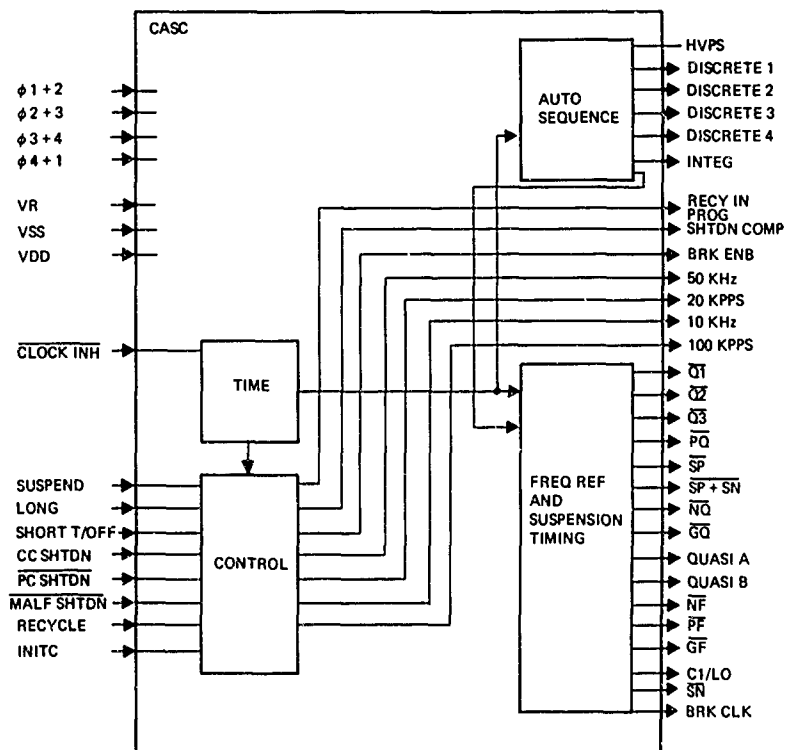


Figure 6-40. CASC Block Diagram

50 kHz	Square wave output controlled by $\overline{SP}$ .
20 KPPS	Timing output with 20 percent duty cycle
10 kHz	Square wave timing output
QUASI A QUASI B	10 kHz signals used to generate sine wave lift off signals
$\Delta VPS$ DISCRETE 1 DISCRETE 2 DISCRETE 3 DISCRETE 4 INTEG	Discrete outputs used to sequence the suspension during power up/down and recycle modes.
SHTDWN COMP RECY IN PROG	Signals used to show status of the sequencing operations.
BRK ENB	Signal to TRGC device which indicates the start of the long shutdown sequence. Used for SMC braking.
BRK CLK	Signal used to reset and clock the 3 $\phi$ SMC brake logic.
$\overline{SN}$ $\overline{SP}$ $\overline{SN + SP}$ $\overline{Q1}$ $\overline{Q2}$ $\overline{Q3}$ $\overline{PQ}$ $\overline{NQ}$ $\overline{GQ}$ $\overline{NF}$ $\overline{PF}$ $\overline{GF}$	These signals are used in the gap and charge monitor logic and charge amp logic.

c. QFRG Device Functional Description. The quasi reference frequency generator for one ESG is mechanized on this device. Two devices per system are used. This logic consists of a 12-bit register and a 12-bit rate multiplier. The output from this section is a pulse train whose period is not generally symmetrical, but is a frequency whose average rate is equal to  $f_c X$  where  $f_c$  is the clock frequency (1 MHz) and  $0 \leq X < 1$ . In particular,  $X = \frac{N}{4096}$  where N is a 12-bit binary number  $0 \leq N \leq 4095$ . This pulse train is an input to a divide-by-16 counter whose output drives a modulo 24 counter. The outputs of the modulo 24 counter, together with  $\overline{SP}$ ,  $\overline{SN}$ , CM Discrete, and HEAT are used to generate sine, cosine waveforms. One device is used for each ESG frequency, and the SELECT GYRO 1/2 input selects which device will drive the spin motor control signals. A block diagram of this device is provided in Figure 6-41. A functional description of the interface signals follows.



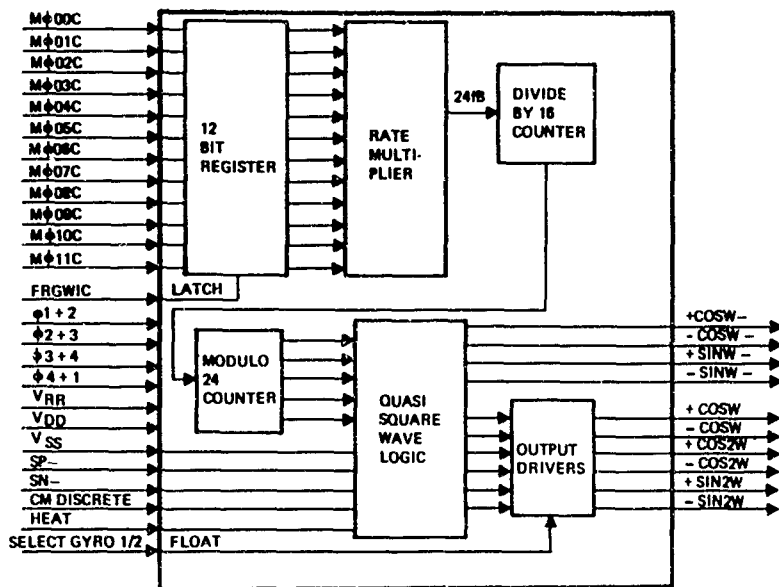


Figure 6-41. Block Diagram of QRFG Device

<u>Signal</u>	<u>Signal Description</u>
SELECT GYRO 1/2	This signal causes the spin motor control outputs to float.
HEAT	Causes a square wave on +COS2W and -COS2W.
CM DISCRETE SP SN	These signals cause switching of the SINW1, COSW1, ESG signals.
MO(00-11)C	Memory output data bus.
FRGWIC	Commands the frequency generator holding register to copy the data on the memory bus. This signal is coincident with the data.
+COSW -COSW +COS2W -COS2W -SIN2W -SN2W	Outputs to spin motor control chip.
+COSW1 -COSW1 +SINW1 -SINW1	These signals are the quasi sine, cosine waveforms for the ESG's.

d. DMAC Functional Description. The DMAC device is designed as a sequencer and controller for data transfers between the System Electronics Unit (SEU) and the Dedicated Processor's Memory. The data words are transferred in a set sequence to or from dedicated memory locations.

This sequence, which is controlled by the DMAC, is initiated by the fast cycle interrupt input. The DMAC then proceeds to store a set number of words into memory and output a set number of words from memory. The DMAC provides the memory address, read/write and cycle commands to control the memory only after issuing a memory cycle-steal request and receiving an acknowledge. To select one source or destination from among the many, the DMAC provides appropriate enables, strobes and a six bit user's address. Figure 6-42 contains a block diagram of the DMAC device. This device as reflected by the block diagram is "logically" more complex than the other three devices described. A functional description of each DMAC input/output signal follows.



<u>Signal</u>	<u>Signal Description</u>
ENXC ENYC ENZC	These signals enable one of the three EMA counters to drive the node which gets latched in the read-out register.
FLTMXC	Gates the EMA register onto the internal data-to-memory bus.
SEUDMC	Memory cycle steal request.
SEUMRC	Used to start a memory cycle (either a READ or WRITE).
SEURDC	READ/ $\overline{\text{WRITE}}$ command to memory.
TFLTC	This signal enables the test word register onto the internal data-to-memory bus.
BGN (SC)	Starts a conversion in the A/D device. The MUX enables and address lines must be set up $1 \mu\text{sec}_{\text{min}}$ before this signal is issued.
MUMUX1 MUMUX2 MUMUX3 MUMUX4 MUMUX5 MUMUX6	These signals are the disable signals to the six 8:1 multiplexers on the input to the A/D converter.
A0 A1 A2 A3 A4 A5	<p>These six address lines are used for three purposes:</p> <ol style="list-style-type: none"> <li>(1) They provide address to the MUX's which enable data to the A/D converter.</li> <li>(2) They provide a coded destination address going to two Spin Motor Control (SMC) devices.</li> <li>(3) They provide coded destination address for the synchro D/A devices.</li> </ol> <p>For data to the SMC's, the address must be set up at least <math>1.0 \mu\text{sec}</math> before the strobe. For MUX addressing (data to the A/D), the address must be set up <math>1.0 \mu\text{sec}</math> before issuing BGIN and must be held until REDO is received.</p>
FLTADL	This signal enables the A/D converter output drivers onto the internal data-to-memory bus.
SMC DMC	These signals are the strobes to the two Spin Motor Control chips. They command the addressed register to copy the data from the input bus.

SYNCLA	This signal causes a data word to be copied from the memory bus into a buffer register. The data are subsequently copied into 1 of 11 synchro D/A devices.
SYNCEN	This signal causes the data to be copied from the synchro buffer register into the addressed D/A device.
TWØC	Loads the test word latch from the memory output bus.
STDLYD	Defines the start of the 2 msec window during which the MUM data must be stored.
FAST/SLOW	This input is used to specify whether a 1 µsec or 2 µsec read cycle is being used.
INITC	Initializes the device. Will reset and float memory address, reset mode control, reset user address and set all outputs to non-active state.
64 Hz (Fast Cycle Interrupt)	This input starts the entire input/output sequence.
CCLCRC	This signal is used to clear the EMA counters (by loading zero) after they have been read.
DR (Data Ready)	Indicates the A/D conversion is complete. The data may be read from the output register and the next conversion started.
SEUAKC	Indicates the next memory cycle may be used by the DMAC. This signal is in response to a cycle steal request, "SEUDMC." This acknowledge will be issued as long as the DMAC continues to request memory and no higher priority requests preempt. In the absence of SEUAKC, the DMAC must relinquish the memory for the next cycle.
NMA(09-15)C	Internal memory address bus. These seven lines provide the dedicated memory addresses for reading/writing the SEU data in memory.
FRGW1C FRGW2C	These signals command the respective QRFG devices to copy the 12-bit data word from the memory bus.
ENDMUC	Issues interrupt request to CPU after storing 12 words of MUM data.
CMPLTC	Issues interrupt request to CPU after the entire fast cycle sequence has been completed.

Development status of the above devices is as follows. The apportionment and preliminary logic design of all four device types have been completed. Simulation of the logic of the QRFG, TRGC, and the DMAC has been completed. Layout design of the QRFG and the TRGC has been completed. Development of these devices will continue in Phase 28.

#### 6.2.9.2 MOS A/D Converter

Cost tradeoff studies showed that a cost savings could be realized (about \$148 per converter) by improving the design of the MOS A/D Converter. The N57A A/D converter utilized the 65003 MOS chip. The improved design will eliminate the requirement for an additional four-phase clock to drive the converter and the tri-state latches which interface with the computer data bus. The new design incorporates the additional capability for the Digital/Synchro Converter and linear Digital/Analog Converter applications. The part number for this new device is 65008. It is estimated that devices will be ready for delivery by mid-September, 1975.

A simplified functional block diagram of the 65008 chip is shown in Figure 6-43. The 65008 is the same as the 65003 with the following exceptions:

1. Inputs and outputs are now TTL compatible.
2. The phase clock generator is on the chip. Only a single phase sync clock is needed for clock input.
3. Output drivers are now tri state.
4. Multiplex switches were deleted.

#### 6.2.9.3 MOS Spin Motor Control Circuit

The MOS Spin Motor Circuit part number is 65010. It was designed primarily to reduce the cost and complexity of the spin motor electronics. Cost savings realized with this circuit were estimated to be about \$275. This circuit generates all the spin motor control signals required for heating, spinup and damping of the gyro rotor. The circuit can also be used as a 12-channel temperature controller. Three lots of devices have been fabricated. Probe testing indicated a defect on the first lot processing technique. A design defect has also been discovered which produces a large transient overshoot on the modulated output signals. Design changes are being made to correct for this problem. Good devices are expected in September 1975.

The MOS Spin Motor Control circuit will interface directly with the computer output data buss. A block diagram of this circuit is shown in Figure 6-44.

The chip contains 12 separate digital to analog converters (DAC) and one 6 bit holding register with a common 6 bit input word. A 4 bit address line with a strobe selects one of 12 DACs or the register. The 12 DACs generate 4 separate functions of 3 DAC's each. One set generates straight analog outputs and the other 3 sets generate outputs that are modulated by a 2 bit signal line.

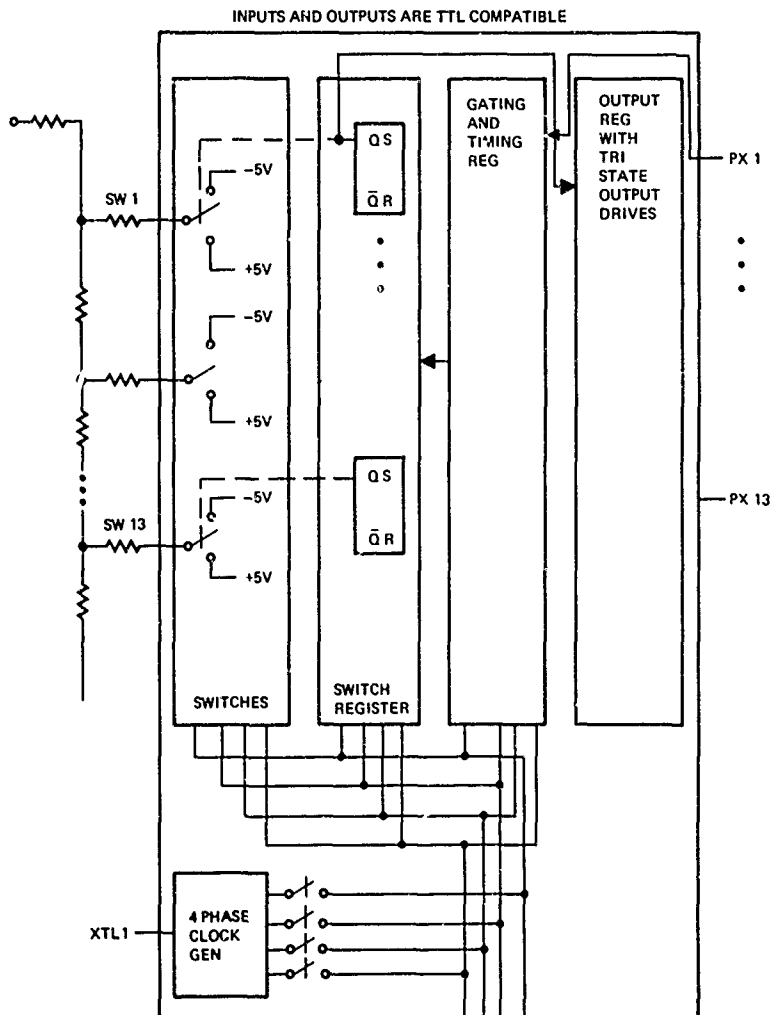


Figure 6-43. Functional Block Diagram of 65008 Chip

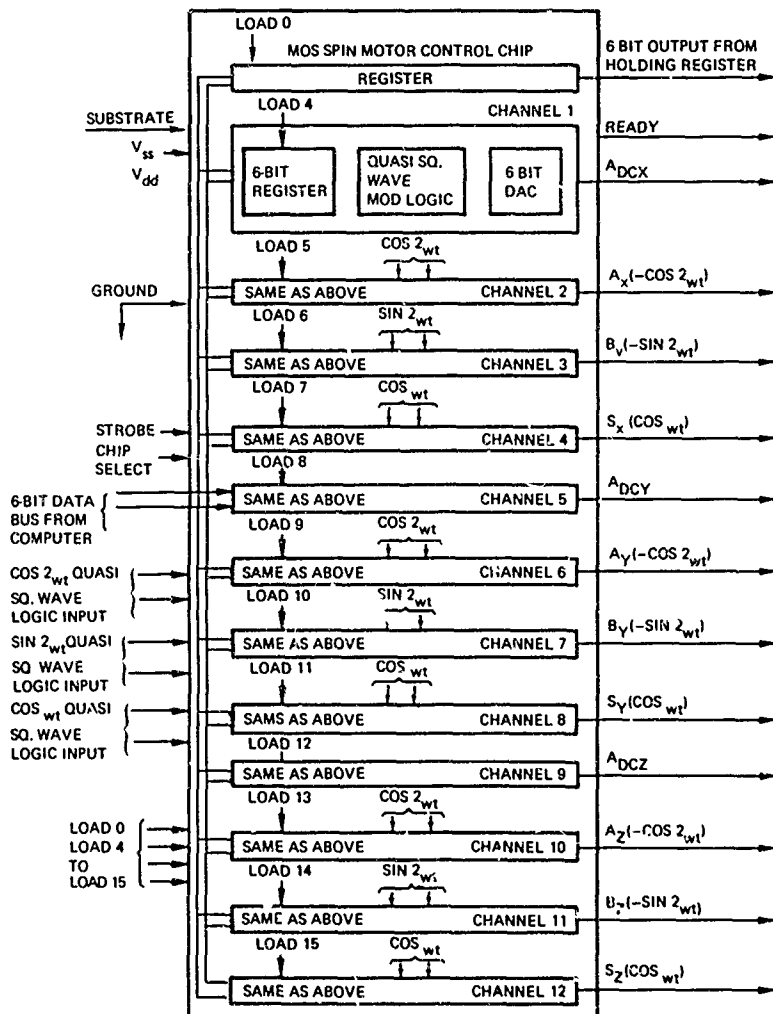


Figure 6-44. Functional Block Diagram of Spin Control MOS Chip



The MOS Spin Motor Control circuit implements the following equations:

1.  $V_1 = A_{DCX} + A_X (-\cos 2 \text{ wt}) + B_X (-\sin 2 \text{ wt}) + S_X (\cos \text{ wt})$
2.  $V_2 = A_{DCY} + A_Y (-\cos 2 \text{ wt}) + B_Y (-\sin 2 \text{ wt}) + S_Y (\cos \text{ wt})$
3.  $V_3 = A_{DCZ} + A_Z (-\cos 2 \text{ wt}) + B_Z (-\sin 2 \text{ wt}) + S_Z (\cos \text{ wt})$

Each term in the equation is an output from one of the 12 DACs. The  $\cos 2 \text{ wt}$ ,  $\sin 2 \text{ wt}$  and  $\cos \text{ wt}$  terms are the 2 line modulation signals. The summing is done externally by connecting 4 outputs together into an operational amplifier sum amp.

### 6.3 SYSTEM ENGINEERING

In Task 5.3, System Engineering, Autonetics developed the 8-Plate MESGA Multisensor, investigated means to eliminate the vacuum pump from the MESGA, developed the 4-Plate gyro, performed mechanization and modeling improvements, investigated MESG/MESGA design improvements, initiated an investigation of MICRON design alternatives, and performed design tradeoffs on the DPU. Autonetics also investigated methods to simplify the gyro electronics and mechanical design and performed electronics design alternatives.

#### 6.3.1 Develop 8-Plate MESGA

##### 6.3.1.1 Develop 8-Plate MESGA Instrument

The intent of this task was to develop an instrument which would serve as a combined gyro and accelerometer. The effort was to consist of two distinct areas:

1. Develop a ceramic header for the metal vacuum housing which would minimize stray capacitance between electrode pins and between electrode pins and ground.
2. Test and evaluate instrument performance and redesign and refabricate as required.

The above two efforts were to be accomplished and be compatible and complementary with fast reaction development.

The task to develop a ceramic header was attempted in 1972 but an apparently qualified vendor failed to produce a satisfactory part. Several new ideas and methods were developed and efforts were again made to fabricate parts. Component parts were designed and fabricated in the April, May, June 1974 time frame and delivered to a qualified vendor. The parts were returned to Autonetics in early October 1974 but were not satisfactory. The ceramic had cracked. In an effort to produce a part which would support MESGA test and evaluation it was decided to fabricate parts using a glass header. While this was recognized as unsuitable for the ultimate instrument, it would serve the purpose for MESGA evaluation. Parts were delivered to the vendor in October 1974 and were returned to Autonetics in mid-December. The glass units had also failed. Parts were again designed and fabricated and shipped to the vendor in January 1975 and were returned to Autonetics in late March 1975. The failure of the final parts when returned to Autonetics at the end of March 1975 concluded the

effort with the vendor. In parallel with this particular effort, some work has been performed using a technique provided by Northrop Corporation and is reported in Para 6.3.6, Design Alternatives Task.

A satisfactory ceramic header was not developed and the effort was discontinued when MESGA development and test was discontinued (see Para. 6.3.5.5). Standard Phase 2A MESG units (beryllium base) were used in support of the test and evaluation of the MESGA subassembly.

#### 6.3.1.2 Develop 8-Plate MESGA Electronics

The development of the 8-Plate MESGA electronics followed tradeoff studies and analyses of the sensitivity to error sources for different types of suspension systems. Studies showed that a low-preload suspension system would give the best chance of meeting the performance specifications because of the lower sensitivity to stray capacitance and preload charge variations. It was determined that the best system for implementing low preload with the capability of digitizing the data with the required accuracy was the pulswidth modulation (PWM) suspension. The N57A system utilizes pulse-amplitude modulation (PAM) suspension. PAM suspension is inherently a high preload mechanism. A decision was therefore made to develop PWM electronics for MESGA. The low-preload PWM electronics were very complex compared to PAM. The complexity makes the PWM electronics considerably more costly than PAM electronics. Figure 6-45 shows a block diagram of the mechanization used for the pulswidth modulation suspension electronics.

##### 6.3.1.2.1 Electronics Sensitivity Tests and Design Improvement

The electronics designs which were being utilized in existing suspension systems were reviewed with respect to the error budgets developed for the MESGA application. It was found necessary to improve the performance of the Sample and Hold, Gap Monitor, and Charge Amplifier by making design improvements in these electronics. In addition, a totally new set of suspension electronics had to be developed since low preload PWM had not previously been developed.

A discussion of the electronics which have the greatest effect on MESGA acceleration errors and the performance requirements of these electronics is summarized in the following:

1. Sample and Hold and Gap Monitor - The average position of the rotor must be stable to approximately 6.75 nano-inches of the nominal center position. Since the Sample and Hold is only one of the error sources which can affect centering, the offset stability of the Sample and Hold must be maintained to about 0.2 millivolts. The N57A Sample and Hold circuit was found to be approximately an order of magnitude higher than this. A new Sample and Hold circuit was designed and evaluated, to provide the required performance. Extensive tests were conducted on this circuit.

A Gap Monitor Circuit was also designed which would provide the required gap measurement stability of  $6.75 \times 10^{-9}$  in.

2. Charge Amplifier - The Charge Amplifier must meet the following requirements for MESGA.

- a. Rise and fall time variations between channels  $\leq 0.24 \times 10^{-9}$  sec
- b. Propagation delay variation between channels  $\leq 0.12 \times 10^{-9}$  sec
- c. Charge error due to high voltage transistor gain variation  $\leq 17$  ppm
- d. Nonlinear force from slew rate limiting  $\leq 25$   $\mu$ g
- e. Stray capacitance variation  $\leq 191$  ppm
- f. DC offset stability must give less than  $6.75 \times 10^{-9}$  in centering stability

A number of improvements were made to the first amplifier stage of the Charge Amplifier. Sensitivity tests were conducted on this first stage. The results are shown in Table 6-31.

Table 6-31. Rise Time and Propagation Delay Sensitivity to Temperature Variations for the Charge Amplifier First Stage

Volts Input	Temperature Variations (nanoseconds per degree C)		Jitter (nanoseconds)	
	Prop Delay	Rise Time	Prop Delay	Rise Time
5.75	0.08	0.09	Negligible	0.5
3.00	0.09	0.09	Negligible	1.0
1.00	0.07	0.07	Negligible	2.0

There is a relatively large sensitivity of propagation delay and rise time to input amplitude change for the first stage of the Charge Amplifier. When the input signal is varied from 1 to 5.75 volts a 10 nanosecond propagation delay and an 11 nanosecond rise time variation occurs. This is not a serious problem if the system is operated at one or two discrete preload values.

The pulse amplitude sensitivity to pulsewidth change for the first stage was originally 600 ppm for a 40 microsecond pulsewidth change. The 600 ppm was reduced to 25 ppm by making design improvements in the first stage.

The amplitude sensitivity of the first stage to temperature variations were found to be less than 5 ppm/ $^{\circ}$ C.

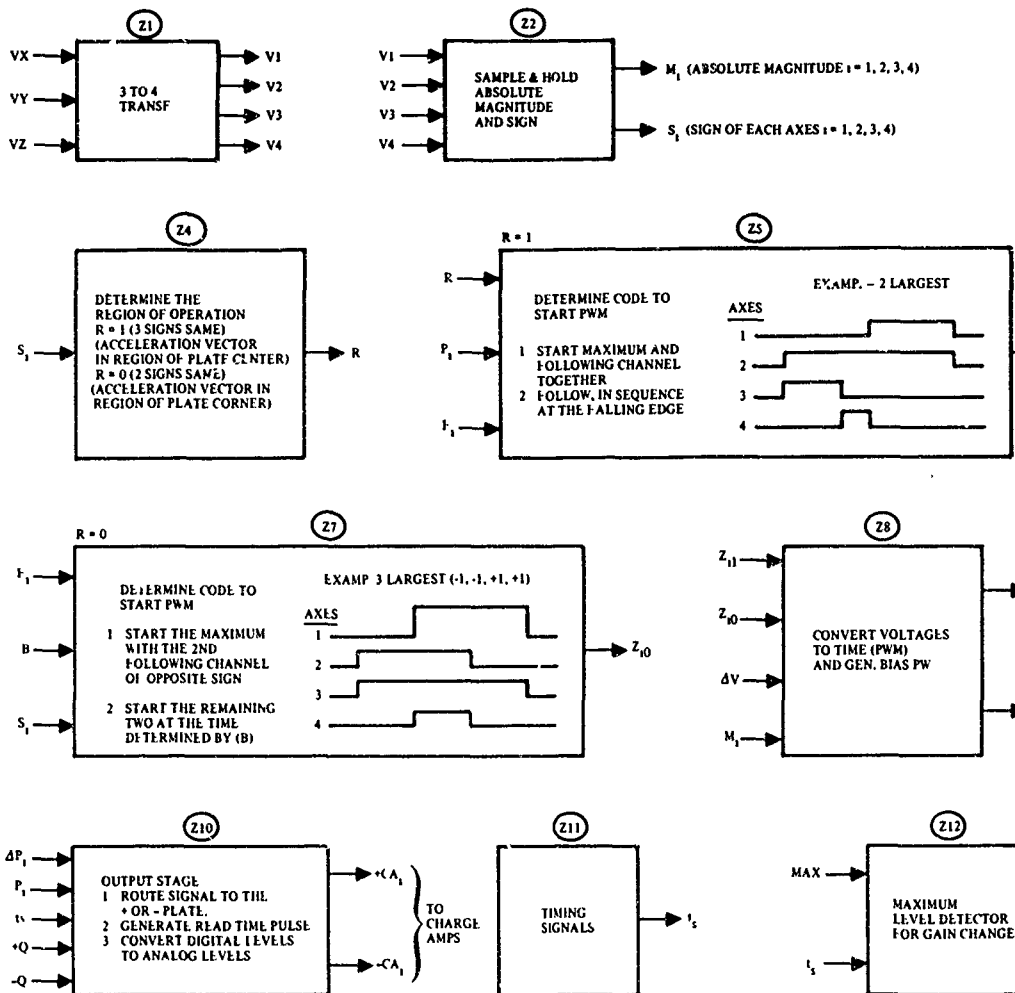


Figure 6-45. Block Diagram

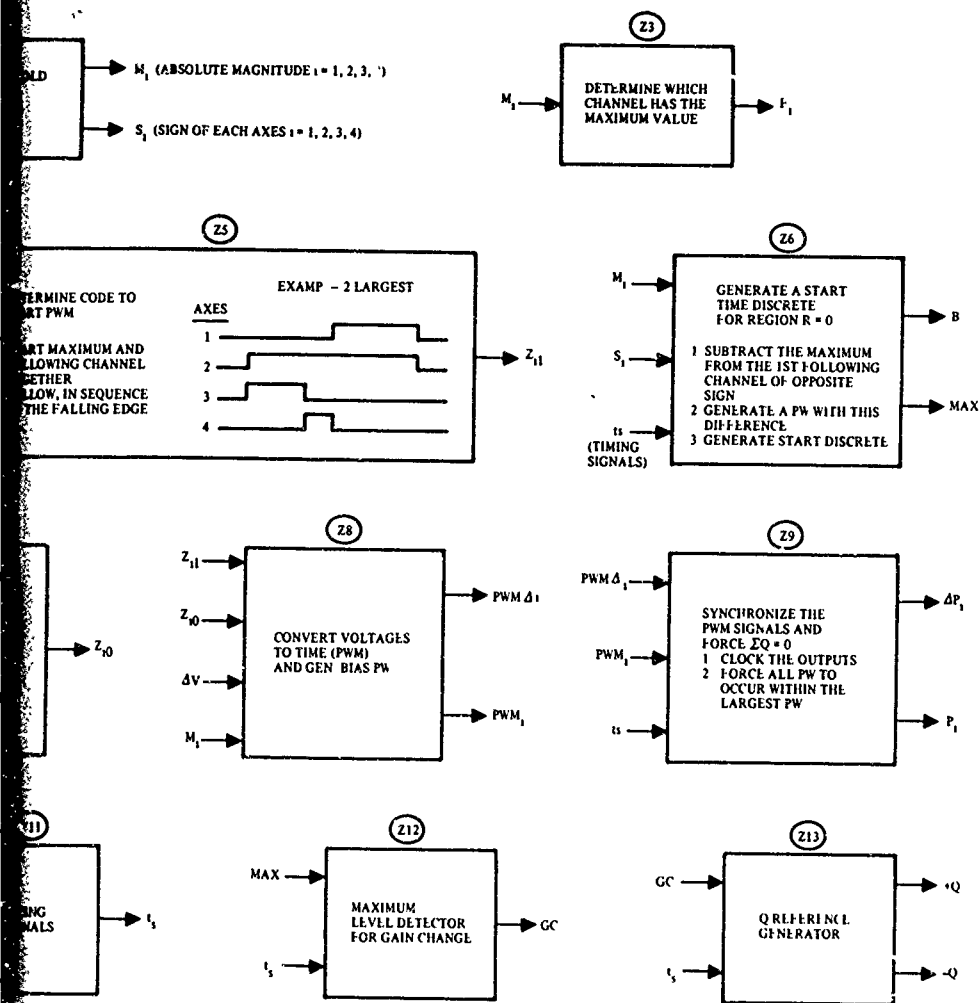


Figure 6-45. Block Diagram of Pulsewidth Modulation Suspension Electronics

The Charge Amplifier was designed so that the charge error would be independent of the high voltage transistor gain. It was also designed to that it was not slew rate limited since acceleration errors would result from this condition. The charge amplifiers were mounted in a stable mechanical configuration close to the gyro to minimize stray capacitance variations. The effects of Charge Amplifier offset were minimized by using capacitor coupling to the output.

3. Gyro and Electronics Temperature Control - The gyro temperature must be stable and maintained within  $0.035^{\circ}\text{F}$ . This required an improved temperature controller design.
4. Acceleration Digitizer - A modification of the EMA acceleration digitizer was obtained. A demodulator precedes the digitizer. This demodulator is a precision type with errors which are substantially less than 25 ppm.

Consideration was given to digitizing the acceleration sensing signal at the Charge Amplifier output as suggested by TASC. It was decided to digitize at the Charge Amplifier input as originally planned. The reasons for this are discussed in Para 6.3.5. Figure 6-46 shows the position of the Acceleration Digitizer in the suspension electronics.

6.3.1.2.2 8-Plate MESGA Electronics Modules. The function of the 8-Plate MESGA electronics suspension modules is described below.

1. Timing Generator, Part Number (P/N) 11835-507-1

This module contains the timing signals and clocks for both the 8-plate and the 4-plate suspension system.

2. Suspension Servo Module, P/N 12075-507-1

This module contains the speed control Notch Filter, the suspension servo compensation network, the Precision Sample and Holds, and the 50 KC buffer.

3. Sign and Magnitude (PWM No. 1), P/N 11840-507-1

The three axes network output from the Suspension Servo Module is fed to this module. The signals are converted to a 4-axes sign and magnitude signal. This module also provides the capability of applying a test signal to each axis. The module will also be utilized for the 4-Plate GSA.

4. 8-Plate PWM Logic (PWM No. 2), P/N 11845-507-1

This module provides the logic codes for the start and stop times of the eight pulsewidth signals. This module is used for the 8-plate system only.

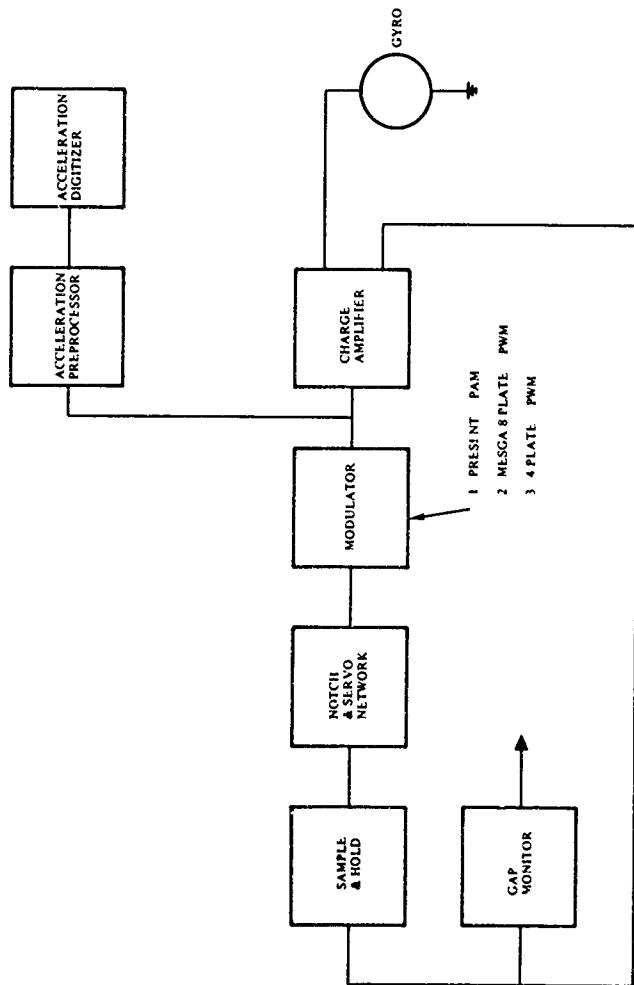


Figure 6-46. Block Diagram of MIESGA 8-Plate Suspension Electronics and Acceleration Digitizer

5. PWM Output (PWM No. 3), P/N 11850-507-1

This module generates the precision voltage pulsewidth modulated signals. The outputs of this module go to the Precision Charge Amp inputs and the acceleration digitizer.

6. PWM Converter (PWM No. 4), P/N 11855-507-1

This module converts the analog signals from the servo network to pulsewidth signals that are proportional to the signal magnitudes. This conversion is mechanized by integrating a reference voltage and comparing it with the signal magnitude. This module is used in the 4-plate GSA in a modified configuration.

7. Modulator Logic and Reference Generator, P/N 11880-507-1

Three distinct functions are generated in this module: (1) the precision voltage references for the pulsewidth modulated signals, (2) a four-bit code that indicates the maximum channel, (3) a discrete which indicates that one of the channels is close to saturation.

8. Precision Sample & Hold, P/N 11805-507-1

One Precision Sample & Hold is mounted on the Suspension Servo Module (P/N 12075-507-1) and one is mounted on the Sign and Magnitude Module (P/N 11840-507-1). The Sample and Hold that is mounted on the Suspension Servo Module, converts the eight charge amp readout signals to three signals. The three outputs are then sampled synchronously at a 10K rate. The Sample & Hold substrate on the Sign and Magnitude module converts the three axes signals to a 4 axes signal which is sampled at a 10KC rate.

9. Q Ref, Max Channel & Max Sense, P/N 11870-507-1

This substrate is mounted on the Modulator Logic and Reference Generator Module (P/N 11880-507-1). This substrate provides the functions as defined in 7 above.

10. Output Control Logic, P/N 11890-507-1

Two substrates of this type are mounted on the PWM Output Module. This substrate provides the logical elements to synchronize the 8 pulsewidth modulated signals.



### 6.3.2 Vaecon Pump Elimination

#### 6.3.2.1 Objective and Approach

Elimination of the Vaecon pump could be a significant step in reducing the cost of the gyro if the following technical objectives are attained:

1. Low voltage or passive pumping at a relatively low cost.
2. Quick starting or continuous pumping.
3. Gyro configuration must not require redesign of system packaging.
4. Rotor speed at, or near, 2434 Hz.
5. Rotor speed stable to 2 Hz per year.

It soon became apparent that these objectives would best be pursued by replacing the Vaecon pump with a getter since exploratory experiments established the necessity for some sort of pumping. The zirconium/graphite getter manufactured by SAES, Milan, Italy, was judged the most promising device. This getter pumps almost all gas species except hydrocarbons and inert gases. It has a capacity of 40 torr-cc per activation and, through multiple reactivations, has a total capacity of 270 torr-cc. Its initial pumping speed, which decreases with mass pumped, is approximately 0.5 litre/sec.

It was also soon apparent that in using this getter the most elusive technical objectives was rotor speed stability. The mechanism causing unacceptable rotor speed changes was taken to be changes in the pressure of non-getterable gases inside the gyro. Such changes have two sources:

1. Outgassing from interior surfaces and from "virtual leaks" (such as material interface surface volumes and screw threads).
2. Leakage of atmosphere through the case seals.

To evaluate the getter it was decided to treat the interior source problems first and external leakage second.

#### 6.3.2.2 Rotor Speed Change, Internally Originating

Outgassing of interior surfaces was initially considered on a component part basis. The various component parts with surfaces within the sealed volume of the gyro were analyzed for relative magnitudes of contribution. The cavities and the getter were judged to have the greatest contributions.

Four cavity halves were step-heated while being monitored by the residual gas analyzer (RGA). Appreciable amounts of argon were detected. In an attempt to isolate the source(s) of this outgassing, a new BeO biscuit was cleaned, monitored, metallized by sputtering Cr/Au and monitored again with the RGA. No appreciable outgassing was detected.

Following the measurements on the metallized biscuit, the cavities from Vaclon pumped gyros 98 and 130 were step-heated and monitored. Significant outgassing of non-getterable gases was detected.

These observations raised a serious question as to whether cavities were or were not outgassing non-getterable species at unacceptable rates after being conditioned (the foregoing specimens were not) for a gettered gyro. In order to explore this question, it was necessary first to establish the relationships between the mass (torr-litres) of gas present and the signal strength (ion current) of the RGA.

Figure 6-47 presents a typical RGA spectrum: ion current versus mass-charge ratio. Several gas species are identified to mass-charge ratio values.

Figure 6-48 presents the required relationship between partial pressure and ion current for oxygen (total volume is known and constant). Note that oxygen yields a signal at each of two ionization states. Note also that the coordinate scales are both logarithmic. An excellent linear regression on the data was obtained. Equally useful relationships were determined also for helium, nitrogen, argon, methane, propane, and carbon dioxide.

The cavities removed from Gyro 138 were conditioned in a vacuum chamber using the same process as was used for Gyros 118 and 126. After conditioning, the vacuum chamber was sealed and held for 24 hours at 150°F. At the end of this "pinched-off" storage period the chamber was opened and the RGA was used to determine the amounts of argon and propane present. A similar determination was made for the empty vacuum chamber subjected to the same time-temperature-pumping profile. This yielded the background levels.

A comparison of the results from the Gyro 138 cavities with those from the background run showed that significant amounts of gas evolution would be within the "noise level" on small differences between very large numbers.

The other component of concern with respect to outgassing was the getter. A new getter was placed in the vacuum chamber and was subjected to a conditioning process cycle identical to that used on Gyro 126.

This getter was activated twice, "killed" with house nitrogen and then reactivated. RGA sniffing was performed during each activation. During the first activation, massive quantities of many gases including argon, nitrogen, hydrogen and organic compounds were detected. During the second activation, lesser amounts of  $H_2$ ,  $N_2$  and Ar (but essentially no hydrocarbons) were detected. During the third activation, small amounts of  $H_2$ ,  $N_2$  and Ar and hydrocarbons were detected.

Following this, the getter was stored in a "pinched-off" chamber the same as were the cavities from Gyro 138. After 24 hours at 150°F the chamber was opened and gas analysis was performed. As before, a background was also measured and was comparable to that for the cavities from Gyro 138. Although these results were subject to the same unacceptably high errors as those from the Gyro 138 cavities, it was noted that the argon signal saturated the electronics. This did not happen with the cavities.

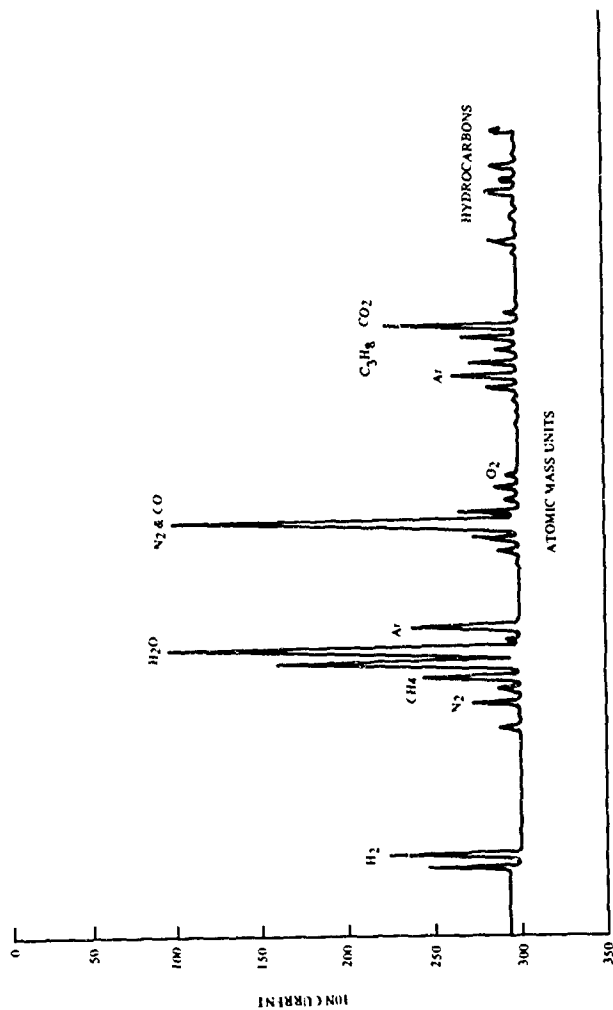


Figure 6-47. RGA Spectrum

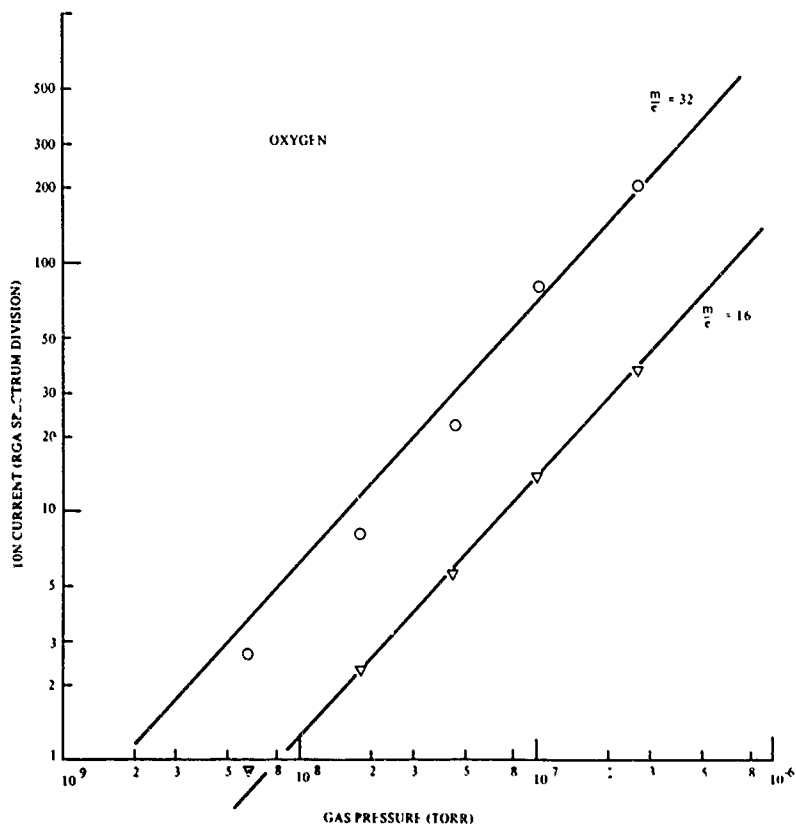


Figure 6-48. RGA Calibration

From this it was concluded that the getter released far greater amounts of non-getterable gas(es) than did the cavities when conditioned as in Gyro 126.

At this time the Research Director of SAES, Milan, Italy was in Anaheim for a technical conference. Consultations with him indicated that our method of getter activation had been counter productive. SAES researchers reported that only nascent hydrogen is released from the getter during activation and this nascent hydrogen interacts with Vacilon pumps. This interaction liberates a variety of previously sorbed gases from the pump.

The liberated species include such non-getterable gases as argon and several hydrocarbons. These liberated gases "poison" the getter. The nascent hydrogen by itself presents no problem since the getter has a very large capacity to re-sorb hydrogen.

SAES recommended using a turbomolecular pump during getter activation since there is no interaction between it and the liberated nascent hydrogen.

Pursuant to the above facts and recommendations a turbomolecular pump was acquired and used during the getter activation of subsequently built gyros (154, 156, and 158) which were speed tested to indicate internal effects.

Measurement of internal effects through gyro speed tests involved changes in design details, changes in fabrication procedures (in addition to the use of the turbomolecular pump), and storage of the entire gyro in a hard vacuum between speed test runs. These efforts are described in the following paragraphs, first gyro-by-gyro and then in a summarizing comparative analysis of the three significant gyros.

6.3.2.2.1 Gyro 118. Figure 6-49 shows the gyro rotor speed change through 36 weeks when stored between speed tests in an air ambient at approximately 150°F. After week 36, the storage environment was changed to a vacuum of approximately  $10^{-8}$  torr at 156°F. The purpose here was to eliminate any contributions to speed change from external leakage.

Figure 6-50 shows speed change trends during the 13-week vacuum storage period. Since a speed determination was not made immediately before starting vacuum storage, the speed change trend must be estimated over the 9-week period ending at week 50. It is possible to pass linear regressions through the data with slopes varying between zero and about 4.8 Hz per year, all of which have approximately the same residual variance. These limits are shown as dashed lines in Figure 6-50.

There is no confident basis for preferring one of these limits over the other as the better single-valued description. However it is interesting to speculate on some details of the dispersion of the data. With the exception of the point at week 41, the data are dispersed in one group of three points (weeks 43 through 47) on a straight line with an extremely small positive slope followed by a group of three points on a straight line with an extremely small negative slope. These two lines are offset from each other by about 0.6 Hz. If one straight line of zero slope is struck through these six points it would make the precision on unique speed determinations

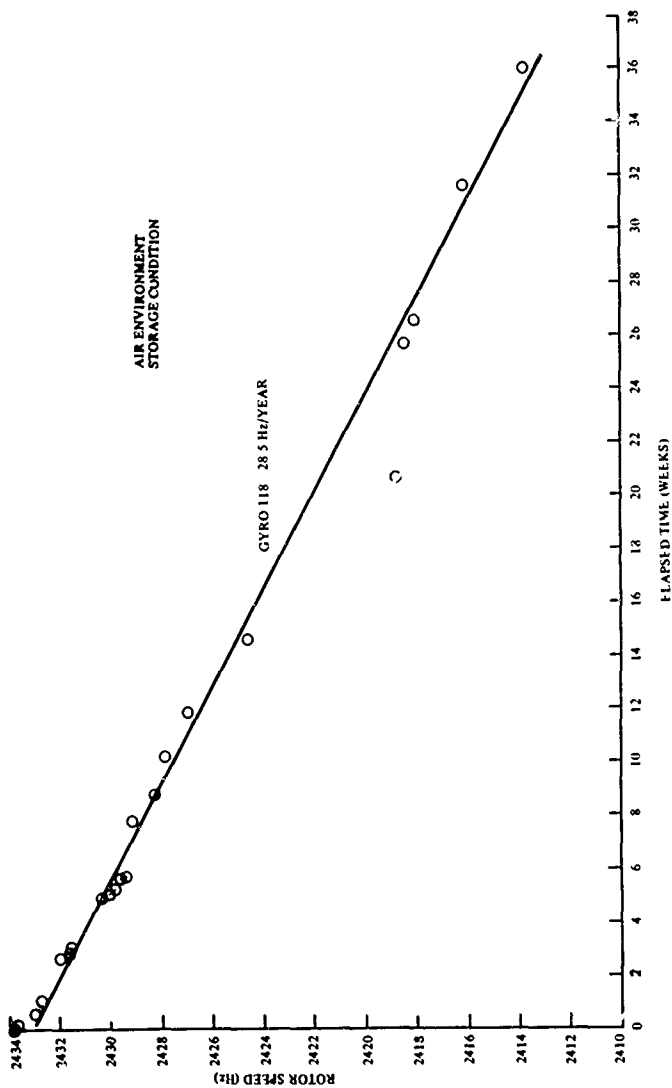


Figure 6-49. Speed Change of Gyro 118

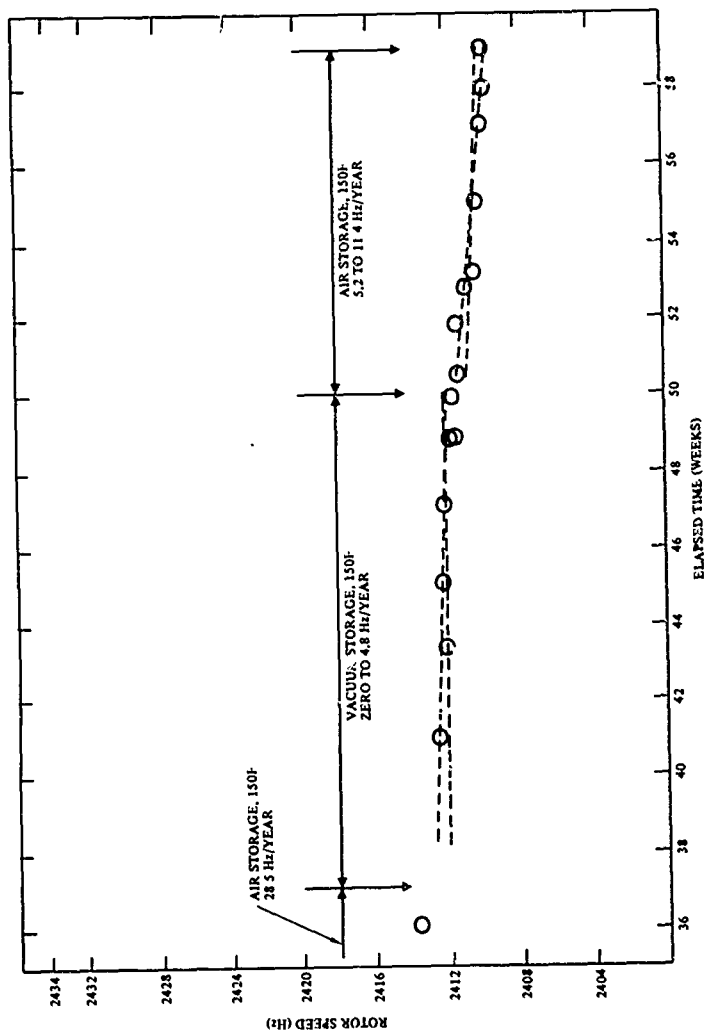


Figure 6-50. Speed Change of Gyro No. 118

appear to be  $\pm 0.3$  Hz. By bringing the point at week 41 back into consideration, the precision would appear to be  $\pm 0.3$  Hz most of the time since this point would deviate from the single zero-slope line by about  $+0.5$  Hz.

In a less detailed vein, the data taken during vacuum storage do indicate that the speed change due to internal outgassing is negligible (or nearly so) after about 40 weeks of storage time. This suggests that the previous speed change rate of 28.5 Hz per year in air storage was due entirely (or nearly so) to external leakage.

In order to check this suggestion, Gyro 118 was stored in air at 150°F from week 50 through week 59. Figure 6-50 shows the results of this testing. The slowdown rate did not return to 28.5 Hz/year following the vacuum storage period but was 5.2 to 11.4 Hz/year. It is judged that the lower value, 5.2, is the better estimate since there seems to be a step of about -0.6 Hz at week 53. The data on either side of week 53 fit a slope of 5.2 Hz/year quite well. However, there is no known reason why a step should have occurred at week 53.

It appears that this gyro slowed down during the first thirty-six weeks primarily because of internally generated gas load changes. It appears that the internally generated changes in gas load has ceased sometime around week 36 or 38 since the slowdown rate in 150°F vacuum storage was negligible (or nearly so) and the slowdown rate in subsequent 150°F air storage was relatively low compared to the initial 150°F air-storage value; i.e., 5.2 Hz/year compared to 28.5 Hz/year. The 5.2 Hz/year rate is not interpreted to be due only to external leaks and is considered to have been constant in magnitude during both 150°F air storage periods.

Gyro 118 was subsequently tested during storage in air at 72°F from week 59 through week 83. The objective was to assess the temperature sensitivity of the external leak. Figure 6-51 shows the results of this testing. The slowdown rate was 3.9 to 5.2 Hz/year. It would seem that external leakage was slightly temperature sensitive.

6.3.2.2.2 Gyro 154. Gettered Gyro 154 was built utilizing both aqueous-detergent and non-aqueous cleaning procedures for the component cleaning. Also, 16 lubricated bolts (instead of 8 non-lubricated bolts) were used at each gold O-ring seal. This gyro was built in a nitrogen environment. Gyro 154 was built in air. After prefunctional test and the vacuum assembly bake on a Vaccon pump, the getter was activated and the gyro getter was activated and the gyro pinched-off. The turbomolecular pump was used instead of the Vaccon pump during getter activation.

Figure 6-52 shows the results of stand testing during vacuum storage at 150°F. This gyro showed a behavior pattern during the first two and one half weeks which suggested either a fast-declining rate of internal outgassing, or an external leak which was closing-up (the gyro was in air at 150°F for about 6 hr for each test run), or a combination of the two. However, data taken subsequently lie 3-Hz below the dashed line. A review of the records showed that the vacuum storage temperature in the interval between weeks 2-1/2 and 3-1/2 was 180°F to 200°F instead of the usual 140°F to 160°F. This was unintentional. It is believed that this difference in storage condition caused the apparent 3-Hz offset.



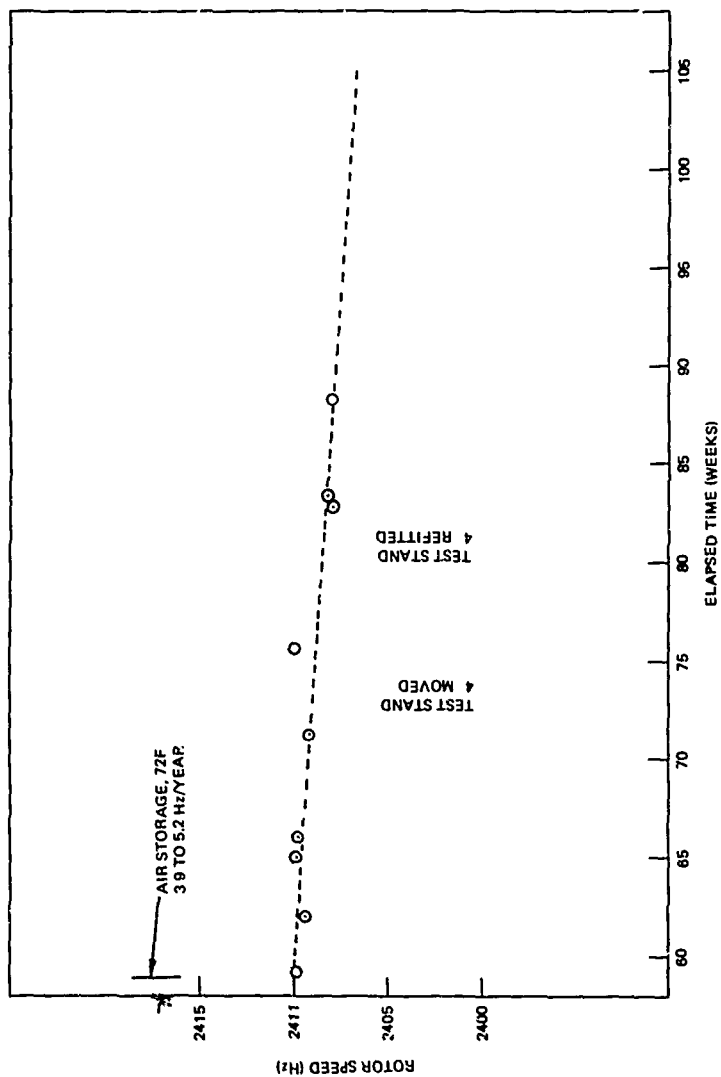


Figure 6-51. Speed Change of Gyro 118

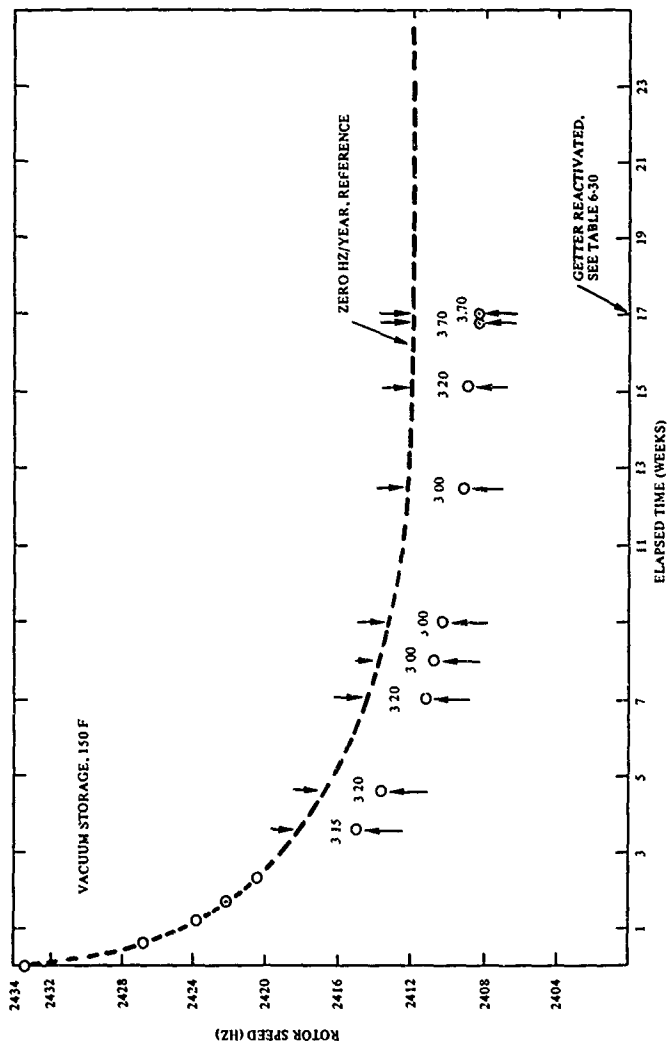


Figure 6-52. Speed Change of Gyro 154

The dashed curve included in Figure 6-52 has been drawn to place the zero Hz/year rate at about week 16. The reference curve is then extended at zero slope. Also shown are the offset values (from the reference) for each data point.

The testing is complete, terminating as shown at week 17. The data shows that the slowdown rate had decayed to some value between zero and 7 Hz/year based on the last four points.

Immediately following the rotor speed determination at week 17, the getter was reactivated and put back on the test stand. At this time, the gyro failed to speed control. Coast-down rates were measured as shown in Table 6-32.

The essential conclusions from the speed data in Table 6-32 are:

1. Reactivation of the getter caused a catastrophic loss of rotor speed presumably from an increase in internal pressure.
2. Reactivation of the getter did not open up a persisting, identifiable external leak.
3. A significantly large external leak was identifiable 16 days after reactivation.

The residual gas analysis, day 21 of Table 6-32 showed the presence of helium at levels which did not correlate with the puncturing operation but persisted throughout the duration of the analysis. The helium pattern was uninterpretable.

The residual gas analysis also showed a strong argon signal which did correlate with the withdrawal of the puncture tool. Other gases were also detected but were identified as being either system background or indigenous to the deformation of the copper pinch-off tube during puncture penetration.

The principal conclusion from the residual gas analysis was that only argon was identifiable as being responsible for the catastrophic degradation of rotor speed.

Helium leak testing, day 22 in Table 6-32, identified several leak paths at each O-ring seal. Each leak path showed a leak rate of about  $6 \times 10^{-9}$  cc-atm/sec helium. The sum of the individual leaks was on the order of  $4 \times 10^{-8}$  cc-atm/sec helium.

Gyro 154 was diagnostically disassembled. The only observation of significance was that the cavities were strongly magnetic (See Table 6-63, Para 6.3.6.1.8). It is believed that the pre-pinch-off baking at 400°F caused this and that the condition did not influence rotor speed stability.

6.3.2.2.3 Gyro 156. Gettered Gyro 156 was built utilizing both aqueous detergent and non-aqueous solvent cleaning procedures for the components. Sixteen lubricated bolts were used at each gold O-ring seal. The electrical feedthrough for getter activation was installed in a "reversed" attitude so as to place its "virtual leaks" on the outside of the case. This gyro was built in a nitrogen environment. The gyro was prefunctionally tested and vacuum assembly baked on a Vacfon pump. The gyro was transferred to the turbomolecular pump for getter activation and pinch-off.

Table 6-32. Gyro 154 After Getter Reactivation

Day	Event	Coast-down Rate (Hz/min) at 2360 Hz
0	Reactivate getter	-
0	Speed test	7
	150F, Vacuum storage	-
1	Speed test	7
	150F, Air storage	-
2	Speed test	7
	150F, Air storage	-
5	Speed test	7
	150F, Air storage	-
14	Changed storage condition	-
	72F, 20 psig helium	-
16	Speed test	54
	72F, Air storage	-
20	Changed storage condition	-
	250 to 300F, Vacuum storage	-
21	Puncture and residual gas analysis	-
	72F, Air storage	-
22	Helium leak checked on Veeco MS17	-

Figure 6-53 shows the results of stand testing during vacuum storage at 150°F. The initial stable speed (at week zero) is shown in a rectangular enclosure since, as will be explained below, it should not be included in speed change estimation. The important feature of the initial stable speed was that it was 2434.6 Hz, 0.6 Hz above nominal. This is interpreted to indicate that the vacuum in this gyro was exceptionally good the day of pinch-off.

During the first week of vacuum storage, Gyro 156 was also exposed to the 180°F to 200°F temperature range (see Para 6.3.2.2.2). When this gyro was tested at week 1 it sparked badly. A stable speed determination was nonetheless obtained. The effect between the week 0 and week 1 points is attributed to these events.

The data from week 1 through week 14 indicate a steadily decreasing slowdown rate which was about 6.6 Hz/year between weeks 1 and 6 but which was zero to 4.0 Hz/year by week 14.

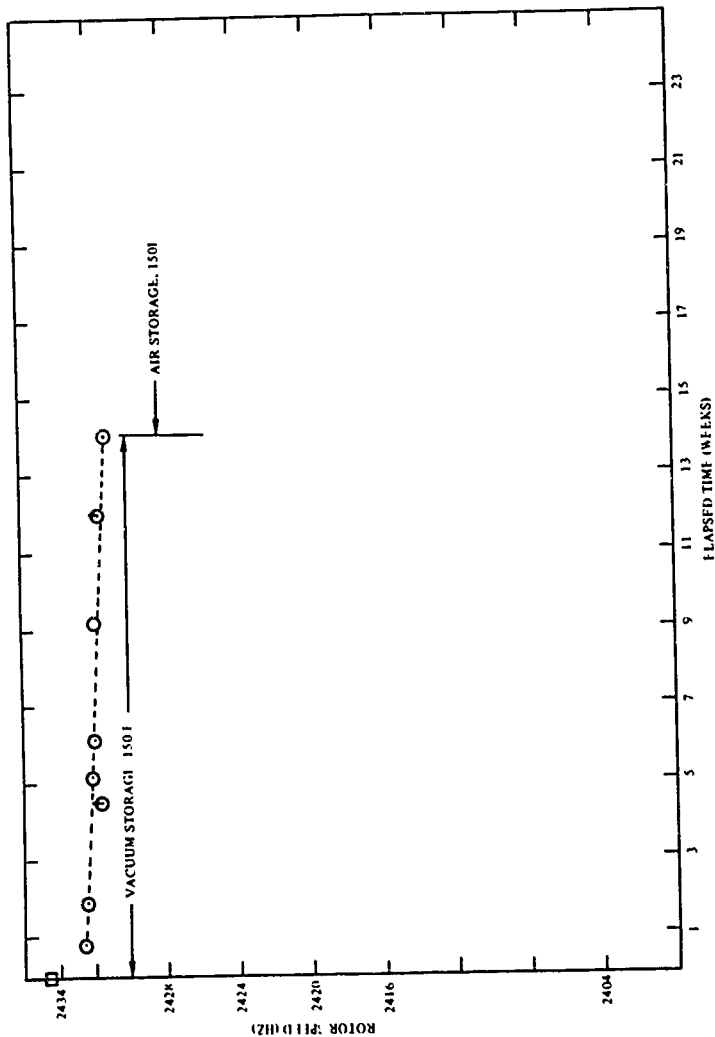


Figure 6-53. Speed Change of Gyro 156

At this point, Gyro 156 was stored in air at 150° F to assess the air leakage correction to vacuum storage data since the gyro was in air at 150° F for about 12 hours for each speed test run during the vacuum storage period.

Figure 6-54 shows the 150° F air storage rotor speed stability data for gettered Gyro 156. No corrections to the 150° F vacuum storage data are required. Even if the true 150° F vacuum storage slowdown rate were zero at week 14, the corrections to the vacuum storage data would be negligible (about 1 Hz on the eighth data point at week 14; progressively less on the preceding ones).

6.3.2.2.4 Comparison of Gyros 118, 154 and 156. Figure 6-55 presents an overview of the three gyros. Curves 1 and 2 are for Gyros 118 and 154 respectively. Curve 3 is for Gyro 156. All three have the characteristic of tending smoothly toward zero slowdown rate (slope) with time. This, of course, is as would be expected when there is no mass transport due to leakage.

Curves 1 and 2 are further similar in that these gyros tended to equilibrate at about the same stable speed although in quite different time periods. Table 6-33 provides some possible reasons for this difference in time to equilibrate. In this table, all of the known differences in design, fabrication features are listed and described.

In comparing Gyros 118 and 154, the high-impact and medium-impact features are the getter feedthrough orientation, the assembly atmosphere, getter packaging, and prefunctional conditioning. All of these would be expected to affect the total mass of non-getterable gas and thus the equilibrium rotor speed of the gyro. These factors do not explain the difference in time to equilibrate except for unknown differences in the effective "virtual" leak rate of the getter feedthrough.

The pump upon which getter activation occurred, a very high impact feature, is probably the most significant consideration. A getter "poisoned" through activation on a vacuum pump would be a very slow virtual leak compared to other possibilities since it is a porous body. Concomitant with this interpretation is the expectancy of a greater mass of trapped, non-getterable gas and thus a lower stable speed in Gyro 118 as compared to Gyro 154. This is not what the speed data show. This suggests that there are other design/fabrication differences affecting rotor speed which are not yet recognized or accounted (such as the magnetic susceptibility of the cavities).

Gyro 156 differs from the other two in that the stable speed was at a much higher value than those of Gyros 118 and 154. The implication is that the mass of trapped, non-getterable gas was comparatively low. Its time to equilibrate was, however, very similar to that of Gyro 154 which, upon examination of the data in Table 6-33 lends some credence to assigning the longer time for Gyro 118 to equilibrate to a "poisoned" getter.

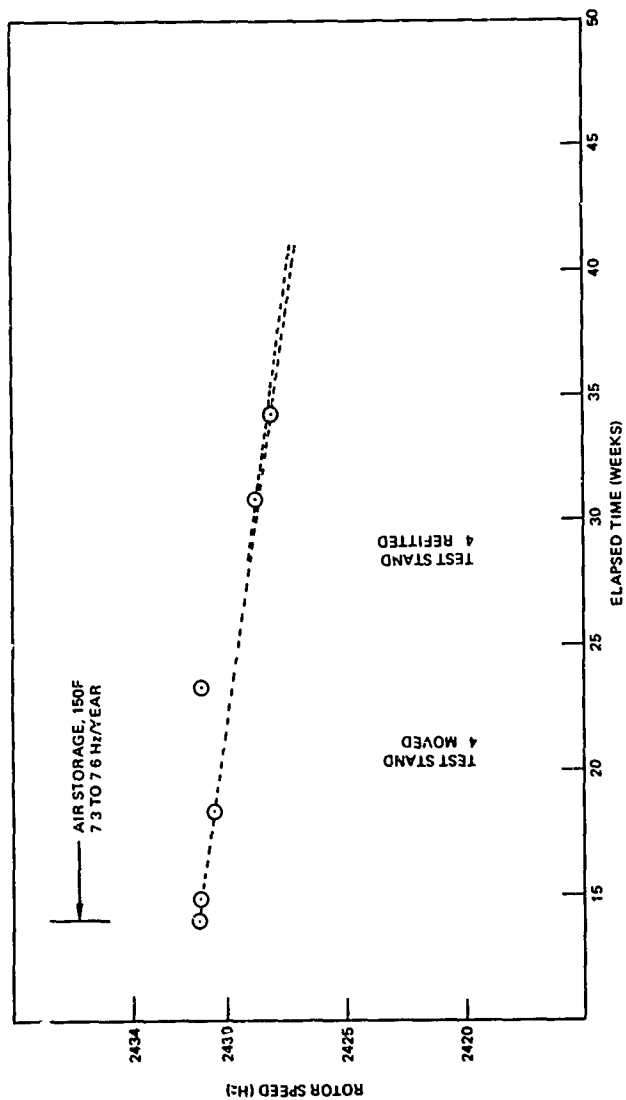


Figure C-54. Speed Change of Gyro 156

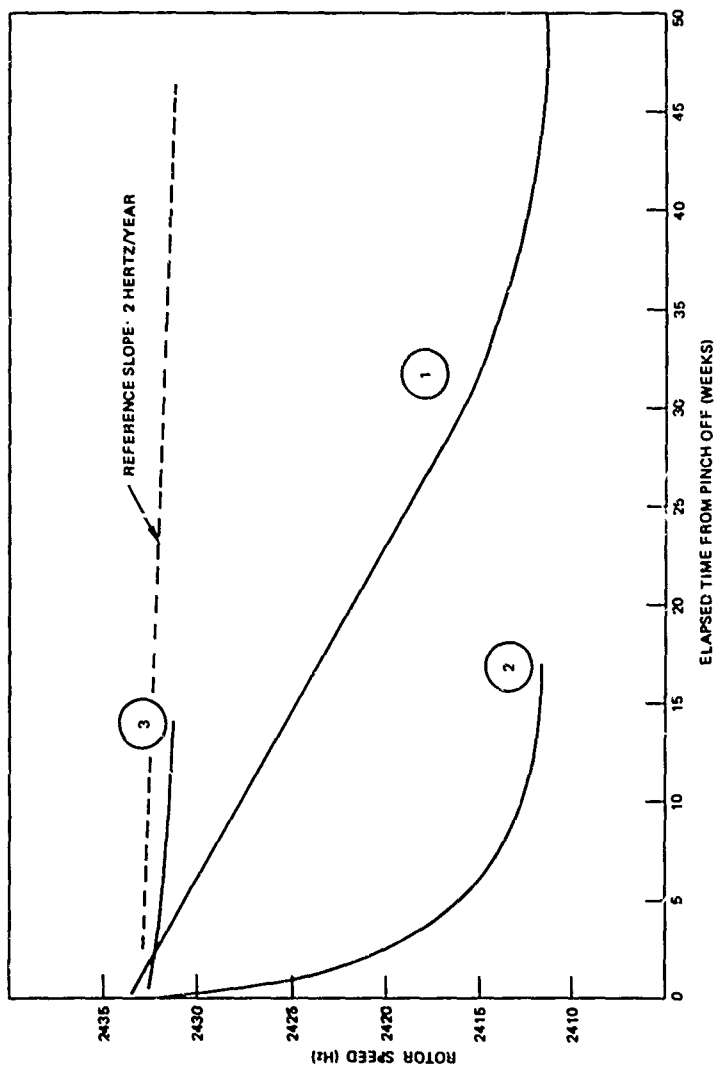


Figure 6-55. Speed Changes from Internal Effects in Gittered Gyros



Table 6-33. Variations in Design/Fabrication of Gettered Gyros

Design/ Fabrication Feature	Gyro 118	Gyro 154	Gyro 156
Getter Feedthru	Normal	Normal	Reversed
Cleaning	Solvent	Detercent & Solvent	Detergent & Solvent
Surface Conditioning:			
Rotor	860°F, Vacuum	Glow Discharge	Glow Discharge
Cavities	400°F In Air	400°F, Vacuum	Glow Discharge
Others	860°F, Vacuum	100°F, Vacuum & 860°F, Vacuum	400°F, Vacuum & 860°F, Vacuum
O-Ring Seals	8 Bolts	16 Bolts	16 Bolts
Assembly	Air, 10 <sup>-1</sup> PPM Ar	N <sub>2</sub> , 10 <sup>-2</sup> PPM Ar	N <sub>2</sub> , 10 <sup>-2</sup> PPM Ar
Getter	Large, Ar-Packed	Large, N <sub>2</sub> -Packed	Large N <sub>2</sub> -Packed
Prefunctional Conditioning	Ar	N <sub>2</sub> , 10 <sup>-2</sup> PPM Ar	N <sub>2</sub> , 10 <sup>-2</sup> PPM Ar
Assembly Bake	400°F, 96 Hrs 10 <sup>-8</sup> Torr	350°F, 120 Hrs 10 <sup>-8</sup> Torr	350°F, 120 Hrs 10 <sup>-8</sup> Torr
Transfer (to Turbomolecular)	N/A	80°F	140°F
Getter Activation	Vaclon Pump	Turbo- molecular	Turbo- molecular
Ion Gage Exposure	Yes	Yes	No
Pinch-Off Soldered	No	Yes	Yes

Neither Gyro 154 nor Gyro 156 had "poisoned" getters. There were, however, two differences between them: the getter feedthrough orientation and the exposure, after getter activation, to an ion gage. Exposure to the ion gage, which is known to outgas significant amounts of non-getterable gases at the moment of turn-on, was probably the lesser factor of the two. Thus the "virtual leak" in the getter feedthrough is probably the more important. In Gyro 154, this "virtual leak" faced the interior of the gyro. In Gyro 156, it faced the exterior.

In summary, the design and the fabrication techniques used for Gyro 156 produced results which closely approached the rotor speed objectives. This is evident from a comparison between curve 3 and the reference slope in Figure 6-55.

6.3.2.2.5 Improving Performance and Lowering Cost. During January 1975, the Research Director from SAES, the getter manufacturer, spent a day at Autonetics to review our experience in detail. Having done this, he identified aspects of fabrication which he considered to be optimum and recommended some alternatives to other aspects which he thought could be improved. The three most salient recommendations were the use of indium seals instead of gold O-rings, the elimination of most of the prepinch-off baking, and elimination of prefunctional conditioning. These recommendations were based on experience from other high vacuum devices and on review of Autonetics' data. This input was used to design the building of Gyro 158.

Gettered Gyro 158 has been built three times (A, B, and C) using minimum processing. "Minimum processing" refers to the exclusion of several process steps which were used to build Gyro 156 and previous gettered gyros. Individual component parts were glow discharge cleaned but were not vacuum baked prior to assembly. Assembly was accomplished in air instead of in the nitrogen-filled glove box. The assembly was not baked under vacuum at 350° to 400°F for 120 hours but under vacuum at 250° to 300°F for 1-1/2 hours prior to getter activation.

The initial attempt to build gettered Gyro 158 (158A) was unsuccessful. The flange-base indium seal of the electrical feedthrough for the getter leaked catastrophically after getter activation. It was subsequently determined that this indium seal configuration would not reliably survive the getter activation step. It is not clear as to why the feedthrough survived getter activation in Gyro 156 but failed in Gyro 158. Their configurations were identical but perhaps this design is marginal.

Gettered Gyro 158B was also unsuccessful due to leaks. On this build, a "deep-well" flange was used to displace the feedthrough from "wrap-around" heating during getter activation. Gold O-ring seals were used instead of indium. Unfortunately the pinch-off tube to base braze sprung a leak.

Gettered Gyro 158C yielded significant data with respect to internally-generated effects. Although this gyro did not speed control, coast-down rates were measured as shown in Table 6-34.

Table 6-34. Gyro 158C

Day	Event	Coast-down Rate (Hz/min) at 2380 Hz
0	Initial getter activation and pinch-off	-
0	Speed test	0.25
	150F, Air storage	-
1	Speed test	6
	150F, Vacuum storage	-
2	Speed test	17
	72F, 20 psig helium	-
8 1/2	Changed storage condition	-
	250 to 300F, Vacuum storage	-
9	Puncture and residual gas analysis	-
	72F, Air storage	-
16	Helium leak checked on Veeco MS17	-

The residual gas analysts, day 9 in Table 6-34 showed no helium at all. The analysis did show a strong argon signal which correlated with the withdrawal of the puncture tool. Other gases were also detected but were identified as being either system background or indigenous to the deformation of the copper pinch-off tube during puncture penetration.

Helium leak testing, day 16 in Table 6-34, showed no leaks (threshold level:  $3 \times 10^{-11}$  atm-cc/sec helium). This testing was performed also with the getter at activation temperature. No leakage was detected under this condition either.

Upon diagnostic disassembly, Gyro 158C parts showed no particular anomalies except for a possible "oil stain" on the 12-hole cavity and a great deal of very fine pitting on the rotor. The origins of these observed anomalies were obscure.

The essential conclusion from gettered Gyro 158C was that "minimum processing" was too minimal. The failure to speed control and the time-degeneration of coast-down characteristics were due to internally-generated changes in non-getterable-gas pressure.

Gettered Gyro 158 was built a fourth time, 158D. The build was similar to that of the 158C except that the traditional ESC solvent cleaning was used instead of the detergent-solvent process. Also, this build was baked after assembly for 336 hours at 300°F with an internal vacuum of about  $10^{-8}$  torr. The residual gases in this vacuum were monitored with the Finnigan Residual Gas Analyzer and were found to reach essentially stable pressure levels after about 160 hours of baking.

Gyro 158D was successfully pinched-off, put on the test stand, and spun-up uneventfully to 1250 Hz. At this point, the motor amplifier was turned off and other parameters were checked out and found to be good. The rotor speed did not decay measurably during this "several second" coast period. As soon as the motor amplifier was turned back on for full spin-up, it was noted that the rotor had dropped. Diagnostic disassembly confirmed that the unit had failed. The reason for the drop in gettered Gyro 158D is unknown. The two most likely possibilities are either that this gyro suddenly became a "high charger" during spin-up, or at the 1250 Hz dwell, or that there was an intermittent defect in the test stand. A suspect cable in the test stand has been redesigned and replaced.

Gettered Gyro 154B was built to replicate 158D. Unfortunately, there was a nonspinning rotor drop on this gyro also. It was subsequently relevelated and found, at this point, to be charging at an unacceptable rate. Gyro 154B is being "tumbled" at about 20 Hertz on the prefunctional test stand in an attempt to decrease the charging rate.

#### 6.3.2.3 Rotor Speed Change, Externally Originating

Since the getter does not pump inert gases and since air contains about one volume percent argon, the gettered gyro must be sealed more efficiently than is necessary for a Vaccon pumped design. Vaccon pumped gyros perform acceptably even when helium leak rates are as high as  $10^{-8}$  atm-cc/sec. With the getter design, calculations indicate that helium leak rates cannot exceed  $10^{-14}$  atm-cc/sec, if the rotor speed stability objective is to be attained.

As described in Para 6.3.2.2, indium seals which "cold weld" to the case surfaces were tried but failed to reliably survive the thermal stresses attendant to getter activation. The 16-bolt gold O-ring design, also mentioned in Para 6.3.2.2, has not generated much confidence either since the rotor speed slowdown rate of Gyro 156 in air, Figure 6-54, is still too high. Other approaches must be tried. In addition, a leak detector more sensitive than those currently commercially available will eventually be required to demonstrate that pre-pinch-off leak rates of gettered gyros are acceptably low. The cost and schedule implications of "buttoning-up" production gyros without this demonstration are quite undesirable.

The following paragraphs describe the efforts to develop a sufficiently sensitive leak detector and to improve the sealing of the gyro case.

6.3.2.3.1 " $10^{-14}$ " Leak Detector. Various pieces of laboratory and test equipment (company) have been assembled to evaluate a " $10^{-14}$ " leak detector. When this assemblage is adequately baked-out it is expected to detect helium leak rates of  $10^{-14}$  torr-litre/sec and possibly  $10^{-15}$  torr-litre/sec. By comparison, commercially available leak detectors will detect helium leak rates of  $10^{-10}$  torr-litre/sec and, under some circumstances,  $3 \times 10^{-11}$  torr-litre/sec. It is expected to replicate those currently operational at Martin-Marietta, Denver, and at General Electric, St. Petersburg.

The leak detector, Figure 6-56, works on the principle of time accumulation of an inert "leaker gas." In this case, helium is the "leaker gas." The residual gas analyzer (RGA) measures the partial pressure of helium as a function of time. During this measurement the VacIon pump is valved-off and the Sorb-Ac pump is used to keep the total pressure at a low enough value to protect the RGA sensor. However, the Sorb-Ac does not pump helium, or any other inert gas.

Leak rates are calculated as:

$$L = SV \frac{\Delta h}{\Delta t}$$

where

L = Leak rate in torr-liters per second

S = RGA scale factor in torr per chart unit

$\frac{\Delta h}{\Delta t}$  = Change in number of chart units with time

V = Volume of the system: 3 liters

Figure 6-57 shows an example of the RGA output. The initial and final changes in signal amplitude ( $\Delta h/\Delta t$ ) were due to internal outgassing plus air leakage when the assemblage and test piece were surrounded by air (which contains 0.0004 percent helium). Between these two slopes is a larger slope due to internal outgassing and air leaks plus leakage through the test piece which was surrounded by 100 percent helium. In this case the helium leak rate of the test piece was calculated as about  $10^{-12}$  torr-liters per second.

Bake-out and minimization of air leaks in the assemblage will continue until the background helium rate is reduced to  $10^{-15}$  torr-liters/sec or less.

6.3.2.3.2 Gyro Case Sealing. Analysis of case sealing alternatives narrowed the attractive options to deformed gold washers and welds. On the basis of experience with welded joints on the vacuum housing and the getter support flange, both of which have been exceptionally reliable with respect to sealing, it was decided to use welding to seal all of the case joints. Figure 6-58 shows a gettered gyro design wherein the gyro case is sealed by electron beam welding. Fabrication tooling for this design has been built and checked-out. Acceptable electron beam welding parameters are being determined for each weld.

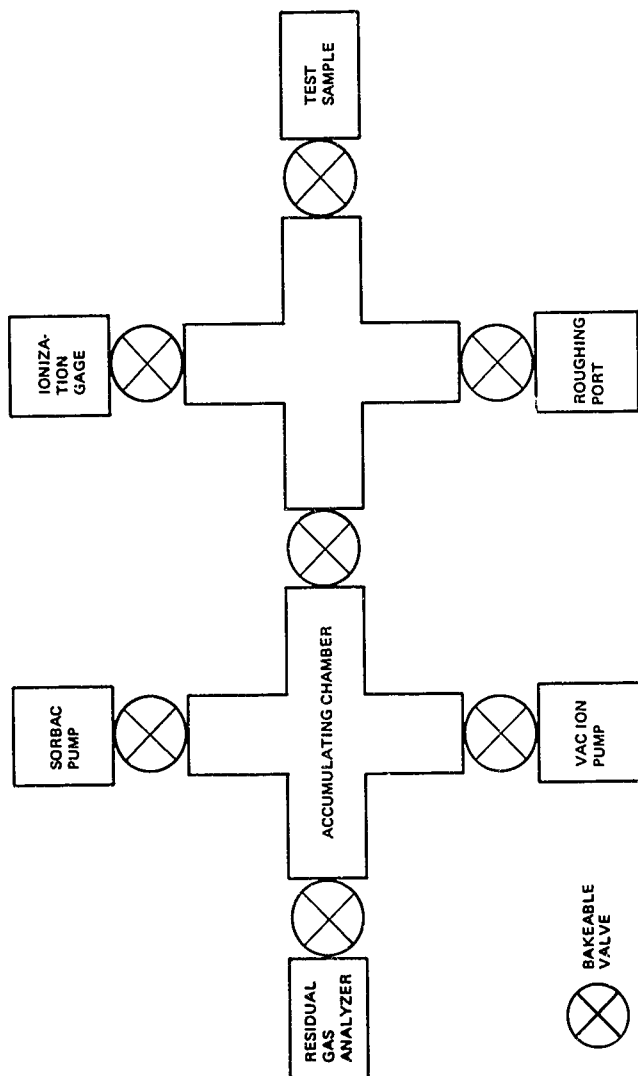


Figure 6-56. " $10^{-14}$ " Leak Detector Schematic

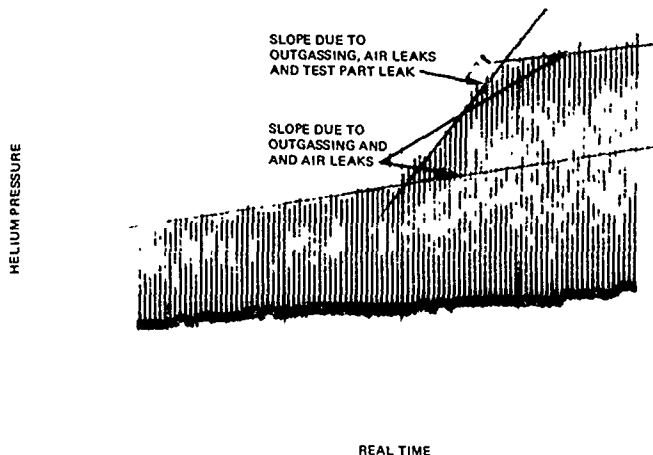


Figure 6-57. Helium Pressure vs Time

### 6.3.3 Develop Four-Plate Gyro

#### 6.3.3.1 Develop Four-Plate Gyro Instrument

The intent of this task was to develop a four-plate MESS instrument for the purpose of cost reduction and potential overall system simplification. The task was to be accomplished without degradation of system performance. The original intent was to accomplish the effort by fabricating four-plate cavity members, assembling instruments with otherwise "standard" parts (N57A type), test and evaluate and then redesign as necessary.

In summary, cavity parts and rotors were fabricated and a number of instrument assemblies were made. The efforts were in support of the electronics lab checkout of the suspension system being developed. The many assembly completions of the four-plate gyro did not include prefunctional burn-in because there is no four-plate suspension capability in that area. The assemblies did include rotor size changes in support of development of a reliable lift-off technique. Also, processing of the instruments at times included vacuum pull down and Vaccon pump initiation while, at other times, included an "air filled" assembly. The pressure in the instrument was thought to enhance or degrade lift off capability because of damping.

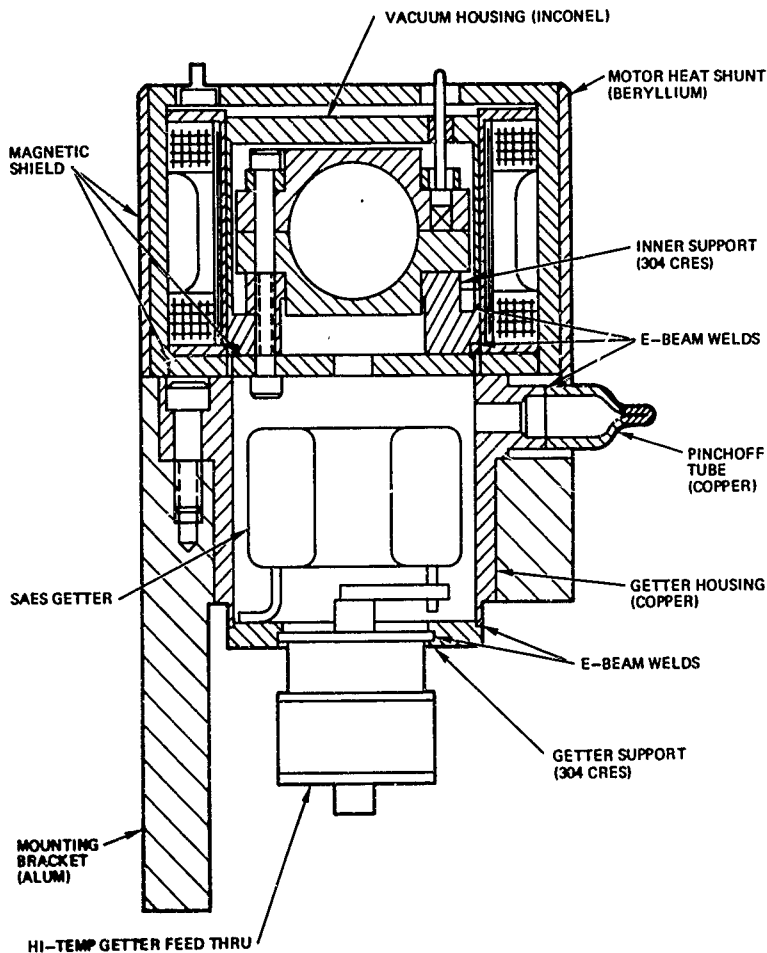


Figure 6-58. Welded Gyro Design



#### 6.3.3.2 Develop Four-Plate Gyro Electronics

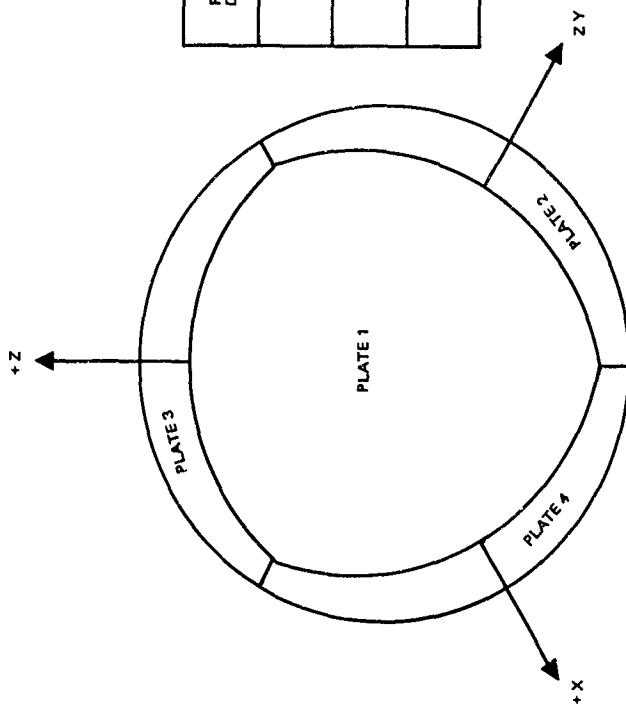
The motivation for developing Four-Plate Gyro Electronics was the potential for suspension electronics cost reduction and drift rate improvements. The potential for cost reduction resulted from the fact that the charge amplifiers were historically a high cost item and one-half as many are required with the four-plate gyro. Although the four-plate suspension electronics are more complex and costly than the PAM eight-plate electronics, the cost could have been reduced by developing MOS circuits. However, it became clear in the course of development and testing of the four-plate electronics that several problems existed with the four-plate gyro electronics that would be very difficult to solve. A list of these problems are summarized in the following:

1. The G capacity was very marginal. In the high G mode, only 12 to 13 G's were available. The ACF system requires 13 G's DC with shock and vibration inputs superimposed.
2. No cavity alignment technique exists for the four-plate gyro.
3. It is not possible to self-calibrate the four-plate gyro as it is with the eight-plate gyro.
4. Higher voltage, more expensive transistors are required for PWM systems than those required for PAM systems. The reason for this is that a High Voltage Switch Power Supply can be used with PAM but cannot be used with PWM.
5. Rotor-liftoff with the four-plate gyro was intermittently bad. This was attributed to the nonlinear forces resulting from the wide span of the four-plate electrodes and the proximity of the rotor to the electrode at liftoff. When an eight-plate gyro was used with the four-plate electronics (one-half of the electrodes used) no liftoff problem occurred.

For the above reasons, it was concluded that the four-plate suspension system is impractical for the ACF application and therefore the task was deemphasized. Although the task was deemphasized, all the design, fabrication and test of the four-plate suspension electronics was completed. A four-plate gyro was suspended with the electronics on many occasions and the electronics were ready for integration with the test station.

Figure 6-59 shows the electrode configuration of the four-plate gyro and the method of application of charge in order to produce a force on each of the orthogonal axes.

Figure 6-60 shows a block diagram of the four-plate gyro electronics and Figure 6-61 shows a typical set of waveforms at the gyro electrodes.



FORE DIRECTION	APPLY CHARGES (±) TO PLATE PAIRS
+Z -Z	1 AND 3 2 AND 4
+Y -Y	1 AND 2 3 AND 4
+X -X	1 AND 4 2 AND 3

Figure 6-59. Four-Plate Gyro Electrode Configuration

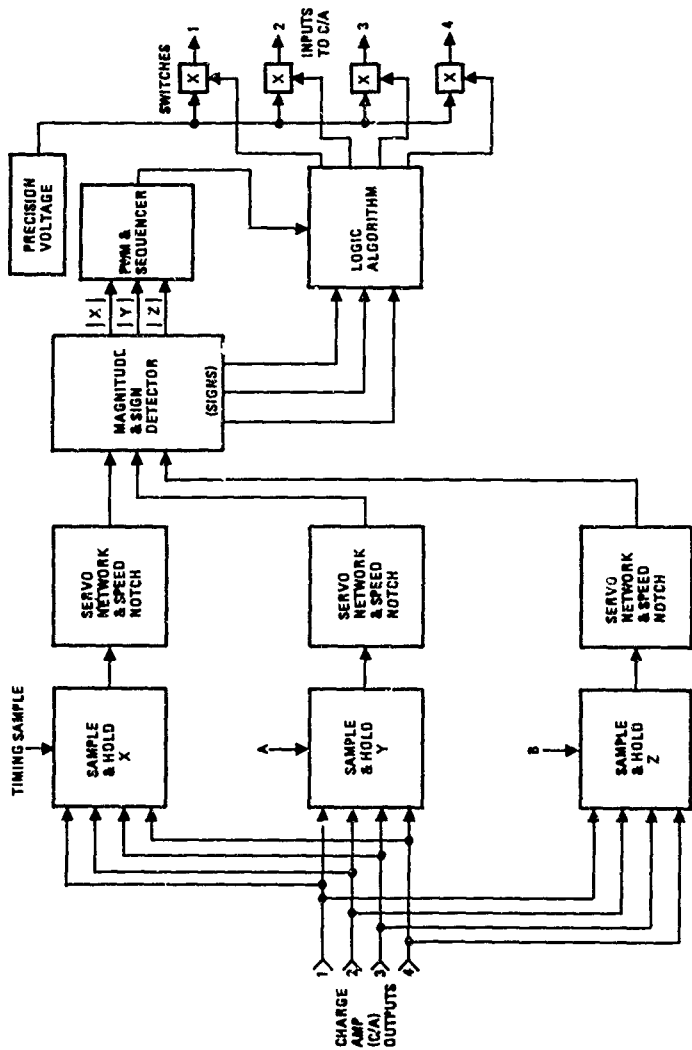


Figure 6-60. Four-Plate Suspension Electronics Block Diagram

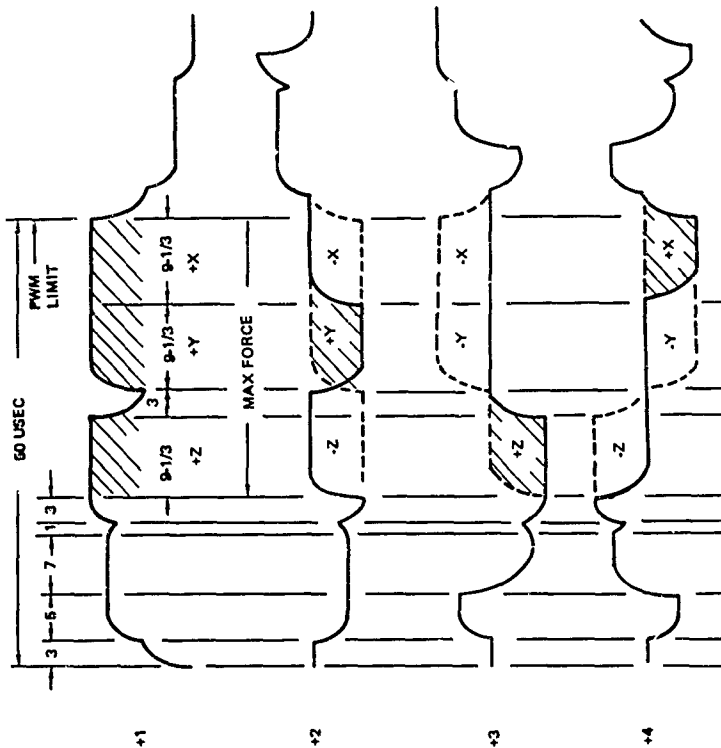


Figure 6-61. Typical Four-plate Waveforms

### 6.3.4 Perform Mechanization and Modeling Improvements

#### 6.3.4.1 Angle Calibration Optimization

The objective of this task was to develop an angle calibration sequence that would meet system calibration requirements at minimum cost. Technical details of the approach used are given in Appendix J.

In order to provide a baseline for comparison with the yet-to-be defined optimum calibration sequence, the "standard" 210-position angle calibration sequence was re-ordered in order of "maximum marginal utility" of the respective calibration data samples. This program is able to optimize the order of 210 samples in about 3-1/2 hours on the IBM 1130 computer. (Evaluation of one calibration sample takes about one minute) The resulting RMS compensation error as a function of the number of calibration samples is shown in Figure 6-62.

The initial estimate of the covariance matrix of uncertainties of the calibration parameters was obtained empirically from the 15 gyros summarized in Table 6-35. A "raw" covariance matrix was obtained by removing the mean of the resulting calibration parameters, and computing the unbiased estimate of sample covariance. The resulting covariance matrix will have rank less than or equal to the number of samples used for generating the estimate. This ill-conditioning is due to sample limitations. To remove this ill-conditioning, all correlation coefficients less than 0.9 in magnitude were eliminated (i.e., set to zero), and all other correlation coefficients were cubed and multiplied by 0.9. This operation preserves the sign of all the larger correlation coefficients, and makes 0.9 the maximum attainable correlation coefficient in the resulting covariance matrix.

The Monte Carlo optimization scheme described in Appendix J was applied to the optimization problem for the two-axis tilt table configuration for the Gyro Subassembly Test Station. (It was expected that this tilt table would be faster for angle calibration table settings than the vernier-type three-axis tables in use on other Test Stations.) The results indicate that, at the end of 30 tilt table settings, the two-axis tilt table is slightly better than the "baseline" three-axis 210-position calibration sequence.

The computer programs for optimizing angle calibration were converted from IBM 1130 computers for implementation on the HP2100 computers, and the differential optimization mechanization was developed and implemented for the GSA tilt table (a two-axis Ultradex table).

The computer programs execute about ten times faster on the Hewlett-Packard 2100 computer system than on the IBM 1130 computer. This meant that more could be accomplished overnight than could previously be accomplished on two weekends of computer processing.

The rms angle compensation error (neglecting drift) from the optimized angle calibration is plotted vs the number of calibration data samples in Figure 6-63. (Each sample takes about 25 sec.) These results are noticeably better than the "standard" 210-sample calibration.

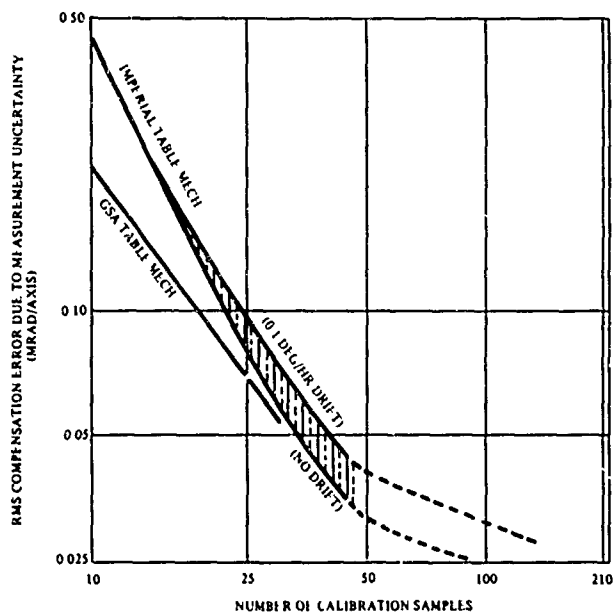


Figure 6-62. RMS Angle Readout Compensation Error vs Number of Calibration Samples

Table 6-35. MESG Angle Calibrations Used in Determining Initial Uncertainty of Calibration Coefficients

System	MESG No.	Calibration Date	Calibration Residual (Mrad, rms per axis)
N57A-1	96	02-27-74	0.072
"	94	02-28-74	0.057
"	66	03-05-74	0.065
"	106	04-29-74	0.096
"	102	05-09-74	0.079
"	112	07-18-74	0.066
"	130	07-18-74	0.052
N57A-2	98	07-05-74	0.043
"	110	07-05-74	0.049
Test Sta. 4	66	03-14-74	0.088
"	96	05-02-74	0.067
"	124	07-11-74	0.069
"	134	07-19-74	0.054
"	68	08-07-74	0.086
"	96	08-14-74	0.056

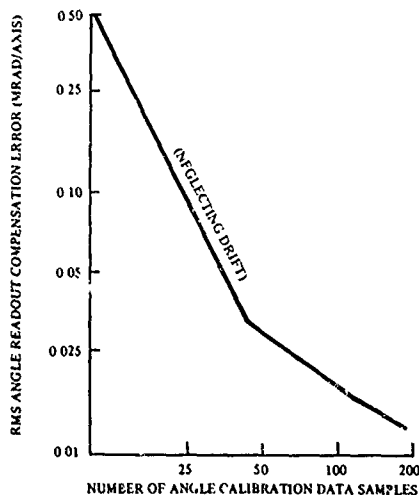


Figure 6-63. RMS Angle Compensation Error vs Number of Calibration Samples

The resulting optimized angle calibration sequence was modified to decrease the total number of distinct table settings on the outer axis. This, in effect, "optimizes" the angle calibration sequence from the standpoint of operational simplicity. In order to perform the selection of decreased tilt table angle settings, a histogram was computed, showing the number of calibration points with the tilt table set within  $\pm 5$  deg of each angle. This distribution was sufficiently "lumpy" that there were thirteen distinct angle settings with most of the optimized tilt table angle settings within  $\pm 5$  deg of the thirteen settings. The angle calibration sequence was then modified by forcing the outer axis angle settings to the closest of the thirteen selected values and allowing the inner axis angle setting to change to the value minimizing the expected squared compensation error. The optimized calibration sequence was truncated at 155 samples including samples for drift observability (the so-called "closure points" of the standard angle calibration). The resulting calibration contains 155 samples, as compared to 230 samples in the standard calibration. This calibration was specified for the two-axis Ultradex tilt table configuration of the GSA test stations. However, it can also be implemented on the Goerz automatic table. An equivalent set of Ultradex/Goerz angles for the 230-sample calibration has also been generated.

An optimized angle calibration sequence, developed for the 2-axis Ultradex tilt table configuration, was run on the Goerz automatic tilt table. This 155-sample calibration was run on the same day as a standard 230-sample calibration. Both calibrations used the Holloman Gyro Subassembly with Gyro No. 104. The rms calibration residuals were 0.046 and 0.086 milliradians per axis for the optimized and standard calibrations, respectively. The lower residuals do not necessarily imply improved calibration accuracy at an arbitrary point on the cavity. The optimized angle calibration has fewer data points to fit the model parameters and hence should give a smaller residual on the calibration data points.

The computer program for analytical comparison of different sets of angle calibration parameters was converted to HP2100 Fortran and de-bugged. The main difficulty was with a zero-divisor default in the IBM 1130 computer, which had been used to advantage in model orthonormalization, one of the main algorithms. In finding the "pseudo square root" or "pseudo inverse" of an ill-conditioned or singular matrix, this default had allowed us to proceed to the correct answer without worrying about division by zero. The zero-divisor default is different in the HP2100 computer, with the result that the "old" algorithms give the wrong answers. This was corrected by adding appropriate logical changes to the algorithm. A comparison of the analytical parameters characterizing the model orthonormalization is given in Table 6-36. Differences in the last digit of the figures shown in the table may be due to differences between the IBM 1130 output formatter (which truncates to the next smaller integer) and the HP2100 formatter (which rounds to the nearest integer). The extended precision word format in the HP2100 computer has a 40-bit mantissa, eight more than the IBM counterpart. This may account for the differences on the last model, where arithmetic errors would become most apparent.

In Table 6-37, the two sets of angle readout parameters obtained from Gyro No. 104 on the "Holloman" Gyro Subassembly are compared by model "groups." One set of angle readout parameters was obtained by the "Standard," 230-sample calibration technique. The other set was obtained by an "optimized" technique, using 155 samples. In order to provide a baseline for comparison, two "Standard" calibrations on Gyro No. 134, ran in February on the Holloman Gyro Subassembly, are compared in the same manner. The results show about a factor of two difference in the two gyros.



Table 6-36. Comparison of IBM 1130 Results with HP2100 Results from Angle Parameter Comparison Program (CMPZE)

MODEL NO.	IBM 1130 RESULT	HP2100 RESULT
"MODEL OVERLAP" <sup>(1)</sup>		
1	0.000000	0.000000
2	0.000000	0.000000
3	0.250000	0.250000
4	0.000000	0.000000
5	0.000000	0.000000
6	0.250000	0.250000
7	0.250000	0.250000
8	0.500000	0.500000
9	1.000000	1.000000
10	0.814345	0.814345
11	0.814345	0.814345
12	0.814345	0.814345
13	0.000000	0.000000
14	0.423659	0.423659
15	0.423659	0.423659
16	0.423659	0.423659
17	0.000000	0.000000
18	0.951189	0.951190
19	0.943456	0.943456
20	0.943456	0.943456
21	0.943456	0.943456
22	0.801783	0.801784
23	0.801783	0.801784
24	0.801783	0.801784
25	0.627645	0.627646
26	0.906363	0.906363
27	0.960362	0.960363
28	0.960714	0.961120
29	1.111244 <sup>(2)</sup>	0.969620
"MODEL MAGNITUDE" <sup>(3)</sup>		
1	0.516397	0.516398
2	0.516397	0.516398
3	0.500000	0.500000
4	0.365148	0.365148
5	0.516397	0.516398
6	0.500000	0.500000
7	0.500000	0.500000
8	0.316227	0.316228
9	0.000000	0.000000
10	0.349148	0.349149
11	0.349148	0.349149

Table 6-36. (Cont)

MODEL NO.	IBM 1130 RESULT	HP2100 RESULT
12	0.349148	0.349149
13	0.676123	0.676123
14	0.450748	0.450749
15	0.450748	0.450749
16	0.450748	0.450749
17	0.195180	0.195148
18	0.054985	0.054986
19	0.190476	0.190476
20	0.190476	0.190476
21	0.190476	0.190476
22	0.251976	0.251976
23	0.251976	0.251976
24	0.251976	0.251976
25	0.022008	0.022008
26	0.011023	0.011023
27	0.001565	0.001566
28	0.000247	0.000246
29	0.000023	0.000013

NOTES:

- (1) "Model overlap" is the ratio of the magnitudes of (a) the component of the model in the functional subspace spanned by the previous models and (b) the full model
- (2) A value greater than 1.0 for this parameter is theoretically impossible
- (3) This is the magnitude (in radians) of the component of the model orthogonal to all previous models

It is believed that the standard calibrations provide the "correct" parameter values, because they perform well in navigation tests. These results would then indicate some deficiency in the optimized calibration. This could be due, in part, to the functional character of the unmodeled errors. The standard calibration has, in effect, 460 scalar measurements (230 samples  $\times$  two error components) for determining 56 parameters. The measurements are sufficiently diverse that no unmodeled error mechanism is likely to be confused with one of the errors modeled by the 56 parameters under all those sample conditions. By restricting the number of samples, we always run the risk that the unmodeled errors may be confused with modeled errors at a more limited set of sample conditions.

There are two factors in these results which should be removed before discarding the optimized calibration technique. One is the fact that the results are for two different gyros. The other factor is that the calibration technique was optimized with respect to an assumed Carlson "square-root" filter mechanization which accounts for drift as an additional non-stationary parameter. The mechanization used for determining the parameters uses a much different method for estimating drift.

Table 6-37. Comparison of Angle Calibration Parameters from  
Standard (230-Sample) Calibration and Optimized (165-Sample) Calibration

PARAMETER CATEGORY	RMS DIFFERENCE (MRAD)	
	STANDARD vs STANDARD (BASELINE)	STANDARD vs OPTIMIZED
Scale Factor	0.077	0.198
Phase Shift	0.074	0.194
Preload Charge Unbalance and Even Rotor Shape Harmonics in Phase with Radial Mass Unbalance	0.030	0.099
Preload Charge Unbalance and Even Rotor Shape Harmonics out of Phase with Radial Mass Unbalance	0.032	0.084
Electrode Edge Effects and Rotor Shape Harmonics in Phase with Radial Mass Unbalance	0.066	0.093
Electrode Edge Effects and Rotor Shape Harmonics out of Phase with Radial Mass Unbalance	0.086	0.075
Odd Rotor Shape Harmonics in Phase with Radial Mass Unbalance	0.009	0.020
Odd Rotor Shape Harmonics out of Phase with Radial Mass Unbalance	0.039	0.029
All Odd Models	0.105	0.244
All Even Models	0.168	0.313
Symmetrical Scale Factor	0.009	0.160
Asymmetrical Scale Factor	0.076	0.078
Diagonal Scale Factor	0.012	0.088

### 6.3.4.2 Drift Model Improvement

6.3.4.2.1 Objective. The purpose of this task was to develop models for the (heretofore) residual drift rates which exceed the error budget and to eliminate unnecessary terms in the present model (designated K44W).

6.3.4.2.2 Approach. In order to evaluate models on actual gyro drift data, it was necessary to develop a "data bank" of sampled drift rates. Programs for loading and manipulation of the data bank were developed, and the data bank was loaded with 3287 drift rate samples from 20 different gyros. (The total number of independent sets of drift rate patterns is greater than 20, because the data bank includes data from the same "gyro number" taken with different sets of suspension electronics and, in some cases, with different rotors.) The data bank was later pared to a population of 33 sets of gyro data shown in Table 6-38.

As an initial estimate of the relative magnitudes of the terms in the K-44W drift rate model, the statistic:

$$\sigma_k = \left\{ \frac{1}{N} \sum_{j=1}^N \frac{\left[ \frac{1}{n_j} \sum_{i=1}^{n_j} \dot{\gamma}_{ij} * \dot{\gamma}_k \right]^2}{\left[ \frac{1}{n_j} \sum_{i=1}^{n_j} \dot{\gamma}_k * \dot{\gamma}_k \right]} \right\}^{1/2}$$

where

$\dot{\gamma}_k$  = drift rate due to unit value of calibration coefficient on  $k^{\text{th}}$  drift rate model

$\dot{\gamma}_{ij}$  = measured value of drift rate on  $i^{\text{th}}$  sample of  $j^{\text{th}}$  data set

$n_j$  = number of drift rate samples in  $j^{\text{th}}$  data set

$N$  = total number of data sets (=42, at present)

$\sigma_k$  = rms magnitude of drift rate due to  $k^{\text{th}}$  drift rate model, if it were the only model

was computed for each model. The functional forms of these terms are shown in Table 6-39. (The histograms of the magnitudes of each calibration coefficient, as distributed over the data sets, were also computed.) The resulting rms magnitudes of drift rates due to individual drift rate models range from 0.019 to 0.092 deg/hr in magnitude, which is a significant spread. These statistics are not the final answer on the relative magnitudes of the respective drift rate models, because they do not take into account the functional non-orthogonality of the models.

Table 6-38. Drift Rate Data Bank Description

Data Set	Gyro	System (1)	Date	Data Type Description (2)
1	56	N57A12	12/18/74	56 Polar + 144 MSA
2	56	N57A12	01/10/75	56 Polar + 24 MSA
3	62	T. S. 4	08/25/72	55 Pos Cal + 24 St
4	74	T. S. 4	08/14/73	48 Pos Polar
5	77	?	12/19/74	51 Pos Polar
6	86	N57A11	08/1-3/73	124 Pos Moving RSA
7	86	N57A12	08/7-9/73	166 Pos Moving RSA
8	86	T. S. 4	09/13/74	51 Pos Polar Calibration
9	86	HOLGSA	01/15/75	56 Pos Polar Calibration
10	90	T. S. 4	07/13/73	51 Pos Polar Calibration
11	90	N57A11	08/16/73	51 Pos MSA Calibration
12	96	T. S. 4	08/21/73	51 Pos Polar Calibration
13	96	N57A22	09/21/74	56 Polar + 22 MSA
14	96	N57A22	12/6/74	56 Polar + 43 MSA
15	98	T. S. 4	12/04/73	51 Pos Polar Calibration
16	9C	N57A12	07/31/74	65 Polar + 22 MSA
17	102	T. S. 4	08/28/73	51 Pos Polar Calibration
18	102	N57A12	12/05/74	56 Pos Polar Calibration
19	110	N57A11	01/10/75	56 Polar + ??? MSA
20	110	N57A11	12/18/74	56 Polar + 144 MSA
21	112	N57A12	07/18/74	56 Pol + 24 Hr MSA
22	118	T. S. 4	11/14/73	51 Pos Polar Calibration
23	124	T. S. 4	07/10/73	51 Polar + 144 MSA
24	124(3)	T. S. 4	02/13/75	56 Polar + MSA
25	130	N57A11	07/31/74	56 Polar + 22 MSA
26	134	N57A21	12/06/74	56 Polar + 43 MSA
27	134	N57A22	02/26/75	56 Polar + 24 MSA
28	136	T. S. 4	09/19/74	51 Polar + 380 MSA
29	140	T. S. 4	10/08/74	51 Pos Polar Calibration
30	142	T. S. 4	10/31/74	51 Pos Polar Calibration
31	142	N57A21	02/23/75	56 Polar + 24 MSA
32	142	HOLGSA	02/28/75	56 Pos Polar Calibration
33	144	T. S. 4	10/11/74	51 Polar + 380 MSA

## Notes:

(1) N57A12 = N57A1, Gyro No. 2 Position, etc

(2) "Pos" = Number of Tilt Table Positions

"Polar" = Rotor Spin Axis Polar

"MSA" = Moving Spin Axis" (not polar)

(3) Narrow Gap Gyro



When the histograms of the distributions of magnitudes of the drift rate models over the data bank had been computed, it was decided to develop a special perspective plotter for representing a third dimension in plotting, so that the third dimension could be made equal to the drift rate model number (there are 35 models). This way, all the information relating to the frequency distributions of model magnitudes could be represented on one page.

The resulting plot is shown in Figure 6-64. Each wiggly line running from upper left to lower right is a histogram. In this figure, the vertical dimension is frequency of occurrence. The axis running from upper left to lower right represents the magnitude, in degrees per hour, that would be assigned to a particular functional drift model on any of the 33 data sets in the data bank if that particular model were the only model being considered. That is, the magnitudes do not take into account the relative non-orthogonality of the models. The third axis in the figure, running from upper right to lower left, represents the drift rate model number. Consequently, this third axis is used for plotting the histograms one behind the other in perspective view.

Some characteristics of this plot have significant interpretations when related to the data bank.

Model number 24 shows a significant number of occurrences of large magnitude values. (This model is, in fact, the model with the largest rms value over the 33 data sets.) This particular model relates to the axial mass unbalance of the rotor. Because it is so easily calibrated and compensated, there is no penalty in drift rate errors associated with large magnitudes of this model.

One reason that these histograms show so much "weight" toward the larger magnitudes is that each model was considered separately, as though it were the only drift rate model. This characteristic expected to be changed significantly when all models are treated simultaneously.

The model evaluation method described above is just the first step of the so-called "Cholesky decomposition" for least-squares problems. The standard solution for the least-squares problem:

$$Az = y$$

is

$$x = (A^*A)^{-1} A^*y$$

where

\* denotes a matrix transposition

A is an m-by-n matrix

x is an n-rowed column vector

y is an m-rowed column vector

m is greater than n

The Cholesky decomposition is an algorithm for finding the upper-triangular "square-root" of  $A^*A$ . That is, an n-by-n matrix U which has zeros below the main diagonal and such that

$$U^*U = A^*A$$

# HISTOGRAMS OF K-44W

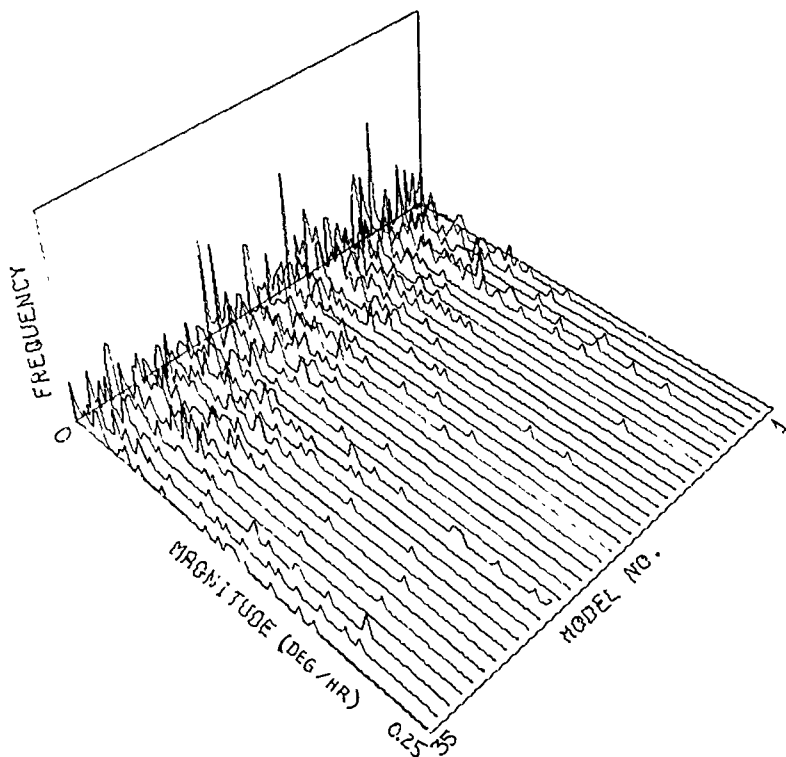


Figure 6-64. Composite Histograms of Individual Drift Rate  
Model Magnitudes, Models Evaluated Independently



If one defines the vector  $z$  by the following formula:

$$z = (U^*)^{-1} A^* y$$

then

$$\begin{aligned} x &= (A^* A)^{-1} A^* y \\ &= (U^* U)^{-1} A^* y \\ &= U^{-1} (U^*)^{-1} A^* y \\ &= U^{-1} z \end{aligned}$$

and, consequently,

$$\begin{aligned} y &= A x \\ &= A (U^{-1} z) \\ &= (A U^{-1}) z \end{aligned}$$

The associated least-squares problem for the vector  $z$  has the virtue that its associated matrix  $(AU^{-1})$  is such that

$$(AU^{-1})^* (AU^{-1}) = I \text{ (identity matrix)}$$

In other words, the models associated with the "z-states" (the components of  $z$ ) are orthonormalized with respect to the conditions of the data sample. (The Cholesky decomposition is equivalent to the Gram-Schmidt orthonormalization sequence, in this respect.) The Cholesky decomposition is used for marginal orthonormalization of the drift rate models with respect to each of the 33 drift rate data sets. This algorithm has the additional advantage that it can be "arrested" at each step, so that the marginally most significant model can be identified at each step, and the orthonormalization sequence can be accomplished in the order of the marginally most significant drift rate models. Because there are 33 different data sets, models will be more significant on some data sets than on others. The marginally most significant model, in this case, is defined as the model with the largest mean-squared coefficient value over the 33 data sets.

In the drift rate model evaluation problem, the vector  $y$  is the drift rate data from one particular data set. (For example, the direction cosine rates observed on Gyro No. 124 on Test Station IV on 10 July 1973.) The matrix  $A$  is the ensemble of partial derivatives of direction cosine rates with respect to drift rate calibration coefficients, and the  $x$ -states are the respective drift rate calibration coefficients for that data.

**6.3.4.2.3 Results.** Intermediate results of the "marginal" utility ordering are shown in Figures 6-64 through 6-67. These are the histograms of the magnitudes of marginal drift model coefficient values after orthonormalization of zero, five, ten and twenty models, respectively. The histograms of coefficients of models which have been orthonormalized are indicated by arrowheads in the figures. These figures demonstrate how the weighting of the histograms of the remaining states becomes shifted

# HISTOGRAMS OF K-44W

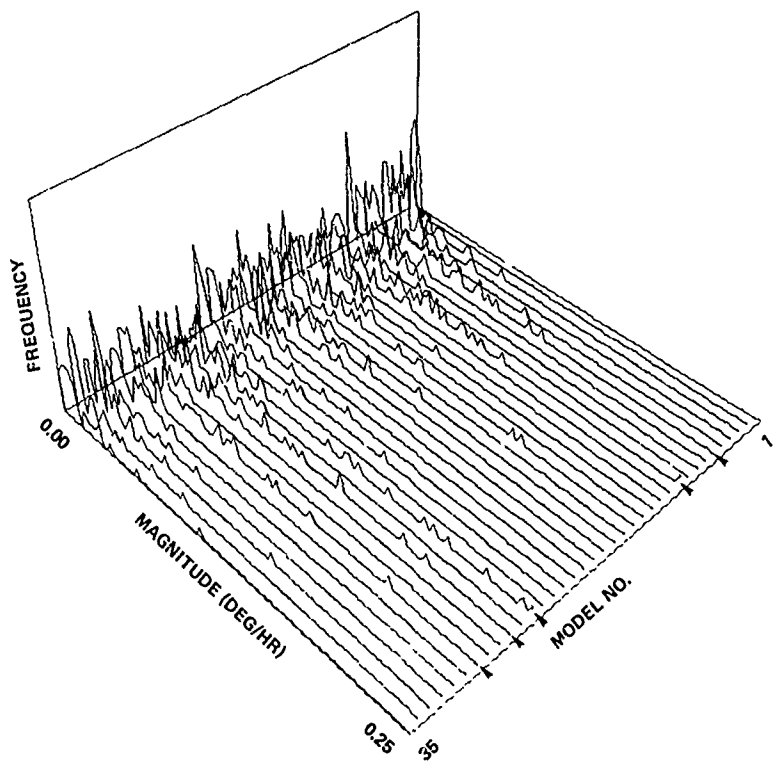


Figure 6-65. Histograms of Marginal Drift Model Coefficients  
after Orthonormalization of Five Models

# HISTOGRAMS OF K-44W

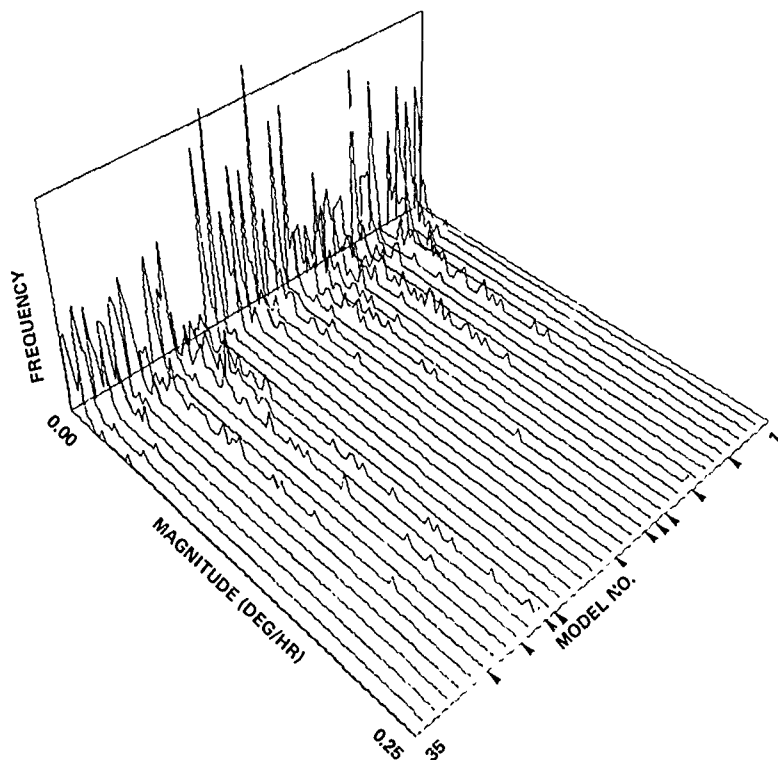


Figure 6-66. Histograms of Marginal Drift Model Coefficients after Orthonormalization of Ten Models

# HISTOGRAMS OF K-44W

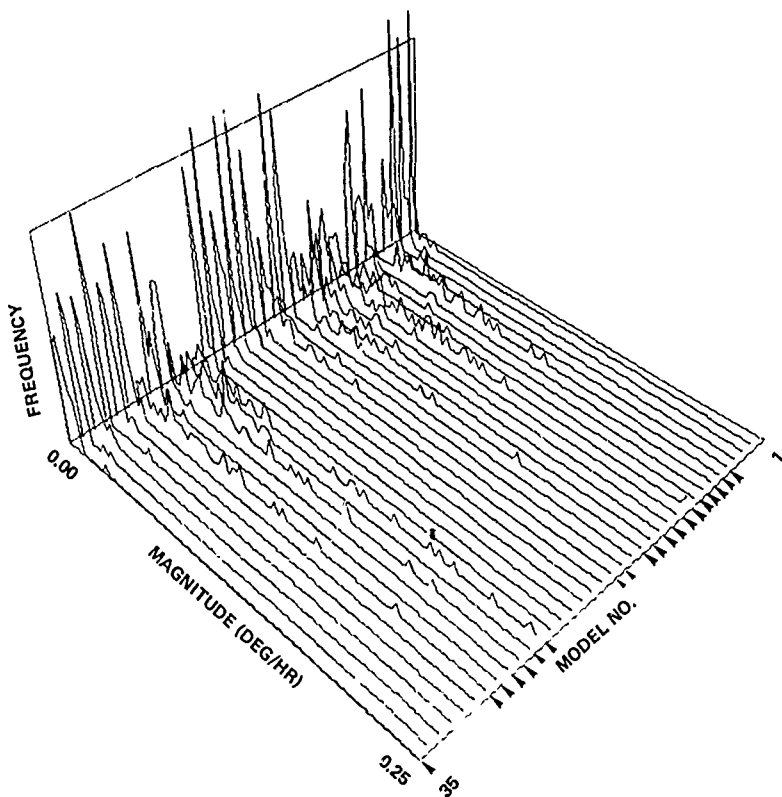


Figure 6-67. Histograms of Marginal Drift Model Coefficients after Orthonormalization of Twenty Models

toward zero as the orthonormalization progresses. Figure 6-68 is the final set of histograms, after orthonormalization of all 35 states. The sequence of orthonormalization is shown by the small typed numbers along the lower right edge of the figure. The larger typed numbers are the associated drift calibration coefficient numbers.

The histograms are plotted in the order of the orthonormalization sequence, in Figure 6-69. This sequence shows the ordering much more dramatically, with the weight of the histograms shifting toward zero from right to left across the figure. In other words, the distributions themselves are rather well behaved. This indicates that the test population of gyros does not contain many wildly different characteristics. There are some drift rate mechanisms that are insignificant on all gyros.

The rms values of the histograms shown in Figure 6-69 are plotted in the same order in Figure 6-70. In this order, each rms value represents the marginal drift rate compensation obtained by adding the associated functional model to the composite drift rate model. In the process of computing these values, the coefficients have been re-ordered so that, at each step, the next functional model was chosen so as to maximize the marginal rms compensation. If the functional models were sufficiently functionally independent, the rms marginal compensation would be a non-increasing function of the number of calibration coefficients. Because this is not the case, there are a few "blips" in the generally decreasing trend of the curve. The interesting feature of this curve is that the last three coefficients contribute 0.0025 deg/hr/axis or less to drift rate compensation on the test population of gyros. The rms coefficient values, their associated functional models and physical interpretations of the five least significant drift model terms are given in Table 6-40. It is interesting to note that two of the three least significant terms are of the same type, i. e. models associated with suspension servo errors at rotor spin frequency and rotor shape. There are no other model terms of this type. The next-to-least significant term is associated with preload charging errors and rotor "pear shape". There are no other terms of this type. Model term No. 30, which was ranked 32nd, is of the same general type as No. 29, which was ranked 2nd. Model term No. 18 is of the same general type as No. 14, which was ranked 6th. Consequently, one should not discard model terms No. 30 and 18, even though they are marginally relatively unimportant, because they represent the same type of physical effect as other model terms which are quite significant.

The model terms of drift model K44W were "re-arranged" functionally into "Model K44WR". This re-arrangement involved only the coefficients numbered 5 through 12 and 14 through 18, and their associated functional models, as given in the formulas below:

$$P'_5 = P_5 + P_9$$

$$P'_6 = P_5 - P_9$$

$$P'_7 = P_{10} + P_{12}$$

$$P'_8 = P_7 + P_{11}$$

# HISTOGRAMS OF K-44W

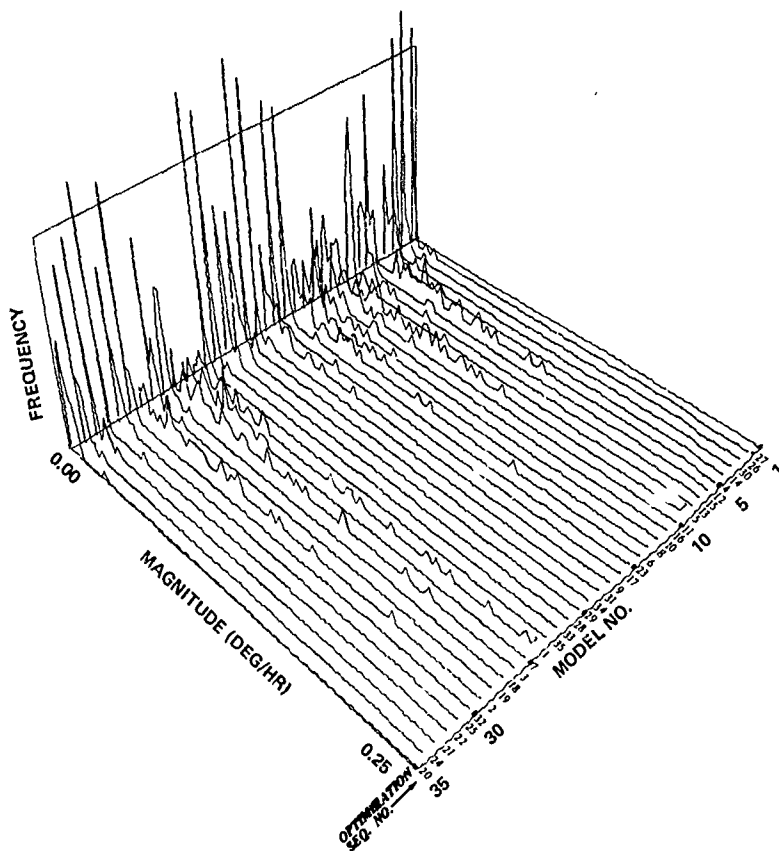


Figure 6-68. Histograms of Marginal Drift Model Coefficients after Orthonormalization of all 35 Models

# HISTOGRAMS OF K-44W

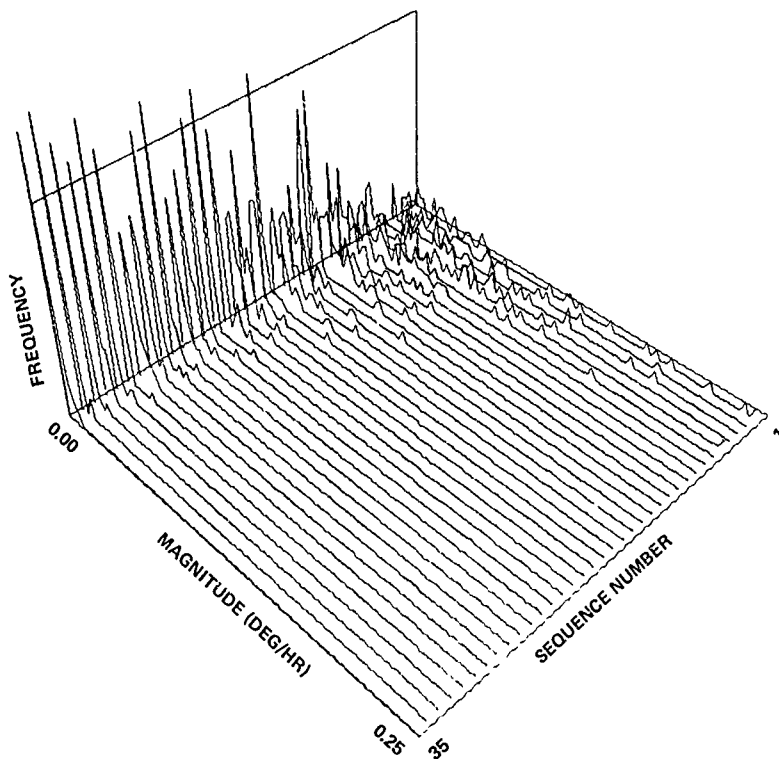


Figure 6-69. Histograms of Marginal Drift Model Coefficients in Sequence of Maximum Marginal Compensation

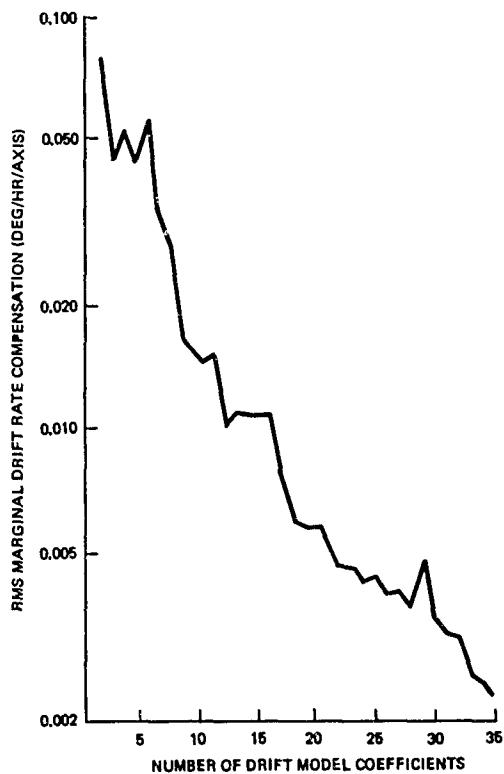


Figure 6-70. Magnitude of rms Marginal Drift Rate Compensation vs Number of Drift Model Coefficient Used



Table 6-40. Five Least Significant Drift Models

Model Coefficient Number	Marginal Compensation (Deg/Hr/Axis)	Model Functional Form ( $F_n$ )*	Physical Interpretation
23	0.0023	$\begin{bmatrix} \gamma_1 \\ \gamma_2 \\ \gamma_3 \end{bmatrix} \times \begin{bmatrix} \gamma_1 \gamma_3^2 \\ 0 \\ \gamma_3 \gamma_1^2 \end{bmatrix}$	Channel-to-channel suspension servo mismatch at rotor frequency and rotor shape harmonics of degree three and type 1. Models No. 22 and 23 are for servo response in quadrature to radial mass unbalance; No. 19 is for servo response in phase with rotor unbalance.
19	0.0024	$\begin{bmatrix} \gamma_2 \gamma_3 \\ \gamma_3 \gamma_1 \\ \gamma_1 \gamma_2 \end{bmatrix}$	
22	0.0025	$\begin{bmatrix} \gamma_1 \\ \gamma_2 \\ \gamma_3 \end{bmatrix} \times \begin{bmatrix} 0 \\ \gamma_2 \gamma_3^2 \\ \gamma_3 \gamma_2^2 \end{bmatrix}$	
30	0.0031		
18	0.0032		

\*The composite drift rate model has the functional form

$$\frac{dY}{dt} = Y \times \sum_{n=1}^{35} P_n F_n(Y, a) + \text{non-drift terms}$$

where  $Y$  is the vector of direction cosines of the rotor spin axis with respect to gyro-fixed coordinates,  $\times$  denotes the vector cross-product,  $P_n$  denotes the nth calibration coefficient and  $F_n$  is a vector-valued function of  $Y$  and  $a$ , the sensed acceleration.

$$P'_9 = P_6 + P_8$$

$$P'_{10} = P_{12} - P_{10}$$

$$P'_{11} = P_7 - P_{11}$$

$$P'_{12} = P_8 - P_6$$

$$P'_{14} = P_{14} + P_{17}$$

$$P'_{15} = P_{14} - P_{17}$$

$$P'_{16} = P_{18}$$

$$P'_{17} = P_{16}$$

$$P'_{18} = P_{15}$$

where the primed (') values represent the re-arranged coefficients and the unprimed values are the original coefficients. This re-arrangement divides the model terms into sequential groups with distinct physical interpretations. The new terms numbered 10 through 12 now model residual magnetic field effects, as distinct from the rotor-oblateness effects modelled by the other states numbered 5 through 9. The new term numbered 14 models the mismatch of the z-channel speed control servo from the x and y channel servos, and number 15 models the mismatch between the x and y channels. The new terms numbered 16 through 18 model 4-space servo effects. The results of performing the orthonormalization technique with respect to this drift model were very enlightening, and resulted in a major improvement in isolation of insignificant states. The resulting ordering of model terms in K44WR is shown in Table 6-41, along with the marginal compensation values. The comparison of marginal compensation curves between K44W and K44WR is given in Figure 6-71. The most remarkable feature of this result is that the antisymmetric part of the matrix of coefficients P5 through P12 in K44W is insignificant compared to the symmetric part. (The antisymmetric part is modelled by the terms numbered 10 through 12 in K44WR. The symmetric part is modelled by the terms numbered 5 through 9 in K44WR.) Also, the fifth model term in K44WR is second only to axial mass unbalance (the 24th model term in K44WR) as a drift mechanism. The term numbered 5 is K44WR models the effect of cavity prolateness and rotor oblateness. This is caused by (1) the rotor operating below its "round" temperature (i. e. the temperature at which anisotropic thermal expansion cancels spin strain) and (2) not enough lapping on the cavity hemisphere "equatorial plane" (i. e. the flat surfaces on which the two halves are joined).

The K44WR model terms gave a sharper separation of least significant terms, and added the complete group of three antisymmetric matrix terms to the six least significant terms of K44W. It was decided to experiment with replacing these six terms with new models. The objective was to find new terms which were even more significant than the ones replaced. Dr. J.C. Pinson had suggested considering more models of the form:

Table 6-41. Ordering of K44WR Models Compared to K44W Models

Marginal Utility Order	K44WR		K44W	
1	24	0.0780	24	0.0780
2	5	0.0727	29	0.0477
3	27	0.0449	26	0.0528
4	26	0.0538	5	0.0449
5	15	0.0333	9	0.0565
6	6	0.0212	14	0.0337
7	7	0.0204	25	0.0276
8	25	0.0183	13	0.0169
9	14	0.0170	17	0.0154
10	13	0.0166	12	0.0146
11	9	0.0143	10	0.0153
12	8	0.0137	6	0.0103
13	4	0.0128	8	0.0112
14	29	0.0083	4	0.0108
15	17	0.0078	7	0.0107
16	3	0.0067	11	0.0107
17	35	0.0061	16	0.0077
18	28	0.0058	27	0.0059
19	34	0.0051	28	0.0058
20	32	0.0046	35	0.0057
21	18	0.0045	33	0.0052
22	31	0.0045	32	0.0046
23	2	0.0043	15	0.0046
24	1	0.0041	34	0.0043
25	33	0.0040	31	0.0044
26	21	0.0039	2	0.0040
27	20	0.0052	1	0.0040
28	16	0.0034	21	0.0038
29	30	0.0031	20	0.0049
30	10	0.0029	3	0.0035
31	11	0.0026	18	0.0032
32	22	0.0025	30	0.0031
33	19	0.0025	22	0.0025
34	23	0.0023	19	0.0024
35	12	0.0019	23	0.0023

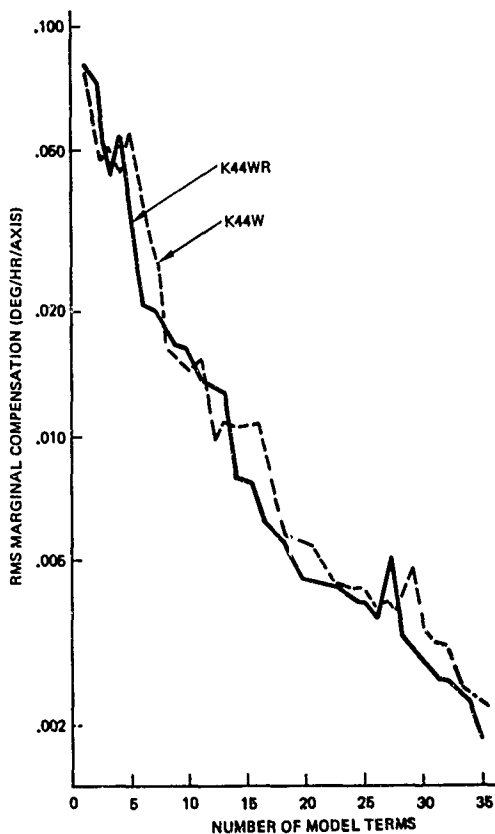


Figure 6-71. Comparison of K44WR and K44W Marginal Compensation

$$\dot{\gamma} = \gamma \times \frac{\partial}{\partial \gamma} (a^* \gamma)^n ; n = 1, 2, 3, \dots$$

where the vector "a" is the sensed acceleration vector. The first term (n=1) of this series is the most significant model (axial mass unbalance), and the second term is somewhat akin to the acceleration-squared model (the fourth term in K44W), which is also quite significant. Therefore, the 10th through the 12 models in K44WR were replaced by three such models. The new functional models are the following:

$$F'_{10} = (a^* \gamma) \begin{bmatrix} a_1 \\ a_2 \\ a_3 \end{bmatrix} = (aa^*) \gamma$$

$$F'_{11} = (a^* \gamma)^2 \begin{bmatrix} a_1 \\ a_2 \\ a_3 \end{bmatrix}$$

$$F'_{12} = (a^* \gamma)^3 \begin{bmatrix} a_1 \\ a_2 \\ a_3 \end{bmatrix}$$

The new functional model  $F'_{10}$  differs from the acceleration-squared model  $F_4$  only slightly, the difference being that  $F'_{10}$  has terms along the main diagonal in the matrix of acceleration-squared terms.

The other classes of experimental models suggested by Dr. Pinson were extensions of the series of acceleration-dependent models represented by the 33rd through 35th terms in K44W, and the "interelectrode groove" models of the 25th through 31st terms in K44W. In the latter case, the suggested extensions were to allow for non-uniform groove effects, which were to be modelled by allowing additional degrees of freedom on the three model components. Therefore, the 19th term of K44R was replaced by the following functional model:

$$F'_{19} = \begin{bmatrix} a_1 (2\gamma_1^2 - 1)^4 \\ a_2 (2\gamma_2^2 - 1)^4 \\ a_3 (2\gamma_3^2 - 1)^4 \end{bmatrix}$$

and the 22nd and 23rd terms were replaced by the new functional models:

$$F'_{22} = \begin{bmatrix} 0 \\ 0 \\ \gamma_3(2\gamma_3^2 - 1)^3 \end{bmatrix}$$

$$F'_{23} = \begin{bmatrix} \gamma_1(2\gamma_1^2 - 1)^3 \\ -\gamma_2(2\gamma_2^2 - 1)^3 \\ 0 \end{bmatrix}$$

The results of the marginal utility ordering with respect to this model (called "K45") are listed in Table 6-42 where they are compared to K44WR. These results show that four of the "replacement" models for the six least significant terms in K44WR remain in the six least significant places. The only worthwhile replacement models appear to be the following functional forms:

$$F'_{11} = (a^* \gamma)^2 \begin{bmatrix} a_1 \\ a_2 \\ a_3 \end{bmatrix}$$

$$F'_{22} = \begin{bmatrix} 0 \\ 0 \\ \gamma_3(2\gamma_3^2 - 1)^3 \end{bmatrix}$$

Another characteristic that has been invariant over the last three models (K44W, K44WR and K45) has been the noticeable increase in marginal compensation that occurs after the 20th or 21st model term is picked as the marginally most significant. This suggests that some common linear combination of these models is prevalent in all the drift data. Upon examination of the functional form of these models, it appears that their sum is equivalent to the functional model:

$$F''_S = \begin{bmatrix} 0 \\ 0 \\ \gamma_3(2\gamma_3^2 - 1)^3 \end{bmatrix}$$

(plus lower-order terms equivalent to  $F'_5$ ) and their difference is equivalent to the functional model:

Table 6-42. Ordering of K45 Models Compared to K44WR

Marginal Utility Order	K45		K44WR	
1	24	0.0780	24	0.0780
2	5	0.0727	5	0.0727
3	27	0.0449	27	0.0449
4	26	0.0538	26	0.0538
5	15	0.0333	15	0.0333
6	6	0.0212	6	0.0212
7	7	0.0204	7	0.0204
8	25	0.0183	25	0.0183
9	14	0.0170	14	0.0170
10	13	0.0166	13	0.0166
11	11	0.0146	9	0.0143
12	9	0.0154	8	0.0137
13	8	0.0150	4	0.0128
14	4	0.0098	29	0.0083
15	17	0.0078	17	0.0078
16	29	0.0074	3	0.0067
17	28	0.0060	35	0.0061
18	22	0.0055	25	0.0058
19	33	0.0050	34	0.0051
20	18	0.0048	32	0.0046
21	2	0.0046	18	0.0045
22	31	0.0043	31	0.0045
23	34	0.0042	2	0.0043
24	1	0.0037	1	0.0041
25	35	0.0035	33	0.0040
26	16	0.0034	21	0.0039
27	30	0.0032	20	0.0052
28	21	0.0031	16	0.0034
29	20	0.0047	30	0.0031
30	32	0.0029	10	0.0029
31	12	0.0028	11	0.0026
32	10	0.0025	22	0.0026
33	3	0.0023	19	0.0025
34	19	0.0020	23	0.0023
35	23	0.0020	12	0.0019

$$F_d'' = \begin{bmatrix} \gamma_1(2\gamma_1^2 - 1) \\ -\gamma_2(2\gamma_2^2 - 1) \\ 0 \end{bmatrix}$$

(plus lower-order terms equivalent to  $F'_6$ ). In order to see whether one of these "re-arranged" model terms was the favored form, the evaluation program was run once again with these equivalent model terms in the 20th and 21st locations. At the same time, the following changes were made in other model terms:

$$F_{20}'' = \begin{bmatrix} 0 \\ 0 \\ \gamma_3(2\gamma_3^2 - 1) \end{bmatrix}$$

$$F_{21}'' = \begin{bmatrix} \gamma_1(2\gamma_1^2 - 1) \\ -\gamma_2(2\gamma_2^2 - 1) \\ 0 \end{bmatrix}$$

$$F_{22}'' = \begin{bmatrix} 0 \\ 0 \\ -\gamma_2(2\gamma_2^2 - 1)^3 \end{bmatrix}$$

$$F_{23}'' = \begin{bmatrix} 0 \\ 0 \\ \gamma_3(2\gamma_3^2 - 1)^4 \end{bmatrix}$$

$$F_{19}'' = \begin{bmatrix} 0 \\ 0 \\ \gamma_3(2\gamma_3^2 - 1)^2 \end{bmatrix}$$



$$F_{10}'' = \begin{bmatrix} 0 \\ 0 \\ \gamma_3(2\gamma_3^2 - 1)^5 \end{bmatrix}$$

$$F_{11}'' = (a^*\gamma)^2 \begin{bmatrix} a_1 \\ a_2 \\ a_3 \end{bmatrix}$$

$$F_{12}'' = \begin{bmatrix} 0 \\ 0 \\ \gamma_3(2\gamma_3^2 - 1)^6 \end{bmatrix}$$

These changes retain the only two new model forms in K45 which were significant, and continue the expansion of the model in the direction started with the 22nd term of K45. That is, to give the model independent freedom in fitting a coefficient to the third component of the terms numbered 25 through 31 in all the models. There are only enough "spare" terms to carry this process from 25 through 30, at this point. There is a physical interpretation of this process. These terms model the effects of interelectrode grooves and zonal spherical harmonics of rotor shape of even degree greater than 2. Allowing independent coefficients on the third components of these functional model terms is equivalent to allowing the "equatorial" interelectrode groove (i.e. the one in the plane along which the cavity halves are joined) to have a different effective width. Due to the method of manufacture, there is probable cause for this to be true.

The drift model incorporating the above changes was designated "K46". The functional form of this composite model is given in Table 6-43. The results of the marginal utility ordering of this model with respect to the data bank are summarized in Table 6-44.

These results show the hoped-for separation of the 20th and 21st terms. They also show significant presence of the "equatorial groove" effect: K46 model terms numbered 10 and 19, which model this effect, are all in the most significant 16 terms. Also, the new 20th term is much more significant than the 21st, and this 20th term also belongs to the class of models influenced by equatorial grooves. It is probable that this effect can be modelled by a single parameter, nominally unity, which multiplies the third component of all the interelectrode groove models. This type of model is non-linear from the standpoint of calibration, but we have had reasonable success with nonlinear models in angle compensation.

Table 6-43 Functional Formulas for Drift Model K46

$F(\gamma, a)$	$=$	$\begin{bmatrix} p_1 \\ p_2 \\ p_3 \end{bmatrix} + p_4 \begin{bmatrix} 0 & a_1 a_2 & a_1 a_3 \\ a_1 a_2 & 0 & a_2 a_3 \\ a_1 a_3 & a_2 a_3 & 0 \end{bmatrix} \begin{bmatrix} \gamma_1 \\ \gamma_2 \\ \gamma_3 \end{bmatrix} + \begin{bmatrix} p_5 + p_6 & p_9 & p_8 \\ p_9 & p_5 - p_6 & p_7 \\ p_8 & p_7 & 0 \end{bmatrix} \begin{bmatrix} \gamma_1 \\ \gamma_2 \\ \gamma_3 \end{bmatrix} + \begin{bmatrix} p_{14} + p_{15} & p_{18} \\ p_{18} & p_{14} - p_{15} \\ p_{17} & p_{16} \end{bmatrix} \begin{bmatrix} \gamma_1 \\ \gamma_2 \\ \gamma_3 \end{bmatrix}$
	$+$	$p_{13} \begin{bmatrix} \gamma_1 \\ \gamma_2 \\ \gamma_3 \end{bmatrix} + p_{21} \begin{bmatrix} \gamma_1 (2\gamma_1^2 - 1) \\ -\gamma_2 (2\gamma_2^2 - 1) \\ 0 \end{bmatrix} + p_{11} (a_1 \gamma_1 + a_2 \gamma_2 + a_3 \gamma_3)^2 \begin{bmatrix} a_1 \\ a_2 \\ a_3 \end{bmatrix}$
	$+$	$\begin{bmatrix} 0 \\ \gamma_3 (2\gamma_3^2 - 1) \left\{ p_{20} + (2\gamma_3^2 - 1) \left\{ p_{19} + (2\gamma_3^2 - 1) \left\{ p_{22} + (2\gamma_3^2 - 1) \left\{ p_{23} + (2\gamma_3^2 - 1) \left\{ p_{10} + (2\gamma_3^2 - 1) p_{12} \right\} \right\} \right\} \right\} \right\} \right\} \right\} \right\}$
	$+$	$\begin{bmatrix} \gamma_3 (2\gamma_1^2 - 1) \left\{ p_{25} + (2\gamma_1^2 - 1) \left\{ p_{26} + 2\gamma_1^2 - 1 \right\} \left\{ p_{27} + (2\gamma_1^2 - 1) \left\{ p_{28} + (2\gamma_1^2 - 1) \left\{ p_{29} + (2\gamma_1^2 - 1) \left\{ p_{30} + (2\gamma_1^2 - 1) p_{31} \right\} \right\} \right\} \right\} \right\} \right\} \right\}$
	$+$	$\gamma_3 (2\gamma_2^2 - 1) \left\{ p_{25} + (2\gamma_2^2 - 1) \left\{ p_{26} + 2\gamma_2^2 - 1 \right\} \left\{ p_{27} + (2\gamma_2^2 - 1) \left\{ p_{28} + (2\gamma_2^2 - 1) \left\{ p_{29} + (2\gamma_2^2 - 1) \left\{ p_{30} + (2\gamma_2^2 - 1) p_{31} \right\} \right\} \right\} \right\} \right\} \right\}$
	$+$	$\gamma_3 (2\gamma_3^2 - 1) \left\{ p_{25} + (2\gamma_3^2 - 1) \left\{ p_{26} + 2\gamma_3^2 - 1 \right\} \left\{ p_{27} + (2\gamma_3^2 - 1) \left\{ p_{28} + (2\gamma_3^2 - 1) \left\{ p_{29} + (2\gamma_3^2 - 1) \left\{ p_{30} + (2\gamma_3^2 - 1) p_{31} \right\} \right\} \right\} \right\} \right\} \right\}$
	$+$	$\begin{bmatrix} a_1 \left\{ p_{24} + (2\gamma_1^2 - 1) \left\{ p_{33} + (2\gamma_1^2 - 1) \left\{ p_{34} + (2\gamma_1^2 - 1) p_{35} \right\} \right\} \right\} \right\} \\ a_2 \left\{ p_{24} + (2\gamma_2^2 - 1) \left\{ p_{33} + (2\gamma_2^2 - 1) \left\{ p_{34} + (2\gamma_2^2 - 1) p_{35} \right\} \right\} \right\} \right\} \\ a_3 \left\{ p_{24} + (2\gamma_3^2 - 1) \left\{ p_{33} + (2\gamma_3^2 - 1) \left\{ p_{34} + (2\gamma_3^2 - 1) p_{35} \right\} \right\} \right\} \right\} \end{bmatrix} \begin{bmatrix} \gamma_1 \\ \gamma_2 \\ \gamma_3 \end{bmatrix}$
	$+$	$p_{32} \begin{bmatrix} a_3 & 0 & a_1 \\ a_2 & a_1 & 0 \end{bmatrix} \begin{bmatrix} \gamma_1 \\ \gamma_2 \\ \gamma_3 \end{bmatrix}$

NOTE: SEE TABLE 6-39 FOR EXPLANATION OF TERMS

Table 6-44. Marginal Utility Ordering of Model K46

Order	Term No.	RMS Marginal Compensation (Deg/Hr/Axis)
1	23	0.078026
2	5*	0.072652
3	27	0.044900
4	26	0.053753
5	15*	0.033332
6	6*	0.021171
7	7*	0.029370
8	25	0.018263
9	14*	0.016975
10	13	0.016636
11	11**	0.014630
12	9*	0.015423
13	8*	0.014971
14	4	0.009814
15	19**	0.007761
16	10**	0.007762
17	17*	0.007669
18	29	0.006246
19	28	0.005226
20	33	0.004678
21	2	0.004603
22	18	0.004546
23	20*	0.004255
24	31	0.004340
25	34	0.003477
26	16*	0.003363
27	1	0.003380
28	35	0.003127
29	32	0.002966
30	30	0.002820
31	3	0.002571
32	21*	0.001983
33	23**	0.001523
34	12**	0.001475
35	22**	0.001478
*Functional forms re-arranged from K44W model		
**New functional forms added to drift model		

#### 6.3.4.2.4 Conclusions

There are 6 terms which can be eliminated from the drift model K44W without significant impact upon drift compensation, based upon the results from a test population of 33 combinations of gyros and electronics. This leaves only 28 of the original 34 terms related to gyro drift (The 13th term models test stand misalignment, in so far as it affects the data.)

There is an apparent acceleration-cubed sensitive drift rate effect. The functional form of the associated model term is such that it would not be distinguished from drifts due to axial mass unbalance on calibration data sampled when the rotor spin axis is polar. Therefore, drift calibration data must be taken with the spin axis at different angles from the local vertical. In particular, polar calibrations alone will not suffice.

The drift model terms for the effects due to interelectrode grooves appear to reflect a different effective width of the equatorial groove, along which the suspension cavity halves are joined. It is likely that this can be accomplished by adding one non-linear model term. This and the model term from the preceding paragraph bring the total number of recommended drift compensation coefficients to 30. (Down from 34).

The above conclusions were derived by an approach which essentially determines how much of a "bite" each model term takes from the data. This approach does not measure how much is left, however. Consequently, we are not in a position, at this time, to draw any conclusions relating to how these model changes will impact residual drift rates. These changes will be made in the drift rate model.

### 6.3.5 Develop Hardware and Software Improvements

#### 6.3.5.1 Introduction and Summary

MESGA development efforts, both experimental and analytical, were initiated prior to 1 April 1974 under company funding.

MESA tests on Test Station IV (T/S IV) were begun in March 1974. These tests were planned to obtain "rough order of magnitude" MESGA sensitivities. Based on Phase 1A test data, and theoretical analyses, it was not expected that the T/S IV tests would demonstrate required performance. It was expected that these tests would support MESGA requirements definition, and the analytical and modelling studies. Both expectations have been borne out by the test data taken on T/S IV.

MESGA error sensitivities were calculated prior to 1 April 1974. These theoretical analyses show that tight tolerances on system parameters are required to limit acceleration sensing errors. The theoretical error sensitivities were in reasonable agreement with test data taken on T/S IV.

Based on the results of the error sensitivity analyses, and the T/S IV test data, it was concluded that there was essentially no chance of meeting performance with a pulse amplitude modulation (PAM) suspension servo mechanism. It was decided that a pulsewidth modulation (PWM) suspension servo would have to be developed for MESGA, and that MESGA development would be restricted to the eight-plate gyro. Requirements implied by MESGA were derived and incorporated in the specification for the eight-plate gyro subassembly (GSA). A MESGA test plan for GSA tests was also developed after the specification for the GSA and GSA Test Station had been completed.

MESGA test data had been obtained on T/S IV (using PAM) for four different gyros by 8 July 1974. Test data for three of the gyros (124, 96 and 102) were generally comparable. The fourth gyro (68) exhibited an anomalously large transient of about 0.1 g which appeared to be some form of "two-state" phenomenon. The test data for gyros 124, 96 and 102 tended to imply that required improvement factors in system parameter stabilities ranged from about 10 to 1000, even assuming FWM. The required improvement factors were larger for PAM than for PWM. It was concluded as a result of these comparisons (test data, present capability estimates and calculated requirements) that MESGA testing on T/S IV should be discontinued. It was recommended that TASC review the analyses and test data to obtain an independent evaluation of the MESGA development effort. The review by TASC was in general agreement with the results obtained by Autonetics which were documented in C74-455.3/201 (Phase 2A status report for the time period 30 June through 3 August 1974) and are presented in Para 6.3.5.4 below.

A summary of the GSA test results is presented in Para 6.3.5.5.

#### 6.3.5.2 MESGA Error Sensitivities

MESGA error sensitivities for most of the major error sources were calculated prior to 1 April 1974. These preliminary calculations were updated and expanded to include additional error sources during the Phase 2A program. These theoretical calculations show that tight tolerances on system parameter stabilities are required

to limit acceleration sensing errors. These analyses also show that tolerances are tighter for PAM than for PWM, because the preload for PAM is higher. This results in a larger bias error for a given error source. It was assumed in these early analyses that the effective PWM preload would be  $1/12$  times the PAM preload. This implies PWM allows larger tolerances on bias error sources by a factor of 12. For example, if bias error is limited to  $25 \mu\text{g}$ , then variation in preload or nominal charge must be limited to less than 4.6 PPM for PAM and to less than 58 PPM for PWM. Similarly, requirements for rotor miscentering are less than  $1.9 \times 10^{-9}$  inch for PAM and less than  $23 \times 10^{-9}$  inch for PWM. As a point of comparison, the ball miscentering repeatability requirement for the N57A system is  $200 \times 10^{-9}$  inch.

The allowable error mechanism variations for MESGA are listed in Table 6-45. The assumptions made in deriving these allowable variations are as follows:

1. Required bias repeatability is  $25 \mu\text{g}$
2. Required scale factor repeatability is 50 PPM
3. A calibration residual of  $30 \mu\text{g}$  is assumed obtainable
4. The forcing duty cycle is  $40 \mu\text{sec}$  maximum for PWM (out of  $40 \mu\text{sec}$  interval)
5. The forcing level is 2.6 g per electrode
6. The preloads for PAM and PWM are:  
 $2.6 \text{ g}$  per electrode for PAM  
 $0.22 \text{ g}$  per electrode for PWM
7. Charge is reversed every  $50 \mu\text{sec}$
8. Each error mechanism is allowed to give maximum error

The last assumption, (8), implies no safety margins exist in the calculated sensitivities. However, even with this assumption, the tolerances are very tight.

The theoretical error sensitivity analyses imply there is essentially no chance of meeting MESGA performance requirements with PAM. Thus it was decided that a PWM suspension servo would have to be developed for MESGA. It had been also decided that MESGA development would be restricted to the eight-plate gyro, because there are sources of acceleration sensing errors in the four-plate gyro which are not present in the eight-plate gyro.

In Table 6-45 each individual error source has been allowed to give the maximum allowed acceleration sensing error ( $25 \mu\text{g}$  for bias or 50 PPM for scale factor). It was decided that a better comparison of present capability versus MESGA requirements would result if the individual error sources were budgeted so as to yield an RSS error equal to the allowed acceleration sensing error. This budget was prepared by allotting RMS errors of  $10 \mu\text{g}$  bias and 20 PPM in scale factor to the digitizer electronics, and then treating the remaining errors as independent errors of equal RMS magnitude. Error budgets were calculated for PAM and PWM, as given in Tables 6-46, and 6-47.

Table 6-45. Allowable Variations for MESGA

Critical Parameter	Pulse Amplitude Modulation		Pulsewidth Modulation	
	Bias	Scale Factor	Bias	Scale Factor
Variation in Nominal or Preload Charge	936 PPM/x 4.6 PPM	- 50 PPM	11200 PPM/x 58 PPM	- 25 PPM
Variation in Rotor Miscentering	$1.87 \times 10^{-9}$ in.	-	$2.25 \times 10^{-8}$ in.	$3.33 \times 10^{-8}$ in.
Gap Measurement Capability	$1.87 \times 10^{-9}$ in.	-	$2.25 \times 10^{-8}$ in.	$3.33 \times 10^{-8}$ in.
Charge on Rotor Measurement Capability	$15000 \text{ PPM} / \frac{Q_B}{Q} \times$	-	$15000 \text{ PPM} / \frac{Q_B}{Q} \times$	-
Variation in Stray Capacitance	10200 PPM/x 51 PPM	550 PPM	638 PPM	275 PPM
Propagation Delay Variation Between Channels	$0.39 \times 10^{-9}$ sec	$0.44 \times 10^{-9}$ sec	$0.39 \times 10^{-9}$ sec	-
Rise Time Variations Between Channels	$0.78 \times 10^{-9}$	-	-	-
Temperature Variations	-	$0.88 \times 10^{-9}$ sec	$0.78 \times 10^{-9}$ sec	-
Case	$0.38^\circ\text{F}$	$0.2^\circ\text{F}$	$4.6^\circ\text{F}$	$0.1^\circ\text{F}$
Rotor	$0.19^\circ\text{F}$	$0.1^\circ\text{F}$	$2.3^\circ\text{F}$	$0.05^\circ\text{F}$

x is displacement of rotor center of mass from the center of the envelope, in microinches  
 $Q_B$  and  $Q$  are ball charge and nominal electrode charge respectively, in coulombs

Table 6-46. MESGA Error Budget (PAM)

Critical Parameter	Requirements		Remarks
	Bias**	Scale Factor	
Variation in Nominal or Preload Charge	280 PPM* 1.4 PPM	21 PPM	$Q_B$ is Ball Charge $Q$ is Nominal Plate Charge, Both in Coul  Nominal Stray Capacity to Ground Assumed to be 5 PF
Variation in Rotor Miscentering	$0.56 \times 10^{-9}$ in.	-	
Gap Measurement Capability	$0.56 \times 10^{-9}$ in.	-	
Charge on Rotor Measurement Capability	$4500 \text{ PPM} / \frac{Q_B}{Q}$		
Variation in Stray Capacity	15 PPM	225 PPM	
Propagation Delay			
Variation Between Channels	$0.12 \times 10^{-9}$ sec	$0.55 \times 10^{-9}$ sec	
Rise Time Variations Between Channels	$0.24 \times 10^{-9}$ sec	$1.1 \times 10^{-9}$ sec	
Temperature Variations			
Case	$0.12^\circ\text{F}$	$0.08^\circ\text{F}$	
Rotor	$0.06^\circ\text{F}$	$0.04^\circ\text{F}$	
Digitizer Electronics	10 $\mu\text{g}$	20 PPM	Assumed Values
RSS	25 $\mu\text{g}$	50 PPM	MICRON System Req.

\*Per  $\mu$ inch displacement of rotor center of mass from envelope center (larger displacement implies a smaller tolerance)

\*\*Assumes a preload of 2.6 G per electrode



Table 6-47. MESGA Error Budget (PWM)

Requirements			
Critical Parameter	Bias**	Scale Factor	Remarks
Variation in Nominal or Preload Charge	3360 PPM* 17.4 PPM	10.3 PPM	
Variation in Rotor Miscentering	$6.75 \times 10^{-9}$ in.	$1.37 \times 10^{-8}$ in.	
Gap Measurement Capability	$6.75 \times 10^{-9}$ in.	$1.37 \times 10^{-8}$ in.	
Charge on Rotor Measurement Capability	$4500 \text{ PPM} / \frac{Q_B}{Q}$		$Q_B$ is ball charge Q nominal plate charge, both in Coulombs
Variation in Stray Capacity	191 PPM	113 PPM	Nominal stray capacity to ground assumed to be 5 PF
Propagation Delay Variation between Channels	$0.12 \times 10^{-9}$ sec		
Rise Time Variations Between Channels	$0.24 \times 10^{-9}$ sec		
Temperature Variations			
Case	1.4°F	0.04°F	
Rotor	0.7°F	0.02°F	
Digitizer Electronics	10 $\mu$ g	20 PPM	Assumed values
RSS	25 $\mu$ g	50 PPM	MICRON System required

\*Per  $\mu$  inch displacement of rotor center of mass from envelope center (larger displacement implies a smaller tolerance).

\*\*Assumes a preload of 0.22 G per electrode.

### 6.3.5.3 MESGA Tests on Test Station IV

MESGA tests on T/S IV were started in March 1974 and continued through 8 July 1974. A series of tests were planned including calibration (angle, drift acceleration), gamma sensitivity and stability tests. These tests were planned to obtain "rough order of magnitude" MESGA sensitivities. It was not expected that the T/S IV tests would demonstrate required performance. The MESGA sensitivity calculations and previous test results obtained in Phase 1A both implied that the T/S IV data would be nowhere near the required values of 25  $\mu\text{g}$  in bias and 50 PPM in scale factor. However, it was expected that the T/S IV tests would support MESGA requirements definition and the MESGA analytical and modelling studies. These different expectations have been borne out by the test data taken on T/S IV.

Figure 6-72 shows the test setup for the T/S IV MESGA tests. Table 6-48 gives a summary of the MESGA tests on T/S IV.

Calibration and gamma sensitivity tests were performed over the periods 29 March - 1 April 1974 and 3 May - 6 May 1974. Gyro No. 124 was used in the first test sequence, gyro No. 96 in the second.

In the 29 March - 1 April test about 20 hours of data were taken with the RSA polar and about 24 hours with the RSA cross-polar. The cross-polar data exhibited sizable first, second, third, and fifth harmonics, (see Figure 6-73). The third harmonic (8 hour period) was the largest and was of similar magnitude ( $\sim 800 \mu\text{g}$ ) in x, y, and z, indicating a bias effect since the z axis was vertical in this test. The second and fifth harmonics were of roughly comparable magnitude in the three axes, about 500  $\mu\text{g}$  and 200  $\mu\text{g}$  respectively. The first harmonic was about 5 times larger in z than in x and y, indicating a scale factor effect. Higher harmonics (6th through 16th) were observed in the data, however, it is thought that these were probably due to very low frequency "noise." An RMS noise level of about 100  $\mu\text{g}$  with a 1 hour correlation time was found to exist in the data. Figures 6-74, 6-75, and 6-76 are plots of the acceleration residuals (measured minus true values) versus sample. Each sample corresponds to an average over 33 minutes, so that about 20 hours of stability data are plotted. Note the transient shifts of up to 1000  $\mu\text{g}$  which occur over a time period of about one to two hours. Trends are present in the data, but these appear to be smaller than the transient shifts.

The RSA cross-polar data for gyro 124 exhibited trends of 0.4  $\mu\text{g}/\text{min}$  in x, 1.2  $\mu\text{g}/\text{min}$  in y and 2.6  $\mu\text{g}/\text{min}$  in z. The trend in Z over 24 hours was about 3700  $\mu\text{g}$ . The RMS residuals for the cross-polar data (after removal of a bias, a ramp or trend and harmonics through the 10th) were about 100  $\mu\text{g}$  per axis. A correlation time of about 50 minutes would be required to explain the 6th through 16th harmonics, assuming 100  $\mu\text{g}$  noise.

The acceleration sensing calibration model had 12 states (9 scale factor and misalignment terms and 3 bias terms). However, the model was varied for the 3 May - 6 May test data to determine how much reduction in calibration residuals could be achieved with more complex models. A second harmonic scale factor effect was predicted by theoretical analyses. Thus these additional scale factor terms involving "gamma-squared" were included in the model and it was found that the calibration residuals were reduced by about 10 percent. However, this also resulted

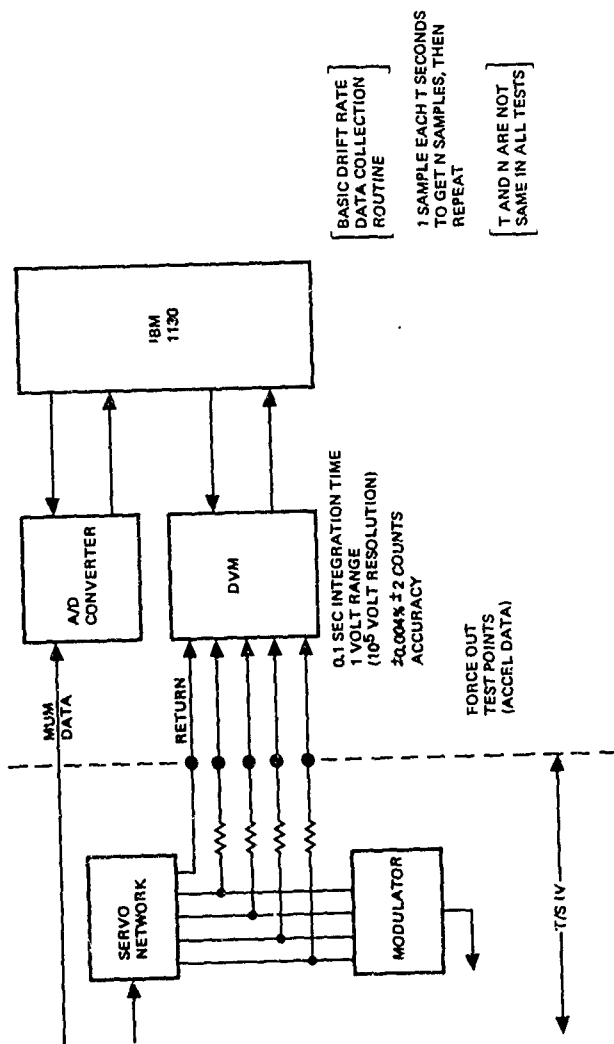


Figure 6-72. MESGA Test Setup, T/S IV

Table 6-48. MESGA T/S IV Test Summary

Date (1974)	Gyro	Tests
3/20	68	Noise 100 $\mu$ g RMS/axis, 4 Point "Calibration".
3/29-4/1	124	Two 13-Point Calibrations (3/29, 4/1), One 51-Point Calibration (During Drift Calibration), RSA Polar 20 Hours, RSA Cross-Polar ~24 hours.
5/3-5/6	96	Two 13-Point Calibrations (5/3, 5/6), Two RSA Polar 24-Hour Runs.
6/27-7/1	68	No Acceleration Calibration, RSA Polar 16.5 Hours 6/27-6/28, RSA Polar 3.5 Hours 7/1.
7/3-7/8	102	Three 13-Point Calibrations (7/3, 7/5, 7/8), Three-1 Hour Noise Tests, RSA Polar 5 Hours on 7/3, RSA Polar 40 Hours 7/3-7/5, RSA Polar 56 Hours 7/5-7/8.
<b>TOTALS</b> 7 13-Point Calibrations - 3 Different Gyros 1 51-Point Calibration 189 Hours RSA Polar - 4 Different Gyros 24 Hours RSA Cross-Polar - 1 Gyro		

in larger apparent shifts in scale factors than those observed using only the 12 state model. The shifts refer to acceleration calibrations performed on 3 May and on 6 May. The third harmonic observed in the 29 March - 1 April test (gyro No. 124) was found to depend upon the  $Y_x Y_y Y_z$ . The 3 May calibration data were also compensated using 3 additional bias states containing this product. The improvement in residuals was negligible (for this different gyro, No. 96).

It was concluded as a result of these experiments that the existing noise level (~100  $\mu$ g RMS with a 1 hour correlation time) was effecting the attempts to calibrate out gamma dependent terms. Thus it was decided to run a dummy load test. In this test the gyro was replaced by 8 capacitors and "acceleration" was measured as before. The RMS noise and noise correlation time were found to be about 350  $\mu$ g and 15 seconds respectively in the dummy load test.

A special test was performed to determine whether or not the instrumentation interface was contributing to the noise. It was found that the noise due to the instrumentation was about 10  $\mu$ g rms.

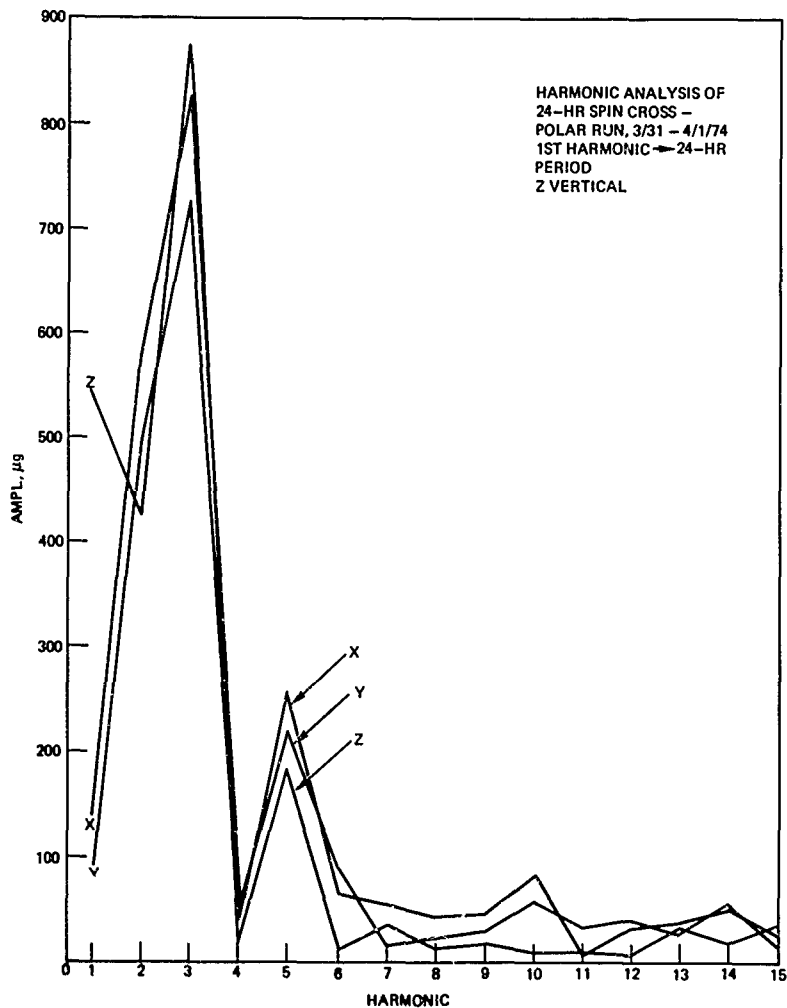


Figure 6-73. Gyro 124 Harmonic Analysis

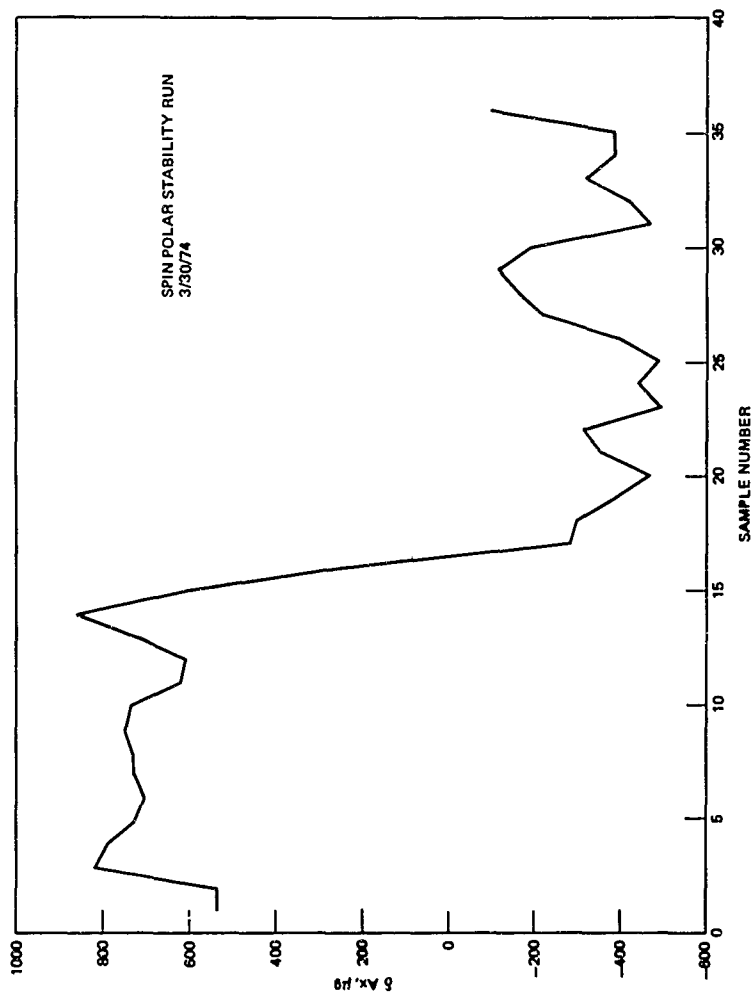


Figure 6-74. Gyro X-Axis Stability Data

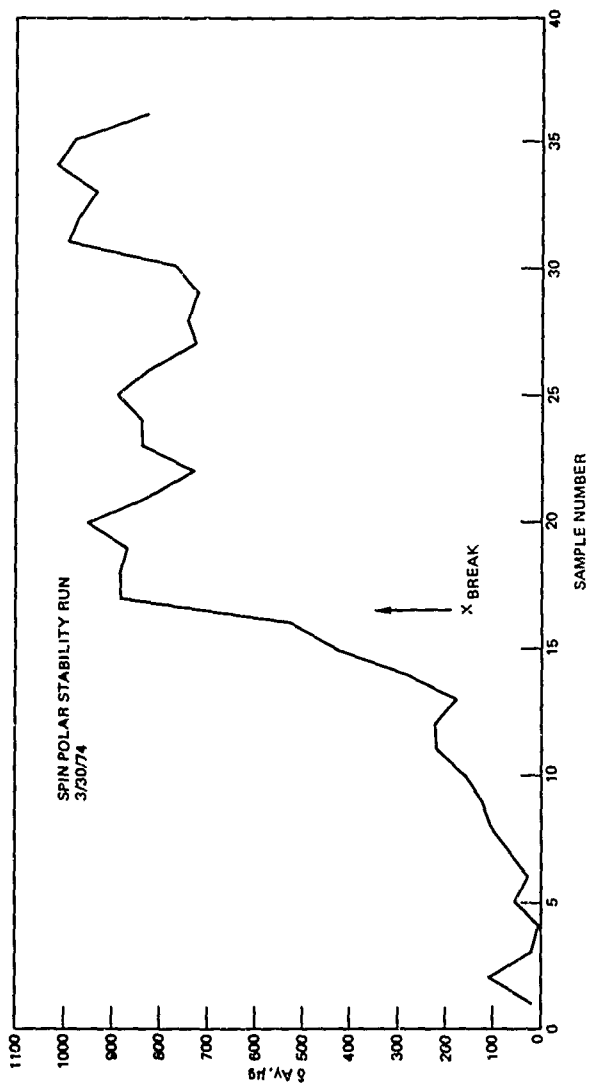


Figure 6-75. Gyro Y-Axis Stability Data

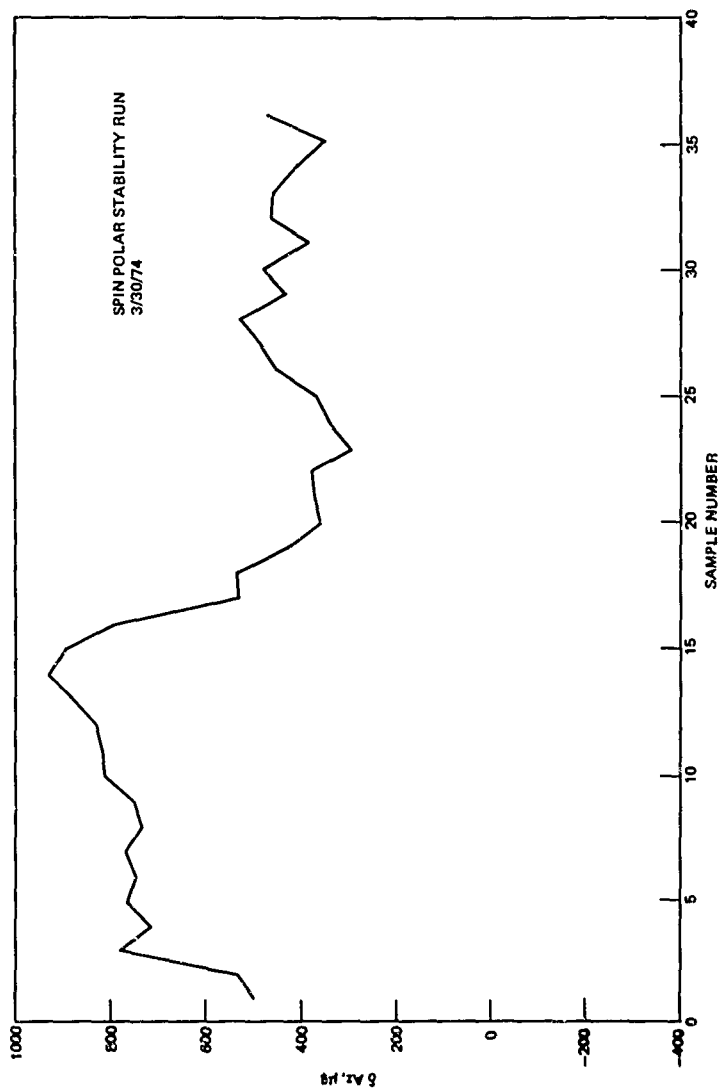


Figure 6-76. Gyro 124 Z-Axis Stability Data



Calibration residuals obtained in the 29 March - 1 April test ranged from about 700  $\mu\text{g}$  to 1000  $\mu\text{g}$ . Three calibrations were performed: 13 point RSA polar, 51 point RSA polar and 13 point RSA cross polar. The smallest residual was obtained for the 13 point RSA cross-polar data, the largest for the 51 point RSA polar data. These calibrations all used the 12 state model.

Calibration residuals obtained in the 3 May - 6 May test ranged from about 600  $\mu\text{g}$  to 2000  $\mu\text{g}$ . The calibration models used were the 12 state, the 12 state plus 3 SF(Y) and 12 state plus 3 B(Y) models as discussed above. The calibration residuals ranged from about 1750  $\mu\text{g}$  to 2000  $\mu\text{g}$  for the 13 point calibration on 3 May. The calibration residuals were about 600  $\mu\text{g}$  and 650  $\mu\text{g}$  for the 13 point calibration on 6 May. The cause of this large difference in residuals is not known. It is known that the difference is not a result of table angle errors. This was determined by processing the calibration data through a special program designed to detect table angle errors in EMA calibration.

Calibration data for gyro 96 are summarized in Table 6-49. It is clear from the table that bias and scale factor shifts are larger for the SF(Y) + 12 state model than for the 12 state model, as noted. The table also shows that use of the SF(Y) + 12 state model results in about a 10 percent decrease in calibration residuals, also as noted above.

Table 6-49. Gyro 96 Calibration Data

Scale Factor and Bias Deltas			
Change in Scale Factor or Bias from May 3 to May 6 Calibrations (Gyro 96)			
$\delta\text{SF}_x$	$\approx +0.6\%$	$= 6000 \text{ PPM}$	} SF(Y) + 12 state
$\delta\text{SF}_y$	$\approx -1\%$	$= -10,000 \text{ PPM}$	
$\delta\text{SF}_z$	$\approx +0.3\%$	$= +3000 \text{ PPM}$	
$\delta b_x$	$\approx -1500 \mu\text{g}$		
$\delta b_y$	$\approx +450 \mu\text{g}$		
$\delta b_z$	$\approx -1000 \mu\text{g}$		
$\delta\text{SF}_x$	$\approx +0.12\%$	$= 1200 \text{ PPM}$	} 12 state
$\delta\text{SF}_y$	$\approx -0.14\%$	$= -1400 \text{ PPM}$	
$\delta\text{SF}_z$	$\approx -0.33\%$	$= -3300 \text{ PPM}$	
$\delta b_x$	$= -870 \mu\text{g}$		
$\delta b_y$	$= -1200 \mu\text{g}$		
$\delta b_z$	$= -140 \mu\text{g}$		
Calibration Residuals:	May 3	1978 $\mu\text{g}$ RMS/Axis	12 state
		1976 $\mu\text{g}$ RMS/Axis	12 state + B(Y)
		1746 $\mu\text{g}$ RMS/Axis	12 state + SF(Y)
	May 6	645 $\mu\text{g}$ RMS/Axis	12 state
		602 $\mu\text{g}$ RMS/Axis	12 state + SF(Y)

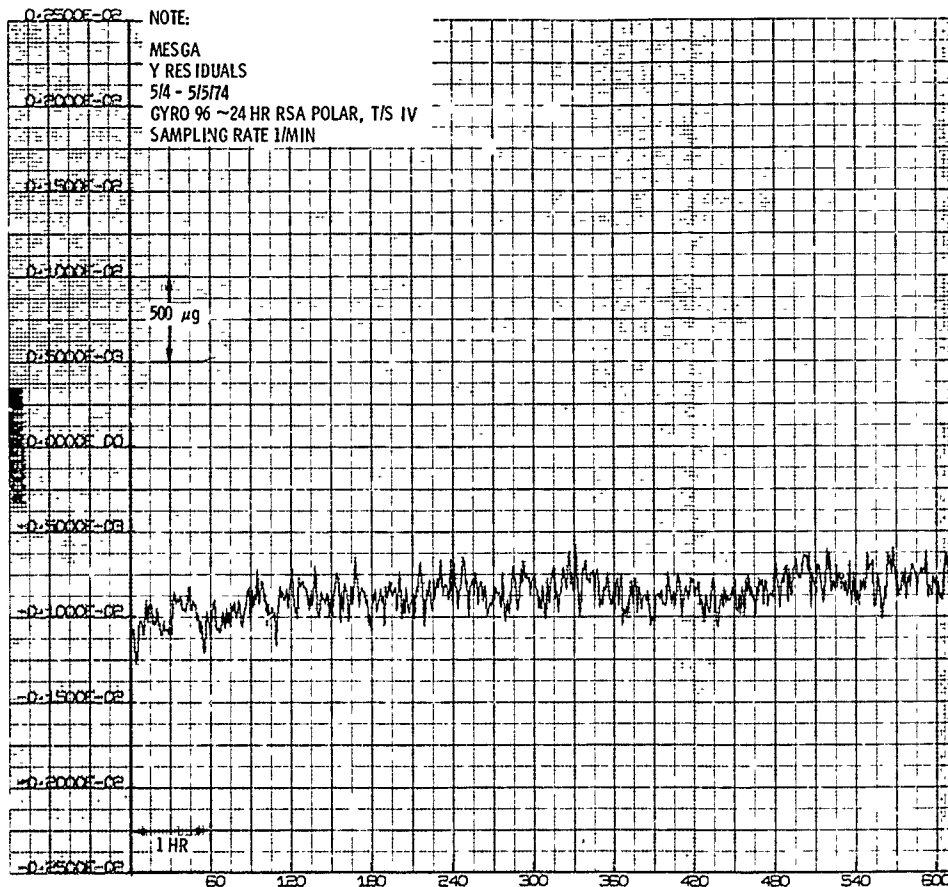
Figures 6-77 and 6-78 are plots of y-axis residuals for gyro 96, taken during the 24 hour RSA polar test on May 4 - May 5, 1974. Bias and trend are obviously present in the data shown in Figure 6-77. These same data are plotted in Figure 6-78, but with bias and trend removed. The RMS noise after removal of bias and trend was 112  $\mu$ g. An autocorrelation function was calculated and is shown in Figure 6-79. The correlation time was estimated to be about 60 minutes and the corresponding RMS noise value was about 90  $\mu$ g.

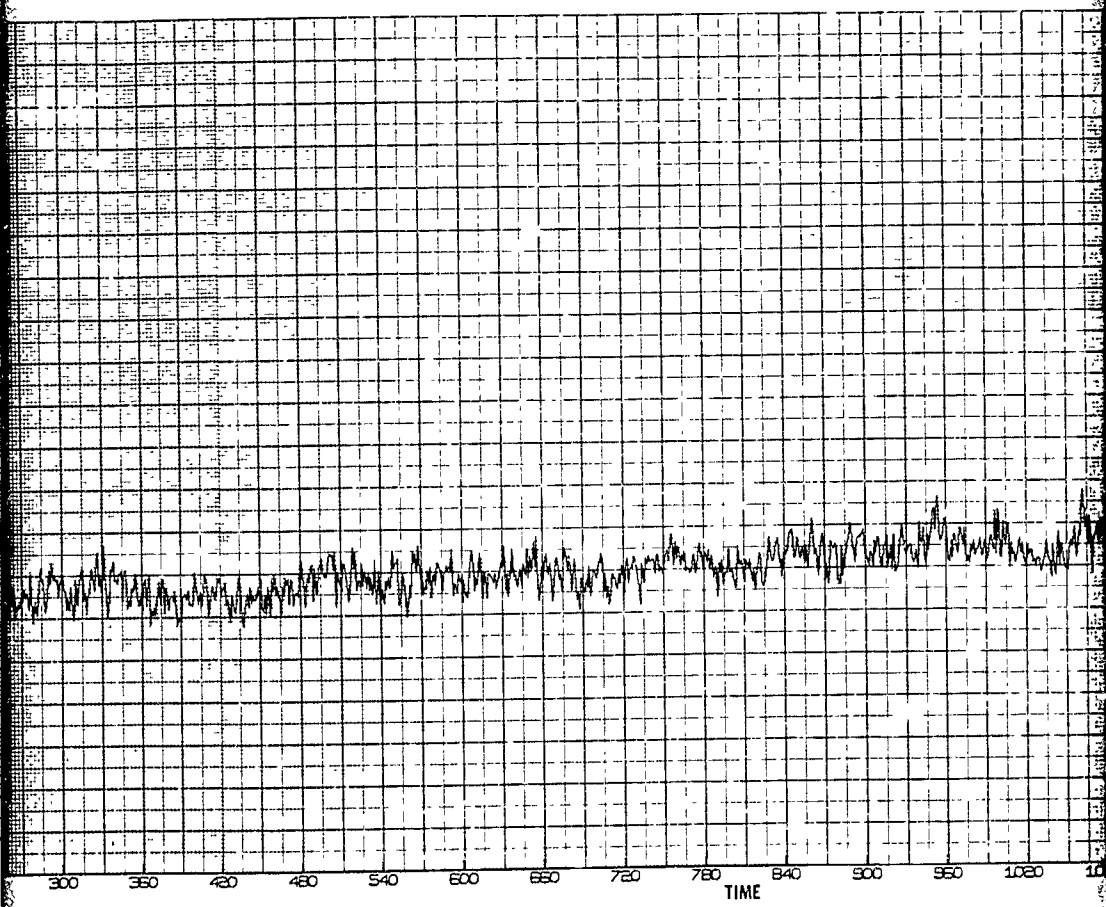
A test was run on gyro 68 on 27 and 28 June 1974 while the gyro was stabilizing in temperature. Large transients were observed in all three axes at the same time. The transient occurred in one sampling interval (in a 1 minute time period), and was largest in magnitude (greater than 0.1 g) of any such observed in the MESGA tests. Figures 6-80, 6-81, and 6-82 are plots of the gyro 68 data showing the transient. Note that the noise is much larger before than after the transient (on the order of 7000  $\mu$ g peak-to-peak versus 300  $\mu$ g peak-to-peak). Figures 6-83 and 6-84 are plots of the noise before and after the transient for the X axis.

The extremely large transient observed in the gyro 68 data was certainly anomalous. This occurrence was the only one of its type in the MESGA tests. The cause of this transient was never isolated. It does appear that the electronics and gyro can operate in two different states, since gyro 68 operated about 10 hours in the abnormally noisy state before suddenly changing to the quieter state.

MESGA tests were performed over the time period 3 July 1974 through 8 July 1974 on Test Station IV. Gyro 102 was used in these tests. One of the objectives of these tests was to obtain data on MESGA calibration repeatability over a time period of several days. This was suggested by the calibration repeatability problem noted in the Gyro 96 tests (3 May 1974 to 6 May 1974). The calibration repeatability in the Gyro 102 tests was comparable with that obtained earlier on Gyro 124 (29 March 1974 to 1 April 1974). Another objective of the Gyro 102 tests was to obtain more data on the trends and transients ("two state" phenomena) observed in previous long term tests. Trends and transient effects in the Gyro 102 test data were generally comparable to those noted in tests on Gyros 124 and 96.

Calibration data for gyro 102 are summarized in Table 6-50. The calibration repeatability is probably as good as can be expected based on earlier test data and analyses. The calibration repeatability problem observed for gyro 96 did not occur for gyro 102. It is of interest to note that the ratio of Z to X scale factors is 0.95 for gyro 102. The corresponding ratio for gyro 124 was  $\frac{3.62}{3.65} \approx 0.99$ . Gyro 102 has a "Z-hole", while gyro 124 does not. This effect (different scale factor ratio) was predicted by theoretical analyses. However, the absence of the Z-hole in gyro 124 is not enough to explain a change from 0.95 to 0.99 in the scale factor ratio. Differences between equatorial grooves which intersect at the Z axis can also result in differences between Z and X scale factors. The largest bias for gyro 102 was about 0.05 g. The largest bias observed in the MESGA tests on the T/S IV was that for gyro 68, which was about 0.17 g.





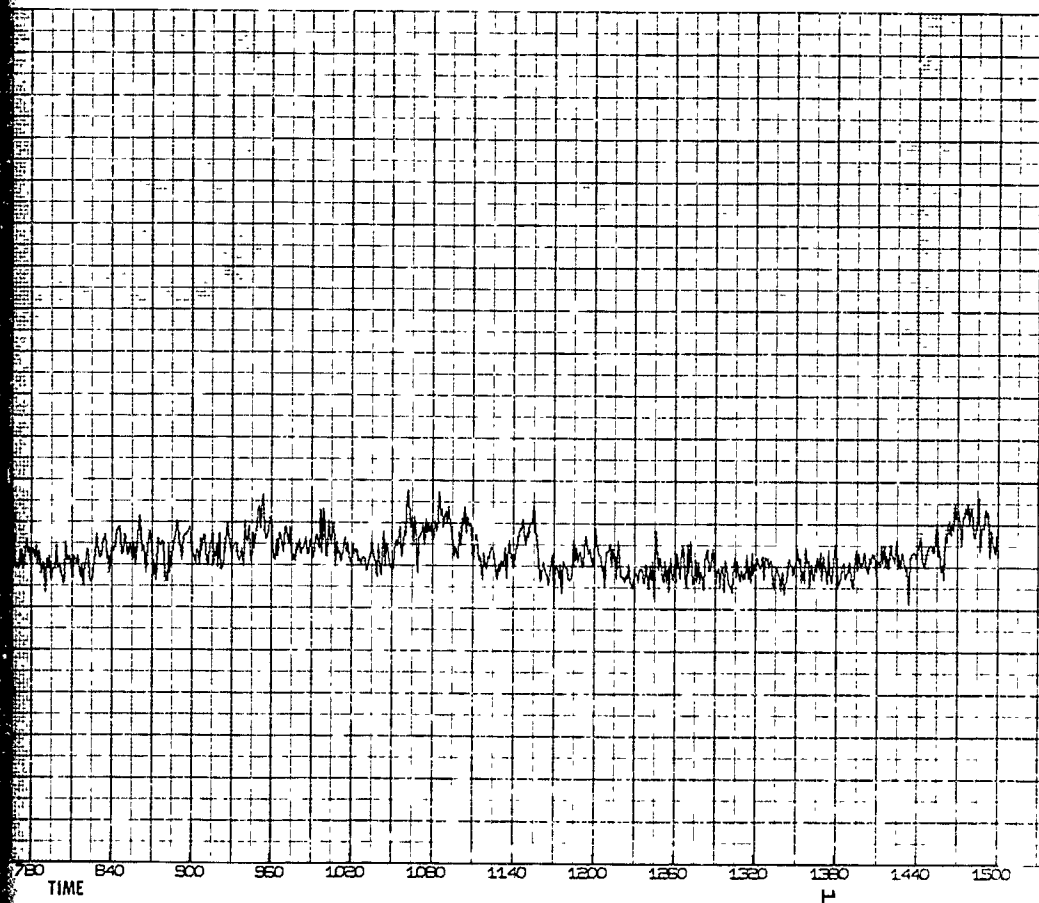
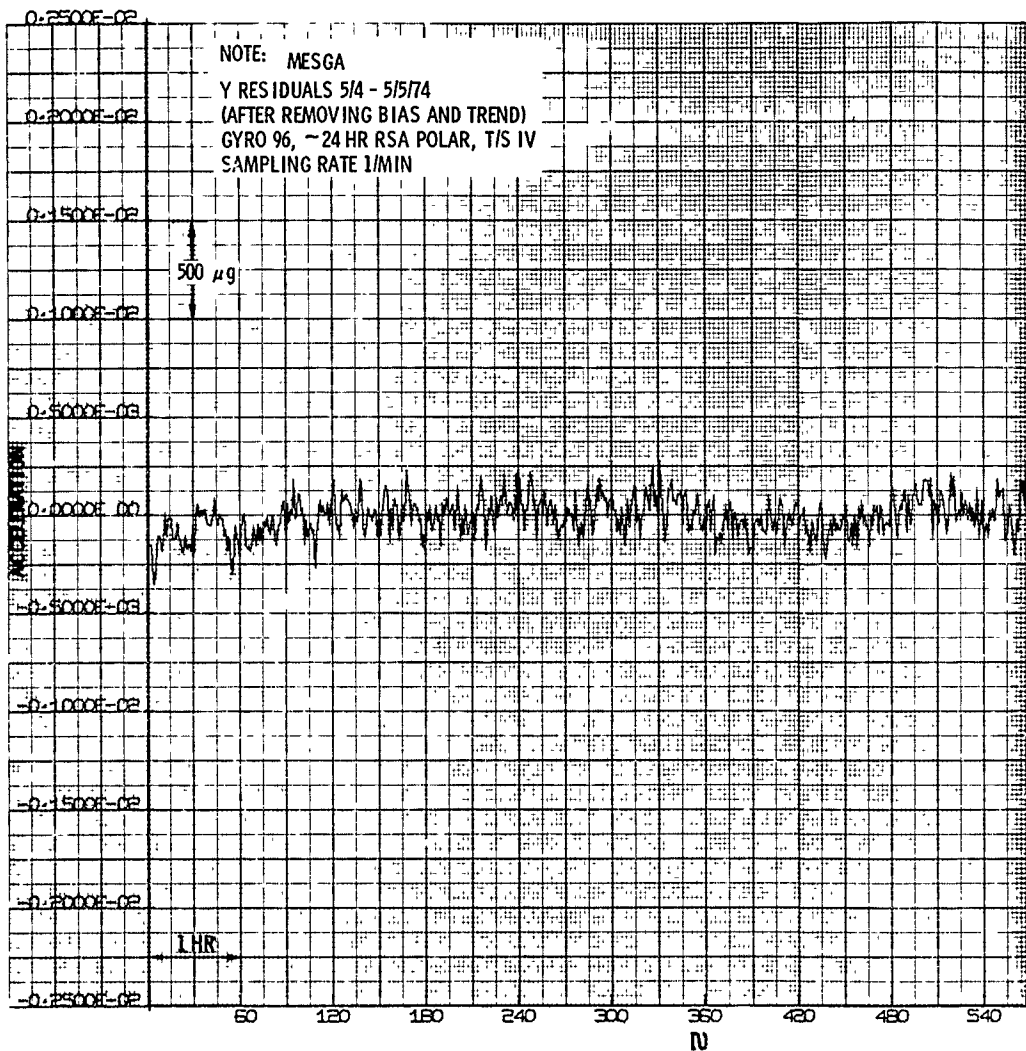
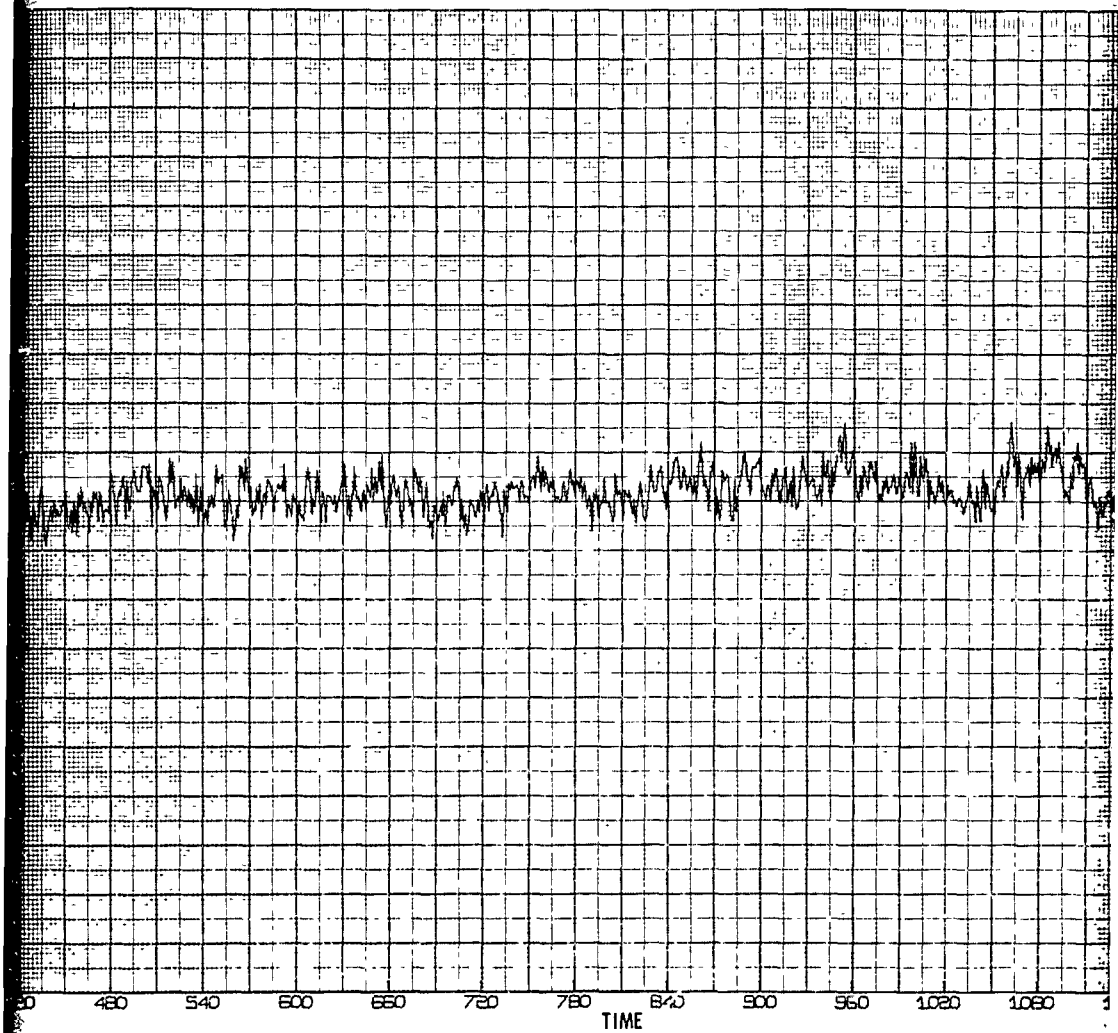


Figure 6-77. Gyro 96 Y Residuals





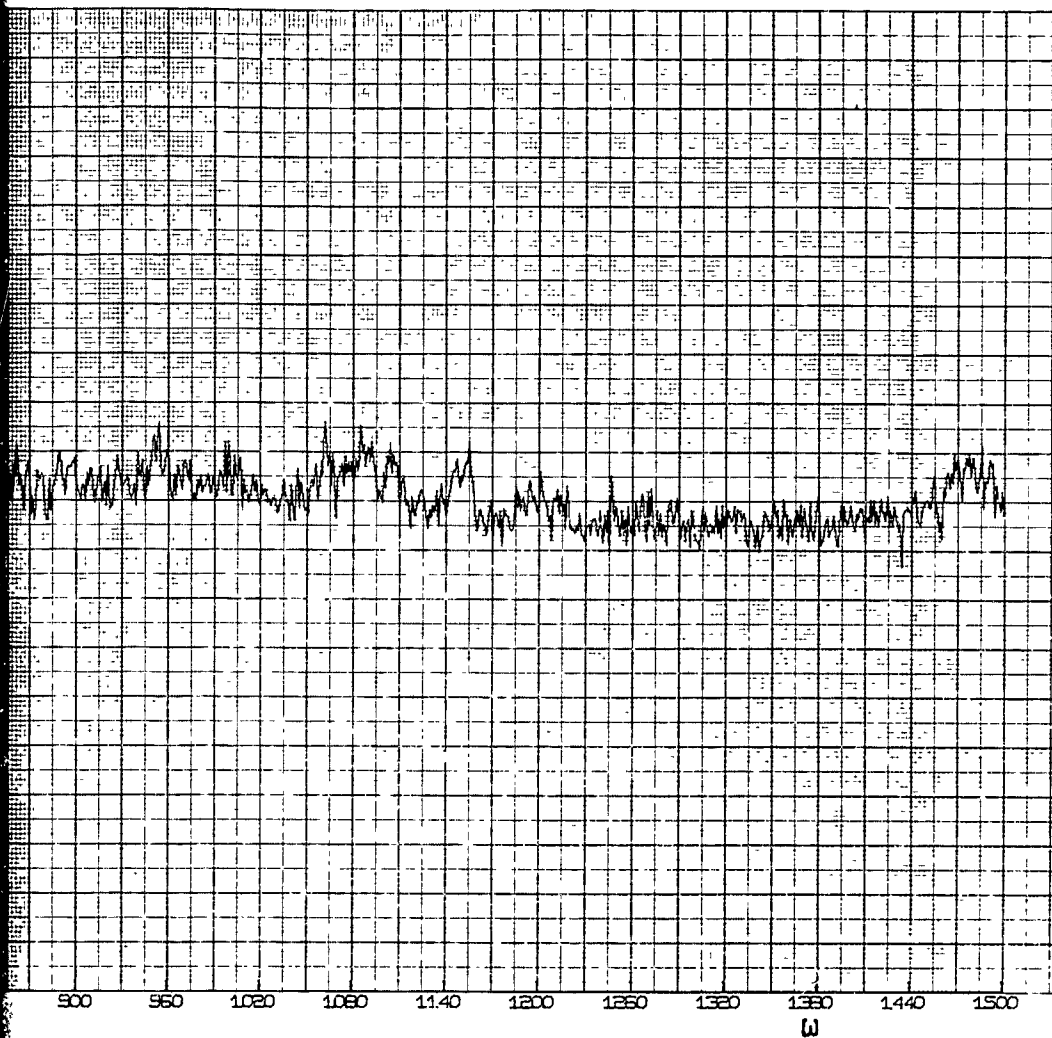
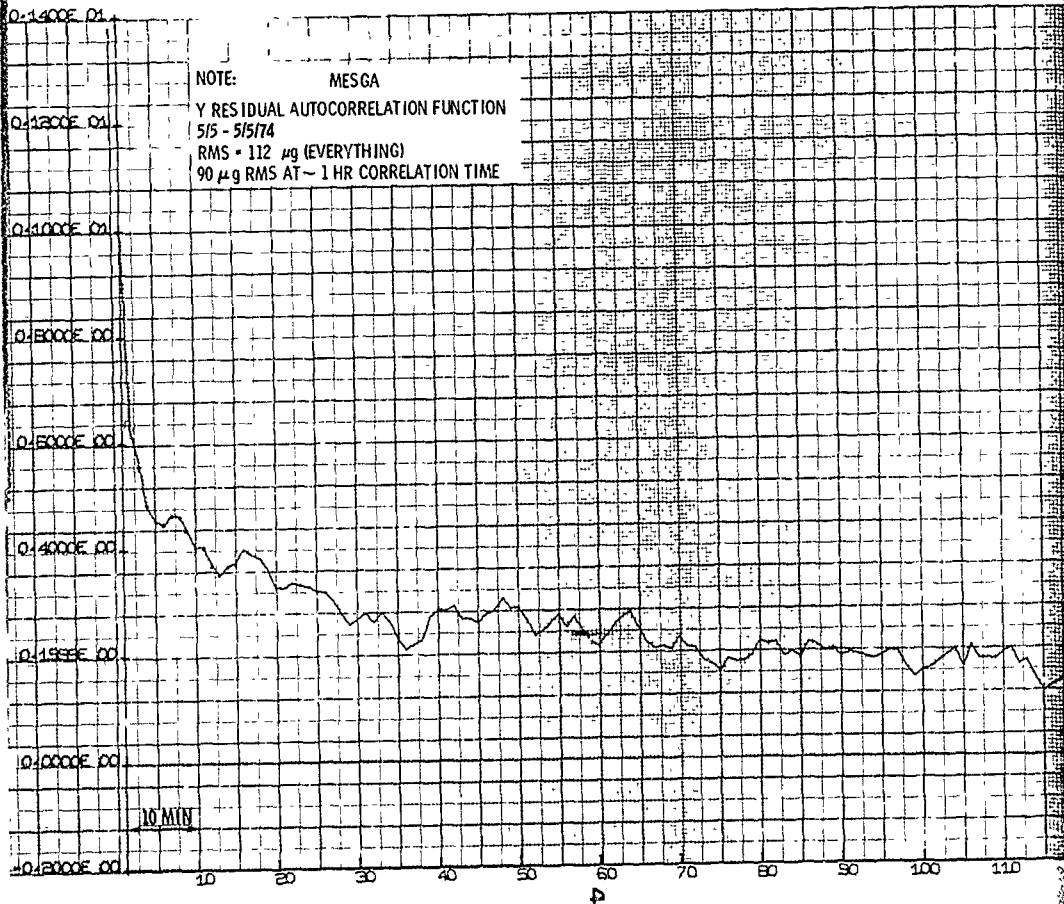
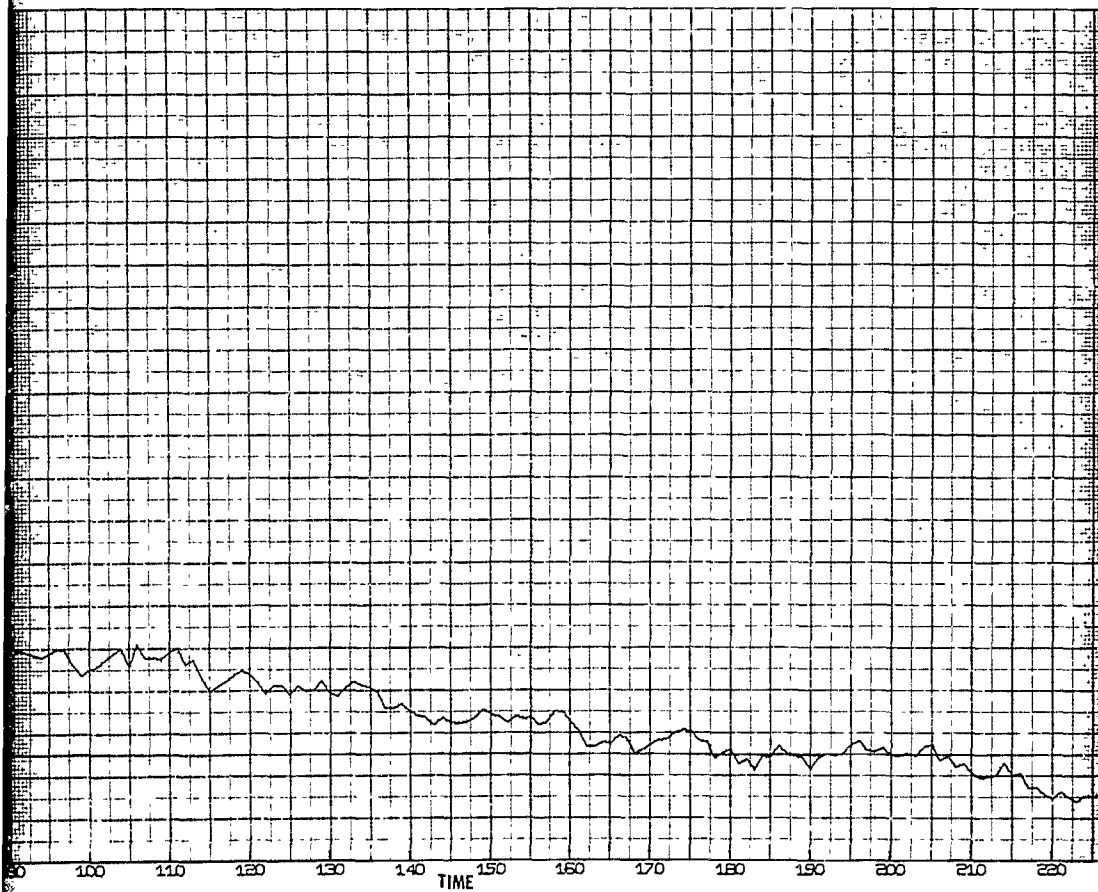


Figure 6-78. Gyro 96 Y Residuals (Bias and Trend Removed)







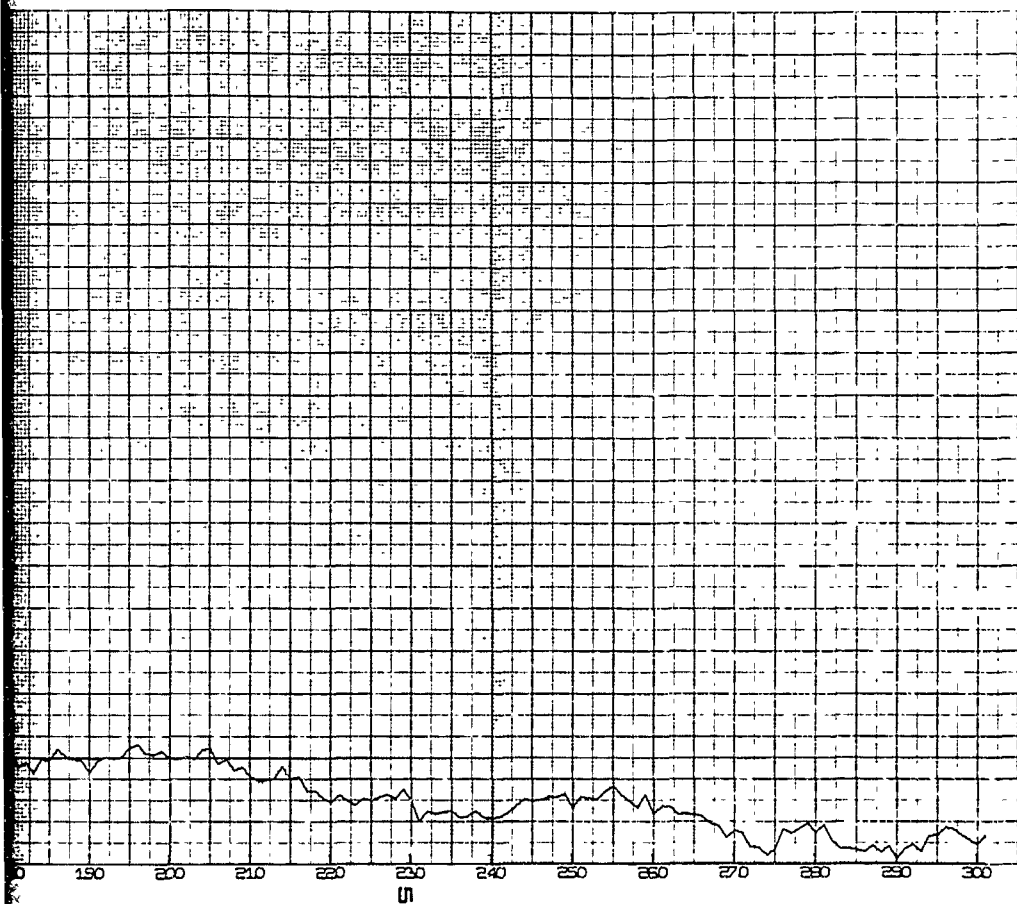
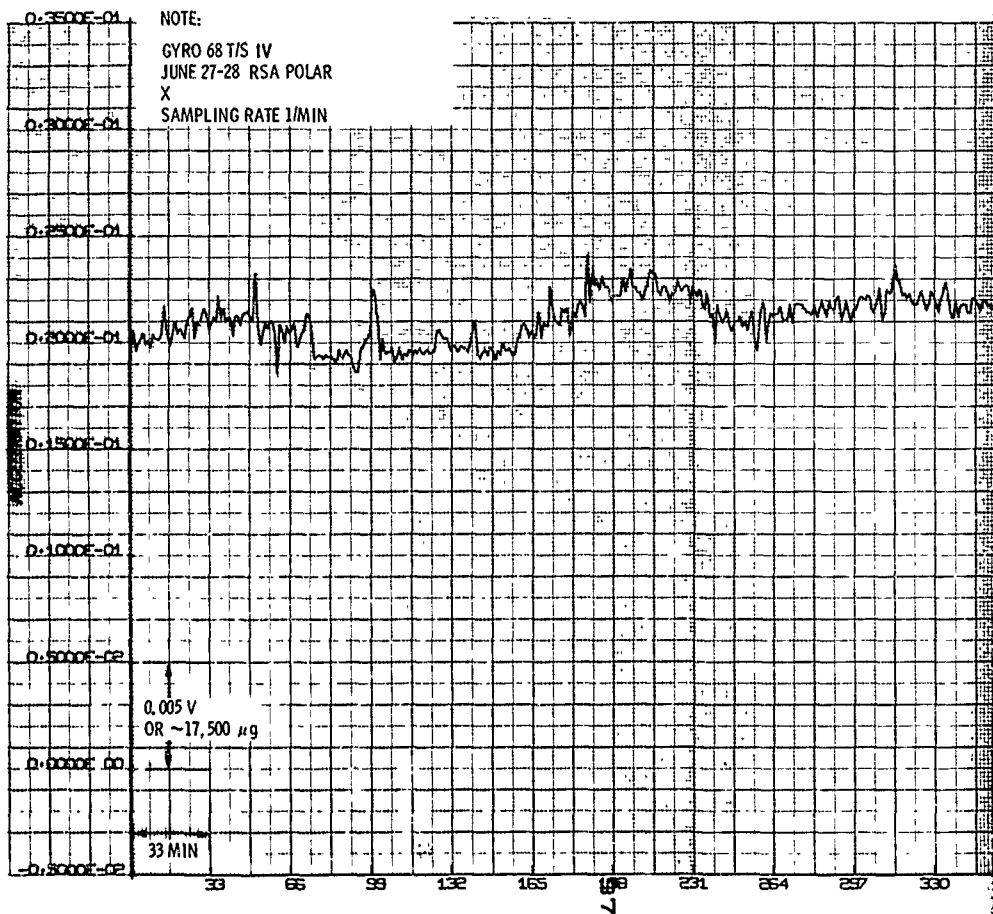
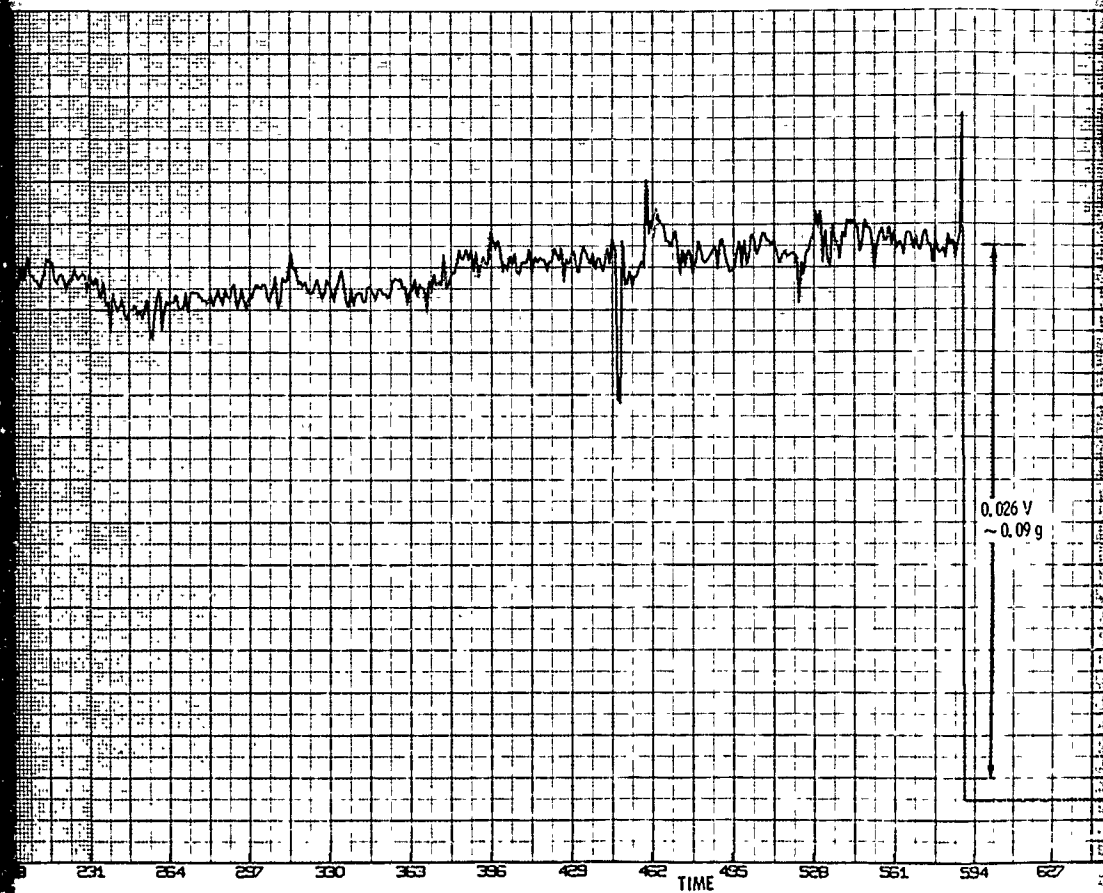


Figure 6-79. Gyro 96 Y Residual Autocorrelation Function





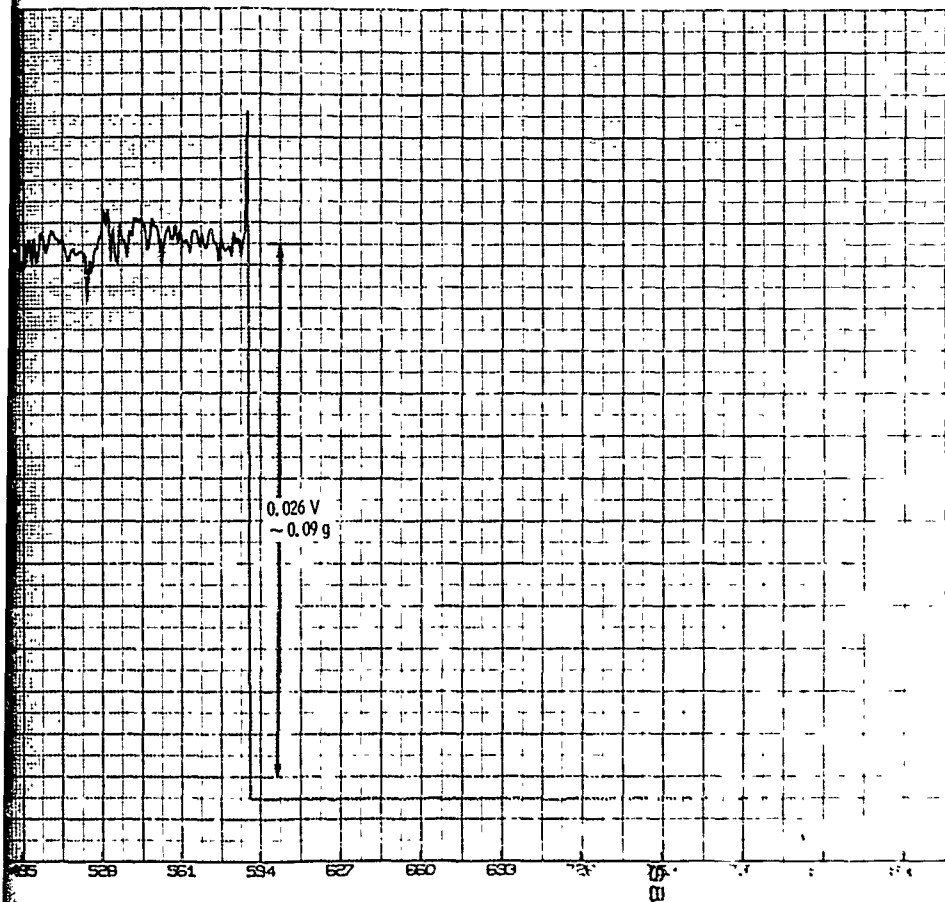


Figure 6-80. Gyro 68 X Axis Transient

COMPLUT

-0.2000E-01

NOTE:

GYRO 68 T/S IV

JUNE 27-28

Y

-0.2500E-01

-0.3000E-01

-0.3500E-01

-0.4000E-01

-0.4500E-01

-0.5000E-01

-0.5500E-01

-0.6000E-01

0.005 V  
OR ~17,500  $\mu$ g

33 MIN

33

66

99

132

165

198

231

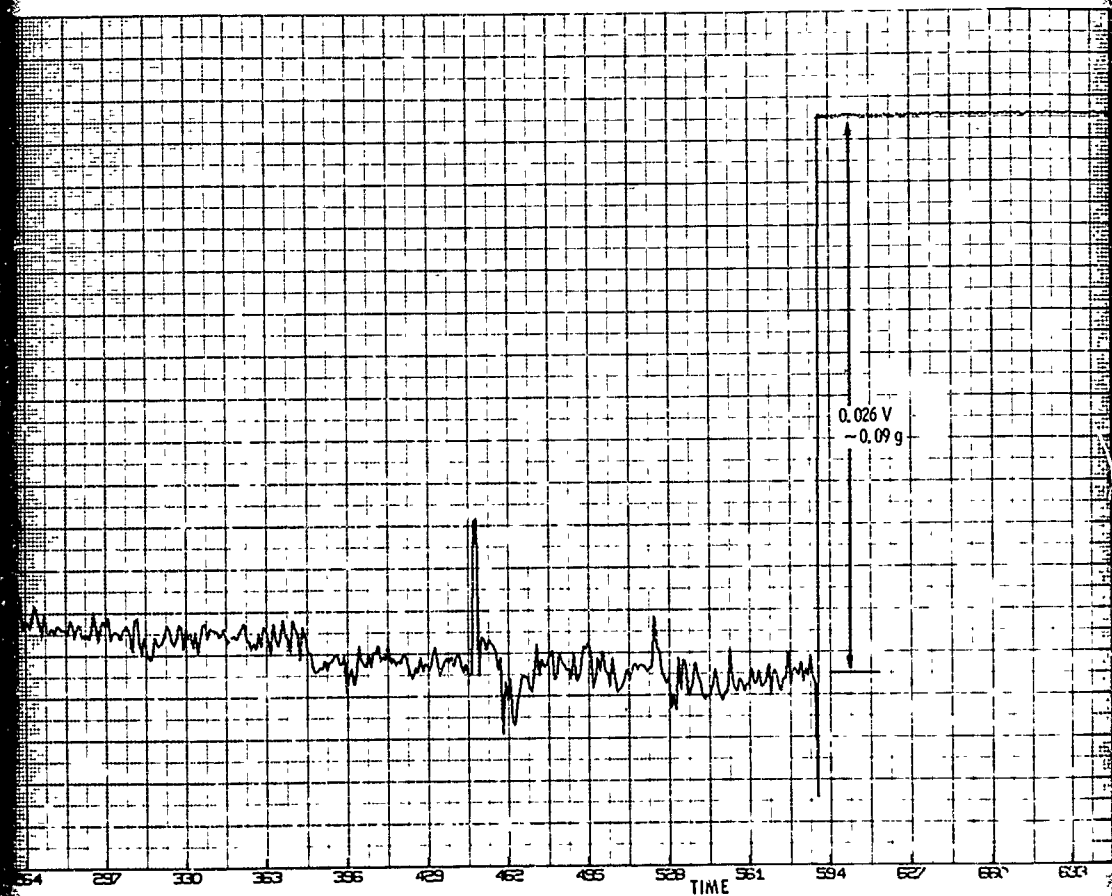
264

297

330

363

U





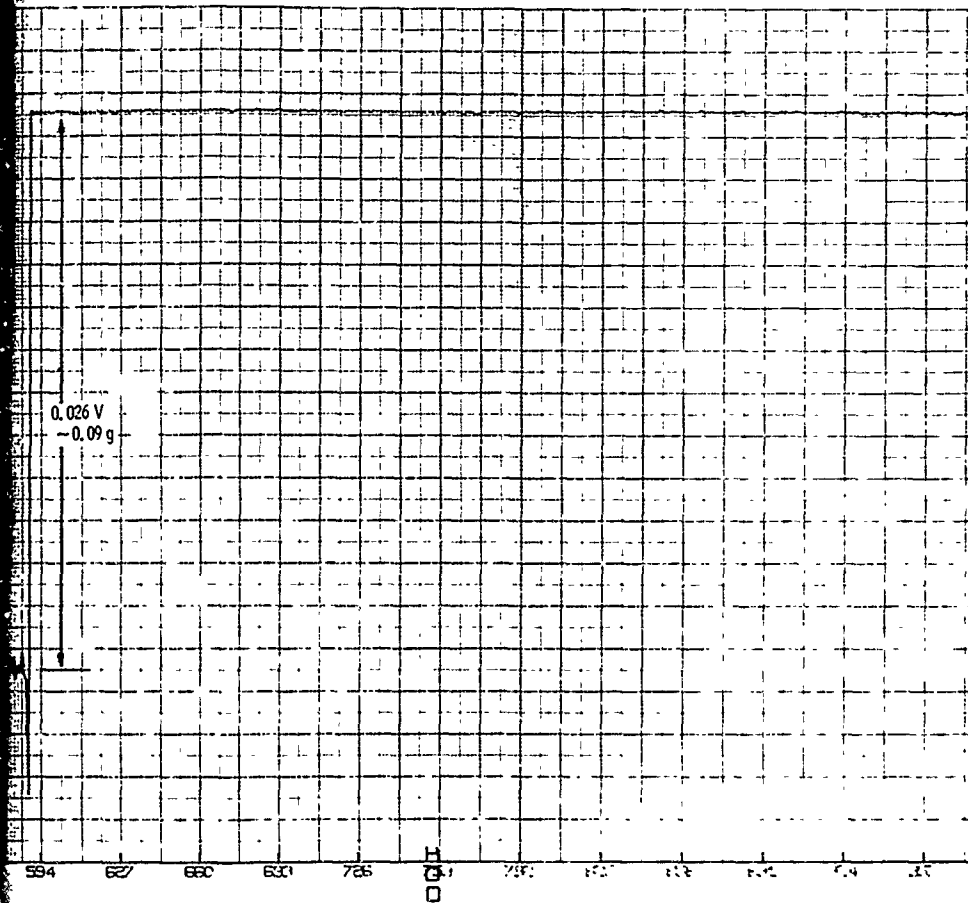
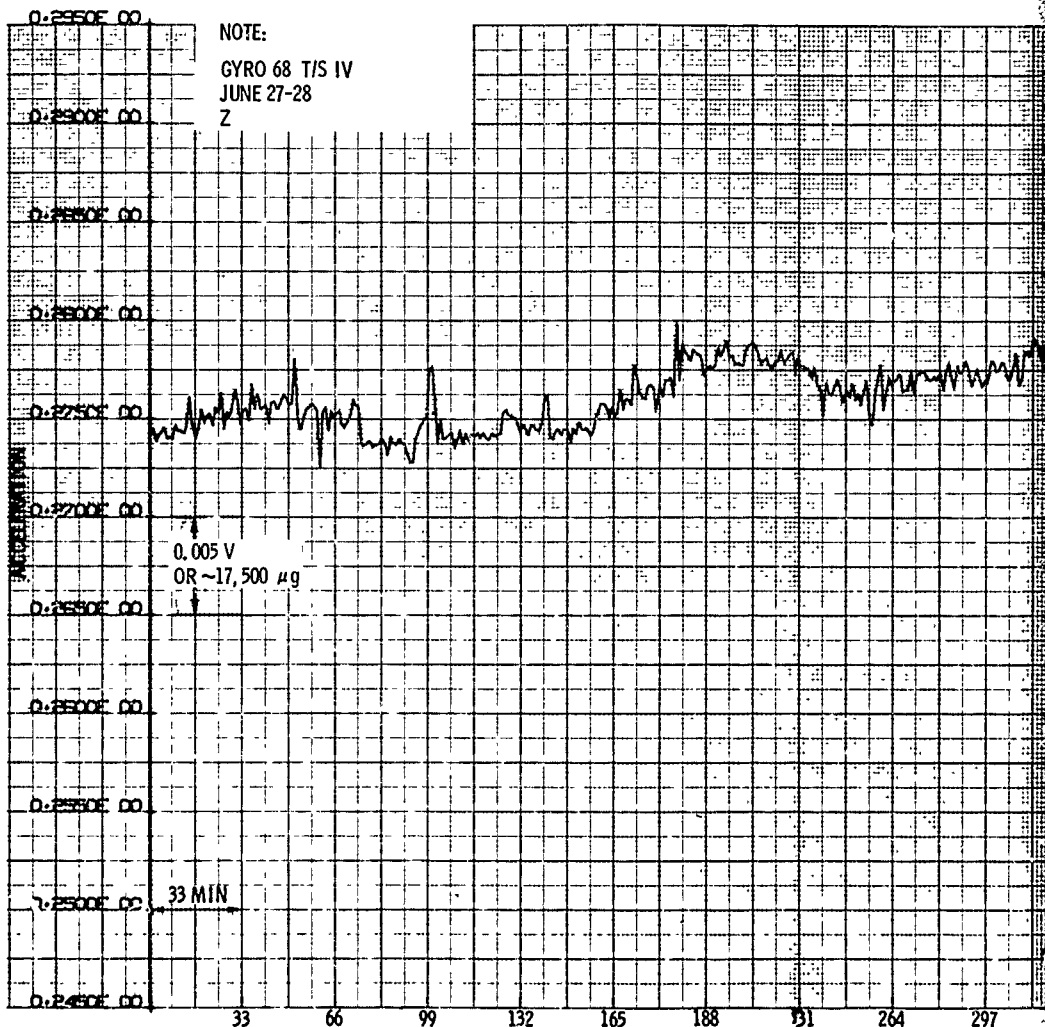
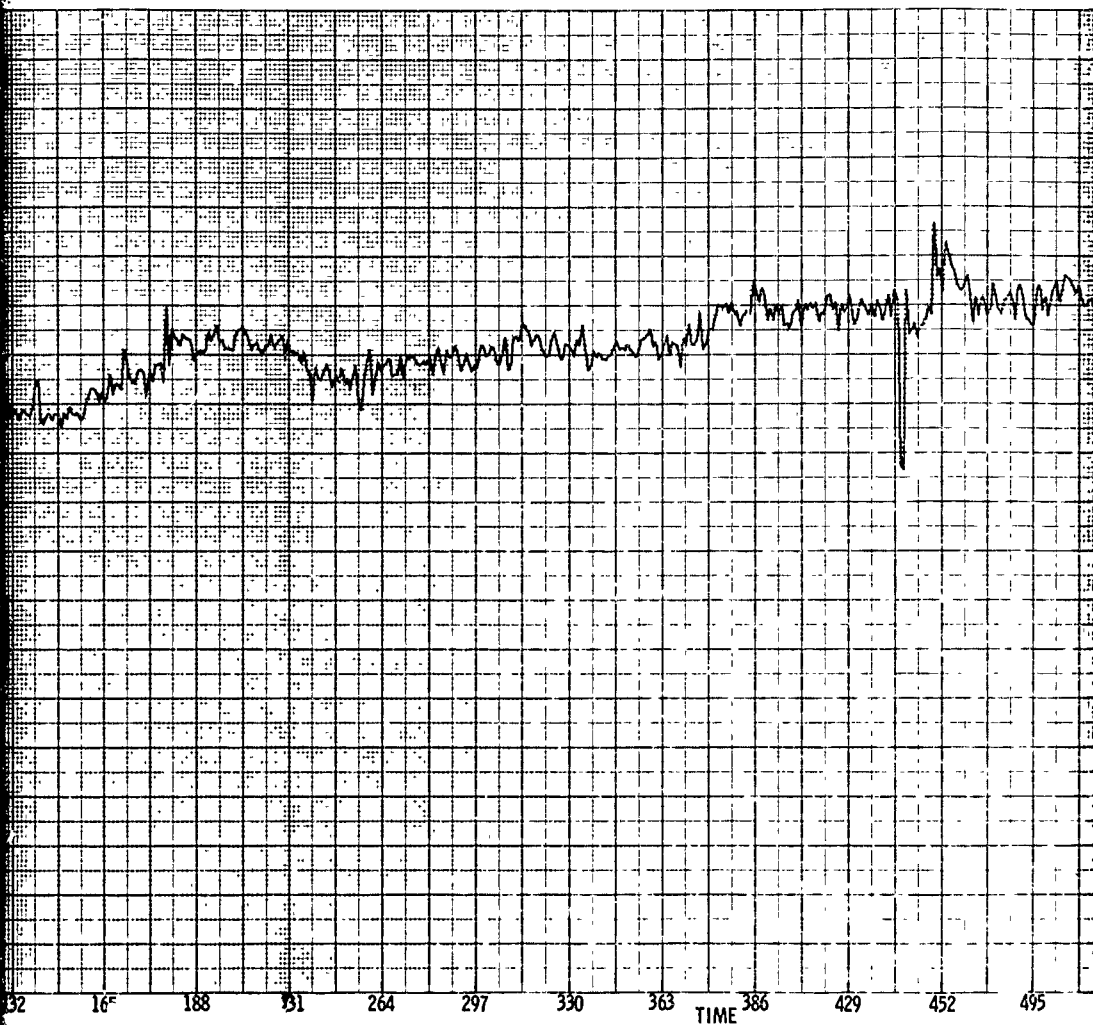


Figure 6-81. Gyro 68 Y Axis Transient





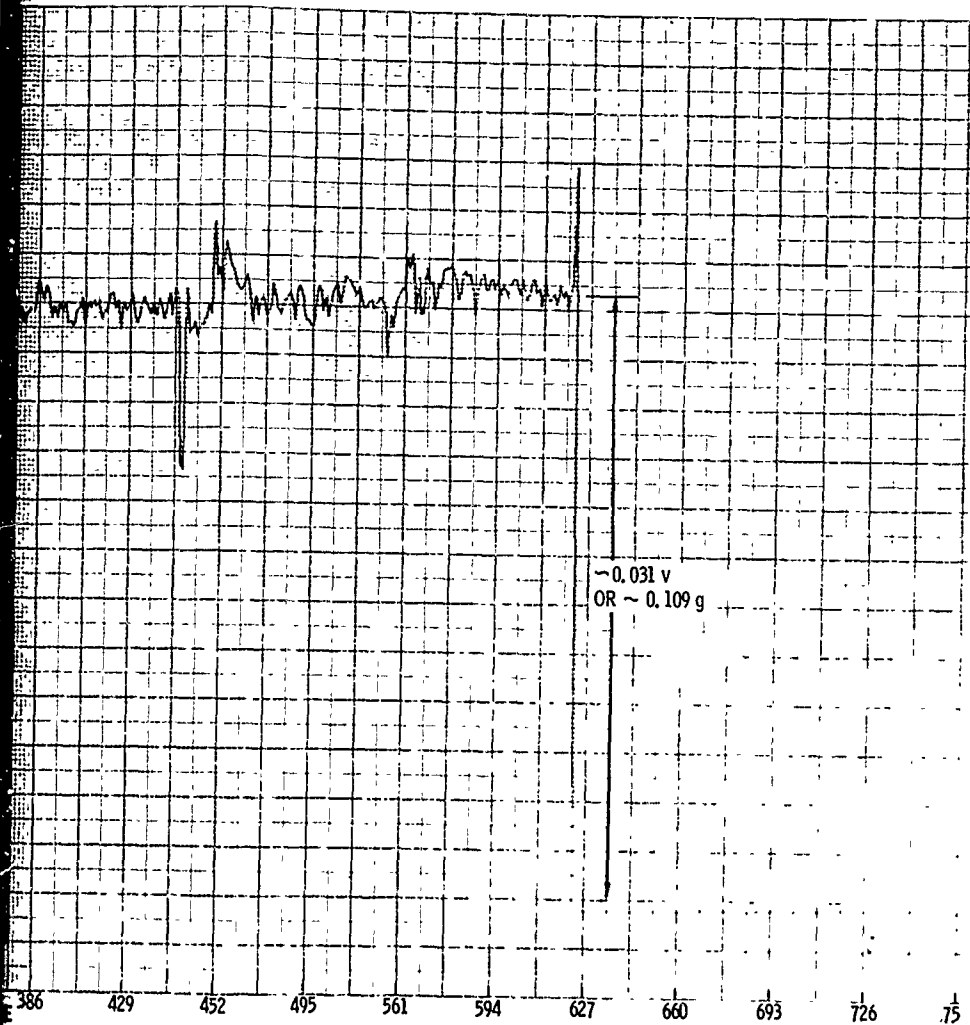
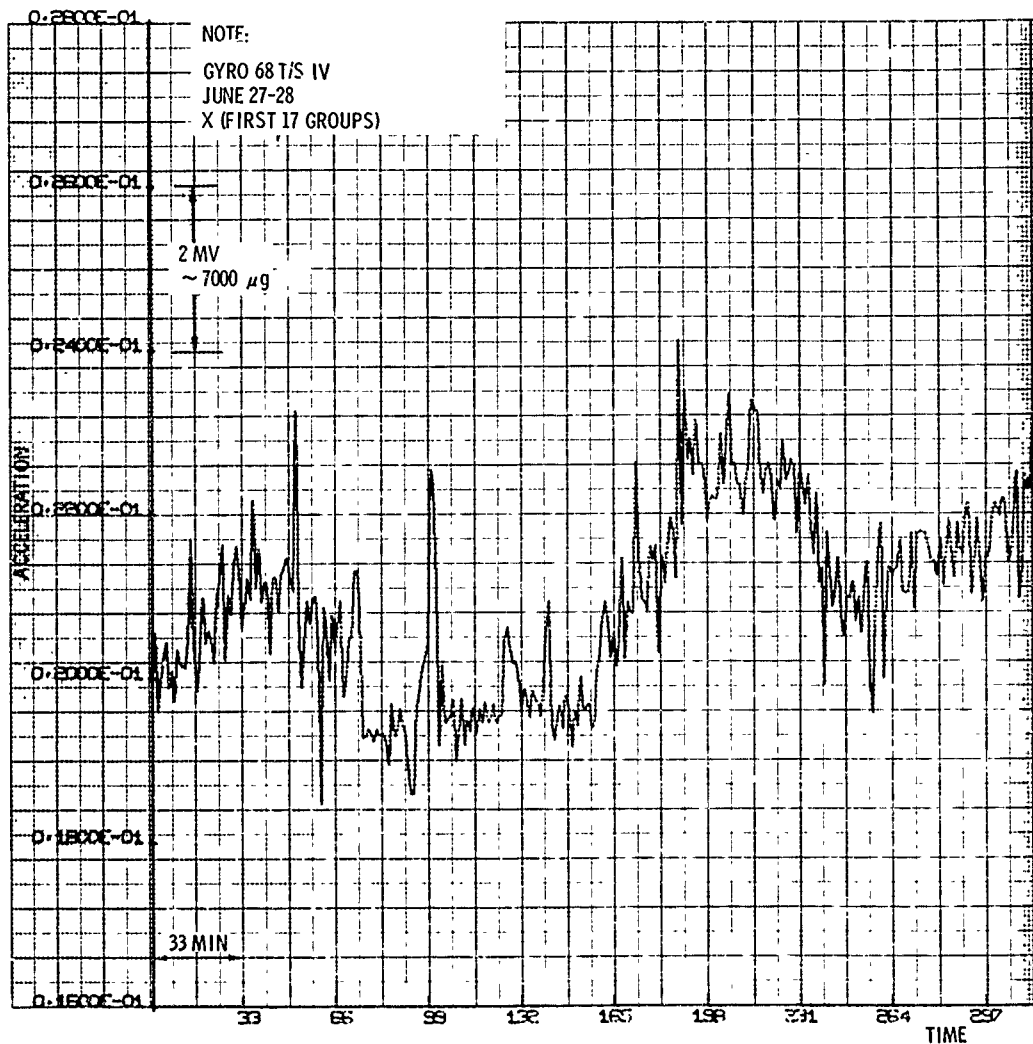


Figure 6-82. Gyro 68 Z Axis Transient



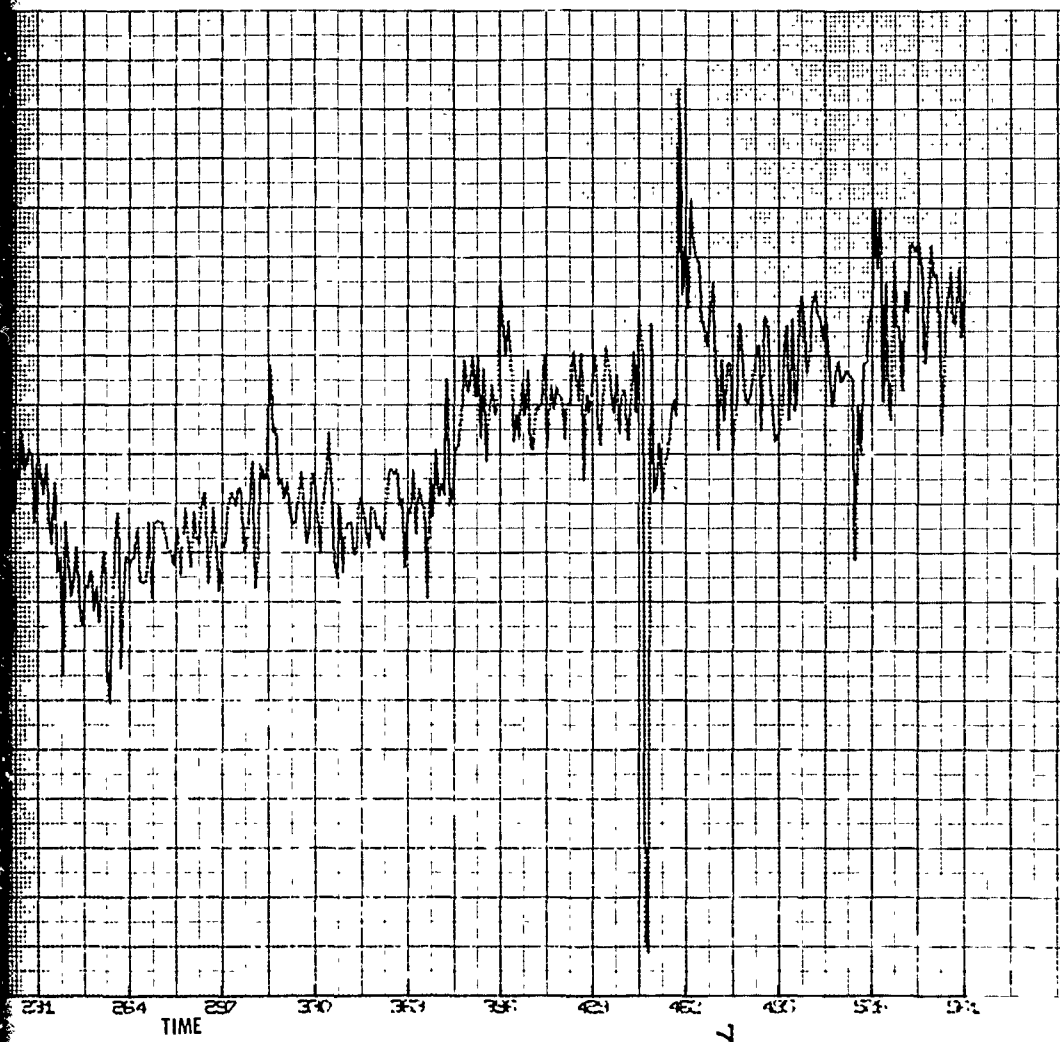


Figure 6-83. Gyro 68 Noise Before Transient

-0.1900E-02  
NOTE:  
GYRO 68 T/S IV  
JUNE 27-28 RSA POLAR  
X (LAST 12 GROUPS)  
(DATA AFTER LARGE TRANSIENT)

-0.1850E-02  
50  $\mu$ V  $\sim$ 175  $\mu$ g

-0.1800E-02

-0.1750E-02

-0.1700E-02

-0.1650E-02

-0.1600E-02

33 MIN.

33 66 99 132 165 198 231 264 297  
TIME

Figure

A POLAR  
PS)  
(GE TRANSIENT)

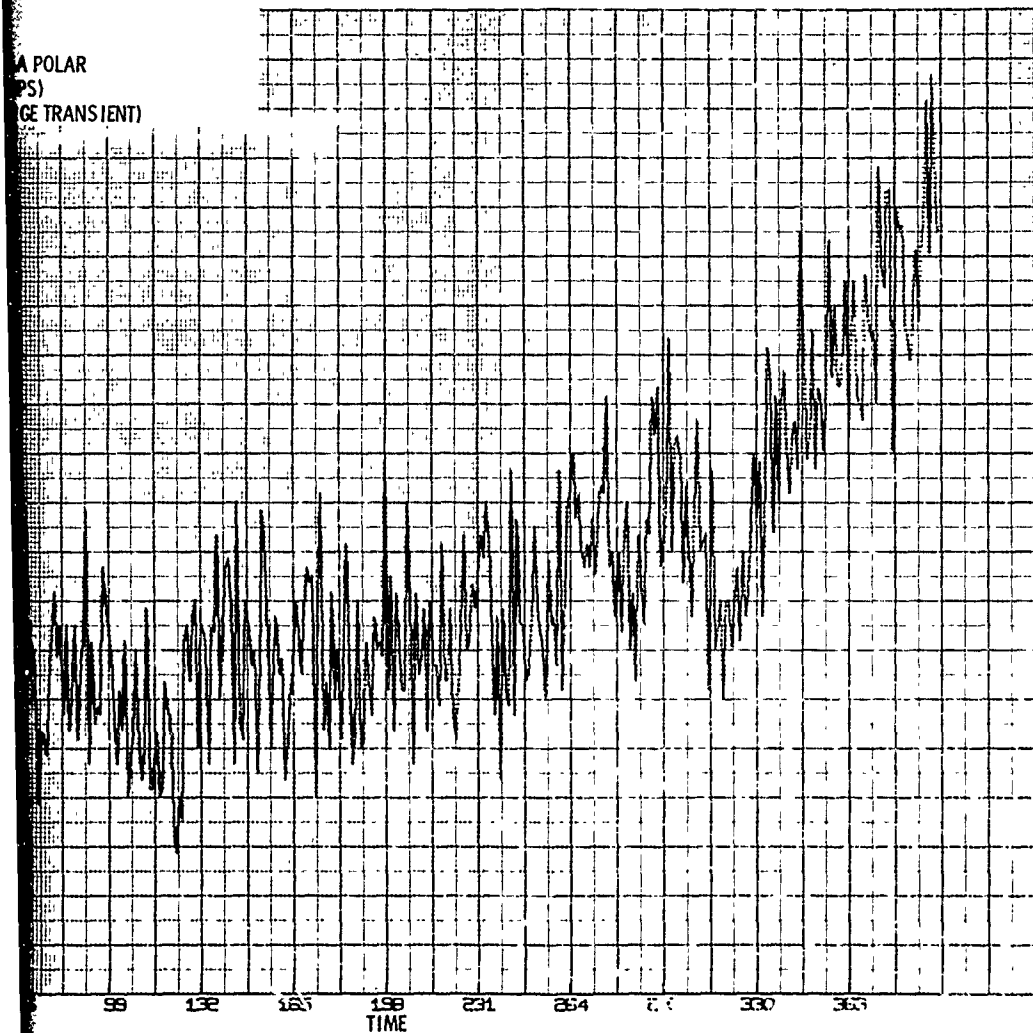


Figure 6-84. Gyro 68 Noise After Transient



Table 6-50. Gyro 102 Data

Three calibrations (No. 1 on 7/3, No. 2 on 7/5, No. 3 on 7/8); changes in scale factors and biases were as follows:

Cal No. 2 - Cal No. 1

$$\delta SF_x = +0.015\%$$

$$\delta SF_y = +0.022\%$$

$$\delta SF_z = +0.041\%$$

$$\delta b_x = -1800 \mu g$$

$$\delta b_y = -1910 \mu g$$

$$\delta b_z = +680 \mu g$$

Cal No. 3 - Cal No. 1

$$\delta SF_x = +0.02\%$$

$$\delta SF_y = +0.022\%$$

$$\delta SF_z = -0.023\%$$

$$\delta b_x = -730 \mu g$$

$$\delta b_y = -1370 \mu g$$

$$\delta b_z = +2020 \mu g$$

Cal No. 1 RMS/axis residual = 624  $\mu g$

Cal No. 2 RMS/axis residual = 658  $\mu g$

Cal No. 3 RMS/axis residual = 506  $\mu g$

RMS/axis residual for Cal No. 1 data using Cal No. 2 S's = 1714  $\mu g$

RMS/axis residual for Cal No. 2 data using Cal No. 1 S's = 1726  $\mu g$

Cal "repeatability"

$$\text{No. 1, } [(1714)^2 - (624)^2]^{1/2} = 1560 \mu g$$

$$\text{No. 2, } [(1726)^2 - (658)^2]^{1/2} = 1600 \mu g$$

$$\frac{SF_z}{SF_x} \approx \frac{3.36}{3.55} \approx 0.95$$

$$SF_x \approx 0.2\% \text{ smaller than } SF_y$$

$$\left. \begin{array}{l} b_x = -0.00951 g \\ b_y = -0.04465 g \\ b_z = -0.04674 g \end{array} \right\} \text{ Cal No. 1}$$

A number of serious problems manifested themselves in the MESGA tests on T/S IV. These problems have been discussed above; they are listed below for emphasis:

1. Transient shifts - The pattern of shifts in the gyro 124 and gyro 96 test data is similar, with the gyro 124 test data exhibiting somewhat larger shifts than that for gyro 96. Much larger (and faster) transient shifts were observed in the gyro 68 test data.
2. Long term trends - Trends have been observed of up to 3700 g in 24 hours. These trends were worse in the gyro 124 tests (and in particular the RSA cross-polar test) than in the gyro 96 tests. This may have been related to the fact that the rotor was heated in torquing to cross-polar and only about 12 hours was allowed for temperature stabilization before starting the RSA cross-polar test. Trends are also apparent in the June 27 - June 28 test data for gyro 68.
3. Low frequency noise - Noise of about 100  $\mu$ g rms and 1 hour correlation time has been observed in the gyro 124 and gyro 96 test data. Noise of this magnitude and spectral characteristic implies large alignment errors.
4. Calibration repeatability - Large differences in calibration residuals and in calibration terms were observed in the two acceleration calibrations for gyro 96.

Gyros 124, 96 and 102 were average, or better than average, with respect to angle and drift calibration residuals. These residuals are listed in Table G-51. Gyro 68 had not been calibrated in angle and drift when it was used for MESGA tests.

Table G-51. Angle and Drift Calibration Data

Gyro 124	
Angle Cal Residual	0.161 mrad rms/axis (blind)
Angle Cal Residual	0.078 mrad rms/axis (with drift comp)
Drift Cal Residual	0.0157 deg/hr rms/axis
Above calibrations were performed on March 29, 1974	
Gyro 96	
Angle Cal Residual	0.067 mrad rms/axis (blind)
Drift Cal Residual	0.007 deg/hr rms/axis
Angle calibration performed on May 2, 1974	
Drift calibration performed on May 9, 1974	
Gyro 102	
Angle Cal Residual	0.14 mrad rms/axis (blind)
Angle Cal Residual	0.086 mrad rms/axis (with drift comp)
Drift Cal Residual	0.00814 deg/hr rms/axis
Gyro 102 calibrations were performed on July 2, 1974	

#### 6.3.5.4 Comparison of Requirements, Test Data and Capability Estimates

MESGA test data taken on gyros 124, 96 and 102 were generally comparable, except for the calibration repeatability problem with gyro 96. Furthermore, these data showed that a large improvement would be required to meet performance. Thus it was decided after the gyro 102 tests (July 1974) that it was a good time to ask "How does present capability compare with the MESGA error budget?"

The error budget of Table 6-47 was used to determine the most severe requirement (bias or scale factor) as listed in Table 6-52. Estimates of present capability were obtained and these are also listed in Table 6-52. The corresponding improvement factor is the ratio:

$$\frac{\text{Present capability}}{\text{Most severe requirement}}$$

The last column in Table 6-52 gives the required improvement factor. It should be noted that the data in Table 6-52 are based upon a time interval of one year between calibrations. It should also be noted that the "most severe requirements" column assumes PWM mechanization. Many of these requirements are even more severe for PAM mechanization.

Most of the data in Table 6-52 are expressed in terms of error source parameter values. For example, preload charge measurement capability required is 10 ppm of preload charge. The notation "(SF)" indicates that the 50 ppm scale factor requirement determines the tolerance on preload charge measurement capability in this case.

Table 6-53 presents the acceleration sensing errors for PWM that are implied by the error source parameter values in the "present capability" column of Table 6-52. For example, if preload charge measurement capability is 200 ppm, the corresponding scale factor error is 400 ppm. This results from the fact that a charge variation of 25 ppm results in a scale factor error of 50 ppm. Table 6-53 shows that about one order of magnitude improvement is required in scale factor error, and over two orders of magnitude improvement in bias error is required, even with PWM mechanization. The corresponding improvement factors for PAM are about 60 for scale factor and over 1000 for bias.

The conversion factor used in Table 6-53 to convert from PWM to PAM is five for both bias and scale factor. This factor was chosen as a reasonable estimate of the overall improvement that should result from the PWM mechanization. The reason for making this conversion is to allow a comparison of recent PAM test data with the expected PWM errors based on present capability. This comparison can be made using the data presented in Table 6-54. The entries in Table 6-54 under the heading "Demonstrated Capability, PAM, RMS" were obtained from PAM test data. The values of 10,000  $\mu\text{g}$  for bias and 1800 ppm for scale factor were obtained from Gyro 102 calibration repeatability data. Bias changes and scale factor changes were multiplied by  $(365/4)^{1/2}$  to allow for a one year interval between calibrations. The time interval between Gyro 102 calibrations was four days, and it is assumed that errors grow with the square root of elapsed time. The values of 10,000  $\mu\text{g}$  for bias and 1800 ppm for scale factor in Table 6-54 are in reasonable agreement with 33,000  $\mu\text{g}$  and 3000 ppm entries in Table 6-53. The last row in Table 6-54 lists data for the dual mode or "two state" phenomenon such as was observed in Gyro 68 data. The transients in the

Table 6-52. MESGA Error Budget (PWM)

Parameter	Most Severe Reqmt, RMS	Present Capability, RMS	Improvement Factor Req'd
Preload Charge Measurement Capability	10 ppm (sf)	200 ppm	20
Rotor Centering Stability	$6.8 \times 10^{-9}$ in (bias)	$10^{-7}$ in	15
Gap Measurement Capability	$6.8 \times 10^{-9}$ in (bias)	$10^{-7}$ in	15
Rotor Charge Measurement Capability	15% (bias)	15%	None
Stray Capacitance Stability	116 ppm of 5 pf (sf)	2000 ppm (0.01 pf)	20
Propagation Delay Variation Between Channels	$0.12 \times 10^{-9}$ sec (bias)	$100 \times 10^{-9}$ sec	800
Rise Time Variations Between Channels	$0.24 \times 10^{-9}$ sec (bias)	$100 \times 10^{-9}$ sec	400
Temperature Stability	0.02°F on Rotor (sf)	0.1°F	5
Digitizer Electronics	10 ug bias 20 ppm sf	20 ug 20 ppm	2 None

Table 6-53. MESGA Errors

Parameter	Errors for Present Capability Estimates, PWM Bias, ug      Scale Factor, ppm	
Preload Charge Measurement Capability	90	400
Rotor Centering Stability	110	140
Gap Measurement Capability	110	140
Rotor Charge Measurement Capability	8	-
Stray Capacitance Stability	80	400
Propagation Delay Variation Between Channels	6,000	-
Rise Time Variation Between Channels	3,000	-
Temperature Stability	8	100
Digitizer Electronics	20	20
RSS	6,700 ug	610 ppm
Overall Improvement Factors Required	270	12
Multiplying by 5 for PAM Gives RSS =	33,000 ug	3,000 ppm

Table 6-54. MESGA Errors - Recent Test Data

Parameter	Requirement, RM%	Demonstrated Capability, PAM, RMS	Improvement Factor Required
Short Term Random Output Variation (15 sec corr. time)	3.5 ug	350 ug (40 min az error)	100
Long Term Scale Factor and Bias Stability (One Year)	25 ug bias 50 ppm s.f.	10,000 ug bias ± 800 ppm s.f. (Assuming Random Walk)	400 (bias) 35 (s.f.)
Dual Mode (Two-State) Phenomenon	7 ug (Assumes Random Walk)	70,000 ug	10,000

Gyro 102 data were on the order of 1000  $\mu\text{g}$ , and the RMS value of this and the 0.1 g type transient for Gyro 68 is 70,000  $\mu\text{g}$ .

The PAM test data obtained on Test Station IV are in reasonable agreement with the estimated PAM errors. The estimated PAM errors are based on present capability estimates and calculated MESGA requirements. It can be concluded that the present capability estimates are not excessively large and that the calculated MESGA requirements are not excessively small. For, if not, then the test data would be much better than predicted.

It was concluded as a result of the above comparison (of test data, present capability estimates, and calculated requirements), that MESGA testing on Test Station IV should be discontinued.

It was recommended at the July Design Review that TASC make an independent assessment of MESGA status (requirements and test data). Some test data were given to TASC personnel on 26 July 1974. Copies of computer plots of test data were made, and were mailed to TASC early in August, 1974, at the request of TASC. Some additional MESGA data were collected together at the request of TASC, and were hand-carried to TASC by Dr. J. C. Pinson on his trip to MIT in August 1974.

TASC presented a review of their MESGA analyses at the MICRON informal design review on 17 October 1974, (see TASC Document SP-445-3 "MICRON Analysis" dated 16 October 1974). One point emphasized by TASC was that sensitivity to voltage errors introduced after the acceleration pickoff was about 3000 times that for voltage errors introduced before the acceleration pickoff. One implication of this is that the acceleration pickoff should be as close to the gyro as possible, i.e., at the charge amplifier output. The acceleration pickoff point for the GSA is at the modulator output (or charge amplifier input). The TASC presentation implies the background of the decision to locate the pickoff at the modulator output should be reviewed.

In the initial MESGA analyses (performed by Dr. R. R. Duncan) it was assumed that the acceleration pickoff would be at the charge amplifier output. This pickoff point was selected to minimize errors. However, when actual design of the 8-plate GSA was initiated it became apparent that the modulator output pickoff point would be much simpler to mechanize than the charge amplifier output pickoff point. It was also felt at the time that the error reduction resulting from the charge amplifier output pickoff point was not sufficient to justify the additional mechanization complexity. Thus it was decided that the acceleration pickoff point should be at the modulator output.

Sensitivity to two major error sources (charge variations and timing variations) would be less for a pickoff at the charge amplifier output than for a pickoff at the modulator output. However, there are problems with the charge amplifier output measurement which result in less error reduction than might otherwise be expected.

1. An ideal measurement of acceleration would be of the form  $KQ_0^2 T$  where  $Q_0$  is the charge amplifier output charge and  $T$  is the time it is applied. The measurement actually made at the charge amplifier output would be of the form  $KQ_0 T$ . Thus in order to obtain acceleration it is necessary to multiply by a reference charge  $Q_R$  to get estimated acceleration  $KQ_R Q_0 T$ . The estimated acceleration for the modulator output pickoff would be  $KQ_R^2 T$ . Thus the errors due to variations in  $Q_R$  for the two pickoff points are

$$\left(\frac{\delta A}{A}\right)_{C/A} = \frac{\delta Q_R}{Q_R}$$

$$\left(\frac{\delta A}{A}\right)_{MOD} = \frac{2\delta Q_R}{Q_R}$$

The charge amplifier output measurement would be better by a factor of 2 than the modulator output measurement, with respect to charge variation errors.

2. The advantage of the charge amplifier output measurement over the modulator output measurement is about a factor of 3, with respect to timing errors. This assumes that no attempt is made to detect and compensate for timing errors. The factor of 3 arises as follows. Assume the turnoff of say the +1 plate is delayed while all the others are off. Then the actual charge on the +1 plate is  $7/8 Q_0$  and  $-1/8 Q_0$  on all the other plates. Thus the error for the modulator output is proportional to  $3/4 = (7/8)^2 - (1/8)^2$ , since the error occurs downstream of the measurement. The measurement at the charge amplifier output would be proportional to  $1 = 1^2 - 0^2$ , while the actual acceleration is proportional to  $3/4$ . Hence the error in the charge amplifier output measurement would be proportional to  $1 - 3/4 = 1/4$ . Thus the charge amplifier output measurement would be better by a factor of 3 than the modulator output measurement.

The question naturally arises as to what could be done to increase the advantage of the charge amplifier output over the modulator output. In the case of charge variations, if  $Q_0^2$  could be integrated over a charge cycle (instead of  $Q_0$ ), the charge variation error would be reduced. The problem with this is that analog squaring circuitry is not nearly accurate enough to make this feasible. In the case of timing variations, if it were possible to detect the existence of unbalance

$$\sum_{i=1}^8 Q_i = 0$$

in the commanded charge, and the duration of such an unbalance, then it would be possible to reduce timing errors by compensation. One problem with this approach is that it requires large bandwidth (~100 MHz) in the differential amplifier buffer circuits. Also, it would be impractical to try to detect more than a few of the combinations (e.g., all off but one plate) which produce errors.

There is another problem with the charge amplifier output pickoff which has not been discussed; the common mode rejection requirement for the differential amplifier buffer. The information signal consists of about a 3 volt variation between two points at roughly a 100 volt level. This implies the common mode rejection ratio for the difference amplifier buffer must be about  $7 \times 10^6$ . This follows from the requirement to limit common mode error to 5 PPM of the nominal output voltage, in order to keep bias error small enough. Achievement of such a common mode rejection ratio while maintaining 100 MHz bandwidth is probably beyond the state-of-the-art. If no attempt



is made to detect and compensate for timing errors, the required difference amplifier buffer bandwidth would be about 200 kHz. The required common mode rejection ratio would be difficult to achieve at this bandwidth.

TASC Document TIM No. 445, "Analysis of Acceleration Readout Error Sensitivities for MICRON", dated 5 December 1974 was received in December and reviewed in January 1975. The sensitivities calculated by TASC and presented in this document tend to be within a factor of about three of the sensitivities calculated by Autonetics. TASC combines errors statistically and distinguishes carefully between four space and three space components. The Autonetics calculations were less statistically refined, and did not always make clear distinctions between four space and three space components. However, it must be noted that typical sensitivities imply required improvements in performance of factors on the order of 100 to 1000 or more. Therefore, given T/S IV data, factors of three differences are not considered significant. Analysis of MESGA data obtained on the eight plate GSA and GSA Test Station may require a closer look at error sensitivities.

#### 6.3.5.5 MESA Tests on the GSA - GSA Test Station

In early May 1975 a review of the planned MESGA testing was performed. A revised plan was written to provide the minimum data set needed to evaluate noise, stability and repeatability of the MESGA function. This revised plan bypassed the angle and drift calibrations in an effort to get to a point where acceleration data could be collected utilizing the GSA improvements such as temperature and gap monitoring to assist in evaluating MESGA performance.

The revised MESGA plan is summarized in Table 6-55.

A MESGA test log summary appears in Table 6-56. Note that gyro 14Y was used in all the tests.

The table angles used in the MESGA calibration are listed in Table 6-57.

Table 6-55. Summary of Revised MESGA Test Plan

1. Perform MESGA calibration (with non-spinning rotor).
2. Spin up and polhode damp at 500 Hz with RSA approximately polar.
3. Despin without damping to TBD Hz
4. Temperature stabilize for 24 hours monitoring temperature and gaps.
5. Perform two MESGA calibrations.
6. Perform MESGA data collection as follows:
  - a. Determine rotor speed and position.
  - b. Collect data for 4 hours with +Z vertical and up (plate corner)  
 $TA1 = 0, TA2 = 55, TA3 = 150$
  - c. Collect data for 4 hours with Y vertical and up (plate corner)  
 $TA1 = 0, TA2 = 55, TA3 = 270$
  - d. Collect data for 4 hours with -1 vertical and up (plate corner)  
 $TA1 = 0, TA2 = 0, TA3 = 150$
  - e. Collect data for 4 hours with -3 vertical and up.  
 $TA1 = 0, TA2 = 70, TA3 = 330$
  - f. Collect data for 24 hours with Z horizontal and +X and +Y 45 degrees from vertical and up (plate edge)  
 $TA1 = 0, TA2 = 35, TA3 = 330$
  - g. Determine rotor speed and position. Repeat steps (b), (c), and (d).
  - h. Shutdown, room temperature soak for at least 12 hours.
  - i. Repeat 2, 3, 4, 6a, 6b, 6c, 6d, and perform one MESGA calibration.

Table 6-56. ME3GA Test Log Summary

Date	Activity
07/09/75	Installed Be base gyro No. 14Y. Suspended 1300 hours.
07/10/75	Ran overnight - Charge monitoring and temperature stabilizing.
07/11/75	Continued as on 07/10/75. Stable gap = -3.249 volts. Shut down for weekend at 1656 hours, no problems. NOTE: Gyro was suspended (but not spinning) for about 52 hours.
07/12/75	Shutdown for weekend.
07/13/75	
07/14/75	Suspended at 0810 hours. Spun up, polhode damped and despun to 442 Hz at 1700 hours, gap = -3.301.
07/15/75	0923 $f_R = 386$ Hz, gap = -3.254 0935 Started spinning cal No. 1 1045 Completed spinning cal No. 1, $f_R = 377$ Hz 1145 Completed spinning cal No. 2, $f_R = 371$ Hz 1412 Gap = -3.252 1430 $f_R = 367$ Hz 1830 Start 4 hour +Z run, TA1 = 0, TA2 = 55, TA3 = 150 2330 Start 4 hour +Y run, TA1 = 0, TA2 = 55, TA3 = 270
07/16/75	0815 Gap = -3.249, $f_R = 322$ Hz 1015 Start 4 hour +1 run, TA1 = 0, TA2 = 0, TA3 = 150 1512 Start 4 hour -3 run, TA1 = 0, TA2 = 70, TA3 = 330 gap = -3.252, $f_R = 307$ Hz 2050 Start 24 hour run +Z horizontal, +X and +Y 45° from vertical and up, TA1 = 0, TA2 = 35, TA3 = 330 gap = -3.250, $f_R = 298$ Hz
07/17/75	2102 Completed 24 hour run. gap = -3.251, $f_R = 285$ Hz 2340 Repeat +Y vertical run, TA1 = 0, TA2 = 55, TA3 = 270 gap = -3.250, $f_R = 286$ Hz
07/18/75	Completed Y vertical run. 1015 Repeat +1 vertical run, TA1 = 0, TA2 = 0, TA3 = 150 gap = -3.247, $f_R = 284$ Hz 1515 Completed +1 vertical run. 1830 Started second +Z vertical run, TA1 = 0, TA2 = 55, TA3 = 150 gap = -3.250, $f_R = 286$ Hz 2330 Completed second +Z run and shut system down. No problems during shutdown.

Table 6-56. (Cont.)

Date	Activity
07/19/75	Shutdown for weekend.
07/20/75	
07/21/75	Suspended at 0800. Spun up and polhode damped at 1300. $f_R = 650$ Hz, gap = -3.501.
07/22/75	Fan overnight, temperature stabilizing 0800 gap = -3.285, $f_R = 464$ Hz 1000 gap = -3.277 1200 No 64 Hz interrupt to computer, could not get IIP 2100 program going. 1400 Replaced MUM + Timing Module and got 64 Hz clock OK 1530 Spun up and polhode damped gap = -3.551, $f_R = 833$ 1730 gap = -3.476, $f_R = 495$ Hz Fan overnight, temperature stabilizing.
07/23/75	Continued temperature monitoring in morning. Started collecting data (+Z vertical and up) at 1407 TA1 = 0, TA2 = 55, TA3 = 150 1400 gap = -3.275, $f_R = 395$ Hz 1430 gap = -3.274, $f_R = 395$ Hz 1900 Completed data taking at 0, 55, 150 position gap = -3.270, $f_R = 385$ Hz 1905 Set table angles to TA1 = 0, TA2 = 55, TA3 = 270 for Y vertical and up and started data collection. 2358 Completed data collection at 0, 55, 270 position 0000 gap = -3.266, $f_R = 359$ Hz 0005 Set table angles to TA1 = 0, TA2 = 0, TA3 = 150 for +1 vertical and up and started data collection
07/24/75	0930 gap = -3.263, $f_R = 309$ Hz 1135 Start calibration 1235 End calibration.

Table 6-57. MESGA Calibration Table Angles

Position	TA1	TA2	TA3
1	0	0	152
2	0	0	242
3	0	0	332
4	0	0	62
5	90	0	152
6	180	0	152
7	270	0	152
8	0	25	152
9	0	25	212
10	0	25	272
11	0	25	332
12	0	25	32
13	0	25	92
14	0	50	152
15	0	50	272
16	0	50	32
17	0	90	152
18	0	90	212
19	0	90	272
20	0	90	332
21	0	90	32
22	0	90	92

Three MESGA calibrations were performed with the rotor spinning at low speed (~300 to 400 Hz, see Table 6-56). Two of these calibrations were performed before shutdown, and one was performed after shutdown to obtain some indication of repeatability across a shutdown. Data were taken at 22 table positions (Table 6-57). The digitizer-counter outputs were sampled 64 per second for 1 minute at each table position. (See Figure 6-85 for a block diagram of the GSA acceleration pickoff.) Thus 3840 data samples were obtained at each table position for each of the 4-space pickoffs. These data were converted to 3-space and the means and standard deviations were stored for later processing off-line. The calibration coefficients and RMS calibration residuals were computed after all the MESGA test data had been acquired (see Table 6-58).

The diagonal (scale factor) terms in Table 6-58 have a magnitude of about 0.2. This must be multiplied by 0.0156 to get the actual scale factor (~0.003 fps per pulse). The bias entries have to be divided by 32.2 to obtain acceleration in units of g's. The RMS residuals are in units of  $\mu$ g's.

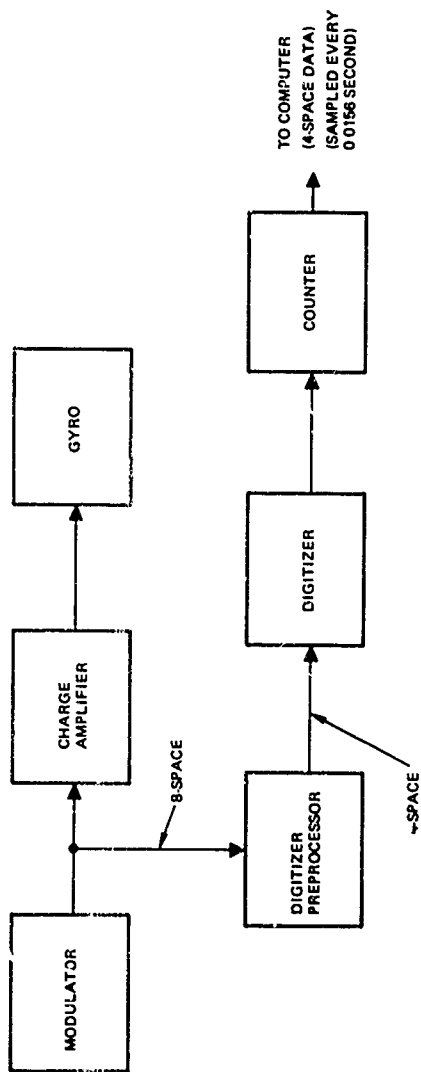


Figure 6-85. GSA Acceleration Pickoff Block Diagram

Table 6-58. GSA MESGA Calibration Data, Gyro 14Y

	Cal A	Cal B	Cal C
Scale Factor and Misalignment Terms	-0.201179	-0.201097	-0.203403
	+0.357387 ( $10^{-2}$ )	+0.363551 ( $10^{-2}$ )	+0.461048 ( $10^{-2}$ )
	-0.348572 ( $10^{-2}$ )	-0.334184 ( $10^{-2}$ )	-0.356424 ( $10^{-2}$ )
	-0.161845 ( $10^{-2}$ )	+0.156285 ( $10^{-2}$ )	+0.141625 ( $10^{-2}$ )
	-0.200872	-0.200955	-0.203561
	-0.143427 ( $10^{-2}$ )	+0.140186 ( $10^{-2}$ )	-0.759946 ( $10^{-3}$ )
	-0.124423 ( $10^{-2}$ )	-0.138634 ( $10^{-2}$ )	-0.169766 ( $10^{-2}$ )
	-0.143300 ( $10^{-2}$ )	+0.151436 ( $10^{-2}$ )	-0.134632 ( $10^{-2}$ )
	-0.207344	-0.207285	-0.209871
Bias, X, Y, Z	-0.677300	-0.722017	-0.122661 ( $10^1$ )
	-0.238095	-0.207103	-0.518526
	-0.147691 ( $10^1$ )	-0.141847 ( $10^1$ )	-0.191778 ( $10^1$ )
RMS Residuals X, Y, Z	2470 $\mu$ g	2561 $\mu$ g	3076 $\mu$ g
	1993 $\mu$ g	2105 $\mu$ g	2785 $\mu$ g
	2076 $\mu$ g	2303 $\mu$ g	2579 $\mu$ g

Differences (shifts) in the calibration parameters between the three calibrations are summarized in Table 6-59. The calibration shifts from Cal A to Cal B are on the order of the shifts seen on gyros 102 and 96 in the T/S IV tests described earlier. The Cal C to Cal A shifts are larger than those seen in the T/S IV tests; however, there was an intervening shutdown in the GSA tests, but not in the T/S IV tests. It should also be noted that the GSA calibrations were back-to-back, while the different calibrations compared in the T/S IV tests were two or three days apart. Based on this one sample, it appears that the calibration repeatability on the GSA was no better than that on T/S IV, and may be worse.

The RMS residuals for Cals A and B are comparable. The RMS residuals for Cal C are bigger than for Cal A or B. It should be noted that the GSA calibration residuals are generally larger than those seen in the T/S IV tests. The 3 May '974 calibration of gyro 96 on T/S IV had an RMS per axis calibration residual of about 2000  $\mu$ g, which is comparable with the Cal A and B residuals. However, this calibration of gyro 96 was considered to be anomalous. The 1000  $\mu$ g transient shifts discussed later may have affected the calibration residuals.

Table 6-59. GSA MESGA Calibration Parameter Shifts

Cal B - Cal A	Cal C - Cal B
$\frac{\delta C_{xx}}{C_{xx}} \approx 0.0004$ (400 PPM)	$\frac{\delta C_{xx}}{C_{xx}} \approx -0.0115$ (-11,500 PPM)
$\frac{\delta C_{yy}}{C_{yy}} \approx -0.0004$ (-400 PPM)	$\frac{\delta C_{yy}}{C_{yy}} \approx -0.013$ (-13,000 PPM)
$\frac{\delta C_{zz}}{C_{zz}} \approx +0.0003$ (400 PPM)	$\frac{\delta C_{zz}}{C_{zz}} \approx -0.0129$ (-12,900 PPM)
$\delta b_x \approx -1400 \mu g$	$\delta b_x \approx -15,700 \mu g$
$\delta b_y \approx +650 \mu g$	$\delta b_y \approx +22,500 \mu g$
$\delta b_z \approx +1800 \mu g$	$\delta b_z \approx +15,500 \mu g$

The bias values in Table 6-58 are comparable with those obtained in the T S IV tests. The largest bias is the  $z$  component, and this was generally true in the T S IV tests. (The  $y$  and  $z$  bias terms for gyro 102 were about the same in magnitude.) Based on this one example, it would appear that bias magnitude depends more on the gyro than on the suspension servo mechanism. The causes of bias variations have not been definitely determined.

The  $x$  and  $y$  diagonal (scale factor) terms are smaller than the  $z$  scale factor. This is the opposite of the pattern noted in the T S IV PAM tests. The  $z$  coefficient is about 3 percent larger than the  $x$  and  $y$  coefficients. In the T S IV tests gyro 124 (no  $z$ -hole) had  $x$  and  $y$  coefficients about 1 percent larger than  $z$ , while gyro 96 and 102 had  $x$  and  $y$  coefficients about 5 percent larger than  $z$ . Gyro 14y (used in GSA MESGA tests) has the new (and narrower) crack dimension of 0.010 inch, and also has no  $z$  hole. The new scale factor pattern may be a result of the new crack size.

MESGA stability data were collected for over 64 hours. There were 10 four hour stability runs at four different orientations ( $\theta$  with  $g$  through a plate corner and  $\theta$  with  $g$  through a plate center). One 24 hour run was made with  $z$  horizontal and  $x$  and  $y$  45 deg from vertical ( $g$  through the center of a plate edge). These tests are listed in Table 6-60 along with date and start time. Figure numbers are also given in Table 6-60 for the plots of measured acceleration versus time which are included herein. These plots were made using raw three-space data. Each data point corresponds to the average (over one minute) of the samples obtained from the digitizers (64 sec). The four-space digitizer outputs have been converted to three-space. Time is plotted, on the abscissa, (actual or real time is about 1.22 times the listed values). Acceleration (in pulse counts) has been plotted on the ordinate, the equivalent acceleration is 500  $\mu g$  per division. Plots of over half the stability data have been included herein because this is their first publication, and also to exhibit enough data that typical patterns can be observed. All the data have been stored on cards.



Table 6-60. Stability Test Summary

Date	Start Time	Orientation	Table Angles	Figure Numbers
7/5	1830	+z vertical	0, 55, 150	6-86, 6-87, 6-88
7/15	2330	+y vertical	0, 55, 270	none
7/16	1015	+1 vertical	0, 0, 150	6-89, 6-90, 6-91
7/16	1512	-3 vertical	0, 70, 330	6-92, 6-93, 6-94
7/16	2050	z horizontal (x & y 45° from vertical)	0, 35, 330	6-95, 6-96, 6-97
7/17	2340	+y vertical	0, 55, 270	6-98, 6-99, 6-100
7/18	1015	-1 vertical	0, 0, 150	none
7/18	1830	+z vertical	0, 55, 150	6-101, 6-102, 6-103
7/23	1407	+z vertical	0, 55, 150	none
7/23	1905	-y vertical	0, 55, 270	none
7/24	0005	-1 vertical	0, 0, 150	none

Figures 6-84 through 6-101 are reviewed individually below. A summary appears at the end of this section.

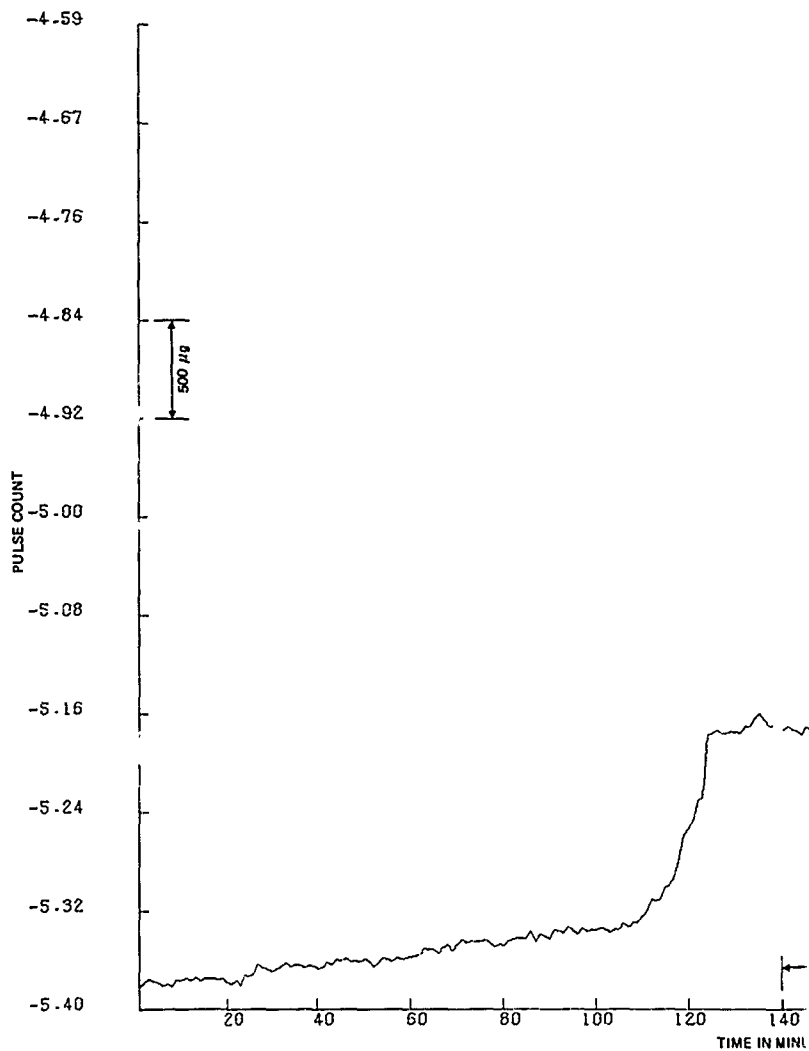


Figure 6-86. X Acceleration

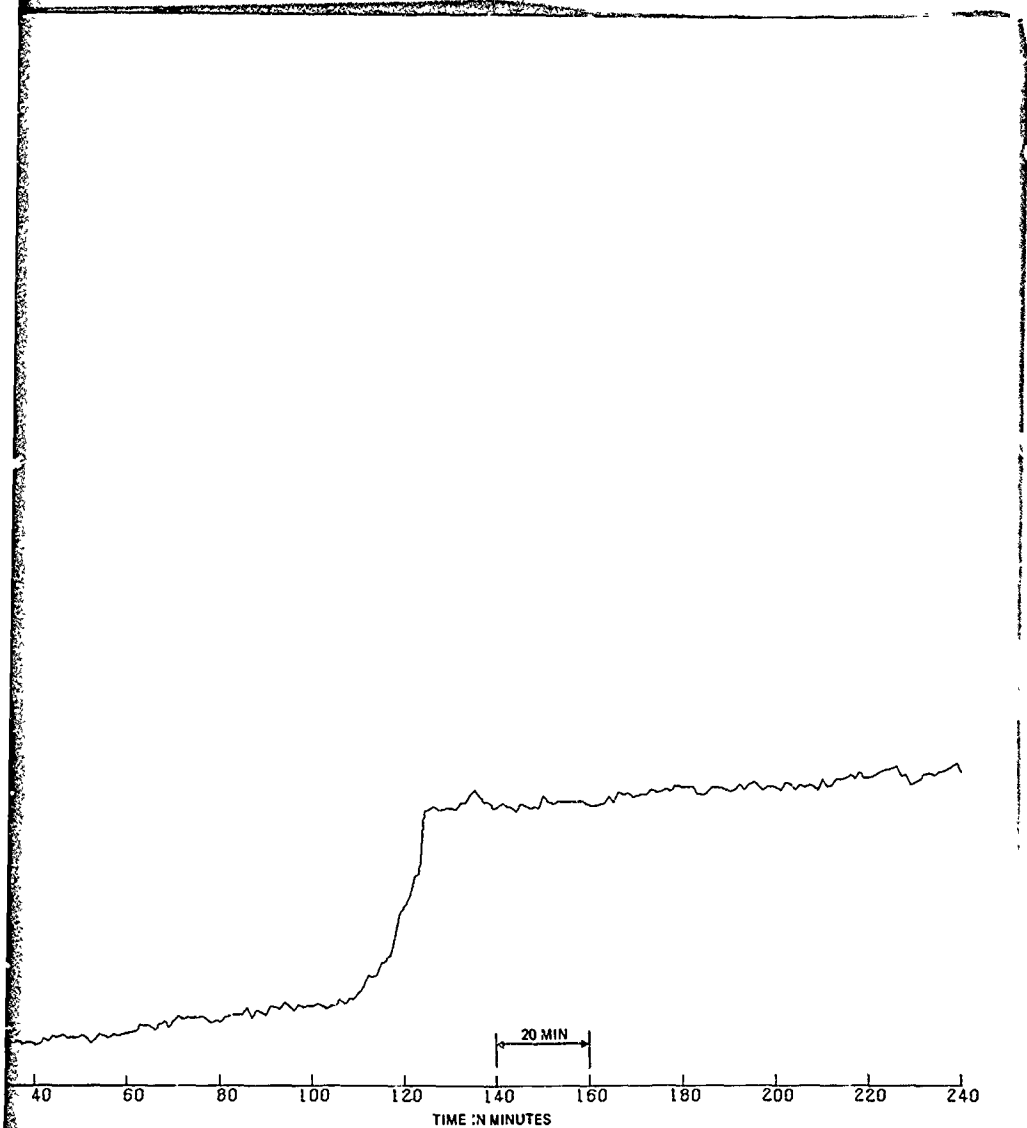


Figure 6-86. X Acceleration Component vs Time; 7-15-75, 1Z Vertical Position

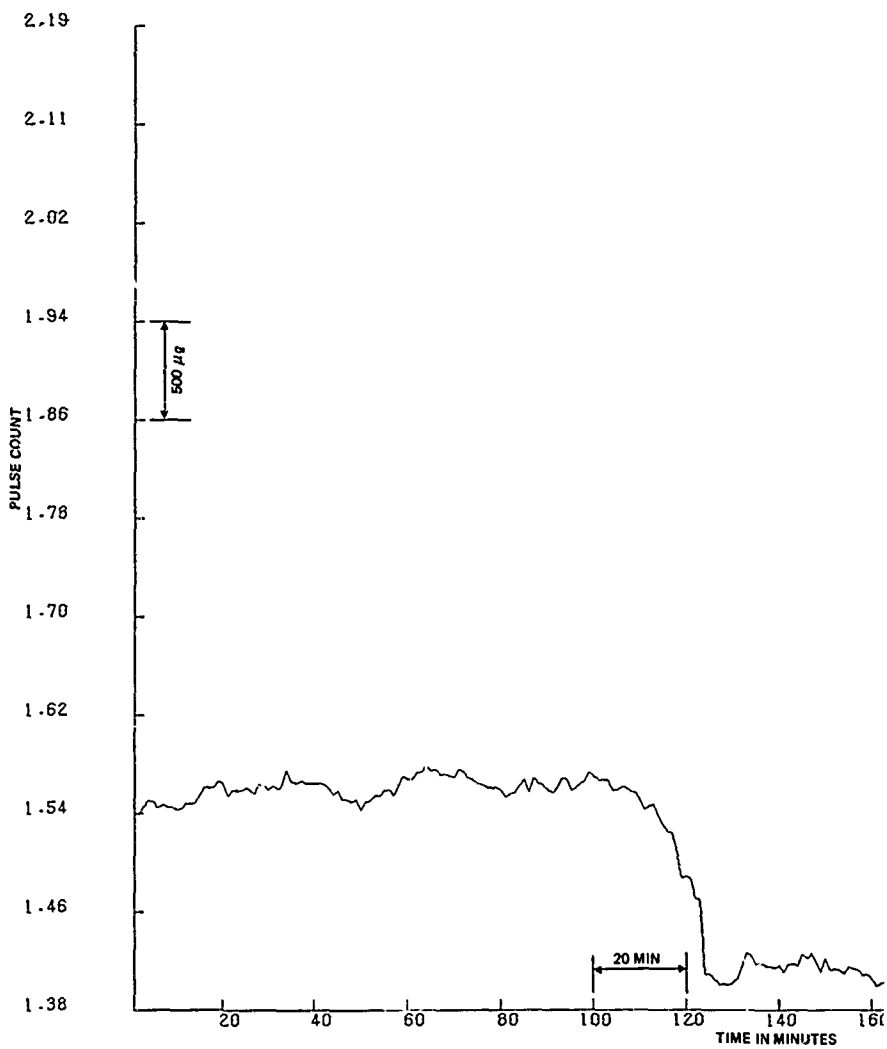


Figure 6-67. Y Acceleration Component

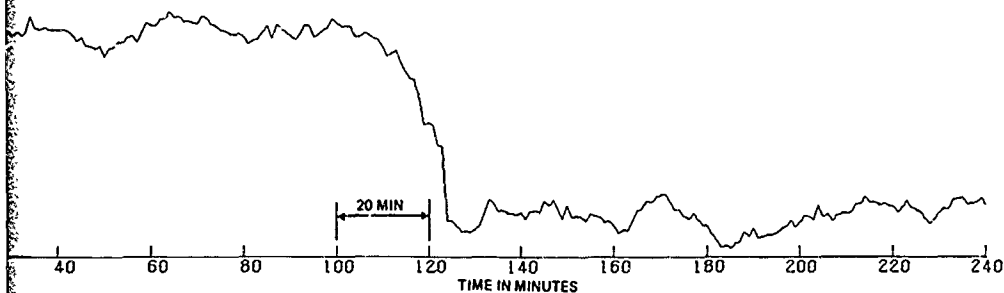


Figure 6-87. Y Acceleration Component vs Time, 7-15-75, +Z Vertical Position

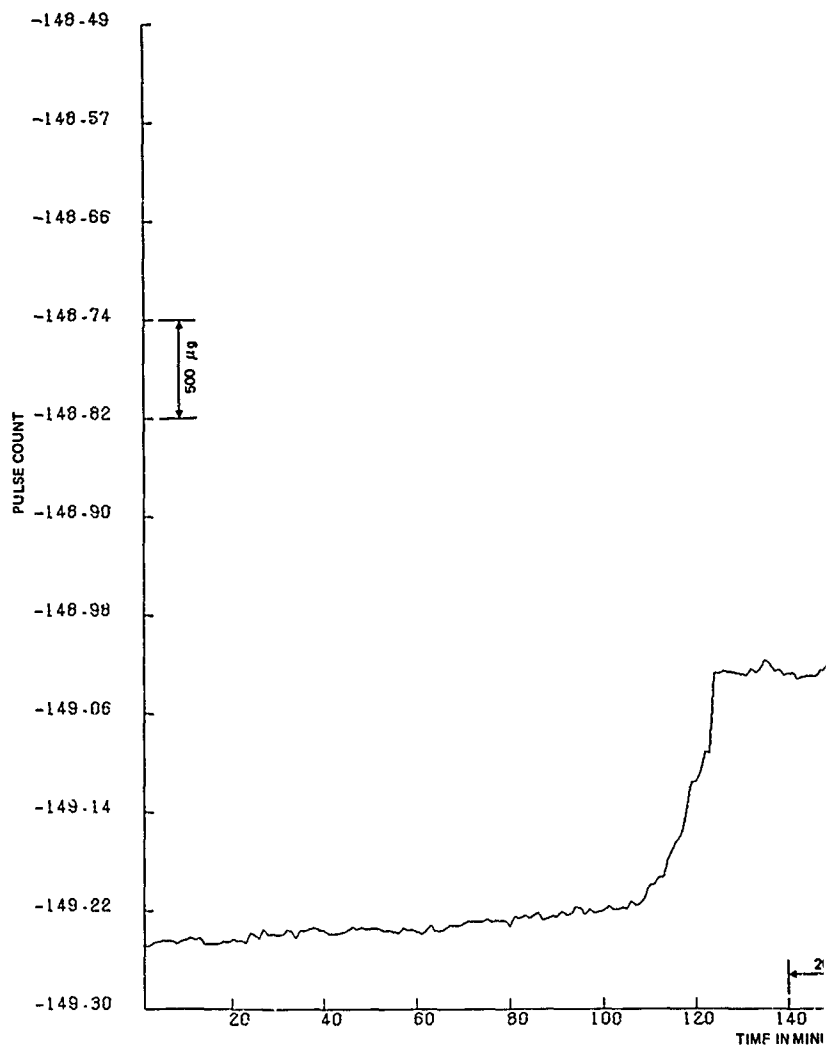


Figure 6-88. Z Acceleration (

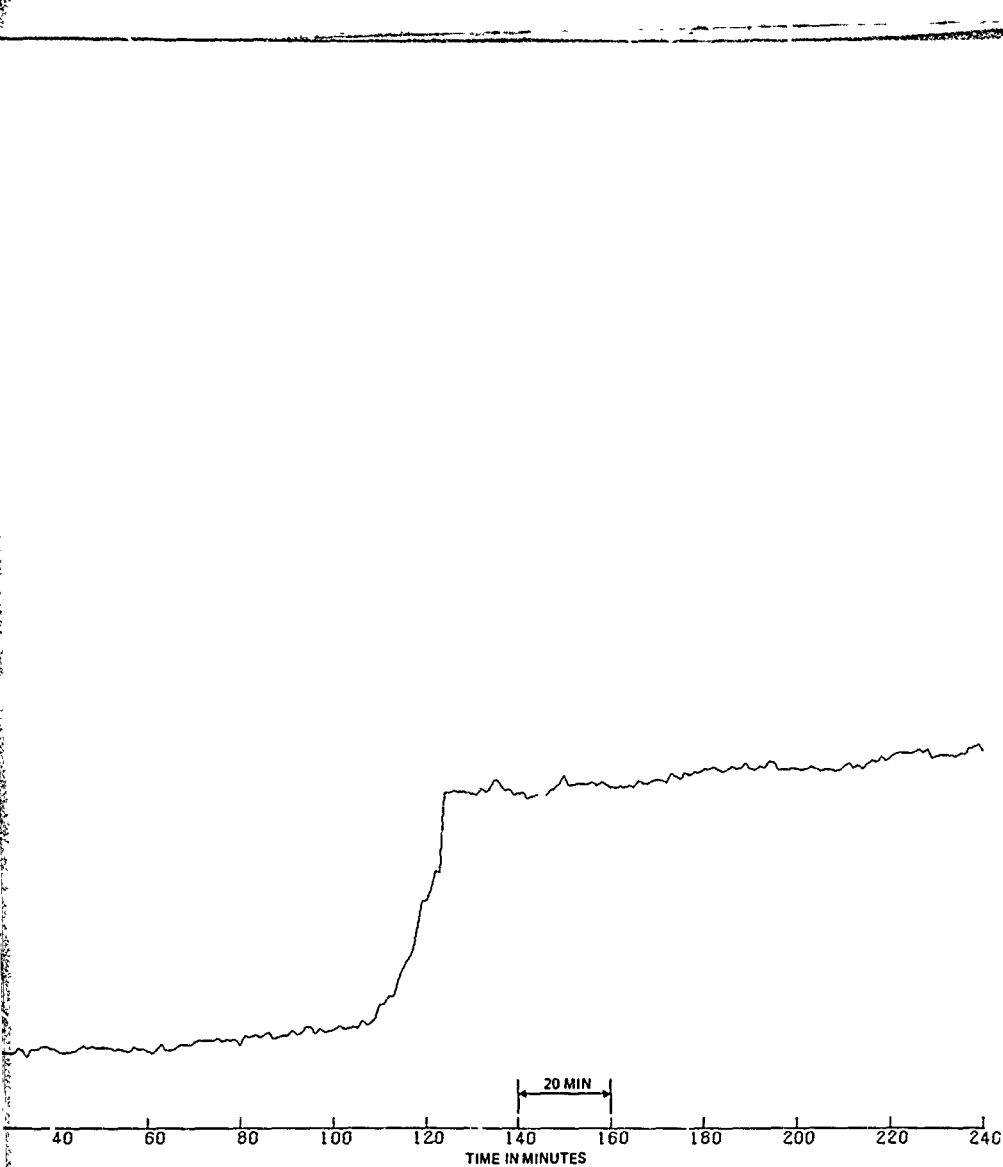


Figure 6-88. Z Acceleration Component vs Time; 7-15-75 - Z Vertical Position

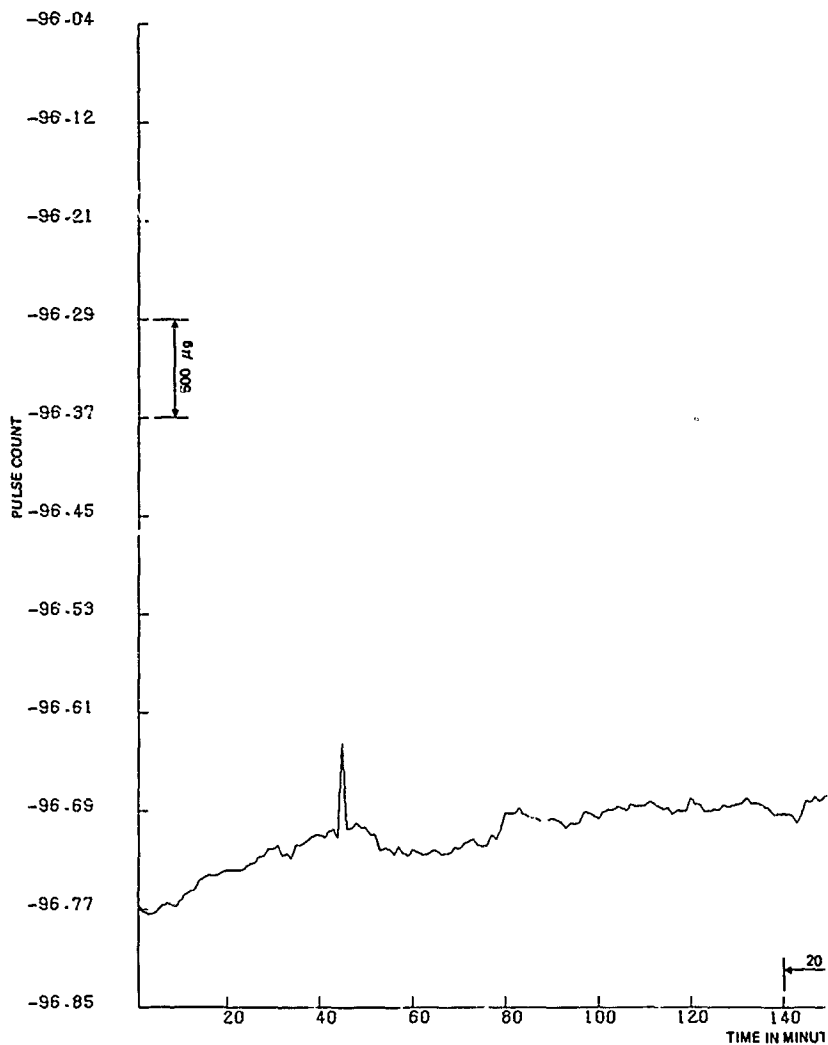


Figure 6-89. Acceleration Cc



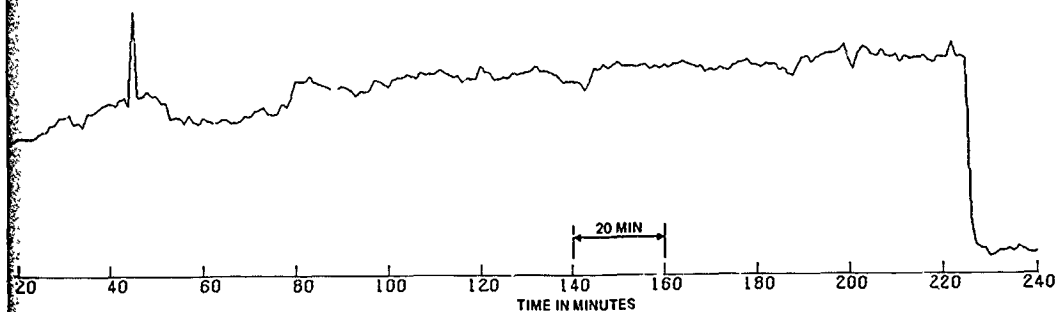


Figure 6-89. X Acceleration Component vs Time, 7-16-75, 1 Vertical Position

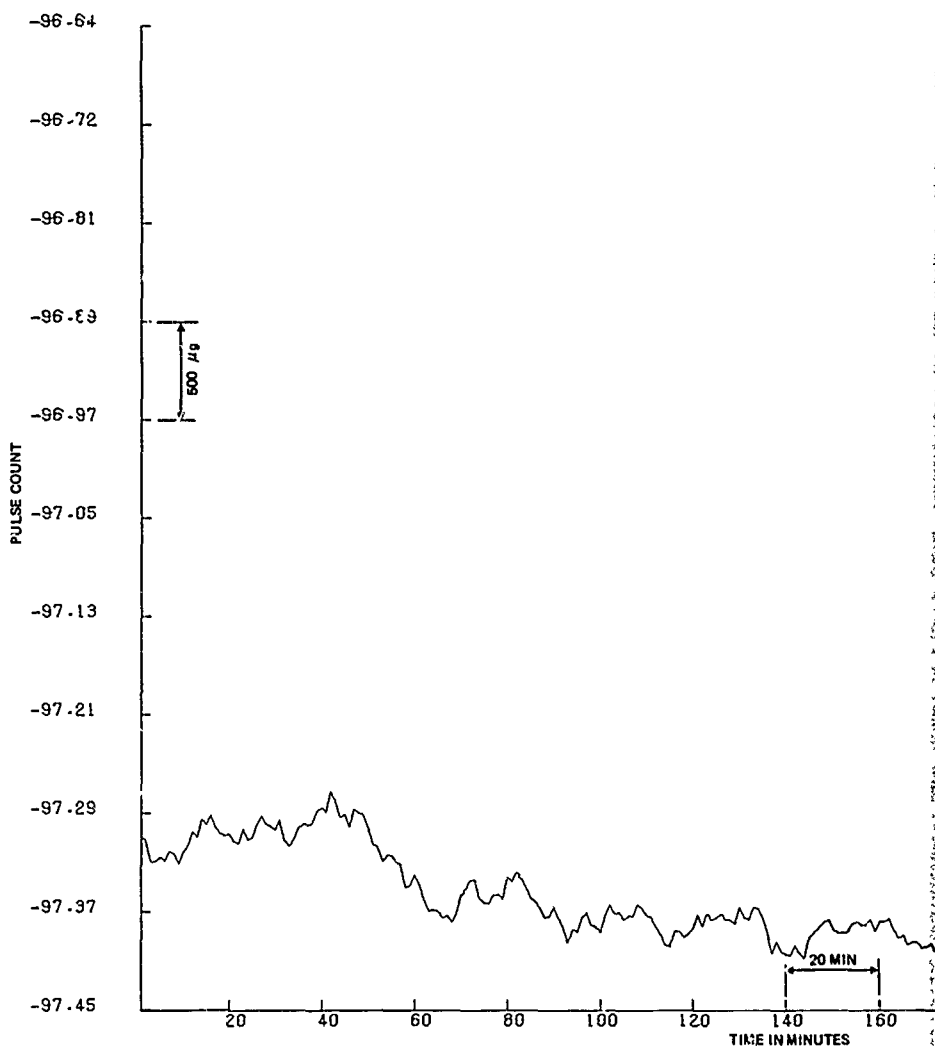


Figure 6-90. Y Acceleration Component vs

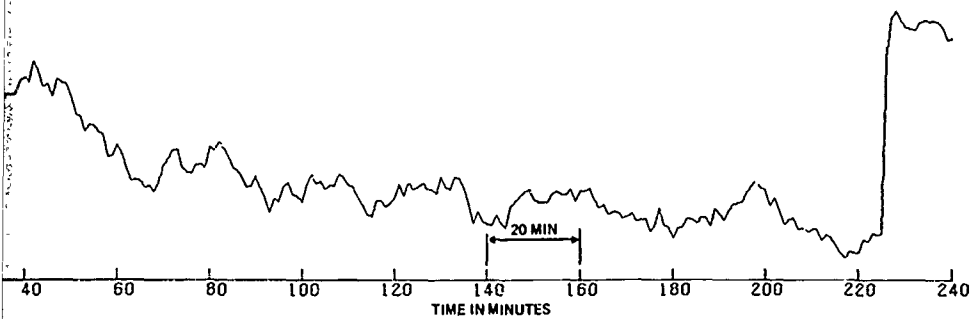


Figure 6-90. Y Acceleration Component vs Time; 7-16-75, +1 Vertical Position

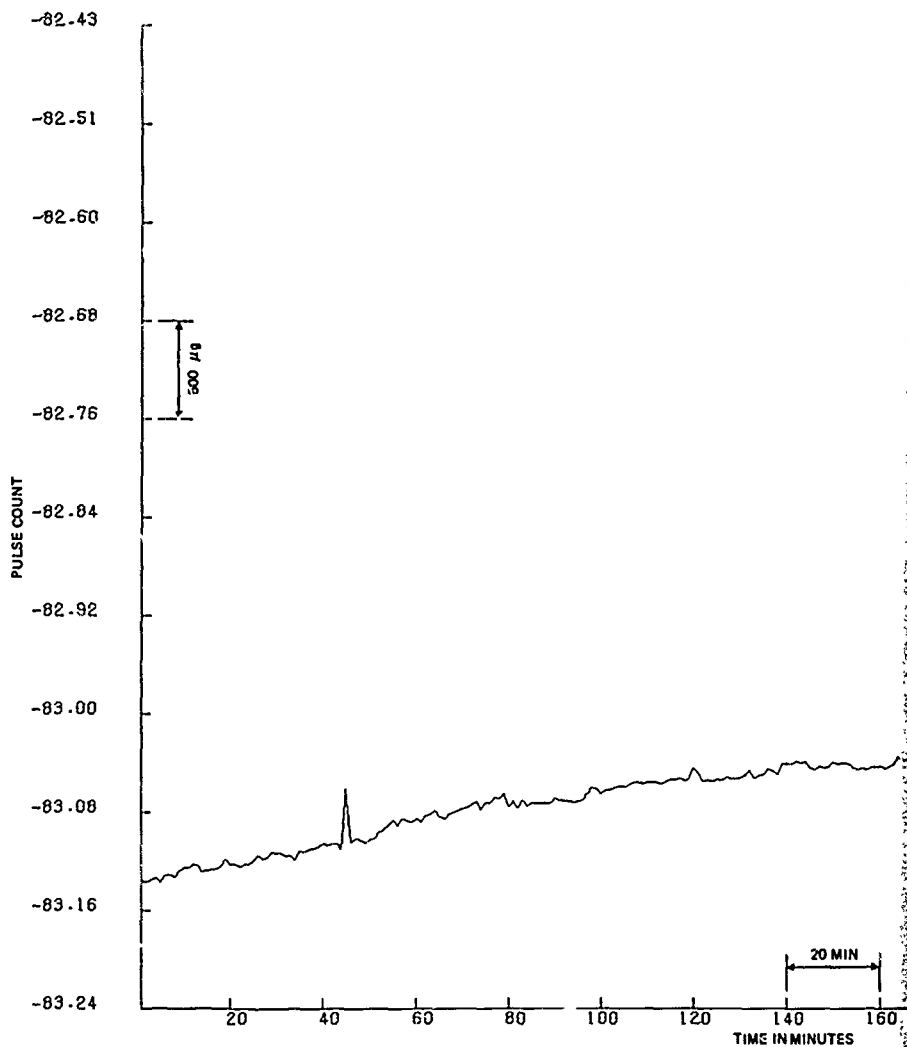


Figure 6-91. % Acceleration Component

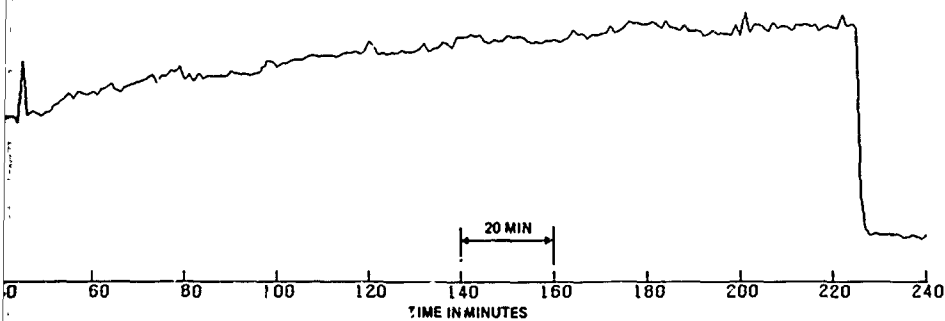


Figure 6-91. Z Acceleration Component vs Time; 7-16-75, 1 Vertical Position

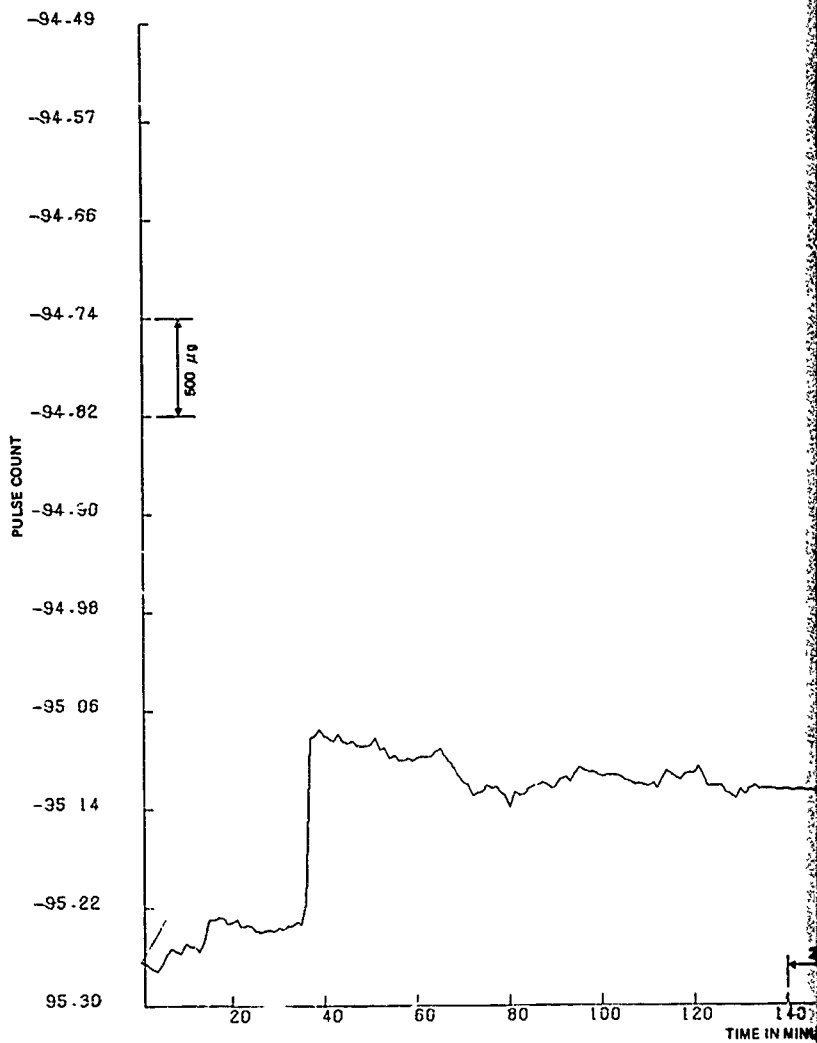


Figure 6-92. X Acceleration

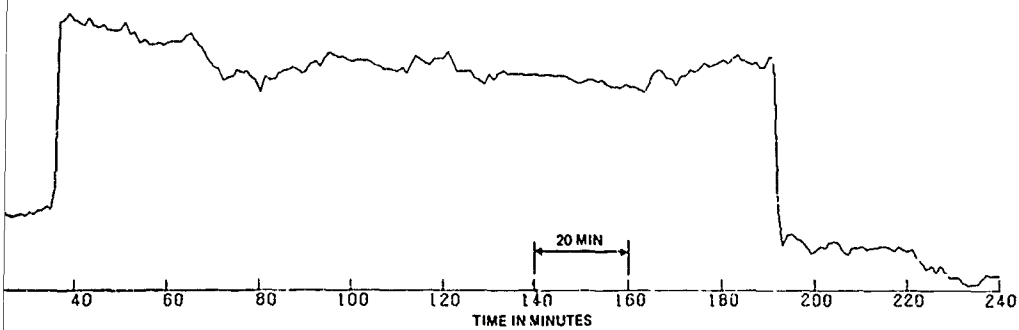


Figure 6-92. X Acceleration Component vs Time; 7-16-75, -3 Vertical Position

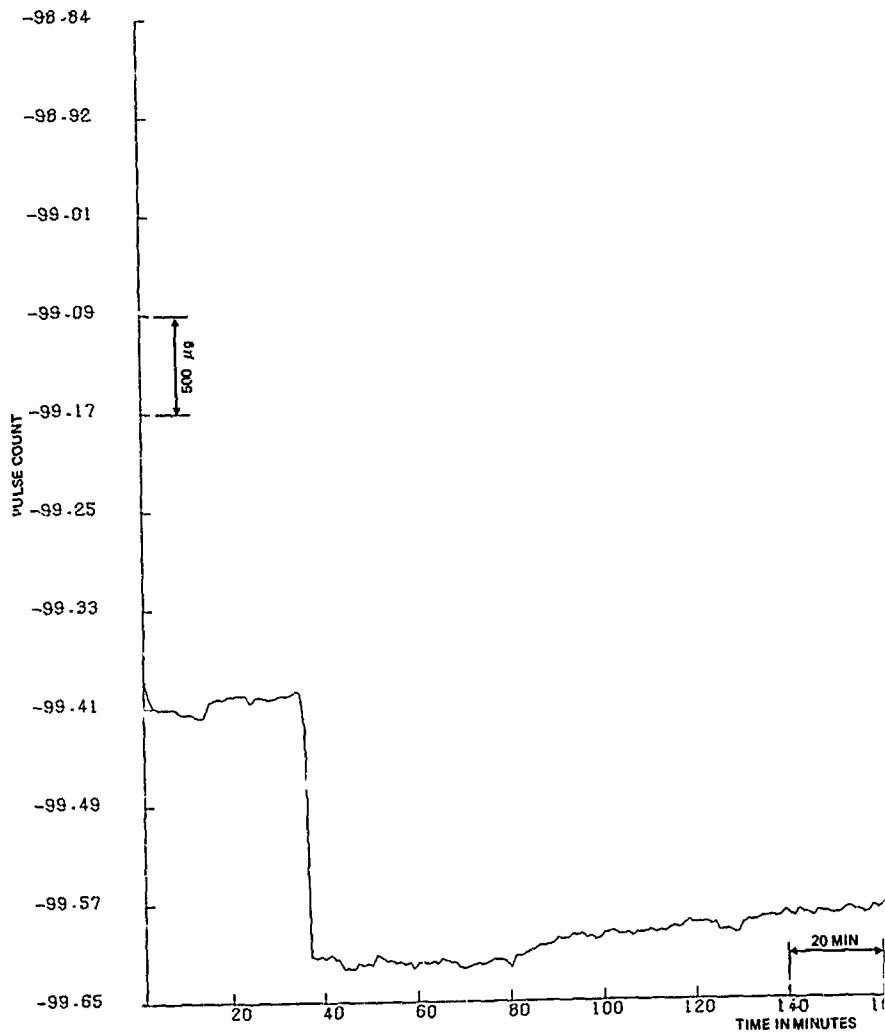


Figure 6-93. Y Acceleration Component



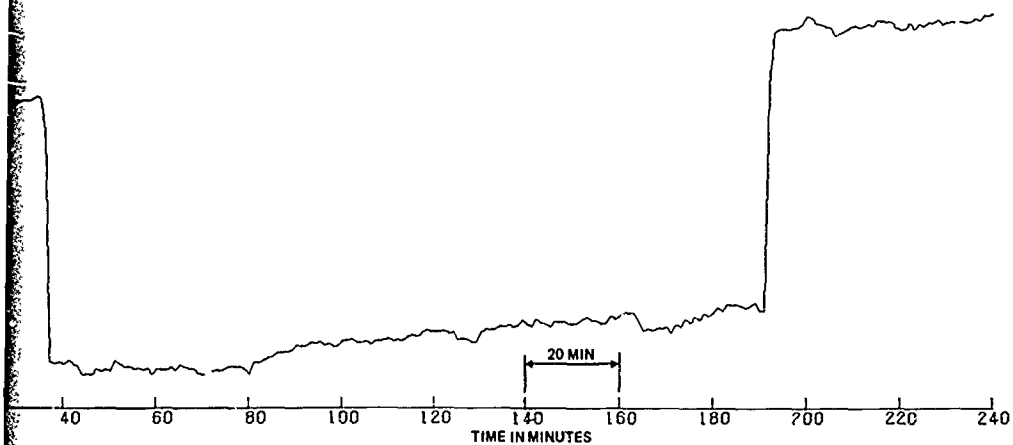


Figure 6-93. Y Acceleration Component vs Time; 7-16-75 -3 Vertical Position

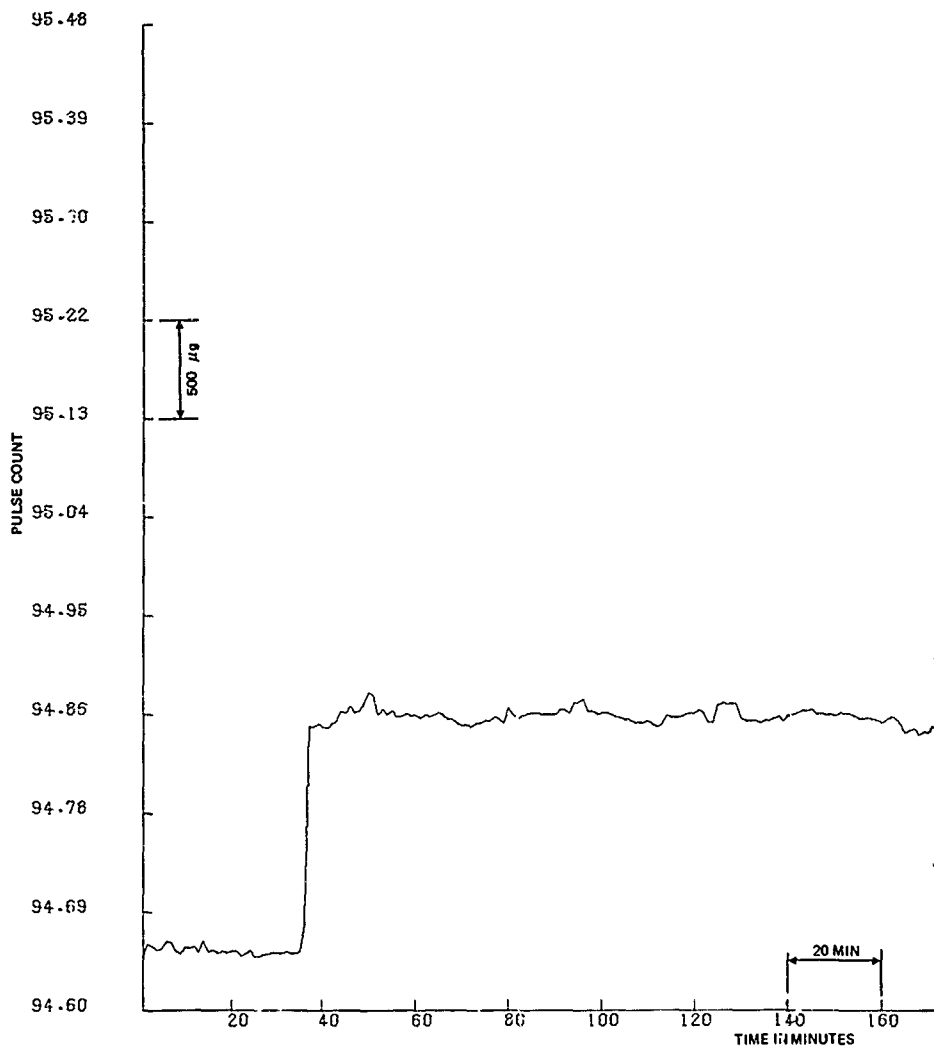


Figure 6-94. Z Acceleration Component v

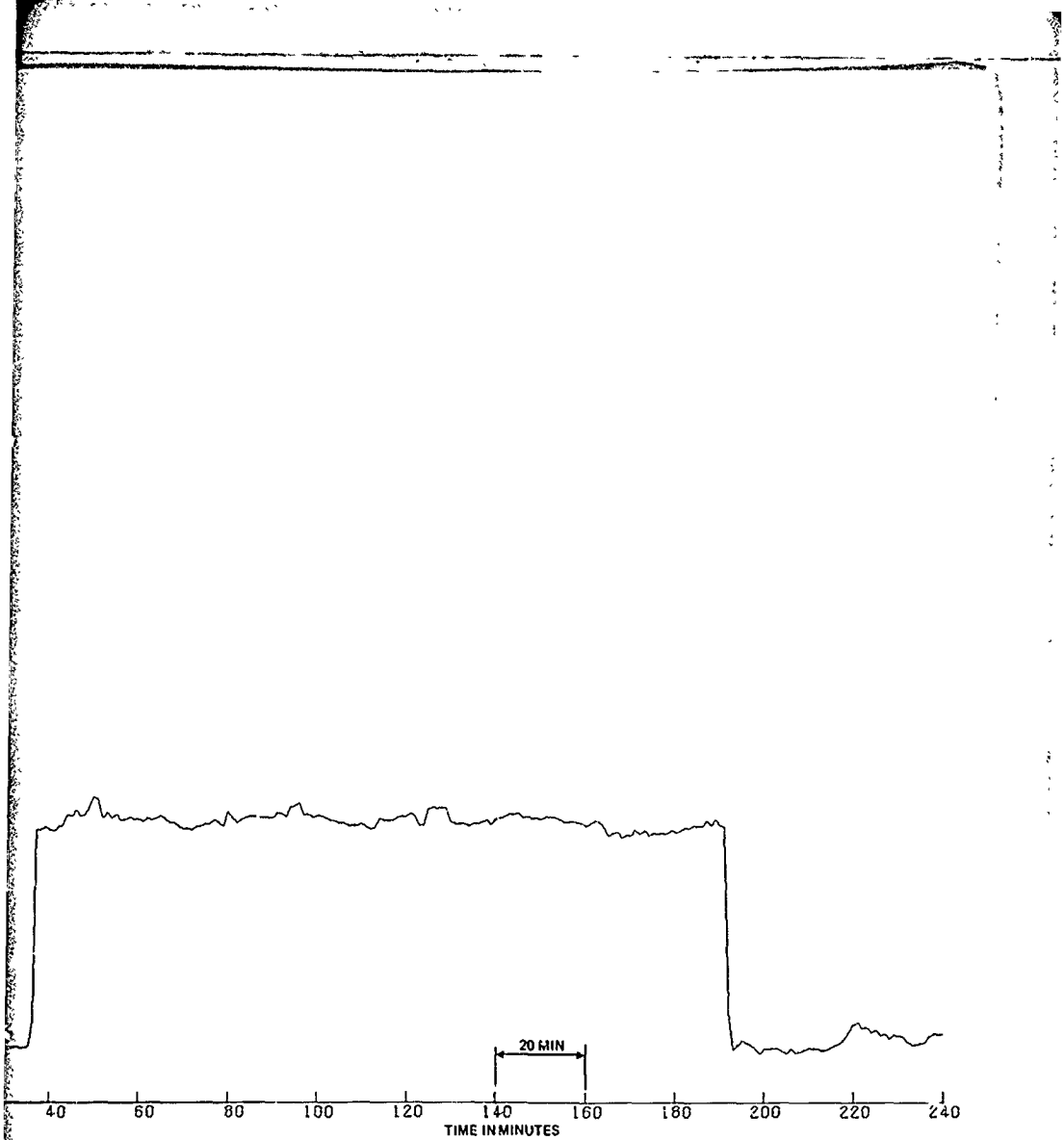
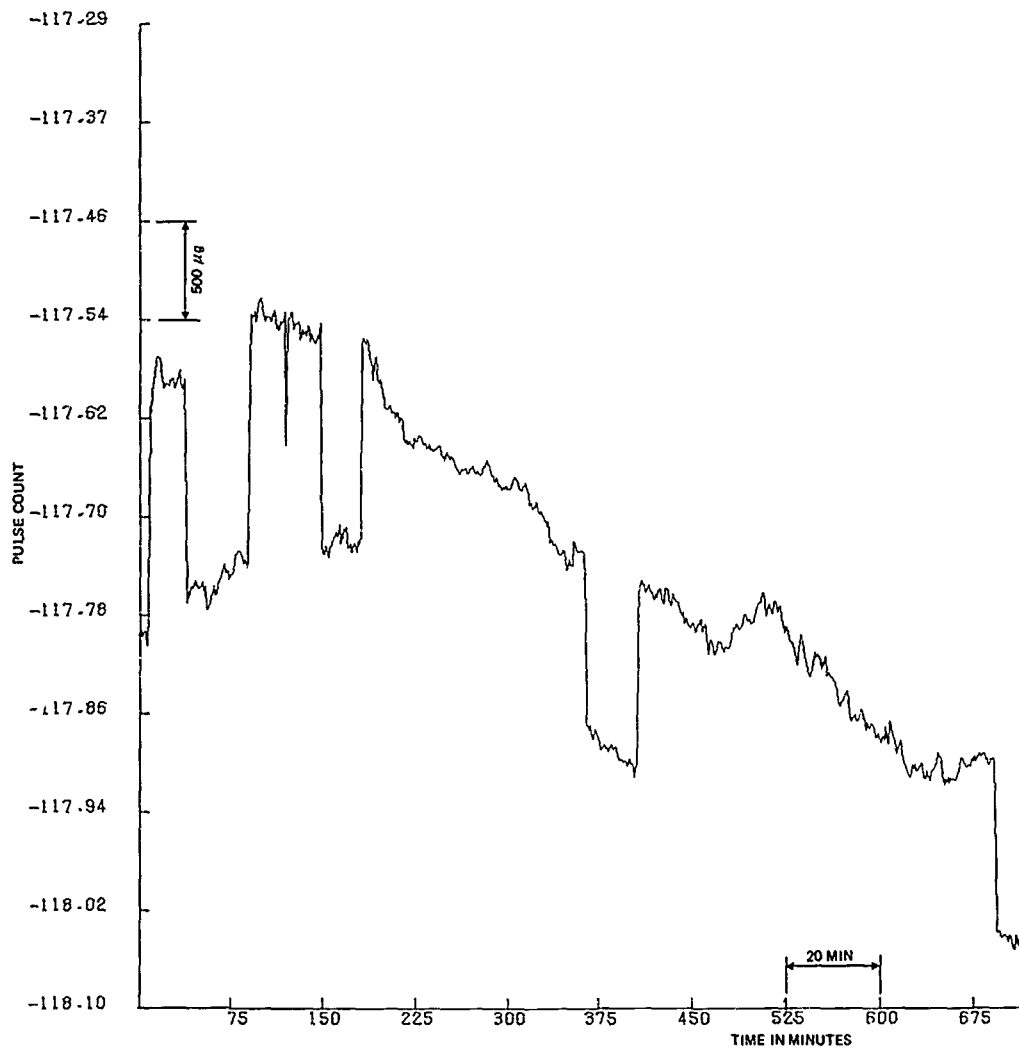


Figure 6-94. Z Acceleration Component vs Time; 7-16-75 -3 Vertical Position



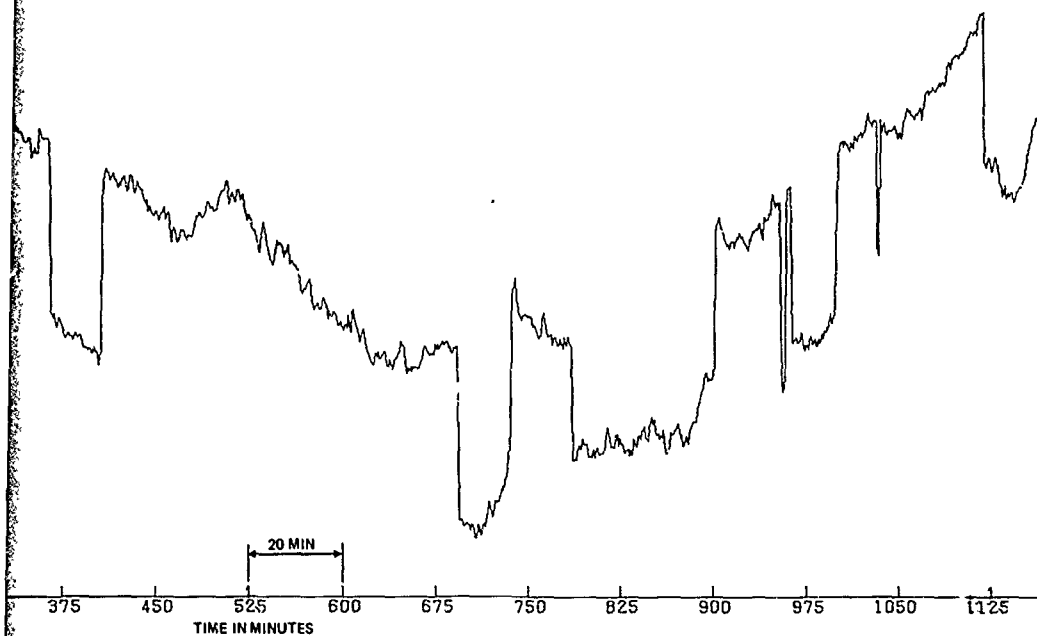
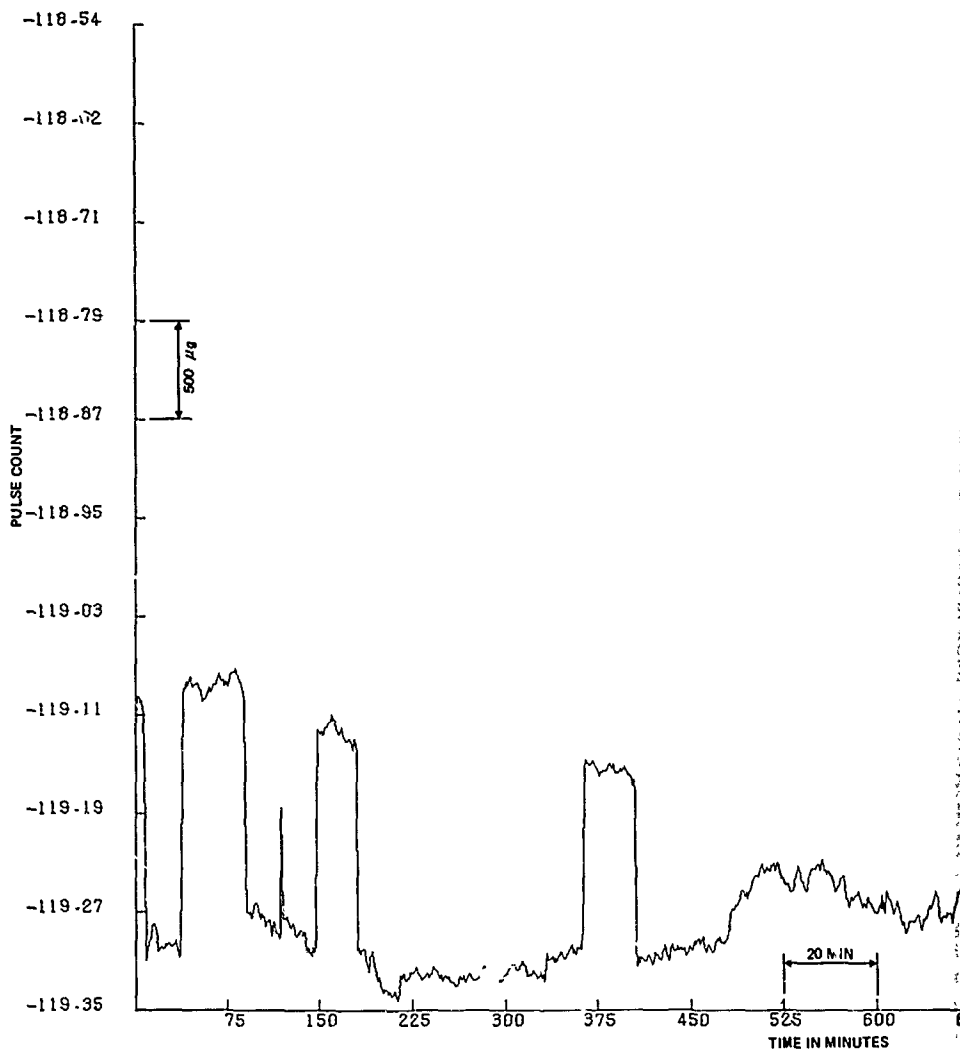


Figure 6-95. X Acceleration Component vs Time; 7-16-75  
7-17-75, Z Horizontal Position



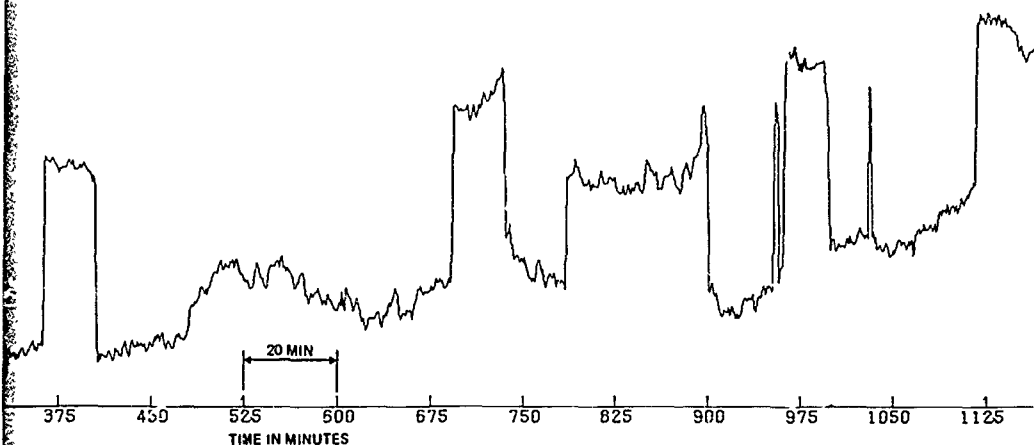
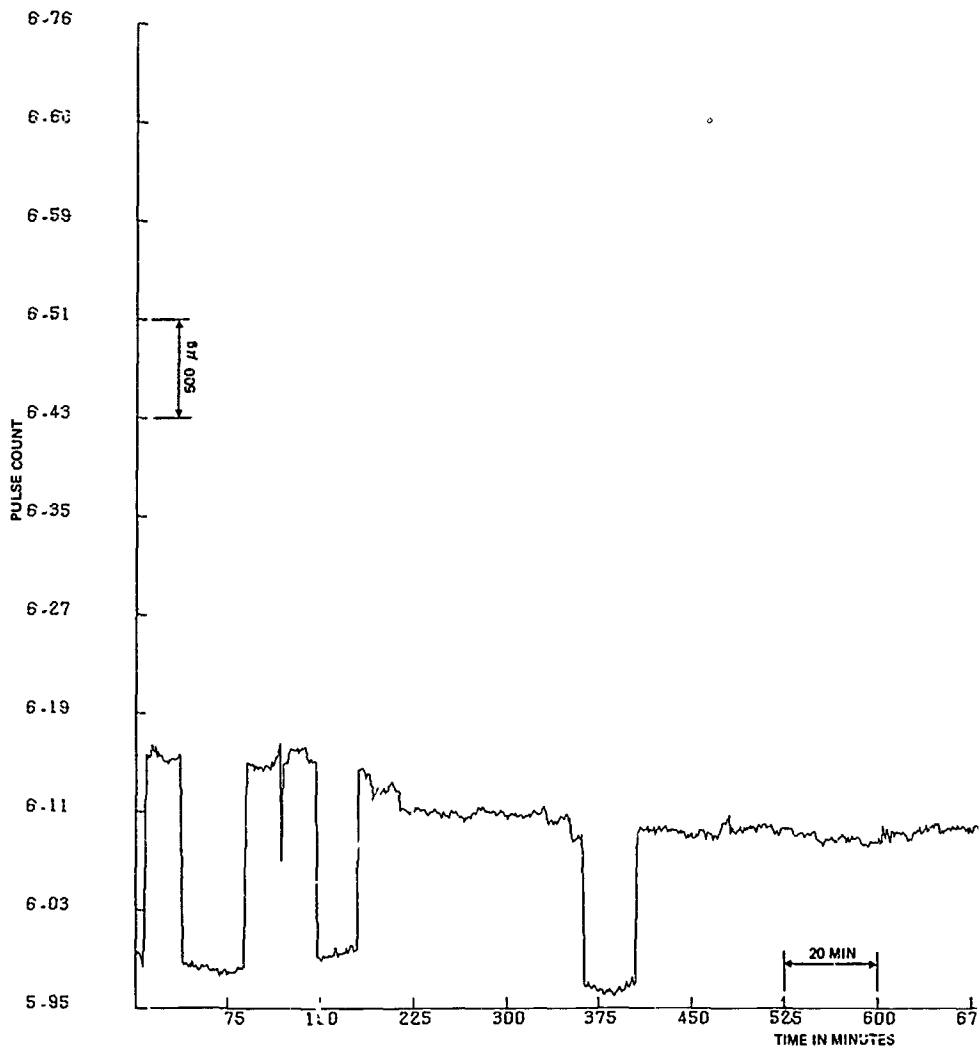


Figure 6-96. Y Acceleration Component vs Time; 7-16-75  
7-17-75, Z Horizontal Position





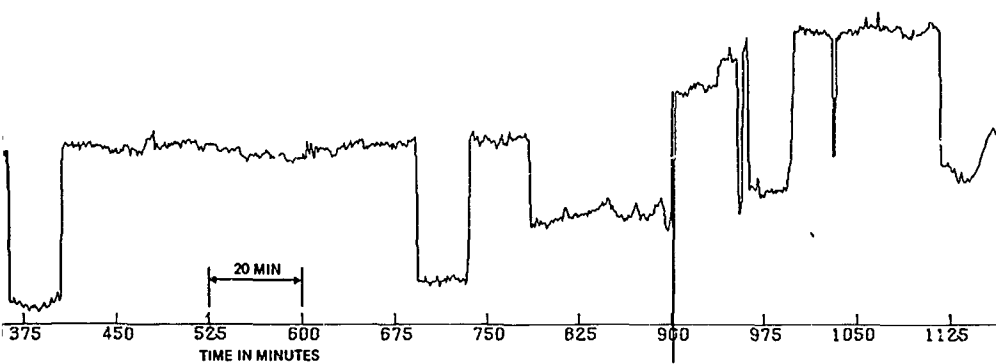


Figure 6-97. Z Acceleration Component vs Time; 7-16-75  
7-17-75, Z Horizontal Position

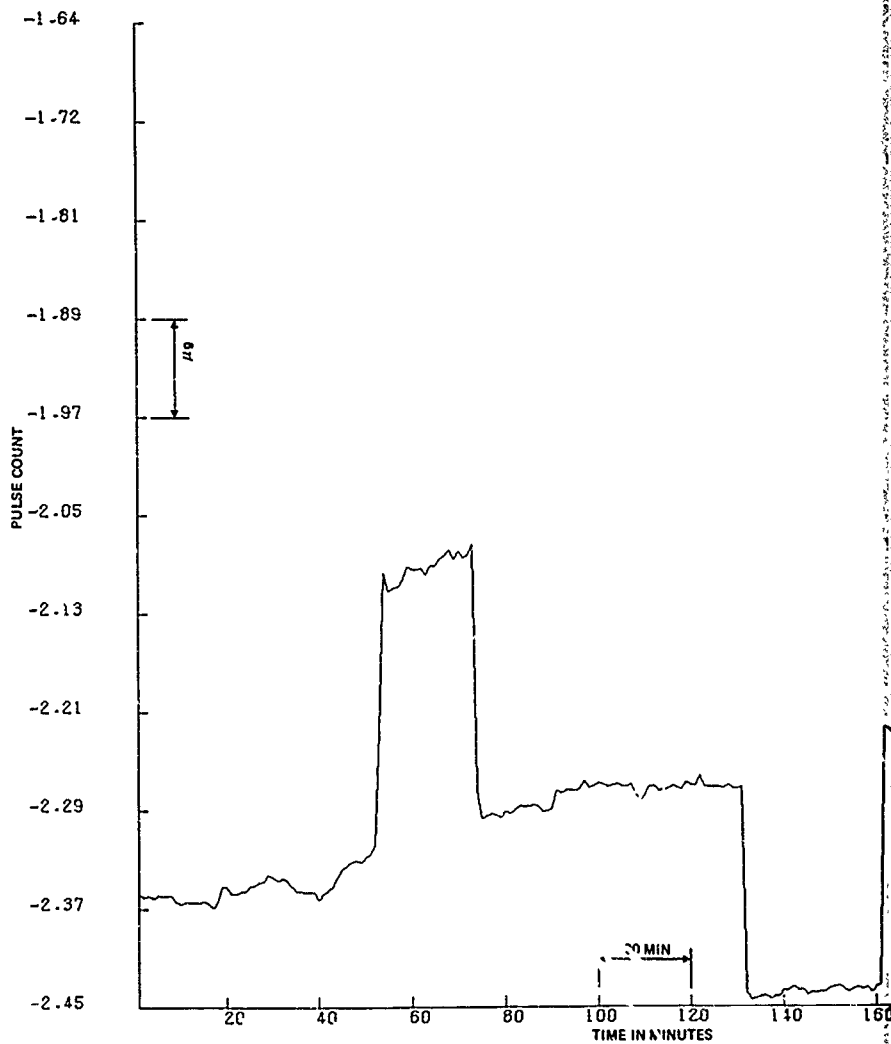


Figure 6-98. X Ac  
7-18

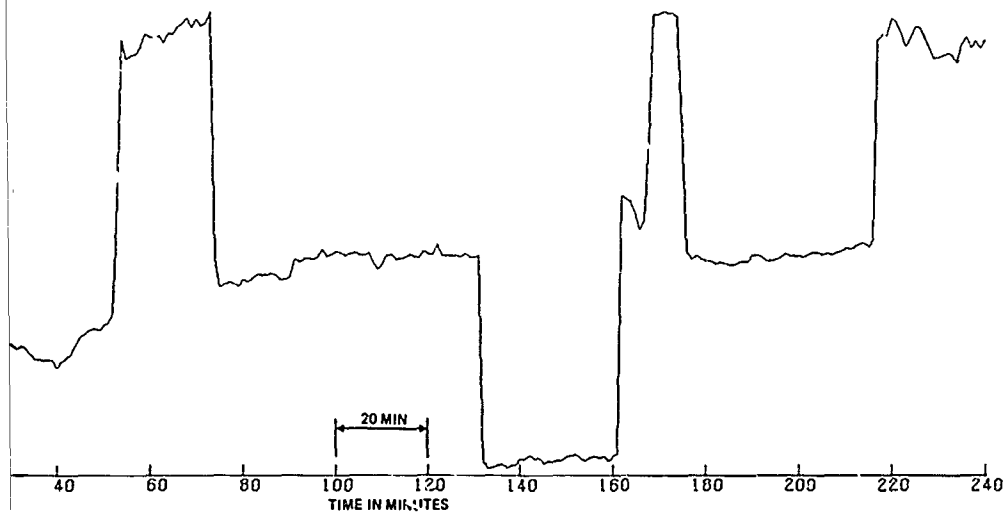


Figure 6-98. X Acceleration Component vs Time, 7-17-75  
7-18-75, -Y Vertical Position

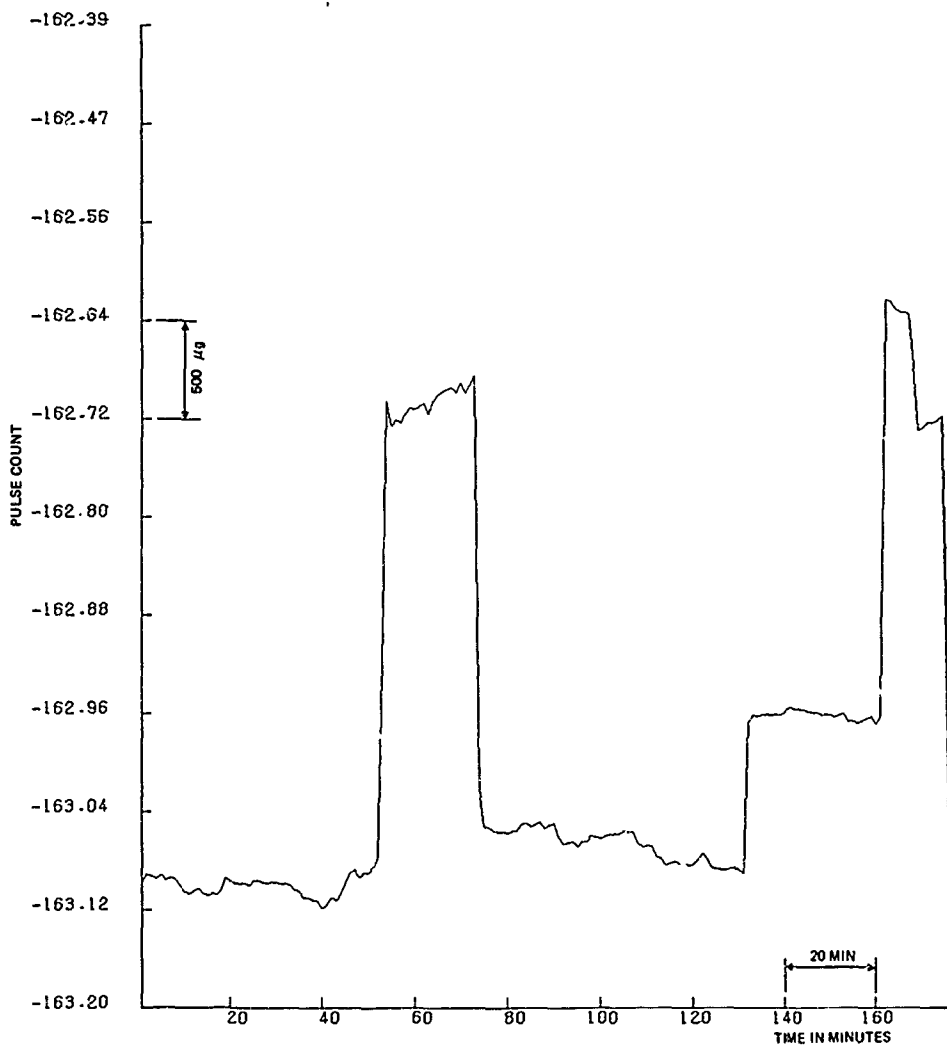


Figure 6-99. Y Acceleration  
7-18-75, -

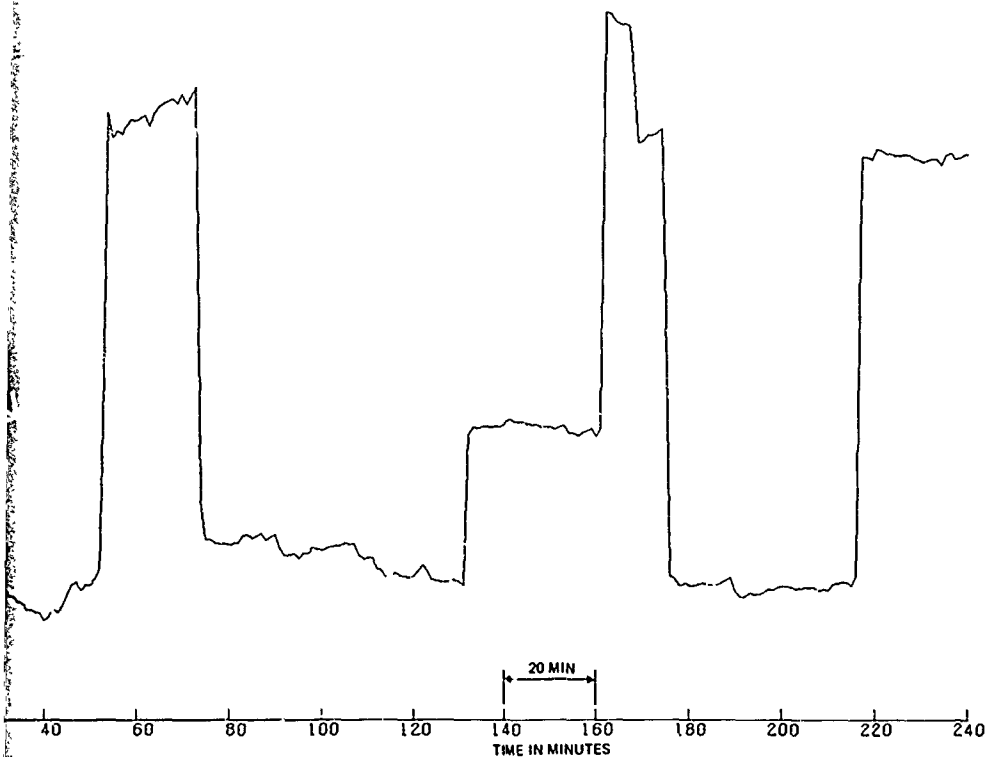


Figure 6-99. Y Acceleration Component vs Time; 7-17-75  
7-18-75, -Y Vertical Position

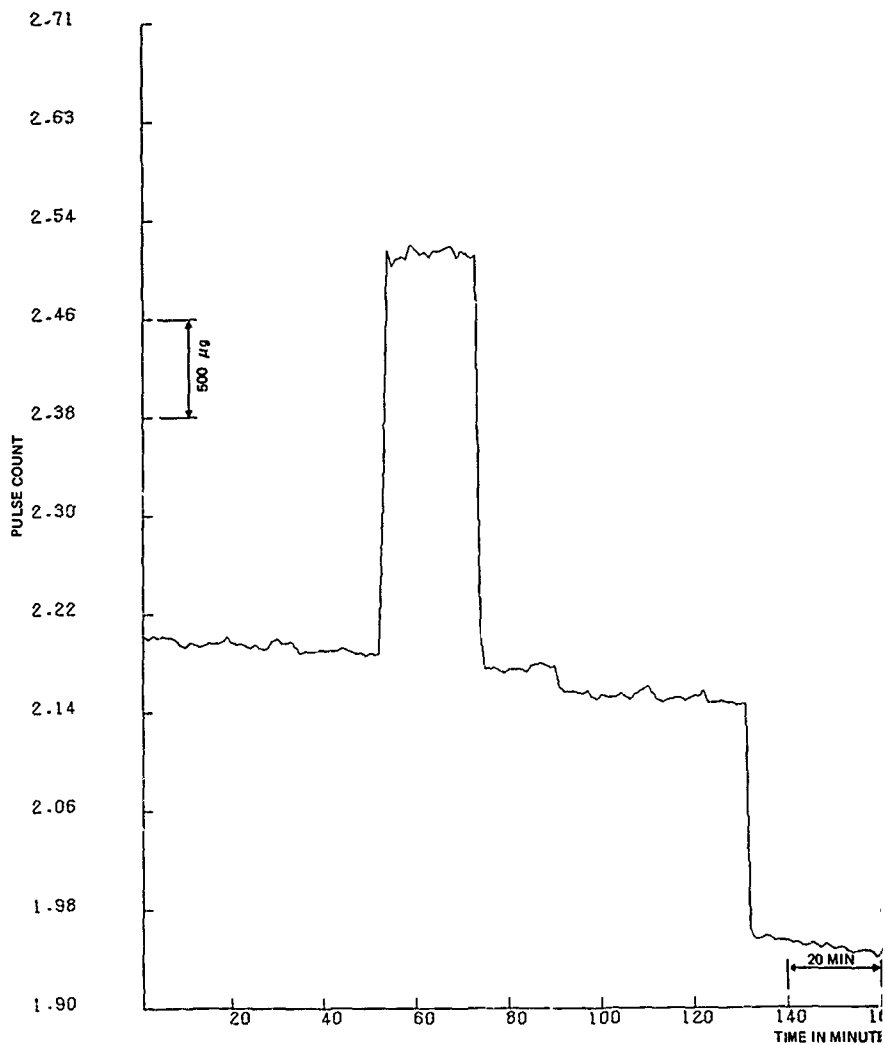


Figure 6-100. Z.  
7-]

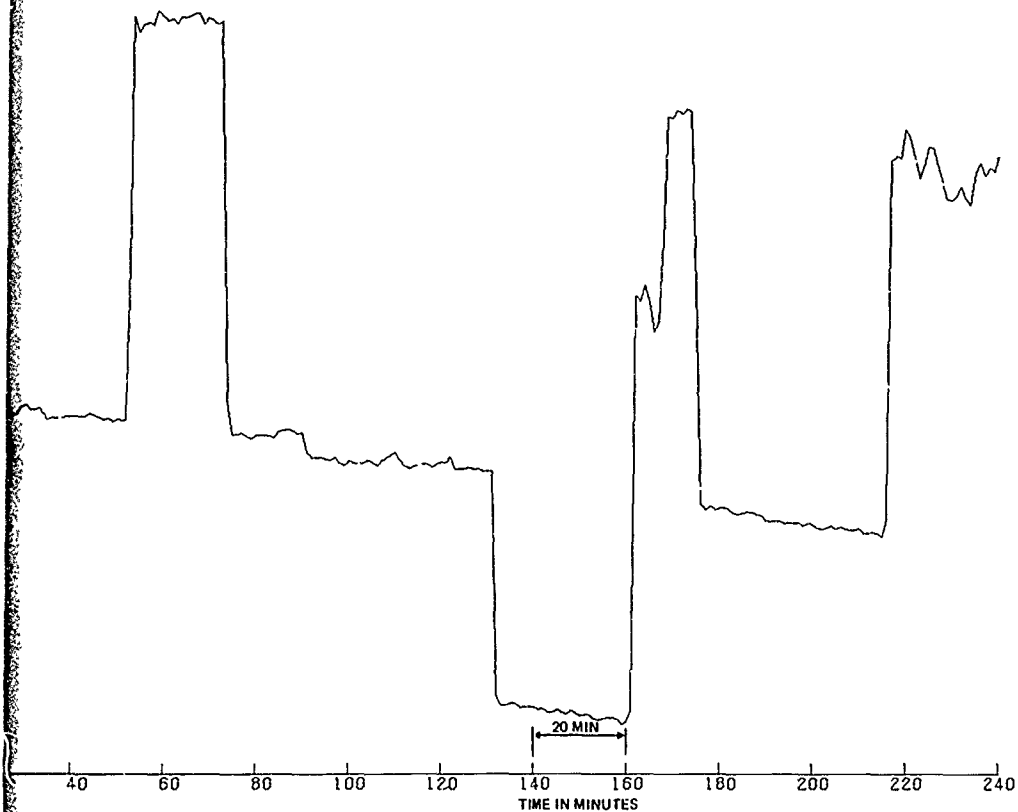


Figure 6-100. Z Acceleration Component vs Time; 7-17-75  
7-18-75, Y Vertical Position

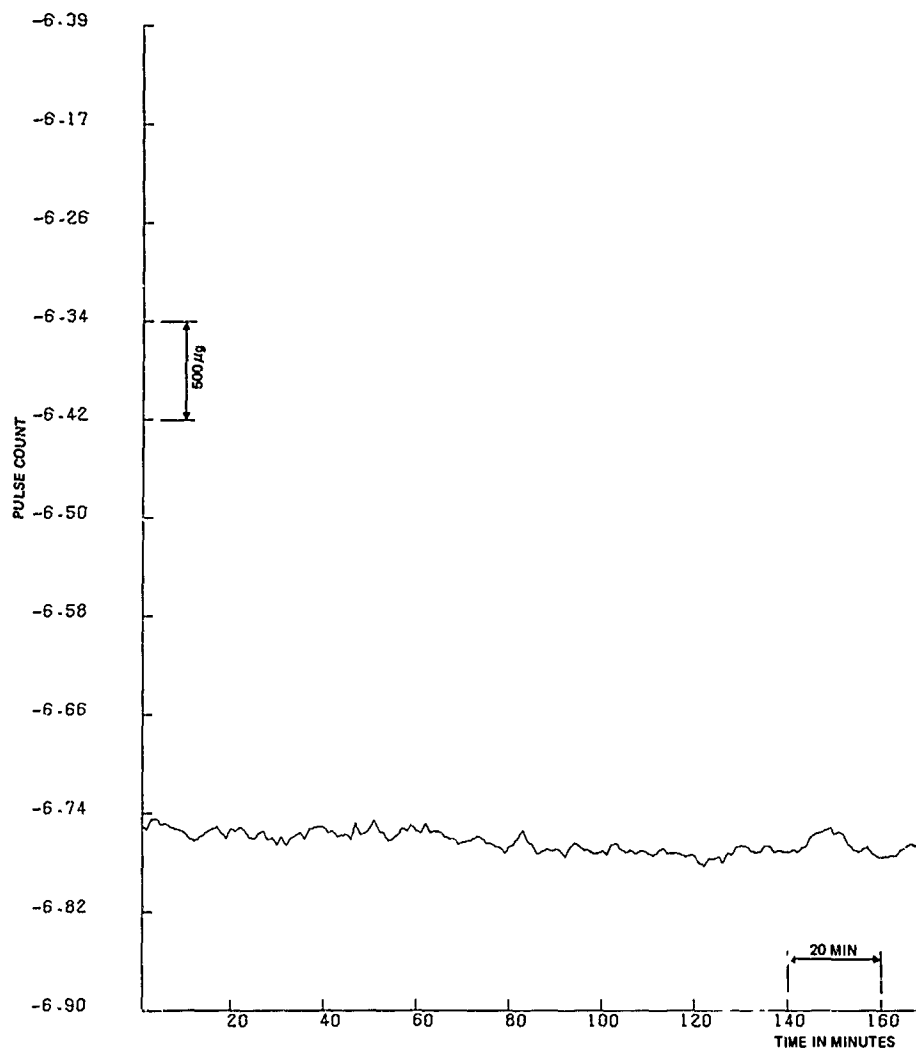


Figure 6-101. X Accel  
-Z



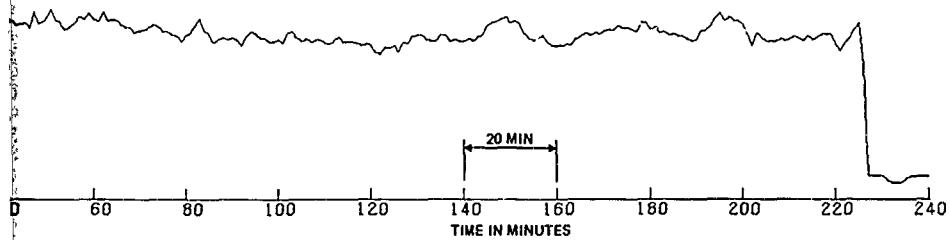


Figure C-101. X Acceleration Component vs Time; 7-18-75,  
-Z Vertical Position

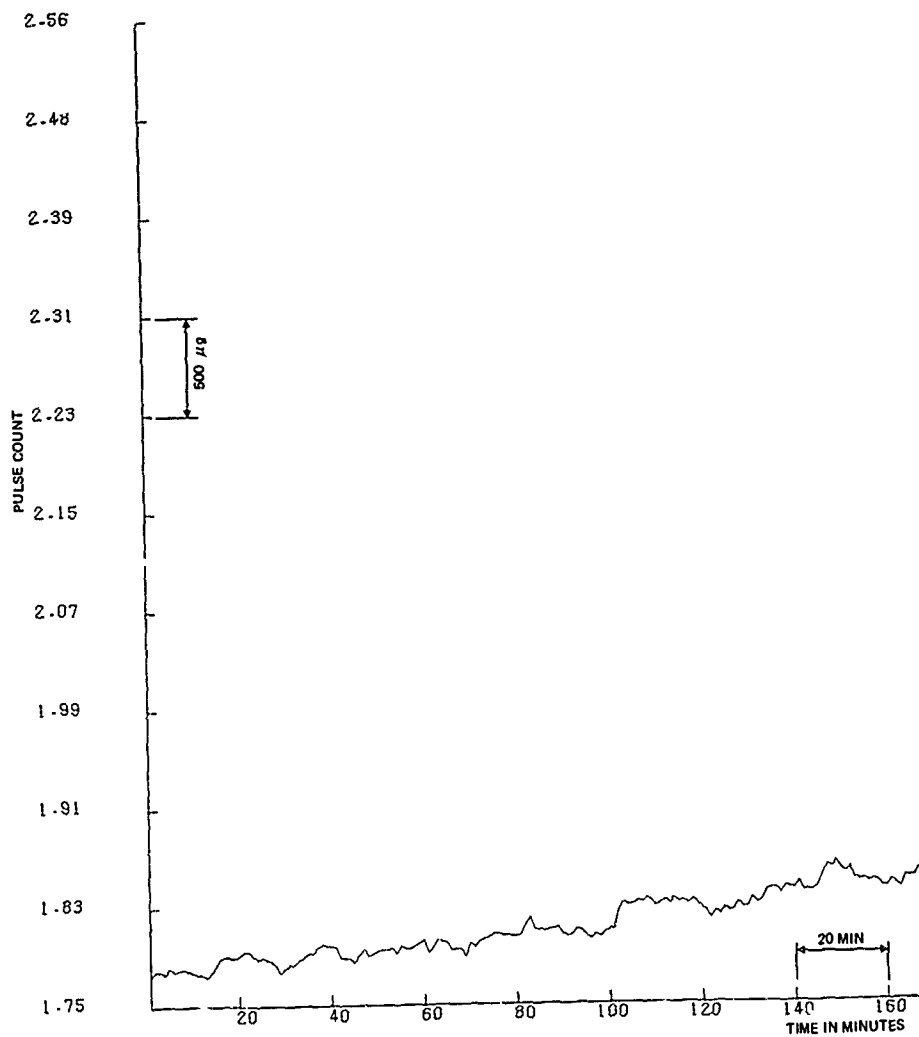


Figure 6-102. Y Acc

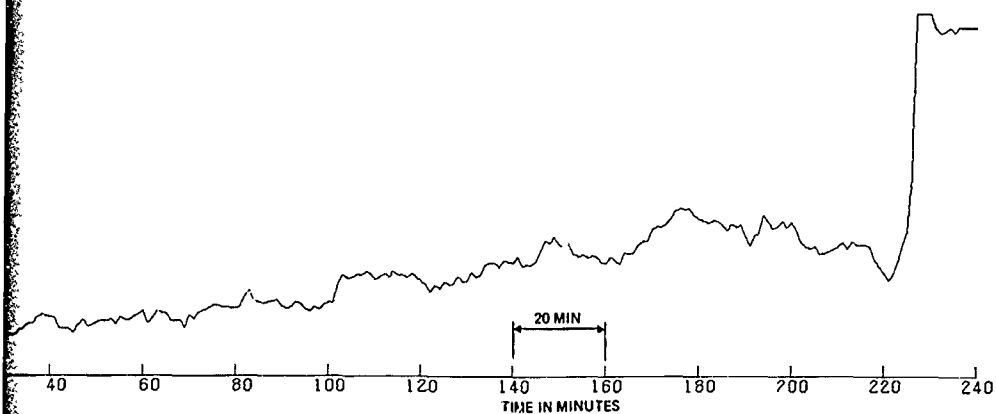


Figure 6-102. Y Acceleration Component vs Time; 7-18-75  
-Z Vertical Position

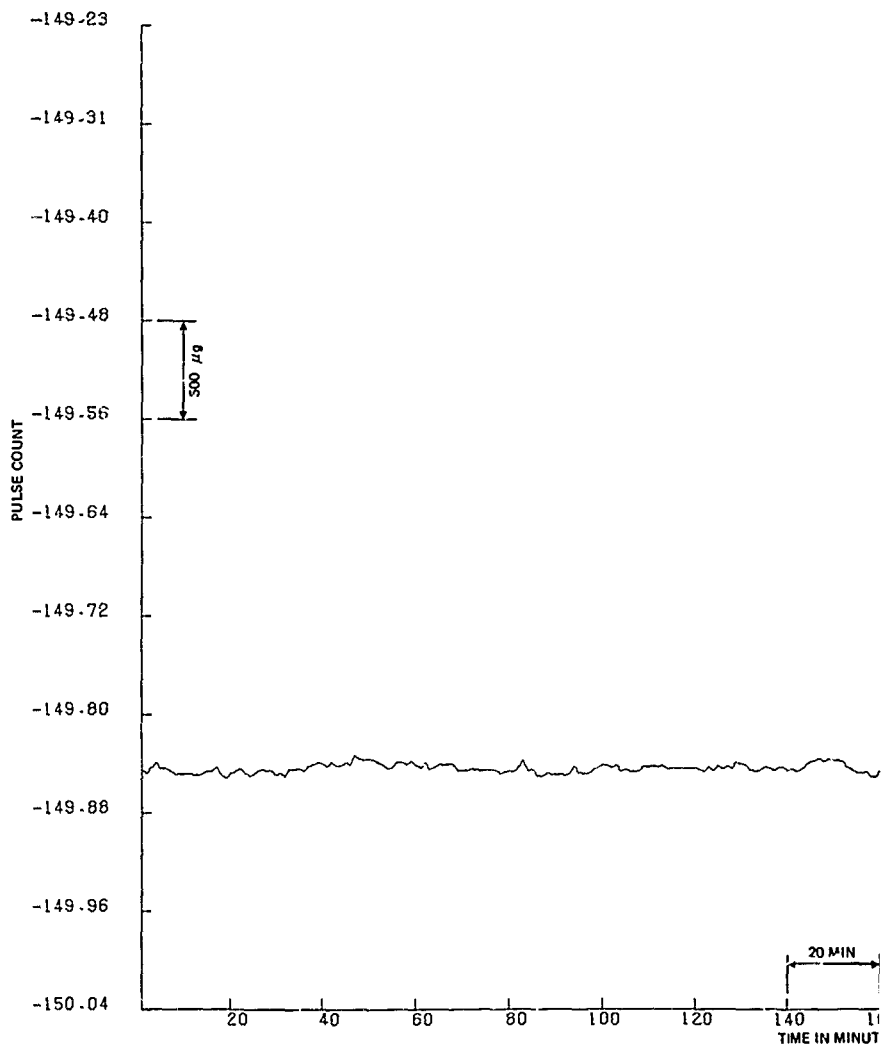


Figure 6-103. Z Ac

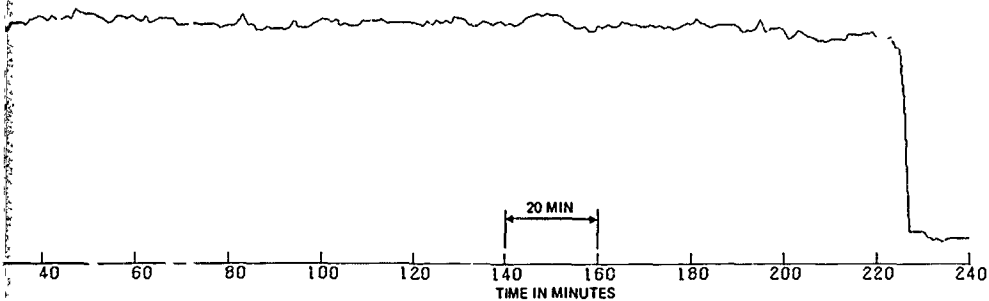


Figure 6-103. Z Acceleration Component vs Time; 7-18-75,  
-Z Vertical Position

Figures 6-86, 6-87, and 6-88 are plots of the x, y and z components of measured acceleration for the z axis vertical test of 15 July 1975. The short term noise (less than 10 minute "period") appears to be about 60  $\mu\text{g}$  peak-to-peak. This is less than the typical value of about 200  $\mu\text{g}$  seen in the PAM tests, see, e.g., Figure 6-78 for gyro 96. The transient level shift with midpoint at a time count of -120 (in all three axes) is of a magnitude similar to those observed in the PAM tests, see, e.g., Figures 6-74, 6-75, and 6-76. The duration of the transient appears to be shorter now, about 20 minutes vs an hour or so in the PAM tests. A change in one four-space axis (+2) could result in such a three-space change. The y axis (which sees the smallest acceleration) appears to have a periodic noise component with about a 50 minute period. The ramps in x and z are about the same, around 2  $\mu\text{g}/\text{min}$ ; this value of trend is similar to that observed in the 24 hr test on gyro 124 over a longer time period.

Figures 6-89, 6-90, and 6-91 are plots of the x, y and z components of measured acceleration for the +1 axis vertical test of 16 July 1975. As has been noted earlier, the z scale factor is larger than that of x and y (by about 3 percent); however, the difference between z and x and y in these figures is even greater (~17 percent) which implies some additional sources of asymmetry. The y axis again appears to have a noise component with about a 50 min period. The trends in x and z are similar as was the case for the +z axis test data of 15 July 1975. It is not known if the spike at a time count of 45 in x and z is real or not. The transient shift occurs in all three axes at the same time (-230 time count), and appears to be faster than the transient change seen in the z axis test on 15 July 1975. Note that the pattern of the change is the same (same direction in x and z, opposite direction in y) which could correspond to a +2 axis change.

Figures 6-92, 6-93, and 6-94 are plots of the x, y and z components of measured acceleration for the -3 axis vertical test of 16 July 1975. The magnitudes of the x and z components are within 1 percent of each other, but the magnitude of the y component is about 5 percent larger than x or z. Note that two transient changes occurred in this four hour test. The z measurement returns very nearly to its original level at the second change while x and y return to somewhat different levels. The pattern of the changes is again the same (x and z change in the same direction, y in the opposite direction). The magnitudes of the steps are on the order of 1000  $\mu\text{g}$  as before.

Figures 6-95, 6-96, and 6-97 are plots of the x, y and z components of measured acceleration for the 24 hr run with z horizontal and x and y 45 deg from vertical. This orientation results in g through the center of a plate edge. The pattern of changes in the transients is the same as before (x and z change in one direction and y in the opposite direction). The magnitudes of the changes are comparable to those occurring in other orientations (~1000  $\mu\text{g}$ ). The x axis appears to have a 24 hr variation present, with a magnitude on the order of 3000  $\mu\text{g}$ . The y axis may also have such a variation present, but z does not. The transients in the data make it difficult to analyze for periodicities and correlations. The actual time span of the data shown in these figures is about 24 hours.

Figures 6-98, 6-99, and 6-100 are plots of the x, y and z components of measured acceleration for the y axis vertical test of 17, 18 July 1975. This run had the most transients of all the four hour runs which were plotted. Also it should be noted that the transient pattern is different than that for the other stability runs. Some of the transient changes correspond to a +2 channel change as before; however, some correspond to a +1 channel change, for example the one at a time count of -52 is in the same direction for all three axes. The plot for the y axis run of 15 July 1975 (not included herein) was examined, and it exhibited the +2 channel type of transient change seen consistently in the other runs. There appears to be a trend in x and z of about 2  $\mu\text{g}$  per minute. However, initial and final values of y are about the same.

Figures 6-101, 6-102, and 6-103 are plots of the x, y and z components of measured acceleration for the z axis vertical test of 18 July 1975. If initial values here are compared with the corresponding final values in Figures 6-86, 6-87, and 6-88, it appears that x and z have shifted in a negative direction (-9900  $\mu\text{g}$  and 5300  $\mu\text{g}$  respectively), while y has shifted about 2300  $\mu\text{g}$  in a positive direction. These shifts occurred during a time interval of about 72 hours, during which the gyro had been in operation. Short term noise characteristics appear to be similar for the two runs. The trend in the 18 July 1975 data appears to be mostly in the y axis. The transients, in the 18 July 1975 data are faster than in the 15 July 1975 test, and are the +2 channel type which have occurred in the other runs.

Data were plotted for the +1 vertical run of 24 July 1975, which was the last stability run before the final calibration on the same date. There was an initial exponential decay transient of about 3700  $\mu\text{g}$  magnitude from start to maximum under-shoot in the x axis, with smaller ones in y and z. Such initial transients were also observed in the y vertical run of 15 July 1975, but were smaller in magnitude (-2000  $\mu\text{g}$  maximum).

The nominal acceleration values for the +1 axis vertical runs of 16 July 1975 and 24 July 1975 are considerably different in y and z. For example y on 16 July 1975 was -97.3 and -93.1 on 24 July 1975 for a change of about 26,000  $\mu\text{g}$ . The change in z was from -83.1 to about -78.7, which corresponds to a change of about 27,000  $\mu\text{g}$ . The change in x was on the order of 600  $\mu\text{g}$ . The scale factors in the 24 July 1975 calibration were larger in magnitude than those of the 15 July 1975 calibration. This is in agreement with the shift in y and z outputs. The change in the x scale factor was about the same as that for y and z; however, the change in x bias was opposite in sign to that for y and z. This bias shift in x could mask a scale factor shift for the +1 vertical data of 24 July 1975.

One of the differences between the GSA PWM suspension servo and the T/S IV PAM suspension servo is that the preload is lower for the FWM servo. (Preload is defined to be the force applied when no external force is present.) In the case of PAM, the reference charge  $Q_{PAM}$  is applied during 45 out of 50  $\mu\text{sec}$ , or 90 percent of the time. During the PAM forcing period (35 out of 50  $\mu\text{sec}$  or 70 percent of the time) the charge is  $Q_{PAM} + \Delta Q$  where  $\Delta Q$  is adjusted to keep the rotor centered. In the case of PWM a reference charge  $Q_{PWM}$  is applied during the readout period and the rotor position is determined. A restoring signal is then generated which is constant in amplitude but whose duration is proportional to the rotor position error. Thus the PWM preload is the force applied by the readout charge.

The readout period for the GSA is 8  $\mu$ sec out of 50  $\mu$ sec. The command signal during this time is 2.8 v, and the corresponding signal during forcing is 3.2 v. If it is assumed that 2.8 v corresponds to -120 v on a plate, and the corresponding plate voltage for T/S IV was 100 v, then the PWM preload is about  $(\frac{8}{45})(1.2)^2 \approx 0.25$  times the PAM T/S IV preload. The PWM forcing acceleration capability corresponding to 3.2 v would be about  $(0.7)(12g) = 8.4 g$ . Thus it is estimated that the GSA PWM servo should be about four times less sensitive to bias error sources than the T/S IV PAM servo. It should be noted that the high g/low g mode capability originally planned for the GSA was deleted because of switching transient problems. Therefore, when the MESGA tests were run on the GSA only a single  $\gamma$  mode capability was mechanized.

An error source which can be related to charge will result in a scale factor error for PWM which is twice that for PAM. The reason is that the force error depends upon charge-squared ( $Q_c^2$ ) in PWM and on charge ( $Q_o$ ) for PAM. It follows that the PWM servo is twice as sensitive to scale factor error sources (related to charge) as the PAM servo.

The overall advantage of PWM over PAM depends upon which error sources dominate. It was crudely estimated early in Phase 2A ( July 1974) that the PAM errors would be about 5 times the PWM errors, see Table 6-53.

One compromise was made in the electronics design which may contribute to the PWM errors being larger than expected: the acceleration preprocessor is blanked during the readout pulses, acceleration measurement occurs only during the interval allowed for forcing. This approach was adopted in order to simplify the preprocessor (demodulator) mechanization. If any change occurs in the force applied during readout, this will result in a change in the measured force and hence in an error. If the measurement included the readout period, then a change in readout force would be balanced by an opposite change in command force, and the sum (the measured force) would not change.

Gyro 14y has a beryllium base, which is different from the gyros (68, 124, 96, and 102) used in the T/S IV tests. The crack size (plate separation) is smaller for gyro 14y than for the earlier gyros. The possible effects on acceleration readout of the smaller crack size have already been discussed. It is not expected that the base material should affect acceleration readout. Stray capacity from plate to ground for gyro 14y should be lower than that for gyros 68, 96 and 102. Gyro 124 already incorporated the bare equator design which is also present in gyro 14y. Test data have shown that the bare equator design results in less capacity from plate to ground than the old plated equator design.

The results of MESGA testing on the GSA and GSA T/S can be summarized as follows:

1. One gyro (14y, beryllium base) was used.
2. Test data were acquired over the time period 15 July 1975 through 24 July 1975.
3. Three calibrations (one hour each) were performed; over 64 hours of stability data were acquired.



4. Data were acquired in two time periods separated by a shutdown.
5. Two calibrations were performed back-to-back, and one calibration was performed after a shutdown.
6. Parameter shifts in the back-to-back calibrations (370 PPM RMS in scale factor and 1370  $\mu\text{g}$  RMS in bias) were comparable with those obtained in PAM tests, in particular on gyro 102.
7. Parameter shifts across a shutdown were very large (12,500 PPM RMS in scale factor and 18,200  $\mu\text{g}$  RMS in bias).
8. Stability tests were run at three types of orientations of the g vector.
  - a. Plate corner (24 hours with y and z vertical)
  - b. Plate center (16 hours with +1 and -3 vertical)
  - c. Plate edge (24 hours with z horizontal and x and y 45 deg from vertical).
9. Calibration repeatability for the GSA and GSA T/S MESGA tests was no better than that obtained in the PAM tests on T/S IV.
10. Stability data is reviewed below.
  - a. Short term noise (<10 min period) was about 60  $\mu\text{g}$  peak-to-peak, which is about 1/3 to 1/4 that seen in the PAM tests.
  - b. Two state transients were generally about 1000  $\mu\text{g}$  in magnitude and occurred in all the plotted runs except one (+1 plate vertical on 24 July 1975). In all runs where they did occur, they could be a result of +2 axis changes except for one run (17 July 1975 y axis vertical test).
  - c. The largest two state transients were about 3000  $\mu\text{g}$  in magnitude and could be a result of +1 axis changes. These occurred in the 17 July 1975 y axis vertical test only. Nothing like the 100,000  $\mu\text{g}$  steps seen on gyro 68 were observed. In particular, the noise characteristics before and after the step changes were similar.
  - d. Trends on the order of 2  $\mu\text{g}/\text{min}$  were observed. These were comparable with trends observed in the PAM tests on T/S IV.
11. The system requirements for acceleration sensing are 50 PPM in scale factor and 25  $\mu\text{g}$  in bias. The measured performance on the GSA and GSA T/S was between two and three orders of magnitude worse than these requirements.

### 6.3.6 Design Alternatives

#### 6.3.6.1 MESG/MESGA Design Alternatives

The intent of the design alternatives task was to design an instrument and to update the instrument design as required to assure adequacy of the MESG to perform in the MICRON system environment. It was necessary that the task complement other efforts such as eight-plate MESG/MESGA, four-plate MESG and Vaclon pump elimination efforts. The culmination of the effort resulted in a design and fabrication of hardware typically represented by Figures 6-104 and 6-105.

At the initiation of Phase 2A, the MESG instrument had proven itself satisfactory for system operation with regard to angle calibration, drift calibration, and performance in a non-hostile system environment. The ability to hold critical tolerances on the rotors and cavities was proven.

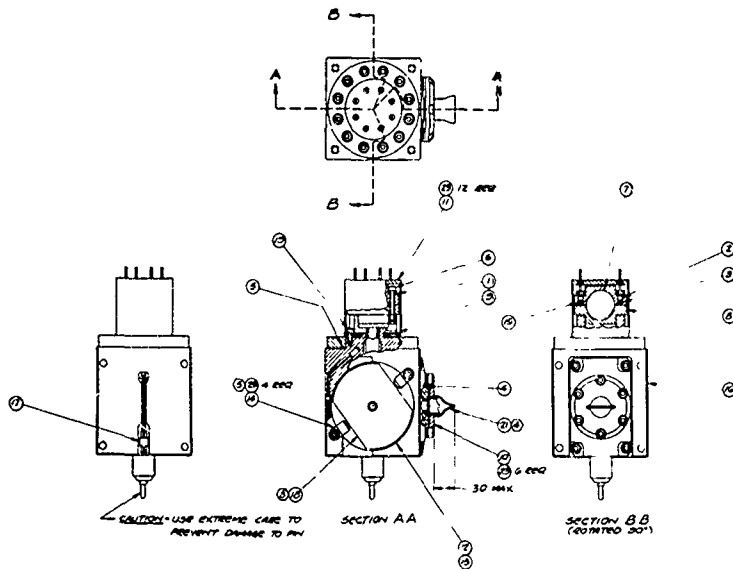
At the initiation of Phase 2A it was recognized that the greatest challenge with regard to the instrument was to develop its fast reaction capability. The significant areas of major development required to produce a functional instrument was primarily with regard to:

1. Reduced case-to-cavity thermal time constant.
2. Motor and motor function development with regard to  $80^{\circ}\text{F}$ . minute rotor heating, spin up, polhode damping, spin down, Z-coil heating and rotor precessing.
3. Development of a fast polhode period rotor with reliable polhode pattern or "signature" as required by computerized polhode damping.

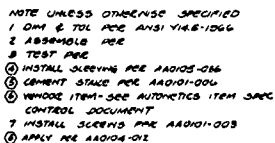
Other alternatives were considered and are presented below along with the reason for their consideration.

**6.3.6.1.1 Reduce Cavity-to-Case Thermal Time Constant.** A gyro design was initiated to reduce the thermal time constant from the MESG/System mounting surfaces up to and including the cavity. The 1 April 1974 N57A type MESG had a time constant in excess of five minutes, and the new desired goal was to achieve a 30-second time constant. Various layouts and designs were accomplished and the final design resulted in a one piece beryllium base structure.

The one piece beryllium base structure was incorporated to provide a very fast heating path and to provide a firm, non slipping configuration planes (in the fast reaction environment) between the cavity and IMU mounting surfaces. In order to incorporate the beryllium base however it was necessary to redesign the Vaclon pump (for thermal coefficient of expansion match to the base) and to develop a brazing technique required to assure vacuum integrity in the fast reaction environment. The Vaclon pump and base were designed first in order to get the long lead items (Vaclon pumps) on order.

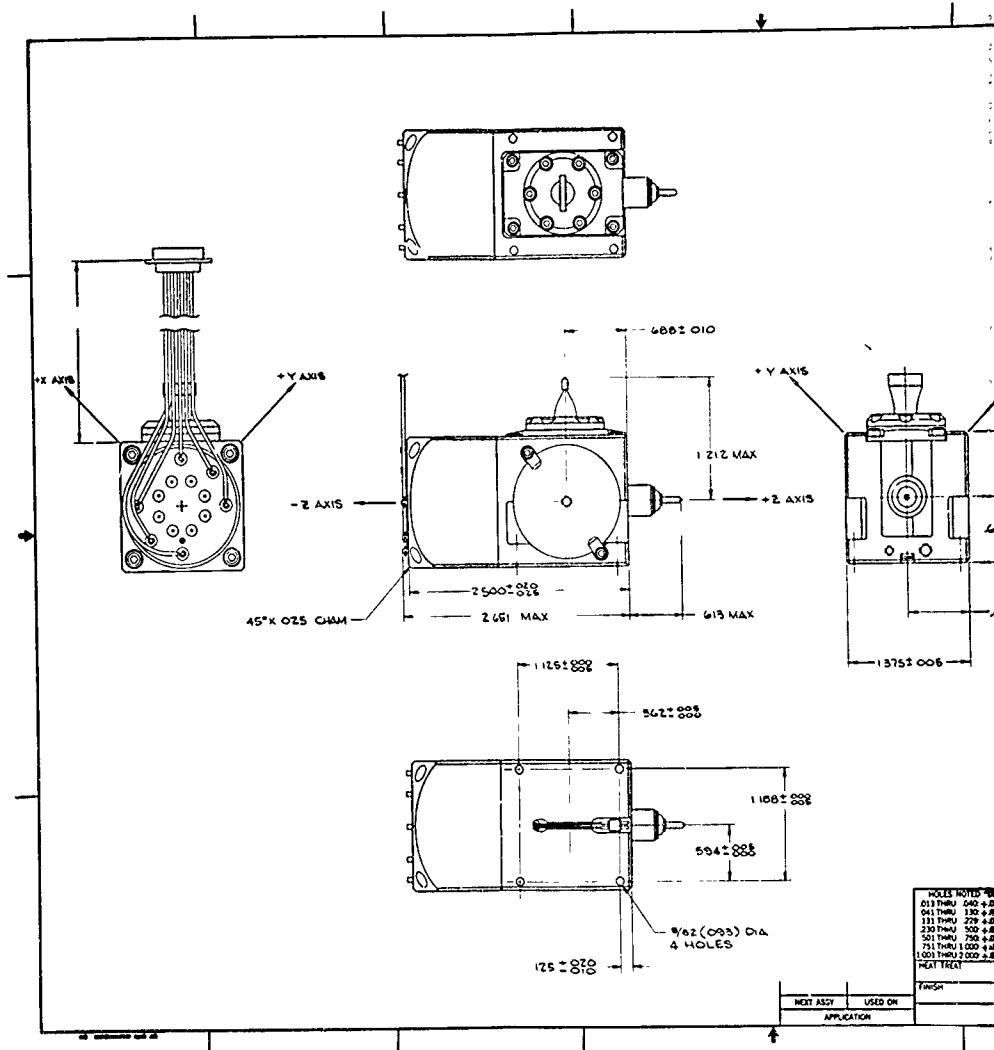


25	
24	
23	
22	
21	
20	
19	
18	
17	
16	
15	
14	
13	
12	
11	
10	
9	
8	
7	
6	
5	
4	
3	
2	
1	
0	
25	
24	
23	
22	
21	
20	
19	
18	
17	
16	
15	
14	
13	
12	
11	
10	
9	
8	
7	
6	
5	
4	
3	
2	
1	
0	
25	
24	
23	
22	
21	
20	
19	
18	
17	
16	
15	
14	
13	
12	
11	
10	
9	
8	
7	
6	
5	
4	
3	
2	
1	
0	



**Preceding page blank**

383



Figure

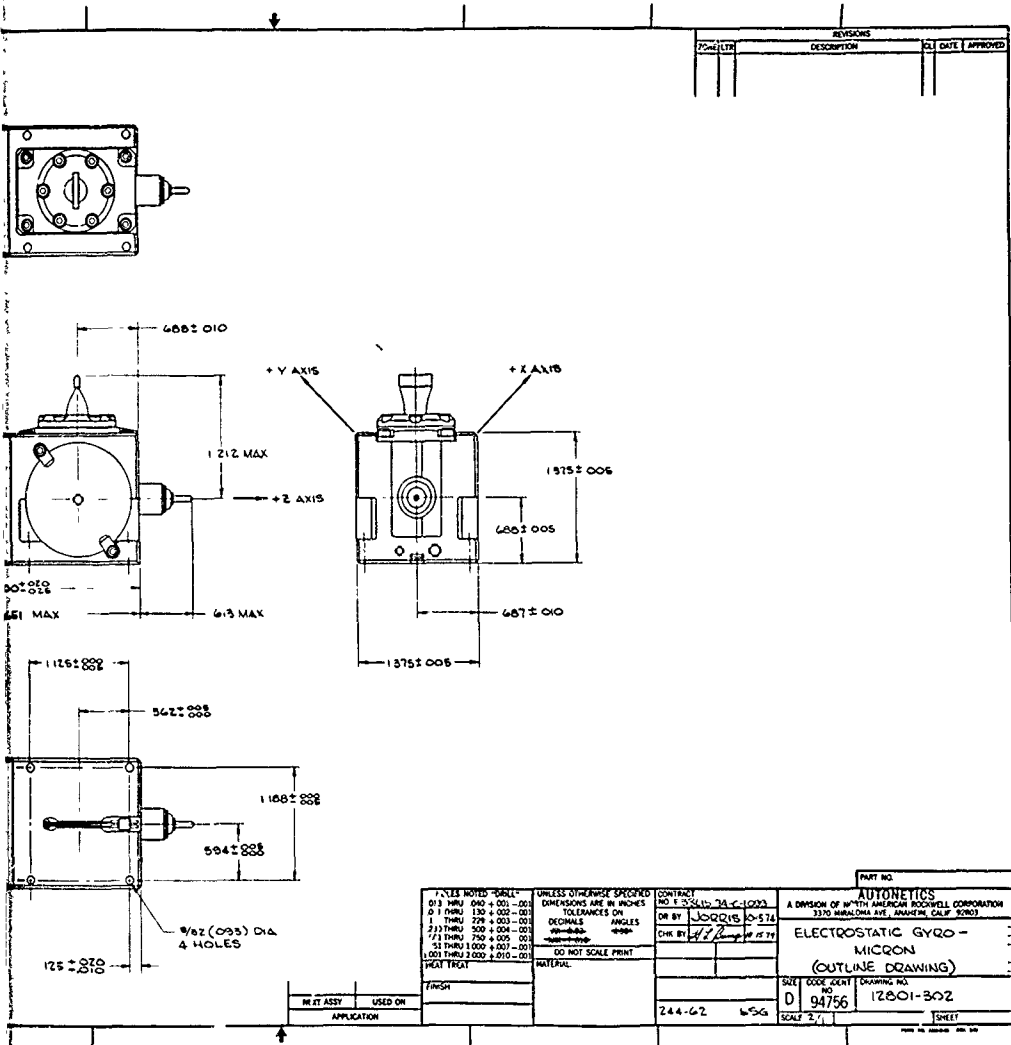


Figure 6-105. Electrostatic Gyro - MICRON (Outline Drawing)

A thermal sensor well was also designed into the instrument to allow measurement of the near-cavity temperature in the event that the thermal time constant of the newly designed instrument was too long. The beryllium base also included a large surface area to provide intimate thermal contact with the IMU support surface thereby reducing the thermal impedance path across the interface. It is noted that redesign of the Vacfon pumps was necessary (and rework thereof) for two reasons: (1) The titanium buttons within the Vacfon pump were falling off from shock (physical and thermal); (2) Sure-start incorporation was becoming highly desirable because of the long start-up time of units which were being tested at HAFB on the N57A system and because the Getter was not developed enough to commit to a Gettered MESG design.

6.3.6.1.2 Motor and Motor Function Development. Eighty degrees fahrenheit per minute MESG heating rates will be required in the MICRON system in order to meet the goals of fast reaction. The MESG case must heatup at  $80^{\circ}\text{F}/\text{minute}$  and therefore the MESG rotor heating capability should be near  $80^{\circ}\text{F}/\text{min}$ . The present accepted method of rotor heating is via Z-coil induction heating.

The development of this capability was sponsored to a large extent by the ECOM Fast Reaction Program, Contract No. DAAB07-73-C-0188 where technique, method, and capability were demonstrated. Also, the ECOM program efforts demonstrated fast spin up, fast polhode damping, and fast spin down capabilities.

The changes imposed by other MICRON requirements, however, affected changes in the MESG (30 sec time constant required MESG base change) and changes in the motor power supply (smaller size, design for non-sinusoidal output) which in turn caused additional design and test activity.

A potentially serious problem with the Z-coil heating was that the motor  $I^2R$  losses could heat the motor windings excessively and damage them: A means of providing a thermal conductive path from the copper motor coils to the IMU chassis was required. Essentially two techniques reduced the magnitude of this problem:

1. Coil to Mu metal motor case time constant reduction.
2. Mu metal motor case to IMU time constant reduction.

The copper coil to Mu metal motor cover time constant reduction was accomplished by use of a good thermal conduction potting compound. Also thermal conductive materials (BeO and injection molding of Stycast) was considered as materials upon which the motor coils could be wound and provide a good thermal path.

A mold was designed and fabricated for encapsulating the coil assembly in the motor cover. This mold fits in the molding machine located in the electromechanical lab. In order to ease the moldability, minor changes were made to the coil form and the motor cover.

The first attempt was to mold the assembly with Stycast 2850 KT compound. This compound was selected because it has a thermal conductivity of  $30 \text{ BTU-in/ft}^2\text{-hr-}^\circ\text{F}$ . This compound is produced by Emerson & Cuming, Inc. and was mixed with Catalyst 11. The molding temperature was  $200^\circ\text{F}$  and the pressure was 1500 psi. The top of the coils were completely covered while only the upper part of the x and y coils were covered. It was concluded that an increase of the space between the O.D. of the Z coil and the I.D. of the motor cover would give a better flow. Also, an increase of the I.D. of the xy coils before molding would improve the flow. So the motor cover was undercut for the length of the coil. A plug was made to push the xy coils against the I.D. of the coil form. Another mold was designed to mold the coil form which is presently fabricated from Fiberglass.

Stycast material type 2850 KT was ordered and received from Emerson & Cuming. Before molding another part the compound was analyzed by the PM lab. It was found that some particles were as large as 0.10 in. Effort was made to crush these particles, but without success. Emerson & Cuming was contacted to request a reduction in particle size and their answer was that in no way can they deliver 2850 KT with smaller particles. The next coil assembly was molded with 2850 FT compound which has a thermal conductivity of  $10 \text{ BTU-in/ft}^2\text{-hr-}^\circ\text{F}$ . This assembly was molded under a pressure of ~1500 psi and a temperature of  $165^\circ\text{F}$ . The part was then cured in the mold for 16 hrs at  $212^\circ\text{F}$ . The disassembling of the mold was difficult and minor rework of the mold has been done to make the disassembling easier next time. The molded assembly was then postcured in an oven at 300 F for 4 hrs. This allows optimum high temperature performance. It is anticipated the unit will be tested during July.

An existing forming fixture has been reworked, so that the O.D. of the x and y coil equals the I.D. of the form coil and the I.D. of the x and y coil large enough to allow for sufficient coverage of the molding compound. One wound coil was clamped in this fixture and put in an oven at  $350^\circ\text{F}$  for 4 hrs. The coil was set and kept its desired shape.

A molding tool was designed to permit injection molding of the motor coil form. The parts were completed during the latter part of July 1975 and a first molding effort was performed. The part looks promising and will be tested for fit/function in early Phase 2B.

It was determined that the BeO material considered for motor coil bobbin fabrication would have been too costly from the standpoint of machining time. The idea was abandoned.

6.3.6.1.3 3-Wire Rotor. Computerized fast reaction requires a rotor with an approximate one second polhode period and a consistent family polhode signature. The development of the rotor has been as a follow-on effort of a company funded effort which developed the first three wire material and rotors thereof ("B" material). The B material rotors were tested and based on those results and the results of a theoretical analyses of the various parametric sensitivities another design was completed, parts were fabricated for the billet ("E" material). The "E" material rotors were in their final stages of fabrication at the end of Phase 2A.



6.3.6.1.4 180°F Rotor Operational Temperature. The purpose of this task was to develop the processes/capability of fabricating rotors which would be capable of operating (functionally and reliably) in a 180°F MESG operational environment. This capability was to be one possible solution to requirements of system fast turn-around, restart and/or high temperature soak environment prior to system startup.

The final design was completed (final rotor size, lapping temperature) and a rotor (W4) was processed through the finishing cycle to determine the integrity of the lapping process/technique at the new elevated temperature.

There was no degradation of surface finish or controlled out-of-roundness. The unit was judged good for inertial grade instrument quality. Rotor W4 was placed on the storage shelf to be assembled into a MESG unit as a 180°F MESG test capability became available. (T/S IV does not have the capability of operating at 180°F.)

6.3.6.1.5 Sure-Start. The design of a Vacion pump sure-start technique was initiated in the December 1974 time frame. The task complements the total fast reaction developments. The effort was started because: (1) N57A MESG units being tested at HAFB were requiring too much time to start (hours); and (2) the Getter had not been developed to the extent that a firm design/commitment could be made. The initial sure-start effort was to consider methods such as:

1. Tungsten Filament
2. Spark Plug
3. Pump Optimized Physical Design
4. Radioactive Source
5. External Fix

An effort was immediately started with regard to incorporation of the tungsten filament while "ground work" was still in progress in the other listed areas. The tungsten filament tests were very successful and caused the abandonment of the other sure-start activities.

The latest design of the sure-start capsule and the manner in which is is incorporated into the Vacion pump is shown in Figure 6-106.

Essentially there have been five units fabricated to test the sure-start feasibility: Build No. 1 consisted of a standard N57A type MESG unit but the rotor and cavity volumes were regions wherein the filaments were placed for the initial tests. The filaments were connected to the standard vacuum housing feedthroughs. Build No. 2 consisted of an N57A type gyro (MESG No. 59) and the filament was incorporated by installation onto the pinch-off flange. The unit also tested well and it was on this unit that it was determined that the filament initiation did not cause charge buildup on the rotor. Build No. 3, 4, and 5 were all on beryllium base units.

All tests to date on hard starting units have been encouraging. Units which average one-half hour for turnon consistently start within three seconds using sure-start initiation.

6.3.6.1.6 Pump and Housing Assembly. The brazing process to fabricate the Pump and Housing Assembly, Part No. 12797-36L, has been developed and qualified. The process produces joints between beryllium and Inconel X-750 which meet requirements with respect to strength, thermal conductivity, vacuum integrity, and freedom from magnetic effects.

This brazing process was selected after evaluation of specimens produced by two alternative processes proposed by Grant and Kamper, Inc. One process employed a Cu-Ag-Li alloy brazed at 1650°F and required Cu plating on the Inconel. The other employed a Cu-Ag-Sn alloy brazed at 1435°F and did not require plating. The specimens were evaluated for vacuum integrity, before and after thermal cycling; for braze integrity by radiography; for braze alloy surface integrity by microscopic examination; for microstructural characteristics by metallographic examination; and for shear strength. Both processes met requirements. The Cu-Ag-Sn system was selected based upon superior surface and microstructural characteristics.

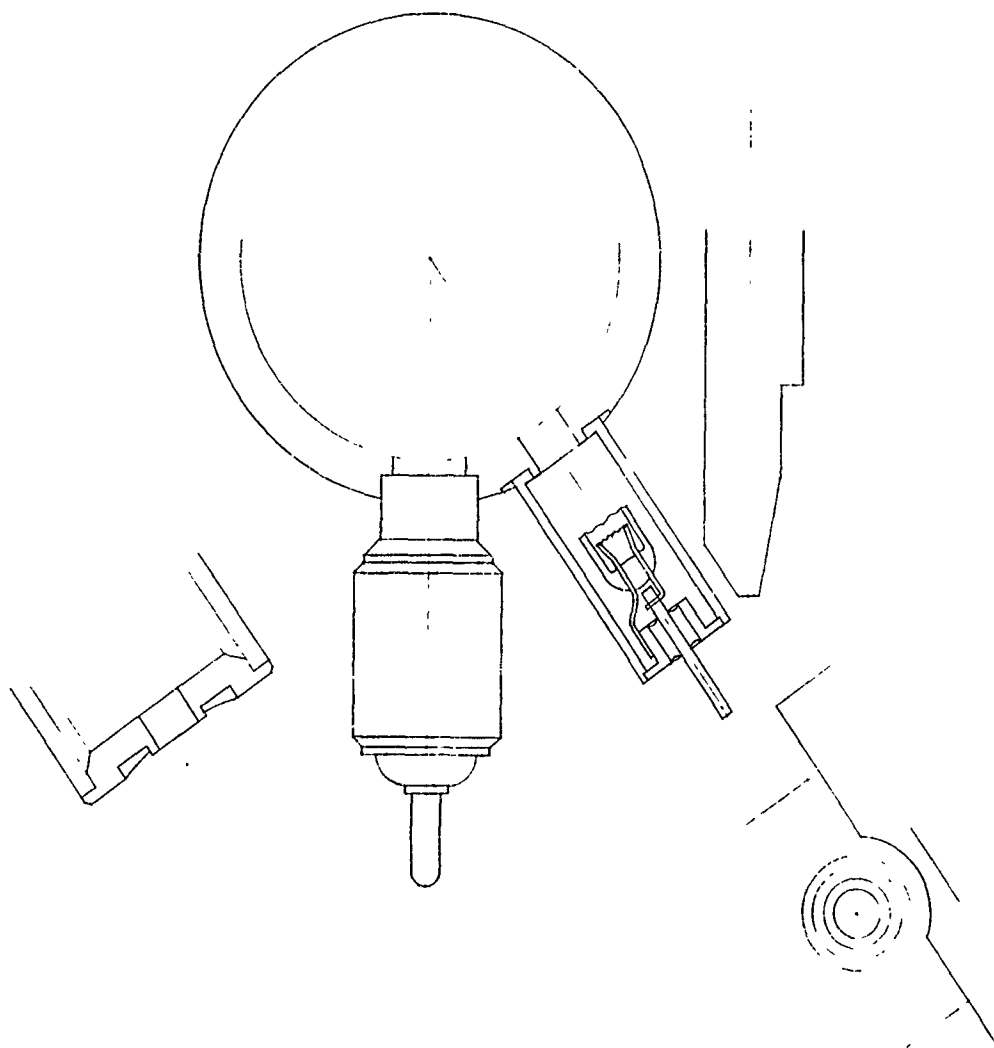
A second batch of three specimens brazed with the Cu-Ag-Sn system was fabricated and evaluated. These Inconel X-750 to beryllium joints were hermetically leak tight (leak rate less than  $10^{-10}$  atm cc/sec. helium). The three specimens were up and down quenched between boiling water and liquid nitrogen ten times. They were still leak tight. Metallographic sections were examined and acceptable microstructural characteristics were observed.

Grant and Kamper submitted a process specification draft for Autonetics' review. This draft was reviewed and accepted. Grant and Kamper then fabricated one pump and housing assembly in accordance with the draft specification. This assembly was evaluated and found acceptable.

A second part was attempted by Grant and Kamper. It was unsuccessful in two respects. The titanium anode inside the pump detached from the pump wall and the braze alloy did not melt. Analysis of the second Pump and Housing Assembly confirmed that the wrong brazing alloy had been used. The parts were cleaned up and brazed successfully with the correct alloy. The titanium cathode was reattached to the pump wall to make this a usable unit.

Subsequently, three more assemblies were brazed. The titanium anodes remained attached to the pump wall. All three assemblies showed acceptable vacuum integrity.

In a related but separate effort, the titanium hydride approach to brazing was investigated. Exploratory attempts to braze beryllium to Inconel X-750 using the titanium hydride approach, indicated feasibility. Joints were produced with each of two standard brazing alloys, BT720, and BT721. Metallographic cross-sections were examined. The joints looked acceptable.



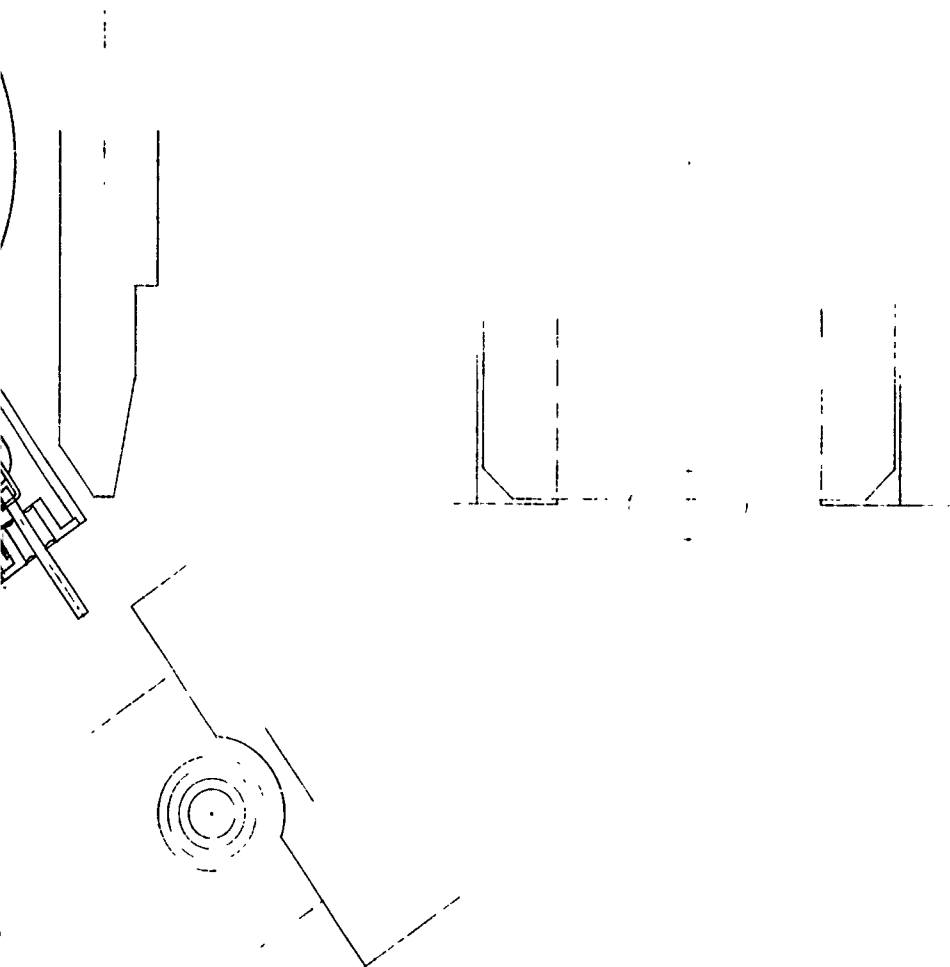


Figure 6-106. "Sure-Start" Modification

Subsequently, three assemblies consisting of an Inconel X-750 tube fitted into a through-hole in a beryllium disc, were brazed using the titanium hydride. Each assembly was prepared in a slightly different manner with respect to the technique of applying the titanium hydride activator. Brazing alloy BT720 (Handy & Harmon) was used. The assemblies were heated in vacuum (approximately  $10^{-6}$  torr) to flow the braze alloy. Visually acceptable wetting and capillary flow occurred in all three assemblies. As-brazed, all three assemblies showed non-detectable leak rates (less than  $10^{-10}$  atm-cc/sec. helium).

The assemblies were thermally cycled by alternately quenching in boiling water and liquid nitrogen with a one minute dwell time in each liquid. Four cycles were applied. After thermal cycling, one of the three leaked at a rate greater than  $10^{-5}$  atm-cc/sec. helium, while leaks in the other two were again non-detectable (less than  $10^{-10}$  atm-cc/sec. helium). Metallographic examinations indicated that the maximum temperature reached during brazing was higher than optimum.

Two more assemblies were brazed using a lower maximum temperature. These two assemblies showed no detectable helium leakage as-brazed. They were thermally cycled as described above. Ten cycles were applied. Helium leakage was again non-detectable. Metallographic examination showed an acceptable structure.

The titanium hydride approach is considered to be developed to the point where fabrication of qualification hardware could be undertaken.

6.3.6.1.7 Feedthroughs in Ceramic Vacuum Housing. The objective of this effort was to emplace electrically conductive, vacuum tight feedthrough pins in beryllium oxide (BeO). Brazing, using the titanium hydride activation process, was chosen as the emplacement method. A variety of pin materials was considered. These included ceramics since the brazing alloy could provide electrical conductivity.

In the first brazing run both molybdenum (Mo) and BeO pins were brazed into through-holes in BeO wafers. The BeO was cleaned per "practice 1", Table 6-61. Two values of diametral clearance between the pin and the hole were used in each case: 0.002 inch and 0.008 inch. The BeO pins were coated with titanium hydride, as were the holes, so that the braze alloy would wet these surfaces. Thus an electrically conductive layer of braze alloy covered the surface of the BeO pin after the brazing cycle.

Metallographic sections of the brazed pins showed joints with braze metal which was exceptionally free of defects. From this evidence, acceptable vacuum integrity would be expected. However, as shown in Figures 6-107 and 6-108, cracking in the BeO wafer occurs at both thicknesses of brazement but the orientations are at 90 deg to each other. In the case of the thinner brazement, Figure 6-107, the cracks in the wafer are associated with the pad on the wafer surface around the hole. Since these cracks are perpendicular to the pin axis, they do not pose a threat to vacuum integrity. In the case of the thicker brazement, Figure 6-108, the cracks are associated with the filler metal in the hole. These cracks are parallel to the pin axis and pose obvious threats to vacuum integrity and to load-carrying capability.

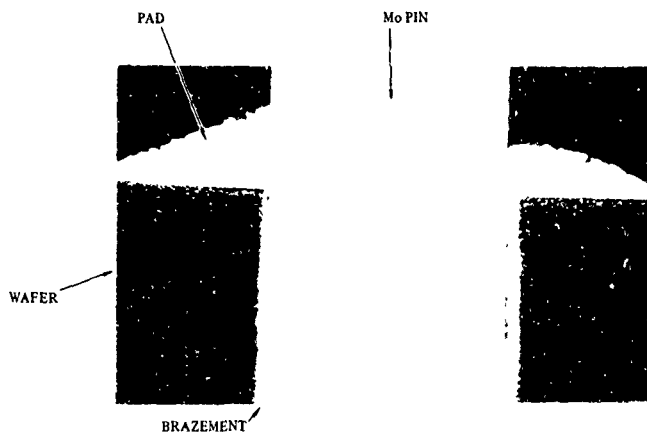
In a second brazing run, the attempt to braze molybdenum, aluminum oxide, beryllium oxide, and Inconel X-750 pins in beryllium oxide wafers was largely

Table 6-61. Feedthrough Brazements: Cleaning Practices  
for Beryllium Oxide

Step	Practice No. 1	Practice No. 2	Practice No. 3	Practice No. 4
1	Ultrasonic, Acetone	Ultrasonic 2 parts/vol Toluene 3 parts/vol Acetone 2 parts/vol Freon TF	Same as 1, Step 1	Same as 2, Step 1
2	Rinse, DI H <sub>2</sub> O	Blow Dry, N <sub>2</sub>	Same as 1, Step 2	Blow Dry, Air
3	Air Bake 1 hr at 150-180F	Etch in 3 parts/vol HCl 1 part/vol HNO <sub>3</sub>  Immerse at room temperature and heat to boiling.	Same as 1, Step 4	Same as 2, Step 3
4	Etch for 0.5 hr in 10 vol % HNO <sub>3</sub> 10 vol % HF	Rinse, DI H <sub>2</sub> O	Same as 1, Step 5	Same as 2, Step 4
5	Rinse, DI H <sub>2</sub> O	Etch for 1 hr in 90 vol % HNO <sub>3</sub> 10 vol % HF	Air bake 2 hr at 500 F	Same as 2, Step 5
6	Air Bake 1 hr at 150-180 F	Rinse, DI H <sub>2</sub> O	---	Same as 2, Step 6
7	---	Air Bake 1 hr at 1000 F	---	Air Bake 1 hr at 1600 F

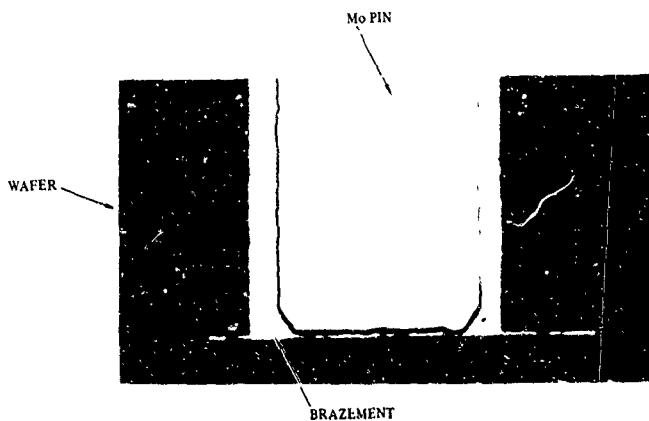
unsuccessful. A concurrent attempt to braze Incoloy 903 pins was successful. All of these attempts were made in the same vacuum furnace run.

The unsuccessful attempts failed due to the absence of any titanium reaction with the surfaces of the holes in the BeO wafers and with the pin surfaces adjacent thereto. The braze alloy then failed to "wet" these surfaces and thus did not enter the gaps between the pins and holes. Wetting did occur on other surface areas.



BRAZEMENT THICKNESS IS APPROXIMATELY 0.004 INCH.  
NOTE CRACKS IN WAFER PARALLEL TO PIN AXIS.

Figure 6-107. Pin Brazed into Beryllium Oxide Wafer



BRAZEMENT THICKNESS IS APPROXIMATELY 0.001 INCH  
NOTE CRACKS IN WAFER PERPENDICULAR TO PIN AXIS

Figure 6-108. Pin Brazed into Beryllium Oxide Wafer

Table 6-61 presents the cleaning practice (No. 1) used on the successful brazes. Also presented is the practice (No. 2) used on those wafers which failed to braze. The No. 2 practice is very similar to that used to prepare BeO for cavity plating. In that case, however, it was suspected that the time-duration of the HNO<sub>3</sub>-HF etch was too great and/or the final bake should have been at 1600F instead of 1000F. Another attempt was thus undertaken.

The third attempt to braze (using only molybdenum, aluminum oxide pins in beryllium oxide wafers) was essentially a repeat of the second. The principal variations from that attempt were the cleaning practices 3 and 4, Table 6-61. The braze alloy failed to wet the BeO hole surfaces cleaned by practice 4 but did wet those cleaned by practice 3.

The data thus show successful brazing with practices 1 and 3, and unsuccessful results with practices 2 and 4. The reason for this is not known with any confidence. It is speculated that the extremely aggressive etching in practices 2 and 4 may be creating excessive surface area in the BeO hole which overwhelms the amount of titanium hydride which will fit in the gap.

Cracks observed in the BeO wafers adjacent to the pins have been a source of constant concern. Figure 6-109 summarizes the data in terms of the radial clearance between the feedthrough pin and the surface of the hole in the BeO wafer. These observations derive from one cross-section per pin. The planes of observation contained, or very nearly contained, the centerline of the hole. This yielded two observations per pin which was not always centered in the hole.

In using these data, stresses induced by cooling the solidified brazement must be kept in mind. Table 6-62 provides an approximate indication of the relative contraction rates of the materials of interest referenced to BeO. This information suggests that thermal-contraction-mismatch induced cracking in the BeO wafer parallel to the feedthrough (the most undesirable case for vacuum integrity) is best avoided by keeping the brazement thickness very small and by using molybdenum or alumina (Al<sub>2</sub>O<sub>3</sub>) as the pin material. The observations in Figure 6-109 are compatible with this generalization. They are also compatible with the corollary that those conditions which minimize cracking parallel to the pin axis, maximize the stresses which would cause cracking perpendicular to the pin axis.

With this in mind, the optimum design would be a feedthrough pin of BeO with a nearly-zero brazement thickness. This optimum involves two drawbacks however.

First, the ceramic pins are so fragile that they could not be allowed to protrude more than one diameter beyond the planar surfaces of the BeO wafer. This constraint would dictate a complete redesign of contacts for each end of the feedthrough pins. Second, brazement thicknesses of less than 0.002 inch, would pose serious yield/reliability risks in a production situation. It is extremely difficult to place the pins into the holes while retaining the continuous titanium hydride coating in the hole when the diametral clearance is less than 0.004 inch. This was quite apparent in the case of the alumina pins with a 0.002 inch diametral clearance.



YIELD/RELIABILITY

**Figure 6-109. Feedthrough Brazements: Cracking in BeO Wafers**

Table 6-62. Feedthrough Brazements - Relative Thermal Contraction

Material	Approximate Thermal Contraction Rates (Relative to BeO)
BeO	1.0
BT720 Braze Alloy	3
Mo	0.9
Al <sub>2</sub> O <sub>3</sub>	1.1
Inconel X-750	2.1
Incoloy 903	1.5

The best compromise is judged to be a molybdenum pin with about 0.005 inch diametral clearance in the hole (0.0025 inch brazement thickness). The risk of inducing cracks in the BeO perpendicular to the pin axis can be reduced by making the wafer thickness as small as practical, probably 1/16 inch instead of 1/8 inch, and by cooling very slowly from the solidification temperature, allowing the brazement a chance to stress relieve itself.

It should also be noted that a 0.0025 inch thick brazement gap which was devoid of braze alloy (one of the unsuccessful attempts using cleaning practice No. 4) exhibited a crack parallel to the pin axis on one side. This was unique among the 22 observations made on 11 unbrazed pins. This case suggests that at least some cracks are attributable to cause(s) other than the thermal-contraction-mismatch stresses in a brazement.

6.3.6.1.8 Cavity Plating. The currently used "Nicoloy" electrodes are not as damage-tolerant as might be desired and tend to become magnetic when subjected to the vacuum baking in fabricating gettered gyros. Five alternatives to "Nicoloy" have been investigated. The following paragraphs describe these efforts.

a. Tantalum Nitride

Four rate runs were made using a variety of sputter-deposition-parameter values. Deposition rates ranged from zero to  $0.5 \times 10^{-6}$  in. per min. These variations included reactive sputtering in Argon/1 percent Nitrogen.

At the end of the fourth run it was observed that the conductive cement bond between the target and the copper backup was failed. The initial bond was made with Eccobond No. 53 after abrasive-conditioning of the faying surfaces. It is not known whether the bond was acceptably conductive on any of the rate runs.

Another bonding approach was formulated. The faying surfaces were etched and them bonded with Ablebond No. 58-1. There were no more problems with the target.

Three rate runs were made using 100 percent Ar at  $5 \times 10^{-3}$  torr. Approximately 5000Å were deposited at a rate of 254Å/minute (1 microinch/minute). Adhesion (celluloid tape) was acceptable and the electrical conductivity was the same as the target material. The deposit had a very smooth surface.

Three more rate runs were made using 97 percent Ar/3 percent N<sub>2</sub> at  $4 \times 10^{-3}$  torr. Approximately 3300Å were deposited at a rate of 330Å/minute (1.3 microinch/minute). Adhesion was acceptable and electrical conductivity was the same as the target material. The deposit had a lumpy or grainy surface. Microprobe analysis detected only tantalum and nitrogen in the deposit.

A BeO cavity, tilted at 45 deg to the target and rotated at 40 rpm about its Z axis, was coated using 97 percent Ar/3 percent N<sub>2</sub> at  $4 \times 10^{-3}$  torr. A flat BeO wafer was coated along with the cavity (but was neither tilted nor rotated). The total run time was 11 hours and included overnight interruption in a vacuum of  $10^{-7}$  torr.

The coating thickness was estimated from the 330Å/minute deposition rate as being  $2.18 \times 10^5$  Å (850 microinches). Adhesion was acceptable and the electrical conductivity was the same as the target material. The deposits had lumpy or grainy surfaces. The BeO cavity coated with this material was lapped and evaluated. The coating thickness in the cavity was measured as  $2.8 \times 10^4$  Å (110 microinches). Some bare spots (BeO showing) were observable. It was judged that this material shows promise but will need more deposition process development.

#### b. Zirconium Nitride

Six rate runs were made using a variety of sputter-deposition-parameter values. Deposition rates ranged from  $0.5 \times 10^{-6}$  to  $1.0 \times 10^{-6}$  in. per min. These variations included reactive sputtering in Argon/1 percent Nitrogen.

At the end of the sixth run the same bond failure as was described for Tantalum Nitride was observed. The validity of the results from the six rate runs in thus questionable.

The target was rebonded as described for the Tantalum Nitride target. There were no more problems with this target either.

One rate was made using 100 percent Ar at  $5 \times 10^{-3}$  torr. Approximately 300Å were deposited at a rate of 100Å/minute (0.4 microinch/minute). Adhesion was acceptable and the electrical conductivity was about one-third that of the target material. The deposit had a very smooth surface. Microprobe analysis detected only zirconium and nitrogen in the deposit.

One rate run was made using 100 percent Ar at  $3 \times 10^{-3}$  torr. Approximately 1000Å were deposited at a rate of 610Å/minute (0.6 microinch/minute). Adhesion was acceptable and the electrical conductivity was the same as the target material. The deposit had a lumpy or grainy surface. Microprobe analysis detected only zirconium and nitrogen in the deposit.

Three rate runs were made using 97 percent Ar/3 percent N<sub>2</sub> at  $4 \times 10^{-3}$  torr. Approximately 1300Å were deposited at a rate of 200Å/minute (1.2 microinch/minute). Adhesion was acceptable and the electrical conductivity was the same as the target material. The surface of the deposit was very smooth.

A BeO cavity, tilted at 45 deg to the target and rotated at 40 rpm about its Z-axis, was coated using a composite approach. A flat BeO wafer (not tilted, not rotated) was coated at the same time. The composite approach consisted first of depositing tantalum nitride and then overcoating with zirconium nitride. In both cases, 97 percent Ar/3 percent  $N_2$  at  $3 \times 10^{-3}$  torr was used. The initial deposition was carried on for 7 hours at which time the system was opened to atmosphere and the zirconium nitride target was substituted for the tantalum nitride target. This took about five minutes. Sputtering was then re-established and carried on for five hours.

The total thickness of the composite coating was estimated as  $2.29 \times 10^5 \text{ \AA}$  (800 microinches). Adhesion was acceptable and the electrical conductivity was the same as the target materials (which are about the same as each other). These specimens were evaluated for lapping characteristics and for film thickness. The results are reported below.

Another BeO cavity was similarly coated using only zirconium nitride. A flat BeO wafer was coated at the same time. The atmosphere was 100 percent Ar at  $4 \times 10^{-3}$  torr. The deposition was carried on for 12 hours.

Adhesion was acceptable and the electrical conductivity was the same as the target material. The surface of the deposit was very smooth.

Both cavities were lapped and evaluated. The first one, zirconium nitride over tantalum nitride on the BeO, was too powdery to lap acceptably. The coating just seemed to disintegrate under the lap. The second one, zirconium nitride on BeO, showed relatively large areas of inadequate adhesion under the lap. Neither specimen was judged to show promise.

#### c. Zirconium Diboride

Eight rate runs were made using a variety of sputter-deposition-parameter values. Deposition rates varied from  $1 \times 10^{-6}$  to  $1.6 \times 10^{-6}$  in. per min. The higher value is the limiting rate for acceptable adhesion and coating density (absence of a powdery condition).

Following this, three trial runs on cavities were made. In the first run, the cavity equator was positioned parallel to the target and reactive sputtering was accomplished in Argon/1 percent Nitrogen. The deposition rate was  $1.5 \times 10^{-6}$  in. per minute. The cleavage strength (perpendicular to the substrate) of the bond of the film to the beryllium oxide substrate was approximately 2000 psi. The film was very difficult to lap.

The second run was performed with the same specimen-target position, again in the reactive gas, but with other parameters at different values. The deposition rate was  $1.6 \times 10^{-6}$  in. per minute. The cleavage strength was again approximately 2000 psi. Again the film was difficult to lap.

The third run was performed using a fixture which positioned the cavity equator at 45 deg to the target and rotated the cavity about its Z-axis. Deposition parameters were the same as those used in the second run. Adhesion was acceptable and the electrical conductivity was the same as the target material. However the lapped cavity showed a significant amount of voids (bare BeO). Since it was suspected that it would be very difficult to solve this problem, work on zirconium diboride was suspended pending review of results from the other materials.

#### d. Zirconium/Zirconium Diboride

In the light of the lapping difficulty on the straight zirconium diboride, it was postulated that a target composed of a 50:50 mixture of zirconium and zirconium diboride would be a more acceptable alternative.

Using the same sputtering-parameter values as were used in runs 2 and 3 for zirconium diboride, it was found that zirconium deposited at  $2.5 \times 10^{-6}$  in. per minute. This rate was considered sufficiently compatible with that of the zirconium diboride to attempt co-deposition from a composite target. The expected film would also be a composite richer in zirconium than the 50:50 target mixture.

One rate run was made using the composite target and 100 percent Ar at  $3 \times 10^{-3}$  torr. The deposition rate was approximately 250Å/minutes (1.0 microinch/minute). Approximately 2000Å were deposited. Adhesion was acceptable and the electrical conductivity was the same as the target material. The surface of the deposit was very smooth.

Seven more rate runs were made using 100 percent Ar at  $4 \times 10^{-3}$  torr. The deposition rates ranged from 317Å/minute to 343Å/minute (1.25 to 1.35 microinch/minute). Approximately 3300Å were deposited. Adhesion was acceptable and the electrical conductivity was the same as the target material. The surfaces of the deposits were very smooth.

A BeO cavity was coated in the tilted, rotating mode previously described. An atmosphere of 100 percent Ar at  $3$  to  $4 \times 10^{-3}$  torr was used. Deposition time was 6-1 1/2 hours. A cleavage test on a flat coated in this run showed the bond strength between the coating and the ceramic substrate to be equal to, or greater than, 5200 psi.

This cavity has been lapped and evaluated. The coating thickness in the cavity was measured as  $2.8 \times 10^4$  Å (110 microinches). The coating lapped very nicely to a good finish. The cavity was evaluated for magnetic characteristics. These results are in Table 6-63, Specimen No. 3. This material looks very promising.

#### e. Inconel X-750

Four rate runs were made using 100 percent Ar at  $3 \times 10^{-3}$  torr. Approximately 3800Å were deposited at rates ranging from 370Å/minute (1.46 microinches/minute) to 394Å/minute (1.55 microinches/minute). Adhesion (celluloid tape) was acceptable and the electrical conductivity was the same as the target material. The surface of the deposit was very smooth.

A BeO cavity, tilted at 45 deg to the target and rotated at 40 rpm about its Z-axis, was coated using 100 percent Ar at  $3 \times 10^{-3}$  torr. Several flats were coated in the same run (not tilted, not rotated). The total run time was 7-1 1/2 hours.

Table 6-63. Magnetic Susceptibility of Cavities

Deflection Distance (Inches) From Autometrics Comparative Magnetic Susceptibility Test								
Specimen No.	Material and Coating Condition	As Coated	Baked 120 Hours At 400°F	Baked 144 Hours At 400°F	Baked 240 Hours At 400°F	Baked 300 Hours At 400°F	Baked 60 Hours At 600°F	Baked 5 Hours At 900°F
1	Inconel X-750; Z-Axis At 45 Deg to Flat Cathode; 3X10 <sup>-3</sup> TORR	Zero (1)	Slight Trace	(2)	(2)	(3)	0.100	(2)
2	Inconel X-750; Z-Axis At 30 Deg to Flat Cathode; 2X10 <sup>-2</sup> TORR	Zero (1)	Trace	(2)	(2)	(2)	(2)	0.086
4	Inconel X-750; Z-Axis Parallel To Conical Cathode; 4.5X10 <sup>-3</sup> TORR	0.060 (1)	(2)	(2)	0.060			
5	SAME AS 4	0.010						
6	SAME AS 4	0.015						
7	SAME AS 4	Zero						
3	Zirconium/Zirconium Diboride; Z-Axis at 45 Deg to Flat Cathode; 3 to 4X10 <sup>-3</sup> TORR	Zero (1)	(2)	(2)	(2)	Zero	(2)	(2)
Gyro 154 Spinner Srt Cavities	"NICULLOY"		(2)	2.00	(2)			
	4-Hole 12 Hole		(2)	(2)	(2)	(2)	(2)	(2)

(1) And Lapped

(2) Not Tested and Will Not Be Tested

The flats showed a coating thickness of  $1.525$  to  $1.65 \times 10^5 \text{ \AA}$  (600 to 650 micro-inches). Adhesion (celluloid tape) was acceptable and electrical conductivity was the same as the target material. The coating was very smooth. A cleavage tensile test showed the bond strength of about 1600 psi between the coating and the ceramic substrate. The electron microprobe was used to check the coating composition. Table 6-64 presents the results (see column labeled "Specimen No. 1") and compares them to the target composition.

The cavity was lapped. The machinist reported that it lapped very well. The coating was thickest in the bottom of the hemispherical cavity and was much thinner near the equatorial plane. After lapping, the coating thickness was measured at 100 to 120 microinches per surface except near the equatorial plane which was slightly thinner and did not contact the lap.

This cavity, identified as Specimen No. 1 in Table 6-63 was evaluated for magnetic susceptibility as a function of baking temperature. The results are in Table 6-63.

Another cavity, tilted with the Z-axis at 30 deg to the plane of the target and rotated at 30 rpm, was coated using 100 percent Ar at  $2 \times 10^{-2}$  torr. Several flats were coated in the same run (not tilted, not rotated). The total run time was 7 hours.

These flats showed a coating thickness of  $1.27$  to  $1.40 \times 10^5 \text{ \AA}$  (500 to 550 micro-inches). Adhesion (celluloid tape) was acceptable and electrical conductivity was the same as the target material. The coating was very smooth. The electron microprobe analysis of this coating is presented in Table 6-64 (see column labeled "Specimen No. 2").

The cavity was lapped. The results were almost identical with those from Specimen No. 1.

This cavity, identified as Specimen No. 2 in Table 6-63, was evaluated for magnetic susceptibility as a function of baking temperature. The results are in Table 6-63.

Effort was then directed toward the problem of coating thickness variation within the hemispherical cavity. The objective is to attain thicker deposition near the equatorial plane so as to make it more nearly the same as that in the bottom of the cavity. Changing the Z-axis-to-target-plane angle from 45 deg to 30 deg did not accomplish very much. A conically shaped cathode (target) was postulated to be more effective and was used to investigate the relationship between target shape and coating uniformity in the hemispherical cavity.

Three rate runs with the conical target were first made on planar substrates. The atmosphere was 100 percent Ar at  $4.5 \times 10^{-3}$  torr. Deposition rates were about  $500 \text{ \AA/minute}$  (2 microinches/minute) on two of these and about  $630 \text{ \AA/minute}$  (2.5 microinches/minute) on the third. Adhesion (celluloid tape) was acceptable and the electrical conductivity was the same as the target material. The surfaces of these deposits were very smooth.

Table 6-64. Microprobe Analyses of Inconel X750 Coatings

Chemical Element	Target Supplier's Certification (wt%)	Specimen No. 1	Specimen No. 2	Specimen No. 4	Specimen No. 5	Specimen No. 6	Specimen No. 7
Ni	73.2	72.0	73.0	74.0	72.0	73.0	74.0
Fe	6.73	8.0	10.0	10.0	10.0	7.0	8.0
Ti	2.71	2.0	1.5	1.7	2.0	1.1	1.1
Al	0.85	2.0	1.5	1.0	0.9	2.0	0.8
Cr	15.15	15.0	14.0	14.0	16.0	17.0	16.0
Si	0.20	Trace	Trace	Trace	Trace	Trace	Trace
Nb	-----	Trace	Trace	Trace	Trace	Trace	Trace
Mn	-----	-----	-----	-----	-----	-----	-----



A BeO cavity, Specimen 4, stationary with its Z-axis coincident with the conical axis of the target, was coated using 100 percent Ar at  $4.5 \times 10^{-3}$  torr. The deposition rate was approximately 500Å/minute and the run was 7 hours long. The coating thickness was calculated as 210,000Å (825 microinches).

This coating was lapped back to a uniform 101,500Å (400 microinch) thickness over the entire hemispherical surface. This was the first time a sputtered coating had been thick enough adjacent to the equatorial plane to be contacted by the lap in this region when the cavity is lapped to finished size.

Lapping characteristics were reported to be very good. The coating was reported to be substantially harder (scratch-resistant) than the Niculoy material. Adhesion on the equatorial plane was acceptable and the electrical conductivity was the same as the target. The surfaces were very smooth, both as-deposited and as-lapped. Magnetic susceptibility as a function of baking temperature is shown in Table 6-63.

Three more cavities (Specimens 5, 6, and 7) have been coated with Inconel X-750 using the same process as that which produced the dimensionally acceptable Specimen 4. Table 6-63 shows their as-coated magnetic susceptibilities. These have not yet been lapped. If the coating was as uniform this time as it was last time, Specimens 6 and 7 could be completely configured and tested in an ESG.

Flat coupons, run with each of these three cavities, were chemically analyzed with the electron microprobe. These results are shown in Table 6-64.

#### f. Summary

Tantalum Nitride, Zirconium/Zirconium Diboride, and Inconel X-750 all appear to be promising alternatives to "Niculoy." A major problem in applying these alternatives, uniformity in the spherical cavity has been solved for Inconel X-750. This solution must now be adapted to the other materials. Assuming success in this, the three alternative materials can be more fully evaluated via testing in gyros.

### 6.3.6.2 Packaging/Thermal Design Alternatives

Analyses were completed during October 1974 to define the best design alternative relative to package external cooling concepts. External cooling concept alternatives were, in the order of preference, as follows:

1. No cooling air
2. Ambient cooling air only
3. Specification cooling air

No cooling air was assumed to mean that there is no atmosphere to act as a heat sink, such as in an extremely high altitude application. Ambient cooling air was assumed to mean that an air atmosphere does exist as a heat sink and heat rejection from the MICRON package to the air heat sink is via natural convection and radiation. Specification cooling air implies that an air heat sink is not only available and is ducted to the MICRON package, but is delivered at a pressure head such that flow is sustained and forced convection is obtained.

These studies based on heat transfer considerations, have confirmed that the only reasonable external heat removal method is by forced convection by externally (vehicle) supplied air coolant. All other methods result in an unreasonably large MICRON package, even with an 80°C ESG control temperature. When the coolant is cooling air in the temperature range specified by Figure 3.2-1, Appendix 1 of Attachment 1 to the MICRON Phase 2 Statement of Work, cooling air flow and pressure drops will be within the limits specified by Figures 3.2-2 and Figure 3.2-3, respectively. Required cooling air flow rates are expected to be as shown by Figure 6-110.

Internal packaging studies were initiated during the quarter ending December 1974. The methodology used in these internal packaging studies during Phase 2A was to create several paper designs of reasonable candidate MICRON IMU packages, and, with the assistance of the cost-of-ownership team, identify those aspects or design features of each candidate which are the costliest and should therefore be avoided in the final design.

Seven candidate package designs were described. These packaging design alternatives were as follows:

1. Packaging Design Alternative No. 1 - This design alternative, Figure 6-111, is a completely wet system, based on the liquid cooled Design Evaluation Model (DEM) design.
2. Packaging Design Alternative No. 2 - This design alternative, Figure 6-112, is a completely dry system with all internal cooling accomplished by conduction to air-cooled coldplates, based on the conduction cooled DEM design.

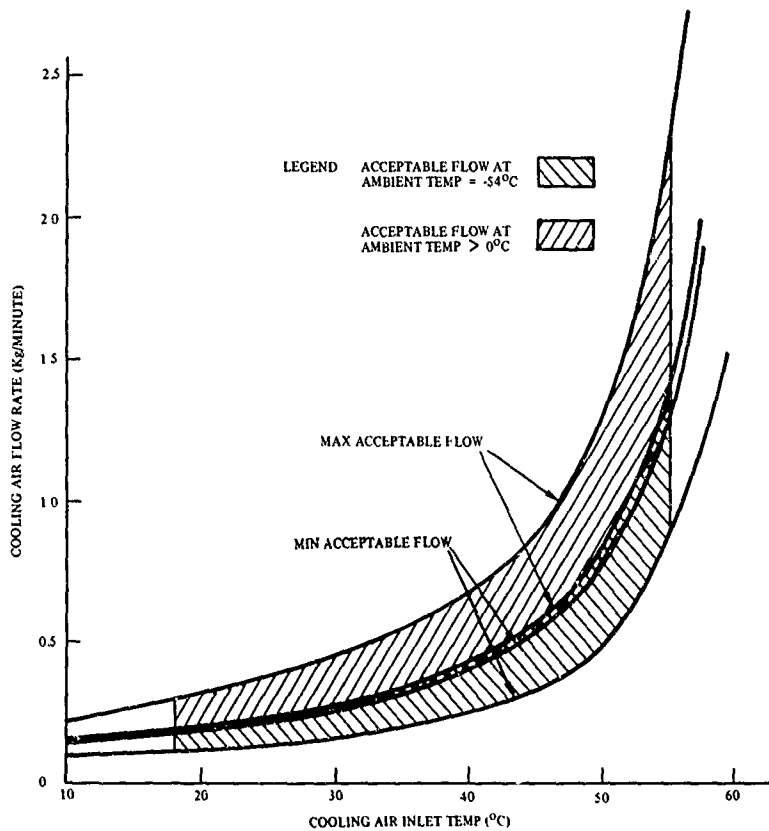


Figure 6-110. Cooling Air Flow Requirements





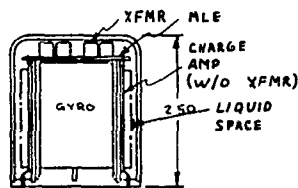
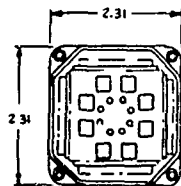




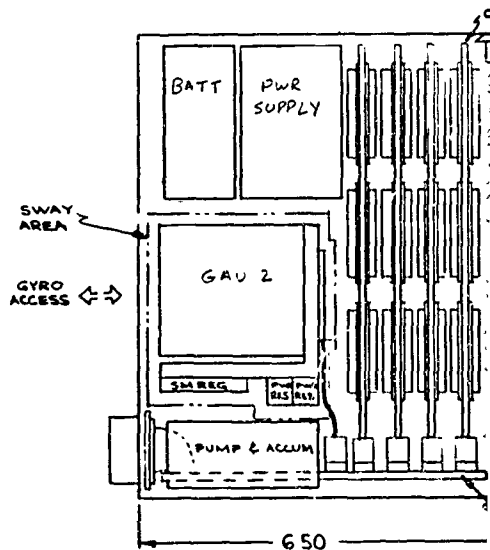
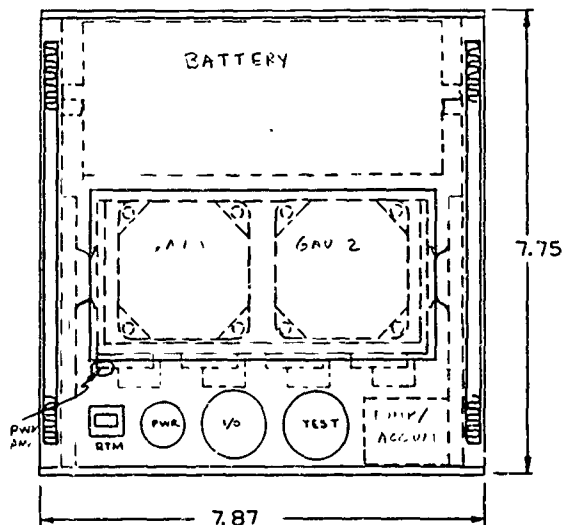
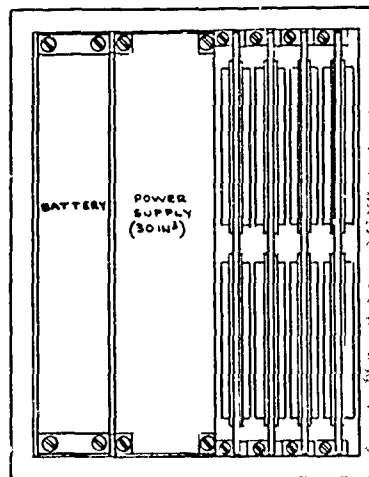
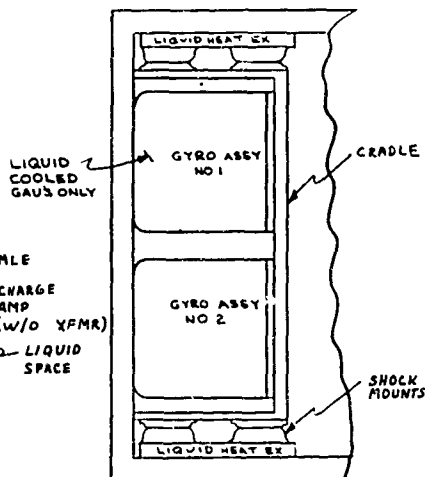
3. Packaging Design Alternate No. 3 - This design alternate, Figure 6-113, is a hybrid liquid cooled system where all electronics are dry and a small liquid coolant loop is used for cooling the GAU (Figures 6-114, 6-115 and 6-116) and power elements of the Spin Motor Power Amplifier.
4. Package Design Alternate No. 4 - This alternate, Figure 6-117, uses identically the same packaging approach and Instrument Assembly as Alternate No. 3. The primary difference is that three standard size electronic subassemblies instead of four of Alternate No. 3 are used.
5. Packaging Design Alternate No. 5 - This alternate, Figure 6-118, is a completely dry design similar to Alternate No. 2, however the standard sized Ceramic Printed Circuits (CPC) and the Aluminum core MLB module packaging concept of Alternate No. 3 and No. 4 are used. Separate EMA's are added, and since the MESC's are not required to operate as MESGA's, the liquid cooling loop of Alternates No. 3 and No. 4 are not required, see Figure 6-119. The GAU uses Jetter gyros and Charge Amp CPC on four sides as in Alternates No. 3 and No. 4 but without the liquid loop.
6. Packaging Design Alternate No. 6 - This alternate, Figure 6-120, is a design based on further reduction of risk by utilizing Vacion MESC's at an inclined angle of 35 deg from horizontal. Because of the Vacion MESC, the packaging of the charge amplifiers are on a single MLB.
7. Packaging Design Alternate No. 7 - This alternate, Figure 6-121, is a multiple LRU version of Packaging Design Alternate No. 6. LRU No. 1 contains Instrument Assembly (Vacion MESC's, charge amps, EMA's, and SMPA power elements on a shock mounted coldplate), IMU electronics, and power supplies and batteries for the above. LRU No. 2 contains the computer, IOU, and additional power supplies, i.e., those equipment whose definitions are dependent upon the application in which it is used.

These packaging design alternatives were reviewed and life-costs were estimated by the cost-of-ownership team, see Section 6.2. Since this task was terminated per the Stop Work Order in December, 1974, packaging studies were continued at a lower level of effort under company sponsorship. The results of both the Phase 2A and company sponsored packaging design studies are directly applicable to the Phase 2B Engineering Prototype MICRON.





GAU DETAIL



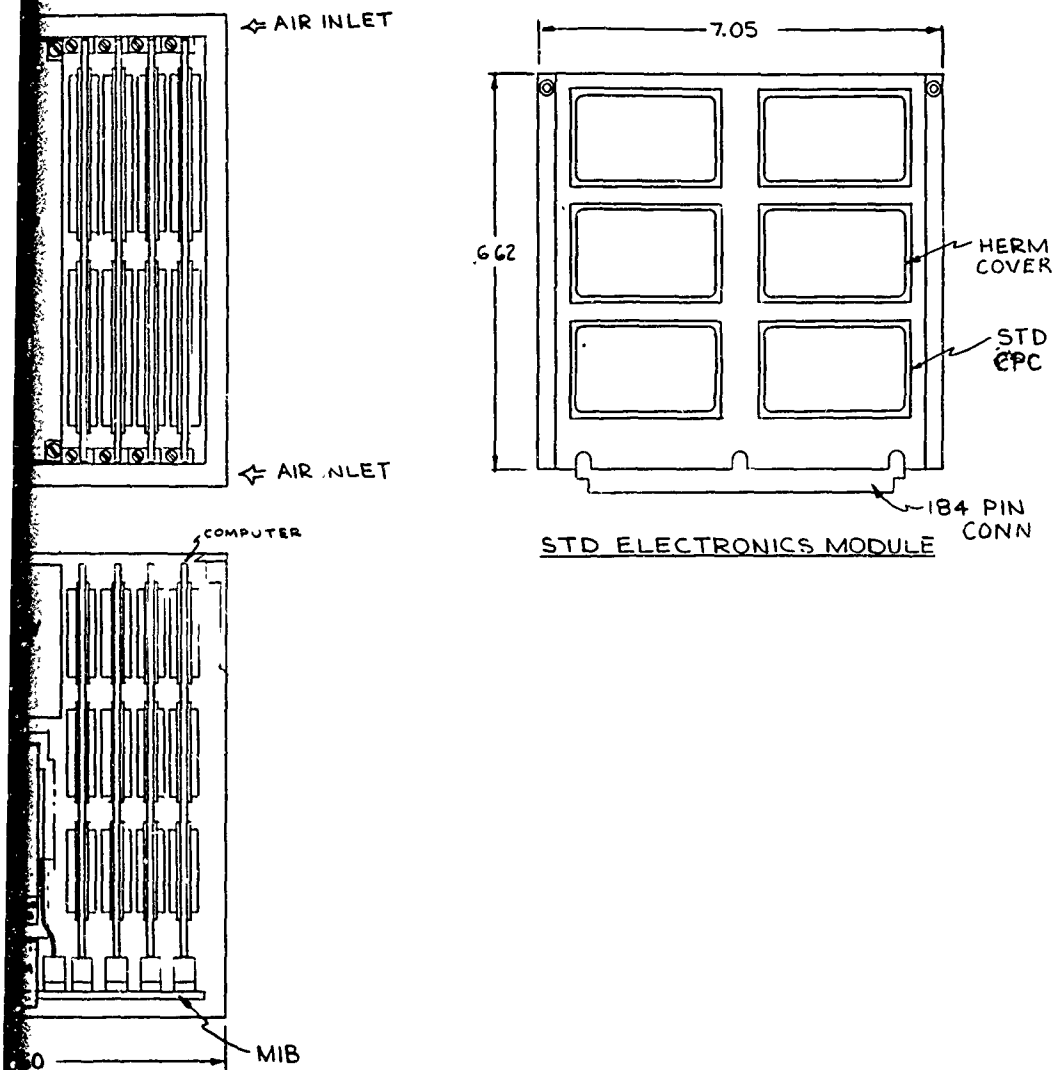


Figure 6-113. Design Alternative No. 3, Approximate Volume 397 In<sup>3</sup>  
W/O Thermal Insulation, Approximate Weight 15 Lb

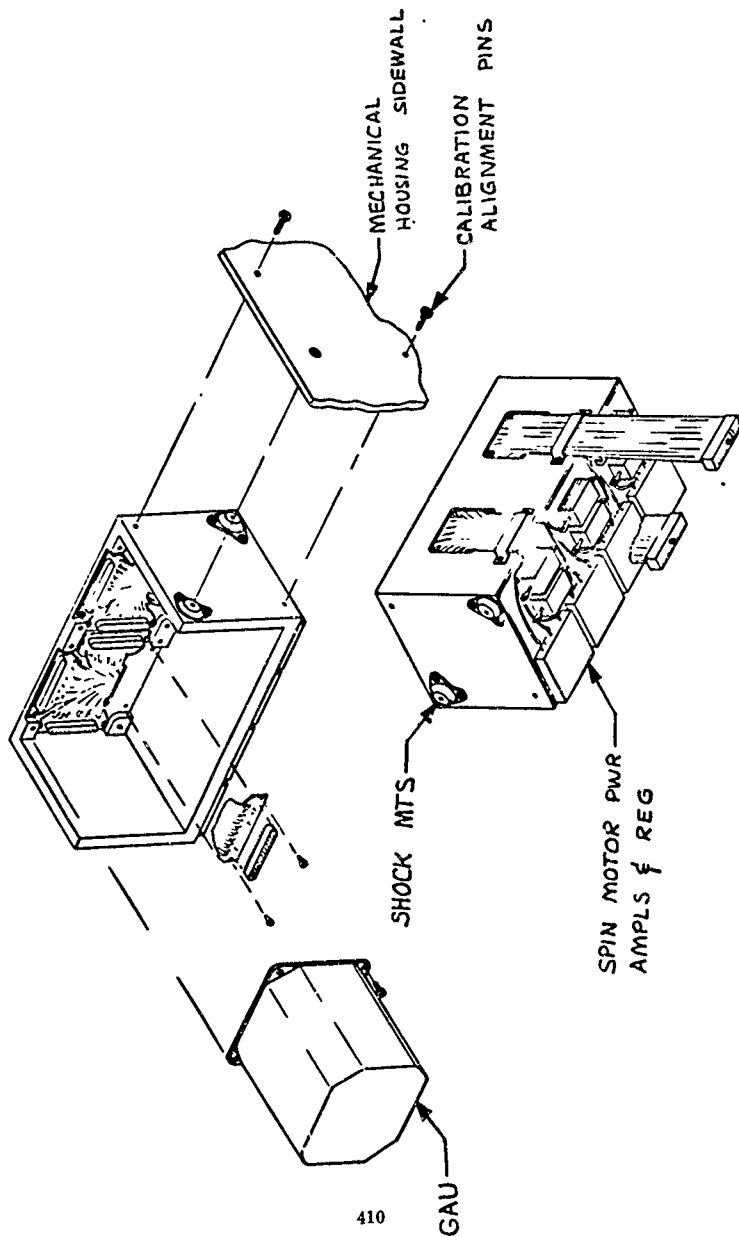


Figure 6-114. Instrument Assembly

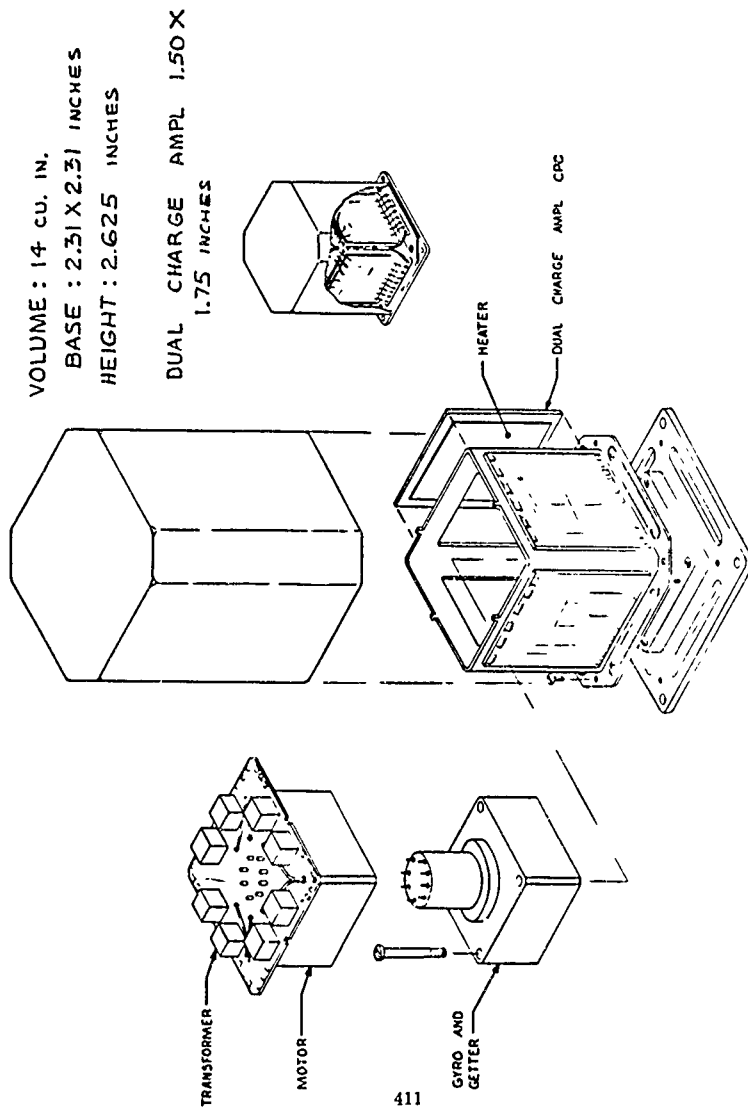


Figure 6-115. Gyro Assembly Unit (GAU)

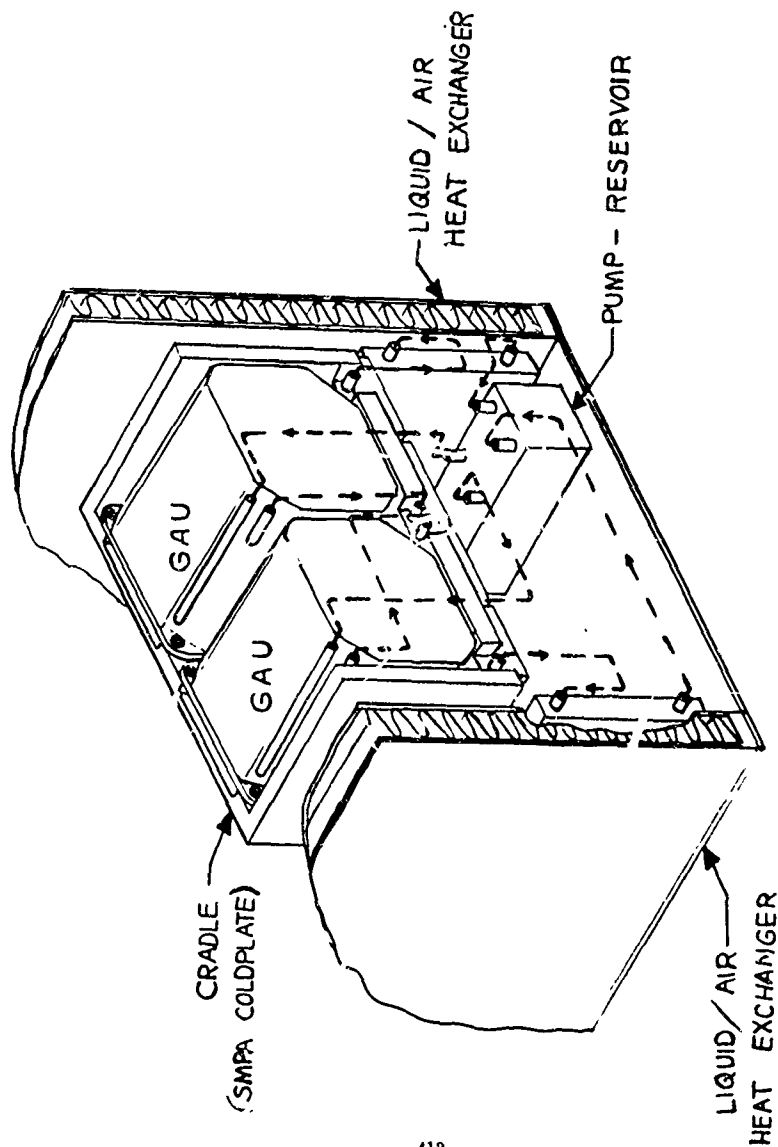
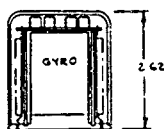
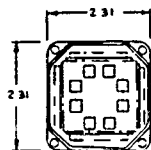
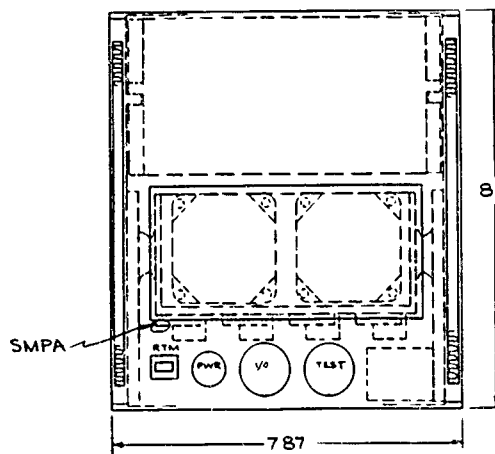
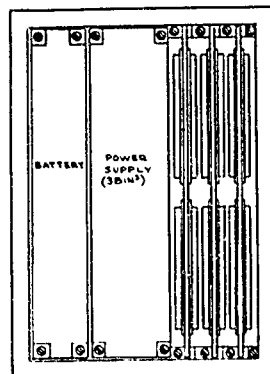
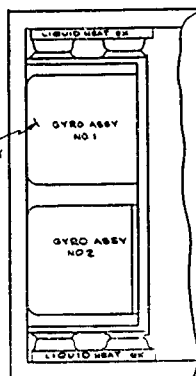


Figure 6-113. Liquid Cooling Loop Flow Schematic



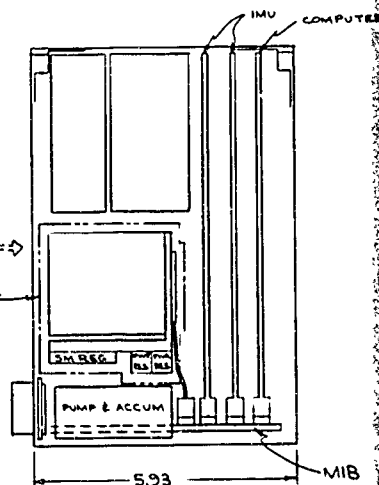
GAU DETAIL

LIQUID COOLED GAU'S ONLY



8.50

GYRO ACCESS  
SWAY ARER



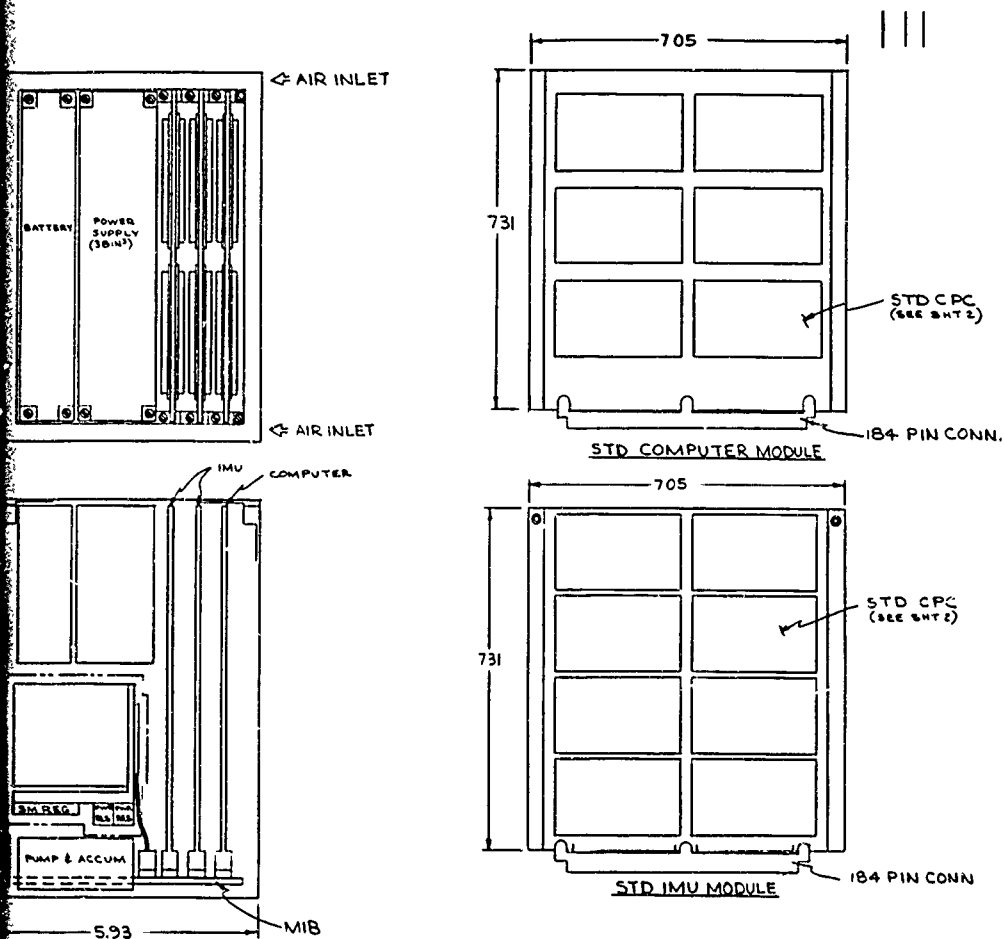
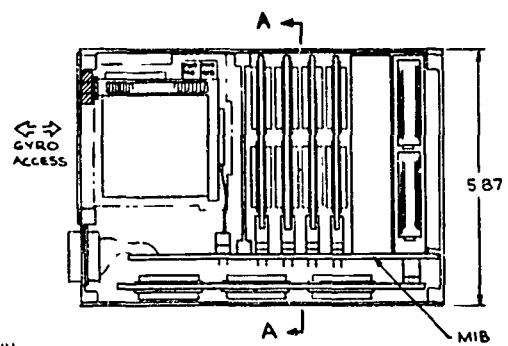
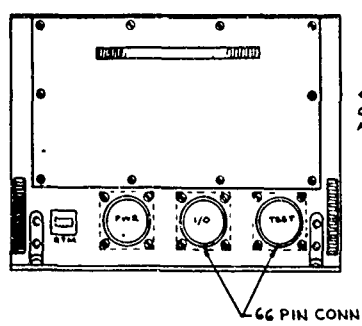
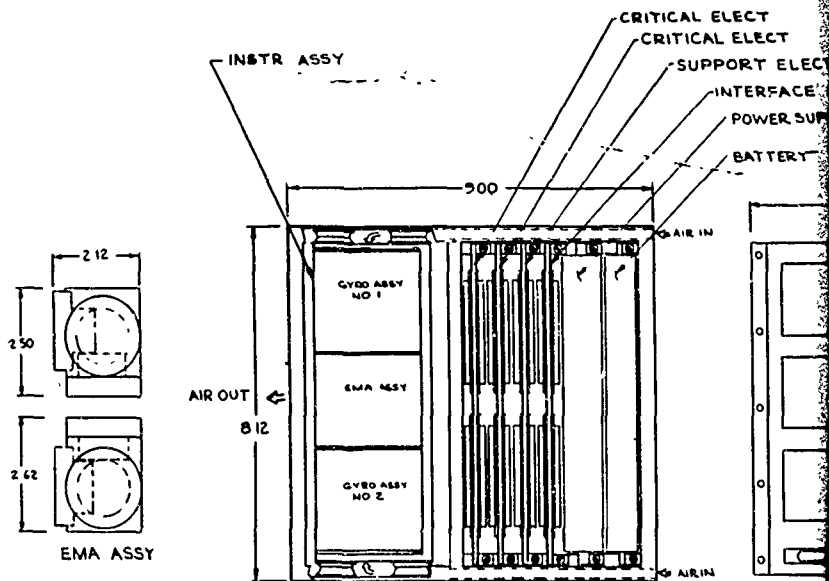


Figure 6-117. Design Alternative No. 4 - Approximate Volume 397 in<sup>3</sup>  
 Approximate Weight 15 Lb





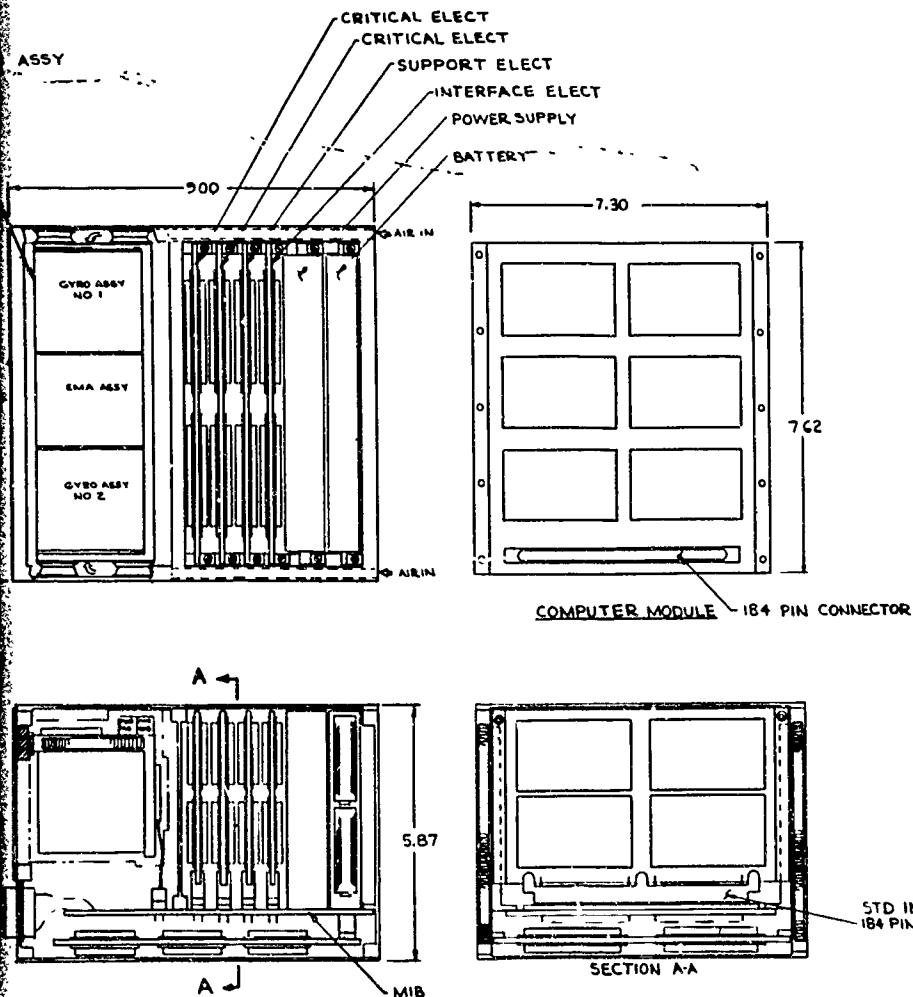


Figure 6-118. Design Alternative No. 5 -  
Approximate Volume 429 In<sup>3</sup> W/O Insulation

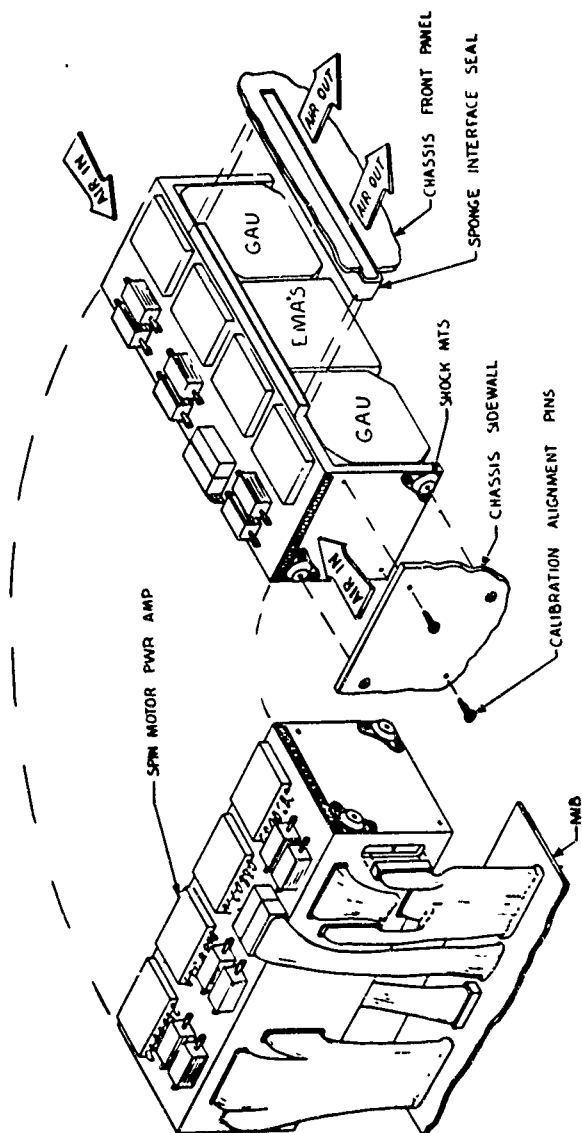


Figure 6-119. Instrument Assembly





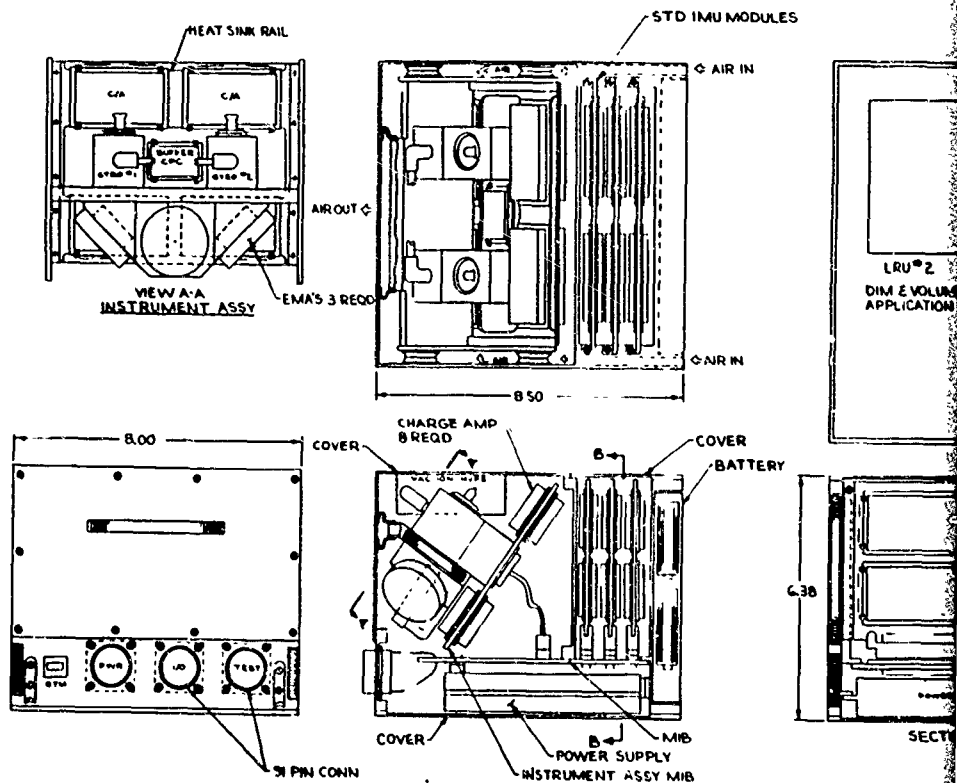


Figure 6-121. Design Alternative  
Estimated Weight 15 LB

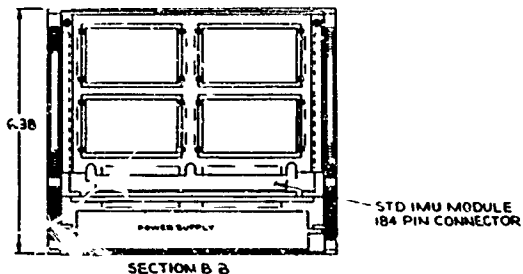
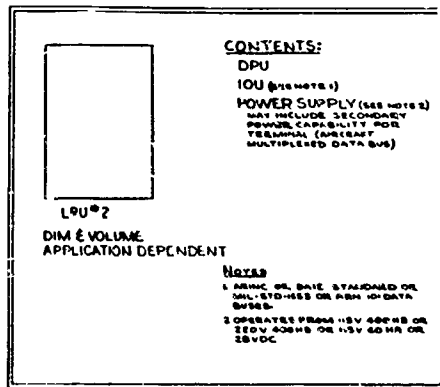
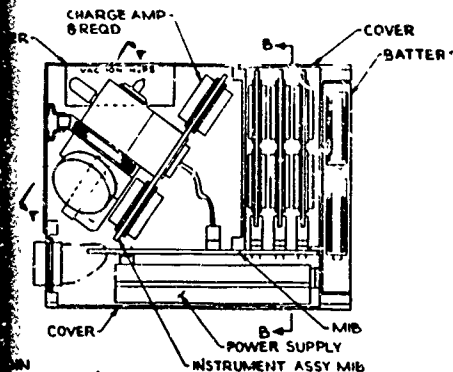
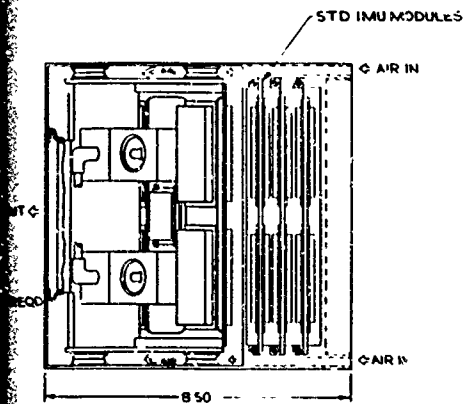


Figure 6-121. Design Alternative No. 7 Volume 434 in<sup>3</sup>  
Estimated Weight 15 Lbs, LRU No. 1 of 2

### 6.3.6.3 DPU Design Alternatives

This task includes tradeoffs performed on the dedicated processor unit. The tradeoffs were conducted with the objectives of reducing size, power and recurring costs.

**6.3.6.3.1 Memory Tradeoffs.** The dedicated processor unit developed for MICRON under separate contract utilized 4096 words of nonvolatile memory implemented with 2-mil plated wire and 4096 words of read-only-memory (ROM) implemented with low voltage P-channel MOS/LSI components. This memory subsystem, and the plated wire in particular, was found to be too expensive for the MICRON cost goals. Tradeoffs were therefore conducted to determine the optimum memory configuration for the MICRON application. These tradeoffs consisted of determining memory organization, nonvolatile storage requirements, power and packaging alternatives. Primary emphasis was placed on utilization of MNOS technology in lieu of plated wire. Hence, electrically alterable read-only-memory (EAROM) MNOS devices were characterized and evaluated. Suitable test techniques and special hardware were developed. The tests were conducted to determine the MNOS retention/access characteristics. A technical memorandum (J175-246-041-02) was prepared which covered the evaluation of the EAROM devices, a detailed description of the devices and the results of the characterization tests. This document is presented in Appendix K.

#### Subsystem Design

One baseline and four alternate memory subsystems were configured. These configurations are:

- |                   |   |                           |
|-------------------|---|---------------------------|
| • Baseline        | 6K ROM<br>1K EAROM<br>1K RWM<br>1 $\mu$ s read cycle<br>Hybrid packaging<br>NCR2100 EAROM   | } 256 word block transfer |
| - Alternate No. 1 | 7K EAROM<br>1K RWM<br>2 $\mu$ s read cycle<br>Hybrid packaging<br>NCR2400 EAROM   | } 1K word block transfer  |
| - Alternate No. 2 | 6K ROM<br>1K EAROM<br>1K RWM<br>1 $\mu$ s read cycle (ROM and RWM)<br>2 $\mu$ s read cycle (EAROM)<br>Conventional packaging<br>NCR2400 EAROM | } 1K word block transfer  |

- Alternate No. 3 Same performance as Baseline  
Conventional packaging
- Alternate No. 4 Same performance as Alternate No. 1  
Conventional packaging

Important features of these configurations are shown in Table 6-65. Preliminary designs for the Baseline and Alternate No. 1 were completed. Both designs require four substrates of three types. The remaining alternates use conventional packaging and will fit on a single module. Power requirements for the two hybrid versions are listed in Tables 6-66 and 6-67. Power requirements for Alternate No. 3 were approximately the same as the baseline, while Alternates No. 2 and No. 4 required essentially the same power as Alternate No. 1. Table 6-68 gives a part count comparison summary for the baseline and Alternate No. 1.

Sixteen 91L02B NMOS static RAMs were used for the read-write memory. These devices were chosen on the basis of speed, power and availability. Each device dissipates 193 mw., worst case for a total of over 3 watts for the RWM. This represents about 1/3 of the total memory power for 1/8 of the memory. As fast 1K static CMOS RAMs (e.g., the Intersil 6508) becomes available, the 91L02B may be replaced, reducing RWM power to around 200 mw.

Table 6-65. Memory Configurations

Feature	Baseline	Configuration			
		Alt. 1	Alt. 2	Alt. 3	Alt. 4
ROM (words)	6144		6144	6144	
EAROM (words)	1024	7068	1024	1024	7068
RWM (words)	1024	1024	1024	1024	1024
Read Cycle Time ( $\mu$ s)	1	2	1 (ROM & RWM) 2 (EAROM)	1	2
Block Transfer RWM- EAROM (words)	256	1024	1024	256	1024
EAROM Device	NCR2100	NCR2400	NCR2400	NCR2100	NCR2400
Packaging Type	Hybrid	Hybrid	Conventional	Conventional	Conventional
CPCs	4	4			
CPC types	3	3			
Memory Devices	44	44	32	44	44
MSI and SSI Devices	51	26	32	45	30
Transistors and Diodes	55	39	19	19	23
Capacitors	30	25	23	21	23
Screen Resistors	102	77			
Discrete Resistors			35	47	53
Relays	4	2		4	2



Table 6-66. Baseline MICRON Semiconductor Memory Power Requirements

Voltage and Tolerance	Mode						Max Power Per Supply	
	RWM or Standby		ROM		EAROM			
	W. C.	Typ.	W. C.	Typ.	W. C.	Typ.	W. C.	Typ.
+5 vdc $\pm 5\%$	8.7	5.8	12.1	8.1	8.9	6.0	12.1	8.1
+12 vdc $\pm 5\%$	0.7	0.5	0.9	0.6	2.0	1.3	2.0	1.3
-12 vdc $\pm 5\%$	0.2	0.1	0.2	0.1	0.6	0.4	0.6	0.4
-17.5 vdc $\pm 5\%$	<u>0.0</u>	<u>0.0</u>	<u>0.0</u>	<u>0.0</u>	<u>0.0</u>	<u>0.1</u>	0.2	0.1
Total	9.6	6.4	13.2	8.8	11.7	7.8		

Values in Watts

W. C. - Worst Case

Typ. - Typical

Table 6-67. MICRON Semiconductor Memory Alternate No. 1 Power Requirements

Voltage and Tolerance	Mode				Max. Power Per Supply	
	Standby, RWM or EAROM Read		On-Board EAROM Write			
	W. C.	Typ.	W. C.	Typ.	W. C.	Typ.
+5 vdc $\pm 5\%$	7.00	4.74	6.42	4.32	7.00	4.74
-12 vdc $\pm 5\%$	2.16	1.52			2.16	1.52
-24 vdc $\pm 5\%$	<u>.53</u>	<u>.48</u>	<u>2.07</u>	<u>1.58</u>	2.07	1.58
Total	9.69	6.64	8.49	5.90		

Values in Watts

W. C. - Worst Case

Typ. - Typical

Table 6-68. MICRON Semiconductor Memory Parts Count Summary

	Baseline	Alternate #1	Change
Substrates	4	4	0
Substrate Types	3	3	0
Memory Chips	44	44	0
Support Chips	36	26	-10
Transistors	38	22	-16
Diodes	17	17	0
Capacitors	30	25	-5
Screen Resistors	102	77	-25
Relays	4	2	-2
Part Types	26	21	-5

#### Conclusions

CMOS technology can meet MICRON requirements using current fabrication techniques. Experience has been gained on the ABC Program where a prototype memory module containing a 12K x 16 MNOS EAROM and 2K x 16 MOS RWM has been fabricated and tested. The ABC uses the same CPU MOS devices and timing as the present MICRON processor.

The only significant potential technical problem using MNOS with MICRON is to provide for a sufficient yield of devices which will meet the speed requirements of the system over the full temperature range. This may be solved by incorporating the DISAG process for the NCR 2100 or screens for the NCR 2400, depending on which device is eventually chosen.

Another possible approach to circumvent speed limitations is to use the EAROM only to hold data during unpowered periods. The contents of the EAROM may then be mapped into RWM at the beginning of a powered interval. Operational data would then be transferred between the processor and the RWM at rated system speed. If this type of approach can be implemented without increasing the size of the RWM, parts count impact will be minimal.

The problem of obtaining multiple sources applies to all memory LSI parts. The Monolithic Memories 5280 8K bipolar ROM, the Advanced Micro Devices 91L02B 1K NMOS RAM and both NCR MNOS EAROMs are single source items. In the case of NCR, no military grade production capability exists or is planned for the future.

## Recommendations

Sufficient data have been generated to estimate development and production costs for five memory subsystem configurations. Performance data for each of these versions have been published. Thus, one of these configurations should now be selected for detailed design and prototype development.

Concurrent with design and development of the prototype, continuing surveillance of MNOS technology should be maintained. Establishment of alternate sources for memory devices should be a prime goal. Technological advances offering potential cost and/or performance improvements should also be monitored for possible incorporation as in-line changes.

6.3.6.3.2 Interface Design. Starting in October 1974, the requirements of the IMU electronics, with respect to the DPU, were reviewed. As a result of this review, the conclusions were reached that the need did not exist for a dedicated, independent, parallel input/output processor capable of block transfers. Further, there is probability not a need for an independent serial processor since a separate serial channel must be included in the IMU in any event for communication with the CCU and other avionics subsystems. Therefore, different techniques were examined which could be used to implement a simplified interface between the DPU and the SEU.

## Implementation Techniques

The approach taken was to eliminate the DPU PIO and IMU computer interface substrates and create a single new substrate which would mechanize a simplified interface between the DPU and IMU electronics. This can be done in two ways:

1. The data exchanges between the DPU and the IMU electronics would be directly to/from the DPU memory via a Direct Memory Access (DMA) channel. The controller for the DMA would require a single substrate. The hardware savings, based on a preliminary implementation of the controller, is 16 bipolar IC's, four MOS IC's, and one CPS. The disadvantage of this method is a loss in flexibility. However, no additional computer capability is required. In fact, less program time is used in this method since a periodic exchange of data would be automatically triggered by the 64 KHz interrupt cycle.
2. The data exchanges between the DPU and IMU electronics would be directly to/from the DPU memory via the memory buses as above, but the memory addresses and the transfer of data would be under program control; that is, three new CPU instructions would be defined:

Load Bus Address Register  
Output Word From Memory  
Input Word To Memory

A strobe would be provided for each of these operations. Once again, a single substrate (which would closely resemble the current "Computer Interface" substrate) would be required. The hardware savings using this method would be 20 bipolar IC's, four MOS IC's and one CPS. The disadvantage of this method is that more computer processing time is

required since an "Input" or "Output" instruction must be executed for each word transferred. However, the assumption is that the MICRON DPU has more than enough throughput for the job.

Based on several factors including results of a cost reduction study, memory bus changes due to all semiconductor memory, and serial I/O requirements, Option 1 above was selected as the preferred approach to the simplification of the interface between the DPU and MUM electronics. A preliminary design of this option was made in bipolar and MOS so that a modified product description could be prepared for cost analysis. The design mechanized a controller which accesses the DPU memory via a DMA channel. The controller is triggered by the 64 Hz cycle and automatically sequences through a fixed routine of writing the MUM and EMA data in memory and reading updated words for spin motor control and for the frequency generator. The logic for the controller should fit into a single custom MOS LSI control device. Data are stored/read from dedicated locations in the DPU memory. The approach would essentially reduce the two substrates of electronics (the "parallel I/O" in the DPU and the "Computer Interface" in the MUM electronics) to a single new control device.

It should be noted that the simplification of the existing parallel channel to the dedicated DMA controller is not contingent on either the development of a new MOS device or the adoption of the proposed remechanization of the other MUM electronics. A bipolar mechanization of the new controller will fit on one substrate which would replace the PIO and Computer Interface substrates.

The IMU electronics allows for two substrates of electronics to mechanize the serial channel to be used for communication with the Control Display Unit (CDU) or a Central Computer Unit (CCU). Since the serial channel for the MICRON system must meet requirements not met by the Serial Input/Output (SIO) in the DPU, the I/O substrates of the IMU would have to receive data from the SIO, reformat, retune and retransmit this data. This inefficiency will be eliminated by the deletion of the SIO. Data for the serial channel will be accessed in parallel from the DPU memory via a DMA channel in the same manner as the parallel channel. The precise mechanization of these two IOU substrates is application dependent and will not be undertaken until the exact specification for the serial channel becomes firm.

6.3.6.3.3 DPU Simplification and Device Reduction. In addition to the redefinition of the memory subsystem, the CPU and IOU (interface between the DPU and SEU) were studied and redefined to (1) simplify the design, and (2) reduce the total parts count and number of parts types used. Alternate packaging schemes were also investigated.

Table 6-69 summarizes the progress made during the DPU component count reduction effort. Selected SEU circuits are included in the totals, as noted, since the mechanization of these circuits is now accomplished in the DPU/SEU interface section of the DPU. As shown in the table, there has been a 42 percent reduction in parts in the non-memory areas, an 86 percent reduction in the memory subsystem, and an overall reduction of 72 percent.

Table 5-69. DPU Component Reduction Summary

	Memory Subsystem		CPU, IOU's, Selected SEU		Totals	
	Developmental Model Memory (Plated Wire Plus ROM)	Semiconductor Memory	Developmental Model CPU and IOU's and Selected SEU Circuits	CPU, IOU's & Selected SEU Circuits Mechanized With MOS	Old DPU's and SEU Mechanization	New DPU's and SEU Mechanization
Total Count of All Components (Excluding Thick Film Resistors)	2861,300 121,323	187	554	321	1771	483
Total Count of All Component Types Excluding Thick Film Resistors	94,24	39	67	33	159,24	58

1. Includes 19 hybrid circuits as single parts.
2. Includes the components in the hybrid.
3. These counts include 139 discrete resistors, but exclude the plated wires.
4. Includes 42 different resistor part types.
5. Except serial channel.

Parts lists were prepared which detailed the reduction in total parts for the DPU as well as the reduction in part types. The parts list has been broken down to the substrate level to facilitate identification of those parts which represent logic previously in the SEU electronics. To the extent possible, the parts selected were beam-leaded parts and were from the list of parts already being used in other portions of the IMU electronics. The parts list may be modified to a small extent when the detailed design of the CPS's is completed. Table 6-70 summarizes the parts usage in the DPU including the electronics previously in the SEU. As discussed in Para 6.3.6.3.1, several alternatives for the memory configuration are being considered. In general, these alternatives require fewer parts than the baseline. Table 6-68 lists the relative parts savings of one alternate memory configuration. Table 6-70 also summarizes the parts usage for a conventionally packaged version of the baseline DPU. This configuration is discussed further in the following section. It is anticipated that as the detailed design of the three IOU/(SEU) substrates progresses, further reductions in the parts quantities can be achieved.

6.3.6.3.3.4 Apportionment of the DPU Logic to Substrates. The apportionment of the DPU logic to substrates has been completed subject to final adjustments as the substrates are actually laid out. The apportionment of the DPU logic, except memory, consists of seven substrates of six types. Two of the types, the program control unit (PCU) and the eight-bit arithmetic and logic units (8ALU) are essentially the same as in the current DPU. There are two 8ALU's per system. The two PCU devices on the PCU have been moved to the 8ALU's to have a more uniform density. The bus logic and clock generation logic have been combined on a single substrate designated BLC. Two new substrates have been defined to mechanize logic functions which were previously in the SEU electronics. These are the Timing Reference Generator (TRG) and the Counter and Automatic Sequencer (CAS) substrates. The last substrate is the Dedicated Processor Interface CPS. This substrate combines the logic required for interrupt request buffering, discrete inputs and outputs, and the controller for word transfers to/from the SEU electronics. The substrate pin-out requirements range between 70 and 232. The number of integrated circuits per substrate ranges between 8 (for all MOS) and 28 (for all TTL).

A few salient points can be made about the apportionment. A distributed clock scheme is to be used in the DPU. A 9 MHz square wave signal is an input to the DPU from the crystal oscillator in the MCM electronics. This signal is divided down on the DPU module and used to form the basic four-phase clocks. These TTL level phase clocks are distributed to each of the substrates where final clock drivers buffer the clocks for use by the MOS devices on that substrate. The memory organization is set up so that there are three basic buses: memory address, data to memory, and data from memory. These buses also extend to a test console external to the IMU enclosure and are therefore buffered by TTL. The organization also utilizes two internal, MOS level buses for memory address and data to memory.

The DPU memory, in the baseline configuration, consists of 1024 words of Read/Write Memory, 1024 words of Electrically Alterable Read Only Memory (EAROM), and 6144 words of ROM. The EAROM is mechanized using NCR 2100's, a 1024-bit device. By using a similar part, which is a 4096-bit device, the 8K word by 16-bit memory could be organized as 1024 words of RWM and 7168 words of EAROM without increasing the total parts count in the memory. Also, the ROM parts are eliminated and the special problems associated with having to change a ROM coding (cost and turnaround time) are eliminated.

Table 6-70. Baseline DPU Parts Summary

	DPU (Hybrid Packaging) Baseline				DPU (Discrete Packaging) Baseline			
	CPU	Memory	IOU/(SEU)	Totals	Module #1 CPU	Module #2 Memory	Module #3 IOU/(SEU)	Totals
Modules	NA	NA	NA	1	1	1	1	3
Substrates	4	4	3	11	NA	NA	NA	NA
Substrate Types	3	3	3	9	NA	NA	NA	NA
MOS LSI or Memory Chips	24	44	24	92	24	44	24	92
Support Chips	34	36	21	91	44	36	29	109
Transistors	50	38	48	136	--	38	--	38
Diodes	--	17	5	22	--	17	5	22
Capacitors	36	30	24	100	16	24	27	67
Relays	--	4	--	4	--	4	--	4
Resistors	70	102	70	242	70	102	70	242
Fat Types	37	26	29	57*	24	26	26	57*

\*Common parts exist among the three sections.

The problem that arises is that the larger EAROM device has a slower read access time. Therefore, the DPU timing must be changed and throughput reduced to some extent to be able to make the change. Assuming that the MICRON mechanization only requires a fraction of the current DPU throughput, then the advantages of alterable ROM may outweigh the decrease in throughput. The read cycle time of this proposed memory would be 2.0 microseconds as opposed to the current read cycle time of 1.0 microsecond.

Three methods of achieving the 2.0 microsecond read cycle were investigated. The first method was to reduce the DPU basic clock rate to 500 kHz. The second method was to re-microprogram the instruction set so that the read access would take two CPU clock cycles. The third method was to generate a pseudo cycle-steal request to the CPU control logic during the second half of a CPU generated memory read operation. The investigation showed this third method to be the best approach for the following reasons: least adverse effect on throughput, changes to the CPU are confined to a single substrate (BLC), same parts increase as the second method, no re-microprogramming required, reversion to a ROM or other memory is not difficult, the required read access time is attainable, and the large instruction set is retained.

Another memory configuration being considered utilizes 1K RWM, 1K EAROM, and 6K ROM as in the baseline except that the EAROM is a 4096 bit device instead of the 1024 bit device. This reduces the number of chips required from 16 to 4. In this scheme, the contents of the EAROM are dumped into the RWM at power turn-on and are not subsequently read from the EAROM during the operational mode. This method protects against the volatility of the RWM while not requiring a slower read-access time due to the more dense EAROM device.

During the latter part of this study, alternative methods of packaging the DPU were examined with the goal of reducing developmental cost. The most economical approach consists of three modules functionally organized to contain the CPU, Memory and IOU/SEU electronics. The modules are 9.3 x 6.6 in. glass boards with heat rails and a 184 pin connector. The boards are 6 to 8 layers with parts mounted on both sides. Table 6-71 is a parts list, by module, of the baseline DPU packaged in this manner.

#### 6.3.6.4 Simplify Gyro Electronics

6.3.6.4.1 Suspension Electronics. The design, breadboarding and most of the evaluation testing has been completed on new suspension electronics designs for Pulse Amplitude Modulation. The new designs include the Charge Amplifier, Sample and Hold Notch Filter, Signal Buffer, Modulator Input and Modulator Output. Thus far, tests have shown good performance as far as the limited data that can be obtained in breadboard tests. Lay outs of the new designs have been completed so that circuits can be fabricated for evaluation on either test station 2M or on the XX77 system. The new Charge Amplifier has reduced the number of transformers from 32 to 24. The Charge Amplifier for the small gap gyro has one-half as many high voltage transistors.



Table 6-71. Discrete Packaging, Baseline DPU Parts List

Part Number	Source	Part Type	CPU Module No. 1 Quantity	Memory Module No 2 Quantity	IOU Module No 3 Quantity
54LS00	T.I.	Quad 2 IN NAND	3		1
54LS02	"	Quad 2 IN NOR	1		6
54LS04	"	Hex Inverter	1	1	3
54LS08	"	Quad 2 IN AND	2	2	2
54LS10	"	Triple 3 IN NAND	1	1	
54LS20	"	Dual 4 IN NAND		1	
54LS76	"	Dual J K F/F W/SET, CLR	3	3	5
54LS138	"	3 → 8 Decoder		1	
54LS153	"	Dual 4 → 1 MUX	5		
54S11	"	Triple 3 IN AND	3		
54S112	"	Dual J K F/F, Neg. Edge Trig	4		
5408	"	Quad 2 IN NAND	3	5	
54157	"	Quad 2 → 1 MUX	2	8	
54173	"	4 Bit Latch W/3 State Out	6	4	
30074	Rockwell MDD	MOS AC	1		
30076	"	MOS MFC	1		
30077	"	MOS AB	4		
30079	"	MOS LAD	2		
30102	"	MOS MXF	8		3
30104	"	MOS PCT	2		8
30105	"	MOS INT	1		
30108	"	MOS BAP			8
A00XX	"	MOS ROM	5		2
30XXX-1	"	MOS TRGC			1
30XXX-2	"	MOS CASC			1
30XXX-3	"	MOS DMAC			1
RM4131BL		Op Amp (Mod. Band)			2
8LC741-B		G.P. Op Amp Comparator			2

Table 6-71. (Cont)

Part Number	Source	Part Type	CPU Module No. 1 Quantity	Memory Module No. 2 Quantity	IOU Module No. 3 Quantity
91L02BM	AMD	1K x 1 RAM		16	
5280	Monolithic Memories	1K x 8 ROM		12	
NCR2100	NCR	256 x 4 EARAM		16	
B2D753A	T.I.	Zener Diode 6.2V			2
B2D751A	T.I.				1
B2D914	T.I.	G.P. Diode		1	
BD3600					2
5082 2837	Hew Pack.	Schottky Diode		16	
M39016/23 004L		SPDT Relay		4	
50R11W475M		Capacitor, 47 $\mu$ f, 50V, 20%			1
50R11W105M		Capacitor, 10 $\mu$ f, 50V, 20%	4		6
50R11W474M		Capacitor, 47 $\mu$ f, 50V, 20%			1
50R11W224M		Capacitor, 22 $\mu$ f, 50V, 20%		11	
50R11W124M		Capacitor, 12 $\mu$ f, 50V, 20%		4	
50R11W104M		Capacitor, 10 $\mu$ f, 50V, 20%	3		11
50R11W103M		Capacitor 01 $\mu$ f, 50V, 20%	4		4
50R11W302M		Capacitor, .003 $\mu$ f, 50V, 20%		9	
50R11W222M		Capacitor, .0022 $\mu$ f, 50V, 20%			2
50R11W101M		Capacitor, 100pf, 50V, 20%			1
50R11W100M		Capacitor 1Gpf, 50V, 20%			1
IM5013	Intersil	Clock Drivers	8		8
2N2222A	T.I.	NPN Transistor (GP)		2	
2N2907	"	PNP Transistor (GP)		2	
2N3467	"	PNP Transistor (Core Driver)		1	
2N3725	"	NPN Transistor (Core Driver)		1	
2N2369A	"	NPN Transistor (Switch)		16	
2N3829	"	PNP Transistor (Switch)		16	
753654	"	Quad MOS Driver		7	
HD6600	Harris	Quad Power Switch Resistors	70	3 102	70

The charge amplifier substrates have been fabricated and testing of these units is commencing. All remaining hybrid CPC's are now in assembly. The MLB board has been received and continuity testing has commenced. In addition, a circuit (Temperature Compensation and Gap Monitor) has been defined which may allow for compensation of all electronics temperature variations except for those in the instruments area (Charge Amplifiers, Signal Buffers), the Crystal Oscillator, and possibly Temperature Compensation and Gap Monitor.

6.3.6.4.2 Attitude Readout Electronics. The MUM Demod Sample and Hold circuits have been evaluated with the low cost CA3130 RCA and LF156 National operational amplifiers. Test results show good performance. Temperature sensitivity tests have been undertaken.

### 6.3.6.5 Simplify Gyro Mechanical Design

The intent of this task is to design the MESH instrument for overall system simplification. The principle efforts have been with regard to the efforts as listed below.

#### 1. Small Gap Gyro

The intent of this task is to reduce the cost of the electronics and yet maintain performance capability. Three small gap units were fabricated in support of the effort; Unit No. 1 had a gap of approximately 225  $\mu\text{in.}$  at 160°F. Angle cal, drift cal, and cross polar drift data were taken to evaluate the MESH performance. Modeling studies will be performed on this data.

Unit No. 2 had a gap of approximately 150  $\mu\text{in.}$  at 160°F but suffered a catastrophic full speed failure on T/S IV on 21 May 1975. The unit offered no particular problems during assembly, burn-in, or bake-out. Problem areas with regard to the small gap were anticipated and corrected prior to instrument test exposure. The unit was mounted on T/S IV and the case (only) was heated to allow good lift-off. The unit was charge monitored (charge was small and stable) and the rotor was heated to approach a 170  $\mu\text{in.}$  gap. At these conditions, a servo response test was conducted to assure adequate servo response with the small gap ESG. All indications were that the unit/system was capable of a good spin up. The rotor was spun up to  $\approx 1200$  Hz and damped into the near C axis such that no problems would be experienced upon spin up to full speed. The charge amp signal, MUM amplitude, and gap size were good and the gyro was spun up to full speed ( $\approx 2430$  Hz). The rotor was then damped toward the A axis. The dividing polhode region was approached and all polhode patterns and signals were normal. It was at this time that the rotor dropped from full speed. No reason was found for the rotor drop.

Unit No. 3 was fabricated and the gap was approximately 170  $\mu\text{in.}$  at 160°F. The unit was evaluated on T/S IV; Angle cal and drift cal were completed on 25 July 1975. The results are presented in Para 6.3.4.

The units evaluated thus far have been of the N57A configuration. A commitment has been made to fabricate all MESH units to give a  $\approx 225$   $\mu\text{in.}$  gap at 160°F. MICRON unit No. A016Y was fabricated with the small gap and will be evaluated on T/S IV early in Phase 2B.

#### 2. 1/2 Impedance Motor

The intent of this task is to design and fabricate a motor with X and Y axis coil impedance one half the value of the ECOM motor coil design which could result in a significant cost reduction in the motor power supply electronics. One motor was fabricated during this reporting period and is available for test as required. Initial baseline testing has been performed in the electronics laboratory.

### 3. MESH Configuration Redesign

Layouts have been made of possible new MESH configurations. They include Vaeon pump and getter layouts. Included are some of the cost cutting features of the getter units currently in fabrication. The base configuration was simplified for ease of machining and alternates for the beryllium base material are being considered. Both these changes are for cost reduction purposes. See Figures 6-122 through 6-125.

### 4. Dual Instrument on a Single Base

It has been suggested that a dual instrument mounted on a single base could represent a cost saving. Initial layouts were made of possible configurations for costing purposes and feasibility studies. The preliminary layout drawings are as shown in Figure 6-126 through 6-128.

### 5. Captured Seal Design

The intent of this task is to perform initial evaluation of the feasibility of alternate seals which would replace present gold o-ring seals. The effort could benefit standard type fabrication or gettered MESH fabrication. Possible seal arrangements are shown in Figures 6-129 through 6-131.

### 6.3.6 Power Supply Design Alternatives

The following tradeoff studies for the power supplies were initiated in Phase 2A and will be continued in Phase 2B:

1. In-house designs vs custom and off-the-shelf designs from power supply manufacturers.
2. Hybrid packaging and discrete parts packaging cost, size, and weight comparisons.
3. Studies to determine the best power hybrid package to use.
4. High-efficiency synchronized and non-synchronized switching regulator circuits design and test.
5. LC-DC Converter design studies.
6. Battery charger (pulse charge vs high current and trickle charge current) tradeoffs.
7. Battery test circuit configuration studies. The battery must be loaded for an adequate test but the length of time is important and must also be defined.
8. Tests to determine if secondary regulators can be eliminated in the power supplies. This would save cost and improve efficiency.

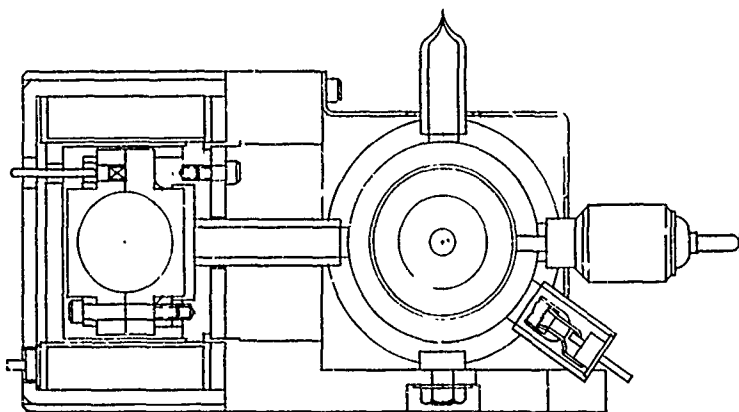
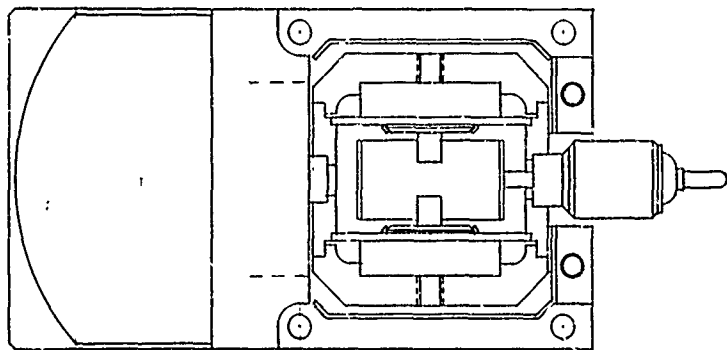


Figure 6-122. Altern

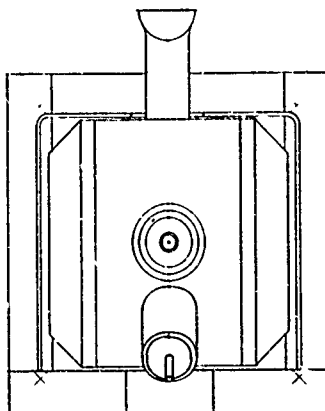
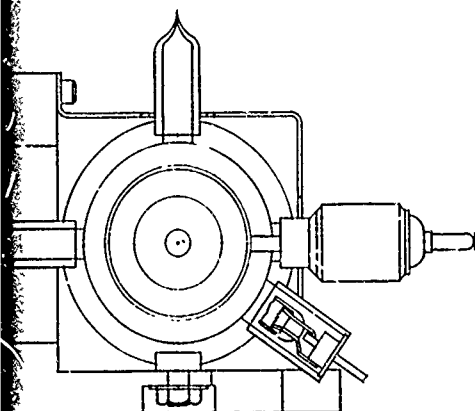
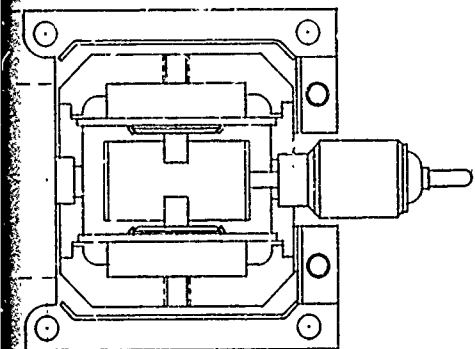


Figure 6-122. Alternative MESC Design No. 1

Preceding page blank

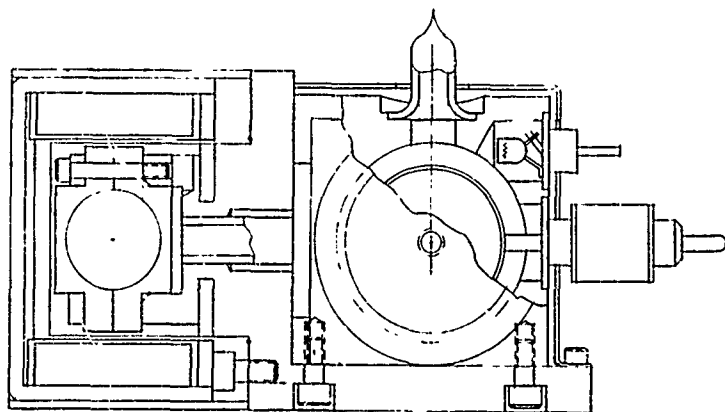
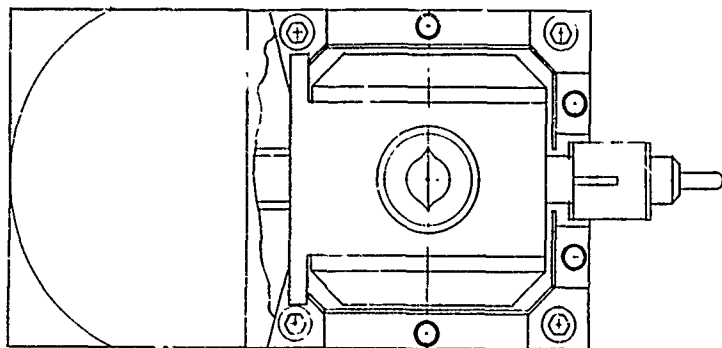


Figure 3-123. Alternas



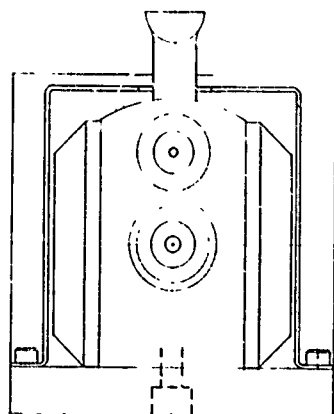
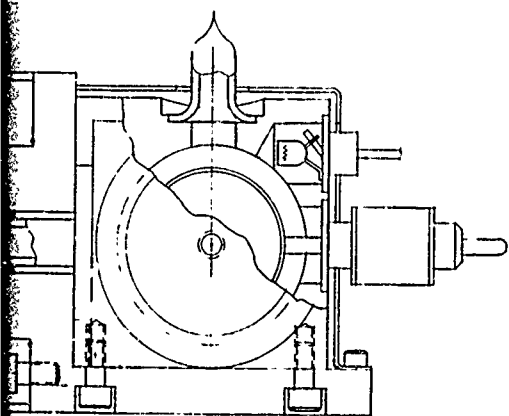
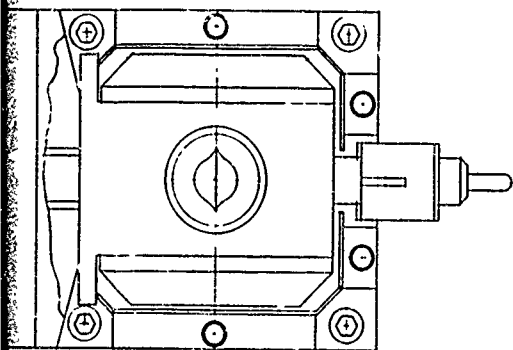


Figure 6-123. Alternative MESG Design No. 2

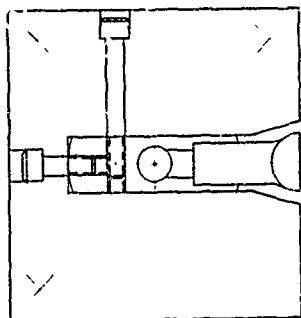
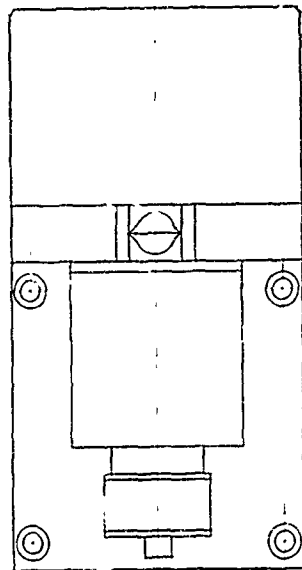
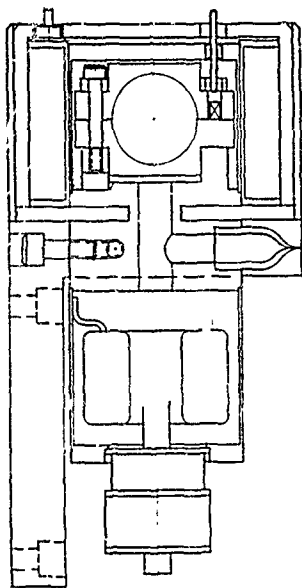
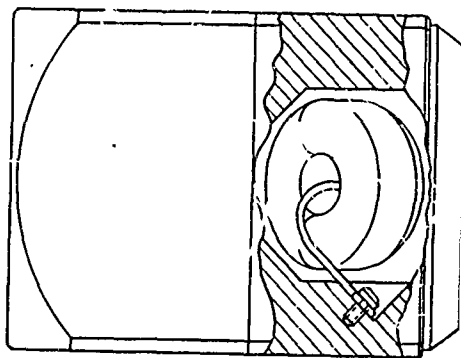
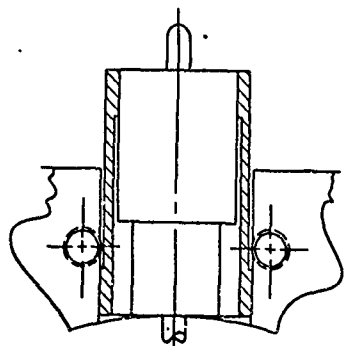
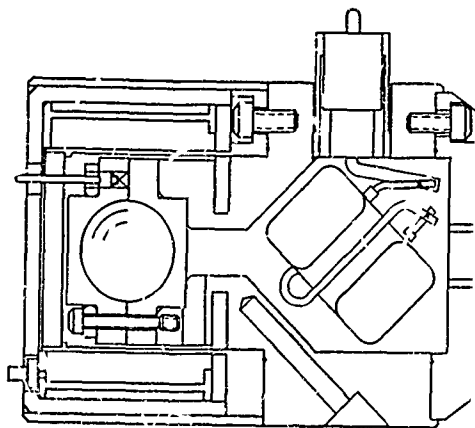
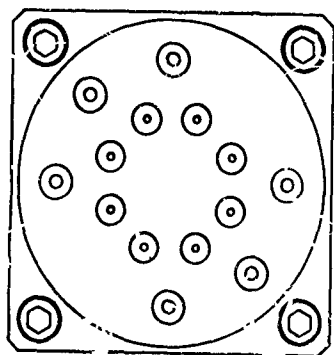


Figure 6-124. Alternative MESG Design No. 3



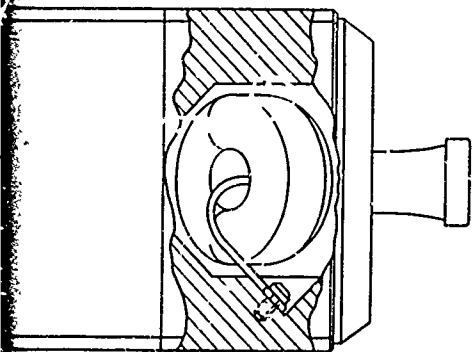
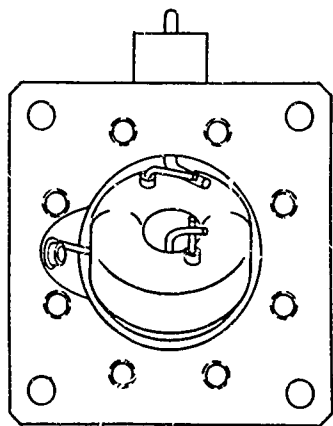
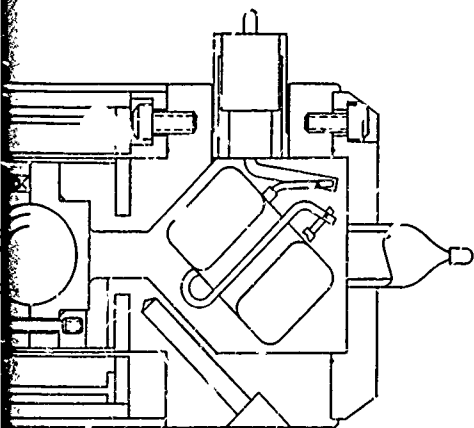


Figure 6-125. Alternative MESG Design No. 4

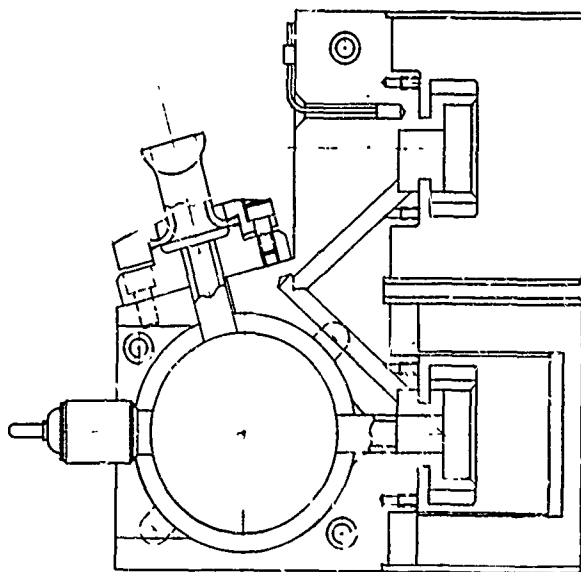
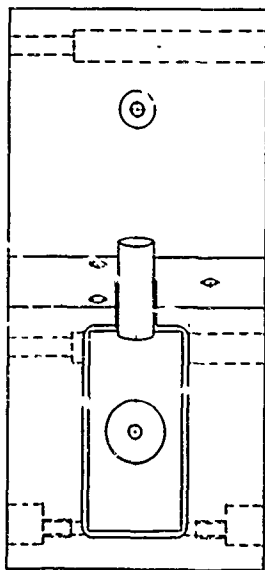
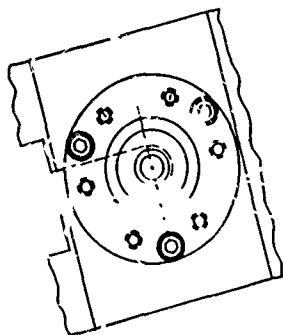


Figure 6-126. Dual Gyro, Singl

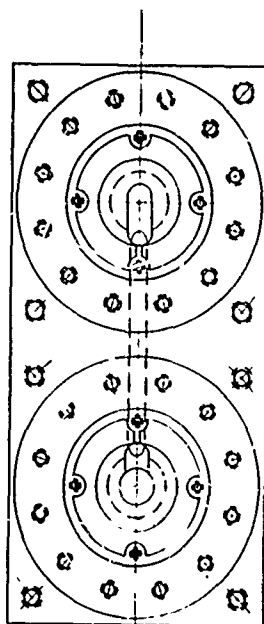
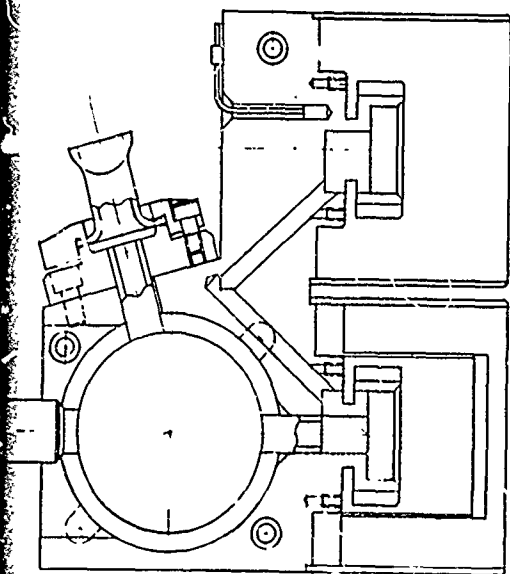
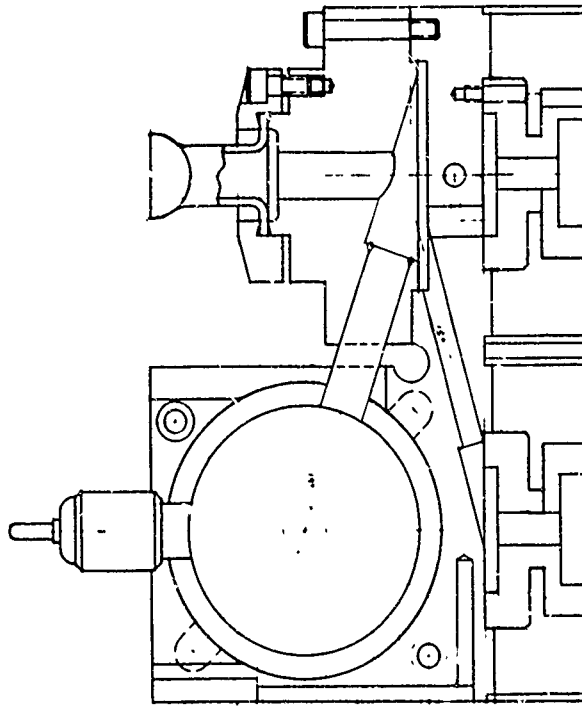
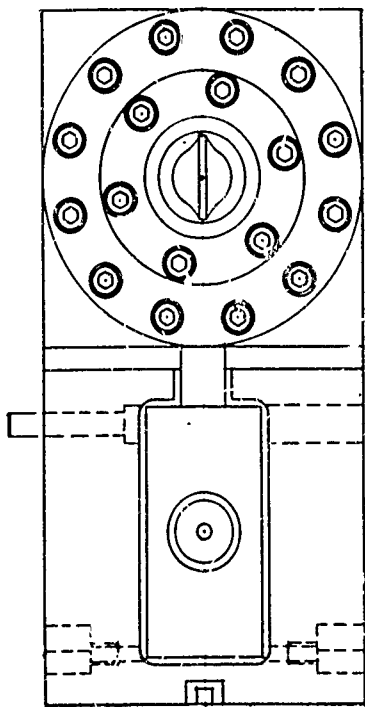


Figure 6-126. Dual Gyro, Single Pump Brazed to Beryllium Base



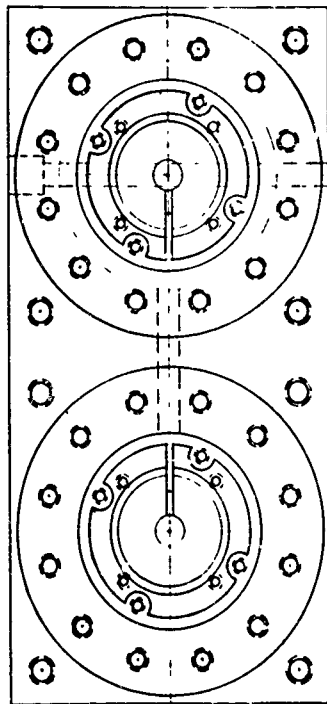
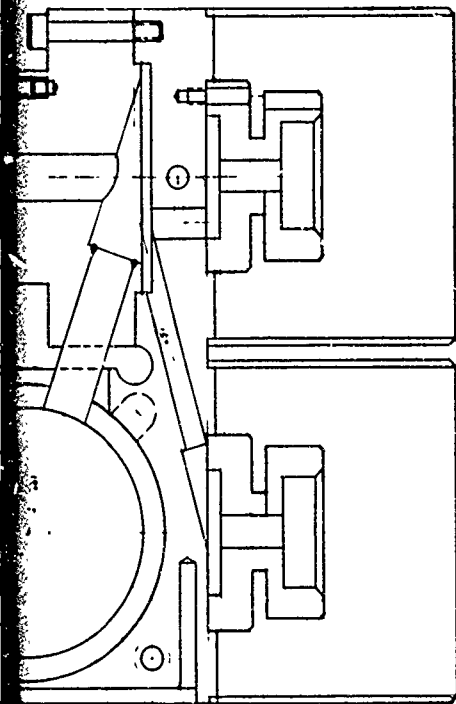


Figure 6-127. Dual Gyro, Single Pump E-Leam Welded to Inconel Adapter



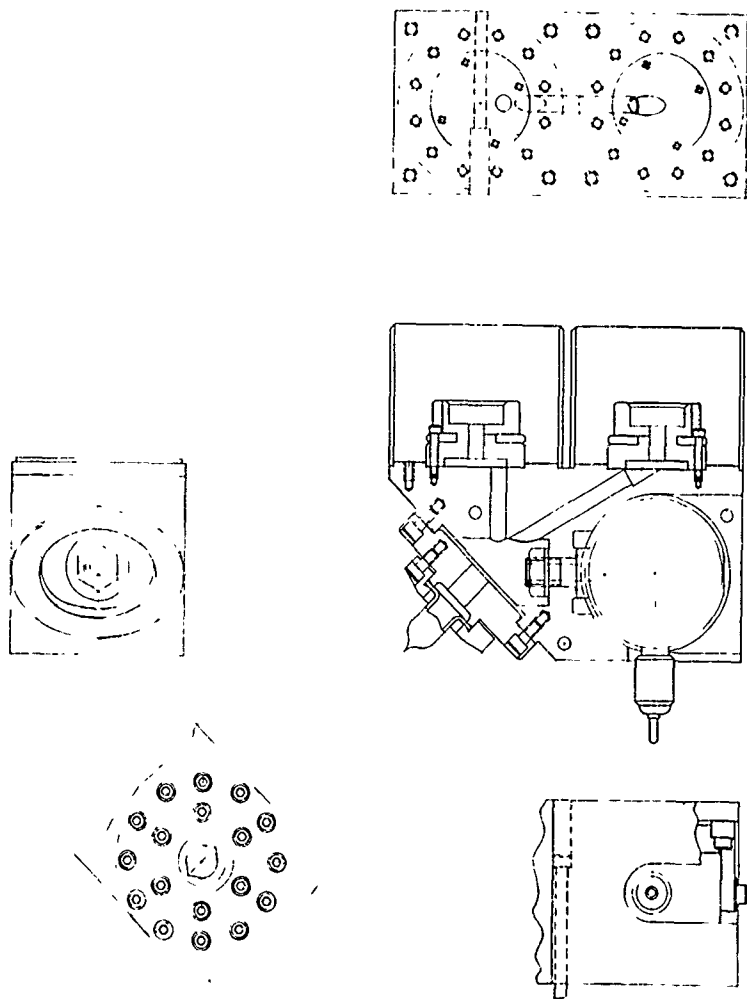


Figure 6-128. Dual Gyro, Sing.

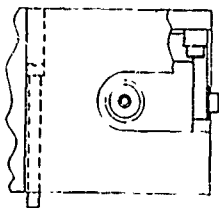
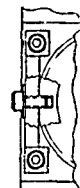
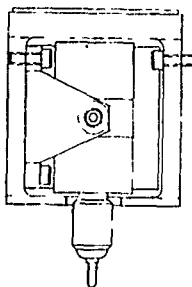
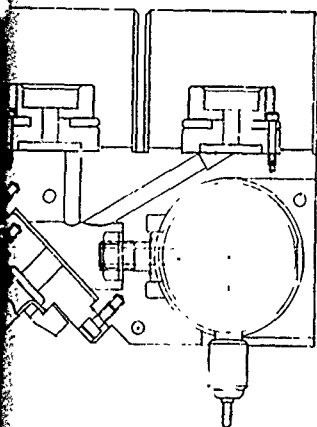
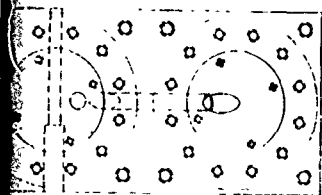
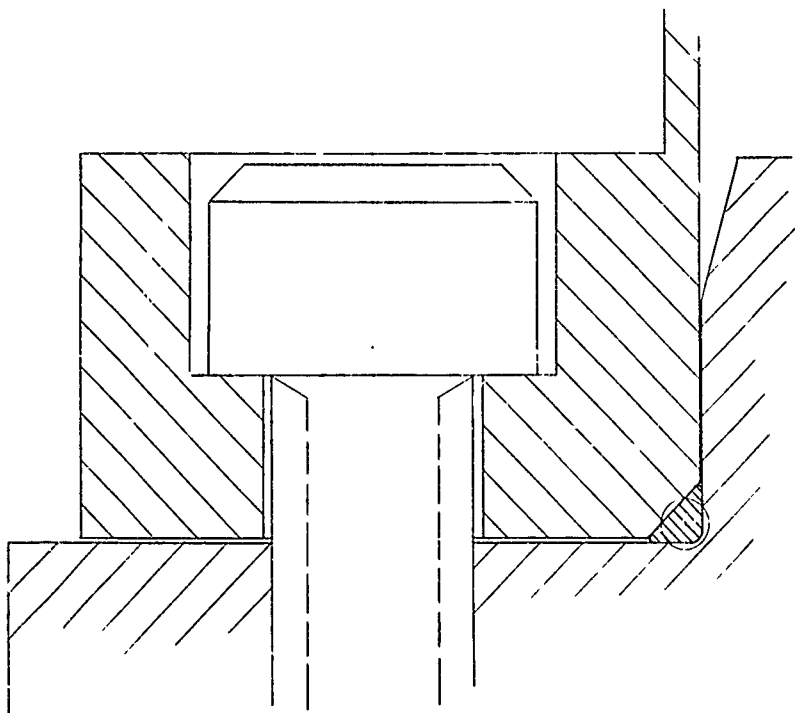


Figure 6-128. Dual Gyro, Single Pump Sealed to Beryllium Base with Gold Gasket



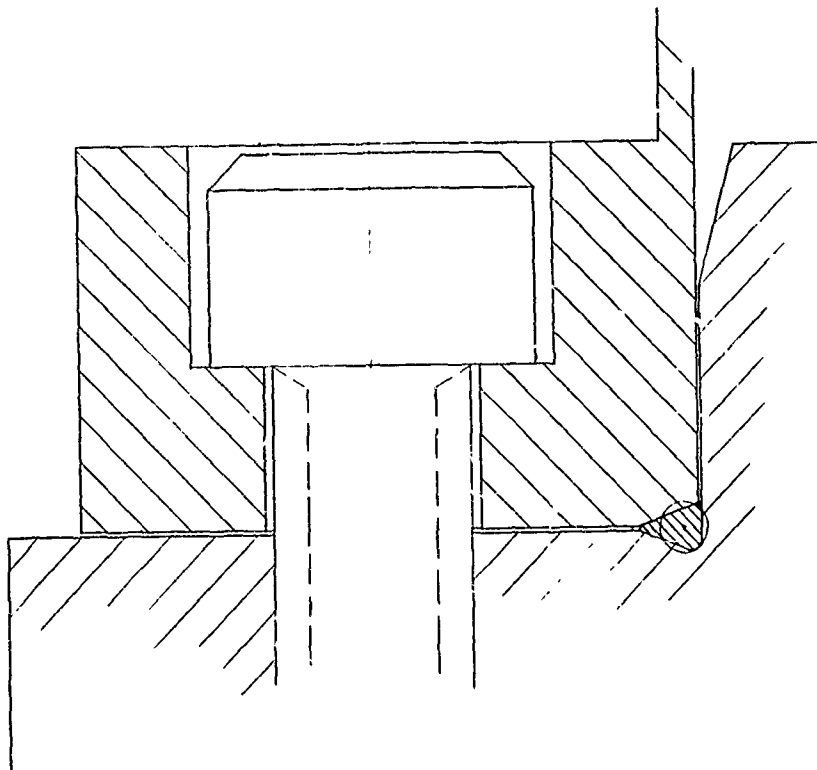
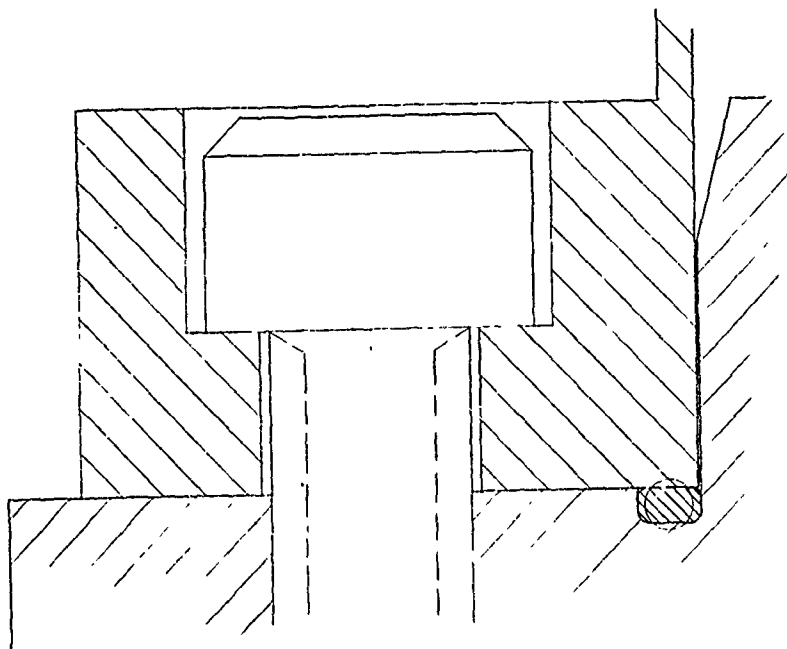
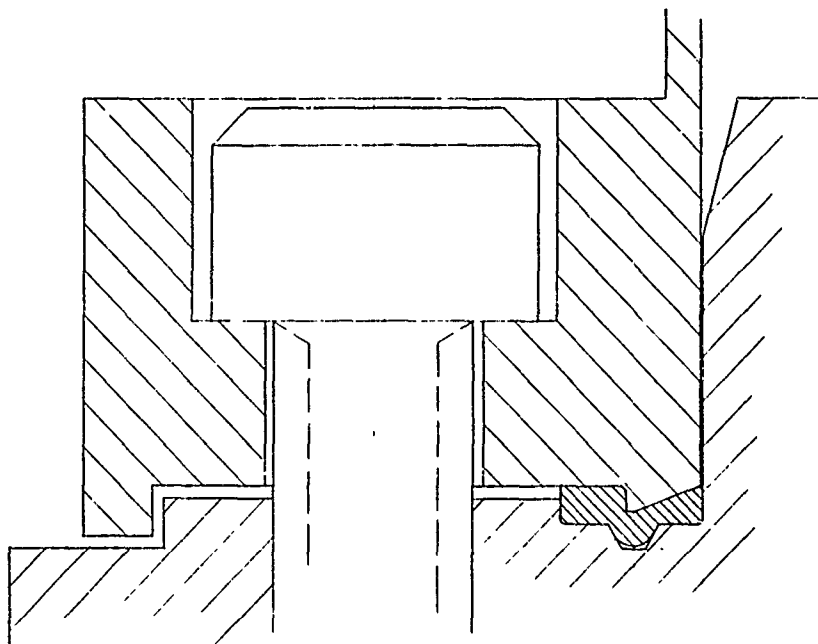


Figure 6-129. Captured Seal Design - Using .020 Diameter Wire

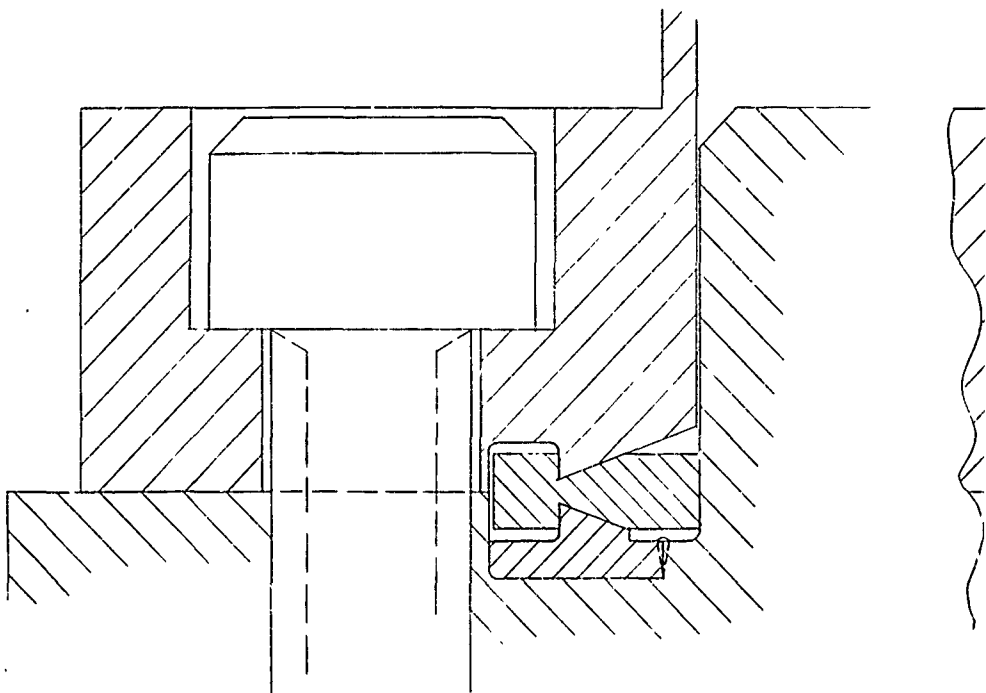


C. 020 DIA WIRE



0.015 ( $\pm$ ) X 0.060 (W) GASKET

Figure 6-130. Captured Seal Design



Figu

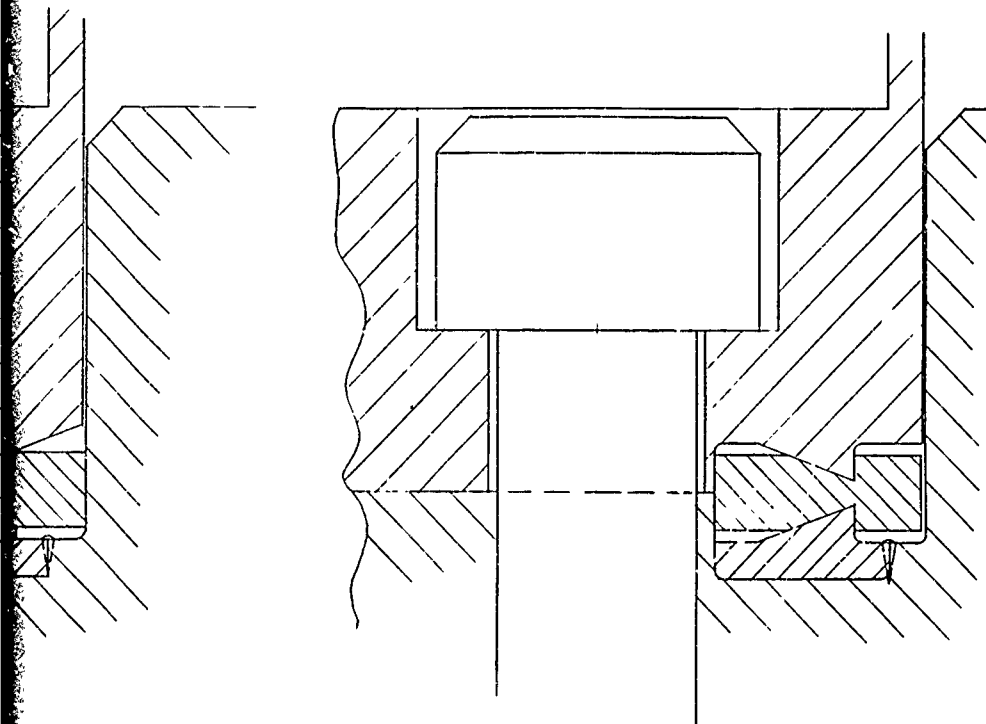


Figure 6-131. Captured Seal Design - Conflat 0.030(t) x 0.089(w) Gasket



Definitions of a hybrid version of the power system package and an all discrete version were completed.

Work was started to develop a high voltage switch which provides bi-level, 10 kHz switching outputs to the charge amplifiers rather than the present 315 vdc voltage. This feature will eliminate the need for the 700 v transistors in the charge amplifiers which should result in very significant cost savings and increase in reliability.

Development breadboarding and tests on the high voltage switch was confirmed in July.

An optimum power system was worked out for 22-32V dc input which included the required redundancy and backup power provision for the critical power. The system included a battery which would store a sufficient amount of energy in a 2 minute "fast charge" cycle to carry the system load during the specified transients as well as the load during the despin mode during prime power failure. Special logic had to be worked out to provide "fast charge" current by "series-parallel" switching of two halves of the battery string during the fast charge mode.

Specifications were prepared for the various power supplies that comprised the power system in order to invite bids from outside suppliers.

Preliminary schematics for the various power circuits were drawn up and major circuits such as the 300 W preregulator, support power supply, and critical power supply were breadboarded and partially tested.

A number of tradeoff studies were performed requiring preliminary packaging design of the entire power system. The tradeoff studies were performed to define cost and size of hybrid versus discrete versus combinations thereof. The study resulted with the conclusion that hybrid circuitry was too high a price to pay for the amount of volume saved. This is due to the fact that approximately 60-70 percent of the components were either magnetic devices or high power devices which were impractical or not obtainable in hybrid form.

The effort at the end of Phase 2A was concentrated on obtaining a definition of an optimum system for 400 Hz, 115 V single phase input. This change from the 24 V dc input to 400 Hz 115 V input requires extensive redesign and various tradeoffs to be considered. This may involve changing spin motor power and battery voltage to between 70 and 80 volts. A scheme to use the battery to filter 400 Hz ripple is being considered which would eliminate some large and heavy filtering components.

In Phase 2B, this effort and preliminary design and breadboarding for 400 Hz will be continued. It is expected that the use of 400 Hz ac input power may result in a saving of cost and space.

#### 6.3.6.7 I/O Design Alternatives

A preliminary I/O design has been defined, with block diagrams and parts lists, for interfacing between the DPU and the following units: the MICRON subsystems (EMA's, SMC, etc.), the digital/synchro converters, and the remote terminal which uses the MIL-STD-1553 serial data bus. The original design scheme for interfacing between the DPU and aircraft avionics incorporated separate holding registers and off-the-shelf digital-to-synchro converters and digital-to-analog converter.

An alternate scheme has been defined for digital-to-synchro conversion that should reduce cost, size, and power from that required for off-the-shelf digital/synchro converters. This scheme saves about \$2000.00. It utilizes  $\sin \theta$  and  $\cos \theta$  digital data from the computer which drive multiplying digital-to-analog converters (DAC's) to obtain 400 Hz signals which are proportional in amplitude to the computer data.

A third low cost mechanization of the Digital/Synchro Converter is presently being evaluated. This new circuit utilizes the new MOS A/D Converter device (65008) which is being designed under the Phase 2A program. Two of the MOS A/D converter devices are required per channel and a total of seven channels are required. The advantage of this particular mechanization is that it requires fewer components than the two previous designs considered and it may also eliminate the need for a separate converter module.

A breadboard of the new scheme was tested with successful results using the NR 65003 NA device as a pre-prototype for the 65008 unit. Further detailed tasks to be undertaken during Phase 2B are determinations of optimum timing for conversion initialization, multiplexing, and strobing the single digital/analog converter circuit and the ten digital/synchro converter circuits. Also, laboratory tests will be continued on the breadboard circuit for harmonic distortion, linearity, and null voltage characteristics.

#### 6.4 APPLICATIONS ENGINEERING

In Task 5.4, Applications Engineering, Autonetics contacted aircraft primes, avionics integration contractors, and other government agencies to gather data on potential applications for MICRON.

Applications Engineering trips made during Phase 2A are discussed in the following paragraphs. Samples of the MICRON Applications Survey questionnaires which were in this task are shown in Appendices L and M.

##### 6.4.1 Applications Engineering Trip to Wright-Patterson Air Force Base (23-25 October 1974)

On 23 through 25 October 1974, Mr. J. A. Schwarz and Mr. L. B. Romine were at Wright-Patterson Air Force Base to visit several offices regarding MICRON and its potential application to various host vehicles. Messrs Schwarz and Romine were joined in this visit by Mr. Ed Toohy and Mr. Ellis Hitt, both of TASC, and Capt. Warzynski and Capt. Radic of AFAL.

Appendix N shows the meeting agenda as well as the audience at each meeting. Appendix O summarizes notes taken during the various meetings as they relate to MICRON and the Applications Engineering task.

So no questions on the MICRON Applications Survey questionnaires were answered during the visit. Additional copies of the questionnaires were left at each of the potential application offices. These offices agreed to fill out the questionnaires and feed the information back to Autonetics through Capt. Radic at AFAL.

#### 6.4.2 Applications Engineering Trip to General Dynamics, Martin Marietta, and McDonnell Douglas (6-8 November 1974)

The subject trip was made by G. W. Sargent and J. A. Schwarz, to (1) General Dynamics in Fort Worth, Texas, on the U. S. AF Air Combat Fighter (ACF) Program, (2) Martin Marietta Corporation in Orlando, Florida, on the USAF Advanced Strategic Air Launched Missile (ASALM) Program, and (3) McDonnell Douglas in St. Louis, Missouri, on the U. S. Navy ACF, USAF ASALM, Stand-Off Missile (SOM), and Cruise Missile Program (CMP). Messers Sargent and Schwarz were joined on this trip by Ed Toohey of TASC.

The purposes of the visits were to (a) inform the various audiences of the MICRON Program status and plans and (b) solicit feedback information from the several programs represented by the audiences regarding their program objectives and requirements related to a navigation system for their application.

Appendix P presents the meeting agenda as well as the audience at each meeting. Appendix Q summarizes notes taken during the various meetings as they relate to MICRON and the Applications Engineering Task.

Copies of both the narrative and the "spec type" Applications Engineering survey questionnaires were left with each audience. Each audience, with the exception of General Dynamics, agreed to fill out the questionnaires and return them to Autonetics.

#### 6.4.3 Applications Engineering Trip to Northrop Co. (12 November 1974)

The subject trip to Northrop Corporation, Hawthorne, California, was made by J. A. Schwarz, G. E. Runyon, D. W. Holmes, and Capt. R. R. Warzynski (AFAL) to discuss the application of MICRON to the F-17 ACF.

The meeting began with a MICRON briefing given by J. A. Schwarz. A question and answer session followed in which the technical requirements on MICRON peculiar to the F-17 application were discussed. The meeting participants are listed in Appendix R.

During the question and answer session, J. A. Schwarz was given a copy of the F-17 INS Specification for our review. Significant areas involved in the discussion included: (1) computer requirements, (2) reaction times, and (3) data buss interface. These requirements are detailed in the INS specification. Northrop personnel were also concerned about MICRON technical risk and whether or not the MICRON schedule would support the ACF schedule. Mr. Ed Light pointed out the go-ahead was expected 1 February 1975 with the production decision date 29 months later, or 1 July 1977. He also noted that purchase of long lead items would necessarily occur somewhat prior to the 1 July 1977 date.

Copies of the applications engineering questionnaires were left with the Northrop Avionics personnel. G. W. Scott requested a second meeting around mid-December at which time they would return the questionnaires and discuss our reaction to the F-17 INS specification.

6.4.4 Applications Engineering Trip to Army ECOM, Sikorsky, Grumman, Fairchild-Republic, and Boeing Vertol (19-21 November 1974)

The subject trip was made by J. A. Schwarz and D. W. Holmes. The agencies and/or companies visited and the related programs were:

1. U.S. Army Electronics Command, Ft. Monmouth, N. J.  
UTTAS (Utility Tactical Transport Aircraft System)  
AAH (Advanced Attack Helicopter)  
ASH (Advanced Scout Helicopter)
2. U.S. Army Security Agency, Ft. Monmouth, N. J.  
Black curtain projects, primarily utilizing fixed-wing aircraft.
3. United Aircraft Corp., Sikorsky Aircraft Division, Stratford, Conn.  
UTTAS  
AAH  
ASW (Anti-Submarine Warfare)
4. Grumman Aerospace Corp., Bethpage, L. I., N. Y.  
MOHAWK  
F-14  
AG  
E-2
5. Fairchild Industries, Inc., Republic Division, Farmingdale, L. I., N. Y.  
A-10
6. The Boeing Co., Vertol Division, Philadelphia, Penn.  
UTTAS  
H1H

Messrs Schwarz and Holmes were accompanied on this trip (except to Boeing) by Mr. R. Clark of ECOM and Mr. J. H. Gilmore, Autonetics representative in the Northeastern region. Mr. Ed Toohey, TASC, participated in the ECOM portion of this trip.

The purposes of the visits were to brief the various audiences on the status of the MICRON Program and the test results obtained on the brassboard system and to request feedback information from the several programs represented by the audiences regarding their program objectives and requirements related to a navigation system for their applications.

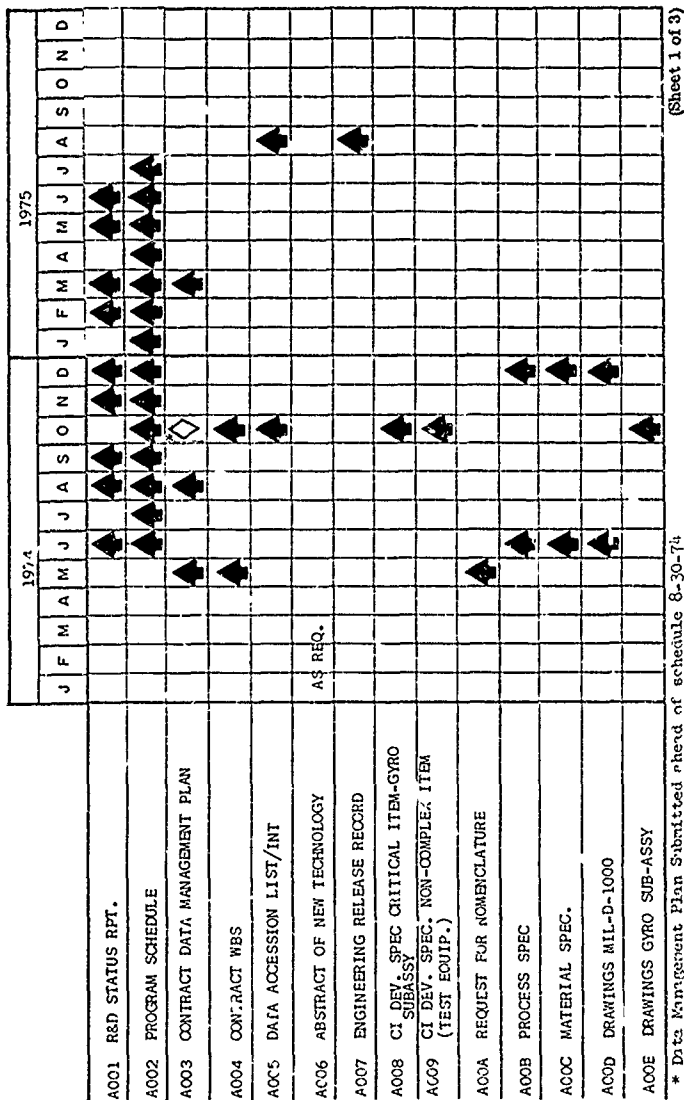
Appendix S lists the audience at each meeting. Appendix T summarizes the various meetings as related to the Applications Engineering Task.

Copies of both the narrative and the "spec type" Applications Engineering survey questionnaires were left with each audience. It was agreed that these questionnaires would be filled out and returned to Autonetics.

No further Applications Engineering activity was performed. This task was terminated per the Stop Work Order received in December 1974.

## 7. TASK 6, DATA

Autoaetics submitted seventy-six data items during Phase 2A in accordance with the Contract Data Requirements List (CDRL). The CDRL data items are shown in Figure 7-1. The black arrows indicate the completed items that were submitted to the Air Force.



\* Data Management Plan Submitted ahead of schedule 8-30-74

(Sheet 1 of 3)

Figure 7-1. Phase 2A MICRON Data Schedule (Sheet 1 of 3)

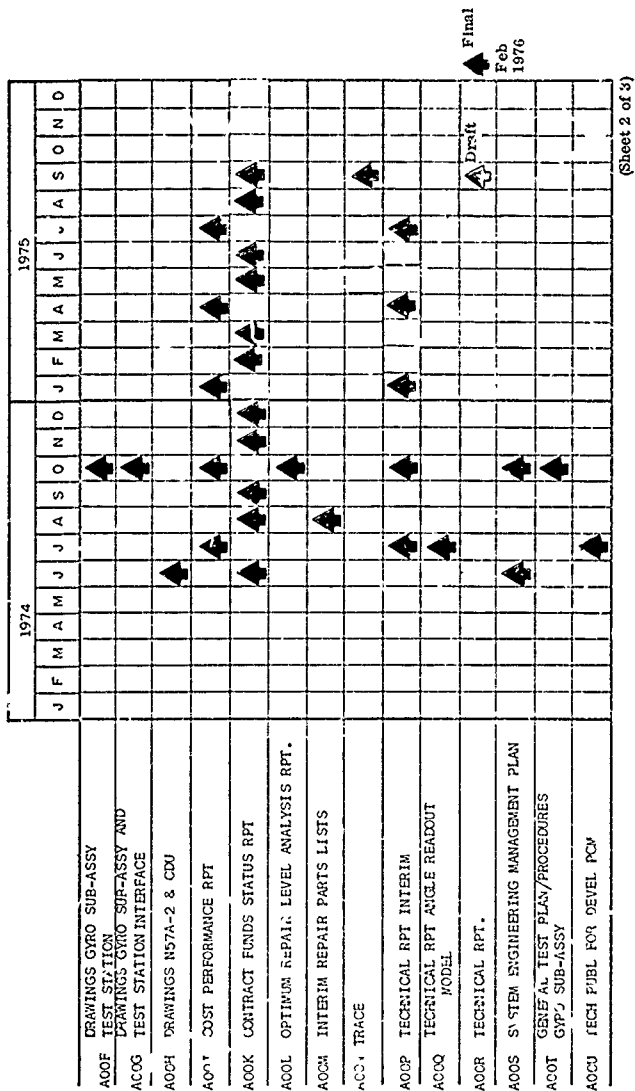


Figure 7-1. Phase 2A MICRON Data Schedule (Sheet 2 of 3)

[illegible]



## 8. PROGRAM SCHEDULE

The MICRON Phase 2A Program Schedule is shown in Figure 11-1. The symbols used are the standard milestone symbols as shown in Figure 11-2.

The line item tasks marked "\*\*\*" were stopped by the reference 4 Stop Work Directive but remain in the reference 5 SOW and are shown on the schedule for completeness. Milestones related to these tasks which extended beyond the effective date of the Stop Work Directive (12/20/75) have been deleted from the schedule to avoid confusion.

The line item tasks marked "\*\*\*\*" were added or extended by the Realigned program (Reference 5). For these tasks which were extended, the arrows were moved to the right per the realigned program without indicating any schedule slip.

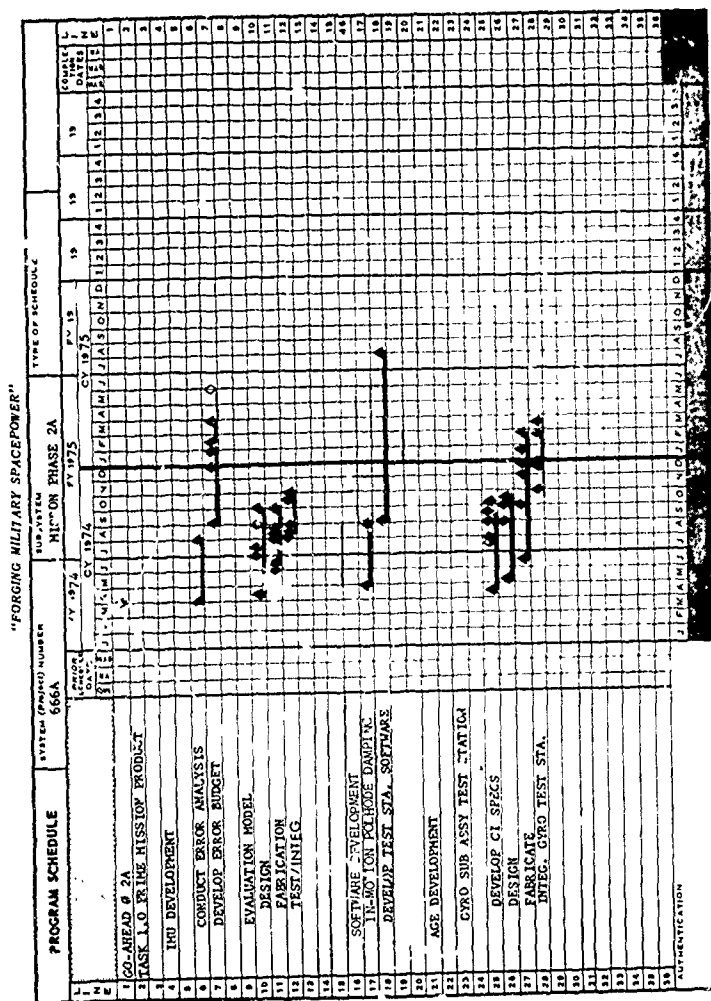
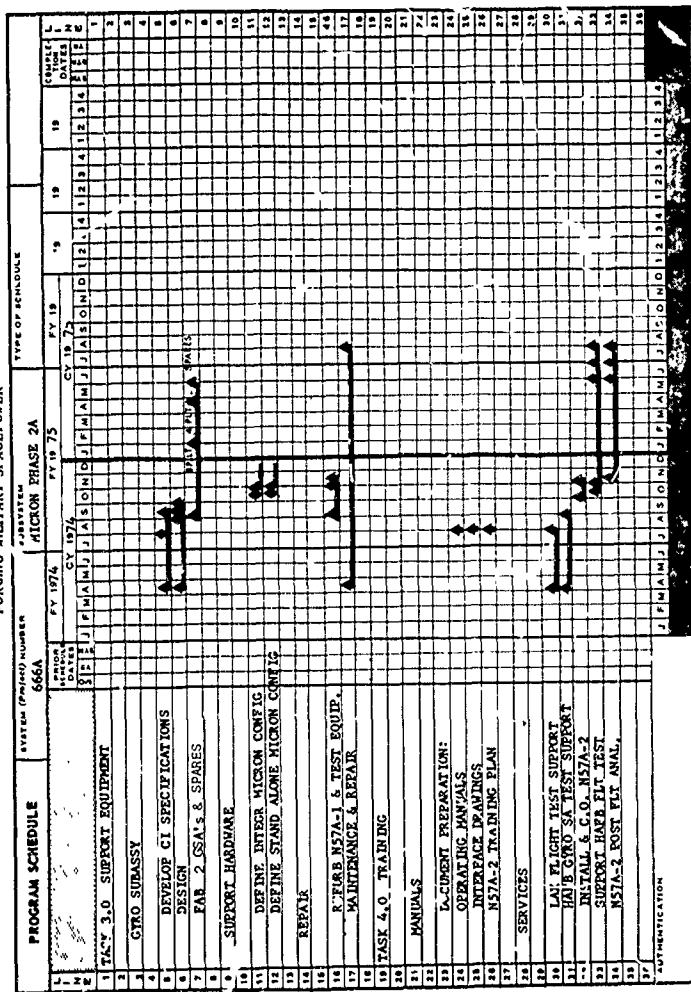


Figure 8-1. Program Schedule (Sheet 1 of 5)



"FORGING MILITARY SPACEPOWER"



"FORCING MILITARY SPACEPOWER"

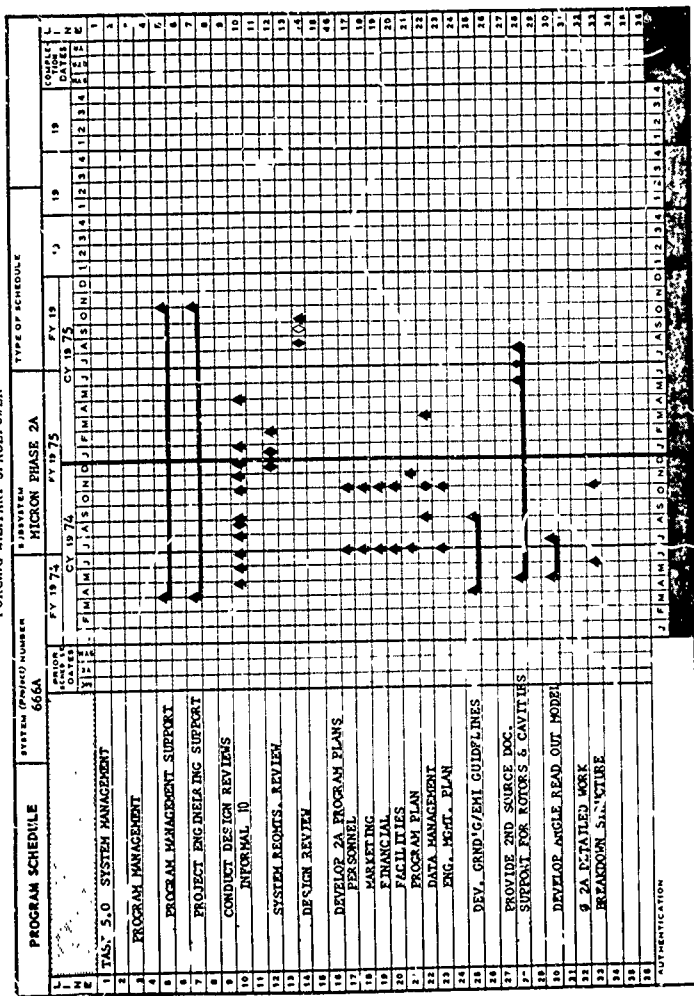


Figure 8-1. Program Schedule (Sheet 4 of 5)

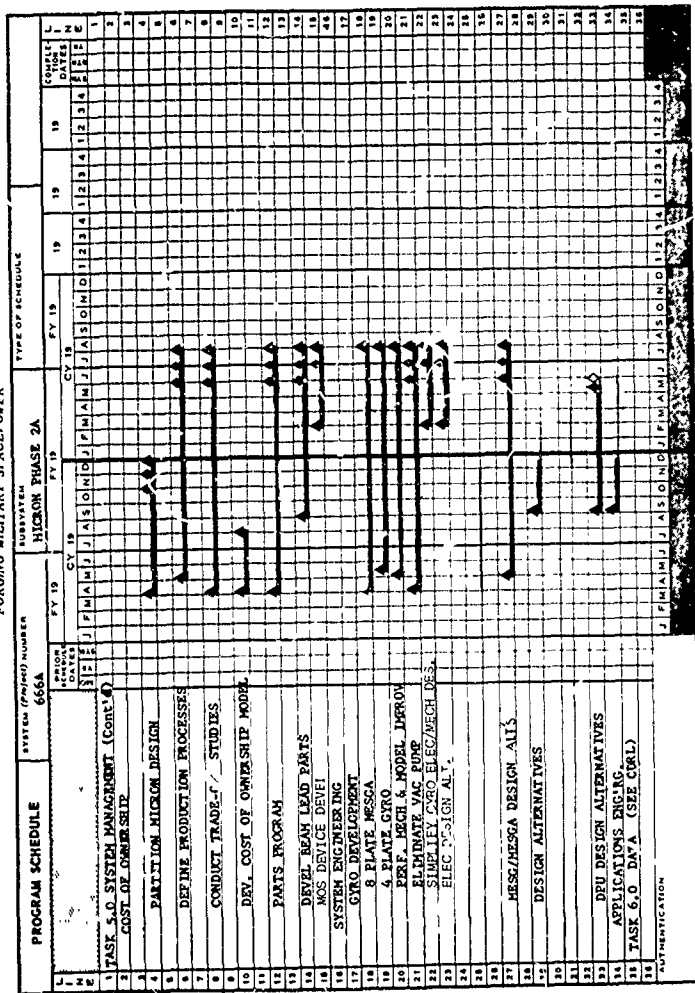


Figure 8-1. Program Schedule (Sheet 5 of 5)















BASIC SYMBOL	MEANING
	Scheduled Completion
	Actual Completion
	Previous Scheduled Completion - Still in future
	Previous Scheduled Completion - Date passed
REPRESENTATIVE USES	MEANING
 	Anticipated Slip - Rescheduled Completion
 	Actual Slip - Rescheduled Completion
 	Actual Slip - Actual Completion
 	Actual Completion Ahead of Schedule
	Time Span Action
	Progress Along Time Span

Figure 8-2. Standard Milestone Symbols

## 9. REFERENCES

1. Purchase Request No. FY11757500472, Attachment No. 1, Statement of Work, dated 10 May 74, MICRON Phase 2A.
2. Purchase Request No. FY1175400472, Appendix I, Specification for the Micro-Navigator (MICRON) Inertial Measurement Unit (IMU) dated 13 May 74.
3. Purchase Request No. FY11757510547, Attachment No. 1, Statement of Work, dated 6 August 1974, MICRON Phase 2A.
4. 4950/PMEB Stop Work Directive, dated 16 December 1974.
5. Purchase Request No. FY11757510680, Attachment No. 1, Statement of Work, dated 29 January 1975, MICRON Phase 2A.